Math-for-industry
Education & Research Hub

ISSN2188-1200

IMI Workshop of the Joint Usage Research Projects

Evolving Design and Discrete Differential Geometry: towards Mathematics Aided Geometric Design

Editors: Makoto Ohsaki and Yoshiki Jikumaru

九州大学マス・フォア・インダストリ研究所

MI Lecture Note Vol.101 : Kyushu University

IMI Workshop of the Joint Usage Research Projects

Evolving Design and Discrete Differential Geometry: towards Mathematics Aided Geometric Design

Editors Makoto Ohsaki and Yoshiki Jikumaru

About MI Lecture Note Series

The Math-for-Industry (MI) Lecture Note Series is the successor to the COE Lecture Notes, which were published for the 21st COE Program "Development of Dynamic Mathematics with High Functionality," sponsored by Japan's Ministry of Education, Culture, Sports, Science and Technology (MEXT) from 2003 to 2007. The MI Lecture Note Series has published the notes of lectures organized under the following two programs: "Training Program for Ph.D. and New Master's Degree in Mathematics as Required by Industry," adopted as a Support Program for Improving Graduate School Education by MEXT from 2007 to 2009; and "Education-and-Research Hub for Mathematics-for-Industry," adopted as a Global COE Program by MEXT from 2008 to 2012.

In accordance with the establishment of the Institute of Mathematics for Industry (IMI) in April 2011 and the authorization of IMI's Joint Research Center for Advanced and Fundamental Mathematics-for-Industry as a MEXT Joint Usage / Research Center in April 2013, hereafter the MI Lecture Notes Series will publish lecture notes and proceedings by worldwide researchers of MI to contribute to the development of MI.

October 2022
Kenji Kajiwara
Director, Institute of Mathematics for Industry

Evolving Design and Discrete Differential Geometry: towards Mathematics Aided Geometric Design

MI Lecture Note Vol.101, Institute of Mathematics for Industry, Kyushu University
ISSN 2188-1200
Date of issue: October 1st, 2025
Editors: Makoto Ohsaki and Yoshiki Jikumaru
Publisher:
Institute of Mathematics for Industry, Kyushu University
Graduate School of Mathematics, Kyushu University
Motooka 744, Nishi-ku, Fukuoka, 819-0395, JAPAN
Tel +81-(0)92-802-4402, Fax +81-(0)92-802-4405
URL https://www.imi.kyushu-u.ac.jp/

Preface

The International Workshop on "Evolving Design and Discrete Differential Geometry - Towards Mathematics Aided Geometric Design" was convened during March 10–13, 2025, in Fukuoka, Japan, under the joint support by Institute of Mathematics for Industry (International Project Research: Workshop (I)) and JST CREST (JPMJCR1911).

Recently, we have been experiencing rapid developments in curved surface design in various fields of design and engineering including architectural design, industrial design, mechanical design, computer graphics, and data processing. In other words, we are facing a kind of paradigm shift in the design and manufacturing process; for example, some of the traditional subtractive manufacturing has been replaced by additive manufacturing. With the development of design tools, demand for designing complex surfaces has increased. Accordingly, design methods for manufacturing and constructing complex continuous/discrete surfaces are becoming important. In this situation, we have growing demand for coordination among the researchers and practitioners in artistic design, structural design, industrial design, as well as those in fabrication and construction.

Discrete differential geometry is an important field of mathematics with applications in curved surface design. The research group of JST CREST with the same title as this workshop has been working on the discrete forms of variational principle and non-Euclidian geometry, and has proposed various methods of designing discrete surfaces with properties such as foldable/retractable surfaces, constant mean curvature surfaces, polyhedral surfaces by rigid origami, aesthetically pleasing surfaces, etc. In order to provide the results of these studies in a publicly accessible form, a prototype of a platform has been developed for performing the design, analysis, and fabrication/construction in an interactive, cyclic, and bi-directional manner on the same surface model.

This meeting provided a forum to exchange information between researchers and practitioners on the theories and techniques underlying the development of design platforms that are based on mathematics, information science, architectural design, and engineering. To enable the design of a structure that has aesthetic value and ensure its safety, 66 researchers and practitioners including nine invited prominent speakers in the related fields discussed during a four day period of meeting to identify common issues through the presentations by experts from all over the world as well as those in the CREST project. The mathematical formulations for new shape design methods based on discrete differential geometry and the variational principle will open a new direction for curved surface design. This meeting has provided an important opportunity to reintegrate knowledge on the geometry of curves and surfaces using mathematics as a hub and sublimate it into a new field of discrete differential geometry for shape design, and to revive Japanese manufacturing, which produces precise and beautiful products but suffers from their high costs.

Chief Editor: Makoto Ohsaki (Kyoto University)
April 2025

2024年度九州大学マス・フォア・インダストリ研究所 共同利用・共同研究　一般研究-研究集会(I)

Evolving Design and Discrete Differential Geometry:

towards Mathematics Aided Geometric Design

2025 3.10 mon ▸ 3.13 thu

九州大学西新プラザ

〒814-0002　福岡市早良区西新2-16-23

参加無料
対面開催
事前申込制

URL:https://joint.imi.kyushu-u.ac.jp/post-15000/

運営責任者、組織委員

大崎 純(京都大学, 責任者)
前川 卓(早稲田大学)
三浦 憲二郎(静岡大学)
梶原 健司(九州大学)
三谷 純(筑波大学)
横須賀 洋平(鹿児島大学)
滝沢 研二(早稲田大学)
中嶋 拓(大林組)
堺 雄亮(ソニーコンピュータサイエンス研究所)

招待講演者

Alexander Bobenko(Technische Universität, Berlin)
Yuri Suris(Technische Universität, Berlin)
Olivier Baverel(Ecole des Ponts ParisTech / Ecole nationale superieure d'architecture de Grenoble)
Robin Oval(Delft University of Technology)
Bert Juettler(Johannes Kepler University)
Rudrusamy U. Gobithaasan(Universiti Sains Malaysia)
Md Yushalify Misro(Universiti Sains Malaysia)
Toby Mitchell(Thornton Tomasetti)
Masaaki Miki(University of Tokyo)

問い合わせ先:共同利用・共同研究拠点事務室　主催:九州大学マス・フォア・インダストリ研究所　共催:JST CREST[数理情報活用基盤]設計の新パラダイムを拓く新しい離散的な曲面の幾何学

九州大学 KYUSHU UNIVERSITY

Institute of Mathematics for Industry Kyushu University

Joint Research Center for Advanced and Fundamental Mathematics-for-Industry
文部科学大臣認定「産業数学の先進的・基礎的共同研究拠点」
九州大学マス・フォア・インダストリ研究所

EDGE

Program

March 10th (Mon.), 2025

9:00-9:30 Opening: Kenji Kajiwara

9:30-10:15 Keynote 1:Olivier Baverel
Make complex structures affordable
Chair: Kazuki Hayashi

10:45-11:30 Keynote 2:Robin Oval
An algebra for topology finding of surface patterns for structural design driven by similarity
Chair: Kazuki Hayashi

11:30-12:00 Kyoto Group 1
Kazuki Hayashi
Deployable auxetic surface structures: From optimized shape to detail design implementation
Chair: Yusuke Sakai

12:00-12:30 Kyoto Group 2
Kentaro Hayakawa
Second-order infinitesimal mechanism for bifurcation analysis and folding path approximation of rigid origami
Chair: Yusuke Sakai

13:45-14:30 Keynote 3:Bert Jüttler
Efficient Matrix Assembly and Adaptive Refinement in Isogeometric Analysis
Chair: Takashi Maekawa

14:30-15:00 Kyoto Group 3
Jingyao Zhang
Shape generation of free-form grid shells with polygonal panels
Chair: Kentaro Hayakawa

15:00-15:30 Kyoto Group 4
Yusuke Sakai

Tessellation as a design principle for mechanical metamaterial
Chair: Kentaro Hayakawa

16:00-16:30 Waseda Group 1
Takashi Maekawa and Felix Scholz
All you need is rotation: Construction of developable strips – Part 1 Theory
Chair: Kenjiro T. Miura

16:30-17:00 Waseda Group 2
Takashi Maekawa and Felix Scholz
All you need is rotation: Construction of developable strips – Part 2 Applications
Chair: Kenjiro T. Miura

17:00-17:30 Waseda Group 3
Maya Okada, Naoyuki Fujita, Takuya Terahara, Yastoshi Taniguchi, Kenji Takizawa and Tayfun E. Tezduyar
Isogeometric Analysis of Membrane and Cable Structures: A Design of Umbrella Zero-Stress State
Chair: Kenjiro T. Miura

17:30-18:00 Waseda Group 4
Takuya Terahara, Kenji Takizawa and Tayfun E. Tezduyar
Continuity and Smoothness in T-Splines Representations of Structures with Different Parametric Dimensions
Chair: Kenjiro T. Miura

March 11th (Tue.),2025
9:30-10:00 Kyushu Group 1
Kenji Kajiwara
Generation of Aesthetic Shapes by Integrable Klein Geometry
Chair: Miyuki Koiso

10:00-10:30 Kyushu Group 2
Yoshiki Jikumaru
Geometry of Michell-Prager type structures and hanging membranes

Chair: Miyuki Koiso

10:45-11:30 Keynote 4: Yuri Suris
Discretization of quadrics and of elliptic coordinates
Chair: Yoshiki Jikumaru

11:30-12:00 Kyoto Group 5
Yoshihiro Kanno
Surface generation for confidence-based data-driven computing in elasticity with application to reliability-based truss topology optimization
Chair: Jingyao Zhang

12:00-12:30 Kyoto Group 6
Makoto Ohsaki
Optimization methods for continuum and latticed shells consisting of developable parts
Chair: Jingyao Zhang

14:00-14:30 Kyoto and Kyushu Group
Kentaro Hayakawa
Introduction to the software platform
Chair: Makoto Ohsaki

14:30-15:15 Keynote 5: Alexander I. Bobenko
Discrete conformality and beyond. Where geometry meets computer graphics and mathematical physics (Online)
Chair: Kenji Kajiwara

16:00-16:30 Tsukuba Group 1
Jun Mitani
Interactive Design and Efficient Simulation of Developable Surfaces with Curved Folds
Chair: Makoto Ohsaki

16:30-17:00 Tsukuba Group 2
Kosuke Horiuchi and Jun Mitani
Modeling of Discrete Developable Surfaces with a Break Using Trace Diagrams on the

Gaussian Sphere
Chair: Makoto Ohsaki

17:00-17:30 Tsukuba Group 3
Aida Safary and Jun Mitani
Parametric Design Tools for 3D Curved-Origami Shapes in Conceptual and Prototype Architectural Design
Chair: Makoto Ohsaki

17:30-18:00 Tsukuba Group 4
Higa Miyashiro Pamela, Yiyang Jia and Jun Mitani
Hoberman's Scissor Mechanism and Digital Fabrication
Chair: Makoto Ohsaki

March 12th (Wed.),2025
9:30-10:15 Keynote 6 Toby Mitchell
Surface Rationalization and Optimization in Structural Engineering Practice
Chair: Yohei Yokosuka

10:45-11:30 Keynote 7 Masaaki Miki
Variable Projection (VarPro) Method and Form-finding of Tension-compression Mixed Shells
Chair: Yohei Yokosuka

11:30-11:50 Kagoshima Group 1
Yohei Yokosuka
Curved Surface Structures with Excellent Mechanical Rationality and Constructability/ Fabricability
Chair: Yoshiki Jikumaru

11:50-12:10 Kagoshima Group 2
Yohei Yokosuka
Lie Spherical Geometry and Design of Curved Surface Structures
Chair: Yoshiki Jikumaru

12:10-12:30 Kagoshima Group 3

Yohei Yokosuka
Form-finding of Composite Tensile Structures by Finite Element Technique based on Nodal Coordinate Assumption
Chair: Yoshiki Jikumaru

14:00-14:30 Kyoto Group 7
Kazuki Hayashi
Piecewise constant mean curvature surfaces
Kentaro Hayakawa
From generation of rigid origami for approximating a curved surface
Chair: Makoto Ohsaki

14:30-15:00 Kyushu Group 4
Miyuki Koiso
Pillow boxes as developable surfaces with curved foldings
Chair: Makoto Ohsaki

15:00-15:30 Kagoshima Group 4
Yohei Yokosuka
Temporary structures with curved folding
Chair: Makoto Ohsaki

16:00-16:30 Poster Short Talks

16:30-18:00 Poster Session
Presenter ＃ 1: Vishesh Bhat (Okinawa Institute of Science and Technology)
Shaping developables – a dual design recipe

Presenter ＃ 2: Kaito Satake (Kanazawa University)
Title: On isothermic coordinate systems for CMC surfaces in the Lorentz-Minkowski 3-space

Presenter ＃ 3: Sanako Suzuki (Mukogawa Women's University)
Title: Geometric Shape Generation by Singular Generalized Miura-ori with Canonical and Non-canonical Arrangements

18:30- Banquet

March 13th (Thurs.),2025

9:30-10:15 Keynote8 Rudrusamy U. Gobithaasan
Local & global property quantification with persistent homology
Chair: Kenjiro T. Miura

10:45-11:30 Keynote 9 Md Yushalify Misro
Advancing precision and smoothness of shape preserving with quintic trigonometric Bézier curves
Chair: Kenjiro T. Miura

11:30-12:00 Shizuoka Group 1
Kenjiro T. Miura
Extension of κ-curve
Chair: Takuya Terahara

12:00-12:30 Kyushu Group 5
Miyuki Koiso
Intrinsic and extrinsic singularities and curvatures of piecewise smooth surfaces
Chair: Shun Kumagai

12:30-13:00 Kyushu Group 6
Yoshiki Jikumaru
Geometric shape generation for ideal lighting
Chair: Shun Kumagai

13:00- Closing:Makoto Ohsaki

Contents

Make complex structures affordable

Olivier Baverel
Ecole Nationale des Ponts et Chaussées / ENSAG

Abstract

The presentation focuses on research proposals that make complex structures more affordable constructions. By reinforcing the links between mechanics of materials, structural engineering, applied mathematics and life cycle analysis, new paths may be explored and building innovations proposed. First a focus is made on the life cycle analysis showing that CO2 is not the only parameter to tackle environmental problems. Secondly proposals based on a rigorous mathematical management of shapes and geometry to rationalize complex situations in a fully integrative way, including cladding and connections will be explained. These knowledges may help to find ways to reuse manufactured goods to limit the environmental impact of construction, many case studied will be shown. Finally, new digital and technological tools such as robot or 3D printing allow to revisit ancient techniques and to generate innovative solutions.

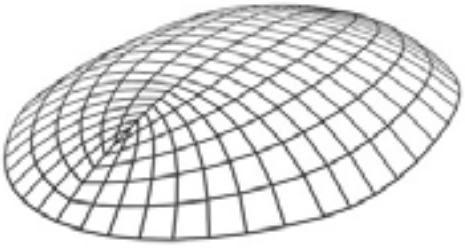

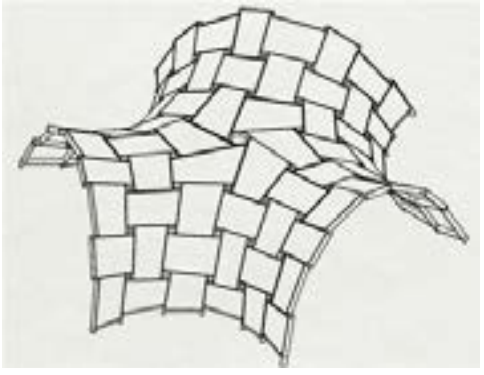

Make complex structures affordable

Prof. Olivier BAVEREL
FIStructE
Prof. Ecole Nationale des Ponts et Chaussées
Prof. ENS Architecture Grenoble
Laboratoire Navier/GSA,

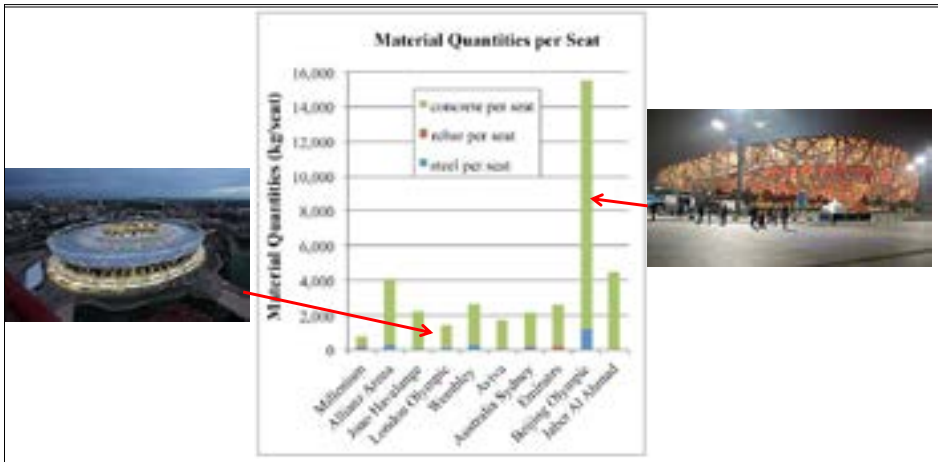

Comparing material quantities and embodied carbon in stadia

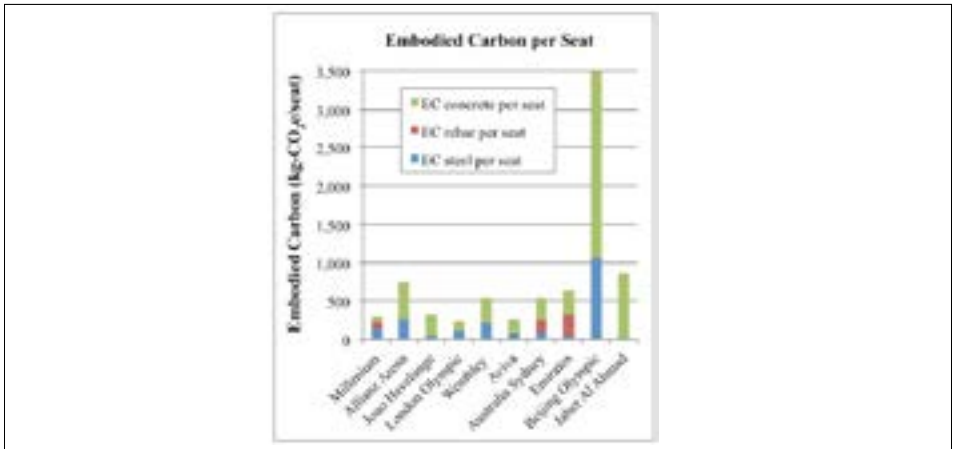

Comparing material quantities and embodied carbon in stadia

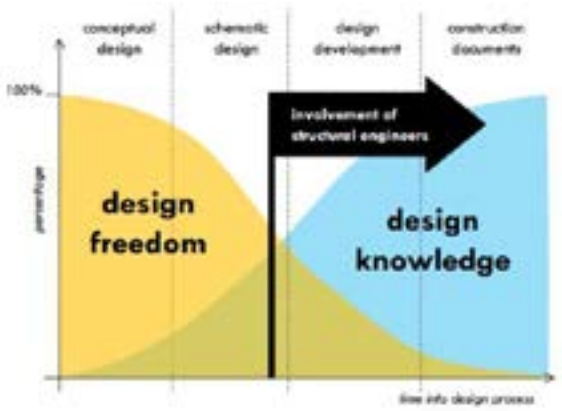

Our challenge

No method

No tool

But we have a strategy

Strategy for a structural innovation

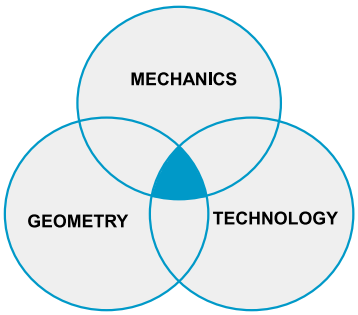

20 YEARS OF RESEARCH ON ELASTIC GRIDSHELLS

2007 Prototypes ENPC

2011 Solidays Festival

2013 Créteil Tem Cathedral

2016 Hybrid Structural Skin

2021

PONTS ParisTech

IP PARIS

T/E/S/S

Navier

VIRY

Classical method for elastic gridshells

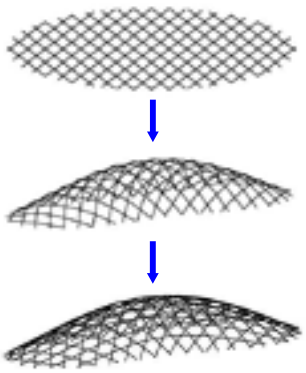

Construction with straight laths

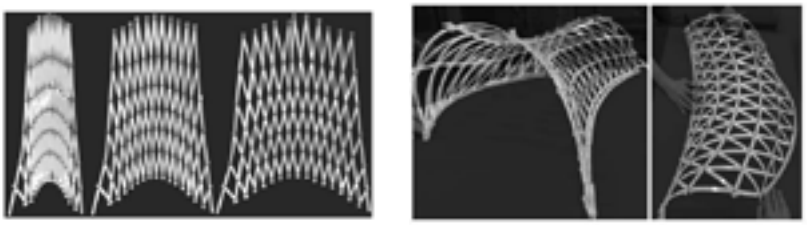

Geodesic gridshells

C. Haskell,

10

Geodesic gridshells

Voss Surfaces

N Montagne , PhD Thesis SXL LAB EPFL/ NAVIER ENPC

Voss surfaces

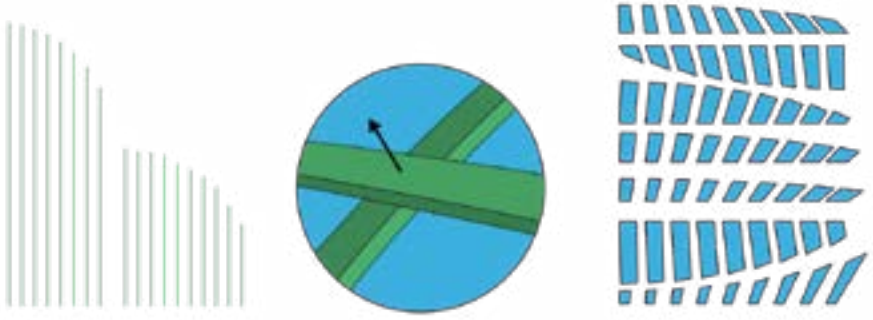

N Montagne , PhD Thesis SXL LAB EPFL/ NAVIER ENPC

Mathematically

A Voss surface is a surface on which there exists two families of geodesic curves forming a conjugate network.

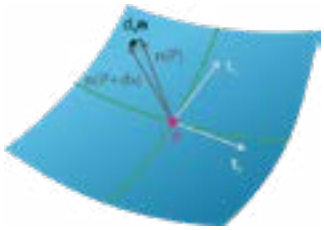

Computationally

A discrete Voss surface in the family of quadrilateral meshes is formed by discrete geodesics and planar facets.

Voss Surface

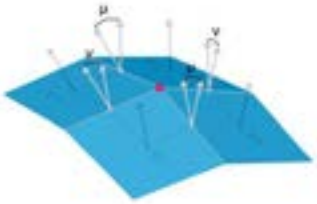

Gauss Map

Figure 2: Spherical projection of dihedral angles. The angles made by adjacent face normals (left) are equal to the arc length of the edge in the Gauss map connecting these normals (right).

Gauss Map

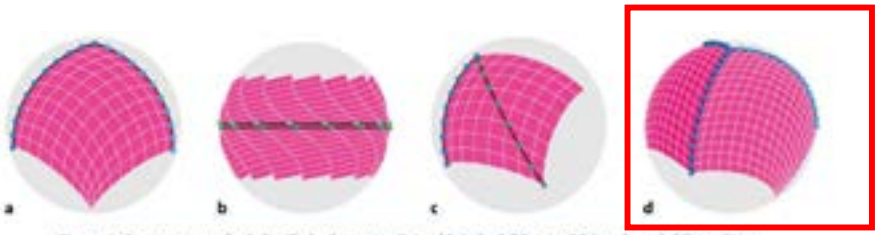

Figure 6: Generation methods for Chebyshev nets : Primal (a), dual (b), mixed (c) and patch (d) conditions.

On a Cheybysev net the integral of curvature cannot exceed Pi

Generation of Voss surface

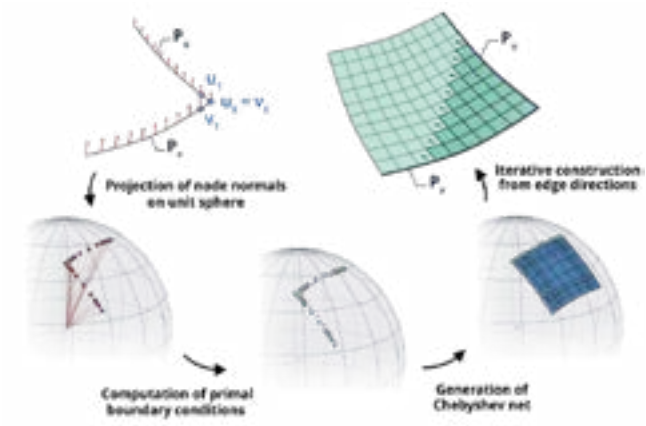

Generation of Voss surface

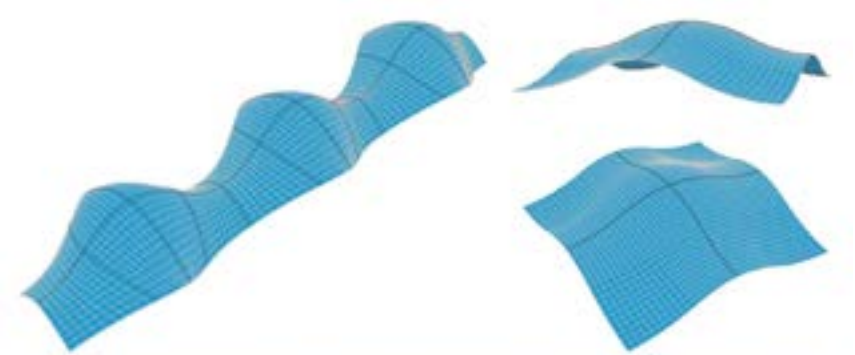

Figure 11: Voss nets created from two boundary curves. Left: Geodesic gridshell inspired by the gridshell of Downland. Right: Geodesic gridshell canopy which can be repeated in both directions.

Isometric Transformation of Voss surface

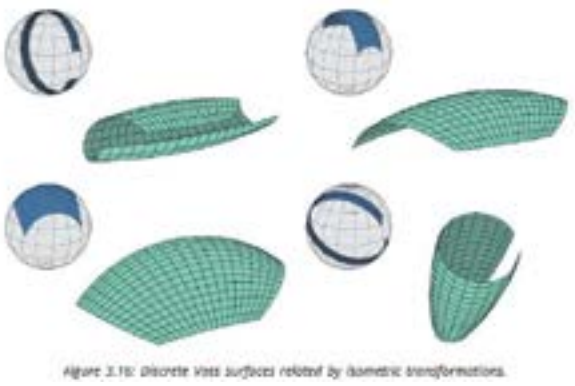

Figure 3.16: Discrete Voss surfaces related by isometric transformations.

N Montagne , PhD Thesis SXL LAB EPFL/ NAVIER ENPC

Geometry of a Pavillion

N Montagne , PhD Thesis SXL LAB EPFL/ NAVIER ENPC

N Montagne , PhD Thesis SXL LAB EPFL/ NAVIER ENPC

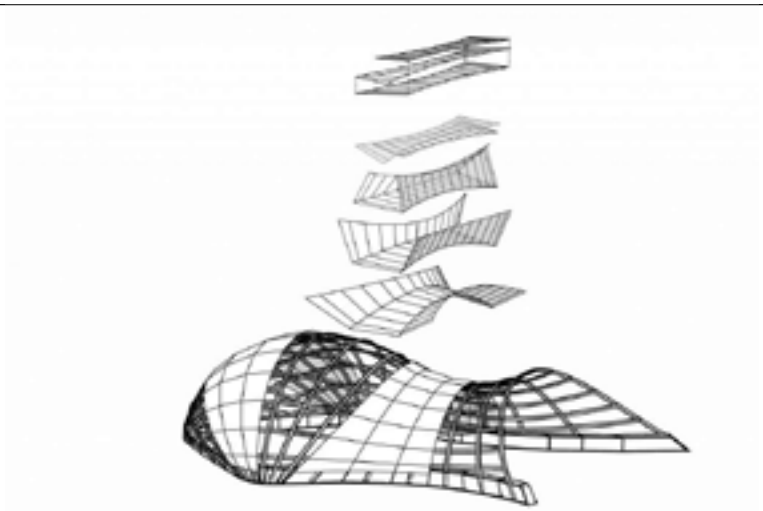

N Montagne , PhD Thesis SXL LAB EPFL/ NAVIER ENPC

N Montagne , P

Tchebidesic Pavillion

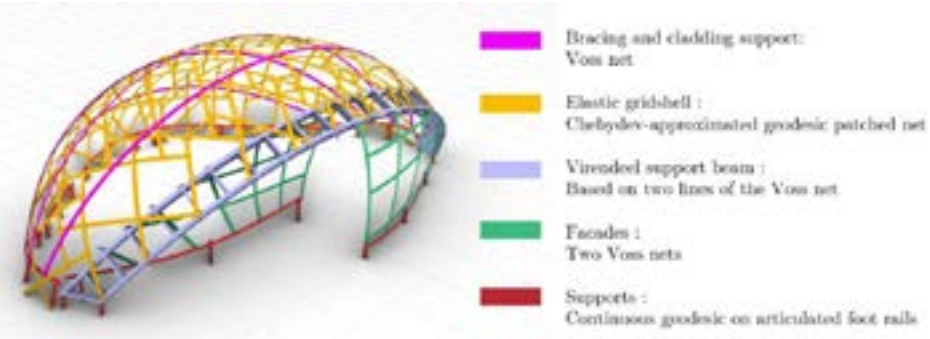

C. Haskell

Tchebidesic Pavillion

C. Haskell

Need for a structural innovation

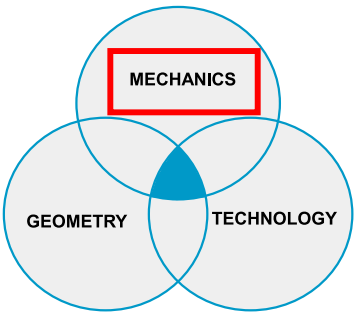

Asymptotic gridshells

Asymptotic gridshells

- Laths laid along asymptotic curves
- Zero normal curvature
- Laths laid ‘perpendicular’ to the surface

Asymptotic network on a minimal surface– Arch. Eike SCHLING

28

Can we get the best from both worlds?

Comparison of morphological approaches

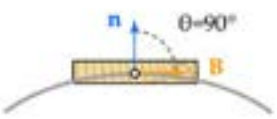

Geodesic gridshell

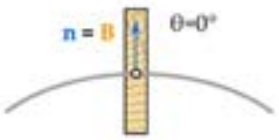

Asymptotic gridshell

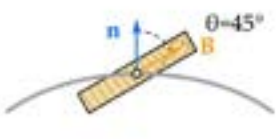

Pseudo-geodesic gridshell (ours)

Comparison of morphological approaches

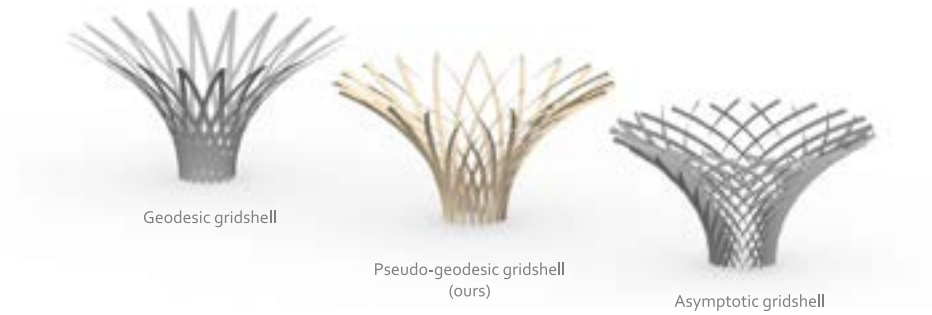

R Mesnil,

Congruent Connector Design

- Axis of connector aligned with surface normal
- Constant angle triangular plates
- Free degree of freedom in rotation
- Patent pending (Mesnil& Baverel 2021)

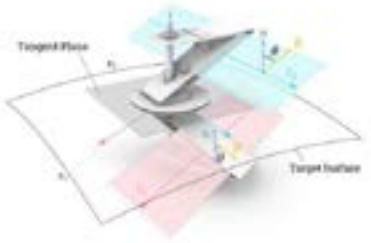

R Mesnil, *O. Baverel*

Implementation

Mesnil, Romain; Muto, Takara; Walia; Krittika; Douthe, Cyril; Baverel, Olivier. « Design and construction of a pseudo-geodesic gridshell." *Advances in Architectural Geometry 2023*.

Grid and shape generation

Parametric shape model (with NURBS)

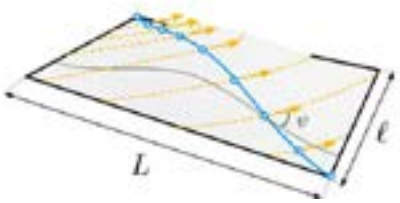

Shooting method from a guide curve (blue). For simplicity, all pseudo-geodesic are shot with the same angle ψ

Fabrication

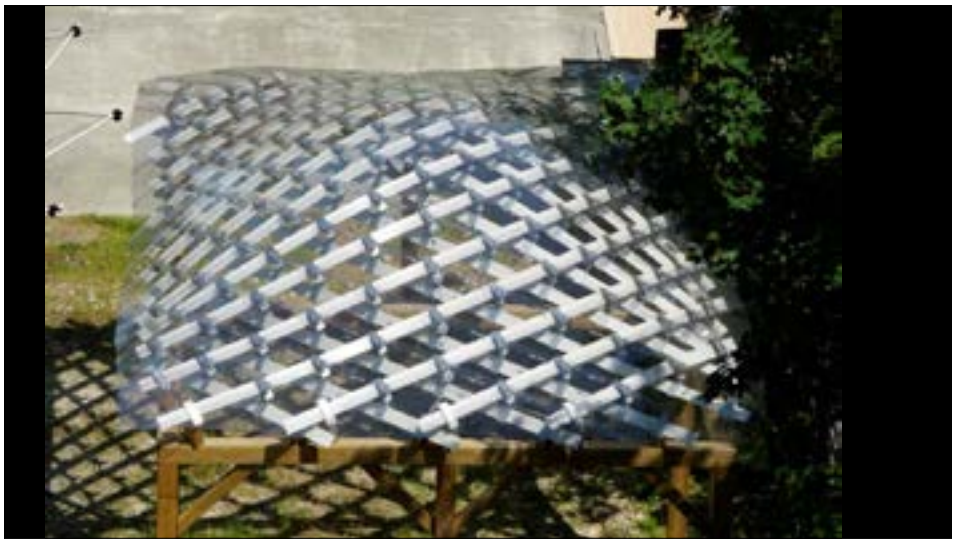

A tool to design?

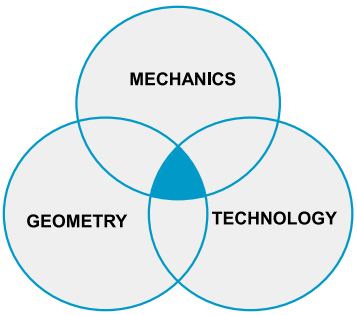

Maxwell's theorem and the Airy stress function

Maxwell's theorem : A planar mesh has a self-stress state if and only if it is the projection of a plane faced polyhedron.

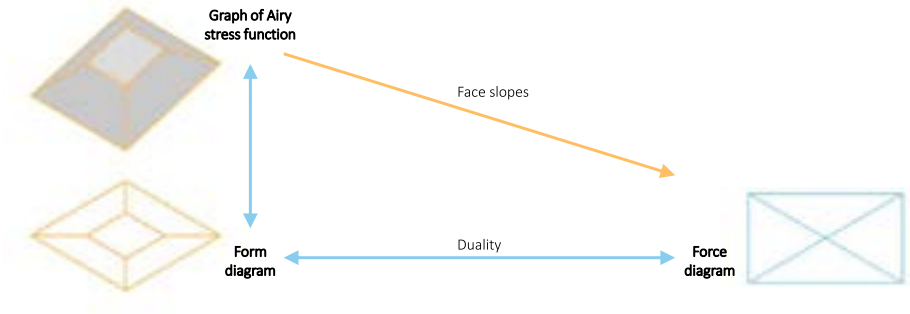

Starting from a plane faced polyhedron: Marionette method

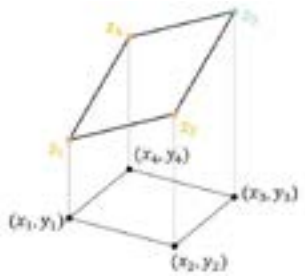

Planar face computation with the Marionette method [1]

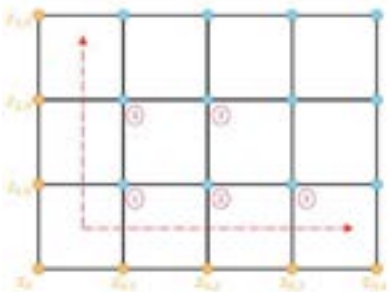

Height propagation principle to obtain the elevation of every node and a three dimensional mesh with planar faces

[1] R. Mesnil et al. "Marionette Meshes: Modelling free-form architecture with planar facets". In: International Journal of Space Structures 32.3 (2017)

A planar panelled shape and its associated funicular loading

given

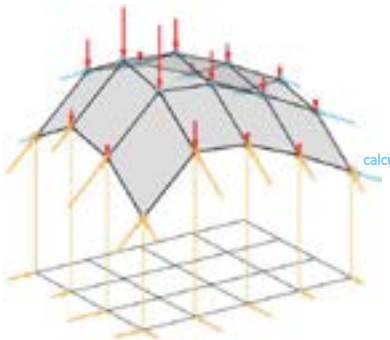

calculated

Equilibrium of a node and propagation

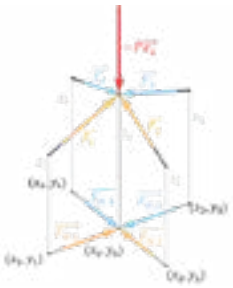

Equilibrium of forces in a vertically loaded node

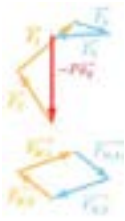

Closure of force polygon in space and in projection

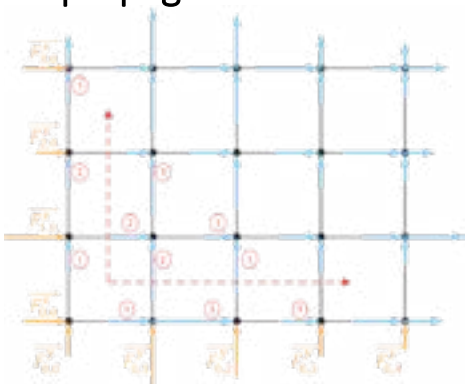

Force propagation principle to obtain the forces in all the bars, and therefore the dual diagram.

Load Finding

given

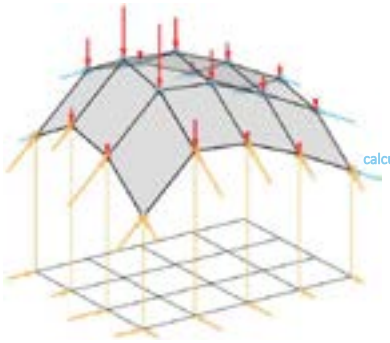

calculated

Optimisation

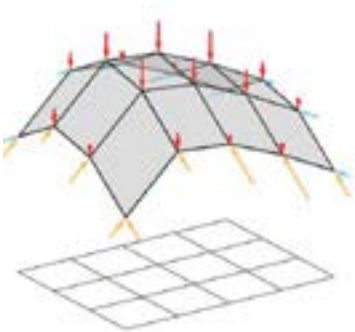

Variation of forces only

Optimisation

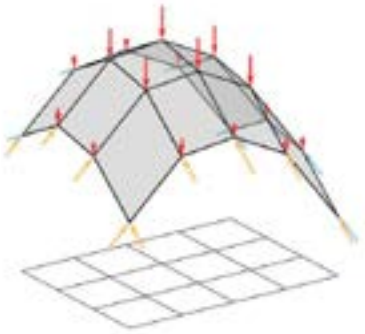

Variation of forces and heights

Funicular deviation as a structural design tool

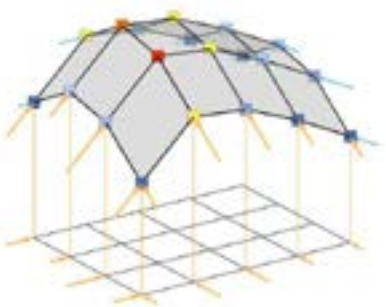

Three-dimensional mesh and the associated vertical loading obtained using the method

Structural innovation

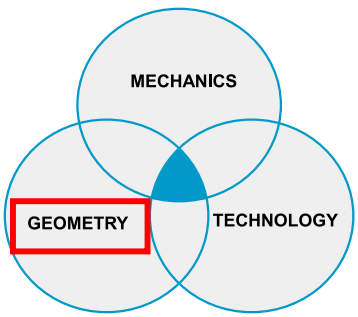

Building with planar curvature lines

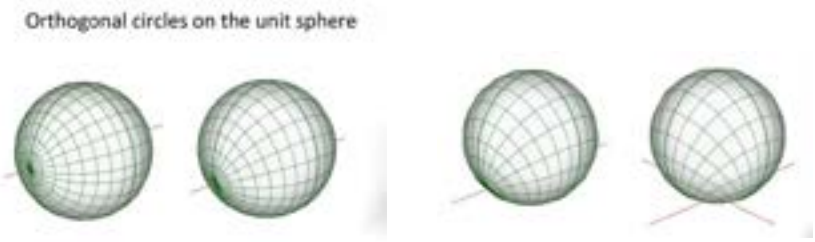

X Tellier, PhD Thesis

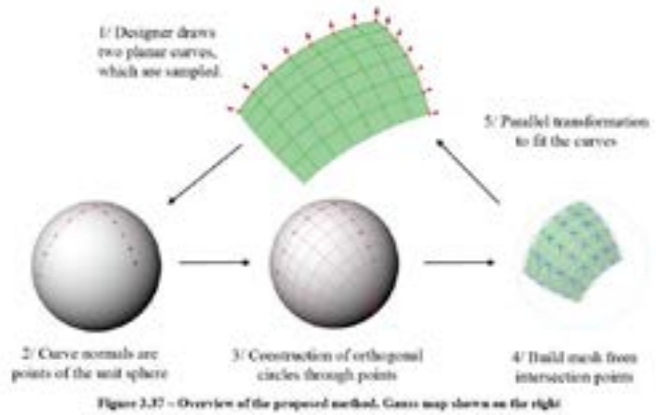

Figure 3.37 – Overview of the proposed method. Gauss map shown on the right

X Tellier, PhD Thesis

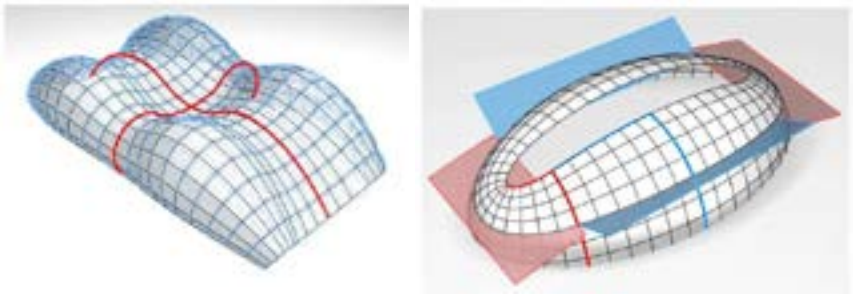

X Tellier, PhD Thesis

CMC Surfaces

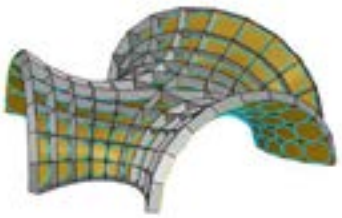

X Tellier, PhD Thesis

Linear Weingarten surfaces

Isotropic LW surfaces

X Tellier, PhD Thesis

Structural innovation

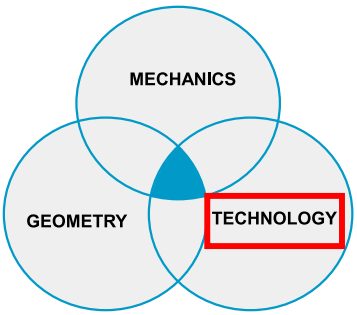

Common space structure

Systèm MERO

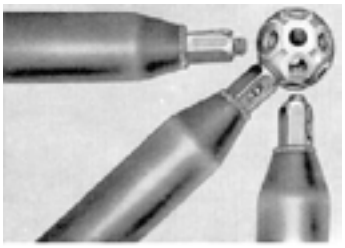

Efficient mechanical behavior
Technologically complex

Space truss

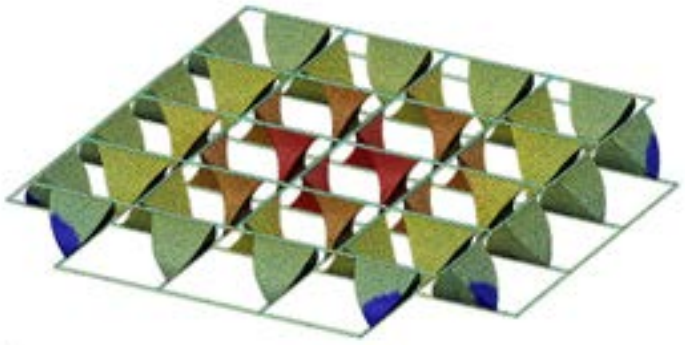

N Leduc, PhD Thesis

N Leduc, PhD Thesis

Structural innovation

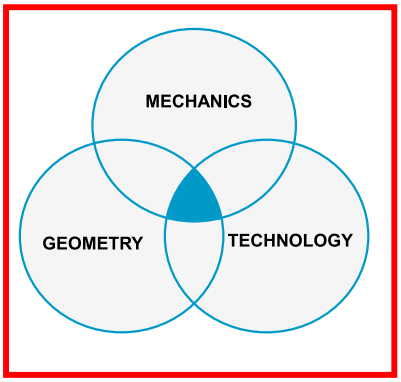

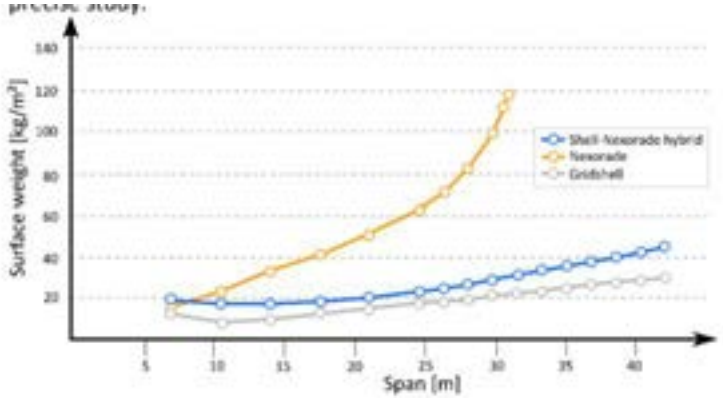

R Mesnil,

Structural innovation

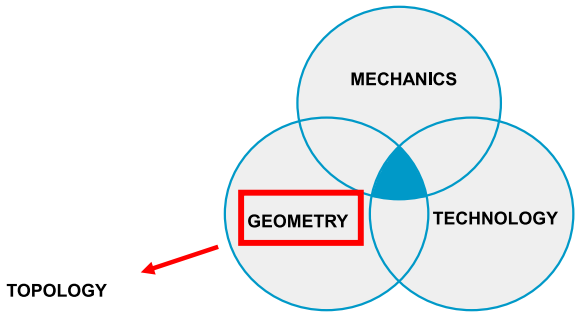

TOWARDS TOPOLOGICAL DESIGN

TOPOLOGICAL DESIGN

PhD of Robin Oval, in collaboration with the Block Research Group (ETH Zürich)

Topology generation of architectural meshes adapted to the support conditions

Romane Boutillier [a,b,*], Cyril Douthe[a], Laurent Hauswirth[b], Olivier Baverel[b,c]

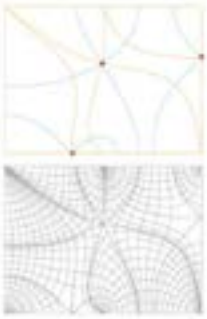

PhD of Romane Boutillier

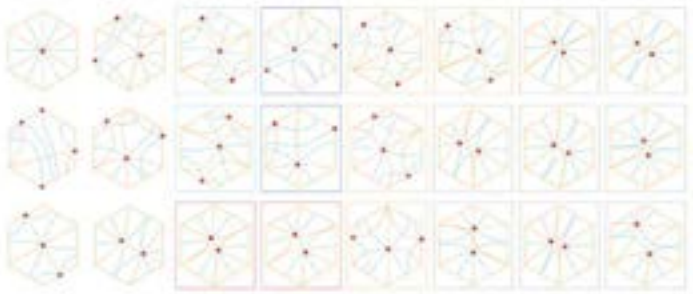

R Boutillier, PhD Thesis

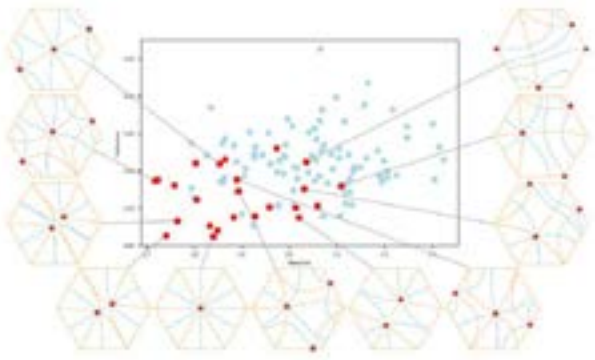

R Boutillier, PhD Thesis

R Boutillier, PhD Thesis

Conclusion

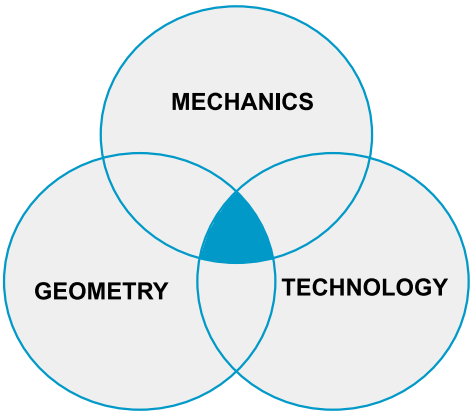

An algebra for topology finding of surface patterns for structural design driven by similarity

Robin Oval
Delft University of Technology, The Netherlands

Abstract

Structural design is a search for the best trade-off between multiple architecture, engineering, and construction objectives, not only mechanical efficiency or construction rationality. Producing hybrid designs from single-objective optimal designs to explore multi-objective trade-offs is common in the design of structural forms, constrained to a single parametric design space. However, producing topological hybrids offers a more complex challenge, as a combinatorial problem that is not encoded as a finite set of real numbers but as an unbonded series of grammar rules. This presentation will focus on a strategy for the generation of hybrid designs of quad-mesh pattern topologies for surface structures. Based on a quad-mesh grammar, an algebra is introduced to measure the distance between designs, find their similar features, and enumerate designs with different degrees of topological similarity. To achieve this, the operators of topological distance, intersection and union of quad meshes will be defined. Structural design applications will be shown to highlight the use of topologically hybrid designs as a surrogate for obtaining multi-objective trade-offs.

An algebra for topology finding of surface patterns for structural design driven by similarity

CREST ED³GE
Hakata, 10/03/2025

Robin Oval
r.oval@tudelft.nl

TUDelft

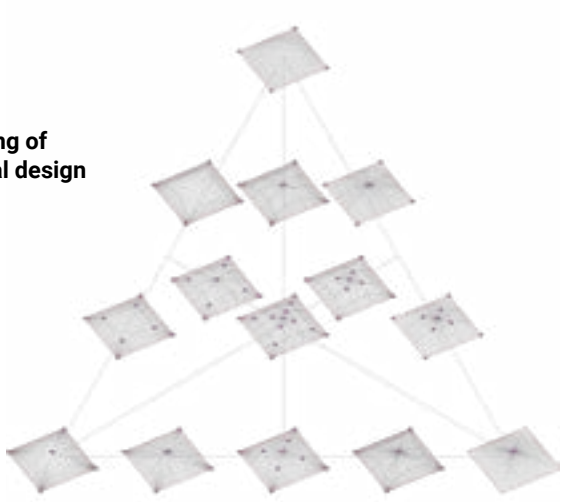

MOTIVATION | Topology at the service of geometry

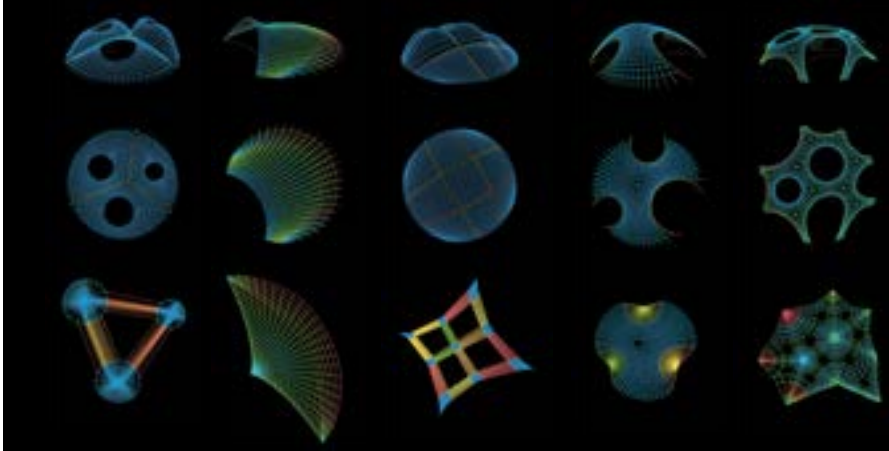

Oval, Rippmann, Van Mele and Block | Beyond the Dome | Architecture Biennale | Venice, Italy | 2016

2

MOTIVATION | Topological optimization

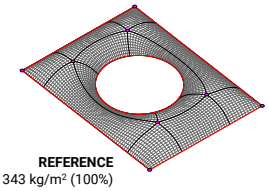

REFERENCE
343 kg/m² (100%)

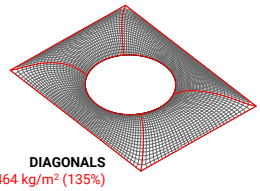

DIAGONALS
464 kg/m² (135%)

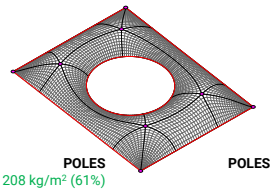

POLES
208 kg/m² (61%)

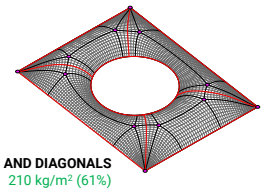

POLES AND DIAGONALS
210 kg/m² (61%)

British Museum | London, UK

MOTIVATION | The challenge of multi-objective search

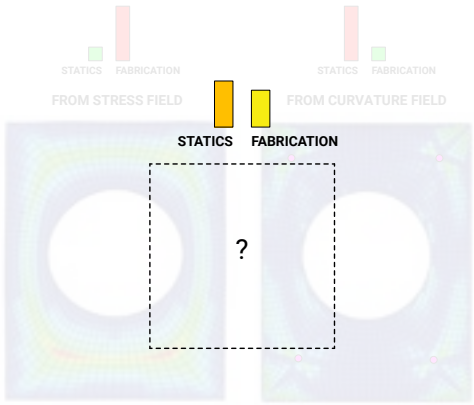

[Schiftner and Balzer, 2010]

4

APPROACH | Quad-mesh topology

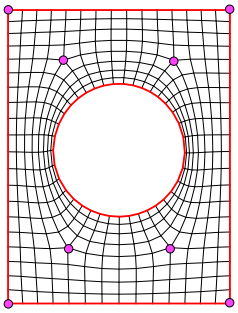

QUAD MESHES = QUADRILATERAL FACES ONLY

SINGULARITIES

VALENCY ≠ 4 OR 3, OFF OR ON BOUNDARY

5

APPROACH | Pole singularities

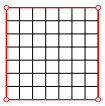

QUAD

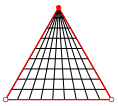

PSEUDO-QUAD
TRIANGLE GEOMETRY
QUAD TOPOLOGY

6

APPROACH | Decoupling design spaces

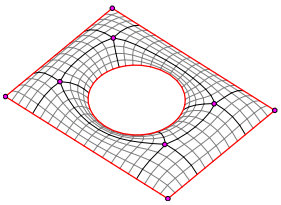

GEOMETRY
QUAD MESH

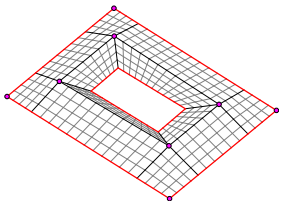

DENSITY
QUAD MESH

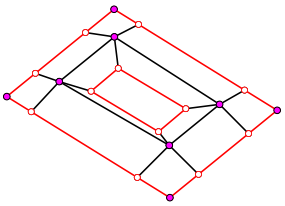

SINGULARITY
COARSE QUAD MESH

7

GRAMMAR | Quad-mesh strip data structure

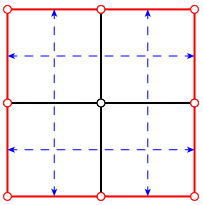

FUNDAMENTAL STRUCTURE OF STRIPS
CONNECTING TOPOLOGICALLY OPPOSITE PAIRS OF EDGE

8

GRAMMAR | Quad-mesh strip data structure

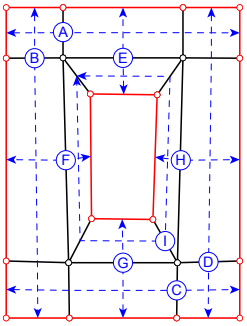

9

GRAMMAR | Two-rule strip grammar

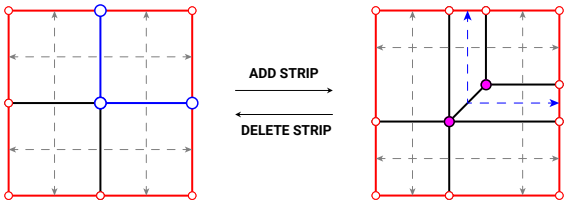

LOW-LEVEL | RECIPROCAL | COMPREHENSIVE

10

GRAMMAR | Rule-based exploration

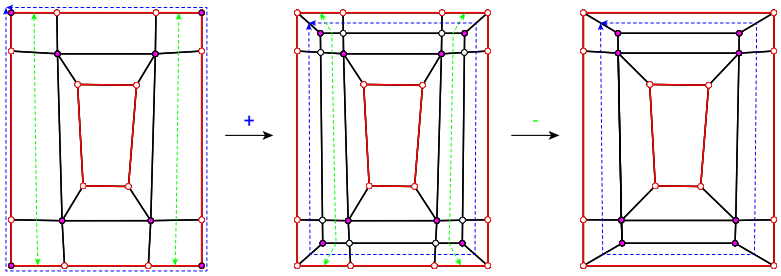

11

GRAMMAR | Rule-based exploration

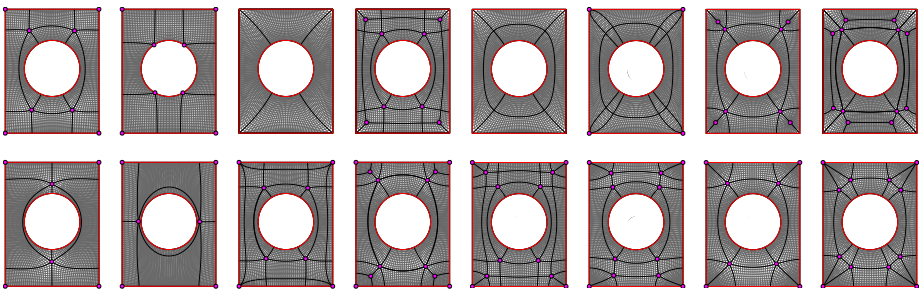

etc.

12

SIMILARITY | Performance-based clusters

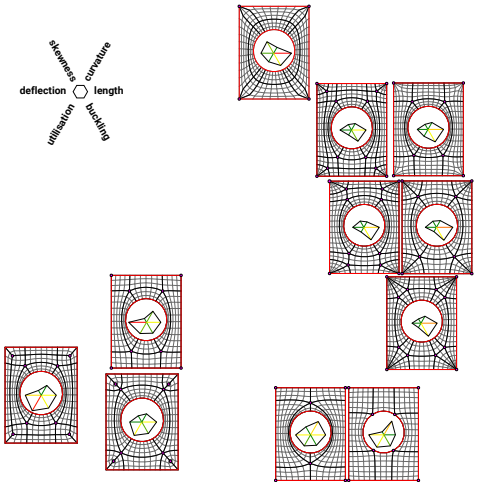

13

SIMILARITY | Performance trade-off

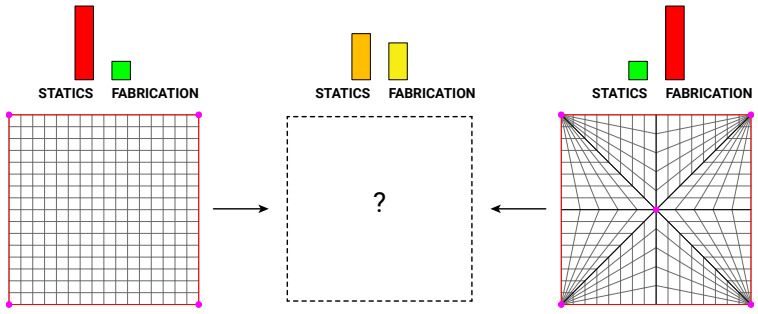

Finding the topological design that provides the performance trade-off

14

SIMILARITY | Surrogate problem

HYPOTHESIS

Designs with similar topologies are likely to have similar performances.

15

SIMILARITY | Topological trade-off

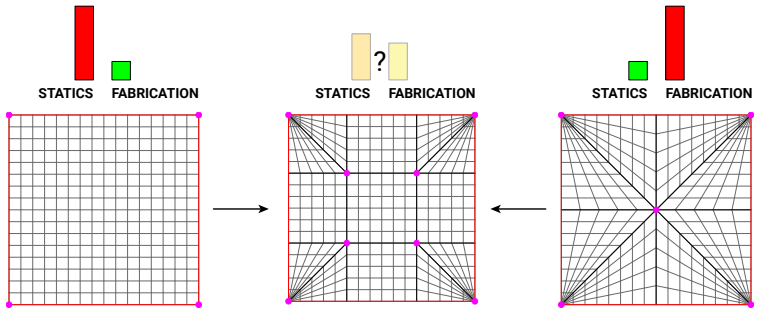

Finding a topological trade-off that may provide a performance trade-off

16

SIMILARITY | Intersection submesh

TOPOLOGICAL SIMILARITY

The largest strip structure in common.

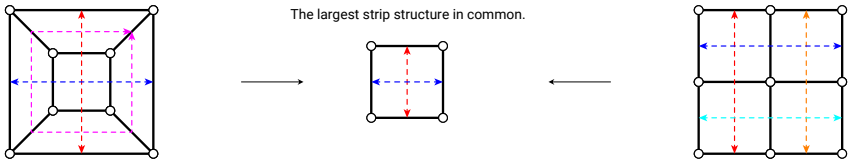

INPUT MESH **INTERSECTION SUBMESH** **INPUT MESH**

17

SIMILARITY | Rule-based topological distance

TOPOLOGICAL DISSIMILARITY OR DISTANCE

The minimum number of rules to convert a mesh into another.

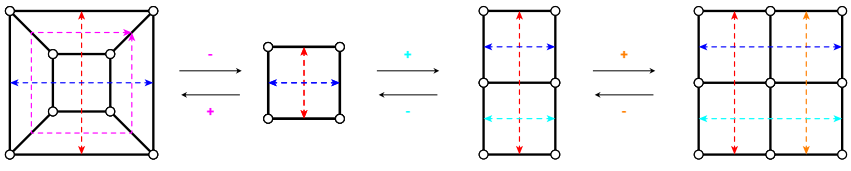

INPUT MESH **INPUT MESH**

DISTANCE = 3

18

SIMILARITY | Union supermesh

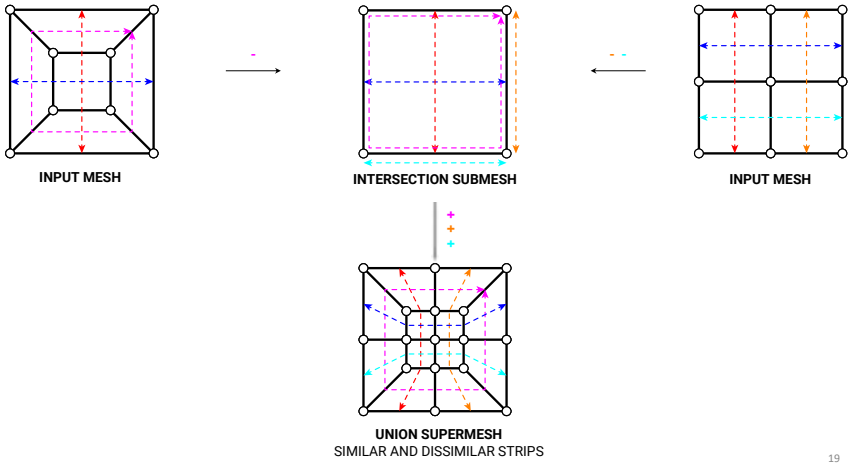

19

SIMILARITY | Intermediary meshes

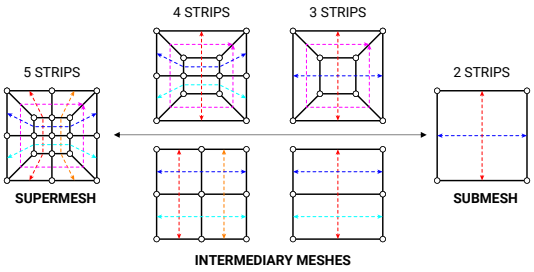

20

Similarity | Gridshell application

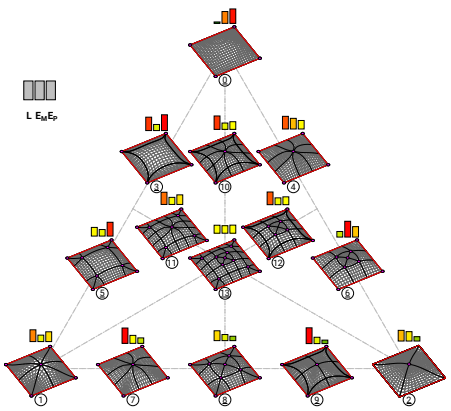

21

Similarity | Gridshell application

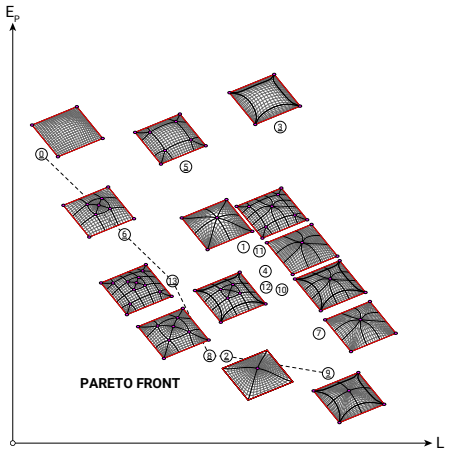

22

Similarity | Gridshell application

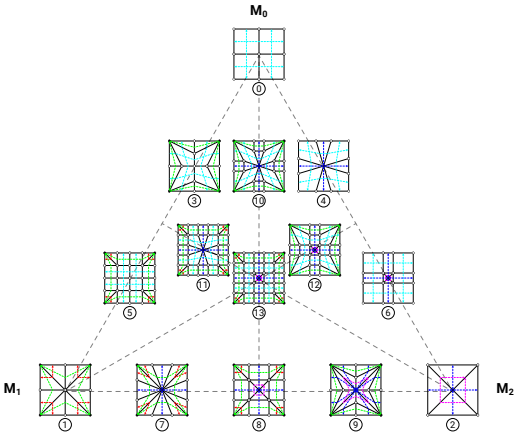

23

Similarity | Dome application

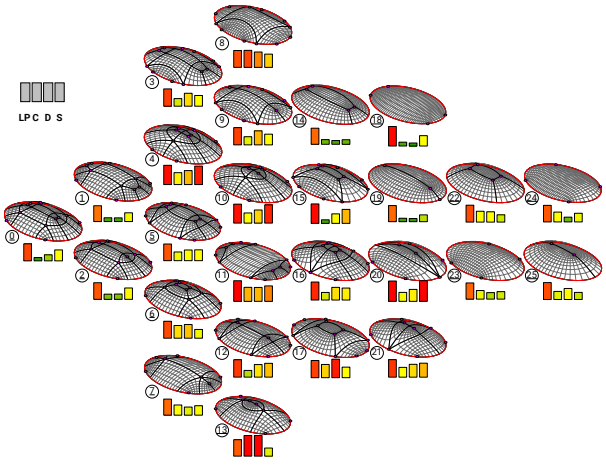

24

Similarity | Dome application

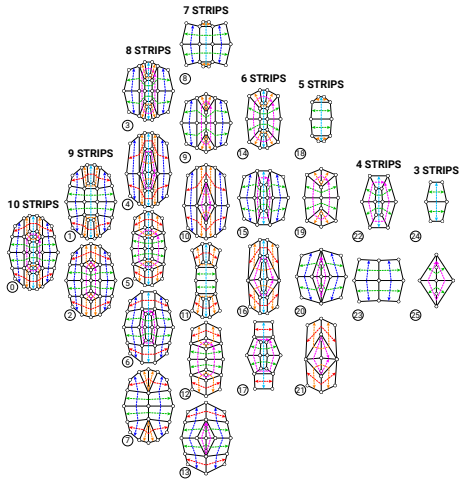

25

Similarity | Floor application

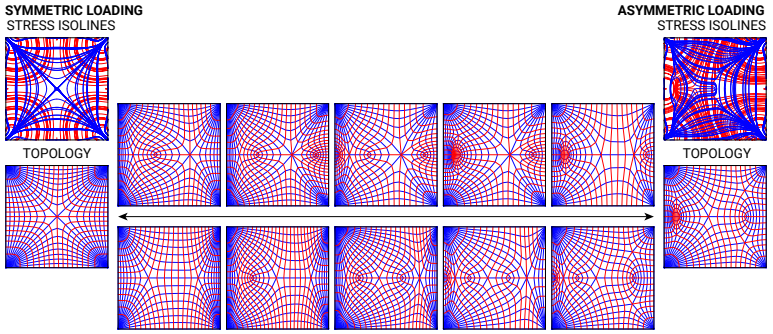

26

OUTRO | Summary

Algebra

Strip data structure, quad-mesh grammar, rule-based topological distance for (dis)similarity, intersection submesh and union supermesh

Application

Hybrid topological designs with variety of multi-objective trade-offs

Performance depends on topology… and its post-processing into a design

References

Oval, R., Rippmann, M., Mesnil, R., Van Mele, T., Baverel, O. and Block, P., 2019. Feature-based topology finding of patterns for shell structures. Automation in Construction, 103, pp.185-201.

Oval, R., Mesnil, R., Van Mele, T., Baverel, O. and Block, P., 2024. Similarity-driven topology finding of surface patterns for structural design. Computer-Aided Design, 176, p.103751.

27

OUTRO | Implementation

https://github.com/BlockResearchGroup/compas_pattern

28

THANK YOU!

Robin Oval | TU Delft | r.oval@tudelft.nl

Deployable auxetic surface structures: From optimized shape to detail design implementation

Kazuki Hayashi
Kyoto University

Abstract

This study presents a streamlined design framework for deployable auxetic surface structures, taking advantage of discrete differential geometry. The process begins by defining basis vectors, informed by a prescribed plan, support locations, and load conditions, to modify the structural shape via Dirichlet energy minimization. Next, a gradient-based optimization algorithm explores the optimal shape to minimize the linear strain energy, adjusting the weights of the basis vectors with gradients that are analytically derived through the chain rule. The final step aims to materialize the optimized geometry using a double-layer auxetic surface structure incorporating kerf joints. This approach achieves the flexibility required for deployment while providing the necessary stiffness for in-service performance.

Deployable auxetic surface structures: From optimized shape to detail design implementation

Kazuki Hayashi (Kyoto University, Japan)

Today's talk

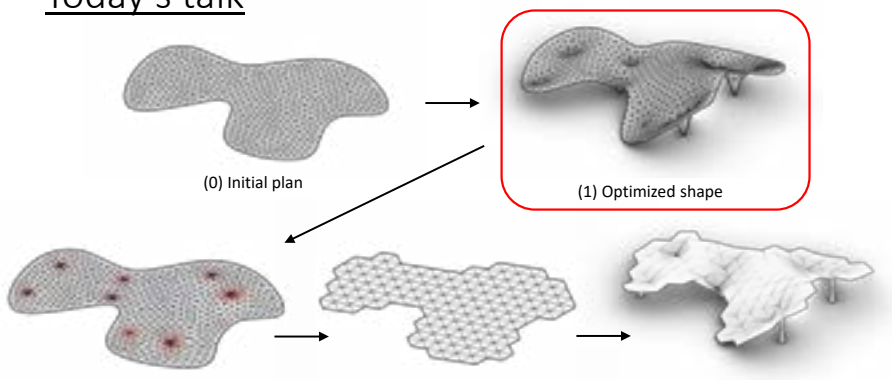

Topic 1/2: Shape sensitivity analysis

- Suppose we have a triangle mesh representing the shell geometry. How to modify its shape to maximize the structural performance?

➡ **Analytically derive shape sensitivity for thin shell structures**

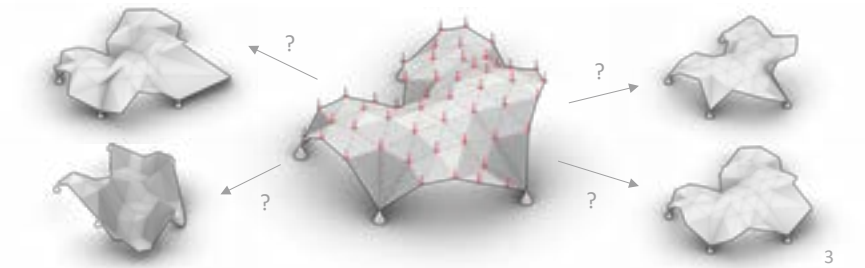

Chain rule for sensitivity analysis

- Chain-ruled computation allows for obtaining the gradient of objective function ($\partial F/\partial x$)

(Example)

$$\begin{cases} F(z) = 2z \\ z(y) = y^2 \\ y(x) = \sin x \end{cases} \longrightarrow \frac{\partial F}{\partial x} = \underbrace{\frac{\partial F}{\partial z} \cdot \frac{\partial z}{\partial y} \cdot \frac{\partial y}{\partial x}}_{\text{chain rule}} = 2 \cdot 2y \cdot \cos x = 4 \sin x \cos x$$

(In our study) F: strain energy (flexibility indicator to be minimized)

x: nodal locations

Chain rule for shape sensitivity analysis

- Chain-ruled computation allows for obtaining the gradient of objective function ($\partial F/\partial x$)

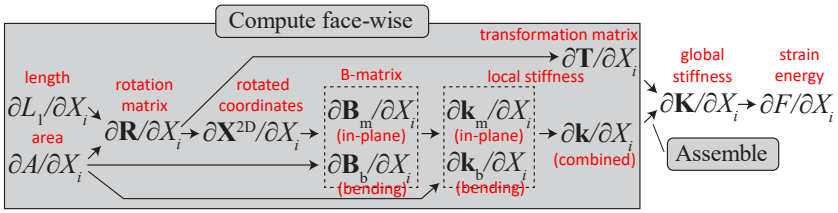

Gradient of edge length

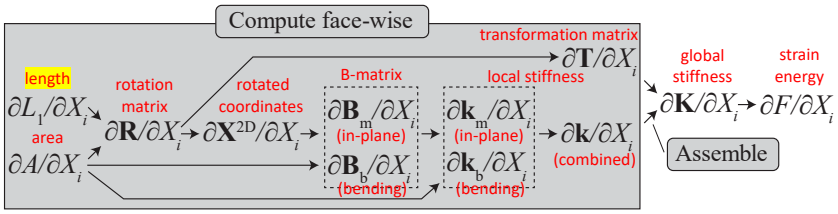

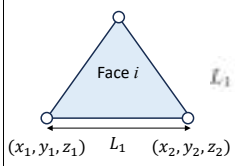

$$L_1 = \sqrt{(x_2 - x_1)^2 + (y_2 - y_1)^2 + (z_2 - z_1)^2}$$

$$\frac{\partial L_1}{\partial X_i} = \begin{cases} \frac{1}{L_1}(x_1 - x_2) & (X_i \equiv x_1) \\ \frac{1}{L_1}(x_2 - x_1) & (X_i \equiv x_2) \\ \frac{1}{L_1}(y_1 - y_2) & (X_i \equiv y_1) \\ \frac{1}{L_1}(y_2 - y_1) & (X_i \equiv y_2) \\ \frac{1}{L_1}(z_1 - z_2) & (X_i \equiv z_1) \\ \frac{1}{L_1}(z_2 - z_1) & (X_i \equiv z_2) \end{cases}$$

Gradient of triangle area

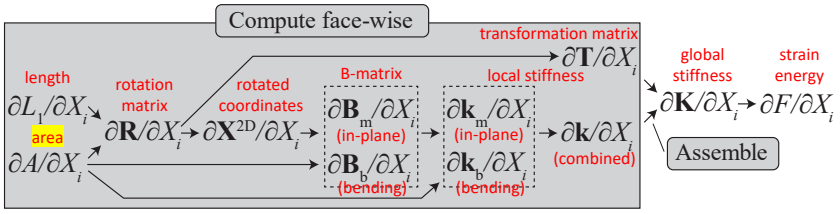

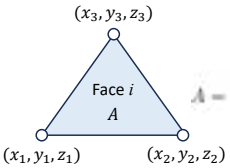

$$A = \frac{\sqrt{a_1^2 + a_2^2 + a_3^2}}{2}$$

$$a_1 = \sum_{p=1}^{3} y_p z_r - y_r z_p \qquad a_2 = \sum_{p=1}^{3} z_p x_r - z_r x_p \qquad a_3 = \sum_{p=1}^{3} x_p y_r - x_r y_p$$

$$\frac{\partial A}{\partial X_i} = \begin{cases} \frac{a_3(y_r - y_q) + a_2(z_q - z_r)}{4A} & (X_i \equiv x_p) \\ \frac{a_1(z_r - z_q) + a_3(x_q - x_r)}{4A} & (X_i \equiv y_p) \\ \frac{a_2(x_r - x_q) + a_1(y_q - y_r)}{4A} & (X_i \equiv z_p) \end{cases}$$

Gradient of rotation matrix

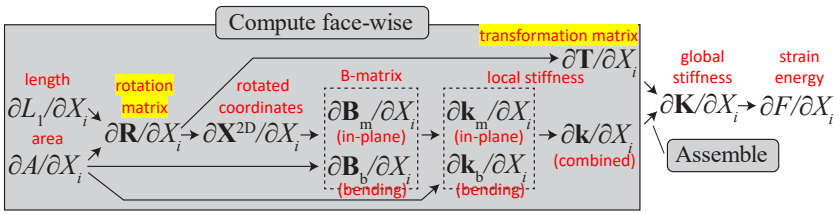

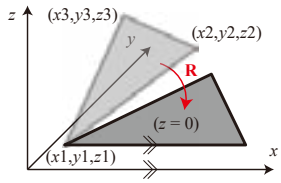

Gradient of rotated nodal coordinates

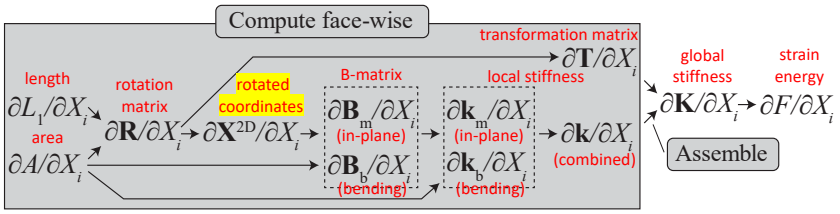

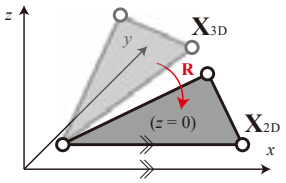

$$\mathbf{X}_j^{2D} = \mathbf{X}_j^{3D}\mathbf{R}_j^{\top} \qquad \frac{\partial \mathbf{X}^{2D}}{\partial X_i} = \frac{\partial \mathbf{X}^{3D}}{\partial X_i}\mathbf{R}^{\top} + \mathbf{X}^{3D}\frac{\partial \mathbf{R}^{\top}}{\partial X_i}$$

(Geometrical strain-displacement relationship)

Gradient of membrane B-matrix

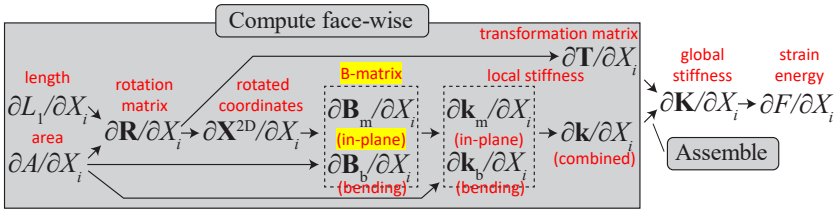

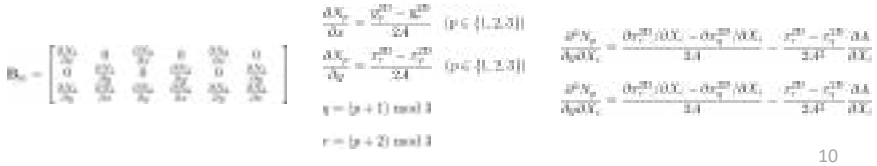

(Geometrical strain-displacement relationship)

Gradient of bending B-matrix

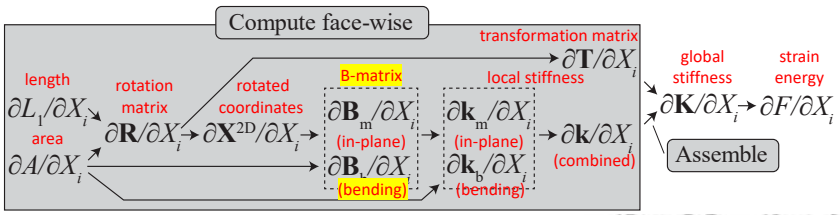

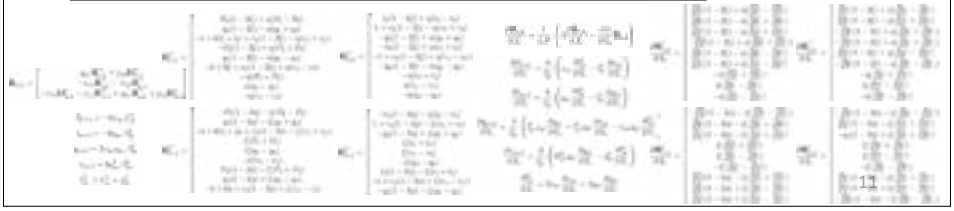

Gradient of local stiffness matrix

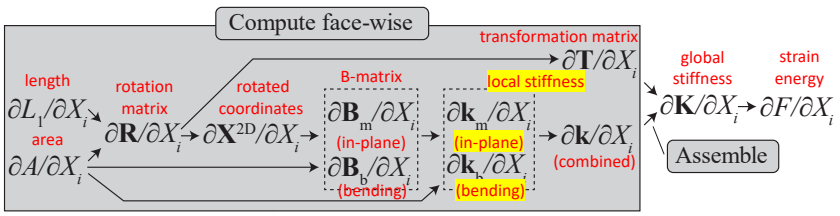

Gradient of global stiffness matrix

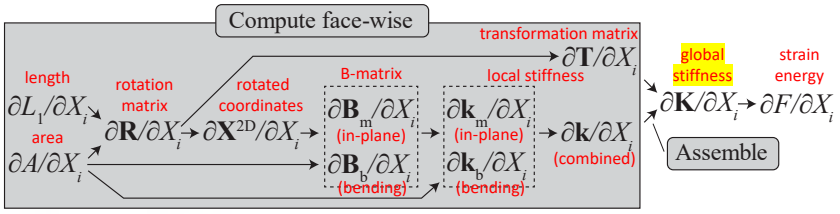

$$\mathbf{k}_j^g = \mathbf{T}_j^\top \mathbf{k}_j \mathbf{T}_j$$

$$\frac{\partial \mathbf{k}_j^g}{\partial X_i} = \frac{\partial \mathbf{T}_j^\top}{\partial X_i}\mathbf{k}_j\mathbf{T}_j + \mathbf{T}_j^\top\frac{\partial \mathbf{k}_j}{\partial X_i}\mathbf{T}_j + \mathbf{T}_j^\top\mathbf{k}_j\frac{\partial \mathbf{T}_j}{\partial X_i}$$

Gradient of strain energy (**objective**)

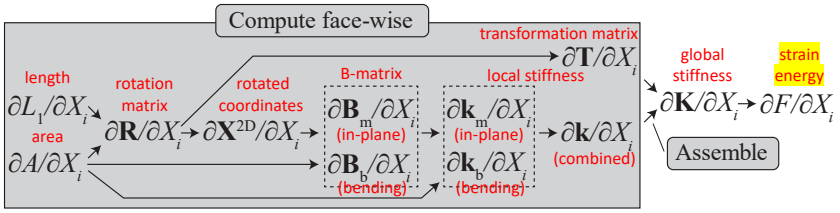

$$F = \frac{1}{2}\mathbf{u}^\top \mathbf{K}\mathbf{u} \qquad \frac{\partial F}{\partial X_i} = -\frac{1}{2}\mathbf{u}^\top\frac{\partial \mathbf{K}}{\partial X_i}\mathbf{u}$$

Displacement caused by load, obtained from stiffness equation

Analytically derived! But why are we happy?

- We can compute how to modify mesh geometry to increase its stiffness if we have the following information:
  (1) mesh (2) thickness (3) material (4) support (5) load

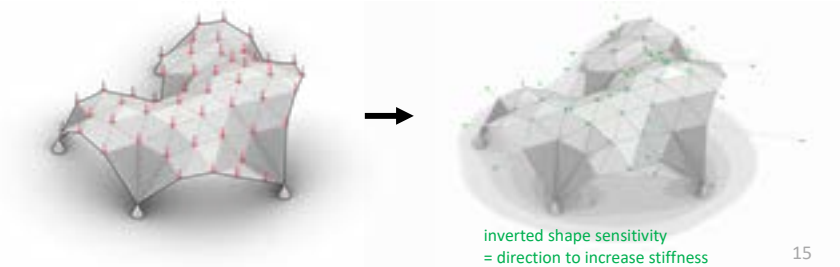

inverted shape sensitivity
= direction to increase stiffness

Q. Is our computation fast?

- If using sparse matrix representation and Just-in-Time (JIT) compilation,
  - Finite difference method: $\approx O(n^2)$
  - Our implementation: $\approx O(n)$

- A. Yes, at the order of approximately $O(n)$

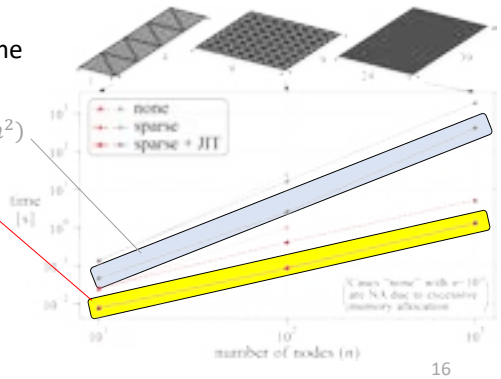

Gradient-based shape optimization

- Many libraries accept sensitivity analysis to speed up optimization

```
from scipy.optimize import minimize

def f(x):                          Objective function
    return x*x                     f(x) = x^2

def f_g(x):                        Gradient function
    return 2*x                     df/dx = 2x

x0 = [1.0]                         Initial x
r = minimize(f,x0,jac=f_g)         Optimize
print(r)                           Display optimization result
```

Run

```
 message: Optimization
          terminated successfully.
 success: True
  status: 0
     fun: 0.0                      Value of f
       x: [ 0.000e+00]             Value of x
     nit: 2                        Iteration
     jac: [ 0.000e+00]             Value of df/dx
hess_inv: [[ 5.000e-01]]           Value of d^2f/dx^2
    nfev: 3   Number of times f(x) was called
    njev: 3   Number of times f_g(x) was called
```

https://docs.scipy.org/doc/scipy/reference/generated/scipy.optimize.minimize.html

Shape optimization (without sensitivity analysis)

Thickness:	20 cm
Young's modulus:	25000 N/mm^2
Poisson's ratio:	0.15
Design load:	1 kN downward at each node

Design variable:	Heights of unsupported nodes
Objective:	Minimizing strain energy
Volume constraint:	$< 1.2 \times$ (initial volume)

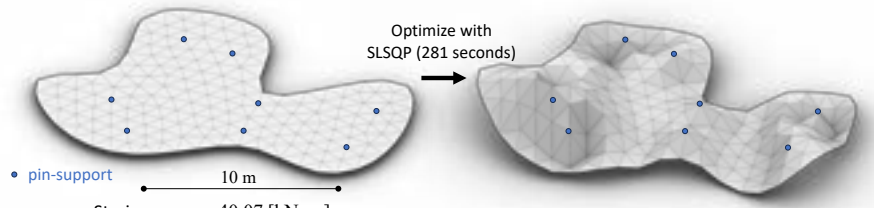

Strain energy = 40.07 [kN·m]
Volume = 28.73 [m^3]
Area = 143.63 [m^2]

Strain energy = 1.18 [kN·m]
Volume = 34.47 ($\cong 1.2 \times 28.73$) [m^3]

Shape optimization (with sensitivity analysis)

Thickness: 20 cm
Young's modulus: 25000 N/mm^2
Poisson's ratio: 0.15
Design load: 1 kN downward at each node

Design variable: Heights of unsupported nodes
Objective: Minimizing strain energy
Volume constraint: $< 1.2 \times$ (initial volume)

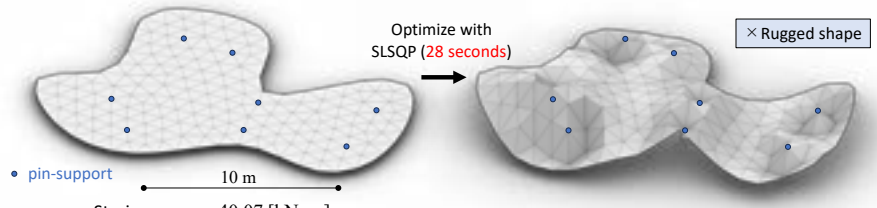

Strain energy = 40.07 [kN・m]
Volume = 28.73 [m^3]
Area = 143.63 [m^2]

Strain energy = 1.28 [kN・m]
Volume = 34.47 ($\cong 1.2 \times 28.73$) [m^3]

19

Filtered shape optimization (Work in Progress)

Thickness: 20 cm
Young's modulus: 25000 N/mm^2
Poisson's ratio: 0.15
Design load: 1 kN downward at each node

Design variable: Weights of smooth deformation modes
Objective: Minimizing strain energy
Volume constraint: $< 1.2 \times$ (initial volume)

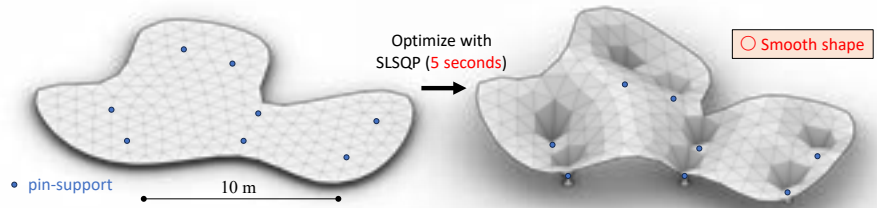

Strain energy = 40.07 [kN・m]
Volume = 28.73 [m^3]
Area = 143.63 [m^2]

Strain energy = 2.90 [kN・m]
Volume = 34.47 ($\cong 1.2 \times 28.73$) [m^3]

20

Today's talk:

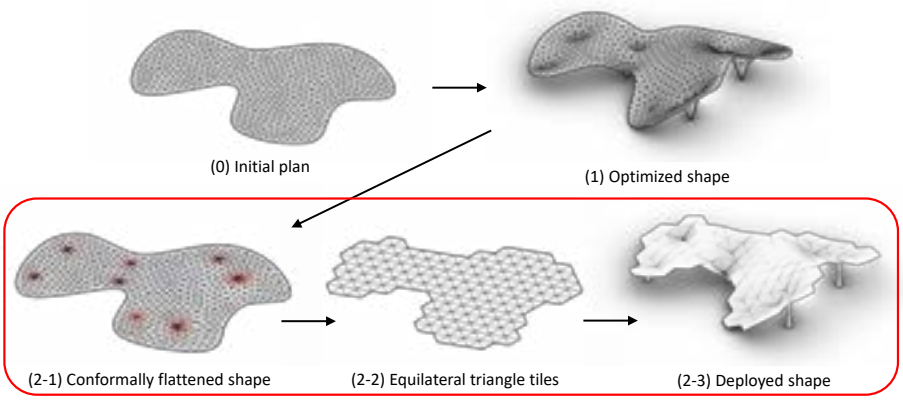

21

Topic 2/2: Deployable auxetic surface

Gaussian curvature

$K = 0$
→ Cylinder, Plane

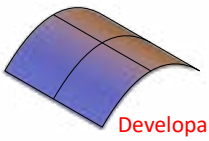

Developable

Easily made by bending a flat sheet

$K > 0$
→ Sphere

$K < 0$
→ Saddle

Non-developable

Cannot be made by bending a flat sheet

Use auxetic surfaces to create non-developable shapes from a flat state

22

Auxetic surface

- Linkage mechanism produced by cutting a sheet material

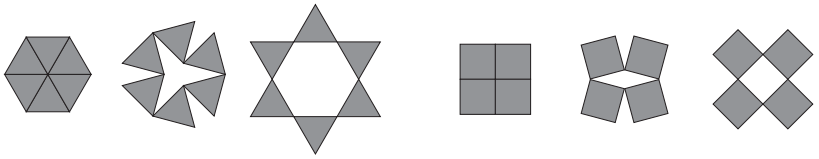

- Characterized by negative Poisson's ratio

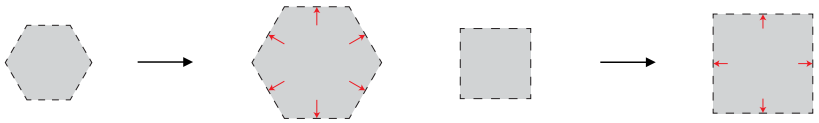

23

Surface construction using an auxetic material

design surface

deployed structure

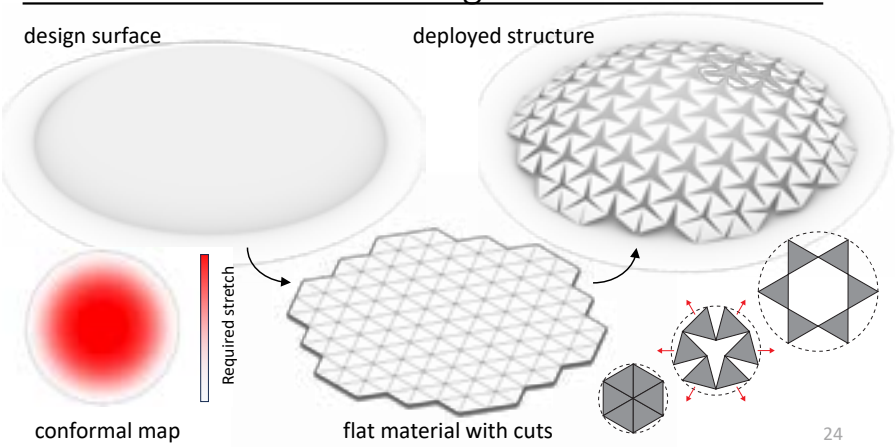

conformal map

flat material with cuts

24

Conformal flattening

Preserve angles, while distorting lengths

output

1: flattened shape preserving angles

2: conformal factors u (required stretch/shrinkage to restore surface)

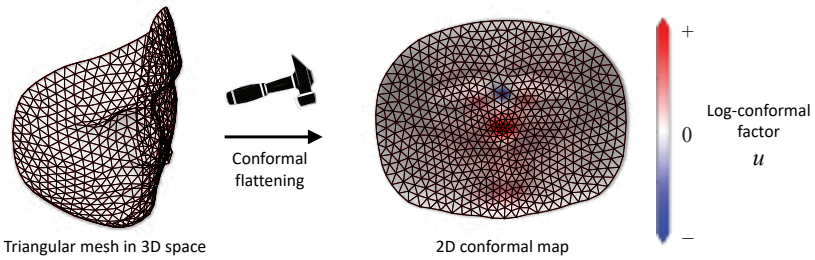

Triangular mesh in 3D space

2D conformal map

Stretch quantification

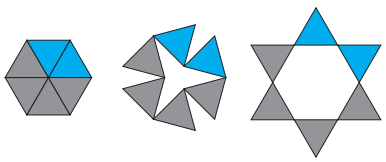

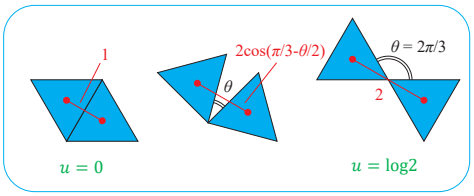

- Expansion in length can be associated with open angle $\theta \in [0, 2\pi/3]$
- Relate log-conformal factor u and open angle θ as

$$\exp(u) = 2\cos\left(\frac{\pi}{3} - \frac{\theta}{2}\right) \in [1.0, 2.0]$$

Deployment analysis

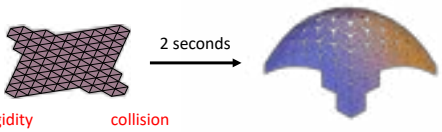

- Minimize $E = w_1 E_{\text{design}} + w_2 E_{\text{rigid}} + w_3 E_{\text{collision}}$ [Konaković et al, 2016]
  (closeness, rigidity, collision)
- Solve a linear system of equations using shape projection operators [Bouaziz et al, 2012]

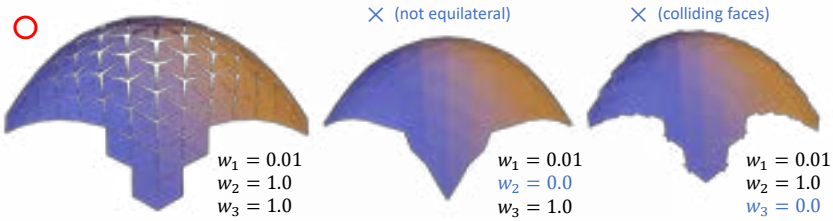

S. Bouaziz et al., "Shape-Up: Shaping discrete geometry with projections," *Eurographics Symposium on Geometry Processing 2012*, vol. 31, no. 5, pp. 1657-1667, 2012.
M. Konaković et al., "Beyond developable: computational design and fabrication with auxetic materials," *ACM TOG*, vol. 35, no. 89, pp. 1-11, 2016.

Elasticity condition of joints is too strict

• $L/d > (\theta/2) \cdot (E/\bar{\sigma})$

Joint shape — Material property

θ : Deployment angle
E : Young's modulus
$\bar{\sigma}$: Elastic limit stress

• Ex.) Suppose $\theta = \pi/3$.

too strict

Glass-Fiber-Reinforced Plastic (GFRP): $E = 15$ [GPa], $\bar{\sigma} = 250$ [MPa] ➡ $L/d > 31.4$
Medium Density Fiberboard (MDF): $E = 4$ [GPa], $\bar{\sigma} = 20$ [MPa] ➡ $L/d > 104.7$

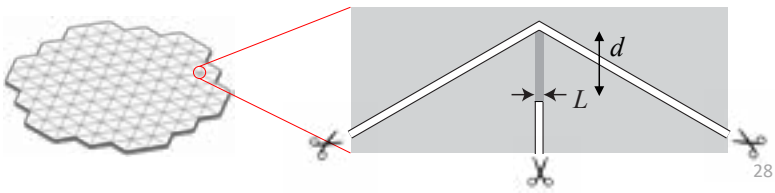

28

Flexibility augmentation through kerfs

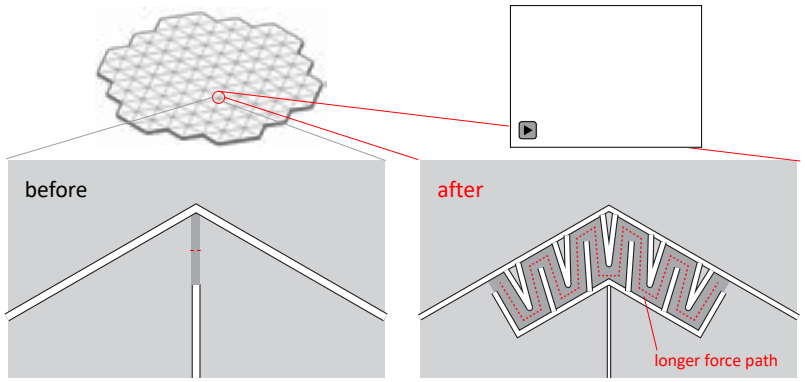

29

Kerf joints enable auxetic behavior

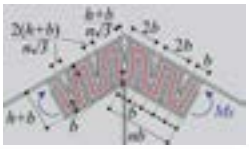

$K_{rz} = \frac{EI_z}{2nh+(2n-1)b}$ (rotational stiffness against deployment)
$K_{rz}\theta_z = M_z$ (bending equilibrium)
$Z_z = b^2t/6$ (section modulus)
$M_z/Z_z = \sigma_{rz} < \sigma_a$ (elastic limit)

$\frac{E}{\sigma_a} < \frac{E}{\sigma_{rz}} = 4n\frac{h}{b} + 4n - 2$

material property — kerf pattern

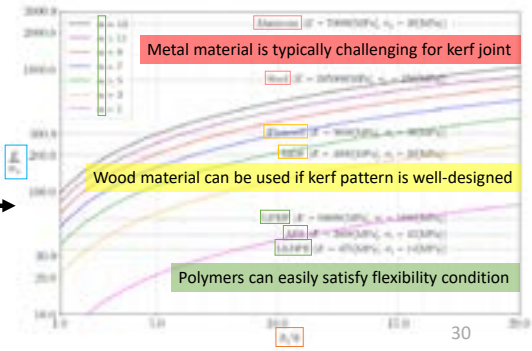

30

Single-layer auxetic material is unstable

- Kerf joints sacrifice stiffness

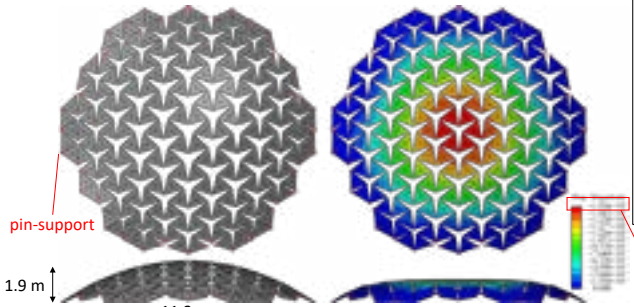

- Material: MDF
  Young's modulus = 4 [GPa]
  Poisson's ratio = 0.25
  density = 700 [kg/m³]
- Kerf parameters
  $n = 9$
  $b = 0.1/n$ [m]
  $h = 0.8/n$ [m]

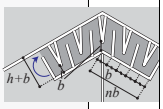

- Assume geometric linearity
- Software: Abaqus 2020

Bilayer scheme for surface stiffening

+ Cancel restoring forces each other
+ Recover in-plane rotational stiffness

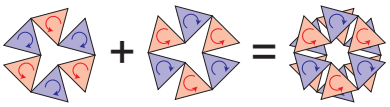

- Suppose surfaces are attached by 3 bolts

➡ Equivalent 6-dof spring stiffnesses are

$$\{K_{tx}, K_{ty}, K_{tz}, K_{rx}, K_{ry}, K_{rz}\}$$
$$= \left\{\frac{3EA}{2t}, \frac{3GA_s}{2t}, \frac{3GA_s}{2t}, \frac{GA_sl^2}{2t}, \frac{EAl^2}{4t}, \frac{EAl^2}{4t}\right\}$$

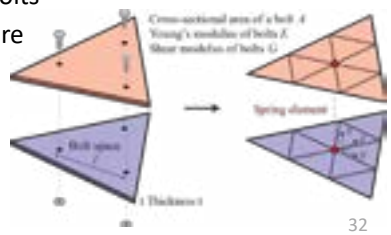

Deformation control by overlaying

Desirable mode
Undesirable mode

Eigenvalue $\hat{\lambda}_1 = 1.00$ $\hat{\lambda}_2 = 1.01$ $\hat{\lambda}_3 = 1.03$ $\hat{\lambda}_4 = 2.71$ $\hat{\lambda}_5 = 3.16$

Single-layer unit cell

Eigenvalue $\hat{\lambda}_1 = 1.00$ $\hat{\lambda}_2 = 1.35$ $\hat{\lambda}_3 = 1.35$ $\hat{\lambda}_4 = 3.05$ $\hat{\lambda}_5 = 6.52$

Double-layer unit cell

Thickness affects open angles

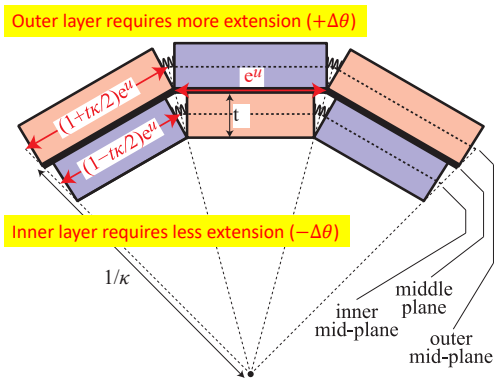

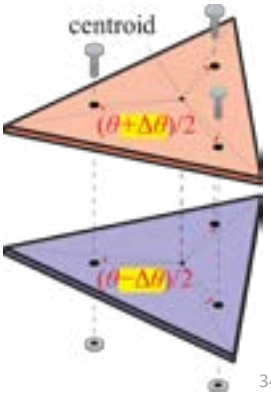

Steiner's formula to modify open angles

- Area of ϵ-offset surface [Hoffmann2009]

$$A_{\text{offset}} = A + 2\epsilon \int HdA + \epsilon^2 \int KdA$$

➡ Offsetting a surface by ϵ increases its area by a factor of $1 + 2\epsilon H + \epsilon^2 K$

- Log-conformal factor of ϵ-offset surface

$$e^{2u_{\text{offset}}} = (1 + 2\epsilon H + \epsilon^2 K)e^{2u}$$

$u_{\text{offset}} \rightarrow \theta + \Delta\theta$; $u \rightarrow \theta$

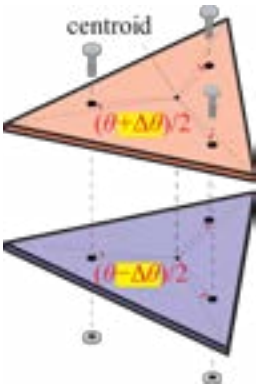

T. Hoffmann, "Discrete Differential Geometry of Curves and Surfaces", COE Lecture Note Series Vol.18, Faculty of Mathematics, Kyushu University, 2009.

Thickness effect on $\Delta\theta$

Larger t and κ increasingly affect the correction of open angle $\Delta\theta$ to approximate the target surface

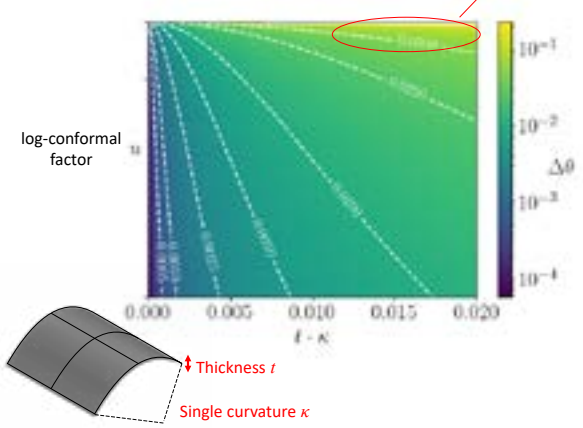

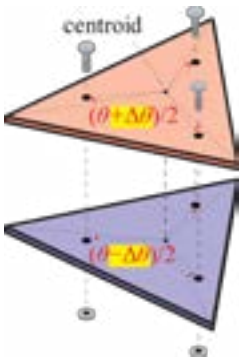

Shapes match between simulation and prototype

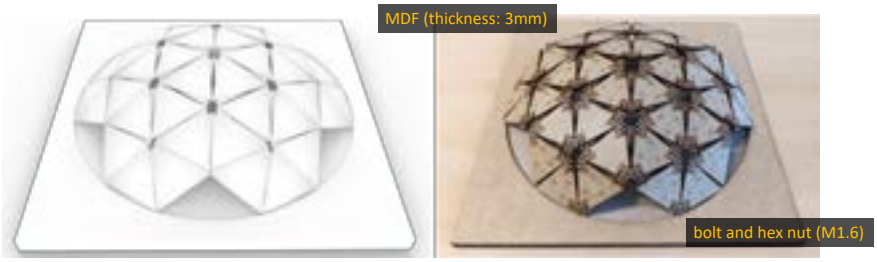

Designed for a maximum mid-surface height of 56.2 mm

Actual maximum mid-surface height: 56 mm

37

Prototypes

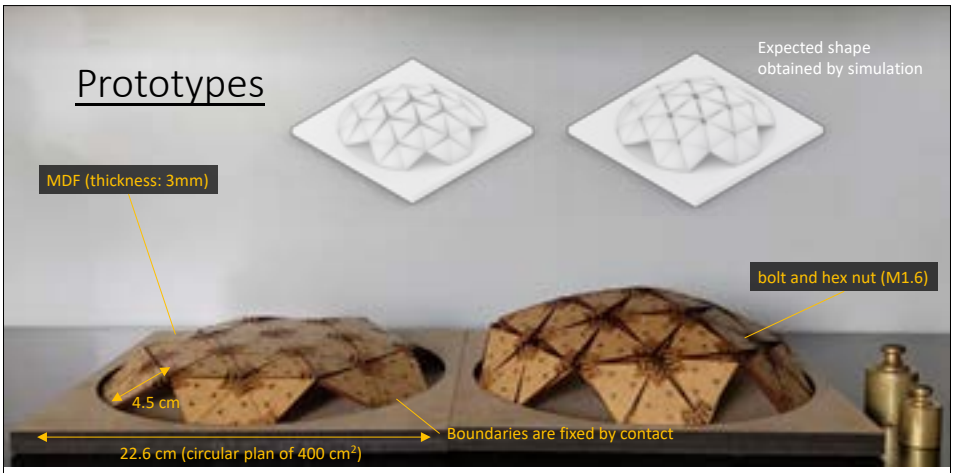

Single-layer

Bilayer

38

Conclusion

- Optimize the shape of shell structures using analytically derived shape sensitivity
- Leveraged conformal geometry to design double-layer deployable auxetic structures with kerf-bending joints

Contact: (Kazuki Hayashi)
hayashi.kazuki@archi.kyoto-u.ac.jp

Second-order infinitesimal mechanism for bifurcation analysis and folding path approximation of rigid origami

Kentaro Hayakawa
Nihon University

Abstract

We investigate the kinematic bifurcation of rigid origami and approximate its folding path with polynomials through the second-order infinitesimal mechanism analysis of a truss model, the assemblage of the pin-connected bars. The motion of the model is constrained by the compatibility condition so that the bar length does not change. The second-order infinitesimal mechanism is obtained from the series expansion of the compatibility condition and its existence condition is the system of homogeneous quadratic equations. The bifurcated mechanisms of rigid origami correspond to the different solutions of the existence condition. In addition, we can use a solution to the existence condition for a polynomial approximation of the folding path of the truss model.

Evolving Design and Discrete Differential Geometry
- towards Mathematics Aided Geometric Design

Second-order infinitesimal mechanism for bifurcation analysis and folding path approximation of rigid origami

Kentaro Hayakawa

Kyoto Group, Nihon University

*Joint work with T. Ohba and M. Ohsaki
@ Kyoto Univeristy

Rigid Origami for Engineering Application

Rigid-folding mechanism

Rigid panels + Rotational hinges

Solar panels on artificial satellite[1)]

Portable shelter[2)]

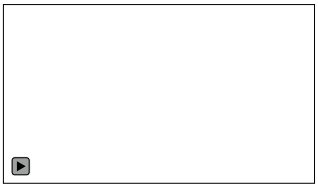

Challenges

Efficient rigid-folding **path tracing**

Exploration of solution space of **multi-degree-of-freedom mechanism** especially with **kinematic bifurcation**

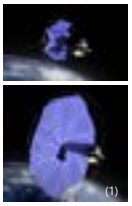

(1)

(2)

1. S. A. Zirbel et al., *J. Mech. Des.*, Vol. 135 (11), paper 111005, 2013.
2. K. Ando et al., *SN Appl. Sci.*, Vol. 2 (12), article 1994, 2020

Analysis of Rigid Folding Mechanism

Analytical solution

Singe vertex[3)]

Periodicity and/or symmetry[4)]

→ Limited to simple crease patterns

Numerical solution

Mechanism on tangent plane of solution space
= first-order infinitesimal mechanism[5)]

→ Insufficient information about kinematic bifurcation[6)]

→ Many iterations for precise path tracing

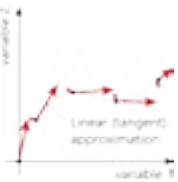

3. J. Farnham et al., *Proc. R. Soc. A*, Vol. 478, paper 20220051, 2022.
4. T. Tachi, in *Origami6*, pp. 97-108, 2015
5. T. Tachi, in Origami4, pp. 175-187, 2009
6. P. Kumar and S. Pellegrino, *Int. J. Solids Struct.*, Vol. 37 (46), pp. 7003-7027, 2000.

Higher-order Infinitesimal Mechanism

1. Kinematic bifurcation[7)]

   Solution space at point of kinematic bifurcation that cannot be obtained from first-order mechanism

   → Prediction of possible folding pattern/motion

2. Efficient and high accuracy path tracing[8)]

   Polynomial expression of folding path with respect to path parameter

   → Small number of iterations for path tracing

   → Folding motion as continuous smooth function in certain range

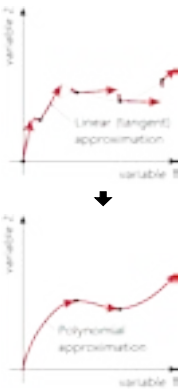

7. K. Hayakawa, T. Ohba, and M. Ohsaki. *Mech. Mach. Theory*, 194 (2024), 105572
8. T. Ohba, K. Hayakawa, and M. Ohsaki. in Proc. 8OSME, 2024

Formulation for Truss Model

Compatibility equation for bar *i*

Constant bar length in folding motion

$$c_i = \frac{1}{2}\left(\left\|\mathbf{x}_j - \mathbf{x}_k\right\|^2 - l_i^2\right) = 0$$

$\mathbf{x}_j$, $\mathbf{x}_k$: position vectors of endpoints of bar i

l_i : Initial length of bar i

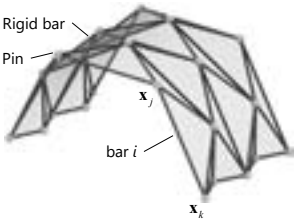

Compatibility equation for entire model

$\mathbf{C}(\mathbf{X}) = \mathbf{0}$ ← $c_i = 0$ for all bars

$$\mathbf{C}(\mathbf{X}) = \begin{pmatrix} c_1 \\ \vdots \\ c_{N_\mathrm{B}} \end{pmatrix} \in \mathbb{R}^{N_\mathrm{B}}$$: incompatibility vector

$$\mathbf{X} = \begin{pmatrix} \mathbf{x}_1 \\ \vdots \\ \mathbf{x}_{N_\mathrm{n}} \end{pmatrix} \in \mathbb{R}^{N_\mathrm{X}}$$: generalized position vector

Infinitesimal Mechanism of Truss Model

Series expansion of compatibility equation w.r.t. path parameter

When $\mathbf{X}$ is a function of the path parameter t (time, arc length etc.)

$$\begin{aligned}\mathbf{C}(\mathbf{X}(t)) &= t\left.\frac{\mathrm{d}\mathbf{C}}{\mathrm{d}t}\right|_{t=0} + \frac{t^2}{2}\left.\frac{\mathrm{d}^2\mathbf{C}}{\mathrm{d}t^2}\right|_{t=0} + \frac{t^3}{6}\left.\frac{\mathrm{d}^3\mathbf{C}}{\mathrm{d}t^3}\right|_{t=0} + \text{h.o.t.} \\ &= t\left[\boldsymbol{\Gamma}^{(0)}\mathbf{X}^{(1)}\right] + \frac{t^2}{2}\left[\boldsymbol{\Gamma}^{(0)}\mathbf{X}^{(2)} + \boldsymbol{\Gamma}^{(1)}\mathbf{X}^{(1)}\right] + \frac{t^2}{6}\left[\boldsymbol{\Gamma}^{(0)}\mathbf{X}^{(3)} + 2\boldsymbol{\Gamma}^{(1)}\mathbf{X}^{(2)} + \boldsymbol{\Gamma}^{(2)}\mathbf{X}^{(1)}\right] + \text{h.o.t.}\end{aligned}$$

$$\boldsymbol{\Gamma}^{(0)} = \left[\begin{array}{ccc} \frac{\partial c_1}{\partial X_1} & \cdots & \frac{\partial c_1}{\partial X_{N_\mathrm{X}}} \\ \vdots & \ddots & \vdots \\ \frac{\partial c_{N_\mathrm{B}}}{\partial X_1} & \cdots & \frac{\partial c_{N_\mathrm{B}}}{\partial X_{N_\mathrm{X}}} \end{array}\right]_{t=0} \in \mathbb{R}^{N_\mathrm{B} \times N_\mathrm{X}}$$: compatibility matrix = Jacobian of $\mathbf{C}(\mathbf{X})$ w.r.t. $\mathbf{X}$

$$\mathbf{X}^{(s)} = \begin{pmatrix} X_1^{(s)} \\ \vdots \\ X_{N_\mathrm{X}}^{(s)} \end{pmatrix} = \left.\frac{d^s\mathbf{X}}{dt^s}\right|_{t=0} \in \mathbb{R}^{N_\mathrm{X}}, \qquad \boldsymbol{\Gamma}^{(s)} = \sum_{k=1}^{N_\mathrm{X}} X_k^{(s)} \left[\begin{array}{ccc} \frac{\partial^2 c_1}{\partial X_1 \partial X_k} & \cdots & \frac{\partial^2 c_1}{\partial X_{N_\mathrm{X}} \partial X_k} \\ \vdots & \ddots & \vdots \\ \frac{\partial^2 c_{N_\mathrm{B}}}{\partial X_1 \partial X_k} & \cdots & \frac{\partial^2 c_{N_\mathrm{B}}}{\partial X_{N_\mathrm{X}} \partial X_k} \end{array}\right]_{t=0} \in \mathbb{R}^{N_\mathrm{B} \times N_\mathrm{X}} \quad (s \geq 1)$$

Infinitesimal Mechanism of Truss Model

Series expansion of compatibility equation w.r.t. path parameter

When $\mathbf{X}$ is a function of the path parameter t (time, arc length etc.)

$$\mathbf{C}(\mathbf{X}(t)) = t\left[\boldsymbol{\Gamma}^{(0)}\mathbf{X}^{(1)}\right] + \frac{t^2}{2}\left[\boldsymbol{\Gamma}^{(0)}\mathbf{X}^{(2)} + \boldsymbol{\Gamma}^{(1)}\mathbf{X}^{(1)}\right] + \frac{t^2}{6}\left[\boldsymbol{\Gamma}^{(0)}\mathbf{X}^{(3)} + 2\boldsymbol{\Gamma}^{(1)}\mathbf{X}^{(2)} + \boldsymbol{\Gamma}^{(2)}\mathbf{X}^{(1)}\right] + \text{h.o.t.}$$

→ $\mathbf{X}^{(1)}$ satisfying $\boldsymbol{\Gamma}^{(0)}\mathbf{X}^{(1)} = \mathbf{0}$: First-order infinitesimal mechanism

Infinitesimal Mechanism of Truss Model

Series expansion of compatibility equation w.r.t. path parameter

When $\mathbf{X}$ is a function of the path parameter t (time, arc length etc.)

$$\mathbf{C}(\mathbf{X}(t)) = t\left[\boldsymbol{\Gamma}^{(0)}\mathbf{X}^{(1)}\right] + \frac{t^2}{2}\left[\boldsymbol{\Gamma}^{(0)}\mathbf{X}^{(2)} + \boldsymbol{\Gamma}^{(1)}\mathbf{X}^{(1)}\right] + \frac{t^2}{6}\left[\boldsymbol{\Gamma}^{(0)}\mathbf{X}^{(3)} + 2\boldsymbol{\Gamma}^{(1)}\mathbf{X}^{(2)} + \boldsymbol{\Gamma}^{(2)}\mathbf{X}^{(1)}\right] + \text{h.o.t.}$$

$\mathbf{X}^{(1)}$ satisfying $\boldsymbol{\Gamma}^{(0)}\mathbf{X}^{(1)} = \mathbf{0}$: First-order infinitesimal mechanism

→ $\left(\mathbf{X}^{(1)}, \mathbf{X}^{(2)}\right)$ satisfying $\begin{cases} \boldsymbol{\Gamma}^{(0)}\mathbf{X}^{(1)} = \mathbf{0} \\ \boldsymbol{\Gamma}^{(0)}\mathbf{X}^{(2)} + \boldsymbol{\Gamma}^{(1)}\mathbf{X}^{(1)} = \mathbf{0} \end{cases}$: Second-order infinitesimal mechanism

Infinitesimal Mechanism of Truss Model

Series expansion of compatibility equation w.r.t. path parameter

When $\mathbf{X}$ is a function of the path parameter t (time, arc length etc.)

$$\mathbf{C}(\mathbf{X}(t)) = t\left[\boldsymbol{\Gamma}^{(0)}\mathbf{X}^{(1)}\right] + \frac{t^2}{2}\left[\boldsymbol{\Gamma}^{(0)}\mathbf{X}^{(2)} + \boldsymbol{\Gamma}^{(1)}\mathbf{X}^{(1)}\right] + \frac{t^2}{6}\left[\boldsymbol{\Gamma}^{(0)}\mathbf{X}^{(3)} + 2\boldsymbol{\Gamma}^{(1)}\mathbf{X}^{(2)} + \boldsymbol{\Gamma}^{(2)}\mathbf{X}^{(1)}\right] + \text{h.o.t.}$$

$\mathbf{X}^{(1)}$ satisfying $\boldsymbol{\Gamma}^{(0)}\mathbf{X}^{(1)} = \mathbf{0}$: First-order infinitesimal mechanism

$\left(\mathbf{X}^{(1)}, \mathbf{X}^{(2)}\right)$ satisfying $\begin{cases} \boldsymbol{\Gamma}^{(0)}\mathbf{X}^{(1)} = \mathbf{0} \\ \boldsymbol{\Gamma}^{(0)}\mathbf{X}^{(2)} + \boldsymbol{\Gamma}^{(1)}\mathbf{X}^{(1)} = \mathbf{0} \end{cases}$: Second-order infinitesimal mechanism

→ $\left(\mathbf{X}^{(1)}, \ldots, \mathbf{X}^{(n)}\right)$ satisfying $\begin{cases} \boldsymbol{\Gamma}^{(0)}\mathbf{X}^{(1)} = \mathbf{0} \\ \boldsymbol{\Gamma}^{(0)}\mathbf{X}^{(2)} + \boldsymbol{\Gamma}^{(1)}\mathbf{X}^{(1)} = \mathbf{0} \\ \vdots \\ \sum_{s=0}^{n-1}\binom{n-1}{s}\boldsymbol{\Gamma}^{(s)}\mathbf{X}^{(n-s)} = \mathbf{0} \end{cases}$: n-th-order infinitesimal mechanism

First-order Infinitesimal Mechanism

Compatibility equation for first-order infinitesimal mechanism

$$\mathbf{\Gamma}^{(0)}\mathbf{X}^{(1)}=\mathbf{0}$$

Solution space of first-order infinitesimal mechanism

Space of $\mathbf{X}^{(1)}$ satisfying $\mathbf{\Gamma}^{(0)}\mathbf{X}^{(1)}=\mathbf{0}$ ⇔ Null space of $\mathbf{\Gamma}^{(0)}$

Dimension of null space $N_{\mathrm{F}}=N_{\mathrm{X}}-\operatorname{rank}\mathbf{\Gamma}^{(0)}$: Number of kinematic indeterminacy

Bases of null space $\boldsymbol{\xi}_1,\ldots,\boldsymbol{\xi}_{N_{\mathrm{F}}}\in\mathbb{R}^{N_{\mathrm{X}}}$: Infinitesimal mechanism modes

$$\mathbf{X}^{(1)}=a_1^{(1)}\boldsymbol{\xi}_1+\cdots+a_{N_{\mathrm{F}}}^{(1)}\boldsymbol{\xi}_{N_{\mathrm{F}}}=\begin{bmatrix}\boldsymbol{\xi}_1 & \cdots & \boldsymbol{\xi}_{N_{\mathrm{F}}}\end{bmatrix}\begin{pmatrix}a_1^{(1)}\\ \vdots\\ a_{N_{\mathrm{F}}}^{(1)}\end{pmatrix}=\bar{\mathbf{X}}\mathbf{a}^{(1)}$$

Second-order Infinitesimal Mechanism

Compatibility equation for second-order infinitesimal mechanism

$$\begin{cases}\mathbf{\Gamma}^{(0)}\mathbf{X}^{(1)}=\mathbf{0}\\ \mathbf{\Gamma}^{(0)}\mathbf{X}^{(2)}+\mathbf{\Gamma}^{(1)}\mathbf{X}^{(1)}=\mathbf{0}\end{cases}$$

$\mathbf{\Gamma}^{(1)}\mathbf{X}^{(1)}$ determined by $\mathbf{X}^{(1)}$

Existence condition of second-order infinitesimal mechanism

($\mathbf{\Gamma}^{(1)}\mathbf{X}^{(1)}$ for first-order infinitesimal mechanism $\mathbf{X}^{(1)}$) ∈ (vector space of $\mathbf{\Gamma}^{(0)}\mathbf{X}^{(2)}$)
⇔ $\mathbf{\Gamma}^{(1)}\mathbf{X}^{(1)}\perp$ (left null space of $\mathbf{\Gamma}^{(0)}$)

Dimension of left null space $N_{\mathrm{S}}=N_{\mathrm{B}}-\operatorname{rank}\mathbf{\Gamma}^{(0)}$: Number of statical indeterminacy

Bases of left null space $\boldsymbol{\omega}_1,\ldots,\boldsymbol{\omega}_{N_{\mathrm{S}}}\in\mathbb{R}^{N_{\mathrm{B}}}$: Self-equilibrium force density modes

$$\begin{cases}\boldsymbol{\omega}_1^{\mathrm{T}}\mathbf{\Gamma}^{(1)}\mathbf{X}^{(1)}=0\\ \vdots\\ \boldsymbol{\omega}_{N_{\mathrm{S}}}^{\mathrm{T}}\mathbf{\Gamma}^{(1)}\mathbf{X}^{(1)}=0\end{cases}\Leftrightarrow\quad\begin{bmatrix}\boldsymbol{\omega}_1 & \cdots & \boldsymbol{\omega}_{N_{\mathrm{S}}}\end{bmatrix}^{\mathrm{T}}\mathbf{\Gamma}^{(1)}\mathbf{X}^{(1)}=\mathbf{\Omega}^{\mathrm{T}}\mathbf{\Gamma}^{(1)}\mathbf{X}^{(1)}=\mathbf{0}$$

Physical Interpretation of Mechanism and Self-equilibrium Modes

Infinitesimal mechanism

$\mathbf{X}^{(1)}=\left.\frac{d\mathbf{X}}{dt}\right|_{t=0}$: velocity, $\mathbf{X}^{(2)}=\left.\frac{d^2\mathbf{X}}{dt^2}\right|_{t=0}$: acceleration

$\boldsymbol{\xi}_1,\ldots,\boldsymbol{\xi}_{N_{\mathrm{F}}}$ ($\mathbf{\Gamma}^{(0)}\boldsymbol{\xi}_i=\mathbf{0}$) : Nodal velocity modes without deformation of bars

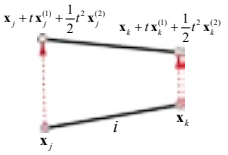

Self-equilibrium force density

$\mathbf{F}^{\mathrm{T}}\mathbf{\Gamma}^{(0)}=\mathbf{0}$ → for node j → $\sum_i F_i\left(\mathbf{x}_j-\mathbf{x}_k\right)=\mathbf{0}$: equilibrium equation

$\frac{\text{axial force}}{\text{bar length}}$ = force density

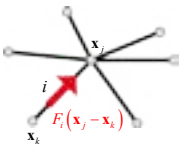

$\boldsymbol{\omega}_1,\ldots,\boldsymbol{\omega}_{N_{\mathrm{S}}}$ $(\boldsymbol{\omega}_i^{\mathrm{T}}\mathbf{\Gamma}^{(0)}=\mathbf{0})$: Self-equilibrium force density modes

Existence of Second-order Infinitesimal Mechanism

Existence condition as a system of homogeneous quadratic equations

$$\mathbf{X}^{(1)} = a_1^{(1)}\boldsymbol{\xi}_1 + \cdots + a_{N_S}^{(1)}\boldsymbol{\xi}_{N_S} = \bar{\mathbf{X}}\mathbf{a}^{(1)}$$

$$\boldsymbol{\Omega}^{\mathrm{T}}\boldsymbol{\Gamma}^{(1)}\mathbf{X}^{(1)} = \mathbf{0} \quad \Leftrightarrow \quad \begin{cases} \mathbf{a}^{(1)\mathrm{T}}\mathbf{Q}_1\mathbf{a}^{(1)} = 0 \\ \vdots \\ \mathbf{a}^{(1)\mathrm{T}}\mathbf{Q}_{N_S}\mathbf{a}^{(1)} = 0 \end{cases}$$

$$\mathbf{Q}_i = \sum_{j=1}^{N_B} \bar{\mathbf{X}}^{\mathrm{T}} \begin{bmatrix} \omega_{i,j}\dfrac{\partial^2 c_j}{\partial X_1^2} & \cdots & \omega_{i,j}\dfrac{\partial^2 c_j}{\partial X_1 \partial X_{N_X}} \\ \vdots & \ddots & \vdots \\ \omega_{i,j}\dfrac{\partial^2 c_j}{\partial X_{N_X} \partial X_1} & \cdots & \omega_{i,j}\dfrac{\partial^2 c_j}{\partial X_{N_X}^2} \end{bmatrix} \bar{\mathbf{X}}$$

Solution of second-order infinitesimal mechanism

$$\mathbf{X}^{(2)} = -\left[\boldsymbol{\Gamma}^{(0)}\right]^{+}\boldsymbol{\Gamma}^{(1)}\mathbf{X}^{(1)} + \bar{\mathbf{X}}\mathbf{a}^{(2)}$$

$\left[\boldsymbol{\Gamma}^{(0)}\right]^{+}$: generalized inverse of $\boldsymbol{\Gamma}^{(0)}$

- $-\left[\boldsymbol{\Gamma}^{(0)}\right]^{+}\boldsymbol{\Gamma}^{(1)}\mathbf{X}^{(1)}$ → complementary solution
- $\bar{\mathbf{X}}\mathbf{a}^{(2)}$ → particular solution determined by $\mathbf{a}^{(1)}$

Degree-six Single Vertex

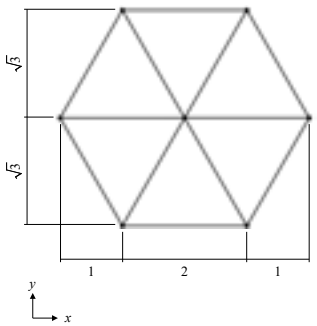

Triangulated regular hexagon

Number of nodes : 7

Number of members : 12

Number of kinematic indeterminacy : 4
(except for rigid-body motion)

Number of statical indeterminacy : 1

Mechanism and Self-equilibrium Force Modes

Infinitesimal mechanism modes

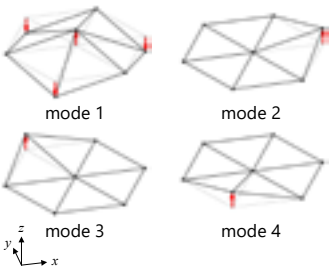

Rigid-body motions are eliminated.
Nodes move only in the z-direction.
Distance: 1.0

Self-equilibrium force density mode

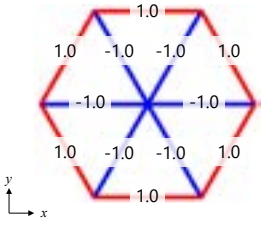

Positive value: tension
Negative value: compression

Axial force of bars
= force density × length

Existence Condition of Second-order Mechanism

Quadratic equation for coefficients of mechanism modes

$$-9\left(a_1^{(1)}\right)^2+\left(a_2^{(1)}\right)^2+\left(a_2^{(1)}\right)^2+\left(a_2^{(1)}\right)^2=0$$

$$\Rightarrow a_1^{(1)}=\pm\frac{1}{3}\sqrt{\left(a_2^{(1)}\right)^2+\left(a_2^{(1)}\right)^2+\left(a_2^{(1)}\right)^2}$$

Kinematic bifurcation

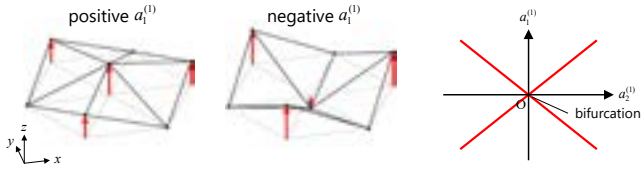

Third-order Infinitesimal Mechanism

Compatibility equation for third-order infinitesimal mechanism

$$\begin{cases}\boldsymbol{\Gamma}^{(0)}\mathbf{X}^{(1)}=\mathbf{0}\\ \boldsymbol{\Gamma}^{(0)}\mathbf{X}^{(2)}+\boldsymbol{\Gamma}^{(1)}\mathbf{X}^{(1)}=\mathbf{0}\\ \boldsymbol{\Gamma}^{(0)}\mathbf{X}^{(3)}+2\boldsymbol{\Gamma}^{(1)}\mathbf{X}^{(2)}+\boldsymbol{\Gamma}^{(2)}\mathbf{X}^{(1)}=\boldsymbol{\Gamma}^{(0)}\mathbf{X}^{(3)}+3\boldsymbol{\Gamma}^{(1)}\mathbf{X}^{(2)}=\mathbf{0}\end{cases}\qquad\left(\boldsymbol{\Gamma}^{(2)}\mathbf{X}^{(1)}=\boldsymbol{\Gamma}^{(1)}\mathbf{X}^{(2)}\right)$$

Existence condition of third-order infinitesimal mechanism

Second-order mechanism: $\boldsymbol{\Omega}^{\mathrm{T}}\boldsymbol{\Gamma}^{(1)}\mathbf{X}^{(1)}=\mathbf{0}\quad\left(\mathbf{a}^{(1)\mathrm{T}}\mathbf{Q}_1\mathbf{a}^{(1)}=\cdots=\mathbf{a}^{(1)\mathrm{T}}\mathbf{Q}_{N_\mathrm{g}}\mathbf{a}^{(1)}=0\right)$

Third-order mechanism: $\boldsymbol{\Omega}^{\mathrm{T}}\boldsymbol{\Gamma}^{(1)}\mathbf{X}^{(2)}=\mathbf{0}$

$$\mathbf{X}^{(2)}=-\left[\boldsymbol{\Gamma}^{(0)}\right]^{+}\boldsymbol{\Gamma}^{(1)}\mathbf{X}^{(1)}+\bar{\mathbf{X}}\mathbf{a}^{(2)}$$

$$\boldsymbol{\Omega}^{\mathrm{T}}\boldsymbol{\Gamma}^{(1)}\bar{\mathbf{X}}\mathbf{a}^{(2)}=\underline{\boldsymbol{\Omega}^{\mathrm{T}}\boldsymbol{\Gamma}^{(1)}\left[\boldsymbol{\Gamma}^{(0)}\right]^{+}\boldsymbol{\Gamma}^{(1)}\mathbf{X}^{(1)}}$$

unknown

determined by the existence of second-order mechanism

Higher-order Infinitesimal Mechanism

Compatibility equation for *n*-th-order infinitesimal mechanism

$$\begin{cases}\boldsymbol{\Gamma}^{(0)}\mathbf{X}^{(1)}=\mathbf{0}\\ \boldsymbol{\Gamma}^{(0)}\mathbf{X}^{(2)}+\boldsymbol{\Gamma}^{(1)}\mathbf{X}^{(1)}=\mathbf{0}\\ \vdots\\ \sum_{s=0}^{n-1}\binom{n-1}{s}\boldsymbol{\Gamma}^{(s)}\mathbf{X}^{(n-s)}=\boldsymbol{\Gamma}^{(0)}\mathbf{X}^{(n)}+\underline{\sum_{s=1}^{n-1}\binom{n-1}{s}\boldsymbol{\Gamma}^{(s)}\mathbf{X}^{(n-s)}}=\mathbf{0}\end{cases}$$

determined by the existence of (*n*-1)-th-order mechanism

Existence condition of *n*-th-order infinitesimal mechanism

Second-order mechanism: $\boldsymbol{\Omega}^{\mathrm{T}}\boldsymbol{\Gamma}^{(1)}\mathbf{X}^{(1)}=\mathbf{0}\quad\left(\mathbf{a}^{(1)\mathrm{T}}\mathbf{Q}_1\mathbf{a}^{(1)}=\cdots=\mathbf{a}^{(1)\mathrm{T}}\mathbf{Q}_{N_\mathrm{g}}\mathbf{a}^{(1)}=0\right)$

Third-order mechanism: $\boldsymbol{\Omega}^{\mathrm{T}}\boldsymbol{\Gamma}^{(1)}\mathbf{X}^{(2)}=\mathbf{0}\quad\left(\boldsymbol{\Omega}^{\mathrm{T}}\boldsymbol{\Gamma}^{(1)}\bar{\mathbf{X}}\mathbf{a}^{(2)}=\boldsymbol{\Omega}^{\mathrm{T}}\boldsymbol{\Gamma}^{(1)}\left[\boldsymbol{\Gamma}^{(0)}\right]^{+}\boldsymbol{\Gamma}^{(1)}\mathbf{X}^{(1)}\right)$

$\vdots$ $\qquad$ $\vdots$

n-th-order mechanism: $\boldsymbol{\Omega}^{\mathrm{T}}\sum_{s=1}^{n-1}\binom{n-1}{s}\boldsymbol{\Gamma}^{(s)}\mathbf{X}^{(n-s)}=\mathbf{0}$

Higher-order Infinitesimal Mechanism

Reformulation of existence condition of *n*-th order mechanism (*n*≥4)

$$\sum_{s=1}^{n-1}\binom{n-1}{s}\boldsymbol{\Omega}^{\mathrm{T}}\boldsymbol{\Gamma}^{(s)}\mathbf{X}^{(n-s)}=\mathbf{0}$$

$$\Leftrightarrow (n-1)\boldsymbol{\Omega}^{\mathrm{T}}\boldsymbol{\Gamma}^{(1)}\mathbf{X}^{(n-1)}+\boldsymbol{\Omega}^{\mathrm{T}}\boldsymbol{\Gamma}^{(n-1)}\mathbf{X}^{(1)}+\sum_{s=2}^{n-2}\binom{n-1}{s}\boldsymbol{\Omega}^{\mathrm{T}}\boldsymbol{\Gamma}^{(s)}\mathbf{X}^{(n-s)}=\mathbf{0}$$

$$\leftarrow \boldsymbol{\Gamma}^{(1)}\mathbf{X}^{(n-1)}=\boldsymbol{\Gamma}^{(n-1)}\mathbf{X}^{(1)}$$

$$\Leftrightarrow n\boldsymbol{\Omega}^{\mathrm{T}}\boldsymbol{\Gamma}^{(1)}\mathbf{X}^{(n-1)}+\sum_{s=2}^{n-2}\binom{n-1}{s}\boldsymbol{\Omega}^{\mathrm{T}}\boldsymbol{\Gamma}^{(s)}\mathbf{X}^{(n-s)}=\mathbf{0}$$

$$\leftarrow \mathbf{X}^{(n-1)}=-\sum_{s=1}^{n-2}\binom{n-2}{s}\left[\boldsymbol{\Gamma}^{(0)}\right]^{+}\boldsymbol{\Gamma}^{(s)}\mathbf{X}^{(n-s-1)}+\bar{\mathbf{X}}\mathbf{a}^{(n-1)}$$

$$\Leftrightarrow \underbrace{\boldsymbol{\Omega}^{\mathrm{T}}\boldsymbol{\Gamma}^{(1)}\bar{\mathbf{X}}\mathbf{a}^{(n-1)}}_{\text{unknown}}=\underbrace{\sum_{s=1}^{n-2}\binom{n-2}{s}\boldsymbol{\Omega}^{\mathrm{T}}\boldsymbol{\Gamma}^{(1)}\left[\boldsymbol{\Gamma}^{(0)}\right]^{+}\boldsymbol{\Gamma}^{(1)}\mathbf{X}^{(n-s-1)}-\frac{1}{n}\sum_{s=2}^{n-2}\binom{n-1}{s}\boldsymbol{\Omega}^{\mathrm{T}}\boldsymbol{\Gamma}^{(s)}\mathbf{X}^{(n-s)}}_{\text{determined by the existence of }(n\text{-}1)\text{-th-order mechanism}}$$

Existence of Finite Mechanism

Existence condition of *n*-th order mechanism

Second-order: $\mathbf{a}^{(1)\mathrm{T}}\mathbf{Q}_i\mathbf{a}^{(1)}=\cdots=\mathbf{a}^{(1)\mathrm{T}}\mathbf{Q}_{N_\mathrm{S}}\mathbf{a}^{(1)}=0$

Third-order: $\boldsymbol{\Omega}^{\mathrm{T}}\boldsymbol{\Gamma}^{(1)}\bar{\mathbf{X}}\mathbf{a}^{(2)}=\boldsymbol{\Omega}^{\mathrm{T}}\boldsymbol{\Gamma}^{(1)}\left[\boldsymbol{\Gamma}^{(0)}\right]^{+}\boldsymbol{\Gamma}^{(1)}\mathbf{X}^{(1)}$

$\vdots$

n-th-order: $\boldsymbol{\Omega}^{\mathrm{T}}\boldsymbol{\Gamma}^{(1)}\bar{\mathbf{X}}\mathbf{a}^{(n-1)}=\sum_{s=1}^{n-2}\binom{n-2}{s}\boldsymbol{\Omega}^{\mathrm{T}}\boldsymbol{\Gamma}^{(1)}\left[\boldsymbol{\Gamma}^{(0)}\right]^{+}\boldsymbol{\Gamma}^{(1)}\mathbf{X}^{(n-s-1)}-\frac{1}{n}\sum_{s=2}^{n-2}\binom{n-1}{s}\boldsymbol{\Omega}^{\mathrm{T}}\boldsymbol{\Gamma}^{(s)}\mathbf{X}^{(n-s)}$

Sufficient condition for existence of finite mechanism

Finite mechanism $\Leftrightarrow$ Existence of $\mathbf{a}^{(1)},\ldots,\mathbf{a}^{(n-1)}$ for arbitrary order of *n*

$$\Leftarrow \begin{cases}\mathbf{a}^{(1)\mathrm{T}}\mathbf{Q}_i\mathbf{a}^{(1)}=\cdots=\mathbf{a}^{(1)\mathrm{T}}\mathbf{Q}_{N_\mathrm{S}}\mathbf{a}^{(1)}=0\\ \mathrm{rank}\left(\boldsymbol{\Omega}^{\mathrm{T}}\boldsymbol{\Gamma}^{(1)}\bar{\mathbf{X}}\right)=N_\mathrm{S}\quad\text{(row full-rank)}\end{cases}$$

n-th Order Polynomial Approximation of Rigid-Folding Motion

1. Calculate $\mathbf{X}^{(1)}$ using manually determined $\mathbf{a}^{(1)}$ satisfying $\begin{cases}\mathbf{a}^{(1)\mathrm{T}}\mathbf{Q}_i\mathbf{a}^{(1)}=0\ (i=1,\ldots,N_\mathrm{S})\\ \mathrm{rank}\left(\boldsymbol{\Omega}^{\mathrm{T}}\boldsymbol{\Gamma}^{(1)}\bar{\mathbf{X}}\right)=N_\mathrm{S}\end{cases}$
2. Calculate $\mathbf{a}^{(2)}=\left[\boldsymbol{\Omega}^{\mathrm{T}}\boldsymbol{\Gamma}^{(1)}\bar{\mathbf{X}}\right]^{+}\boldsymbol{\Omega}^{\mathrm{T}}\boldsymbol{\Gamma}^{(1)}\left[\boldsymbol{\Gamma}^{(0)}\right]^{+}\boldsymbol{\Gamma}^{(1)}\mathbf{X}^{(1)}$ (existence condition of $\mathbf{X}^{(3)}$)
3. Calculate $\mathbf{X}^{(2)}=-\left[\boldsymbol{\Gamma}^{(0)}\right]^{+}\boldsymbol{\Gamma}^{(1)}\mathbf{X}^{(1)}+\bar{\mathbf{X}}\mathbf{a}^{(2)}$
4. Initialize *k* as $k\leftarrow 3$
5. Calculate $\mathbf{a}^{(k)}=\left[\boldsymbol{\Omega}^{\mathrm{T}}\boldsymbol{\Gamma}^{(1)}\bar{\mathbf{X}}\right]^{+}\left\{\sum_{s=1}^{k-1}\binom{k-1}{s}\boldsymbol{\Omega}^{\mathrm{T}}\boldsymbol{\Gamma}^{(1)}\left[\boldsymbol{\Gamma}^{(0)}\right]^{+}\boldsymbol{\Gamma}^{(1)}\mathbf{X}^{(k-s)}-\frac{1}{k+1}\sum_{s=2}^{k-1}\binom{k}{s}\boldsymbol{\Omega}^{\mathrm{T}}\boldsymbol{\Gamma}^{(s)}\mathbf{X}^{(k-s+1)}\right\}$ (existence condition of $\mathbf{X}^{(k+1)}$)
6. Calculate $\mathbf{X}^{(k)}=-\sum_{s=1}^{k-1}\binom{k-1}{s}\left[\boldsymbol{\Gamma}^{(0)}\right]^{+}\boldsymbol{\Gamma}^{(s)}\mathbf{X}^{(k-s)}+\bar{\mathbf{X}}\mathbf{a}^{(k)}$
7. Update *k* as $k\leftarrow k+1$ and go to 4 while $k\le n$
8. Calculate $\mathbf{X}(t)=\mathbf{X}^{(1)}t+\frac{1}{2}\mathbf{X}^{(2)}t^2+\cdots+\frac{1}{n!}\mathbf{X}^{(n)}t^n$

Resch's Pattern

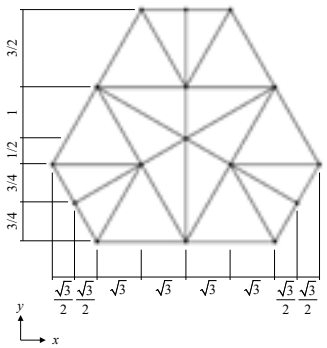

Part of Resch's triangular rigid-foldable tessellation pattern

Number of nodes : 16

Number of members : 33

Number of kinematic indeterminacy : 13
(except for rigid-body motion)

Number of statical indeterminacy : 4

Infinitesimal Mechanism Modes

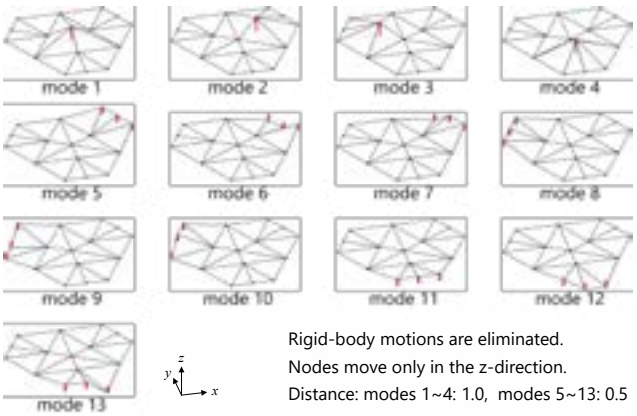

Rigid-body motions are eliminated.
Nodes move only in the z-direction.
Distance: modes 1~4: 1.0, modes 5~13: 0.5

Self-equilibrium Force Density Modes

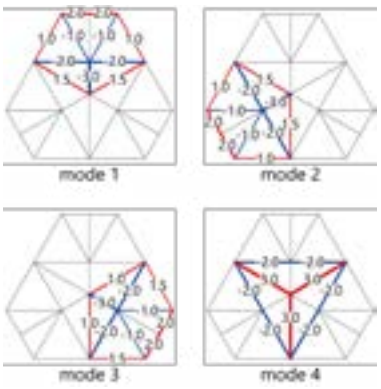

Positive value: tension
Negative value: compression

Axial force of bars
= force density × length

Each Stressed region contains a single interior node

Existence Condition of Second-order Mechanism

Quadratic equations for coefficients of mechanism modes

$$\begin{cases} 6a_1^{(1)}a_2^{(1)} - 9\left(a_2^{(1)}\right)^2 + 2a_2^{(1)}a_5^{(1)} + 2\left(a_6^{(1)}\right)^2 + 2\left(a_7^{(1)}\right)^2 = 0 \\ 6a_1^{(1)}a_3^{(1)} - 9\left(a_3^{(1)}\right)^2 + 2a_3^{(1)}a_8^{(1)} + 2\left(a_9^{(1)}\right)^2 + 2\left(a_{10}^{(1)}\right)^2 = 0 \\ 6a_1^{(1)}a_4^{(1)} - 9\left(a_4^{(1)}\right)^2 + 2a_4^{(1)}a_{11}^{(1)} + 2\left(a_{12}^{(1)}\right)^2 + 2\left(a_{13}^{(1)}\right)^2 = 0 \\ 9\left(a_1^{(1)}\right)^2 - 4\left(a_2^{(1)}\right)^2 - 4\left(a_3^{(1)}\right)^2 - 4\left(a_4^{(1)}\right)^2 = 0 \end{cases}$$

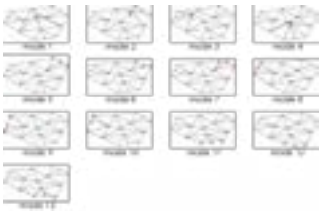

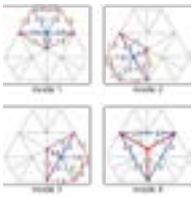

Existence Condition of Second-order Mechanism

Solution to the quadratic equations

$$a_1^{(1)} = \frac{2}{3}s_1\sqrt{p_2^2+p_3^2+p_4^2}, \quad a_2^{(1)} = s_2p_2, \quad a_3^{(1)} = s_3p_3, \quad a_4^{(1)} = s_4p_4,$$

$$a_5^{(1)} = -2s_1\sqrt{p_2^2+p_3^2+p_4^2} + s_2\left(\frac{9}{2}p_2 - b_6^2 - b_7^2\right), \quad a_6^{(1)} = b_6\sqrt{p_2}, \quad a_7^{(1)} = b_7\sqrt{p_2},$$

$$a_8^{(1)} = -2s_1\sqrt{p_2^2+p_3^2+p_4^2} + s_3\left(\frac{9}{2}p_3 - b_9^2 - b_{10}^2\right), \quad a_9^{(1)} = b_9\sqrt{p_3}, \quad a_{10}^{(1)} = b_{10}\sqrt{p_3},$$

$$a_{11}^{(1)} = -2s_1\sqrt{p_2^2+p_3^2+p_4^2} + s_4\left(\frac{9}{2}p_4 - b_{12}^2 - b_{13}^2\right), \quad a_{12}^{(1)} = b_{12}\sqrt{p_4}, \quad a_{13}^{(1)} = b_{13}\sqrt{p_4}$$

s_1, s_2, s_3, s_4 : -1 or 1
p_2, p_3, p_4 : non-negative real value
$b_6, b_7, b_9, b_{10}, b_{12}, b_{13}$: arbitrary real value
} 13 variables (= degrees of freedom)

Existence Condition of Second-order Mechanism

Solution to the quadratic equations

$$a_1^{(1)} = \frac{2}{3}s_1\sqrt{p_2^2+p_3^2+p_4^2}, \quad a_2^{(1)} = s_2p_2, \quad a_3^{(1)} = s_3p_3, \quad a_4^{(1)} = s_4p_4,$$

$$a_5^{(1)} = -2s_1\sqrt{p_2^2+p_3^2+p_4^2} + s_2\left(\frac{9}{2}p_2 - b_6^2 - b_7^2\right), \quad a_6^{(1)} = b_6\sqrt{p_2}, \quad a_7^{(1)} = b_7\sqrt{p_2},$$

$$a_8^{(1)} = -2s_1\sqrt{p_2^2+p_3^2+p_4^2} + s_3\left(\frac{9}{2}p_3 - b_9^2 - b_{10}^2\right), \quad a_9^{(1)} = b_9\sqrt{p_3}, \quad a_{10}^{(1)} = b_{10}\sqrt{p_3},$$

$$a_{11}^{(1)} = -2s_1\sqrt{p_2^2+p_3^2+p_4^2} + s_4\left(\frac{9}{2}p_4 - b_{12}^2 - b_{13}^2\right), \quad a_{12}^{(1)} = b_{12}\sqrt{p_4}, \quad a_{13}^{(1)} = b_{13}\sqrt{p_4}$$

s_1, s_2, s_3, s_4 : -1 or 1 ——— bifurcation of mechanism
p_2, p_3, p_4 : non-negative real value
$b_6, b_7, b_9, b_{10}, b_{12}, b_{13}$: arbitrary real value
} degrees of freedom after bifurcation

Sufficient Existence Condition of Finite Mechanism

Sufficient condition for existence of finite mechanism

$$\operatorname{rank}\left(\boldsymbol{\Omega}^{\mathrm{T}}\boldsymbol{\Gamma}^{(2)}\overline{\mathbf{X}}\right)=4$$

$$\boldsymbol{\Omega}^{\mathrm{T}}\boldsymbol{\Gamma}^{(2)}\overline{\mathbf{X}}=\begin{bmatrix} 3a_2^{(1)} & 3a_1^{(1)}-9a_2^{(1)}+a_5^{(1)} & 0 & 0 & a_2^{(1)} & 2a_6^{(1)} & 2a_7^{(1)} & 0 & 0 & 0 & 0 & 0 & 0 \\ 3a_3^{(1)} & 0 & 3a_1^{(1)}-9a_3^{(1)}+a_6^{(1)} & 0 & 0 & 0 & 0 & a_3^{(1)} & 2a_9^{(1)} & 2a_{10}^{(1)} & 0 & 0 & 0 \\ 3a_4^{(1)} & 0 & 0 & 3a_1^{(1)}-9a_4^{(1)}+a_{11}^{(1)} & 0 & 0 & 0 & 0 & 0 & 0 & a_4^{(1)} & 2a_{12}^{(1)} & 2a_{13}^{(1)} \\ 9a_1^{(1)} & -4a_2^{(1)} & -4a_3^{(1)} & -4a_4^{(1)} & 0 & 0 & 0 & 0 & 0 & 0 & 0 & 0 & 0 \end{bmatrix}$$

Example of solution

$$\mathbf{a}^{(1)}=\left(-\frac{2\sqrt{3}}{3},\ 1,\ 1,\ 1,\ \frac{5+4\sqrt{3}}{2},\ 1,\ -1,\ \frac{5+4\sqrt{3}}{2},\ 1,\ -1,\ \frac{5+4\sqrt{3}}{2},\ 1,\ -1\right)^{\mathrm{T}}$$

Polynomial Approximation of Rigid-folding Path

Direction of first-order mechanism at the initial flat state

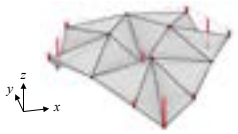

first-order infinitesimal mechanism

+ rigid-body motion

folded state

Folding motion by multiple polynomial approximation

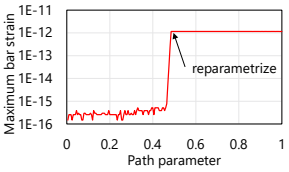

Summary

1. Kinematic bifurcation

   Existence condition of second-order infinitesimal mechanism

   → System of quadratic equations for coefficients of mechanism modes

2. Polynomial approximation of folding path

   Sufficient condition for existence of finite mechanism

   → Row full-rankness of matrix consisting of mechanism modes, self-equilibrium force modes, and Hessian of incompatibility vector

   Series expansion of nodal position vector for path parameter

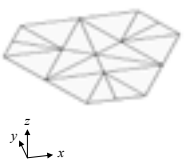

Efficient Matrix Assembly and Adaptive Refinement in Isogeometric Analysis

Bert Jüttler,
Johannes Kepler University

Abstract

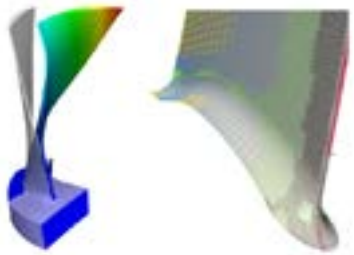

Isogeometric Analysis is a computational framework for numerical simulation, which was introduced by T.J.R. Hughes et al. in 2005 with the aim of bridging the gap between Design and Analysis, by adopting the prevailing mathematical technology of tensor product splines for discretizing of partial differential equations (PDEs). This presentation will address two of the many challenges that arise in this context. First, while the use of spline discretizations clearly offers advantages in terms of the number of degrees of freedom required compared to classical finite elements, these advantages are then compromised by the higher computational cost of matrix assembly in isogeometric analysis. We describe our methods for efficient matrix assembly, which make use of spline projection, pre-computed look-up tables and sum factorization to optimize the computational performance of the entire process. Second, since the rigid structure of tensor product splines is an obstacle to the use of adaptive refinement in isogeometric analysis, various generalizations of them have been proposed in the literature. These include T-splines (introduced by Sederberg et al. in 2003), hierarchical B-splines (invented by Forsey and Bartels in 1988) and the so-called "locally refined" splines (Dokken et al. 2013). In this presentation, we will analyze these approaches and compare them with the truncated variant of hierarchical B-splines, which reconciles the requirements of isogeometric analysis with those of geometric design.

References

[1] C. Giannelli, B. Jüttler, S. K. Kleiss, A. Mantzaflaris, B. Simeon, J. Špeh, "THB-splines: An effective mathematical technology for adaptive refinement in geometric design and isogeometric analysis", Comput. Meth. Appl. Mech. Engrg., vol. 299, pp. 337–365, 2016.

[2] M. Pan, B. Jüttler, A. Giust, "Fast formation of isogeometric Galerkin matrices via integration by interpolation and look-up", Comput. Meth. Appl. Mech. Engrg. vol. 366 (2020), 113005.

Efficient Matrix Assembly and Adaptive Refinement in Isogeometric Analysis

Bert Jüttler

JKU Linz, Austria

joint work with Carlotta Giannelli, Alessandro Giust, David Grossmann, Gabor Kiss, Angelos Mantzaflaris, Dominik Mokris, Maodong Pan, Bernd Simeon, Hendrik Speleers, ...

Outline

- Isogeometric analysis
- Efficient matrix assembly
- Adaptive spline refinement
  - T-splines
  - HB-splines
  - LR B-splines
- Concluding remarks

Motivation: Numerical simulation in practice

Problems

The use of different geometric models causes **different problems with data exchahnge.**

Related experiences

Ship design: Bronsart et al. (2004):

> "On average, generating the panel meshes takes up to 30% to 90% of the total time needed for wave resistance calculations".

Automotive industry: Farouki (SIAM News 1999) quotes Morgan, who

> "presented the following 'typical' breakdown of the effort in a realistic CFD analysis: 1-4 **weeks** for geometry repair and preparation, 10-20 minutes for surface meshing, 3-4 hours for volume meshing, and about 1 hour for the actual flow analysis."

Isogeometric Analysis (IgA)

... is an approach to bridge the gap between
"Geometry" (CAD)
and
"Analysis" (FEM)
... was established by T.J.R. Hughes et al. 2005

☞ Use the same representation for Design and Analysis! ☜

A NURBS volume

$$G(r,s,t) = \sum_{i\in\mathcal{I}} \sum_{j\in\mathcal{J}} \sum_{k\in\mathcal{K}} R_{ijk}(r,s,t)\mathbf{d}_{ijk}, \quad (r,s,t) \in [0,1]^3$$

with

$$R_{ijk}(r,s,t) = \frac{w_{ijk}\beta_{i,\mathcal{R}}(r)\beta_{j,\mathcal{S}}(s)\beta_{k,\mathcal{T}}(t)}{\sum_{i'\in\mathcal{I}} \sum_{j'\in\mathcal{J}} \sum_{k'\in\mathcal{K}} w_{i'j'k'}\beta_{i',\mathcal{R}}(r)\beta_{j',\mathcal{S}}(s)\beta_{k',\mathcal{T}}(t)}$$

$\mathbf{d} = (\mathbf{d}_{ijk})$	(de Boor) control points
$\beta_{i,\mathcal{R}}(r)$, $\beta_{j,\mathcal{S}}(s)$, $\beta_{k,\mathcal{T}}(t)$	B-splines
$\mathcal{R}$, $\mathcal{S}$, $\mathcal{T}$	knot vectors
$\mathcal{I}$, $\mathcal{J}$, $\mathcal{K}$	index sets of the control points
w_{ijk}	weights

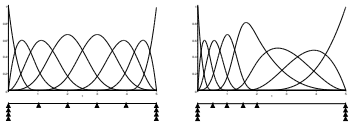

IgA for a real-world example

D. Großmann (MTU Aero Engines) et al., CAGD 2012:

Comparison of Isogeometric and FEM simulations of turbine blades subject to centrifugal forces, pressure, and temperature (linear elasticity with temperature-dependent material properties)

Accuracy: IgA vs. FEM

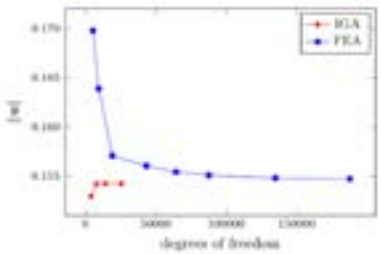

Figure 2.10: Displacements of the top corner at the leading edge of the blade caused by the surface pressure.

⇝ **same accuracy with ≈ 10% of dofs**

Computation time I: solving the linear system

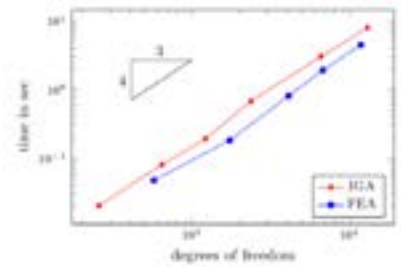

Figure 1.8: Computational time required to solve the linear system.

$\rightsquigarrow$ IGA needs **slightly** more time than FEM (increased bandwidth)

Computation time II: assembling the matrices (Gauss quadrature)

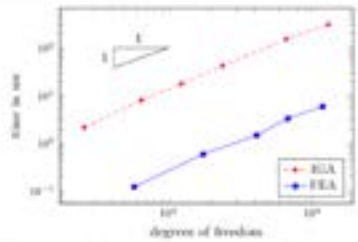

Figure 1.9: Computational time required to assemble the stiffness matrix. A dashed line for the isogeometric method illustrates the currently non-optimized code.

$\rightsquigarrow$ IGA assembly needs **significantly** more time than FEM assembly!
($\approx$ 40 times)

Outline

- Isogeometric analysis
- Efficient matrix assembly
- Adaptive spline refinement
  - T-splines
  - HB-splines
  - LR B-splines
- Concluding remarks

Matrix generation challenge

$\rightsquigarrow$ Several approaches to address this challenge:

(A) special quadrature rules for splines: Auricchio, Calabro, Hughes, Reali & Sangalli '12, Hughes, Reali, Sangalli '10, Schillinger, Hossain & Hughes '14, Barton & Calo '16, ...

(B) computation re-use ("sum factorization"): Antolin, Buffa, Calabro, Martinelli & Sangalli '15 Calabro, Sangalli & Tani '16

(A+B) weighted quadrature: Calabro, Sangalli & Tani'17, Hiemstra, Sangalli, Tani, Calabro, Hughes'19 Giannelli, Kanduc, Martinelli, Sangalli, Tani '22

(C) isogeometric collocation: Schillinger, Evans, Reali, Scott & Hughes '13, De Lorenzis, Evans, Hughes & Reali '14, ...

(D) spline projection: Mantzaflaris & J.'15, Pan, J.& Giust '20

(E) tensor methods [based on (D)] Mantzaflaris, J., Khoromskij & Langer'17

Integration by Spline Projection

Example: Mass matrix

$$M_{\boldsymbol{ij}} = \int_{[0,1]^d} \beta_{\boldsymbol{i}} \beta_{\boldsymbol{j}} w \mathrm{d}\boldsymbol{x}, \quad w = \lambda |\det \tilde{\nabla} \boldsymbol{F}|. \tag{1}$$

Spline projection

$$w(\boldsymbol{x}) \approx \sum_{\boldsymbol{k} \in \mathcal{I}} w_{\boldsymbol{k}} \beta_{\boldsymbol{k}}(\boldsymbol{x}) \tag{2}$$

transforms elements into

$$M_{\boldsymbol{ij}} \approx \int_{[0,1]^d} \beta_{\boldsymbol{i}} \beta_{\boldsymbol{j}} \sum_{\boldsymbol{k} \in \mathcal{I}} w_{\boldsymbol{k}} \beta_{\boldsymbol{k}} \mathrm{d}\boldsymbol{x} = \sum_{\boldsymbol{k} \in \mathcal{I}} w_{\boldsymbol{k}} \int_{[0,1]^d} \beta_{\boldsymbol{i}} \beta_{\boldsymbol{j}} \beta_{\boldsymbol{k}} \mathrm{d}\boldsymbol{x}. \tag{3}$$

Sum Factorization

Use look-up tables

$$L_{\ell, i_\ell j_\ell k_\ell} = \int_0^1 \beta_{\ell, i_\ell} \beta_{\ell, j_\ell} \beta_{\ell, k_\ell} \mathrm{d}x_\ell, \tag{4}$$

and rewrite mass matrix elements as

$$M_{\boldsymbol{ij}} \approx \sum_{\boldsymbol{k} \in \mathcal{I}} w_{\boldsymbol{k}} \prod_{\ell=1}^{d} L_{\ell, i_\ell j_\ell k_\ell}. \tag{5}$$

Efficient evaluation via "sum factorization" (shown for $d = 3$):

$$M_{\boldsymbol{ij}} \approx \underbrace{\sum_{k_3} L_{3,i_3 j_3 k_3} \underbrace{\sum_{k_2} L_{2,i_2 j_2 k_2} \underbrace{\sum_{k_1} L_{1,i_1 j_1 k_1} w_{k_1 k_2 k_3}}_{= A_{(i_1 j_1)(k_2 k_3)}}}_{= B_{(i_1 i_2)(j_1 j_2) k_3}}}_{\approx M_{(i_1 i_2 i_3)(j_1 j_2 j_3)}}, \tag{6}$$

Results: Theory

Symmetry is preserved (unlike weighted quadrature)

Accuracy of overall simulation: is preserved if spline projection uses the same degree as the discretization

Computational complexity: $O(Np^{d+1})$ (same as weighted quadrature, less than any other method)

Results: #flops per dof ($d = 3$):

	$p=1$	$p=2$	$p=3$	$p=4$	$p=5$	asymptotics
GQ	1,672	60,534	794,688	5,890,750	30,326,616	$\mathcal{O}(p^9)$
EGS	512	7,047	47,104	209,375	715,392	$\mathcal{O}(p^7)$
IL	1,390	27,460	202,642	907,960	3,014,326	$\mathcal{O}(p^6)$
GGS	304	2,646	11,904	37,750	96,336	$\mathcal{O}(p^5)$
WQ	190	1,014	3,350	8,446	17,934	$16p^4 + \mathcal{O}(p^3)$
ILS	200	1,202	4,248	11,138	24,248	$24p^4 + \mathcal{O}(p^3)$
ILS-S	88	336	954	2,206	4,428	$3p^4 + \mathcal{O}(p^3)$

GQ: Gauss quadrature; EGS: element-wise GQ with SF, GGS: global GQ with SF, IL: Interpolation and Look-up, WQ: weighted quadrature, ILS: our method, ILS-S: with use of symmetry

Results: Speedup ($d = 3$)

... on a particular geometry. Note that we compare with the highly optimized G+Smo implementation!

	$p=1$	$p=2$	$p=3$	$p=4$	$p=5$
Predicted speedup	8.36	50.36	187.07	528.89	1250.69
Observed speedup	5.42	6.38	12.4	29.9	66.3

Outline

- Isogeometric analysis
- Efficient matrix assembly
- Adaptive spline refinement
  - T-splines
  - HB-splines
  - LR B-splines
- Concluding remarks

The need for adaptive generalizations of TP splines

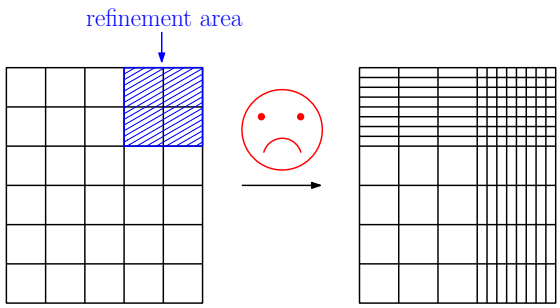

The need for adaptive generalizations of TP splines

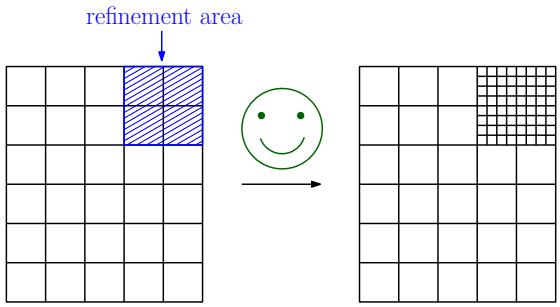

The main competitors

- **T-splines (splines with T-joints)**
- **Hierarchical B-splines**
- **LR splines (Locally Refined Splines)**

Outline

- Isogeometric analysis
- Efficient matrix assembly
- Adaptive spline refinement
  - T-splines
  - HB-splines
  - LR B-splines
- Concluding remarks

T-splines: The most popular approach

History:

- 2003: invented by Sederberg at al. (SIGGRAPH)
- approx. 2003: T-SPLINE INC. established
- T-spline plugin for the RHINO modeling software
- 2010: Use of T-splines in Isogeometric Analysis
- Dec. 2011: AUTODESK acquires T-SPLINE INC.
- 2018: U-splines

T-splines: Definition

Blending functions **(linear independence is not guaranteed!)** associated with T-meshes are products of B-splines with local knot vectors

$$N_{i,j}(s,t) = B_{\sigma(i)}(s) B_{\tau(j)}(t)$$

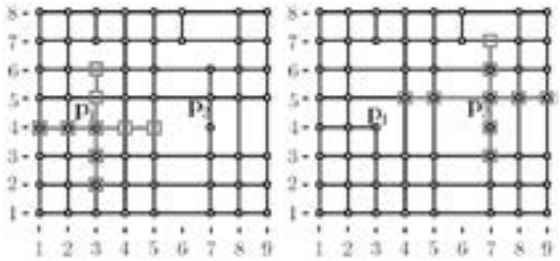

Example: Advection Dominated Advection–Diffusion

Solve $\kappa \Delta u + \boldsymbol{a} \cdot \nabla u = 0$ with diffusion coefficient $\kappa = 10^{-6}$ and advection velocity $\boldsymbol{a} = (\sin\theta, \cos\theta)$ for $\theta = 45°$.

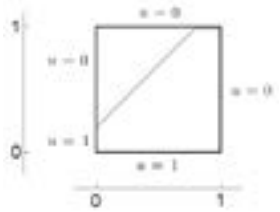

grey: estimated position of sharp layers

is solved using SUPG stabilization

Example: Advection Dominated Advection–Diffusion

T-mesh

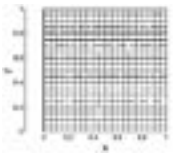

Solution

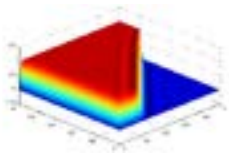

patches marked for refinement

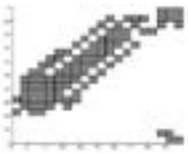

Example: Advection Dominated Advection–Diffusion

T-mesh

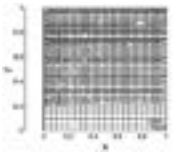

Solution

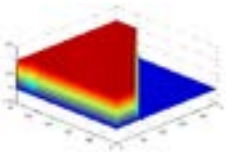

patches marked for refinement

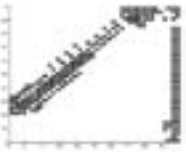

Example: Advection Dominated Advection–Diffusion

T-mesh

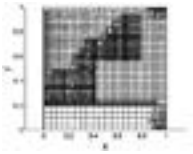

Solution

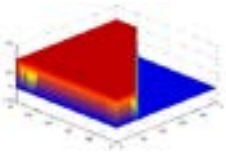

patches marked for refinement

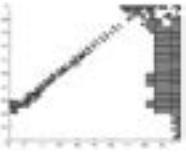

Example: Advection Dominated Advection–Diffusion

T-mesh

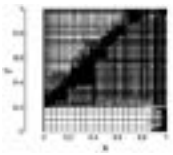

Solution

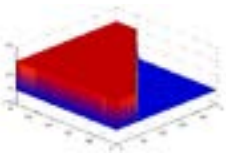

patches marked for refinement

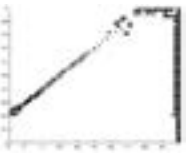

Example: Advection Dominated Advection–Diffusion

T-mesh | Solution | patches marked for refinement

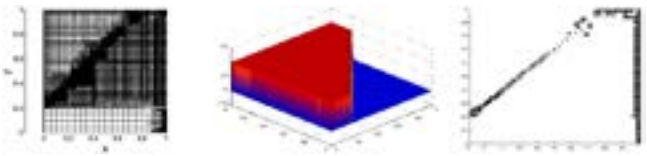

Refinement of T-splines is not as local as we hoped it to be!

Insertion of a grid point may trigger a chain of additional grid point insertions, in order to get a refinement of the previous T-spline space.

Especially bad for refinement along diagonals.

T-splines: Recent Advances

These problems triggered 521 citations and further research:

AST-splines: **sub-class** of "Analysis Suitable T-splines" (M. Scott et al. 2012), a.k.a. **DCT-Splines:** "Dual Compatible T-splines" (Pavia Group)

– are characterized by the fact that knot line extensions do not intersect

– **are linearly independent**

– **have the expected approximation power**

– possess a **sub-sub-class** that admits refinement with **linear complexity** (Morgenstern & Peterseim 2015)

– **refinement algorithm in 3D?**

Outline

- Isogeometric analysis
- Efficient matrix assembly
- Adaptive spline refinement
  - T-splines
  - HB-splines
  - LR B-splines
- Concluding remarks

H(ierarchical) B-splines: The classical approach ...

... with a new twist!

- Forsey & Bartels 1988: HB-spline as sums of B-spline functions
- Kraft 1997: defines a basis and a quasi-interpolant
- Vuong, Giannelli, J., Simeon 2011: Use in IGA, basis for weaker assumptions
- Giannelli, J., Speleers 2012: Truncated HB-splines – a new basis with better properties
- Giannelli, J., Speleers 2013: strong stability & completeness
- Manni & Speleers 2015: Quasi-interpolant $\rightsquigarrow$ approximation power
- Buffa, Giannelli, Morgenstern, Peterseim 2016: Complexity of mesh refinement

HB-splines: Definition

Hierarchy of **nested spline spaces** V^ℓ, spanned by B-spline bases B^ℓ

$$V^\ell = \operatorname{span} B^\ell \subset V^{\ell+1} = \operatorname{span} B^{\ell+1}$$

Hierarchy of **nested domains** $\Omega^\ell \subset \mathbb{R}^d$

$$\Omega^\ell \supseteq \Omega^{\ell+1}$$

The **Kraft basis** is defined by a selection mechanism:

$$\mathcal{K} = \bigcup_\ell \{\beta \in B^\ell : \operatorname{supp}_0 \beta \subseteq \Omega^\ell, \quad \operatorname{supp}_0 \beta \not\subseteq \Omega^{\ell+1}\}$$

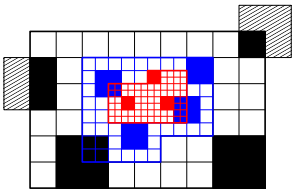

HB-Splines: 2D example ($p = 2$)

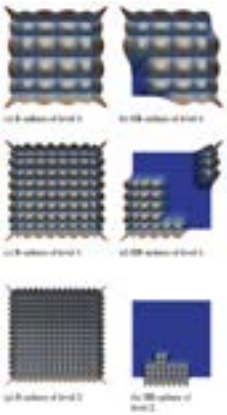

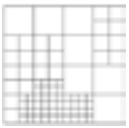

HB-splines: Properties of the Kraft basis

Properties:

Linear independence is implied by local linear independence of B-splines

Weighted partition of unity

$$\sum_{\beta \in \mathcal{K}} w_\beta \beta = 1 \quad w_\beta > 0$$

under certain assumptions on the domain hierarchy
$\rightsquigarrow$ is required for geometric modeling!

HB-Splines: First Use in IGA

.. by A.-V. Vuong et al. 2005 demonstrates the locality of the refinement:

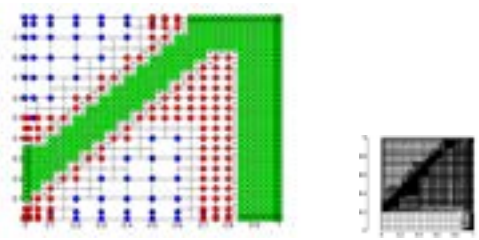

refined grid for the advection-diffusion problem / T-splines

Several papers explore HB splines in IGA: Schillinger et al. 2012, Bornemann & Cirak 2013, Kuru et al. 2013, ...

HB-Splines: Algebraic Completeness (AC)

Question: Given a hierarchical grid, does span $\mathcal{K}$ contain **any** piecewise polynomial function of degree $\mathbf{p}$ and smoothness C^s?

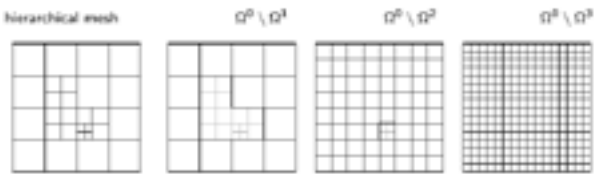

General answer: Only under certain conditions on the "rings" $\Omega^0 \setminus \Omega^{\ell+1}$!

HB-Splines: Answers to the AC question

• Answer for $d = 2$, $\boldsymbol{s} = \boldsymbol{p} - 1$, $\mathbf{p} = (p, p)$ (Giannelli & J. 2013):
Yes if $\Omega^0 \setminus \Omega^{\ell+1}$ **admits offset curves** at distance $(p-1)/2$:

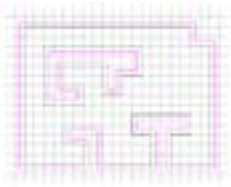

offset for $\mathbf{p} = (2, 2)$

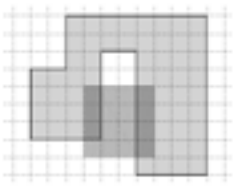

bad case for $\mathbf{p} = (3, 3)$

• Answer for $d = 3$, $\boldsymbol{s} = \boldsymbol{p} - 1$, $\mathbf{p} = (p, p, p)$ (Berdinsky & six co-authors 2014):
Yes if $\Omega^0 \setminus \Omega^{\ell+1}$ **admits offset surfaces** at distance $(p-1)/2$.

• **Answer for any d, any $\boldsymbol{s}$, any $\boldsymbol{p}$,** (Mokriš, J., Giannelli 2014): Yes if the supports of the basis functions in B^ℓ intersected with $\Omega^0 \setminus \Omega^{\ell+1}$ are all connected.

THB-Splines: A novel basis (Giannelli, J., Speleers 2012)

Any function of level ℓ admits a representation of level $\ell + 1$:

$$\beta \in B^\ell, \quad \beta(x) = \sum_{\gamma \in B^{\ell+1}} c_\gamma(\beta)\gamma(x)$$

"two scale relation", basis of subdivision surfaces

(**very beautiful coefficients** for uniform knots!)

We **truncate** the function by **omitting** the functions γ which are selected at the next level:

$$\text{trunc}^{\ell+1}(\beta)(x) = \sum_{\gamma \in B^{\ell+1}, \text{supp}\gamma \not\subseteq \Omega^{\ell+1}} c_\gamma(\beta)\gamma(x)$$

Applying this idea recursively defines the **T(runcated) HB-spline basis** $\mathcal{T}$

HB-Splines: 2D example ($p = 2$)

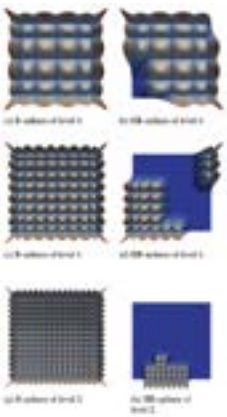

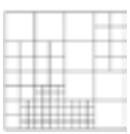

THB-Splines: 2D example ($p = 2$)

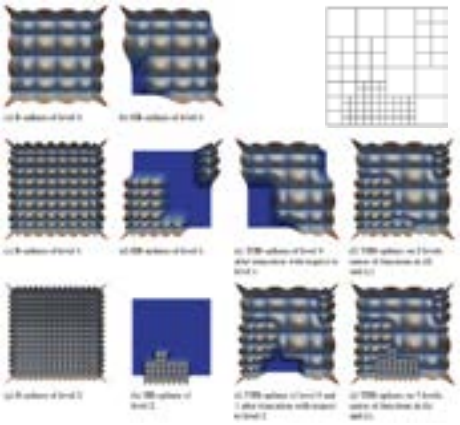

THB-Splines: Preservation of Coefficients (PoC)

THEOREM:

Any function in the THB-spline basis $\mathcal{T}$ has a **unique mother:**

$$\beta = \text{mother}(\tau) \quad \text{if} \quad \tau = \text{trunc}(...\text{trunc}(\beta)...)$$

Consider a function f which has a **representation at all levels:**

$$f(x) = \sum_{\beta \in B^\ell} c_\beta \beta(x) \quad \ell = 0, 1, 2, \ldots$$

The representation of f with respect to the THB-spline basis $\mathcal{T}$ **preserves the coefficients of the mother functions:**

$$f(x) = \sum_{\tau \in \mathcal{T}} c_{\text{mother}(\tau)} \tau(x)$$

THB-Splines: PoC implies Partition of Unity

The B-spline basis form a partition of unity

$$1 = \sum_{\beta \in B^\ell} 1 \cdot \beta(x) \quad \ell = 0, 1, 2, \ldots$$

The representation of 1 with respect to the THB-spline basis $\mathcal{T}$ **preserves the coefficients of the mother functions:**

$$1 = \sum_{\tau \in \mathcal{T}} 1 \cdot \tau(x)$$

HB-Splines vs. THB splines:

HB splines violate THB splines possess
the convex hull property.

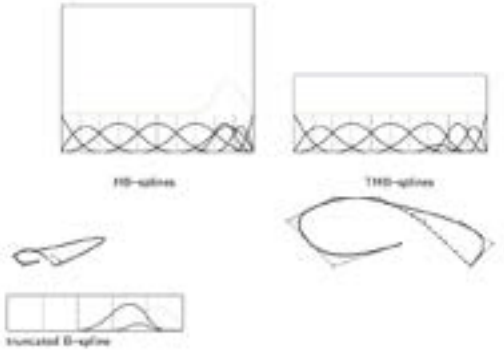

HB-Splines vs. THB splines:

HB splines violate THB splines possess
the convex hull property.

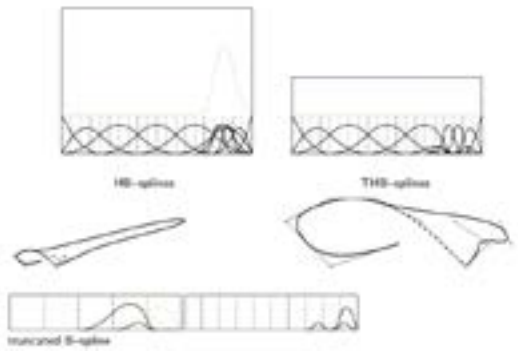

HB-Splines vs. THB splines:

HB splines violate THB splines possess
the convex hull property.

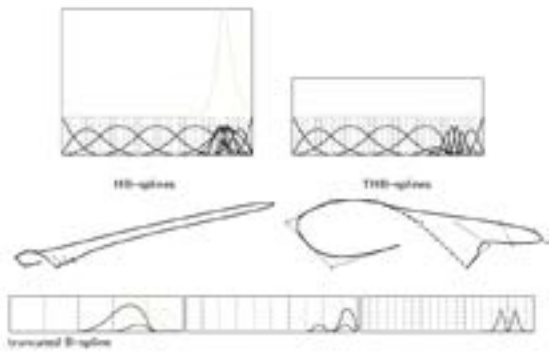

THB-Splines: PoC gives Greville points

Greville points (1D: abscissas) are the coefficients of the coordinate functions.

Used as collocation points in BEM

The **Greville points** of the B-spline basis are well known:

$$x = \sum_{\beta \in B^\ell} \xi_\beta \cdot \beta(x) \quad \ell = 0, 1, 2, \dots$$

The representation of x with respect to the THB-spline basis $\mathcal{T}$ **preserves the coefficients of the mother functions:**

$$x = \sum_{\tau \in \mathcal{T}} \xi_{\text{mother}(\tau)} \cdot \tau(x)$$

The Greville point of a THB-spline function is equal to that of its mother!

THB-Splines: PoC implies strong stability

Theorem:

There exists constants C_1 and C_2 such that

$$C_1 \max\{c_\tau : \tau \in \mathcal{T}\} \leq \left\| \sum_{\tau \in \mathcal{T}} c_\tau \tau \right\|_\infty \leq C_2 \max\{c_\tau : \tau \in \mathcal{T}\}$$

The constants depend neither on the choice of the subdomains nor on the number of levels.

$C_2 = 1$

Proof by PoC.

THB-Splines: Approximation Power

Manni & Speleers 2015:

Using PoC, Quasi-Interpolation operators for THB-splines can be derived from those of standard B-splines and provide **optimal approximation power.**

THB-Splines: Numerical Results (Giannelli et al. 2016)

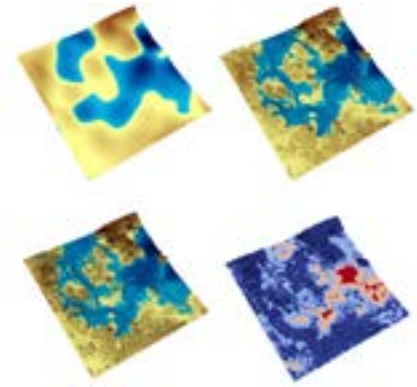

Approximation of geographic data: 1,3,6 levels + level distribution

THB-Splines: Numerical Results (Giannelli et al. 2016)

refinement step	no. of degrees of freedom		maximum error		% below threshold	
	local	global	local	global	local	global
0	100	100	1.02e-01	1.02e-01	10.44	10.44
1	324	324	9.59e-02	9.59e-02	16.58	16.58
2	1,156	1,156	8.68e-02	8.68e-02	27.62	27.62
3	4,356	4,356	6.82e-02	6.82e-02	41.23	41.23
4	16,388	16,900	6.38e-02	6.38e-02	57.62	57.63
5	57,034	66564	2.79e-02	2.79e-02	77.24	77.29
6	164,011	264,196	6.27e-03	6.27e-03	98.58	98.83

THB-Splines: Numerical Results (Giannelli et al. 2016)

refinement step	no. of degrees of freedom		maximum error		% below threshold	
	local	global	local	global	local	global
0	100	100	1.02e-01	1.02e-01	10.44	10.44
1	324	324	9.59e-02	9.59e-02	16.58	16.58
2	1,156	1,156	8.68e-02	8.68e-02	27.62	27.62
3	4,356	4,356	6.82e-02	6.82e-02	41.23	41.23
4	16,388	16,900	6.38e-02	6.38e-02	57.62	57.63
5	57,034	66564	2.79e-02	2.79e-02	77.24	77.29
6	164,011	264,196	6.27e-03	6.27e-03	98.58	98.83

THB-Splines: Numerical Results (Giannelli et al. 2016)

Ad hoc refinement of unit cube

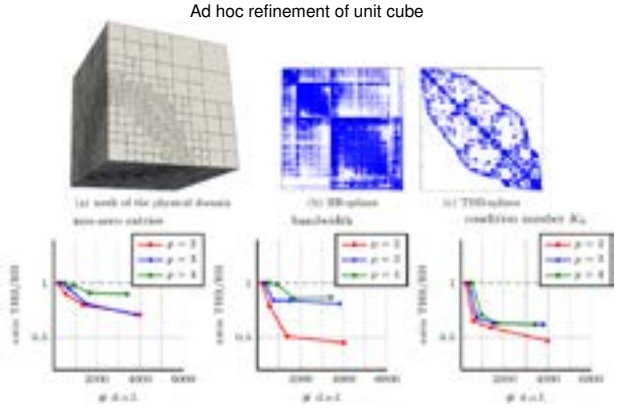

THB-Splines: Numerical Results (Giannelli et al. 2016)

Advection-diffusion on unit square:

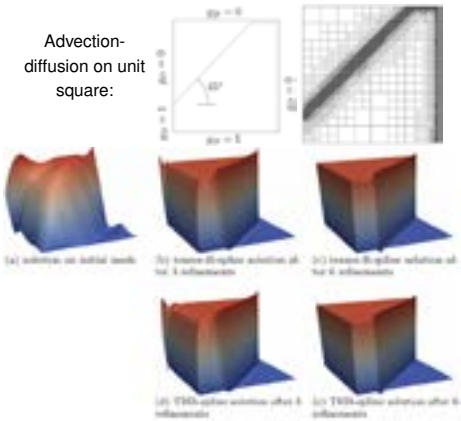

THB-Splines: Numerical Results (Giannelli et al. 2016)

Advection-diffusion on unit square:

		sparsity					
		non-zero entries			bandwidth		
step	#d.o.f.	HB	THB	$\frac{\text{THB}}{\text{HB}}$	HB	THB	$\frac{\text{THB}}{\text{HB}}$
$p = 2$							
0	36	196	196	1.00	11	11	1.00
1	86	1208	1030	0.85	35	22	0.63
2	247	5011	4417	0.88	72	49	0.68
3	650	17170	14048	0.82	176	98	0.56
4	1590	50849	38377	0.75	700	262	0.37
5	3804	134537	95385	0.71	1874	448	0.24
6	9114	333007	231669	0.70	4180	837	0.20

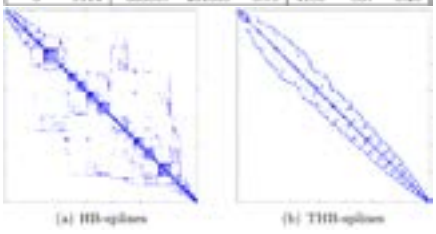

(a) HB-splines (b) THB-splines

THB-Splines: Numerical Results (Giannelli et al. 2016)

Advection-diffusion on Indiana:

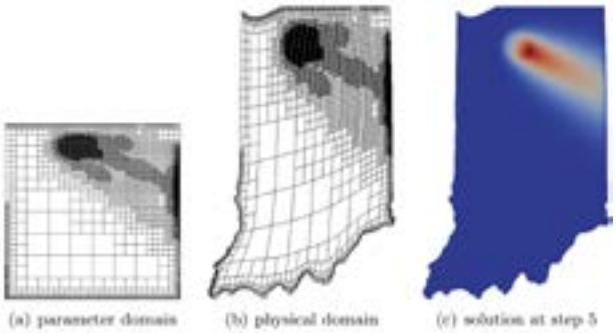

(a) parameter domain (b) physical domain (c) solution at step 5

THB splines are well suited for Geometric Modeling **and** IGA!

THB-Splines: Numerical Results (Kiss et al. 2014)

Turbine blades - cooperation with MTU Aero Engines:

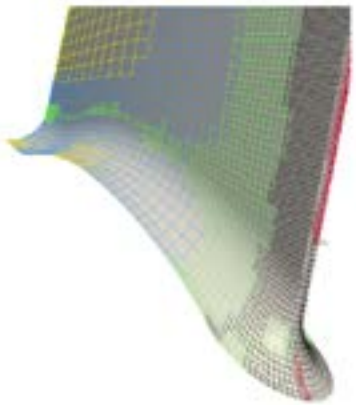

THB-Splines: Numerical Results (Kiss et al. 2014)

Turbine blades - cooperation with MTU Aero Engines:

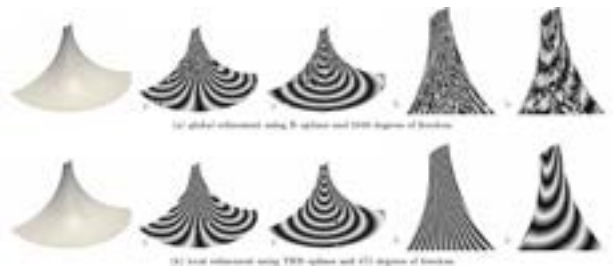

$\rightsquigarrow$ THB splines improve surface quality

THB-Splines: Numerical Results (Kiss et al. 2014)

Turbine blades - cooperation with MTU Aero Engines:

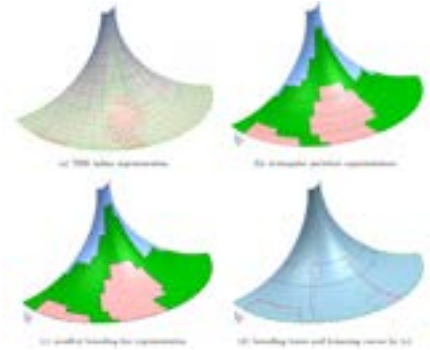

Two strategies for CAD export

Outline

- Isogeometric analysis
- Efficient matrix assembly
- Adaptive spline refinement
  - T-splines
  - HB-splines
  - LR B-splines
- Concluding remarks

LR-splines: The Newcomer

History:

- around 2010: **L**ocally **R**efined Splines invented by Dokken et al.
- since 2010: presentations at various conferences and workshops
- around 2010: patented
- 2013: Theoretical paper appears in CAGD

LR-splines: Definition (Dokken, Lyche and Pettersen 2013)

start with a tensor-product mesh

insert meshline segments

split functions whose support is traversed by meshline segments

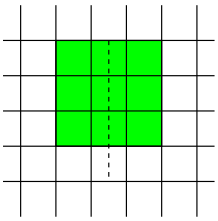

The set of LR splines is independent of the order of meshline insertions.

LR-splines: Properties

LR spline spaces on nested T-meshes are nested.

Linear independence is not guaranteed.

Detecting linear dependencies can be costly.

Current work (PhD thesis of Lisa Groiss, 2023): Mesh refinement for perfect LR B-splines bases (locally linearly independent, partition of unity)

Outline

- Isogeometric analysis
- Efficient matrix assembly
- Adaptive spline refinement
  - T-splines
  - HB-splines
  - LR B-splines
- Concluding remarks

Concluding Remarks

- ♡ Isogeometric Analysis ♡
- Fast matrix assembly via spline projection and sum factorization
- Three approaches to adaptive spline refinement
- Ongoing work: Refinement ensuring local linear independence

Shape generation of free-form grid shells with polygonal panels

Jingyao Zhang
Kyoto University

Abstract

This study addresses the shape generation of free-form grid shells with polygonal panels through two distinct approaches:

(a) For the generation of triangulated meshes with a predefined Gaussian curvature distribution, e.g., Figures 1 and 2, we introduce an efficient two-step method that integrates discrete Ricci flow and optimization techniques [1, 2]. The first step is to find the feasible edge lengths satisfying the predefined Gaussian curvature distribution, making use of circular packings. The second step is to embed these edge lengths into a three-dimensional space, by solving an optimization problem.

(b) For the generation of free-form planar meshes composed of polygonal panels, e.g., the planar quadrilateral mesh as shown in Figure , we propose a mechanical approach, modelling the mesh as a planar tensegrity structure. Self-equilibrated tensegrity units enable planarity of the panels, although this is not explicitly addressed as an objective in solving the form-finding problem.

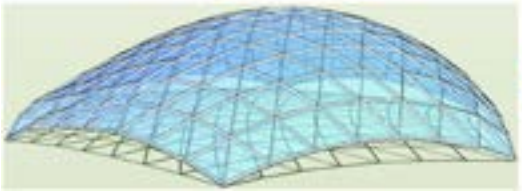

Figure 1: Surface with non-uniform Gaussian curvature

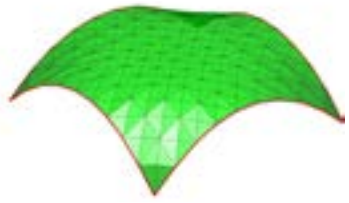

Figure 2: Globally developable surface

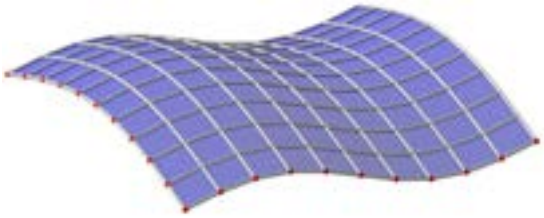

Figure 3: Planar quadrilateral mesh

References

[1] J. Y. Zhang, M. Ohsaki, A design tool for globally developable discrete architectural surfaces using Ricci flow, Japan Architectural Review, Vol. 6 (1), 312410, 2023. 10.1002/2475-8876.12410

[2] S. Kaji, J. Y. Zhang, Finetuning discrete architectural surfaces by use of circle packing, Journal of Asian Architecture and Building Engineering, Vol. 23 (1), pp. 188–203, 2024.

Shape generation of free-form grid shells with polygonal panels

Jingyao ZHANG

Ohsaki Group

Kyoto University

2025/3/10

Grid shells (polygonal panels)

Triangular mesh:

1. Globally developable discrete surfaces

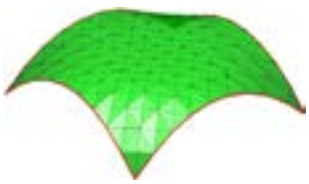

2. Discrete surface with specified Gaussian curvature
   (with Prof. Kaji, Kyusyu Uni.)

Polygonal mesh:

3. Planar polygonal grid shell

hexagonal

quadrilateral

2

Topic 1:
Globally developable discrete surface using Ricci flow

J.Y. Zhang, M. Ohsaki,
A design tool for globally developable discrete architectural surfaces using Ricci flow,
Japan Architectural Review, Vol. 6 (1), 312410, 2023.

CP for Discrete Surface

- Conformality: keep corner angles ➡ too rigid!

⇓

- Preserve intersection angle (edge weight) instead
- Circle packing is defined at vertices of mesh

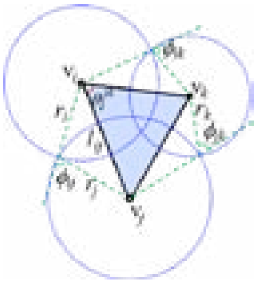

Radius at vertex $r_i^{jk} = \frac{1}{2}(l_{ij} + l_{ki} - l_{jk})$

↓

Mean radius $r_i = \frac{1}{n_i} \sum_{f_{ijk} \in F} r_i^{jk}$

↓

Edge weight $\phi_{ij} = \cos^{-1} \frac{l_{ij}^2 - r_i^2 - r_j^2}{2 r_i r_j}$

↓

Edge length $l_{ij}^2 = \underline{r_i^2} + \underline{r_j^2} + 2 r_i r_j \cos \underline{\underline{\phi_{ij}}}$

variable during Ricci flow — fixed

Discrete Ricci flow

• Chow, B., & Luo, F. (2003). Combinatorial Ricci flows on surfaces. Journal of Differential Geometry, 63(1), 97-129.

- In the smooth case, the Gaussian curvature is determined by the Riemannian metric.
- Two Riemannian metrics g_1, g_2 on a manifold are conformally equivalent if they are related by a positive scaling at each point.

$$g_2 = e^{2u} g_1, \quad u : M \to \mathbb{R}$$

- For a compact surface with Riemannian metric (X, g_{ij}), Hamilton (1988) introduced the 2D Ricci flow

$$\frac{dg_{ij}}{dt} = -K g_{ij}$$

- It was further proved that for any closed surface with any initial Riemannian metric, the solution of the Ricci flow exists for all time (reference?).
- After normalizing the solution to have fixed area, the solution converges to a constant curvature metric conformal to the initial metric as time goes to infinity.

- Chow and Luo (2003) presented the analogous flow in the combinatorial setting, and showed that the discrete Ricci flow has solutions for all time for any initial metric and converges exponentially fast to the circle packing metric constructed by Thurston.

$$\frac{du_i}{dt} = \bar{K}_i - K_i \qquad u_i = \ln r_i \qquad \sum_{i \in V} u_i = 0$$

target curvature — conformal factor — radius in Euclidean space

Procedure 2: Geometry

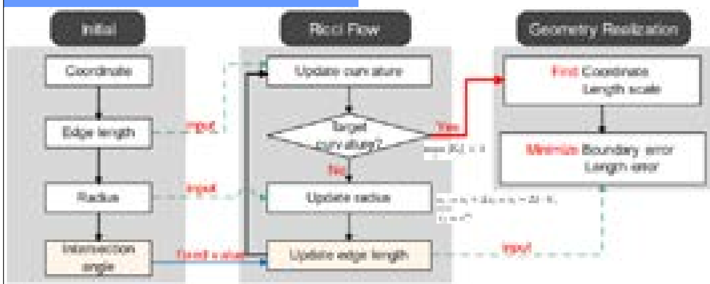

Final geometry by optimization:

SciPy optimizer:

- Trust Region Reflective (trf) algorithm
- Solve a nonlinear least-squares problem with bounds
- Simple but robust

Opt 1:

Find $\{x_i, y_i, z_i\}$ — Coordinates $(v_i \in V)$

Minimize $f_1 = \sum_i \left((x_i - x_i^{tar})^2 + (y_i - y_i^{tar})^2 + (z_i - z_i^{tar})^2 \right)$ — Boundary $(v_i \in B)$

Minimize $f_2 = \sum_{ij} \left(l_{ij} - \lambda l_{ij}^{Ricci} \right)^2$ — Edge length from Ricci flow $(e_{ij} \in E)$

Example 1: Initial Settings

- Span: 30 m
- Height: 20 m

- 169 vertices: 42 boundary, 127 interior
- 462 edges
- 294 faces (triangles)

- Coefficients for objective functions: $a_1 = 1.0, a_2 = 0.01$
- Scaling factor for initial radii: $\alpha = 1.2624$

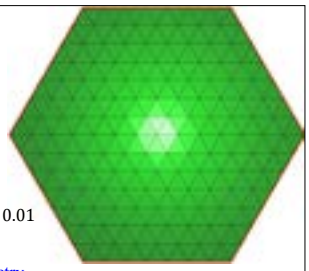

Initial geometry

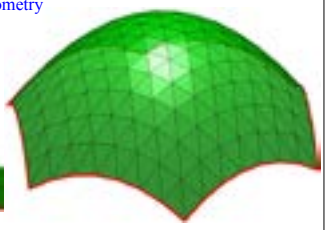

7

Example 1: Modified CP

- Metric embedding: trusted-region

- Scaling factor for edge length: $\beta = 1.6619$

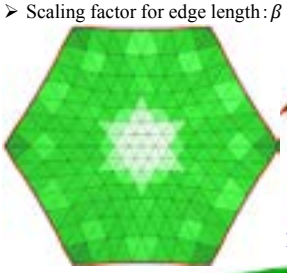

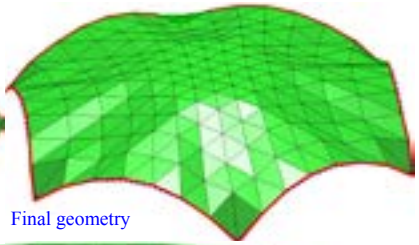

Final geometry

8

Example 1: Curvature

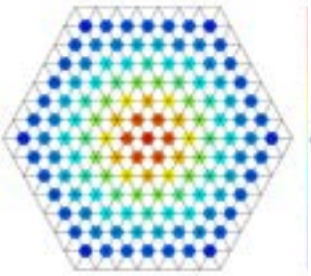

Initial

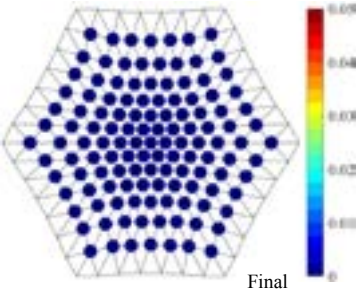

Final
Modified CP

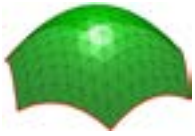

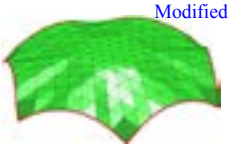

9

Example 1: Efficiency

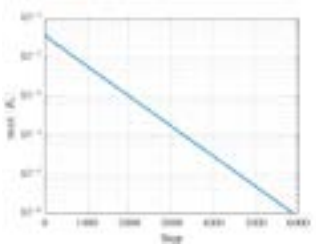

Ricci flow

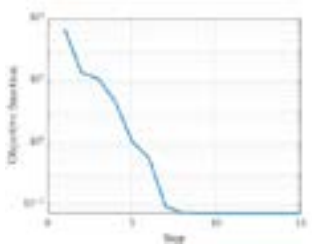

Geometry realization

10

Example 1: Developed

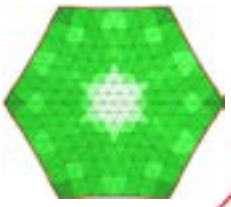

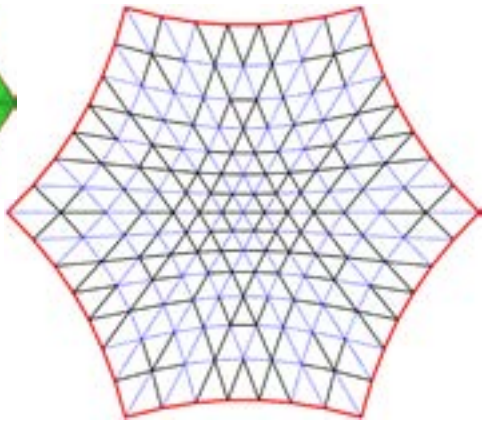

Mountain

Valley

11

Example 2: Initial geometry

- 181 vertices
  - 145 interior vertices (constrained)
  - 36 boundary vertices
- 504 edges
  - 464 interior edges (constrained)
  - 40 other edges
- 324 faces (triangles)

- alpha = 1.2296

Initial geometry

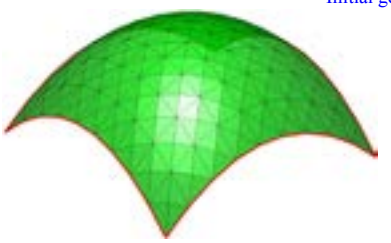

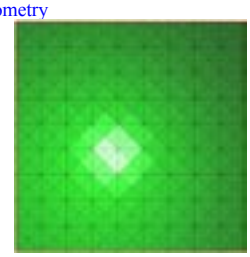

12

Example 2: Final geometry

- Metric embedding: trusted-region
- $\beta = 1.5435$

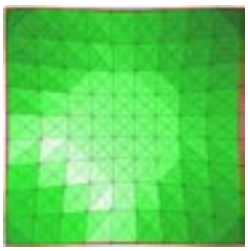

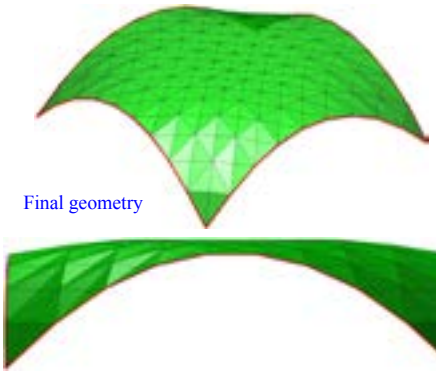

Final geometry

13

Example 2: Curvature

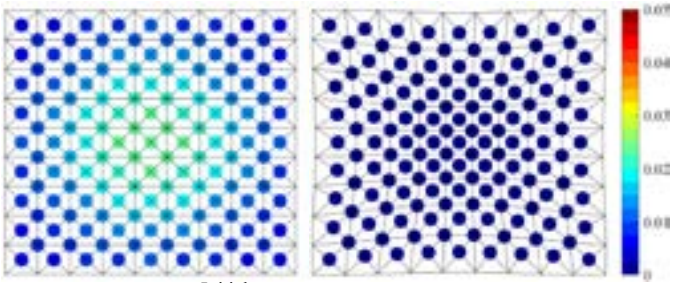

Initial

Final
Modified CP

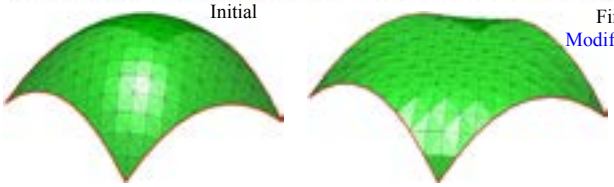

14

Example 2: Efficiency

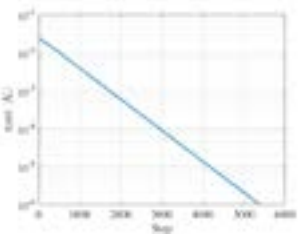

Ricci flow

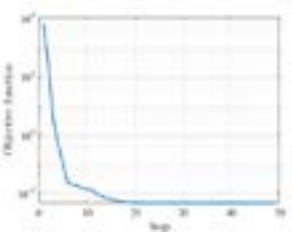

Geometry realization

15

Example 2: Developed

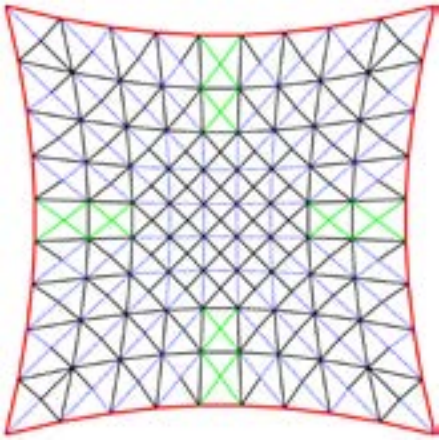

Mountain

Valley

16

Remarks

Current Study:

- An efficient tool for designing discrete architectural surfaces, that are globally developable and span the prescribed boundary
- A simple modified circle packing scheme has better performance in conformality than traditional Thurston's CP

Future Studies:

- The final geometry is not close enough to the initial (usually desired) one
  -> Divide the surface into several components
- Meshes of other shape
- Structural performance

17

Topic 2:
Discrete surface with user-defined Gaussian curvature using Ricci energy

Joint work with Prof. Kaji, Kyusyu Uni.

S. Kaji, J.Y. Zhang,
Finetuning discrete architectural surfaces by use of circle packing,
Journal of Asian Architecture and Building Engineering,
Vol. 23 (1), pp. 188-203, 2024.

Ricci Energy

Specified Gaussian curvature

Specified boundary

- Metric optimisation: Minimize Ricci energy

$$\sum_{i \in V_K} (K_i(\mathbf{u}) - \bar{K}_i)^2 + \lambda_e \sum_{e_{ij} \in E_{fix}} (l_{ij}(\mathbf{u})^2 - \bar{l}_{ij}^2)^2$$

- Embedding optimisation: Minimize coordinate errors

$$\sum_{e_{ij} \in E} (\|v_i - v_j\|^2 - \beta l_{ij}^2)^2 + \lambda_v \sum_{i \in V_{fix}} \|v_i - \bar{v}_i\|^2$$

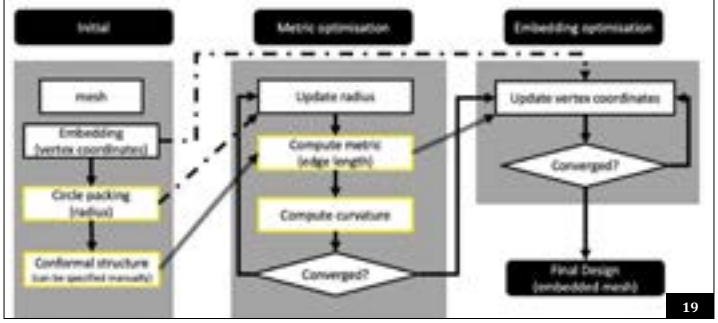

19

Example 2: Initial Settings

- Span: 30 m
- Height: 10 m

- 169 vertices: 42 boundary, 127 interior
- 462 edges
- 294 faces (triangles)

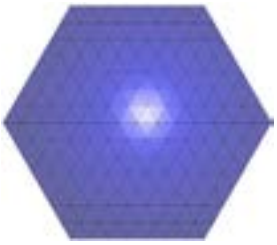

Initial geometry

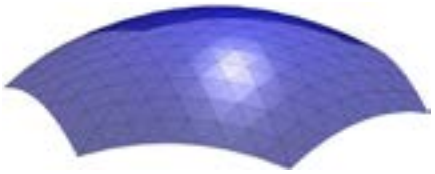

20

Example 2a: Final Geometry

- Discrete Ricci flow (Matlab): 19 sec
- Target Gaussian curvature for interior vertices
  - $\sum \bar{K}_i = 1.5$
  - $\bar{K}_i = \frac{1.5}{127} = 0.0118$

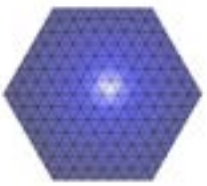

Final geometry

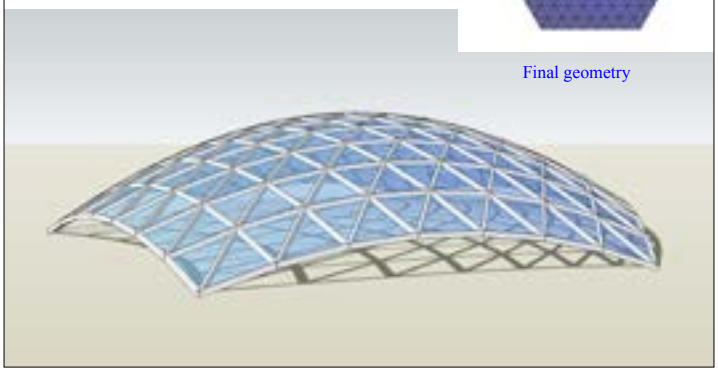

Example 2a: Gaussian Curvature

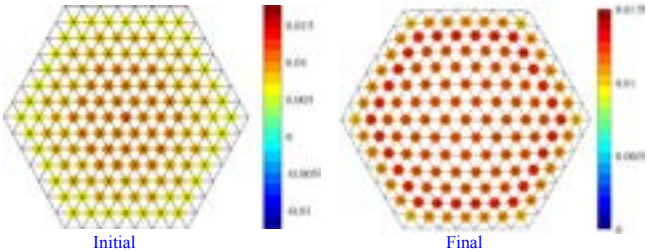

Initial Final

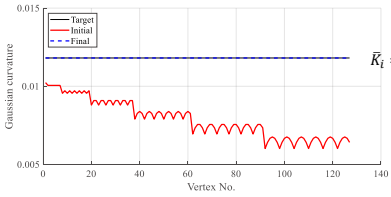

$$\bar{K}_i = \frac{1.5}{127} = 0.0118$$

22

Example 2b: Irregular triangle

- Span: 30 m
- Height: 10 m

- 169 vertices: 42 boundary, 127 interior
- 462 edges
- 294 faces (triangles)

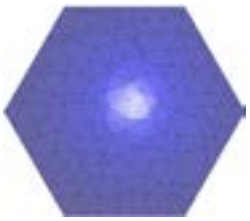

Initial geometry

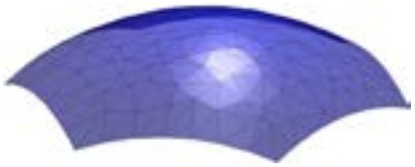

23

Ex2b: regular shape

- Target Gaussian curvature for interior vertices
  - $\sum \bar{K}_i = 1.5$
  - $\bar{K}_i = \frac{1.5}{127} = 0.0118$

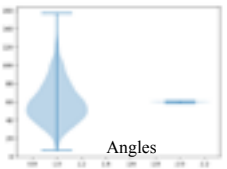

Angles

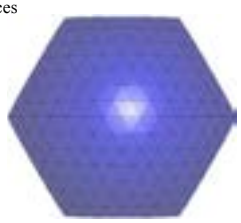

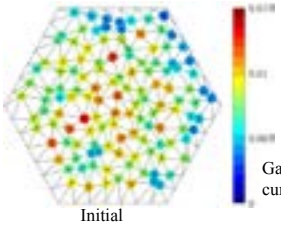

Gaussian curvature

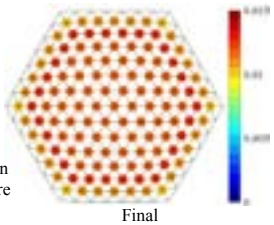

Initial Final

24

Example 3: Various curvature

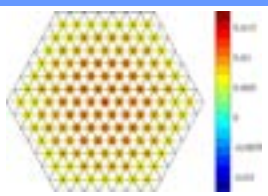

Initial curvature

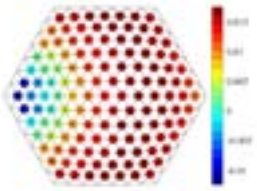

Final curvature

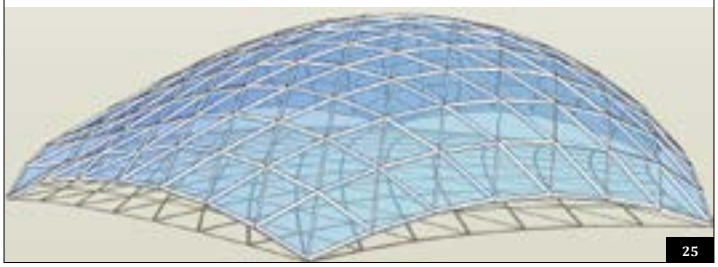

25

Ex4: amplifying curvature

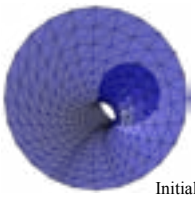

1.1 times of Gaussian curvature

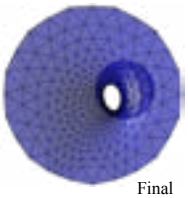

Initial

Final

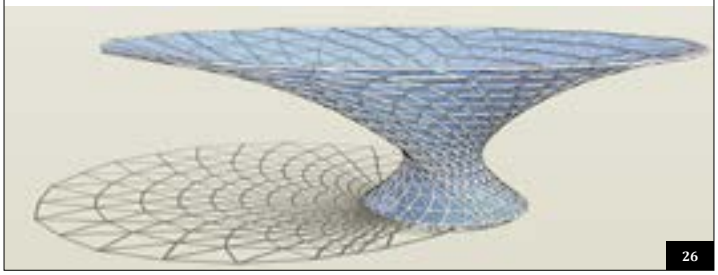

26

Topic 3:
Planar polygonal grid shell using tensegrity theory

J.Y. Zhang, M. Ohsaki,
A mechanical approach to generation of planar polygonal mesh for grid shells, under review

Existing studies

Continuous surface

Discretization

Target geometry

PQ mesh

Geometrical approach

- Circular net
- Chebyshev net
- Conjugate direction field
- Optimization
- …

Objective 1: Planar polygonal mesh
Objective 2: Approximate the target geometry

28

Current study

- Blender + Python
- https://github.com/martinsprojects/trussgen

Continuous surface

Discretization

Target geometry

Mechanical approach

Form-finding & Geometry correction

PQ mesh

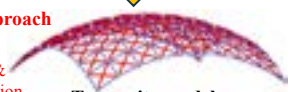

Tensegrity model

Tensegrity = **Tens**ional + Int**egrity**
(R.B. Fuller, 1975)

Tensegrity unit:
4 cables : Quad edges
2 struts : Auxiliary

29

Why tensegrity? (Example 1)

Self-equilibrium
⇒ **Co-planar + Stable**

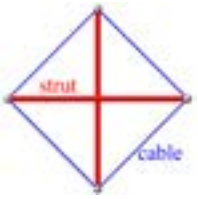

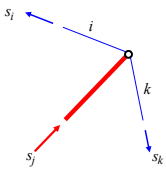

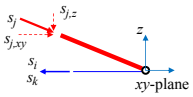

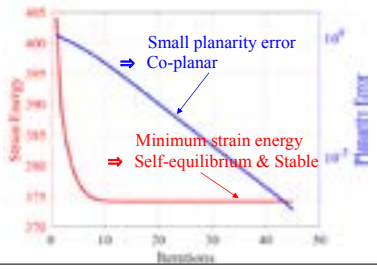

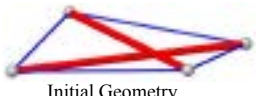

Initial Geometry

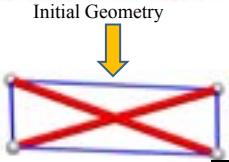

Final Geometry

30

Form-finding Methods

- Introduction to Tensegrity
- Applications
- Stability
- Form-finding (or Shape-finding)
  - Intuition Approaches
  - Analytical Approaches (using symmetry)
  - Numerical Approaches
    - Adaptive Force Density Method
    - Dynamic Relaxation Method
    - **Non-linear Analysis (NLA) Method**
    - Optimization Method

31

NLA for Unstable Structures

D: Equilibrium matrix
s: Prestress vector
f: Unbalanced force vector
K: Stiffness matrix
d: Nodal coordinates

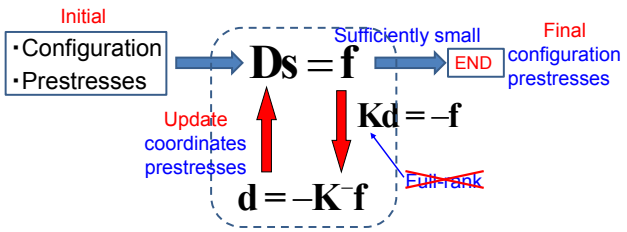

32

Tensegrity Tower by NLA

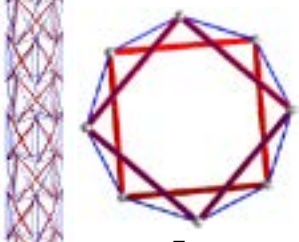

Top

Side

Initial

	Stiffness	Prestress
Struts	100	-1
Cables	10	1

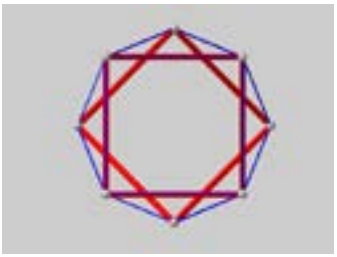

84 Iterations

33

Proposed Method

Objective 1: PQ mesh
Objective 2: Approx. the target geometry

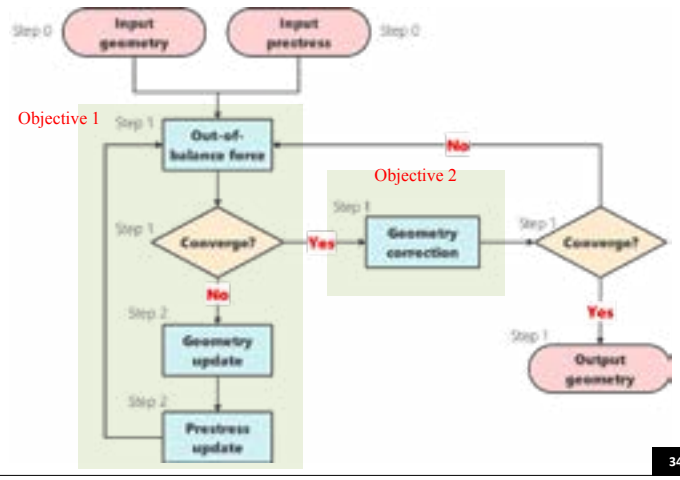

34

Self-equilibrium Equations

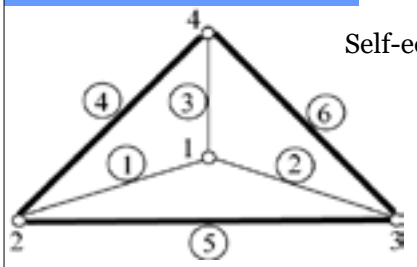

Self-equilibrium Equations:

$$\mathbf{Ex}=\mathbf{Ey}=\mathbf{Ez}=\mathbf{0}$$

E:	Force density matrix
x,**y**,**z**:	Nodal coordinates

Force Density $q_k = f_k / l_k$

$$\mathbf{E}=\begin{pmatrix} q_1+q_2+q_3 & -q_1 & -q_2 & -q_3 = 0 \\ & q_1+q_4+q_5 & -q_5 & -q_4 \\ & & q_2+q_5+q_6 & -q_6 \\ & \text{Sym.} & & q_3+q_4+q_6 \end{pmatrix}$$

35

Self-equilibrium Condition

➢ **Self-equilibrium condition**

$$\bigstar\ \mathbf{Ex}=\mathbf{0} \Rightarrow \mathbf{x},\mathbf{y},\mathbf{z}=\alpha_1\begin{pmatrix}1\\ \vdots \\ 1\end{pmatrix}+\sum_{i=2}^{h}\alpha_i\mathbf{P}_i$$

- $h >= 4$ ⇒ Three-dimensional

☆ **E** has four 0 eigenvalues	Self-equilibrium
☆ Other eigenvalues are positive	Super-stability

➢ **Geometry modification**

$$\mathbf{E}\bar{\mathbf{x}}_i = \mathbf{0} \qquad \mathbf{x} := \mathbf{x}+\sum_{i=1}^{n^E}\beta_i\bar{\mathbf{x}}_i = \mathbf{x}+\mathbf{B}\boldsymbol{\beta}_x$$

Null space

$$\mathbf{E}\left(\mathbf{x}+\sum_{i=1}^{n^E}\beta_i\bar{\mathbf{x}}_i\right) = \mathbf{Ex}+\sum_{i=1}^{n^E}\beta_i\mathbf{E}\bar{\mathbf{x}}_i = \mathbf{0}$$

Self-equilibrium NOT violated!!

36

Geometry Correction

$$\mathbf{x} + \mathbf{B}\boldsymbol{\beta}_x = \mathbf{x}_0$$ Target geometry

$$\boldsymbol{\beta}_x = \mathbf{B}^{+}(\mathbf{x}_0 - \mathbf{x})$$ Least squared solution

$$\mathbf{x} := \mathbf{x} + \sum_{i=1}^{n^E} \beta_i \bar{\mathbf{x}}_i = \mathbf{x} + \mathbf{B}\boldsymbol{\beta}_x$$

New geometry

Geometry correction

$$\mathbf{E}(\mathbf{x} + \sum_{i=1}^{n^E} \beta_i \bar{\mathbf{x}}_i) = \mathbf{E}\mathbf{x} + \sum_{i=1}^{n^E} \beta_i \mathbf{E}\bar{\mathbf{x}}_i = \mathbf{0}$$

37

Errors

- **Planarity error**
  - Distance to approximated tangent plane

$$\text{distance}(\mathbf{v}_{i,j}) = (\mathbf{v}_{i,j} - \mathbf{o}_i) \cdot \mathbf{n}_i$$

Center Normal

  - Sum squared distance

$$\varepsilon_i^q = -n_i(\mathbf{o}_i^\top \mathbf{n})^2 + \sum_{j=1}^{n_i} \mathbf{v}_{i,j}^\top (\mathbf{n}\mathbf{n}^\top)\mathbf{v}_{i,j}$$

  - Planarity error ((average distance)

$$\varepsilon^q = \frac{1}{n_q}\sqrt{\sum_{i=1}^{n_q} \varepsilon_i^q}$$

- **Geometry error**

$$\varepsilon^c = \frac{1}{3n}\sqrt{\|\hat{\mathbf{x}} - \mathbf{x}_0\|^2 + \|\hat{\mathbf{y}} - \mathbf{y}_0\|^2 + \|\hat{\mathbf{z}} - \mathbf{z}_0\|^2}$$

Final geometry Target geometry

38

Tensegrity Model

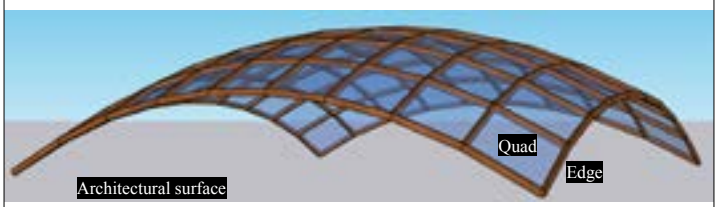

Form-finding
Find the **geometry** (& prestress)
at the state of **self-equilibrium**

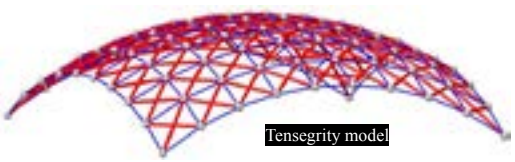

39

Example 2: Quad panels

- Span: 18.0 x 18.0 (m)
- Height: 4.9 (m)
- Nodes: 100 , quads: 81
- Cable stiffness: 10^5 N
- Strut stiffness: 10^3 N
- Strut prestress: -100N
- Computational time: 0.19 sec

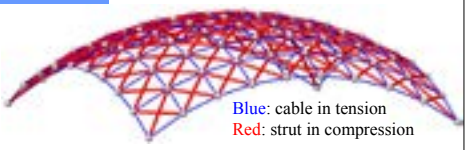

Blue: cable in tension
Red: strut in compression

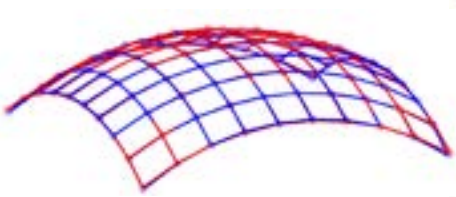

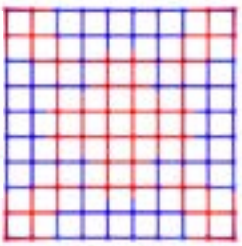

Blue: initial geometry
Red: final geometry

40

Example 2

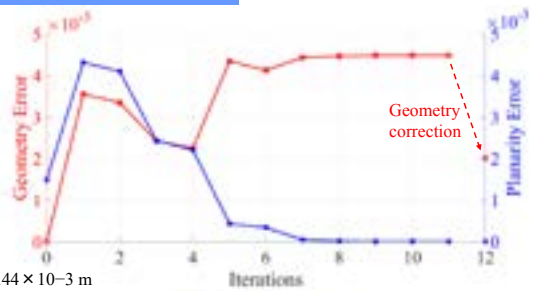

Geometry: 4.44 × 10−3 m
Planarity error: 5.21 × 10−6 m

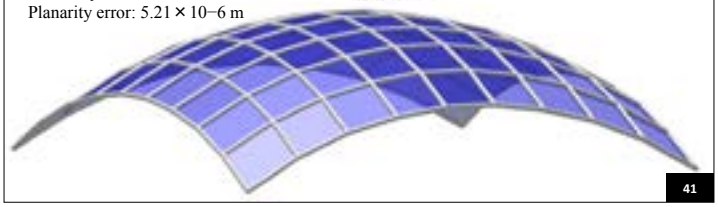

41

Example 3: Hexagonal panels

- Span: 29.9 x 26.0 (m)
- Height: 6.8 (m)
- Nodes: 126 , hexagons: 43
- Cable stiffness: 10^5 N
- Strut stiffness: 10^3 N
- Strut prestress: -100N
- Computational time: 0.42 sec

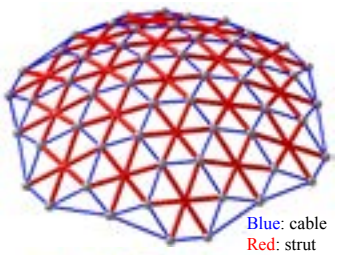

Blue: cable
Red: strut

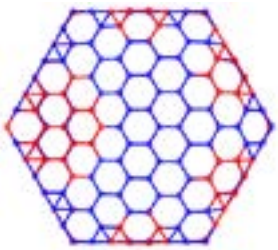

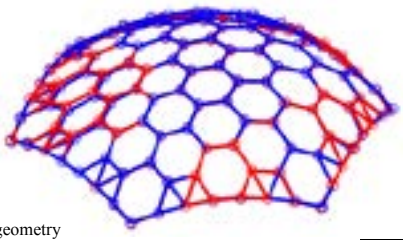

Blue: initial geometry
Red: final geometry

42

Example 3

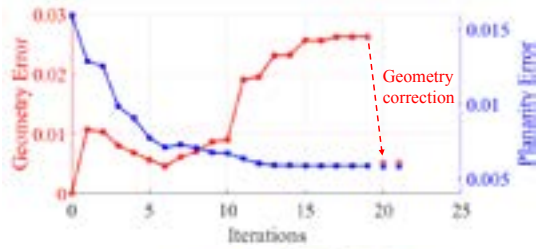

Geometry: 0.0051 m
Planarity error: 0.0058 m

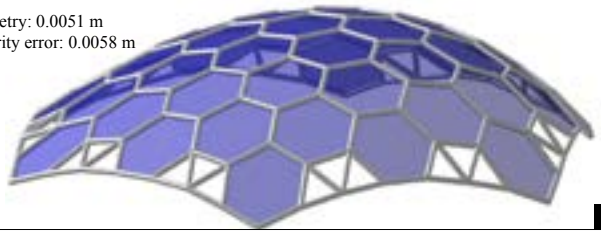

43

Example 4: Hybrid panels

- Span: 24.6 x 19.4 (m)
- Height: 5.8 (m)
- Nodes: 160,
- Octagons: 32, Quads: 31
- Cable stiffness: 10^5 N
- Strut stiffness: 10^3 N
- Strut prestress: -100N
- Computational time: 1.3 sec

Blue: cable
Red: strut

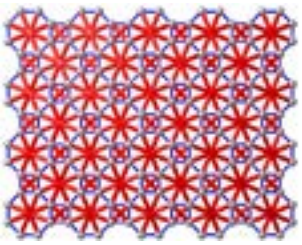

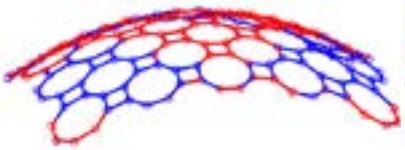

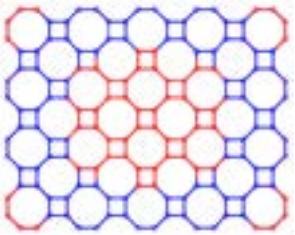

Blue: initial geometry
Red: final geometry

44

Example 4

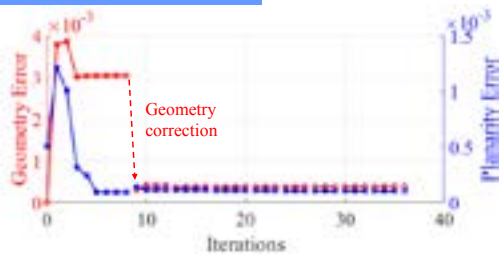

Geometry: 3.80 × 10−4 m
Planarity error: 1.02 × 10−4 m

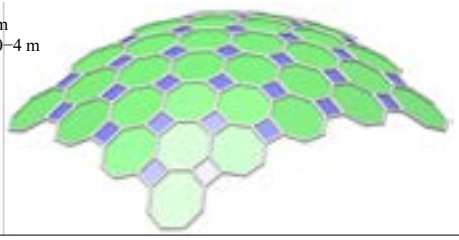

45

Tessellation as a design principle for mechanical metamaterials

Yusuke Sakai
Sony Computer Science Laboratories

Abstract

Tessellation, a geometric pattern filling a plane without any gaps or overlaps, serves as a powerful tool for designing mechanical metamaterials. Mechanical metamaterials are artificial structures engineered for unique and tunable mechanical characteristics. In this talk, we introduce how simple polygonal tessellations can define the internal units of metamaterials, allowing tailorable mechanical responses through geometric design. By adjusting geometric configurations, we demonstrate intuitive tunability in deformation behaviors, leading to applications in transformable curved surfaces and tubular structures with unique mechanical behavior. Designing tessellation offers a systematic design scheme for adaptive and programmable structures, expanding possibilities for applications in aesthetic architectural roofs and mechanical devices.

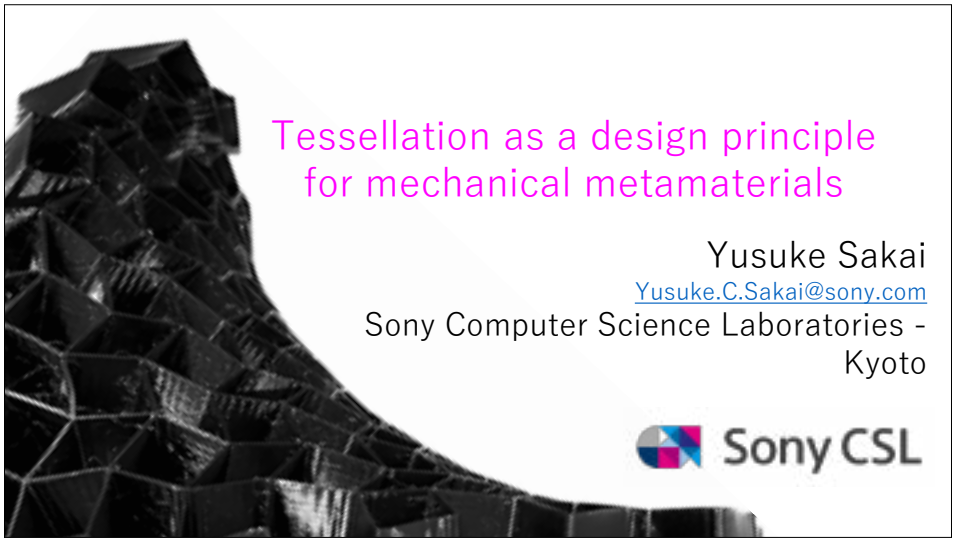

Tessellation as a design principle for mechanical metamaterials

Yusuke Sakai
Yusuke.C.Sakai@sony.com
Sony Computer Science Laboratories - Kyoto

Sony CSL

Tessellation

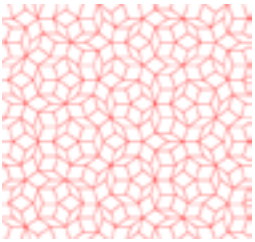

Penrose Tiling

https://www.alhambradegranada.org/ja/info/galeriadefotosalhambra/azulejosalhambra.asp

Metamorphosis III by M.C. Escher, 1968

2

Aperiodic ‘hat’ monotile

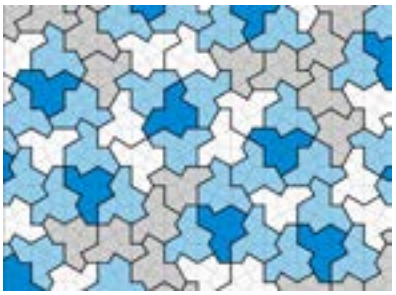

https://cs.uwaterloo.ca/~csk/hat/

[Smith *et al.*, 2023]

[Clarke *et al.*, 2023]

3

Mechanical Metamaterials

Negative Poisson's ratio
[Alderson and Alderson, 2007]

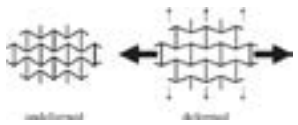

Torsion-compression metamaterial
[Frenzel *et al.*, 2017]

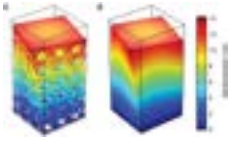

Pentamode metamaterial
[Kadic *et al.*, 2012]

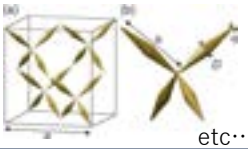

etc…

Energy absorber
[Lee *et al.*, 2019]

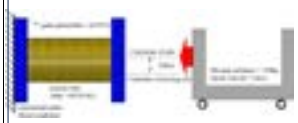

Wave guide system
[Bordiga *et al.*, 2024]

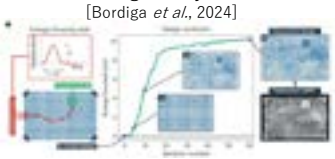

Mechanical cloaking
[Zhang et al., 2015]

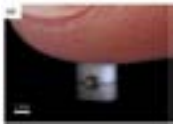

Exotic mechanical properties for enhanced applications

4

From 2D to 3D

Carl Friedrich Gauss
(1777-1855)

Parametric Wood: Image (wordpress.com)

"Morphing a thin plate into a programmed shape is a challenging problem, as highlighted by Gauss…"
[Siéfert *et al.*, Nature Materials, **18**:2019.]

?

Quadrilateral

Other tessellations

5

From tessellation to mechanical metamaterials

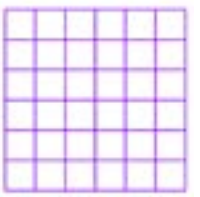

[Sakai, 2024]

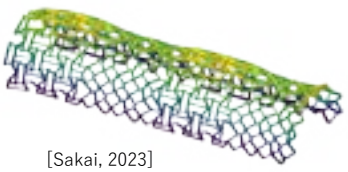

[Sakai, 2023]

6

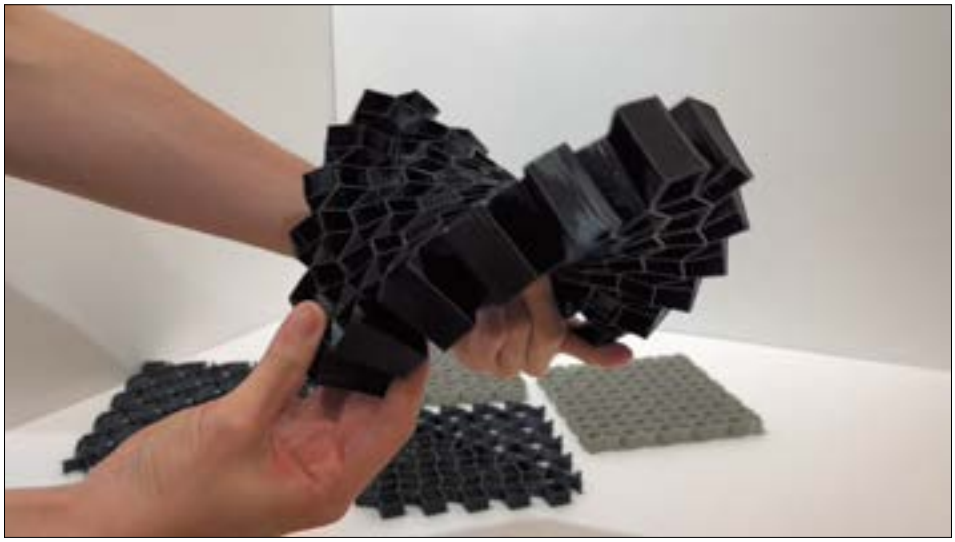

Geometrical Representation

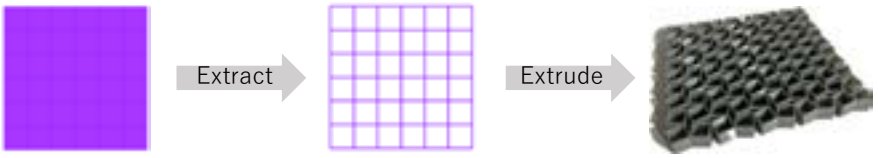

Rotating quadrilateral　　Edges　　Initial flat grid

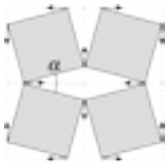

$0^\circ \le \alpha < 180^\circ$

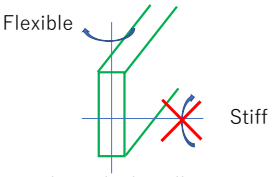

Thin & high wall member

8

Eigenvalue estimates soft and stiff modes

$$\mathbf{K}\,\mathbf{v}_i = \lambda_i \mathbf{M}\,\mathbf{v}_i$$

Stiffness matrix: $\mathbf{K}$
Mass matrix: $\mathbf{M}$
Eigenvalue: λ_i
Eigenvector: $\mathbf{v}_i$

Free boundary constraints

Lanczos method,
(Abaqus Ver. 2022)

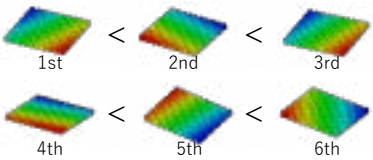

Rigid body mode
(zero-energy mode)

$\lambda \simeq 0$

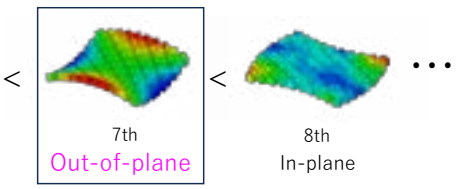

Elastic mode

9

Soft yet stiff

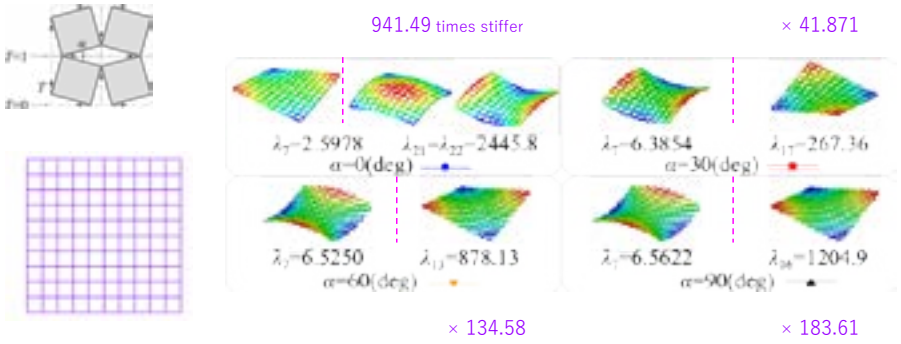

Larger eigenvalue ratio ⇒ Better deformability

10

From tessellation to mechanical metamaterials

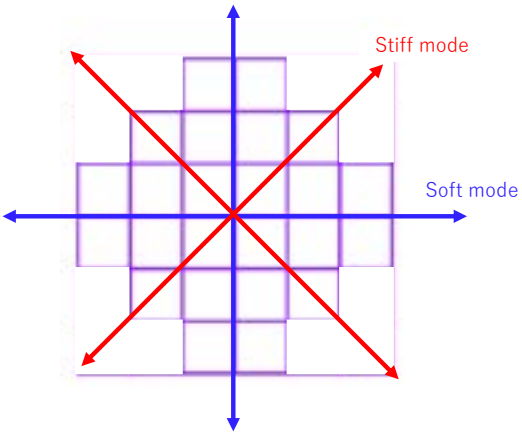

11

New fidget toy?

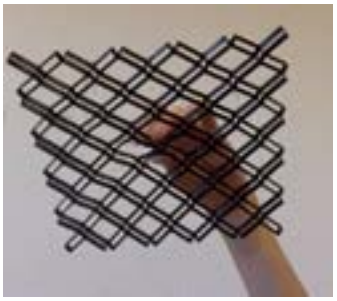

“ぷるぷる (Purupuru)” structures

12

Surface Zoo: Large-deformation analysis

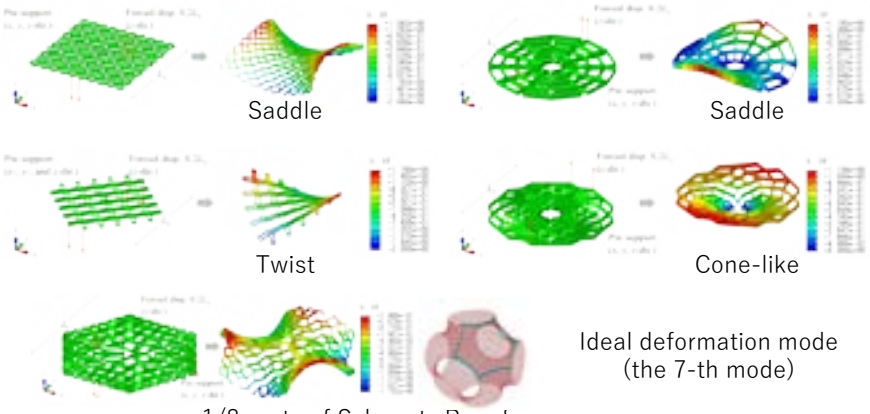

1/8 parts of Schwartz P surface

Ideal deformation mode
(the 7-th mode)

13

Diagonals produce positive Gaussian curvature

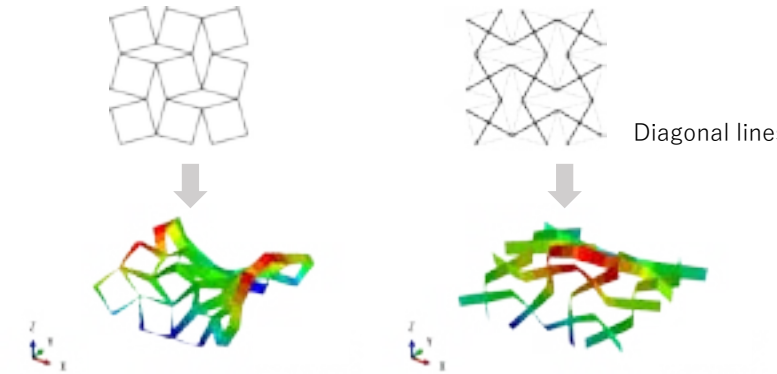

Negative Gaussian curvature

Positive Gaussian curvature

14

Surface Zoo: Hybrid grid pattern

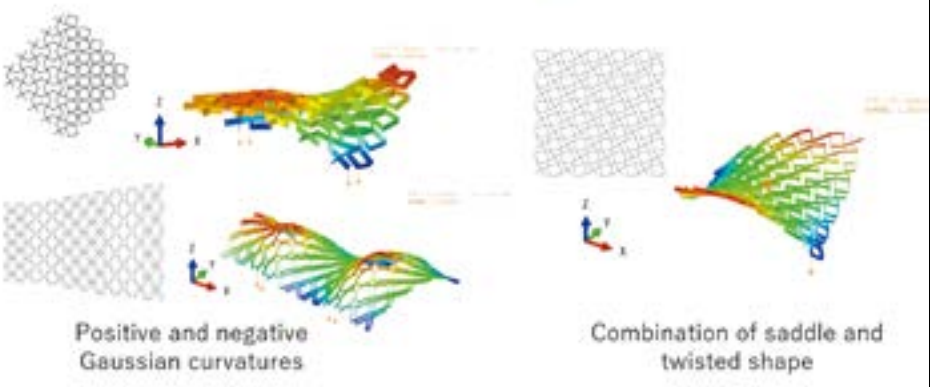

Positive and negative
Gaussian curvatures

Combination of saddle and
twisted shape

Experimental validation

Initial flat grid

Thermoplastic Polyurethane
(Young's modulus 35MPa,
Poisson's ratio 0.4)

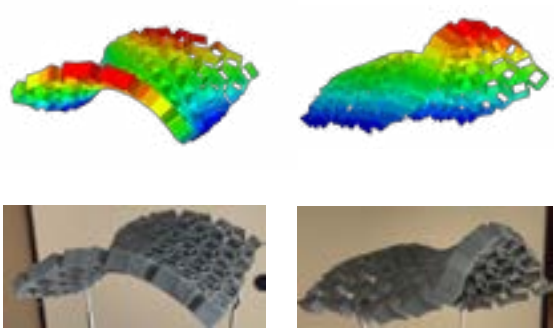

16

Rotating quadrilateral

回転四辺形メタマテリアル

Rotating quadrilateral　Edges　Initial flat grid

特徴
・ヒンジ等の機構を使わずに意図した局面にのみ変形する構造
Without resorting to adding hinge-joints, our target curved surfaces can be obtained under appropriate force distributions.
・硬さと柔らかさの共存する構造で振動の制御にも応用可能
A structure that combines hardness and softness, which can also be applied to vibration control.

From tessellation to mechanical metamaterials

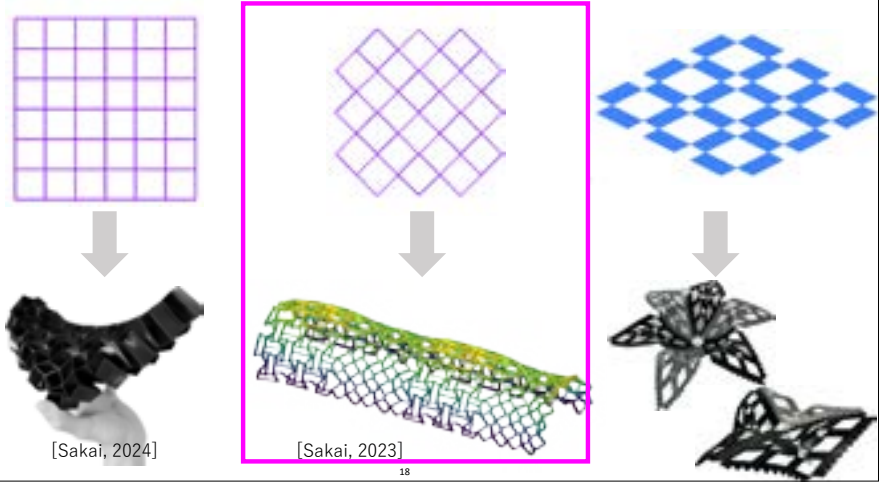

[Sakai, 2024]　[Sakai, 2023]

18

Poisson's ratio and Gaussian curvature

Poisson's ratio $\nu = -\dfrac{\varepsilon_2}{\varepsilon_1}$ $\varepsilon = \left(L_{\text{ini}} - L_{\text{def}}\right) \Big/ L_{\text{ini}}$: Strain

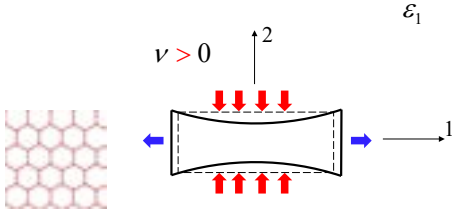

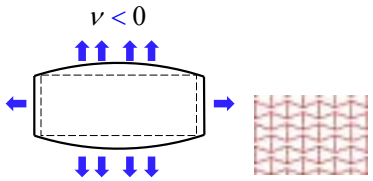

19

3D pentagonal grid

Discrete Gaussian curvature

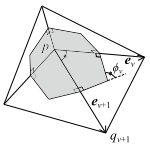

$$K_p = 2\pi - \sum_{v=1}^{4} \phi_v$$

$$= 2\pi - \sum_{v=1}^{4} \cos^{-1}\left(\frac{\boldsymbol{e}_v \cdot \boldsymbol{e}_{v+1}}{|\boldsymbol{e}_v| \cdot |\boldsymbol{e}_{v+1}|}\right)$$

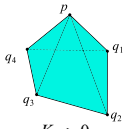

$K_p > 0$

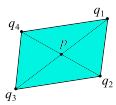

$K_p = 0$

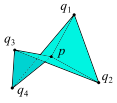

$K_p < 0$

Angle defect

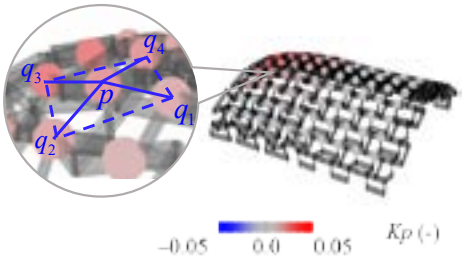

On 4-valent vertices

21

Thickness & discrete Gaussian curvature

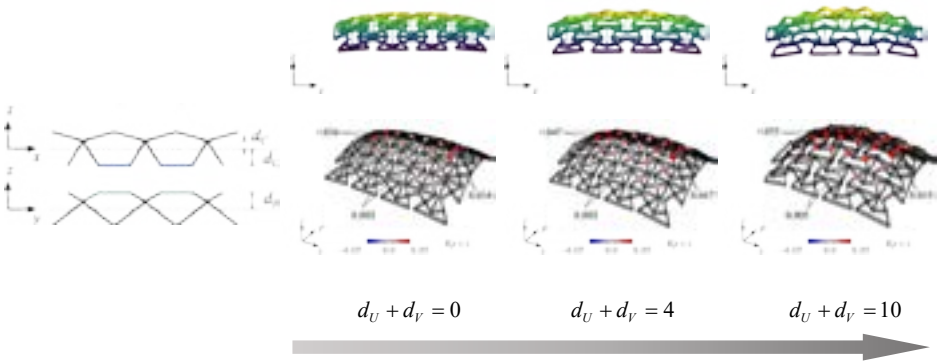

$d_U + d_V = 0$ $d_U + d_V = 4$ $d_U + d_V = 10$

Larger thickness → Larger absolute value of discrete Gaussian curvature

22

Member profile & discrete Gaussian curvatures

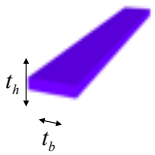

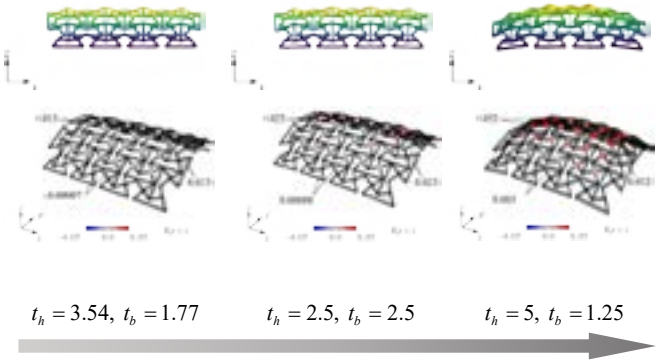

$t_h = 3.54,\ t_b = 1.77$ $t_h = 2.5,\ t_b = 2.5$ $t_h = 5,\ t_b = 1.25$

Thin & high wall member → Larger absolute value of discrete Gaussian curvature

23

Convexity & Concavity → Function

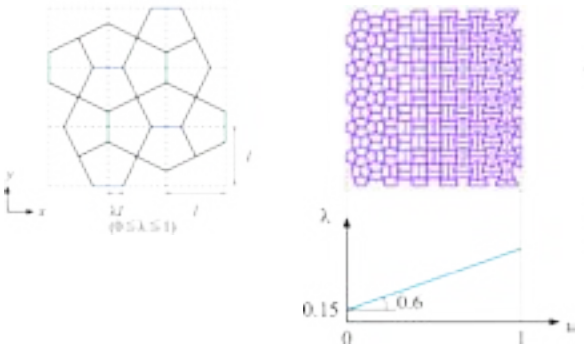

24

Convexity & Concavity → Function

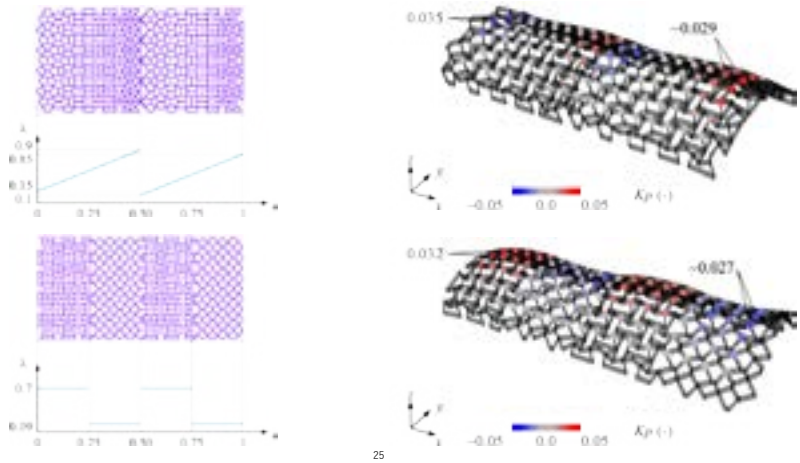

25

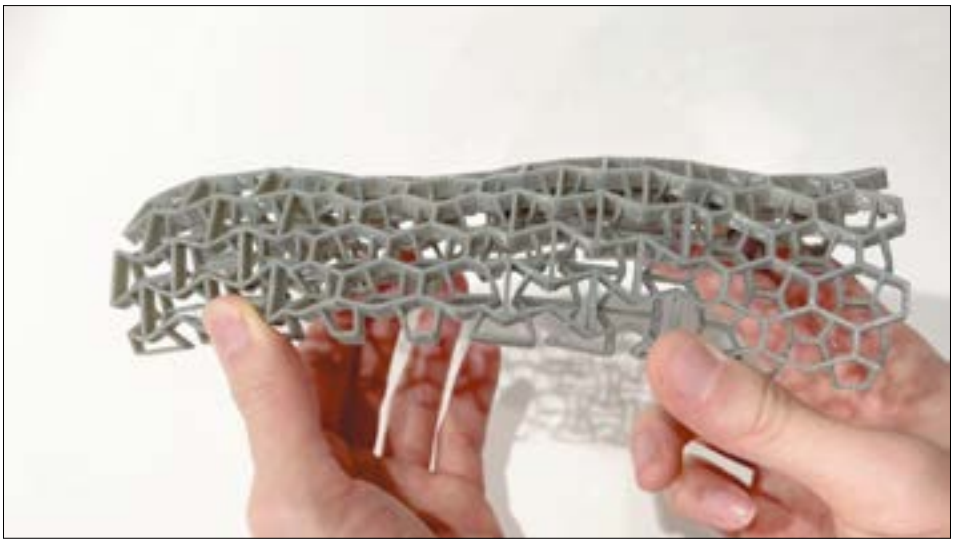

From tessellation to mechanical metamaterials

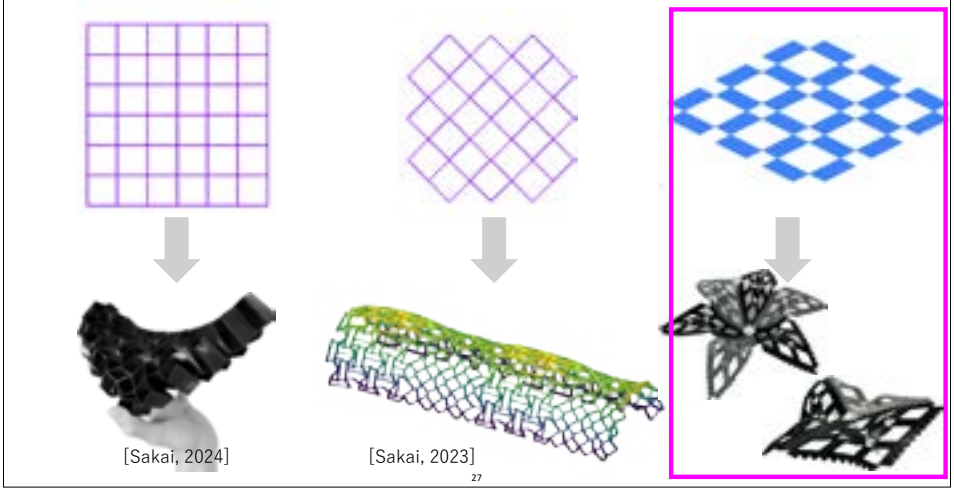

27

Rhombic sheet

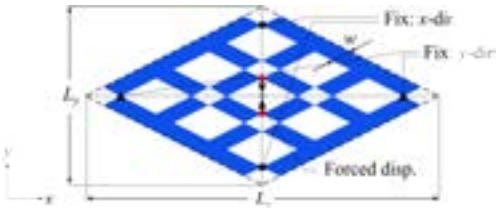

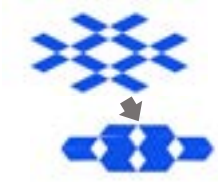

RotQuad tessellation
In-plane deformation

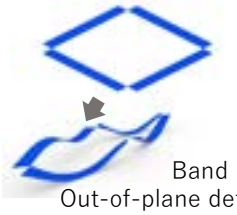

Band
Out-of-plane deformation

28

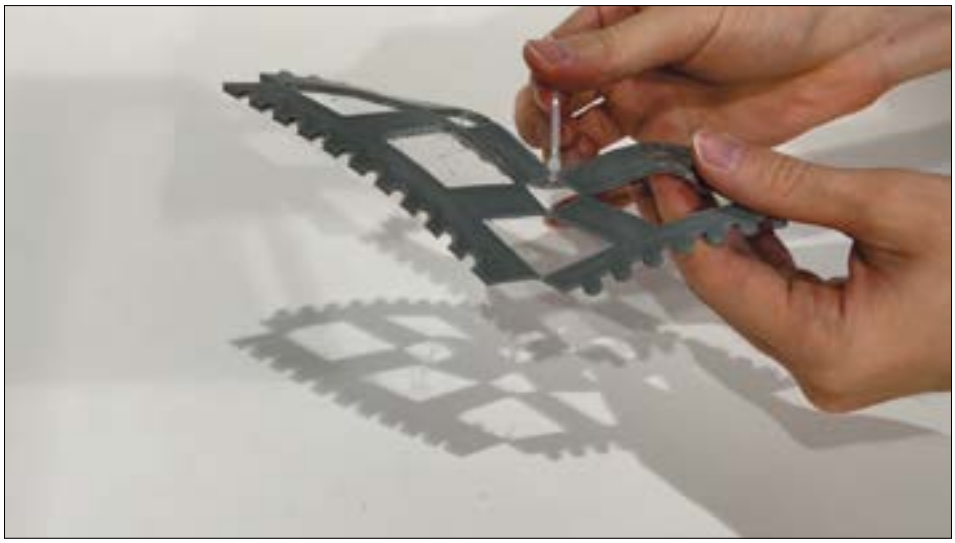

Simulation setting

thickness t
Young's modulus E

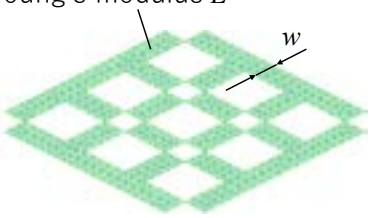

Mesh generation
[Combine & Clean] → [TriRemesh]

In-plane stiffness: Ewt
[EdgeLengths]

Out-of-plane stiffness: $Ewt^3/12$
[Hinge]

Kangaroo2
(Dynamic Relaxation)

30

Comparison

Numerical Simulation

Physical Model

31

Multistability

Snap-through

32

Connection system

Attach & Detach

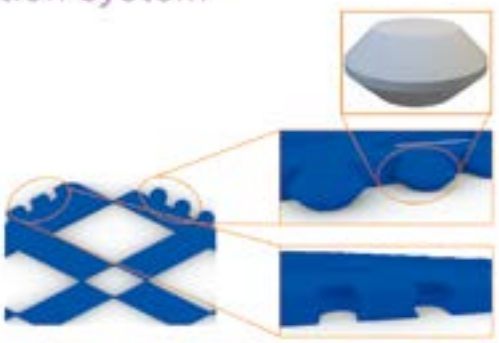

3D Printable without any support parts

33

Surface zoo

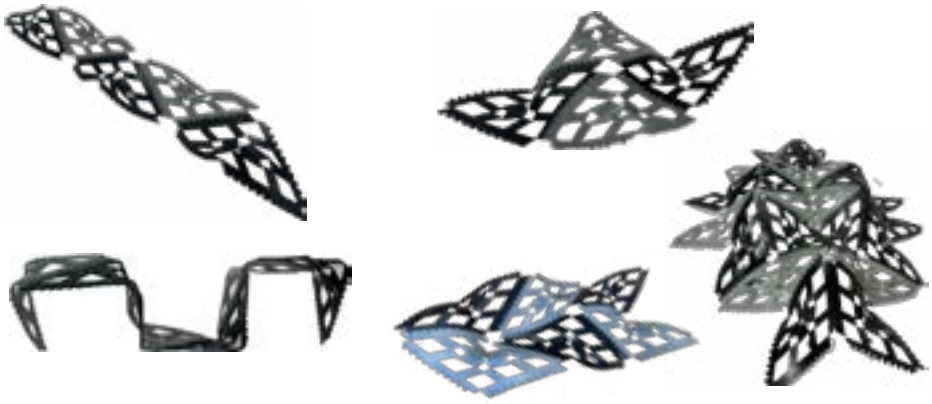

34

Surface zoo

Gaussian curvature
> 0

Gaussian curvature
< 0

Monster with two arms

35

CAADRIA2025 in Univ. Tokyo

Display 25-28th, March

All you need is rotation: Construction of developable strips – Part 1 Theory

Takashi Maekawa
Waseda University

Felix Scholz
Johannes Kepler University

Abstract

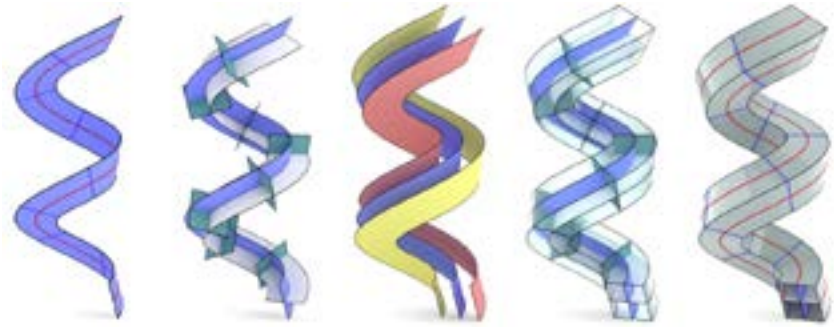

We present a novel method for generating developable strips along a space curve, offering flexible design. Central to this approach is the rotation angle, which governs the relationship between the Frenet frame of the input space curve and the Darboux frame of the curve on the resulting developable strip [1]. By treating this angle as a free design parameter, represented by any differentiable function along the curve, our method enables the creation of diverse developable geometries. This generalization significantly expands the design space, allowing for developable strips that share a common directrix curve. The rotation angle can be specified in various forms, such as constants, linear variations, sinusoidal patterns, or solutions to initial value problems defined by ordinary differential equations. By introducing this versatile framework, we advance the theoretical understanding of developable surface design, providing a powerful toolset for exploring and manipulating developable geometries with exceptional flexibility.

References

[1] T. Maekawa and Felix Scholz, “All you need is rotation: Construction of developable strips”, ACM Transactions on Graphics, vol. 43, no. 6, 2024.

All you need is rotation: Construction of developable strips – Part 1 Theory

Takashi Maekawa
Waseda University

Felix Scholz
Johannes Kepler University

Motivation 1

Ease of designing developable strips

We generate developable strips along a given space curve by designing a suitable **rotation angle** between the Frenet and Darboux frames.

$\varphi(t) = -0.06\,t + \frac{\pi}{6}$ along a helix

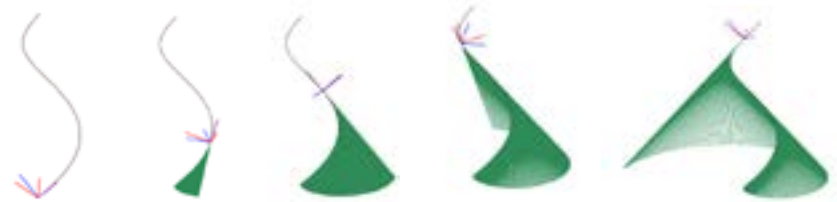

t = 0 t = $\frac{\pi}{2}$ t = π t = $\frac{3\pi}{2}$ t = 2π

Motivation 2

Ease of fabrication for various applications

Design

Flatten

Cut

Fabricate by bending

ED3GE 3-10-2025

Frenet-Serret formula

- Motion of the moving Frenet frame **c**(s)
  Arc-length parametrized curve **c**(s)

$$\begin{bmatrix} \mathbf{t}' \\ \mathbf{n}' \\ \mathbf{b}' \end{bmatrix} = \begin{bmatrix} 0 & \kappa(s) & 0 \\ -\kappa(s) & 0 & \tau(s) \\ 0 & -\tau(s) & 0 \end{bmatrix} \begin{bmatrix} \mathbf{t} \\ \mathbf{n} \\ \mathbf{b} \end{bmatrix}$$

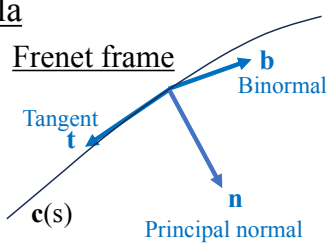

- Arbitrarily parametrized curve **c**(t)

$$\begin{bmatrix} \dot{\mathbf{t}} \\ \dot{\mathbf{n}} \\ \dot{\mathbf{b}} \end{bmatrix} = \Lambda(t) \begin{bmatrix} 0 & \kappa(t) & 0 \\ -\kappa(t) & 0 & \tau(t) \\ 0 & -\tau(t) & 0 \end{bmatrix} \begin{bmatrix} \mathbf{t} \\ \mathbf{n} \\ \mathbf{b} \end{bmatrix}$$

$\dot{\boldsymbol{c}}(t) = \Lambda(t)\, \mathbf{c}'(s)$

↑ Parametric speed

ED3GE 3-10-2025

Motion of Darboux frame

- Arc-length parametrized curve **c**(s)

$$\begin{bmatrix} \mathbf{t}' \\ \mathbf{B}' \\ \mathbf{N}' \end{bmatrix} = \begin{bmatrix} 0 & \kappa_g(s) & \kappa_n(s) \\ -\kappa_g(s) & 0 & \tau_g(s) \\ -\kappa_n(s) & -\tau_g(s) & 0 \end{bmatrix} \begin{bmatrix} \mathbf{t} \\ \mathbf{B} \\ \mathbf{N} \end{bmatrix} \quad (1)$$

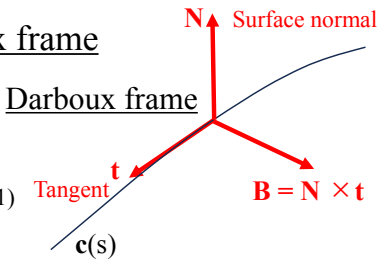

- Arbitrarily parametrized curve **c**(t)

$$\begin{bmatrix} \dot{\mathbf{t}} \\ \dot{\mathbf{B}} \\ \dot{\mathbf{N}} \end{bmatrix} = \Lambda(t) \begin{bmatrix} 0 & \kappa_g(t) & \kappa_n(t) \\ -\kappa_g(t) & 0 & \tau_g(t) \\ -\kappa_n(t) & -\tau_g(t) & 0 \end{bmatrix} \begin{bmatrix} \mathbf{t} \\ \mathbf{B} \\ \mathbf{N} \end{bmatrix}$$

$\dot{\boldsymbol{c}}(t) = \Lambda(t)\, \mathbf{c}'(s)$

↑ Parametric speed

ED3GE 3-10-2025

Rotation angle φ

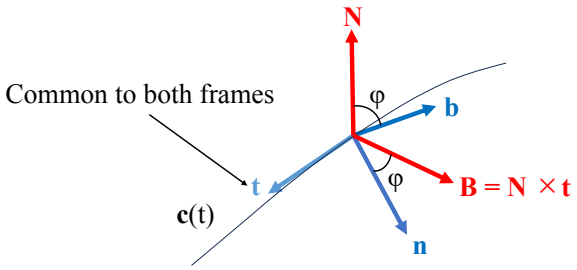

Darboux frame t-B-N

$$\begin{bmatrix} \mathbf{t} \\ \mathbf{B} \\ \mathbf{N} \end{bmatrix} = \begin{bmatrix} 1 & 0 & 0 \\ 0 & \cos\varphi & \sin\varphi \\ 0 & -\sin\varphi & \cos\varphi \end{bmatrix} \begin{bmatrix} \mathbf{t} \\ \mathbf{n} \\ \mathbf{b} \end{bmatrix}$$

Frenet frame t-n-b (2)

κ_n κ_g τ_g in terms of φ

- Plug (2) into (1)

$$\begin{aligned} \mathbf{B}' &= -\kappa_g \mathbf{t} - \tau_g \sin\varphi\, \mathbf{n} + \tau_g \cos\varphi\, \mathbf{b} \\ \mathbf{N}' &= -\kappa_n \mathbf{t} - \tau_g \cos\varphi\, \mathbf{n} - \tau_g \sin\varphi\, \mathbf{b} \end{aligned}$$

- Differentiate the second and third equations of (2)

$$\begin{aligned} \mathbf{B}' &= -\kappa\cos\varphi\, \mathbf{t} - \sin\varphi \left(\tau + \frac{d\varphi}{ds}\right)\mathbf{n} + \cos\varphi \left(\tau + \frac{d\varphi}{ds}\right)\mathbf{b} \\ \mathbf{N}' &= \kappa\sin\varphi\, \mathbf{t} - \cos\varphi \left(\tau + \frac{d\varphi}{ds}\right)\mathbf{n} - \sin\varphi \left(\tau + \frac{d\varphi}{ds}\right)\mathbf{b} \end{aligned}$$

- By comparing B' and N' we get

$$\kappa_n = -\kappa\sin\varphi \qquad \kappa_g = \kappa\cos\varphi \qquad \tau_g = \tau + \frac{d\varphi}{ds}$$

Key idea

The Darboux frame generally exists only if there's a surface containing the curve.

However, in this research, we take a **reverse** approach.

We first define the **rotation angle φ independently of the surface**.

Then construct the developable surface based on this rotation.

Unit ruling direction vector **d**

Do Carmo 76
Developable surface: The envelope of the family of tangent planes along a curve

$$\mathbf{d} = \frac{\mathbf{N} \times \dot{\mathbf{N}}}{|\dot{\mathbf{N}}|} = \frac{\tau_g \mathbf{t} - \kappa_n \mathbf{B}}{\sqrt{\tau_g^2 + \kappa_n^2}}$$

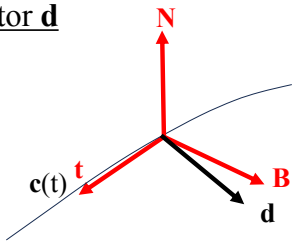

$$\tau_g = \tau + \frac{d\varphi}{ds} \qquad \kappa_n = -\kappa \sin\varphi \qquad \mathbf{B} = \cos\varphi\ \mathbf{n} + \sin\varphi\ \mathbf{b}$$

$$\mathbf{d} = \frac{(\tau + \frac{d\varphi}{ds})\mathbf{t} + \kappa \sin(\varphi)\cos(\varphi)\mathbf{n} + \kappa \sin^2(\varphi)\mathbf{b}}{\sqrt{(\tau + \frac{d\varphi}{ds})^2 + \kappa^2 \sin^2(\varphi)}}$$

B-spline representation

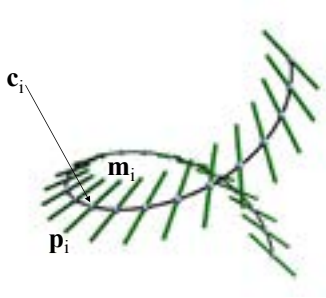

We fit B-spline curves to $\mathbf{p}_i$ and $\mathbf{m}_i$ based on the parametrization of $\mathbf{c}_i$

By linearly interpolating these curves, we generate B-spline developable strip

Rulings become isoparametric lines

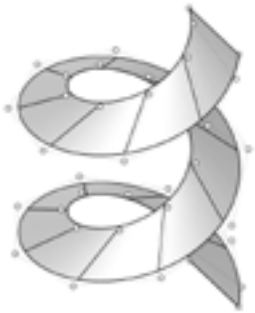

Flattening of developable strips

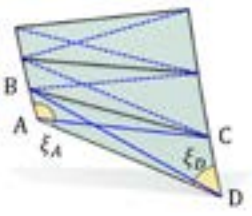

Split the quad ABCD into two triangles ABD and ACD

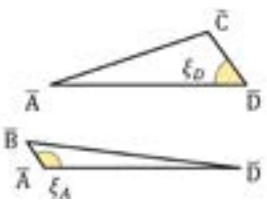

AB, AD, CD
ξ_A, ξ_D are preserved

$\bar{B}$ and $\bar{C}$ are transformed to global coordinates

Well-known rotation angles

Tangential developable (along helix)
$\varphi(t) = 0$

Rectifying developable (along helix)
$\varphi(t) = \frac{\pi}{2}$

Envelope of the family of tangent planes (along a helical curve on torus)
$\varphi(t) = \cos^{-1}(\mathbf{b}\cdot\mathbf{N})$

New rotation angles φ(t)

- $\varphi(t) = q$ (constant)
- $\varphi(t) = pt + q$ (linear function)
- $\varphi(t) = p\sin(\omega t) + q$ (sinusoidal function)
- $\frac{d\varphi(t)}{dt} = f(\varphi)$ (solution to an ordinary differential equation)

φ(t) = q (constant)

$\varphi(t) = \frac{\pi}{4}$ along a cubic Bézier curve

Perspective view

Right view

$\varphi(t) = \frac{\pi}{6}$ along a helix

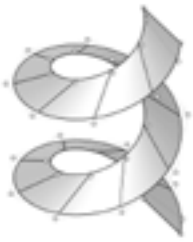

Perspective view

Front view

φ(t) = pt + q (linear function)

φ(t) = -0.06t + q along a helix

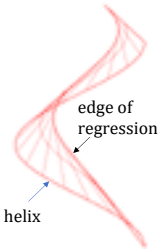

$q = \frac{\pi}{4}(45^\circ)$

$q = \frac{10\pi}{36}(50^\circ)$

$q = \frac{11\pi}{36}(55^\circ)$

$q = \frac{\pi}{3}(60^\circ)$

Edge of regression

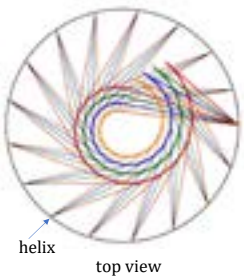

top view

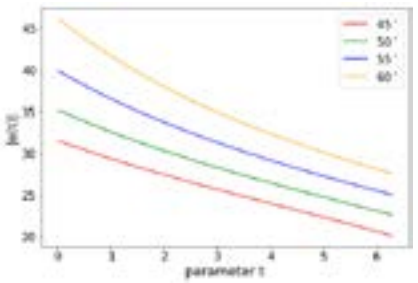

φ(t) = psin(ωt) + q
(sinusoidal function)

Suitable for closed loop strips

Toroidal blade along an ellipse: $\varphi(t) = 0.8\cos(t) + \frac{\pi}{2}$

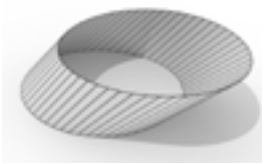

Ribonization

Approximate a surface using multiple developable strips (torus ω=3)

$\mathbf{c}(t) = ((R + r\cos(\omega t))\cos t, (R + r\cos(\omega t))\sin t, r\sin(\omega t))$

$\varphi(t) = cos^{-1}(\mathbf{b} \cdot \mathbf{N})$
Conventional method

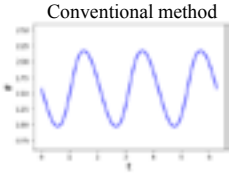

$\varphi(t) = psin(\omega t) - q$

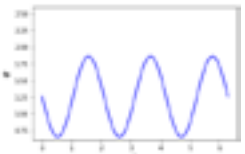

$\varphi(t) = psin(\omega t) + q$

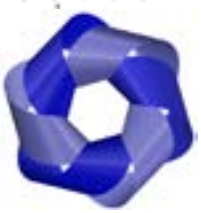

$\frac{d\varphi(t)}{dt} = f(\varphi)$ (solution of o.d.e.)

$$\mathbf{t} \cdot \mathbf{d} = \frac{(\tau + \frac{d\varphi}{ds})}{\sqrt{(\tau + \frac{d\varphi}{ds})^2 + \kappa^2 \sin^2(\varphi)}} = \cos(\theta) = constant$$

$$\frac{d\varphi}{ds} = \pm\frac{\kappa \sin(\varphi)}{\tan(\theta)} - \tau$$

$\theta = \frac{\pi}{6}$

$\theta = \frac{\pi}{4}$

$\theta = \frac{\pi}{3}$

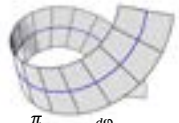

$\theta = \frac{\pi}{2}$, $\tau + \frac{d\varphi}{ds} = \tau_g = 0$
Rotation minimizing frame

Rotation minimizing frame (RMF)

$\theta = \frac{\pi}{2}$

$\tau_g = \tau + \frac{d\varphi}{ds} = \cos\frac{\pi}{2} = 0$

ODE reduces to integration problem $\varphi(t) = -\int_{t_0}^{t} \Lambda\tau(t)dt + \varphi_0$

Log-aesthetic curve
$\varphi_0 = 0$

Log-aesthetic curve
$\varphi_0 = \frac{\pi}{2}$

Orthogonal to each other

Differential geometry of developable strips

Gaussian curvature $K = \frac{LN - M^2}{EG - F^2} = 0$ as $N = M = 0$

Principal curvatures $\kappa_{max} = H + |H|$ $\kappa_{min} = H - |H|$

$H > 0$	$\kappa_{max} = 2H$	$\kappa_{min} = 0$ (ruling)
$H = 0$	$\kappa_{max} = 0$	$\kappa_{min} = 0$
$H < 0$	$\kappa_{max} = 0$ (ruling)	$\kappa_{min} = 2H$

Offsets of developable strip

$$\hat{K} = \frac{K}{1+2Hd+Kd^2}$$

$\hat{K}$: Gaussian curvature of offset surface
K: Gaussian curvature of developable strip
H: Mean curvature of developable strip
d: offset distance

The offset surface of a developable surface is also a developable surface

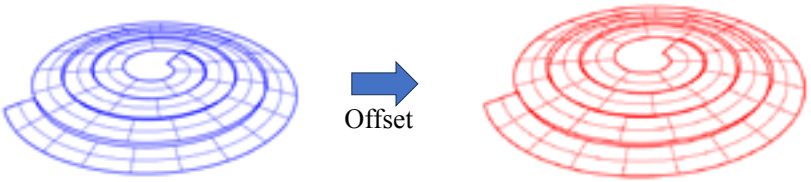

Triply Orthogonal Structure (TOR)

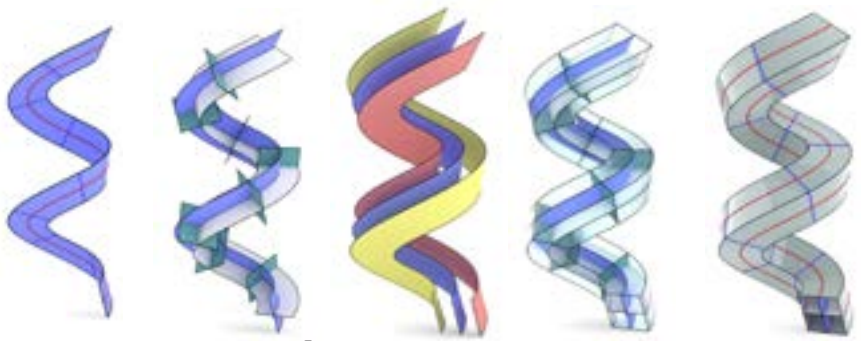

RMF along helix with $\varphi_0 = 0$

RMF with $\varphi_0 = \frac{\pi}{2}$ + square plates

Offsets of blue strip

Offsets of blue and silver strips are added

Triply orthogonal structure

Summary & Conclusions

- This work introduced a method for constructing developable strips along space curves by designing the rotation angle φ as a free design parameter.

  The angle φ defines the relationship between the Frenet frame of the input curve and the Darboux frame of the curve on the resulting developable strip.

- The approach has broad applicability, including in architecture, windmill blade design for papercraft models, and triply orthogonal structures, which will be discussed in Part 2 of the talk.

All you need is rotation: Construction of developable strips – Part 2 Applications

Takashi Maekawa
Waseda University

Felix Scholz
Johannes Kepler University

Abstract

The versatility of the proposed method is demonstrated through both computational and physical examples, showcasing its broad range of applications. These include architecture, windmill blade design, curved folding, triply orthogonal structures, and the creation of surfaces with log-aesthetic curves. Such examples highlight the method's potential in fields like architectural design, industrial design, and papercraft modeling, offering a powerful tool for innovative surface design and fabrication. Specifically, we present:

- Architectural Design: A helical structure spanning the parameter range $0 \leq t \leq 2\pi$
- Inverted Catenary Arch: A model composed of two developable surfaces intersecting to form the shape of an inverted catenary.
- Deltoid Evolute: A construction based on the evolute of a deltoid curve, which intriguingly forms another deltoid when viewed from above. This is expressed through developable surfaces aligned along the deltoid.
- Papercraft Windmill Blade: We designed a vertical papercraft model with a developable surface. Unlike horizontal-axis turbines, vertical-axis turbines are wind-direction insensitive, removing the need for yaw control.
- Additional examples demonstrating the versatility of the method will be presented during the talk.

References

[1] T. Maekawa and Felix Scholz, "All you need is rotation: Construction of developable strips", ACM Transactions on Graphics, vol. 43, no. 6, 2024.

All you need is rotation: Construction of developable strips – Part 2 Application

Takashi Maekawa
Waseda University

Felix Scholz
Johannes Kepler University

Planar curve (ellipse)

$\varphi = \frac{\pi}{2}$ (rectifying developable)

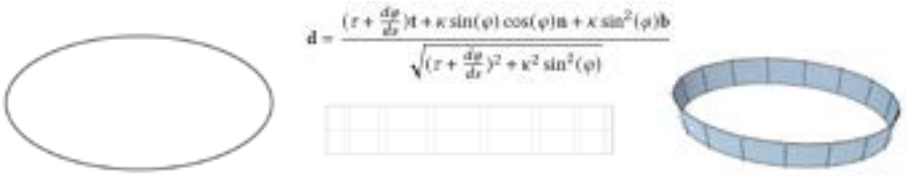

$\varphi(t) = \sin(2t) + \frac{\pi}{2}$

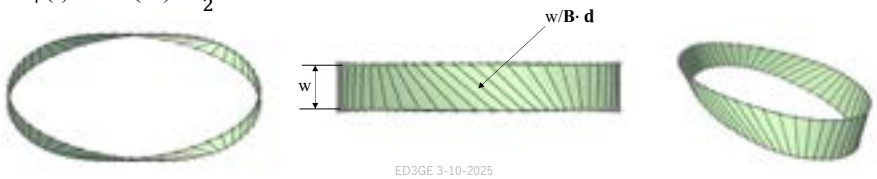

Inverted catenary arch

Directrix: Inverted catenary, $\mathbf{c}(t) = (t, 0, -a\cosh(\frac{t}{a}) + a\cosh(\frac{l}{a}))$

a= 4, ℓ= 10 for $-\ell \le t \le \ell$, w = 1 (half-width of strip)

$\varphi(t) = \cos(\frac{\pi t}{4\ell}) - \frac{3\pi}{2}$

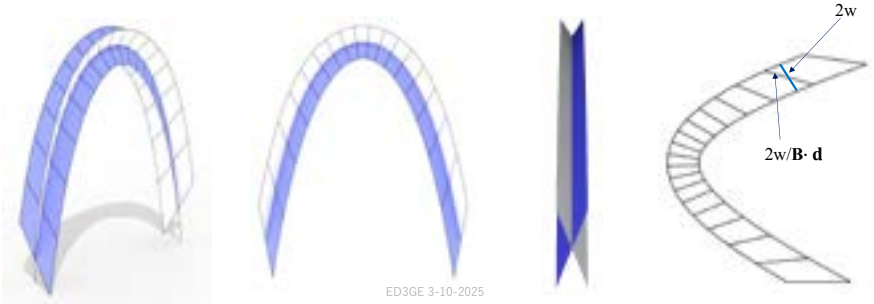

Möbius strip

Directrix: $\mathbf{c}(t) = (\sin(t), (1-\cos(t))^3, \sin(t)(1-\cos(t)))$

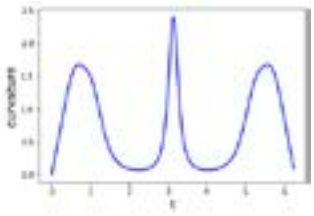

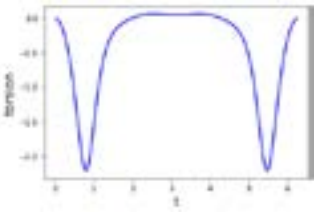

$\varphi = \frac{\pi}{2}$ (rectifying developable)

3D cubic Bézier curve as directrix

$\varphi = \frac{\pi}{2}$

$\varphi = \frac{\pi}{4}$

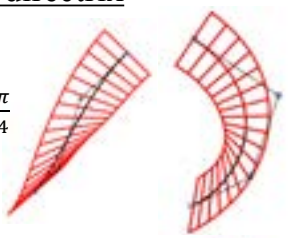

RMF

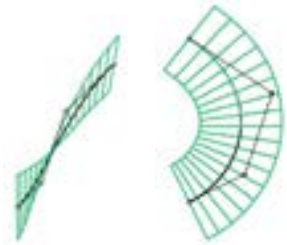

Three developable strips sharing the same Bézier curve

Helical windmill (3 developable blades)

Directrix: Helix, $\mathbf{c}(t) = (a\cos(t), a\sin(t), bt)$ with a = 50, b= 35, $0 \le t \le \frac{2\pi}{3}$

$\varphi(t)$ is determined by RMF

$\varphi_0 = \frac{\pi}{2}$: blades obtain lift rather than drag from the air

Helical windmill

Sea shell surface

https://en.wikipedia.org/wiki/Seashell_surface#/media/File:Seashell_Surface.PNG

$\mathbf{r}(t, \theta) = \mathbf{helix}(t) + rt\,(-\cos(\theta)\mathbf{n}(t) + \sin(\theta)\mathbf{b}(t))$

$a = 20$, $b = 30$ for the helix

$r = 15$, $\theta = 0$, the half-width $w(t) = \frac{rt}{8}$

$\varphi(t) = 0.5\sin(t) + \frac{\pi}{6}$

$\varphi(t) = 0.5\sin(t) + \frac{\pi}{4}$

Difference

Sea shell surface

$\theta = 0, \quad \theta = \pi$

$w^{+}(t) = \frac{rt}{8}(1 + 0.2\sin(30t)), \quad w^{-}(t) = \frac{rt}{8}(1 + 0.2\cos(30t))$

Hemisphere (Reichstag dome)

Hemisphere: $x^2 + y^2 + z^2 = a^2$

Directrix: $\mathbf{c}(t) = (\sqrt{a^2 - b^2 t^2}\cos(\lambda t), \sqrt{a^2 - b^2 t^2}\sin(\lambda t), bt)$, $0 \le t \le \frac{a}{b}$

$\varphi(t)$ is determined by RMF

$a = 1$, $b = 1$, and $\lambda = 108$

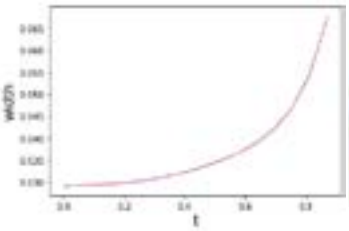

https://en.wikipedia.org/wiki/Reichstag_dome

Deltoid evolute

Directrix: Deltoid, $\mathbf{c}(t) = (a(2\cos(t) + \cos(2t)), a(2\sin(t) - \sin(2t)), 0)$

a = 50 (radius of small circle)

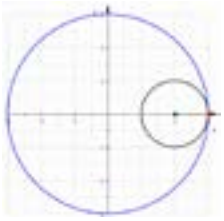

https://en.wikipedia.org/wiki/Deltoid_curve#/media/File:Deltoid2.gif

Evolute of the deltoid

$\varphi = \varphi_{del} = \text{const}$

$\tau_g = 0$, leading to $\mathbf{d} \cdot \mathbf{t} = 0$

$\mathbf{d}_{proj} = (\mathbf{d} \cdot \mathbf{t})\mathbf{t} + (\mathbf{d} \cdot \mathbf{n})\mathbf{n} = \cos(\varphi_{del})\mathbf{n}$

$w(t)\cos(\varphi_{del}) = \frac{1}{\kappa(t)}$

Deltoid evolute

3D Top view

Front view

Perspective view

Flattened strip

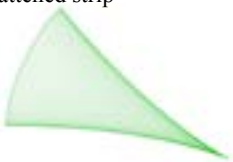

Loxodrome

A loxodrome is a curve on a sphere that intersects all meridians at the same angle α

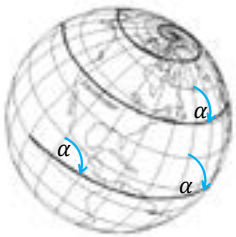

THE LOXODROME ON AN ELLIPSOID
R. E. Deakin, 2010

Sphere: $\mathbf{r}(u, v) = (r \sin u \cos v,\ r \sin u \sin v,\ r \cos u)$,
where $0 \le u \le \pi$ and $0 \le v \le 2\pi$

Directrix: Eqn. of loxodrome $v = \tan\alpha \ln \tan\frac{u}{2} + c$
(c is the integration constant)

$u = 2 \arctan(e^{\frac{v-c}{a}})$

$w(v) = \cos(\frac{\pi}{2} - \alpha)\ \frac{r}{2}\ (u_b - u_a)$

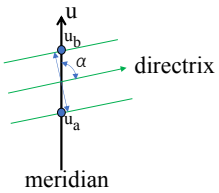

Loxodrome

Integration constant: c = $\frac{\pi}{4}, \frac{3\pi}{4}, \frac{5\pi}{4}, \frac{7\pi}{4}$

The maximum and average deviations from the sphere normalized by sphere's diameter are computed to be 0.629% and 0.327%, respectively

Loxodrome

Curved folding

Directrix: Helix, $\mathbf{c}(t) = (a\cos(t), a\sin(t), bt)$ with a = 50, b= 25, $0.6\,\pi \le t \le 2\pi$
w(t) = 15

Solve $\frac{d\varphi}{ds} = \frac{\kappa \sin(\varphi)}{\tan(\theta)} - \tau$ where $\theta = \frac{\pi}{4}$

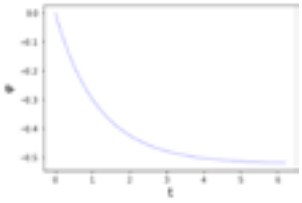

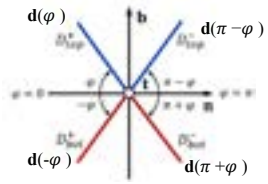

Bottom pair

Curved folding

Directrix: Helix, $\mathbf{c}(t) = (a\cos(t), a\sin(t), bt)$ with a = 50, b= 25, $0.6\,\pi \le t \le 2\pi$
w(t) = 15 (half-width of developable strip), $\theta = \frac{\pi}{4}$

t'= κ**n** using $\kappa = \kappa_g$ and **n**=(0, 0, 1) × **t**

Ribonization of torus by TOR

Directrix curve
c(t) = ((R + r cos(7t)) cos t,
(R + r cos(7t)) sin t,
r sin(7t))
w = 0.2

Directrix curve
c(t) = ((R + r cos(7t)) cos (t + $\frac{\pi}{7}$),
(R + r cos(7t)) sin (t + $\frac{\pi}{7}$),
r sin(7t))
w = 0.2

Flattened strip

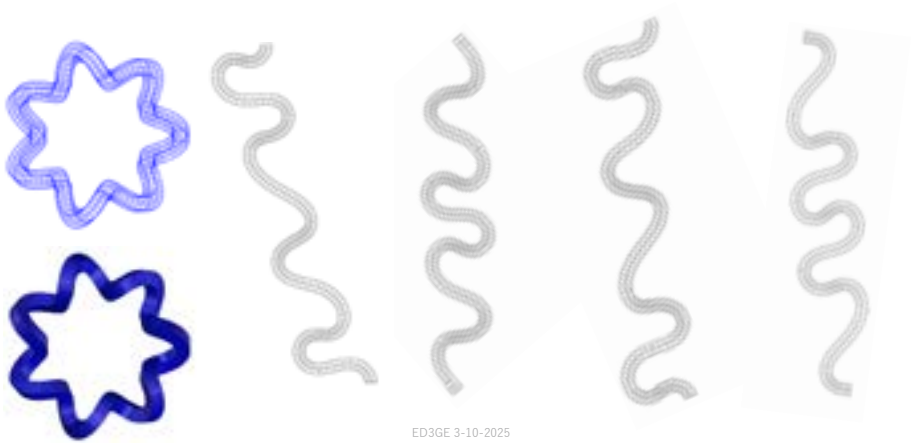

Film-based Perovskite photovoltaic module

Todori, K., Miyauchi, H.: Film-based perovskite photovoltaic module with light weight and flexibility to accommodate various styles of installation.
Toshiba Rev. **76**(3), 17–20 (2021)

Transparent PET films pasted on a 3Dprinted model of the approximated complete log-aesthetic surface.

PVC films of blue alternating with orange pasted on a 3D printed model.

F. Scholz, S. Nishikawa, M. Takezawa, T. Maekawa, "Approximation of doubly curved surfaces by analysis-suitable piecewise surfaces with high Developability", The Visual Computer, 2022.

Walls of Cristo Obrero

https://upload.wikimedia.org/wikipedia/commons/1/19/Parroquia_del_Cristo_Obrero_-_panoramio_%285%29.jpg

$\mathbf{r}(u, v) = (u, a \cos(\omega v) \frac{h-v}{h}, h\text{-}v)$, $0 \le u \le l$, $0 \le v \le h$

When v = const. the isoparametric curve becomes planar.
Thus, $\tau_g = 0$, and hence $\mathbf{d} = -\mathbf{B}$

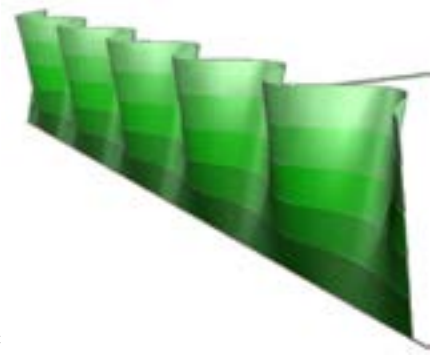

Royan Central Market Hall

Google map: 45° 37' 39.53" N
1° 1' 52.67" W

Completion: 1956

Material: Reinforced concrete structure

Royan Central Market Hall B-spline: Consists of 13 doubly curved surfaces (Courtesy of Prof. Yokosuka)

Piecewise developable B-spline strips

Original model

Approximation by 5 piecewise developable strips per doubly curved surfaces using

$\varphi(t) = cos^{-1}(\mathbf{b} \cdot \mathbf{N})$

F. Scholz, S. Nishikawa, M. Takezawa, T. Maekawa, "Approximation of doubly curved surfaces by analysis-suitable piecewise surfaces with high Developability", The Visual Computer, 2022.

Future work

- Explore more analytical functions and polynomial curves for rotation angles.
- Investigate the potential of triply orthogonal structures in framing freeform surface architecture.

Isogeometric Analysis of Membrane and Cable Structures: A Design of Umbrella Zero-Stress State

Maya Okada / Naoyuki Fujita / Takuya Terahara / Yastoshi Taniguchi / Kenji Takizawa

Waseda University, 1-6-1 Nishi-Waseda, Shinjuku-ku, Tokyo, Japan

Tayfun E. Tezduyar
Rice University, MS 321, 6100 Main Street, Houston, TX 77005, USA

Abstract

An umbrella is a common item that requires aesthetically and functionally good design. A wrinkle-free design is suitable in both directions, and for manufacturing reasons, zero-stress state (ZSS) of each membrane part is flat. We model an umbrella using T-splines, which we developed in [1], and using geometric knowledge [2] and steady-state structural mechanics. We use a newly developed Bézier simplex and combined T-splines to represent the membrane parts (see 1). To design the ZSS, we use the integration-point-based zero-stress state (IPBZSS) technique [3]. The bone parts are connected with the membrane with the method described in [1], and we newly developed the torsion representation (see 2 for a test) to stabilize the bone parts of the umbrella.

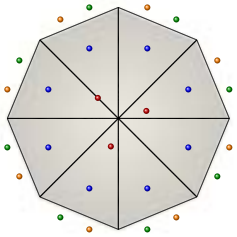

Figure 1: Simplex geometry with higher-order continuous and computational result

Figure 2: Isogeometric analysis of cable structure

References

[1] T. Terahara, K. Takizawa, and T.E. Tezduyar, "T-splines computational membrane–cable structural mechanics with continuity and smoothness: I. Method and implementation", Computational Mechanics, **71** (2023) 657–675.

[2] T. Terahara, S. Nishikawa, A. Suzuki, K. Takizawa, and T. Maekawa, "Geometric modeling of umbrella surfaces", Computer-Aided Design, **175** (2024) 103750.

[3] T. Sasaki, K. Takizawa, and T. E. Tezduyar, "Aorta zero-stress state modeling with T-spline discretization", Computational Mechanics, **63** (2019) 1315–1331.

Continuity and Smoothness in T-Splines Representations of Structures with Different Parametric Dimensions

Takuya Terahara / Kenji Takizawa

Waseda University, 1-6-1 Nishi-Waseda, Shinjuku-ku, Tokyo, Japan

Tayfun E. Tezduyar
Rice University, MS 321, 6100 Main Street, Houston, TX 77005, USA

Abstract

We present a computational method using T-splines discretization for structural mechanics with different parametric dimensions are connected with continuity and smoothness. The Isogeometric analysis (IGA) gives accuracy to structural mechanics computations [1], and higher-order continuity allows use of the higher-order differential equations, such as the Kirchhoff–Love shells [2]. In IGA, connecting a 1D structure, such as a cable, to a 2D structure, such as a shell, is not that straightforward. That is because the control points are not on the cables or surfaces. The simple approach requires an extra refinement to have C^0 continuity functions that represents the position on the cables or surfaces. We proposed a new discretization method using T-splines [3, 4]. We present computations of test and parachute deformation. The computations demonstrate how the method works.

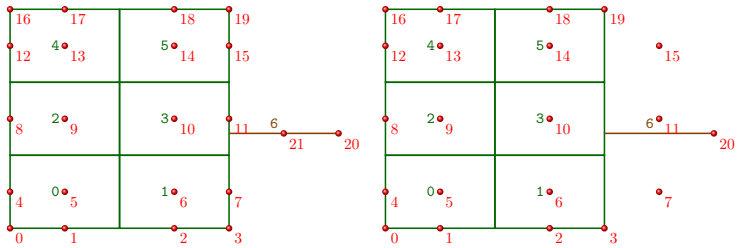

Figure 1: Membran–cable structures with C^0 and C^1 continuous

Figure 2: Parachute deformation

References

[1] K. Takizawa, T. E. Tezduyar, and T. Terahara, "Ram-air parachute structural and fluid mechanics computations with the space–time isogeometric analysis (ST-IGA)", Computers & Fluids, **141** (2016) 191–200.

[2] Y. Taniguchi, K. Takizawa, Y. Otoguro, and T.E. Tezduyar, "A hyperelastic extended Kirchhoff–Love shell model with out-of-plane normal stress: I. Out-of-plane deformation", Computational Mechanics, **70** (2022) 247–280.

[3] T. Terahara, T. Kuraishi, K. Takizawa, and T.E. Tezduyar, "Computational flow analysis with boundary layer and contact representation: II. Heart valve flow with leaflet contact", Journal of Mechanics, **38** (2022) 185–194.

[4] T. Terahara, K. Takizawa, and T.E. Tezduyar, "T-splines computational membrane–cable structural mechanics with continuity and smoothness: I. Method and implementation", Computational Mechanics, **71** (2023) 657–675.

T★AFSM

Isogeometric Analysis of Membrane and Cable Structures: A Design of Umbrella Zero-Stress State

M. Okada, N. Fujita,
T. Terahara, Y. Taniguchi, K. Takizawa
Waseda University

T.E. Tezduyar
Rice University
Waseda University

T★AFSM

Overview

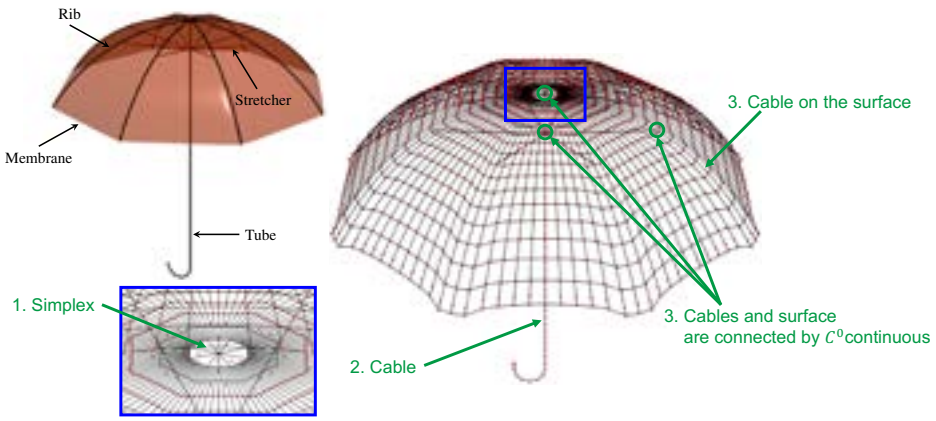

T★AFSM

Smooth Representation for Bézier Simplex Elements

M. Okada, N. Fujita,
T. Terahara, Y. Taniguchi, K. Takizawa
Waseda University

T.E. Tezduyar
Rice University
Waseda University

T★AFSM

Rectangular and Simplex

Umbrella

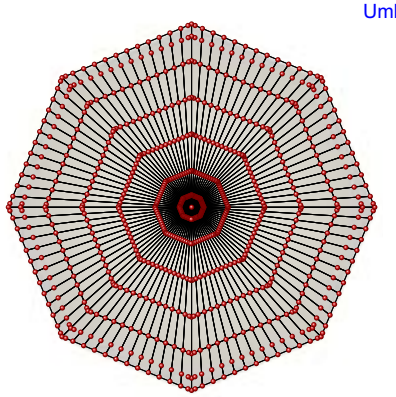

Rectangular mesh

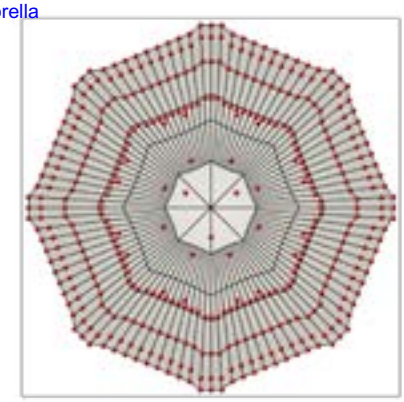

Simplex mesh

T★AFSM

Bézier Simplex

Basis function

$$B^{s}_{p,\boldsymbol{m}}(\boldsymbol{s}) = \frac{p!}{\prod_{k=0}^{n_{pd}} m_k!} \prod_{k=0}^{n_{pd}} {s_k}^{m_k}$$

p: polynomial order of the basis functions
n_{pd}: number of parametric dimensions
s_k: k_{th} Barycentric coordinate
m_k: degree in k_{th} Barycentric coordinate

p=2, n_{pd}=2

$$B^{s}_{2,0} = {s_0}^2 \qquad B^{s}_{2,1} = 2 s_0 s_1$$
$$B^{s}_{2,2} = {s_1}^2 \qquad B^{s}_{2,3} = 2 s_0 s_2$$
$$B^{s}_{2,4} = 2 s_1 s_2 \qquad B^{s}_{2,5} = {s_2}^2$$

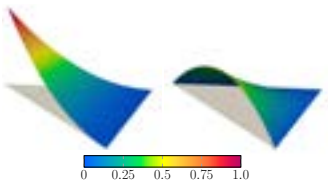

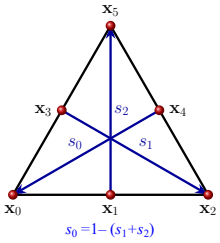

T★AFSM

Bézier Simplex

Bézier extraction

$$\mathbf{B}^{s}_{p,\boldsymbol{m}} = \mathbf{C}_{ST}\mathbf{N}_{p,n}$$

Bézier simplex $\mathbf{B}^{s}_{p,\boldsymbol{m}}$
Product form Bézier $\mathbf{N}_{p,n}$

Extraction-operator

p=2, n_{pd}=2

$$\mathbf{C}_{ST} = \begin{bmatrix} 1 & 0 & 0 & 0 & 0 & 0 & 0 & 0 & 0 & 0 \\ 0 & 1 & 0 & 0 & 0 & 0 & 0 & 0 & 0 & 0 \\ 0 & 0 & 1 & 0 & 0 & 0 & 0 & 0 & 0 & 0 \\ 0 & 0 & 0 & 1 & \frac{1}{2} & 0 & 0 & 0 & 0 & 0 \\ 0 & 0 & 0 & 0 & \frac{1}{2} & 1 & 0 & 0 & 0 & 0 \\ 0 & 0 & 0 & 0 & 0 & 0 & 1 & 1 & 1 & 1 \end{bmatrix}$$

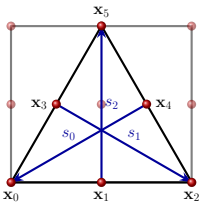

p=3, n_{pd}=2

$$\mathbf{C}_{ST} = \begin{bmatrix} 1 & 0 & 0 & 0 & 0 & 0 & 0 & 0 & 0 & 0 & 0 & 0 & 0 & 0 & 0 & 0 \\ 0 & 1 & 0 & 0 & 0 & 0 & 0 & 0 & 0 & 0 & 0 & 0 & 0 & 0 & 0 & 0 \\ 0 & 0 & 1 & 0 & 0 & 0 & 0 & 0 & 0 & 0 & 0 & 0 & 0 & 0 & 0 & 0 \\ 0 & 0 & 0 & 1 & 0 & 0 & 0 & 0 & 0 & 0 & 0 & 0 & 0 & 0 & 0 & 0 \\ 0 & 0 & 0 & 0 & 1 & \frac{1}{3} & 0 & 0 & 0 & 0 & 0 & 0 & 0 & 0 & 0 & 0 \\ 0 & 0 & 0 & 0 & 0 & \frac{2}{3} & \frac{2}{3} & 0 & 0 & 0 & 0 & 0 & 0 & 0 & 0 & 0 \\ 0 & 0 & 0 & 0 & 0 & 0 & \frac{1}{3} & 1 & 0 & 0 & 0 & 0 & 0 & 0 & 0 & 0 \\ 0 & 0 & 0 & 0 & 0 & 0 & 0 & 0 & 1 & \frac{2}{3} & \frac{1}{3} & 0 & 0 & 0 & 0 & 0 \\ 0 & 0 & 0 & 0 & 0 & 0 & 0 & 0 & 0 & \frac{1}{3} & \frac{2}{3} & 1 & 0 & 0 & 0 & 0 \\ 0 & 0 & 0 & 0 & 0 & 0 & 0 & 0 & 0 & 0 & 0 & 0 & 1 & 1 & 1 & 1 \end{bmatrix}$$

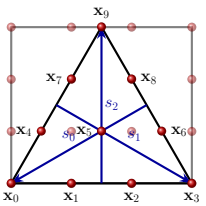

T★AFSM

Constraint of Control Points for a Smoothing Surface

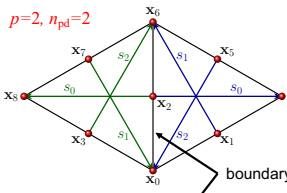

Constraint

$$\begin{cases} \mathbf{A}_3 = x_a\mathbf{A}_1 + y_a\mathbf{A}_2 \\ \mathbf{B}_3 = x_b\mathbf{B}_1 + y_b\mathbf{B}_2 \\ x_a = x_b = x \\ y_a = y_b = y \end{cases}$$

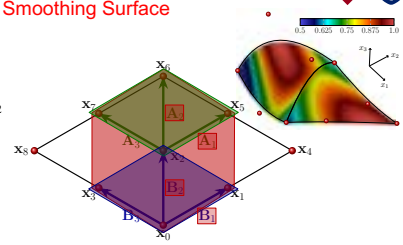

boundary ($s_0 = 0$)

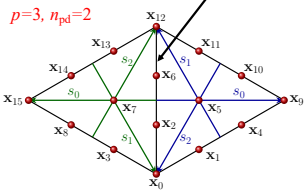

Constraint

$$\begin{cases} \mathbf{A}_3 = x_a\mathbf{A}_1 + y_a\mathbf{A}_2 \\ \mathbf{B}_3 = x_b\mathbf{B}_1 + y_b\mathbf{B}_2 \\ \mathbf{C}_3 = x_c\mathbf{C}_1 + y_c\mathbf{C}_2 \\ x_a = x_b = x_c = x \\ y_a = y_b = y_c = y \end{cases}$$

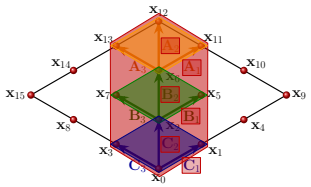

6

T★AFSM

Building Smooth Basis Functions in a Rectangular Octagon Space (p=3, n_{pd}=2)

8 elements, 49 control points

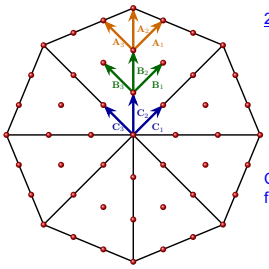

24 boundary conditions

$$\begin{cases} \mathbf{A}_3 = x\mathbf{A}_1 + y\mathbf{A}_2 \\ \mathbf{B}_3 = x\mathbf{B}_1 + y\mathbf{B}_2 \\ \mathbf{C}_3 = x\mathbf{C}_1 + y\mathbf{C}_2 \\ x = -2 + \sqrt{2} \\ y = \sqrt{2} \end{cases}$$

Constraint expression for 49 control points

$$\mathbf{A}\begin{bmatrix} z_0 \\ \vdots \\ z_{48} \end{bmatrix} = \begin{bmatrix} 0 \\ \vdots \\ 0 \end{bmatrix}$$

$$\mathbf{A} \in \mathbb{R}^{24\times 49}$$

Independent solutions: $\dim(\ker \mathbf{A}) = 27$

27 smooth basis functions

Partition of unity
Non-negative
+ Rotational symmetry

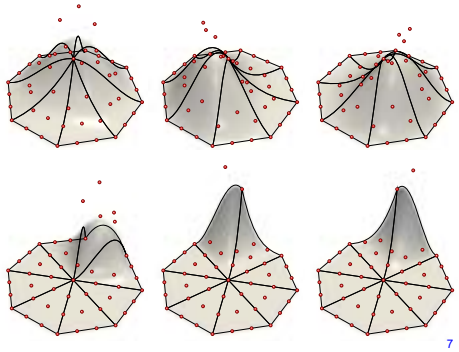

7

T★AFSM

C^1 Basis Functions across the 8 Elements

2D MESH

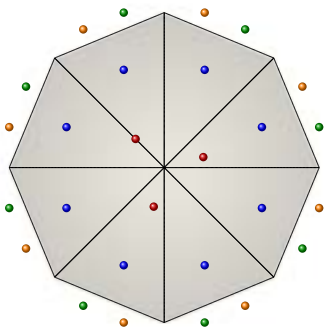

27 smooth basis functions (8 elements)

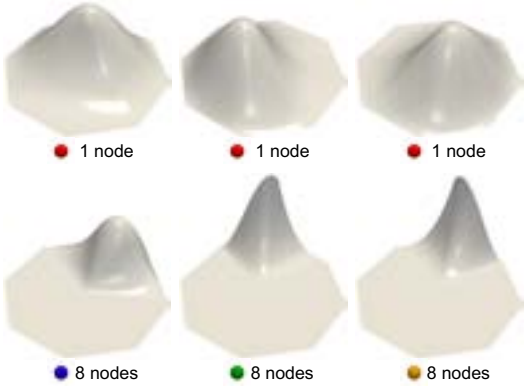

8

T★AFSM

Cable Model

M. Okada, N. Fujita,
T. Terahara, Y. Taniguchi, K. Takizawa
Waseda University

T.E. Tezduyar
Rice University
Waseda University

T★AFSM

Overview

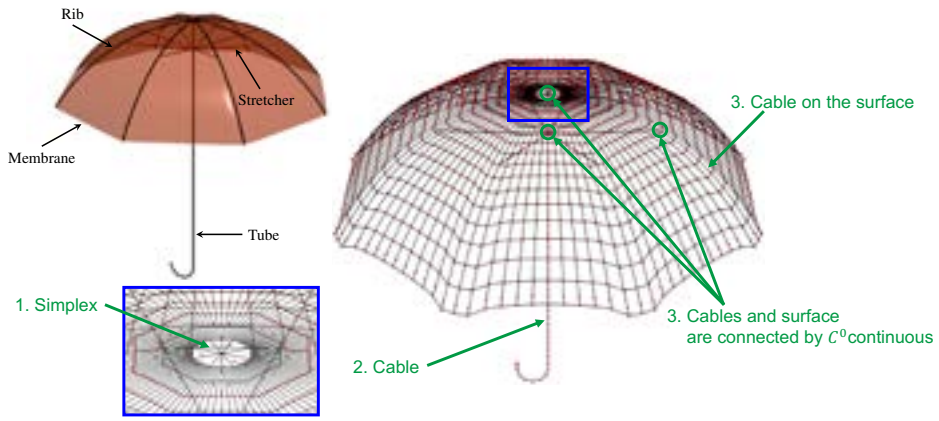

T★AFSM

Rotation-Free Cable Model

Principle of Virtual Work

$$\int_{S_t} \delta\mathbf{x}\cdot\mathbf{h}\mathrm{d}S + \int_{S_0}\rho_0 A_0\delta\mathbf{x}\cdot(\mathbf{f}-\mathbf{a})\mathrm{d}S - \int_{S_0}\frac{E}{\|\mathbf{G}_1\|^4}(\underbrace{A_0\varepsilon\delta\varepsilon}_{\text{Axial}} + \underbrace{I\kappa\delta\kappa}_{\text{Bending}})\mathrm{d}S = 0$$

$$\epsilon = \frac{1}{2}(\mathbf{x}_{,\xi^1}\cdot\mathbf{x}_{,\xi^1} - \mathbf{X}_{,\xi^1}\cdot\mathbf{X}_{,\xi^1})$$

$$\kappa = \mathbf{x}_{,\xi^1\xi^1}\cdot\mathbf{n} - \mathbf{X}_{,\xi^1\xi^1}\cdot\mathbf{N}$$

Cross-sectional area:	A_0
Moment of inertia of area:	I
Density:	ρ_0
Young's modulus:	E
Acceleration:	$\mathbf{a}$
Force per unit mass:	$\mathbf{f}$
Surface force per unit length:	$\mathbf{h}$
Tensile strain:	ε
Virtual displacement:	$\delta\mathbf{x}$
Change in curvature:	κ
Tangent vector of the centerline in undeformed configuration:	$\mathbf{G}_1$
Centerline in undeformed configuration:	S_0
Centerline in deformed configuration:	S_t

Cable Model Considering Rotation

Geometric Description of Cable

$$\mathbf{X}^{3D}(\xi^1,\xi^2,\xi^3) = \mathbf{X}(\xi^1) + \xi^2\mathbf{A}_2(\xi^1) + \xi^3\mathbf{A}_3(\xi^1) \qquad \mathbf{x}^{3D}(\xi^1,\xi^2,\xi^3) = \mathbf{x}(\xi^1) + \xi^2\mathbf{a}_2(\xi^1) + \xi^3\mathbf{a}_3(\xi^1)$$

- Two tensors for geometric description

$$\mathbf{\Lambda}(\mathbf{T}_0,\mathbf{t}) = (\mathbf{T}_0\cdot\mathbf{t})\mathbf{I} + \frac{1}{1+\mathbf{T}_0\cdot\mathbf{t}}(\mathbf{T}_0\times\mathbf{t})(\mathbf{T}_0\times\mathbf{t}) + (\mathbf{T}_0\times\mathbf{t})\times\mathbf{I}$$

$$\bar{\mathbf{R}}_{\mathbf{t}}(\psi) = \mathbf{I}\cos(\psi) + \sin(\psi)\mathbf{t}\times\mathbf{I}$$

- Example of geometric description

$$\mathbf{A}_\alpha = \bar{\mathbf{R}}_{\mathbf{T}}(\Psi)\cdot\mathbf{\Lambda}(\mathbf{T}_0,\mathbf{T})\cdot\mathbf{A}^0_\alpha \qquad \mathbf{a}_\alpha = \bar{\mathbf{R}}_{\mathbf{t}}(\psi)\cdot\mathbf{\Lambda}(\mathbf{T}_0,\mathbf{t})\cdot\mathbf{A}^0_\alpha$$

Cable Model Considering Rotation

Principle of Virtual Work

$$\int_{S_t}\delta\mathbf{x}\cdot\mathbf{h}\,\mathrm{d}S + \int_{S_0}\rho_0 A_0\delta\mathbf{x}\cdot(\mathbf{f}-\mathbf{a})\,\mathrm{d}S - \int_{S_0}\left(\underbrace{\frac{E}{\|\mathbf{A}_1\|^4}(A_0\varepsilon\delta\varepsilon}_{\text{Axial}} + \underbrace{I\kappa_{21}\delta\kappa_{21} + I\kappa_{31}\delta\kappa_{31})}_{\text{Bending}} + \underbrace{\frac{GI_p}{\|\mathbf{A}_1\|^2}\left(\frac{1}{2}\kappa_{32}\delta\kappa_{32} + \frac{1}{2}\kappa_{23}\delta\kappa_{23}\right)}_{\text{Torsion}}\right)\mathrm{d}S = 0$$

$$\mathbf{a}_\alpha = \frac{\partial\mathbf{x}}{\partial\xi^\alpha}$$

$$\mathbf{A}_\alpha = \frac{\partial\mathbf{X}}{\partial\xi^\alpha}$$

$$\epsilon = \frac{1}{2}(\mathbf{x}_{,\xi^1}\cdot\mathbf{x}_{,\xi^1} - \mathbf{X}_{,\xi^1}\cdot\mathbf{X}_{,\xi^1})$$

$$\kappa_{\alpha\beta} = \mathbf{a}_{\beta,1}\cdot\mathbf{a}_\alpha - \mathbf{A}_{\beta,1}\cdot\mathbf{A}_\alpha$$

Cross-sectional area:	A_0
Moment of inertia of area:	I
Polar moment of inertia of area:	I_p
Density:	ρ_0
Young's modulus:	E
Modulus of transverse elasticity:	G
Acceleration:	$\mathbf{a}$
Force per unit mass:	$\mathbf{f}$
Surface force per unit length:	$\mathbf{h}$
Tensile strain:	ε
Virtual displacement:	$\delta\mathbf{x}$
Change in curvature:	$\kappa_{21},\kappa_{31},\kappa_{23},\kappa_{32}$
Tangent vector of the centerline in undeformed configuration:	$\mathbf{A}_1$
Centerline in undeformed configuration:	S_0
Centerline in deformed configuration:	S_t

Yarn Spinning

Method

Principle of virtual work

$$\int_{S_t}\delta\mathbf{x}\cdot\mathbf{h}\,\mathrm{d}S + \int_{S_0}\rho_0 A_0\delta\mathbf{x}\cdot(\mathbf{f}-\mathbf{a})\,\mathrm{d}S - \int_{S_0}\left(\underbrace{\frac{E}{\|\mathbf{A}_1\|^4}(A_0\varepsilon\delta\varepsilon}_{\text{Axial}} + \underbrace{I\kappa_{21}\delta\kappa_{21} + I\kappa_{31}\delta\kappa_{31})}_{\text{Bending}} + \underbrace{\frac{GI_p}{\|\mathbf{A}_1\|^2}\left(\frac{1}{2}\kappa_{32}\delta\kappa_{32} + \frac{1}{2}\kappa_{23}\delta\kappa_{23}\right)}_{\text{Torsion}}\right)\mathrm{d}S + \delta W_{\text{contact}} = 0$$

Augmented Lagrangian method

$$\delta W_{\text{contact}} = \int_{(S_t)_c}(\lambda_N + \epsilon d_N)\,\delta d_N\,\mathrm{d}S$$

Work by contact force:	W_{contact}
Penetrating length:	d_N
Penalty parameter:	ϵ
Lagrange multiplier:	λ_N
domain where contact force acts in deformed configuration:	$(S_t)_c$

Cross-sectional area:	A_0
Moment of inertia of area:	I
Polar moment of inertia of area:	I_p
Density:	ρ_0
Young's modulus:	E
Modulus of transverse elasticity:	G
Acceleration:	$\mathbf{a}$
Force per unit mass:	$\mathbf{f}$
Surface force per unit length:	$\mathbf{h}$
Tensile strain:	ε
Virtual displacement:	$\delta\mathbf{x}$
Change in curvature:	$\kappa_{21},\kappa_{31},\kappa_{23},\kappa_{32}$
Tangent vector of the centerline in undeformed configuration:	$\mathbf{A}_1$
Centerline in undeformed configuration:	S_0
Centerline in deformed configuration:	S_t

T★AFSM

Yarn Spinning

Test Case: Computational Settings

- Rotate fiber ends counterclockwise

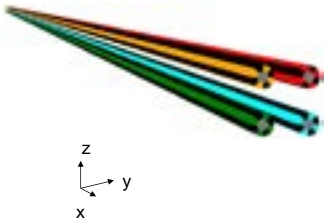

Dimensions and properties (Wool fiber)

Length (m)	0.3
Radius (m)	2.5×10^{-4}
EA_0 (N)	2.501×10^{2}
EI (N · m^2)	3.909×10^{-6}
GI_p (N · m^2)	3.909×10^{-6}
ρ_0 (kg/m^3)	1.316×10^{3}

Number of nodes	103
Number of elements	100

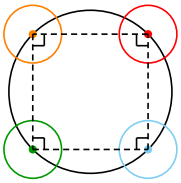

T★AFSM

Yarn Spinning

Contact Analysis

Result

T★AFSM

Yarn Spinning

Contact Analysis

Result

Result (without contact analysis)

T★AFSM

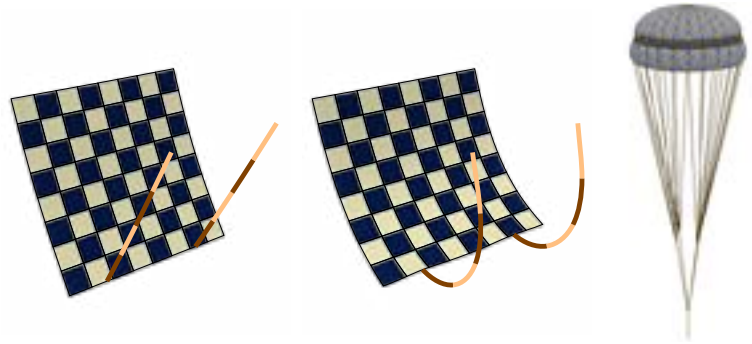

Continuity and Smoothness in T-Splines Representations of Structures with Different Parametric Dimensions

T. Terahara, K. Takizawa
Waseda University

T.E. Tezduyar
Rice University
Waseda University

T★AFSM

Ventricle-Valve-Aorta Flow Analysis with the Space–Time IGA and Topology Change

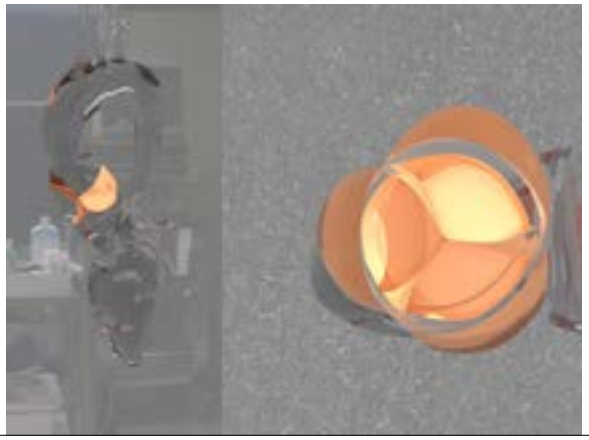

2019 T★AFSM

24

T★AFSM

Ventricle-Valve-Aorta Flow Analysis with the Space–Time IGA and Topology Change
Mitral Valve

2024 T★AFSM

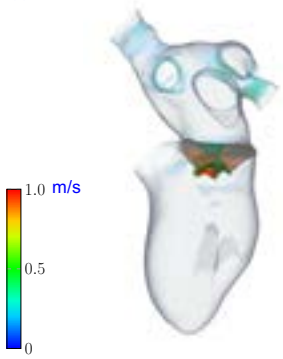

*1

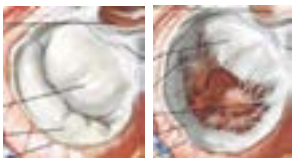

*2

*1 F.H. Netter, "Atlas of Human Anatomy", Netter Basic Science, Page 532.
*2 J.G. Castillo, J. Solis, A.G-Pinto and D.H. Adams, "Surgical echocardiography of the mitral valve", *Revista Espanola de Cardiologia*, 64, 1169–1181, 2011.

25

T★AFSM

Membrane–Cable Structure

Parachute


*1


*2

Umbrella


*3

*1 https://parade.com/904524/marilynvossavant/why-do-skydivers-use-rectangular-parachutes/
*2 https://www.nasa.gov/mission_pages/mars/images/ms0364-20090422.html
*3https://www.komiyakasa.jp/encyclopedia/history-of-japanese-umbrella-industory/

T★AFSM

Membrane–Cable Structure

Ram-Air Parachute

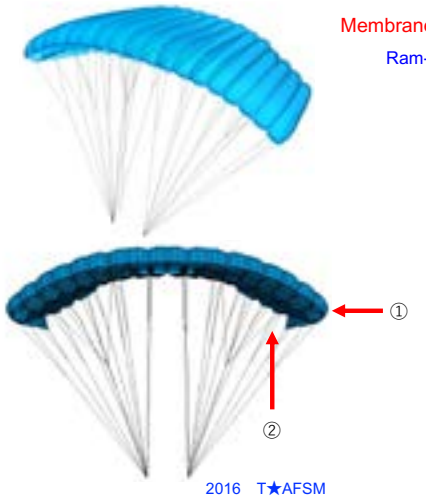

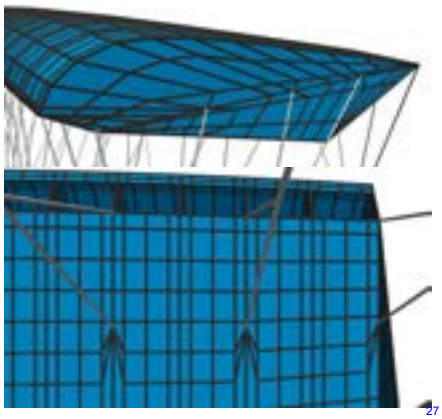

2016 T★AFSM

T★AFSM

Membrane–Cable Structure

Connecting Membrane and Cable

$\Xi^{a,1}$ {0, 0, 0, 1, 2, 2, 2}

$\Xi^{a,2}$ {0, 0, 0, 1, 2, 3, 3, 3}

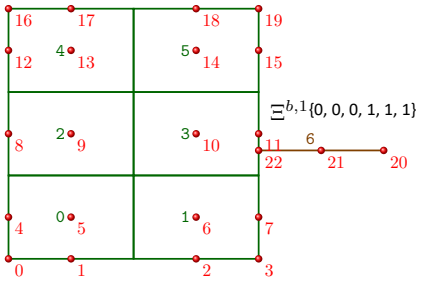

$\Xi^{b,1}$ {0, 0, 0, 1, 1, 1}

$N_k^{e,\alpha}$

e: element number
α: direction
k: local index

Shape function for membrane

$$M_a^e(\xi^1, \xi^2) = N_{a^1}^{e,1}(\xi^1) N_{a^2}^{e,2}(\xi^2)$$

Shape function for line

$$L_b^e(\xi^1) = N_{b^1}^{e,1}(\xi^1)$$

T★AFSM

Membrane–Cable Structure

Connecting Membrane and Cable

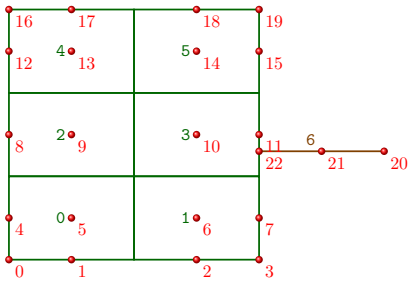

Example

$$\mathbf{C}^{6,1} = \begin{bmatrix} 1 & 0 & 0 \\ 0 & 1 & 0 \\ 0 & 0 & 1 \end{bmatrix}$$

$$\mathbf{C}_0^{6,1} = \begin{bmatrix} 1 & 0 & 0 \end{bmatrix}$$
$$\mathbf{C}_1^{6,1} = \begin{bmatrix} 0 & 1 & 0 \end{bmatrix}$$
$$\mathbf{C}_2^{6,1} = \begin{bmatrix} 0 & 0 & 1 \end{bmatrix}$$

Bernstein polynomial

$$B_k^p(\xi) = \binom{p}{k} 2^{-p} (1+\xi)^k (1-\xi)^{p-k}$$
$$\binom{p}{k} = \frac{k!}{k!\,(p-k)!}$$

Bezier extraction operator

$$\mathbf{C}^{e,\alpha} = [C_{lk}^{e,\alpha}] \in \mathbb{R}^{(p^{e,\alpha}+1)\times(p^{e,\alpha}+1)}$$

Shape function written by Bezier extraction

$$N_l^{A,\alpha}(\xi) = \sum_{k=0}^{p^{A,\alpha}} C_{lk}^{e,\alpha} B_k^{p^{e,\alpha}}(\xi)$$

Bezier extraction row operators

$$\mathbf{C}_k^{e,\alpha} \in \mathbb{R}^{1\times(p^{e,\alpha}+1)}$$

29

T★AFSM

Membrane–Cable Structure

Connecting Membrane and Cable

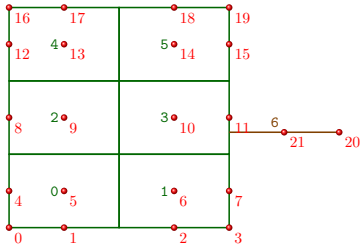

C^0 continuous

Represent the shape function for line using the shape functions of membrane

$$\overline{L}_b^B(\xi^1) = N_{a^2}^A(\xi_c^{A,2}) N_c^{B,1}(\xi^1)$$
$$= \underbrace{\left(\sum_{l=0}^{p^{A,2}} C_{a^2 l}^{A,2} B_l^{p^{A,2}}(\xi_c^{A,2})\right)}_{\text{Scalar}} \left(\sum_{k=0}^{p^{B,1}} C_{ck}^{B,1} B_k^{p^{B,1}}(\xi^1)\right)$$

A: element number of the membrane
B: element number of the cable

30

T★AFSM

Membrane–Cable Structure

Connecting Membrane and Cable

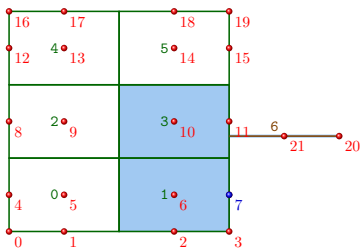

C^0 continuous

$$N_{a^2}^3(\xi_c) = \begin{bmatrix} 0.245 & 0.710 & 0.045 \end{bmatrix}$$

$$\overline{L}_b^B(\xi^1) = N_{a^2}^A(\xi_c^{A,2}) N_c^{B,1}(\xi^1)$$
$$= \left(\sum_{l=0}^{p^{A,2}} C_{a^2 l}^{A,2} B_l^{p^{A,2}}(\xi_c^{A,2})\right) \left(\sum_{k=0}^{p^{B,1}} C_{ck}^{B,1} B_k^{p^{B,1}}(\xi^1)\right)$$

$$\overline{\mathbf{C}}_0^{6,1} = 0.245 \begin{bmatrix} 1 & 0 & 0 \end{bmatrix}$$

31

Membrane–Cable Structure

Connecting Membrane and Cable

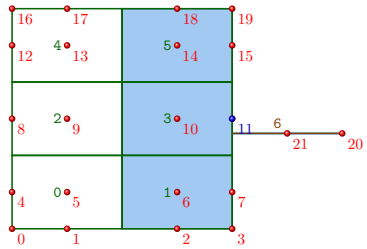

C^0 continuous

$$N^3_{a^2}(\xi_c) = \begin{bmatrix} 0.245 & 0.710 & 0.045 \end{bmatrix}$$

$$\begin{aligned} \overline{L}^B_b(\xi^1) &= N^A_{a^2}(\xi^{A,2}_c) N^{B,1}_c(\xi^1) \\ &= \left(\sum_{l=0}^{p^{A,2}} C^{A,2}_{a^2 l} B^{p^{A,2}}_l(\xi^{A,2}_c) \right) \left(\sum_{k=0}^{p^{B,1}} C^{B,1}_{ck} B^{p^{B,1}}_k(\xi^1) \right) \end{aligned}$$

$$\overline{\mathbf{C}}^{6,1}_1 = 0.710 \begin{bmatrix} 1 & 0 & 0 \end{bmatrix}$$

Membrane–Cable Structure

Connecting Membrane and Cable

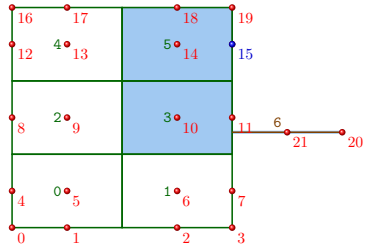

C^0 continuous

$$N^3_{a^2}(\xi_c) = \begin{bmatrix} 0.245 & 0.710 & 0.045 \end{bmatrix}$$

$$\begin{aligned} \overline{L}^B_b(\xi^1) &= N^A_{a^2}(\xi^{A,2}_c) N^{B,1}_c(\xi^1) \\ &= \left(\sum_{l=0}^{p^{A,2}} C^{A,2}_{a^2 l} B^{p^{A,2}}_l(\xi^{A,2}_c) \right) \left(\sum_{k=0}^{p^{B,1}} C^{B,1}_{ck} B^{p^{B,1}}_k(\xi^1) \right) \end{aligned}$$

$$\overline{\mathbf{C}}^{6,1}_2 = 0.045 \begin{bmatrix} 1 & 0 & 0 \end{bmatrix}$$

Membrane–Cable Structure

Connecting Membrane and Cable

C^0 continuous

$$\mathbf{C}^{6,1}_0 = \begin{bmatrix} 1 & 0 & 0 \end{bmatrix}$$
$$\mathbf{C}^{6,1}_1 = \begin{bmatrix} 0 & 1 & 0 \end{bmatrix}$$
$$\mathbf{C}^{6,1}_2 = \begin{bmatrix} 0 & 0 & 1 \end{bmatrix}$$

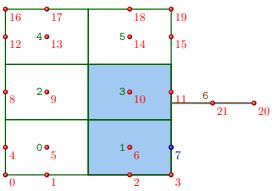

$$\overline{\mathbf{C}}^{6,1}_0 = 0.245 \begin{bmatrix} 1 & 0 & 0 \end{bmatrix}$$

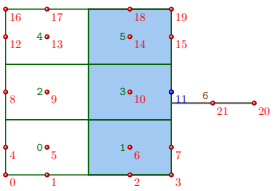

$$\overline{\mathbf{C}}^{6,1}_1 = 0.710 \begin{bmatrix} 1 & 0 & 0 \end{bmatrix}$$

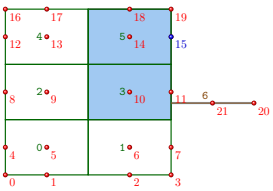

$$\overline{\mathbf{C}}^{6,1}_2 = 0.045 \begin{bmatrix} 1 & 0 & 0 \end{bmatrix}$$

$$\overline{\mathbf{C}}^{6,1}_3 = \begin{bmatrix} 0 & 1 & 0 \end{bmatrix} \quad \overline{\mathbf{C}}^{6,1}_4 = \begin{bmatrix} 0 & 0 & 1 \end{bmatrix}$$

Membrane–Cable Structure

Connecting Membrane and Cable

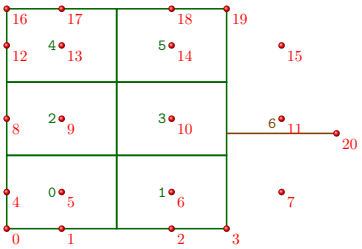

C^1 continuous

$$\mathbf{C}_0^{6,1} = \begin{bmatrix} \frac{1}{2} & 0 & 0 \end{bmatrix}$$
$$\mathbf{C}_1^{6,1} = \begin{bmatrix} \frac{1}{2} & 1 & 0 \end{bmatrix}$$
$$\mathbf{C}_2^{6,1} = \begin{bmatrix} 0 & 0 & 1 \end{bmatrix}$$

Membrane–Cable Structure

Connecting Membrane and Cable

C^1 continuous

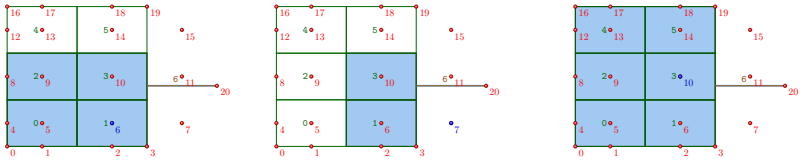

$\bar{\mathbf{C}}_0^{6,1} = 0.245 \begin{bmatrix} \frac{1}{2} & 0 & 0 \end{bmatrix}$ $\bar{\mathbf{C}}_1^{6,1} = 0.710 \begin{bmatrix} \frac{1}{2} & 0 & 0 \end{bmatrix}$ $\bar{\mathbf{C}}_2^{6,1} = 0.045 \begin{bmatrix} \frac{1}{2} & 0 & 0 \end{bmatrix}$

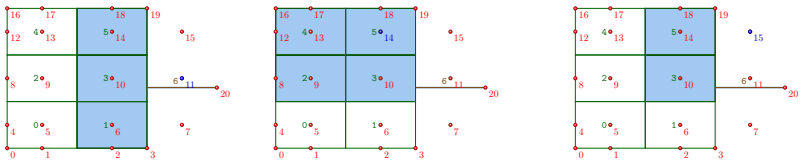

$\bar{\mathbf{C}}_3^{6,1} = 0.245 \begin{bmatrix} \frac{1}{2} & 1 & 0 \end{bmatrix}$ $\bar{\mathbf{C}}_4^{6,1} = 0.710 \begin{bmatrix} \frac{1}{2} & 1 & 0 \end{bmatrix}$ $\bar{\mathbf{C}}_5^{6,1} = 0.045 \begin{bmatrix} \frac{1}{2} & 1 & 0 \end{bmatrix}$

$$\bar{\mathbf{C}}_6^{6,1} = \begin{bmatrix} 0 & 0 & 1 \end{bmatrix}$$

Membrane–Cable Structure

Computational Settings

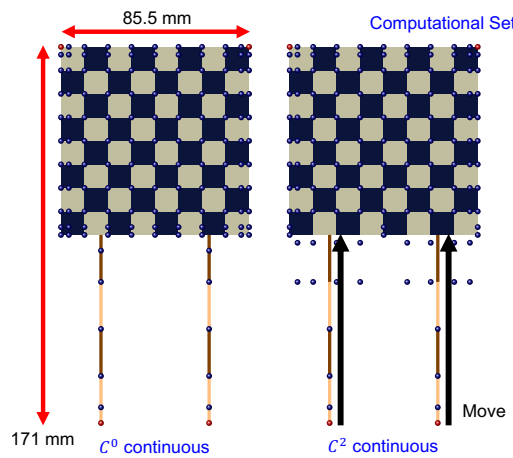

C^0 continuous

C^2 continuous

Models for surface
- Shell
- Membrane

Cable
- With bending stabilized cable
- Without bending stabilized cable

T★AFSM

Membrane–Cable Structure

Results: Membrane

Cable | Bending-stabilized cable | Cable | Bending-stabilized cable

C^0 continuous | C^2 continuous

T★AFSM

Membrane–Cable Structure

Result: Shell

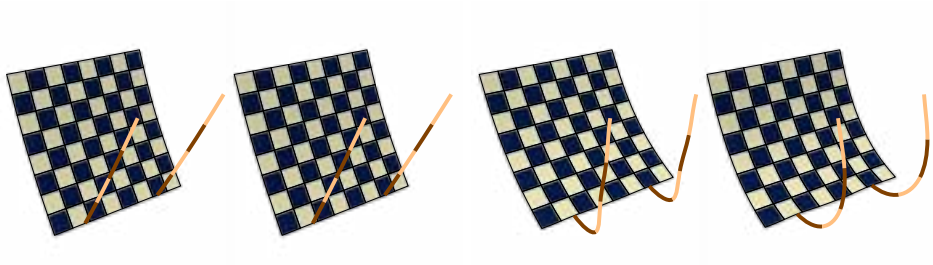

Cable | Bending-stabilized cable | Cable | Bending-stabilized cable

C^0 continuous | C^2 continuous

T★AFSM

Disk-Gap-Band (DGB) Parachute

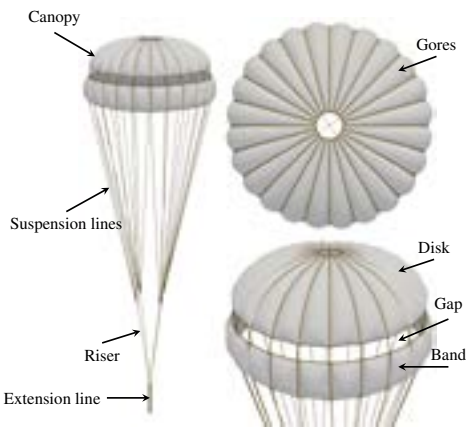

T★AFSM

DGB Parachute

Mesh (DGB-N)

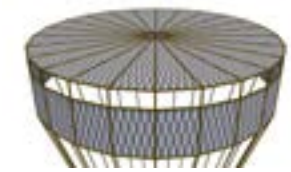

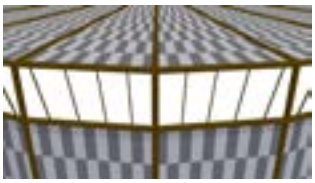

Detail

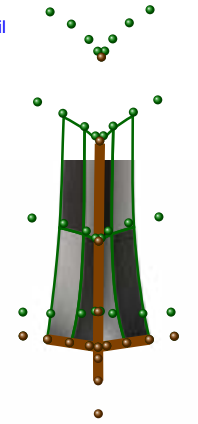

41

T★AFSM

DGB Parachute

Mesh (DGB-T1)

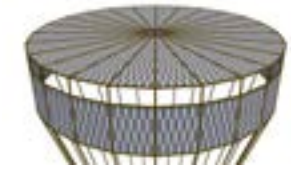

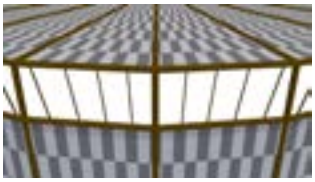

Detail

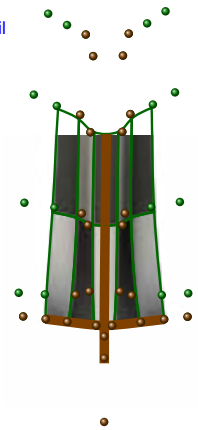

42

T★AFSM

DGB Parachute

Mesh (DGB-T2)

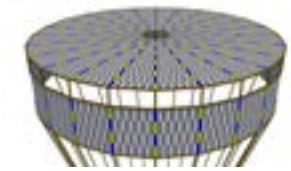

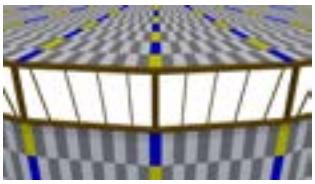

Detail

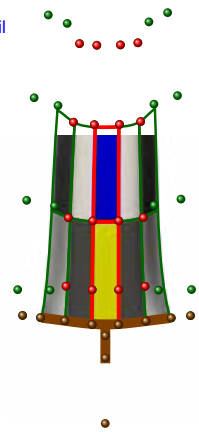

43

T★AFSM

DGB Parachute

Results

DGB-N DGB-T1 DGB-T2

T★AFSM

Umbrella

Geometric Design

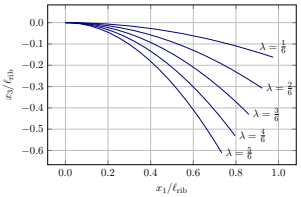

Rib Modeling

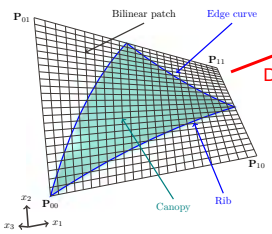

Canopy Modeling

Develop

Manufacturing

T. Terahara, S. Nishikawa, A. Suzuki, K. Takizawa, and T. Maekawa, "Geometric modeling of umbrella surfaces", *Computer-Aided Design*, 175 (2024) 103750.

T★AFSM

Overview

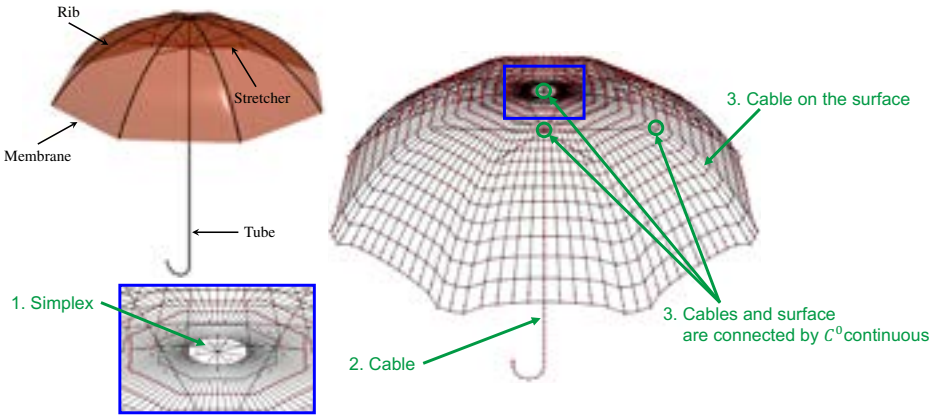

T★AFSM

Umbrella

M. Okada, N. Fujita,
T. Terahara, Y. Taniguchi, K. Takizawa
Waseda University

T.E. Tezduyar
Rice University
Waseda University

47

T★AFSM

Modeling

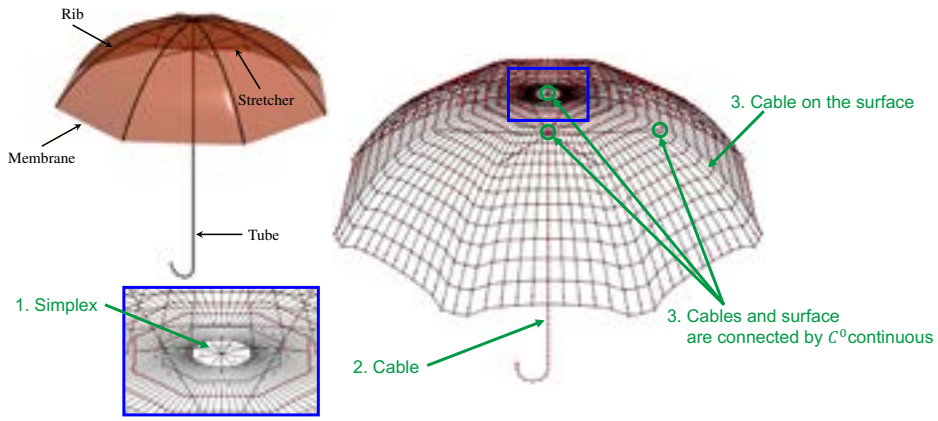

48

T★AFSM

Goals

Strong

Ease of opening

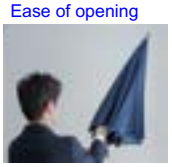

Reducing wrinkle

[1] https://www.komiyakasa.jp/products/long70107srsltid=AfmBOopE_i3jw-Axvyn1vg5RhTvS4474bgk5SXT1Eynh9OSvieMGRX91
[2] https://www.komiyakasa.jp/encyclopedia/history-of-japanese-umbrella-industory/

49

T★AFSM

Umbrella

Umbrella[1]

Wooden pattern for membrane

Bones

Cutting fabric membrane[2]

Sewing membrane peices[2]

Fixing bones on the membrane[2]

[1] https://www.komiyakasa.jp/encyclopedia/history-of-japanese-umbrella-industory/
[2] https://www.komiyakasa.jp/about/how-its-made/

T★AFSM

Structural Analysis

Zero-Stress State (ZSS)

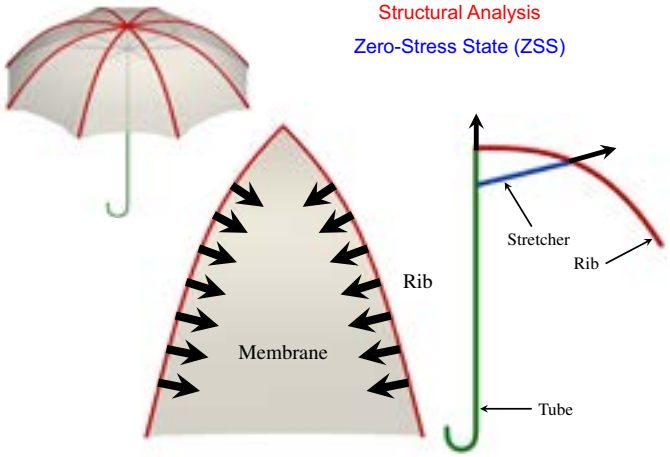

1. Rib curve

2. Membrane surface (Coons patch[1])

3. Flatten membrane

[1] https://www.mathcurve.com/surfaces.gb/patchcoons/patchcoons.shtml

T★AFSM

Structural Analysis

Examples of ZSS and Converged Solutions

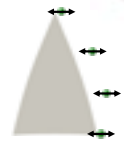

4 control variables
to represent the stretch

0.96-0.96-0.96-0.96

1.00-1.02-1.00-0.96

1.00-1.02-0.96-0.96

1.00-0.98-0.96-0.93

Generation of Aesthetic Shapes by Integrable Klein Geometry

Kenji Kajiwara
Institute of Mathematics for Industry, Kyushu University, Japan

Yoshiki Jikumaru
Faculty of Information Networking for Innovation and Design, Toyo University, Japan

Shun Kumagai
Hachinohe Institute of Technology, Japan

Abstract

In this talk, we consider a class of plane curves called the *log-aesthetic curves* (LAC) and their generalizations which have been developed in industrial design as the curves obtained by extracting the common properties among thousands of curves that car designers regard as aesthetic. We consider these curves in the framework of *similarity geometry* (Klein geometry associated with $\mathrm{CO}^+(2,\mathbb{R}) \simeq \mathrm{SO}(2) \ltimes \mathbb{R}^+$) and characterize them as invariant curves under the integrable deformation of plane curves governed by the *Burgers equation*. We propose a variational principle for these curves, leading to the stationary Burgers equation as the Euler-Lagrange equation[1, 3]. We then extend the LAC to space curves by considering the integrable deformation of space curves under similarity geometry. The deformation is governed by the coupled system of the *modified KdV equation* satisfied by the similarity torsion and a linear equation satisfied by the curvature radius. The curves also allow the deformation governed by the coupled system of the *sine-Gordon equation* and associated linear equation. The space curves corresponding to the travelling wave solutions of those equations would give a generalization of the LAC to space curves. We also consider the surface constructed by the family of curves obtained by the integrable deformation of such curves. A special class of surfaces corresponding to the constant similarity torsion yields quadratic surfaces (ellipsoid, one/two-sheeted hyperboloid and paraboloid) and their deformations, which may be regarded as a generalization of the LAC to surface. We discuss the construction of such curves and surfaces together with their mathematical properties, including integration scheme of the frame by symmetries, and present various examples of curves and surfaces.

Finally we discuss the *self-affinity* of plane curves that has been proposed in the area of industrial design as a characteristic property of the LAC. After some investigations and extending the definition[3], we propose a new class of "aesthetic curves" with self-affinity, which includes the logarithmic spiral (special case of the LAC) and quadratic curves (parabola, hyperbola and ellipse) under the framework of *equiaffine geometry* (Klein geometry associated with $\mathrm{SL}(2,\mathbb{R})$). It may be an interesting problem to investigate the similar class of curves in Möbius geometry.

References

[1] Jun-ichi Inoguchi,Kenji Kajiwara, Kenjiro T.Miura, Masayuki Sato, Wolfgang K.Schief and Yasuhiro Shimizu, Log-aesthetic curves as similarity geometric analogue of Euler's elasticae, Comp. Aided Geom. Design, **61** (2018) 1–5, https://doi.org/10.1016/j.cagd.2018.02.002.

[2] Jun-ichi Inoguchi, Kenji Kajiwara, Kenjiro T. Miura, Yoshiki Jikumaru and Wolfgang K. Schief, Log-aesthetic curves: similarity geometry, integrable discretization and variational principles, Comput. Aided Geom. Design **105**(2023) 102233, https://doi.org/10.1016/j.cagd.2023.10223.

[3] Shun Kumagai and Kenji Kajiwara, Self-affinities of planar curves: towards unified description of aesthetic curves, arXiv:2407.17008v1, https://doi.org/10.48550/arXiv.2407.17008, to appear in Japan J. Indust. Appl. Math. (2025).

Generation of Aesthetic Shapes by Integrable Klein Geometry

Kenji Kajiwara
Institute of Mathematics for Industry (IMI),
Kyushu University, Japan

Joint work with:
Yoshiki Jikumaru (Toyo University)
Shun Kumagai
(Hachinohe Institute of Technology)
Wolfgang Schief (UNSW)

CREST-ED3GE Conference

March 11, 2025
Nishijin Plaza, Fukuoka, Japan

Institute of Mathematics for Industry
KYUSHU UNIVERSITY

Introduction (1) : Log-Aesthetic Curve (LAC)

LAC: Planar curve developed in industrial design - shape elements with built-in artisticity

Extraction of a common property of the curves which car designers regard as "***aesthetic***" → **LAC**

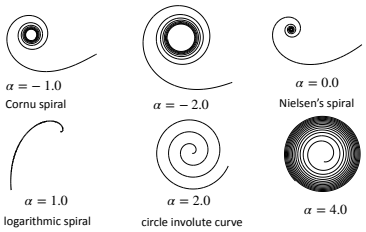

$$q(s) = \begin{cases} (\xi s + \eta)^{1/\alpha} & (\alpha \neq 0) \\ e^{\xi s + \eta} & (\alpha = 0) \end{cases}$$

s: arc length, $q(s)$: curvature radius,
α : "slope"

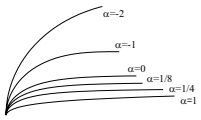

Introduction (2) : LAC and Similarity Geometry

Consultation from a Practitioner of CAD

Extension of LAC: Guiding principle & sound theoretical framework needed!

Logarithmic Spiral LAC (α=1)

$$\gamma = \begin{bmatrix} ae^{b\theta}\cos\theta \\ ae^{b\theta}\sin\theta \end{bmatrix}$$

: self-similar ! → Similarity Geometry

Log-aesthetic curve — Similarity Geometry
- Variational Formulation: "Fairing Energy" = (curvature) ^{2} + (additional term)
- *Shape invariant curve w.r.t. integrable deformation*

Euler's elastic curve — Euclidean Geometry
- Variational Formulation : Elastic Energy = (curvature)^2
- *Shape invariant curve w.r.t. integrable deformation*

Various Extensions

self-adaptive integrable discretization

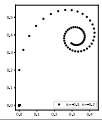

Space curves

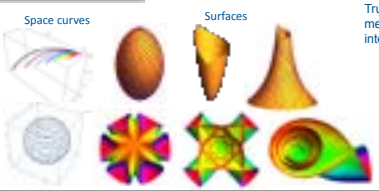

Surfaces

Truss structure with mechanical optimality & integrability & artisticity

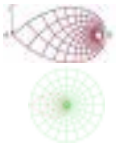

Euclidean Geometry vs Similarity Geometry

Euclidean Geometry

$\gamma(s) = \begin{bmatrix} x(s) \\ y(s) \end{bmatrix} \in \mathbb{R}^2$ s: arc length

$ds = \sqrt{(dx)^2 + (dy)^2} \rightarrow 1 = \sqrt{\left(\frac{dx}{d\theta}\right)^2 + \left(\frac{dy}{ds}\right)^2} = \left\| \frac{d\gamma}{ds} \right\|$

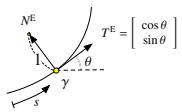

Frenet Frame : $\Phi^E = [T^E, N^E], \quad \frac{d\gamma}{ds} = T^E, \quad N^E = R(\frac{\pi}{2})T^E, \quad \|T^E\| = 1$

Frenet formula $\frac{d\Phi^E}{ds} = \Phi^E \begin{bmatrix} 0 & -\kappa \\ \kappa & 0 \end{bmatrix}, \quad \kappa = \frac{d\theta}{ds}$: curvature

$\frac{d}{ds} = \frac{d\theta}{ds}\frac{d}{d\theta} = \kappa \frac{d}{d\theta} = \frac{1}{q}\frac{d}{d\theta}, \quad q = \frac{1}{\kappa}$: curvature radius

LAC

$\rightarrow \frac{d^2\kappa}{ds^2} + (\alpha+1)\frac{1}{\kappa}\left(\frac{d\kappa}{ds}\right)^2 = 0$

$q^\alpha = as + b$

$\rightarrow \frac{d^2(q^\alpha)}{ds^2} = 0$

$\frac{d}{ds} = \frac{1}{q}\frac{d}{d\theta}$,

$\frac{d^2}{ds^2} = -\frac{1}{q^3}\frac{dq}{d\theta}\frac{d}{d\theta} + \frac{1}{q^2}\frac{d^2}{d\theta^2}$

Similarity Geometry = Klein geometry w.r.t. similarity transformation group (translation + roration + scale transformation)

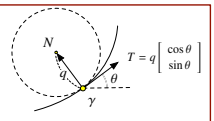

θ : angle function = similarity arc length

Similarity Frenet frame: $F = [T, N], \quad \frac{d\gamma}{d\theta} = T = \frac{1}{\kappa}T^E = qT^E, \quad N = R(\frac{\pi}{2})T$

Similarity Frenet formula: $\frac{dF}{d\theta} = F\begin{bmatrix} u & -1 \\ 1 & u \end{bmatrix}, \quad u = \frac{\kappa_s}{\kappa^2} = -\frac{q_\theta}{q}$: Similarity curvature

$\frac{d^2(q^a)}{d\theta^2} = 0, \quad a = \alpha - 1$

$q^a = \xi\theta + \eta$

$\rightarrow u = -\frac{\lambda}{a\lambda\theta + 1}$

$\rightarrow \frac{du}{d\theta} = au^2 + c$

Riccati equation

Shape Invariant Curve w.r.t. Integrable Deformation

Euclidean Geometry

$\frac{\partial\gamma}{\partial s} = T^E, \quad N^E = R(\frac{\pi}{2})T^E$

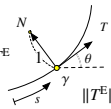

$\Phi^E = [T^E, N^E], \quad \|T^E\| = 1$

$\frac{\partial\Phi^E}{\partial s} = \Phi^E \begin{bmatrix} 0 & -\kappa \\ \kappa & 0 \end{bmatrix}, \quad \kappa = \frac{\partial\theta}{\partial s}$

Integrable Deformation t: deformation parameter

curve deformation: $\frac{\partial\gamma}{\partial t} = f(s,t)T^E + g(s,t)N^E$

compatibility: $\frac{\partial}{\partial t}\left(\frac{\partial\Phi^E}{\partial s}\right) = \frac{\partial}{\partial s}\left(\frac{\partial\Phi^E}{\partial t}\right)$

$\frac{\partial\Phi^E}{\partial t} = \Phi^E \begin{bmatrix} 0 & \kappa_{ss} + \frac{\kappa^3}{2} \\ -\kappa_{ss} - \frac{\kappa^3}{2} & 0 \end{bmatrix}, \quad f = -\frac{\kappa^2}{2}, \quad g = -\kappa_s$

Euler's elastic curve $\kappa'' + \frac{\kappa^3}{2} - \lambda\kappa = c_0$ $\leftarrow$ $X = s - \lambda t$ travelling wave ansatz $\leftarrow$ $\frac{\partial\kappa}{\partial t} + \frac{3}{2}\kappa^2\frac{\partial\kappa}{\partial s} + \frac{\partial^3\kappa}{\partial s^3} = 0$ modified KdV equation

Similarity Geometry

$\|T\| = q$

$\frac{\partial\gamma}{\partial\theta} = T, \quad N = R(\frac{\pi}{2})T$

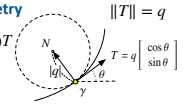

$F = [T, N], \quad \frac{\partial F}{\partial\theta} = F\begin{bmatrix} u & -1 \\ 1 & u \end{bmatrix}, \quad u = -\frac{q_\theta}{q}$

Integrable Deformation t: deformation parameter

curve deformation: $\frac{\partial\gamma}{\partial t} = f(\theta,t)T + g(\theta,t)N$

compatibility: $\frac{\partial}{\partial t}\left(\frac{\partial F}{\partial\theta}\right) = \frac{\partial}{\partial\theta}\left(\frac{\partial F}{\partial t}\right)$

$\frac{\partial F}{\partial t} = F\begin{bmatrix} -u_\theta + u^2 + 1 - bu & b \\ -b & -u_\theta + u^2 + 1 - bu \end{bmatrix} \quad f = b - u, \quad g = -1$

LAC $u' = au^2 + c$ $\leftarrow$ $u \rightarrow au$ $\quad u' = u^2 + c$ $\leftarrow$ $X = \theta + bt$ travelling wave ansatz $\rightarrow$ $\frac{\partial u}{\partial t} = \frac{\partial}{\partial\theta}\left(\frac{\partial u}{\partial\theta} - u^2 + bu\right)$ Burgers equation

Variational Formulation: Elastic Curves & LAC

Euler's Elastic Curves: Critical pt. of Elastic Energy

$E(\gamma) = \frac{1}{2}\int_{s_1}^{s_2} (\kappa^2 + \lambda)\, ds$ $\xrightarrow[\text{Euler-Lagrange equation}]{\text{Variation of Curve}}$ $\kappa'' + \frac{\kappa^3}{2} - \lambda\kappa = 0$

LAC: Critical pt. of Fairing Energy

$\mathcal{F}(\gamma) = \frac{1}{2}\int_{\theta_1}^{\theta_2} \left(a^2u^2 + \frac{\mu}{q^{2a}}\right) d\theta$ $\xrightarrow[\text{Euler-Lagrange eq.}]{\text{Variation of Curve}}$ $a\frac{du}{d\theta} - \frac{\mu}{q^{2a}} = 0, \quad u = -\frac{q_\theta}{q}$ $\leftrightarrow$ $\frac{d^2u}{d\theta^2} = 2au\frac{du}{d\theta}$ $\updownarrow$ $\frac{du}{d\theta} = au^2 + c$

Extension to Space Curves and Surfaces by Similarity Geometry

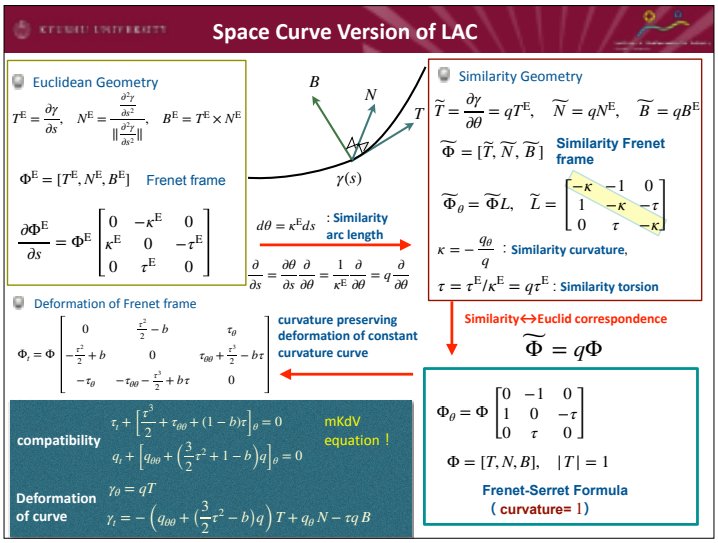

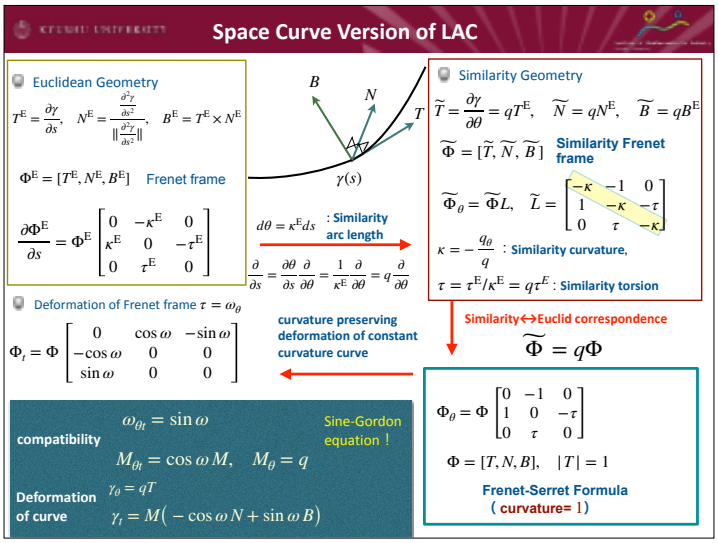

Space Curve Version of LAC

$\gamma_\theta = qT$, q : curvature radius, τ : similarity torsion

$$\tau_t + \left[\frac{\tau^3}{2} + \tau_{\theta\theta} + (1-b)\tau\right]_\theta = 0$$

$$q_t + \left[q_{\theta\theta} + \left(\frac{3}{2}\tau^2 + 1 - b\right)q\right]_\theta = 0$$

Travelling wave solution:

$$q(\theta,t) = q(X), \quad \tau(\theta,t) = \tau(X), \quad X = \theta - ct$$

$\frac{\partial}{\partial\theta} = \frac{d}{dX}$, $\frac{\partial}{\partial t} = -c\frac{d}{dX}$ Shape invariant curve w.r.t. integrable deformation

$$\left[\frac{\tau^3}{2} + \tau_{XX} + (1-b-c)\tau\right]_X = 0$$ Equation of Euler's elastic curve

$$\left[q_{XX} + \left(\frac{3}{2}\tau^2 + 1 - b - c\right)q\right]_X = 0$$ Lamé equation

Elliptic Function Solution

$$\tau = 2\xi\,\mathrm{dn}(\xi\theta+\eta,k),$$
$$q = q_1\,\mathrm{sn}(\xi\theta+\eta,k)\,\mathrm{cn}(\xi\theta+\eta,k),$$
$$1 - b - c = -\xi^2(2-k^2)$$

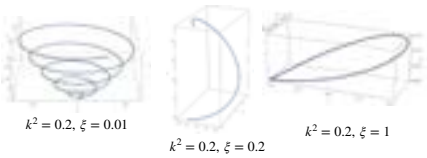

$k^2 = 0.2,\ \xi = 0.01$ $k^2 = 0.2,\ \xi = 0.2$ $k^2 = 0.2,\ \xi = 1$

Shape parameter: Slope α

$$\gamma_\theta = q^{1/a}T$$

slope α $(a = \alpha - 1)$

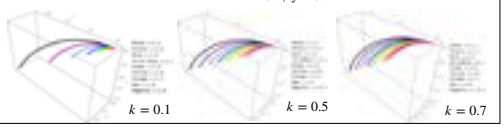

$k = 0.1$ $k = 0.5$ $k = 0.7$

Constant Torsion Curves and Surfaces

Equations for the frame

$$\Phi_\theta = \Phi\begin{bmatrix}0 & -1 & 0\\ 1 & 0 & -\tau\\ 0 & \tau & 0\end{bmatrix} \qquad \Phi_t = \Phi\begin{bmatrix}0 & \frac{\tau^2}{2}-b & \tau_\theta\\ -\frac{\tau^2}{2}+b & 0 & \tau_{\theta\theta}+\frac{\tau^3}{2}-b\tau\\ -\tau_\theta & -\tau_{\theta\theta}-\frac{\tau^3}{2}+b\tau & 0\end{bmatrix}$$

Compatibility

$$\left[q_{XX} + \left(\frac{3}{2}\tau^2 + 1 - b - c\right)q\right]_X = 0 \qquad \left[\frac{\tau^3}{2} + \tau_{XX} + (1-b-c)\tau\right]_X = 0$$

τ : const. $\left[\frac{\tau^3}{2} + \tau_{XX} + (1-b-c)\tau\right]_X = 0 \longrightarrow$ trivial

$$q_{XX} + \sigma^2 q = 0 \qquad \sigma^2 = \frac{3}{2}\tau^2 + 1 - b - c$$

$$\Phi_\theta = \Phi\begin{bmatrix}0 & -1 & 0\\ 1 & 0 & -\tau\\ 0 & \tau & 0\end{bmatrix}$$
$$\Phi_t = \Phi\left(-\frac{\tau^2}{2}+b\right)\begin{bmatrix}0 & -1 & 0\\ 1 & 0 & -\tau\\ 0 & \tau & 0\end{bmatrix}$$

$\longrightarrow$ $\Phi(\theta,t) = \Phi(Z)$, $Z = \theta + \left(-\frac{\tau^2}{2}+b\right)t$ $\longrightarrow$

$$\Phi = \frac{1}{\omega}\begin{bmatrix}\cos\omega Z & -\omega\sin\omega Z & -\tau\cos\omega Z\\ \sin\omega Z & \omega\cos\omega Z & -\tau\sin\omega Z\\ \tau & 0 & 1\end{bmatrix} \quad \begin{matrix}T & N & B\end{matrix}$$

$\omega^2 = 1 + \tau^2$

$\sigma^2 = 0$

$$q = c_1\left(X + \frac{1}{\lambda}\right) \longrightarrow \gamma = \frac{c_1}{\omega^3}\begin{bmatrix}\cos\omega Z + \omega\left(X+\frac{1}{\lambda}\right)\sin\omega Z\\ \sin\omega Z - \omega\left(X+\frac{1}{\lambda}\right)\cos\omega Z\\ \frac{\tau\omega^2}{2}\left(X+\frac{1}{\lambda}\right)^2\end{bmatrix} \xrightarrow[\omega\to 1]{\tau\to 0} c_1\begin{bmatrix}\cos Z + \left(X+\frac{1}{\lambda}\right)\sin Z\\ \sin Z - \left(X+\frac{1}{\lambda}\right)\cos Z\\ 0\end{bmatrix}$$ circle involute

Direct extension of LAC

$$\gamma_3 = \frac{\tau\omega^3}{2c_1}(\gamma_1^2+\gamma_2^2) - \frac{c_1\tau}{2\omega^3}$$ paraboloid

$$\begin{cases}X = \theta + (b-1)t,\\ Z = \theta + bt\end{cases}$$

$\sigma^2 > 0$: ellipsoid or one-sheet hyperboloid $\sigma^2 < 0$: two-sheed hyperboloid

Surfaces Generated from Constant Torsion Curves

Sphere Ellipsoid 1 Ellipsoid 2

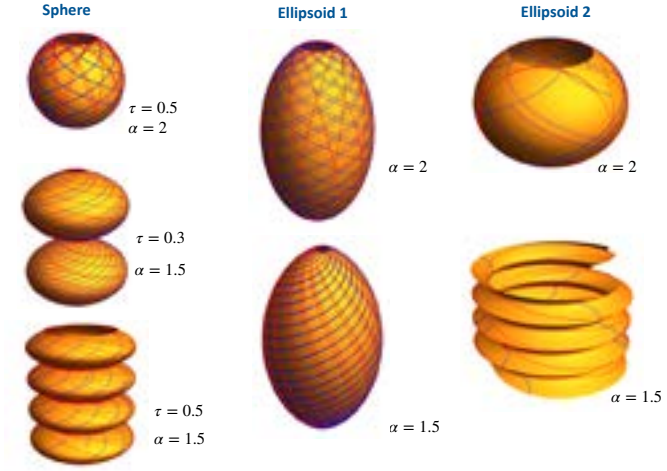

$\tau = 0.5$, $\alpha = 2$ $\alpha = 2$ $\alpha = 2$

$\tau = 0.3$, $\alpha = 1.5$

$\tau = 0.5$, $\alpha = 1.5$ $\alpha = 1.5$ $\alpha = 1.5$

Surfaces Generated from Constant Torsion Curves

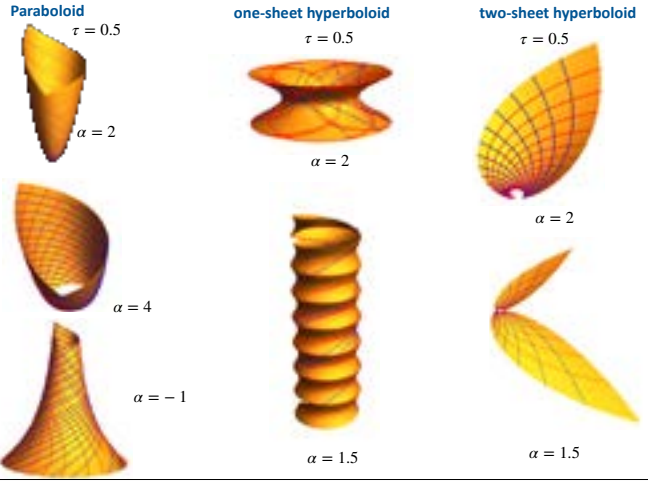

Similarity Pseudospherical Surface

$\Phi = [T, N, B] \in SO(3)$

$$\Phi_\theta = \Phi \begin{bmatrix} 0 & -1 & 0 \\ 1 & 0 & -\tau \\ 0 & \tau & 0 \end{bmatrix} \longrightarrow \begin{aligned} T_\theta &= N, \\ N_\theta &= -T + \tau B, \\ B_\theta &= -\tau N \end{aligned}$$

$$\Phi_t = \Phi \begin{bmatrix} 0 & \cos\omega & -\sin\omega \\ -\cos\omega & 0 & 0 \\ \sin\omega & 0 & 0 \end{bmatrix}$$

$$\gamma_\theta = qT,$$
$$\omega_{\theta t} = \sin\omega,$$
$$M_{\theta t} = \cos\omega\, M$$
$$\tau = \omega_\theta, \quad q = M_\theta$$

Specialization: $q = \tau_\theta \to M = \omega_\theta$

$M_{\theta t} = \cos\omega\, M \longrightarrow \omega_{\theta\theta t} = (\cos\omega)\,\omega_\theta$

$\longrightarrow \boxed{(\omega_{\theta t} - \sin\omega)_\theta = 0}$

consistent!

Integration of tangent vector:

$$\gamma_\theta = \omega_{\theta\theta} T = (\omega_\theta T)_\theta - \omega_\theta T_\theta$$
$$= (\omega_\theta T)_\theta - \omega_\theta N = (\omega_\theta T)_\theta + B_\theta$$
$$= (\omega_\theta T + B)_\theta$$

integration! $\longrightarrow \boxed{\gamma = \omega_\theta T + B}$

Similarity Pseudospherical Surface

Relation with Pseudospherical Surface $\Phi = [T, N, B] \in SO(3)$

$$\Phi_\theta = \Phi \begin{bmatrix} 0 & -1 & 0 \\ 1 & 0 & -\omega_\theta \\ 0 & \omega_\theta & 0 \end{bmatrix} \quad \Phi_t = \Phi \begin{bmatrix} 0 & \cos\omega & -\sin\omega \\ -\cos\omega & 0 & 0 \\ \sin\omega & 0 & 0 \end{bmatrix}, \quad \gamma = \omega_\theta T + B$$

$[T, N, B] = [-\overline{C}, \overline{B}, \overline{A}]$

Gauss-Weingarten equation for pseudospherical surfaces!

$$[\overline{A}, \overline{B}, \overline{C}]_\theta = [\overline{A}, \overline{B}, \overline{C}] \begin{bmatrix} 0 & \omega_u & 0 \\ -\omega_u & 0 & -1 \\ 0 & 1 & 0 \end{bmatrix}, \quad [\overline{A}, \overline{B}, \overline{C}]_t = [\overline{A}, \overline{B}, \overline{C}] \begin{bmatrix} 0 & 0 & -\sin\omega \\ 0 & 0 & \cos\omega \\ \sin\omega & -\cos\omega & 0 \end{bmatrix}$$

$\overline{R} = \overline{R}(\theta, t)$: position vector of the surface,
θ, t : arc length along asymptotic lines

$$\overline{A} = \overline{R}_\theta,$$
$$\overline{B} = -\overline{R}_\theta \times \overline{N} = \frac{\overline{R}_\theta}{\sin\omega} - \frac{\overline{R}_t}{\tan\omega}$$
$$\overline{C} = \overline{N}$$

Similarity Pseudospherical Surface

$$\boxed{\gamma = \overline{R}_\theta - \omega_\theta \overline{N}}$$

Gallery : Similarity Pseudospherical Surfaces


Breather Surface (1)


Breather Surface (2)


Kuen Surface


Pseudosphere

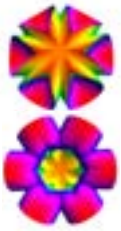
Similarity Breather Surface (1)


Similarity Breather Surface(2)

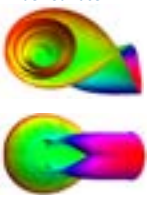
Similarity Kuen Surface

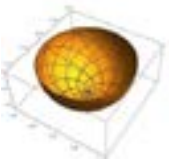
Similarity Pseudosphere

Self-Affinity of Aesthetic Curves

"Aesthetic Curves" and Self-Affinity (1)

Analysis of "Aesthetic Curves" and Verbalization (Harada-Mori-Sugiyama, 1995)

$\gamma(s)$: planar curve with monotonic curvature (s: arc length, s_{all}: total arc length)

Logarithmic Curvature Distribution (LCD)

"Aesthetic curves" have a common property:
the logarithmic curvature distribution becomes linear → "Monotonic Rhythm Curves"

- Divide the values of the curvature radius ρ into small intervals $\overline{\rho}_i$
- $\overline{s}_i$: length of subcurves with curvature radius in the interval $\overline{\rho}_i$
- Log-Log graph of the histogram of $\overline{s}_i/s_{\mathrm{all}}$ vs $\overline{\rho}_i/s_{\mathrm{all}}$:
  "**Logarithmic curvature distribution**"

Horizonatal axis: $\log(\overline{\rho}_i/s_{\mathrm{all}})$, **Vertical axis** : $\log(\overline{s}_i/s_{\mathrm{all}})$

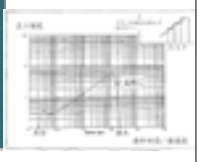

Weber-Fechner's Law: (perception) ∝ log (stimulus)

"Aesthetic Curves" and Self-Affinity (2)

Verbalization (Harada-Mori-Sugiyama, 1995)

monotonic rhythm curves			complex rhythm curves	
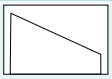	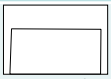		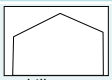	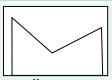
divergent type negative "slope"	constant speed type zero "slope"	convergent type positive "slope"	hill type positive & negative slope	valley type negative & positive slope
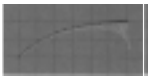		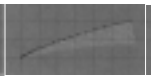		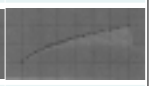
・sharp ・energetic	・stable ・static	・curve with pause ・centripetal	divergent curve changing into convergent at some point	convergent curve changing into divergent at some point

Logarithmic Curvature Graph and LAC (Nakano et al 2003, Miura 2005)

Continuum Limit of LCD: **Logarithmic curvature graph:** $(X, Y) = \left(\log \rho, \log \left| \frac{ds}{d \log \rho} \right| \right)$

Logarithmic curvature graph is a line with slope $\alpha \rightarrow \rho^{\alpha} = c_0 s + c_1$: LAC

Harada's Self-Affinity

Self-Affinity of "Aesthetic Curves" (Harada-Mori-Sugiyama 1995)

‣ **Harada's Self-Affinity for monotonic rhythm curves** *(Harada's original definition)* :

- For a given curve, cut it at arbitrary two points to get a subcurve
- Extend the subcurve in both **horizontal** and **vertical** directions with arbitrary scales
- The obtained curve coincides with the original curve by applying affine transformation

‣ **Harada's Self-Affinity (HSA) for monotonic rhythm curves** :

- $\gamma(s) : [0,1] \rightarrow \mathbb{C}$: planar curve
- For an arbitrary subinterval $[s_0, s_1] \in [0,1]$, there exist a reparametrization $t(s) : [0,1] \rightarrow [s_0, s_1]$ and an affine map $F \in \mathrm{Aff}(\mathbb{C})$ such that $\gamma(s) = F\gamma(t(s))$

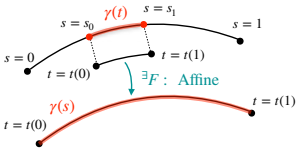

Harada's Claim

‣ Monotonic rhythm curves possess the HSA

Miura's Self-Affinity

‣ **Miura's Self-affinity for LAC** (*Miura's original definition*) :

- For a given curve, cut it at arbitrary two points to get a subcurve
- Extend the subcurve in both **tangential** and **normal** directions with arbitrary scales
- With a suitable reparametrization, the obtained curve coincides with the original curve with a suitable parameter shift.

‣ **Miura's Self-Affinity for LAC** :

- $\gamma(s) : [0,1] \rightarrow \mathbb{C}$: planar curve, $\rho(s)$: curvature radius, s : arc length
- There exist a reparametrization $t(s) : [0,1] \rightarrow [0,1]$ and $\mu(\epsilon), \nu(\epsilon) > 0$ such that for any $\epsilon > 0$, $\rho(t+\epsilon) = \mu(\epsilon)\rho(t)$, $ds(t+\epsilon) = \nu(\epsilon)\, ds(t)$

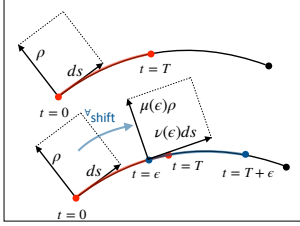

Theorem (Miura 2006, Kumagai - K 2024)

‣ A planar curve possesses **Miura's self-affinity**
↔ The curve is a circle, a line or **a LAC**

Harada's Self-Affinity

Self-Affinity of "Aesthetic Curves" (Harada-Mori-Sugiyama 1995)

- **Harada's Self-Affinity for monotonic rhythm curves *(Harada's original definition)*:**
  - For a given curve, cut it at arbitrary two points to get a subcurve
  - Extend the subcurve in both **horizontal** and **vertical** directions with arbitrary scales
  - The obtained curve coincides with the original curve by applying affine transformation

- **Harada's Self-Affinity (HSA) for monotonic rhythm curves:**
  - $\gamma(s) : [0,1] \to \mathbb{C}$: planar curve
  - For an arbitrary subinterval $[s_0, s_1] \in [0,1]$, there exist a reparametrization $t(s) : [0,1] \to [s_0, s_1]$ and an affine map $F \in \mathrm{Aff}(\mathbb{C})$ such that $\gamma(s) = F\gamma(t(s))$

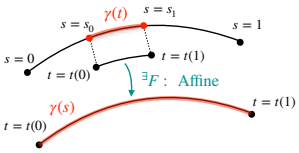

Harada's Claim

- Monotonic rhythm curves possess the HSA

Theorem (Kumagai - K, 2024)

- A planar curve possesses the HSA
  ↔ The curve is a line, or a ***parabola***

Harada's Self-Affinity (2)

Parabola has the HSA

$$\gamma(s) = \begin{bmatrix} s \\ s^2 \end{bmatrix}, \quad s \in [0,1]$$

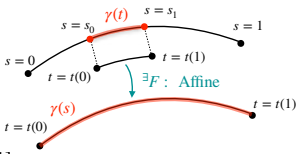

$$0 \le {}^{\forall}s_0 < {}^{\forall}s_1 \le 1, \quad t(s) = (s_1 - s_0)s + s_0, \quad s \in [0,1]$$

$$\longrightarrow \quad t \in [s_0, s_1], \quad s_0 = t(0), \quad s_1 = t(1)$$

Trivial identity: $t^2 = \left((s_1 - s_0)s + s_0\right)^2 = (s_1 - s_0)^2 s^2 + 2s_0(s_1 - s_0)s + s_0^2$

$$\begin{bmatrix} t \\ t^2 \end{bmatrix} = \begin{bmatrix} s_1 - s_0 & 0 \\ 2s_0(s_1 - s_0) & (s_1 - s_0)^2 \end{bmatrix} \begin{bmatrix} s \\ s^2 \end{bmatrix} + \begin{bmatrix} s_0 \\ s_0^2 \end{bmatrix}$$

or:

$$\begin{bmatrix} s \\ s^2 \end{bmatrix} = \begin{bmatrix} -\frac{1}{s_1 - s_0} & 0 \\ -\frac{2s_0}{(s_1 - s_0)^2} & 1 \end{bmatrix} \begin{bmatrix} t - s_0 \\ t^2 - s_0^2 \end{bmatrix}$$

$\longrightarrow$ $\gamma(s)$ has the HSA!

Equiaffine Geometry

Theorem (Miura 2006, Kumagai - K 2024)

- A planar curve possesses **Miura's self-affinity**
  ↔ The curve is a circle, a line or **a LAC**

Theorem (Kumagai - K, 2024)

- A planar curve possesses **Harada's self-affinity**
  ↔ The curve is a line, or **a parabola**

Similarity geometry:

$\mathbf{p} \mapsto rA\mathbf{p} + \mathbf{b}, \quad r \in \mathbb{R}, A \in \mathbf{SO}(2), \mathbf{b} \in \mathbb{R}^2 \quad \kappa^{\mathrm{Sim}} = -\frac{q_\theta}{q}$

circle: $\kappa^{\mathrm{Sim}} = 0$

line: $\kappa^{\mathrm{Sim}} = \infty$

logarithmic spiral: $\kappa^{\mathrm{Sim}} = \mathrm{const.}$

Equiaffine geometry:

$\mathbf{p} \mapsto A\mathbf{p} + \mathbf{b}, \quad A \in \mathbf{SL}(2,\mathbb{R}), \mathbf{b} \in \mathbb{R}^2$

parabola: $\kappa^{\mathrm{SA}} = 0$

line: $\kappa^{\mathrm{SA}} = \infty$

ellipse: $\kappa^{\mathrm{SA}} = \mathrm{const.} > 0$

hyperbola: $\kappa^{\mathrm{SA}} = \mathrm{const.} < 0$

Equiaffine geometry:

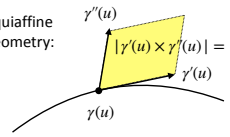

t: arbitrary parameter s.t. $|\gamma_t \times \gamma_{tt}| \neq 0$

$\longrightarrow$ $u = \int |\gamma_t \times \gamma_{tt}|^{\frac{1}{3}} dt$ "equiaffine arc length"

$\Phi^{\mathrm{SA}}(u) = [\gamma_u, \gamma_{uu}]$ equiaffine Frenet frame

$\Phi'(u) = \Phi(u) \begin{bmatrix} 0 & -\kappa^{\mathrm{SA}} \\ 1 & 0 \end{bmatrix}$ equiaffine Frenet formula

κ^{SA} : equiaffine curvature

$$\kappa^{\mathrm{SA}} = \frac{\gamma_{uuu}}{\gamma_{uu}} = \kappa^{\frac{4}{3}} + \frac{1}{3}\kappa^{-\frac{5}{3}}\kappa_{ss} - \frac{5}{9}\kappa^{-\frac{8}{3}}\kappa_s^2$$

Extendable Self-Affinity

- **Extendable Self-affinity** *(rough outline)* :
  - For a given curve, cut it at arbitrary two points to get a subcurve
  - Apply a suitable reparametrization, and then arbitrary parameter shift by $\epsilon > 0$
  - Then the obtained curve coincides with a certain affine map of the original subcurve.

- **Extendable Self-affinity** :
  - $\gamma(u) : [0,1] \to \mathbb{C}$: planar curve (in equiaffine geometry: u = equiaffine arc length)
  - There exist a reparametrization $t(u) : [0,1] \to [0,1]$ and an affine map $F_\epsilon \in \mathrm{Aff}(\mathbb{C})$ such that for any $\epsilon > 0$, $\gamma(t+\epsilon) = F_\epsilon \gamma(t)$

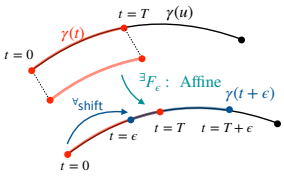

Theorem (Kumagai - K, 2024)

- Choosing $t = u$, then a planar curve posesses ESA
  $\leftrightarrow$ The curve is **a parabola, or an ellipse or a hyperbola**
- For general t, a planar curve possesses ESA
  $\leftrightarrow \kappa^{\mathrm{SA}} = (\xi u + \eta)^{-2}, \quad \xi, \eta \in \mathbb{R}$
  $\leftrightarrow$ the curve is either of the following :
  (i) $y = x^\alpha, e^x$
  (ii) $y = x \log x$
  (iii) logarithmic spiral

New Class of Curves with ESA in Equiaffine Geometry

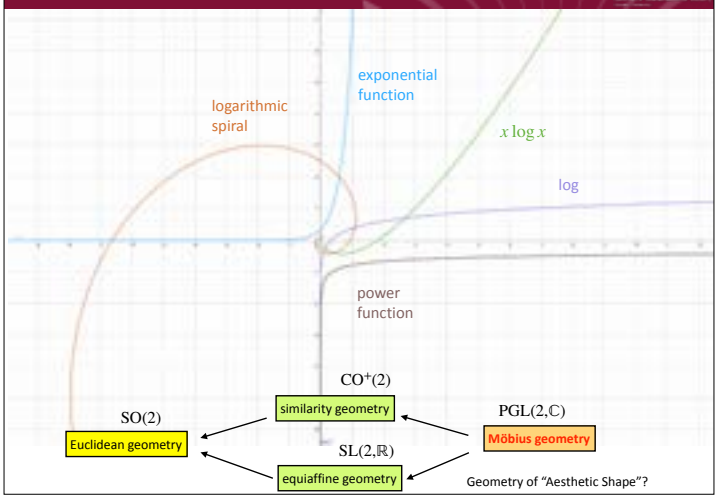

Geometry of Michell-Prager structures and hanging membranes

Yoshiki Jikumaru
Faculty of Information Networking for Innovation And Design, Toyo University, Japan
Kentaro Hayakawa
Department of Conceptual Design, College of Industrial Technology, Nihon University, Japan
Kazuki Hayashi
Department of Architecture and Architectural Engineering, Graduate School of Engineering, Kyoto University, Japan
Kenji Kajiwara
Institute of Mathematics for Industry, Kyushu University, Japan
Yohei Yokosuka
Department of Architecture and Architectural Engineering, Kagoshima University, Japan

Abstract

In this talk, we introduce some geometric objects motivated by the structures in architectural design. In the first part, we focus on so-called Michell-Prager-type structures. This is joint work with Yohei Yokosuka, Kazuki Hayashi, Kentaro Hayakawa, and Kenji Kajiwara [1]. Considering a quadrilateral mesh with such a structure on its diagonals, we can obtain the privileged discrete isothermic surfaces introduced by Bobenko and Pinkall. Their mechanical properties can be derived from the result by Schief. We also introduce the relation with the discrete log-aesthetic curves proposed in [3]. In the second part, we introduce the geometry of hanging membranes. This is joint work with Yohei Yokosuka [2]. We formulate the hanging membranes according to the classical shell membrane theory. Remarkably, the in-plane equilibrium condition can be characterized by the existence of a Combescure transformation of the membrane.

References

[1] K. Hayashi, Y. Jikumaru, Y. Yokosuka, K. Hayakawa and K, Kajiwara, Parametric generation of optimal structures through discrete exponential functions: unveiling connections between structural optimality and discrete isothermicity. Struct. Multidisc. Optim. **67** 41 (2024). https://doi.org/10.1007/s00158-024-03767-1.

[2] Y. Jikumaru and Y. Yokosuka, Differential geometric formulation of hanging membranes: shell membrane theory and variational principle, Int. J. Math. Ind. **14** (2022), https://doi.org/10.1142/S2661335222500046.

[3] J. Inoguchi, K. Kajiwara, K. T. Miura, Y. Jikumaru and W. K. Schief, Log-aesthetic curves: similarity geometry, integrable discretization and variational principles, Comput. Aided Geom. Design **105**(2023) 102233, https://doi.org/10.1016/j.cagd.2023.10223.

Information Networking for Innovation And Design

Geometry of Michell-Prager type structures and Hanging membranes

CREST ED3GE International Conference

Yoshiki Jikumaru (Toyo University)

Collaborators: Kazuki Hayashi (Kyoto University), Yohei Yokosuka (Kagoshima University), Kentaro Hayakawa (Nihon University), Kenji Kajiwara (Kyushu University)

INIAD, Toyo University

March 11th, 2025

Purpose of this talk

In this talk, we introduce (mini) examples of

Mathematics Motivated by Architectural Design.

They consist of the following contents:

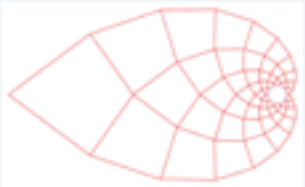

Figure: Michell-Prager type structures and discrete isothermic surfaces

Figure: Formulation of Hanging membranes

Part1: Michell-Prager type structure

References

- K. Hayashi, Y. Jikumaru, Y. Yokosuka, K. Hayakawa and K. Kajiwara, Parametric generation of optimal structures through discrete exponential functions: unveiling connections between structural optimality and discrete isothermicity, *Struct. Multidisc. Optim.* 67, 41 (2024). https://doi.org/10.1007/s00158-024-03767-1
- J. Inoguchi, Y. Jikumaru, K. Kajiwara, K.-T. Miura, W. K. Schief, Log-aesthetic curves: Similarity geometry, integrable discretization and variational principles, *Comput. Aided Geom. Des.*, 105 (2023), 102233.

Michell-Prager structures

Michell structures

The "optimal" structure when B is fixed and the load F acts on point A.

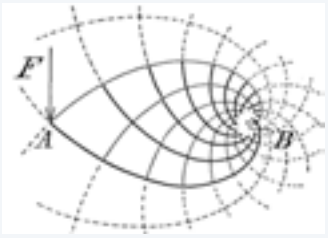

(a) Michell structure (1904)

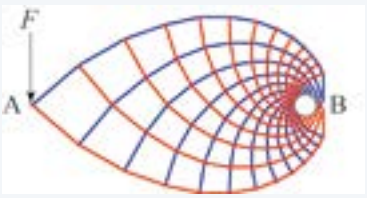

(b) Acting Compression, Tension

A characteristic property of the structure

A "well-known" property

There exists a constant C_0, for every bar member e, we have

$$(\text{Axial force acting on } e) \times (\text{Length of } e) = C_0.$$

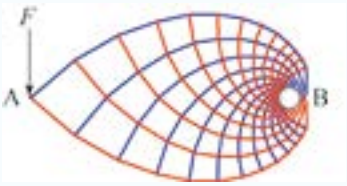

A characteristic property of the structure

We will consider a class of truss structures that have this property in general:

$$(\text{Axial force acting on } e) \times (\text{Length of } e) = C_0.$$

We call such a structure as Michell-Prager type structure.

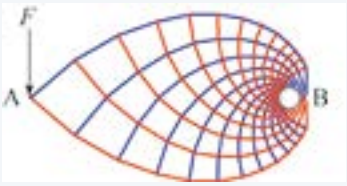

Variational principle

We introduce the signature for each member:

$$q(e) = \begin{cases} +1 & e \text{ is a horizontal edge,} \\ -1 & e \text{ is a vertical edge.} \end{cases}$$

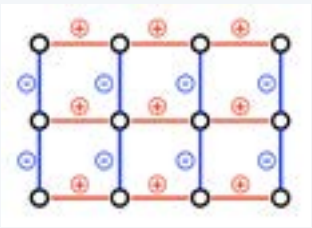

Figure: Definition of the signature q

In discrete differential geometry, q is called P-labelling.

Variational principle

Proposition

Let us consider the following objective functional:

$$E = C_0 \sum_e q(e) \log |e|.$$

Then, in the equilibrium structure, the axial forces satisfying the following relation can be introduced:

$$(\text{Axial force acting on } e) \times (\text{Length of } e) = C_0.$$

- How to find the functional: the “prestressed cable-net structures”.
- An example of discrete holomorphic quadratic differential? (Kenyon-Lam, 2019)
- Q. Relation with discrete harmonic functions?

A relation with discrete differential geometry

It is convenient to consider an “imaginary (dotted) mesh” like the following:

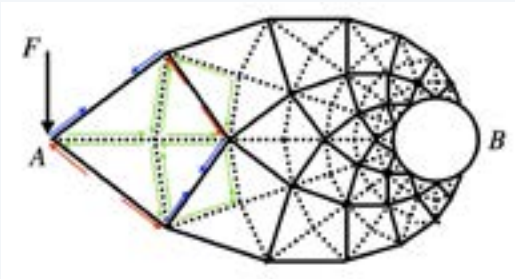

A relation with discrete differential geometry

Moreover, we introduce the following labelling:

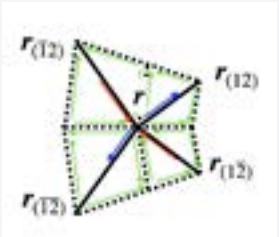

Figure: form diagram

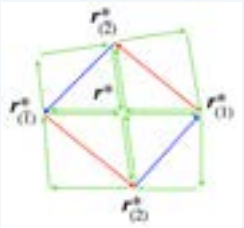

Figure: force diagram

Then, the defining equation for Michell-Prager type structures becomes:

$$\|\boldsymbol{r}_{(12)} - \boldsymbol{r}\| \cdot \|\boldsymbol{r}^*_{(2)} - \boldsymbol{r}^*_{(1)}\| = C_0. \tag{1}$$

A relation with discrete isothermic net

Michell-Prager condition:

$$\|\boldsymbol{r}_{(12)} - \boldsymbol{r}\| \cdot \|\boldsymbol{r}^*_{(2)} - \boldsymbol{r}^*_{(1)}\| = C_0. \tag{2}$$

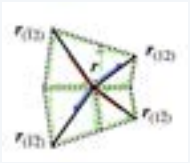

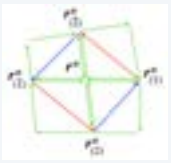

Theorem (Bobenko-Suris, 2009)

If the quad mesh $\boldsymbol{r}$ constitute discrete isothermic net (constant cross ratio), then there exists a constant C_0 such that

$$\|\boldsymbol{r}_{(12)} - \boldsymbol{r}\| \cdot \|\boldsymbol{r}^*_{(2)} - \boldsymbol{r}^*_{(1)}\| = C_0. \tag{3}$$

Remark: The constant C_0 is determined from the cross-ratio condition.

“Pure shear” stress distribution

Theorem (Schief, 2014)

Assume purely tangential forces acting on each edge of the circular net $\boldsymbol{r}$.
Then the quad mesh $\boldsymbol{r}$ is in equilibrium $\iff$ $\boldsymbol{r}$ constitutes a discrete isothermic net.
Moreover, the Christoffel dual $\boldsymbol{r}^*$ corresponds to the “force diagram”.

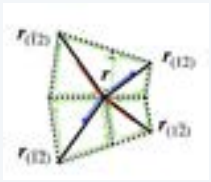

Figure: form diagram

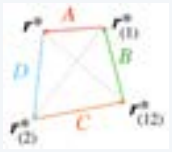

Figure: force diagram

Therefore, we can generate structures from discrete isothermic nets!

Examples of the structure

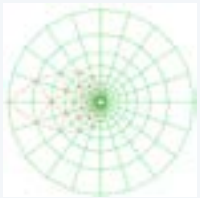

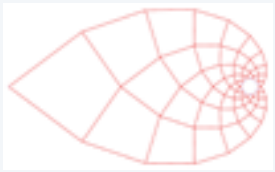

Figure: A structure from discrete exponential function.

A trivial but “Interesting” Property

The discrete curves are discrete log-aesthetic curves (dLAC of slope 1, log-spiral).

Q. dLACs (governed by Riccati type eqn) are consistent with cross-ratio equation???

Non-trivial example: discrete power functions

A discrete analogue of the function $z^{2/3}$:

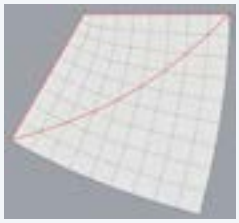

Figure: Force diagram

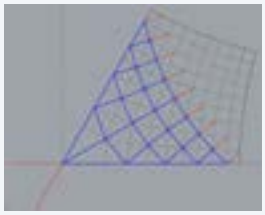

Figure: Form diagram

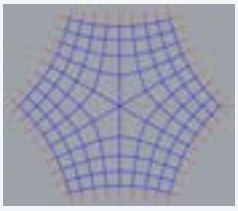

Figure: Form diagram

- In the Christoffel dual $z^{4/3}$, take a closed curve.
- Red vectors are loading or boundary reaction forces acting on blue structure.

General problem (open)

In summary, we can propose a mathematical problem for shape generation:

General problem (open)

1. Find a suitable "boundary", consistent with the cross-ratio equation, which corresponds to the external force and the boundary reaction force.
2. Find the "internal mesh" for a given boundary, and take the Christoffel dual. By taking the diagonals of the dual, we have the Michell-Prager type structure.
3. From the variational point of view, for a given boundary, find the mesh that gives the critical point of the functional $\sum_e q(e) \log |e|$. (Interestingly, a similar problem is discussed in Kenyon-Lam (2019).)

Part 2: Hanging membranes

In this part...

We introduce:

- A shell membrane theoretic formulation of hanging membranes.
- Our formulation is based on the assumption "stress lines = curvature lines".
- In-plane equilibrium $\Longleftrightarrow$ existence of another surface (Combescure transform), which is similar to the theory of membrane 0 surfaces.
- Variational principles.

Reference:

Y. Jikumaru and Y. Yokosuka, Differential geometric formulation of hanging membranes: Shell membrane theory and variational principle, Int. J. Math. Ind. **14**(01) 2250004 (2022).

Background 1 (Hooke's observation)

A model of hanging chain by Robert Hooke (1635–1703):

"Theorem" (Robert Hooke, 1676)

An ideal compression-only geometry for a rigid arch can be obtained by:

abcccddeeeeefggiiiiiiiillmmmmnnnnnooprrsssttttttuuuuuuuux.

Note: The anagram in No. 3

ceiiinosssttuu

is called Hooke's law:

ut tensio, sic vis
(as the extension, so the force).

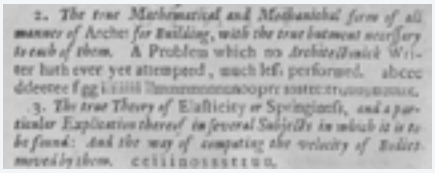
2. The true Mathematical and Mechanical form of all manner of Arches for Building, with the true Botment necessary to each of them. A Problem which no Architect or Writer hath ever yet attempted, much less performed. abcccddeeeeefggiiiiiiiillmmmmnnnnnooprrsssttttttuuuuuuuux.
3. The true Theory of Elasticity or Springiness, and a particular Explication thereof in several Subjects in which it is to be found: and the way of computing the velocity of Bodies moved by them. ceiiinosssttuu.

Figure: Hooke's article in 1676.

Background 1 (Hooke's observation)

The solution of the anagram (Richard Waller, 1705)

Ut pendet continuum flexile, sic stabit contiguum rigidum inversum.
(As hangs the flexible line, so but inverted will stand the rigid arch.)

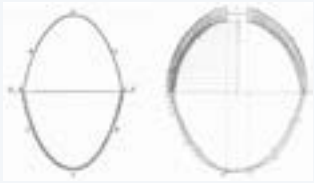

(a) A sketch by Giovanni Poleni (1748)

(b) Gateway arch (Missouri, St. Louis)

Background 2 (Gaudi and Isler's hanging model)

Hanging models by Antoni Gaudi (1852–1926):

(a) Antoni Gaudi (1878)

(b) Sagrada Familia

(c) The model by Gaudi (Gaudi Museum)

Hanging models by Heinz Isler (1926–2009):

(a) A model by Heinz Isler

(b) Gas station in Deitingen (Switzerland)

Background 3 (Previous researches)

Previous researches

1. Hanging membranes (with special symmetry):
   Novozhilov (1964), Brew-Lewis (2007).
2. Thrust Network Analysis: Block-Ochsendorf (2007).
   $\rightarrow$ Graphic statics (horizontal, J. C. Maxwell (1867)),
   $+$ Force density method (vertical, H.-J. Schek (1974)).
3. Relation with isotropic geometry:
   Vouga-Höbinger-Wallner-Pottmann (2012).
4. Singular minimal surfaces:
   Böhme-Hildebrandt-Tausch (1980), U. Dierkes (2003), R. Lopéz (2018).

Notations from classical surface theory

Let $\boldsymbol{r} = \boldsymbol{r}(x, y)$ be a surface (patch) in $\mathbb{R}^3$.
$\boldsymbol{r} = \boldsymbol{r}(x, y)$: the model of the middle surface of a shell membrane.
Assume that the coordinates (x, y) are the curvature line coordinates.
In this case, the 1st and 2nd fundamental forms are given by

$$I = A_1^2\,dx^2 + A_2^2\,dy^2, \quad II = \kappa_1 A_1^2\,dx^2 + \kappa_2 A_2^2\,dy^2. \tag{4}$$

Denote

$$\boldsymbol{r}_x = A_1\boldsymbol{e}_1, \quad \boldsymbol{r}_y = A_2\boldsymbol{e}_2, \quad \boldsymbol{N} = \boldsymbol{e}_1 \times \boldsymbol{e}_2, \tag{5}$$

that is, $\boldsymbol{e}_1$ and $\boldsymbol{e}_2$ are the unit tangent vectors
and $\boldsymbol{N}$ is the unit normal on the surface.

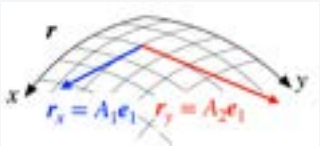

Combescure transformation

Definition (Combescure, 1867)

If the functions $\overline{A}_1$ and $\overline{A}_2$ satisfy the relations

$$\frac{(A_1)_y}{A_2} = \frac{(\overline{A}_1)_y}{\overline{A}_2}, \quad \frac{(A_2)_x}{A_1} = \frac{(\overline{A}_2)_x}{\overline{A}_1}, \tag{6}$$

then there exists a surface $\overline{\boldsymbol{r}}$ given by the relations

$$\overline{\boldsymbol{r}}_x = \overline{A}_1\boldsymbol{e}_1, \quad \overline{\boldsymbol{r}}_y = \overline{A}\boldsymbol{e}_2. \tag{7}$$

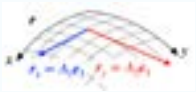

In particular, $\boldsymbol{r}_x \parallel \overline{\boldsymbol{r}}_x$ and $\boldsymbol{r}_y \parallel \overline{\boldsymbol{r}}_y$ at corresponding points.
The surface $\overline{\boldsymbol{r}}$ is called the Combescure transformation of $\boldsymbol{r}$.

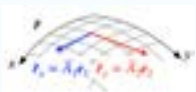

The equilibrium equation

The equilibrium condition for a membrane with "stress line = curvature line":

$$\begin{aligned}(A_2T_1)_x - (A_2)_xT_2 + \langle \boldsymbol{q}, \boldsymbol{e}_1\rangle A_1A_2 &= 0,\\ (A_1T_2)_y - (A_1)_yT_1 + \langle \boldsymbol{q}, \boldsymbol{e}_2\rangle A_1A_2 &= 0,\\ \kappa_1T_1 + \kappa_2T_2 + \langle \boldsymbol{q}, \boldsymbol{N}\rangle &= 0,\end{aligned} \tag{8}$$

where

- $\langle \cdot, \cdot \rangle$: the standard inner product in $\mathbb{R}^3$.
- T_1, T_2: normal stress (resultants) along x- and y-coordinate lines, respectively.
- $\boldsymbol{q}$: the load (vector) acting on the unit area of the membrane.
  In this talk, you can assume the vertical load (self-weight).
- We call in-plane equilibrium and out-of-plane equilibrium conditions, resp.

Existence of the Combescure transformation

The equilibrium condition for a membrane with "stress line = curvature line":

$$\begin{aligned}(A_2T_1)_x - (A_2)_xT_2 + \langle \boldsymbol{q}, \boldsymbol{e}_1\rangle A_1A_2 &= 0,\\ (A_1T_2)_y - (A_1)_yT_1 + \langle \boldsymbol{q}, \boldsymbol{e}_2\rangle A_1A_2 &= 0,\\ \kappa_1T_1 + \kappa_2T_2 + \langle \boldsymbol{q}, \boldsymbol{N}\rangle &= 0.\end{aligned} \tag{9}$$

In this case, we denote

$$\overline{A}_1 = A_1(T_2 + \langle \boldsymbol{q}, \boldsymbol{r}\rangle), \quad \overline{A}_2 = A_2(T_1 + \langle \boldsymbol{q}, \boldsymbol{r}\rangle). \tag{10}$$

Then, if we assume $\boldsymbol{q}$ is constant vector (e.g., self-weight), we can verify

$$\frac{(\overline{A}_1)_y}{\overline{A}_2} = \frac{(A_1)_y}{A_2}, \quad \frac{(\overline{A}_2)_x}{\overline{A}_1} = \frac{(A_2)_x}{A_1}, \tag{11}$$

that is, in-plane equilibrium condition $\iff$ $^\exists$ Combescure transformation $\overline{\boldsymbol{r}}$!

A similarity with membrane 0 surfaces

If $\langle \boldsymbol{q}, \boldsymbol{r}\rangle \approx 0$, that is, for a "shallow shell", we have

$$\overline{A}_1 = A_1T_2, \quad \overline{A}_2 = A_2T_1, \tag{12}$$

and the out-of-plane equilibrium condition becomes the "bilinear form":

$$\begin{pmatrix} H_\circ & A_1 & \overline{A}_1\end{pmatrix}\begin{pmatrix}0 & 0 & 1\\ 0 & q_n & 0\\ 1 & 0 & 0\end{pmatrix}\begin{pmatrix}K_\circ\\ A_2\\ \overline{A}_2\end{pmatrix} = 0, \tag{13}$$

where $q_n = \langle \boldsymbol{q}, \boldsymbol{N}\rangle$ is the normal loading.

Theorem (Rogers-Schief, 2003)

If q_n is constant, the surfaces $\boldsymbol{r}$, $\overline{\boldsymbol{r}}$, $\boldsymbol{N}$ constitute "membrane 0 surfaces".

Remark: the assumption "shallow" is not necessary in Rogers-Schief theory.

Hanging membranes of "symmetric" case

Theorem

For constants λ, b, we assume the relations

$$T_1 + \langle \boldsymbol{q}, \boldsymbol{r} \rangle = \lambda \kappa_2 - b, \quad T_2 + \langle \boldsymbol{q}, \boldsymbol{r} \rangle = \lambda \kappa_1 - b. \tag{14}$$

Then the in-plane equilibrium equation becomes "trivial (Mainardi-Codazzi eqn)". Moreover, the out-of-plane equilibrium equation gives the constraint

$$2\lambda \mathcal{K} - 2\mathcal{H}(\langle \boldsymbol{q}, \boldsymbol{r} \rangle + b) + \langle \boldsymbol{q}, \boldsymbol{N} \rangle = 0, \tag{15}$$

where we put $\mathcal{K} = \kappa_1 \kappa_2$ (Gaussian curvature) and $\mathcal{H} = (\kappa_1 + \kappa_2)/2$ (mean curvature).

If $\lambda = 0$, we have $T_1 = T_2 = -(\langle \boldsymbol{q}, \boldsymbol{r} \rangle + b)$ (known as "singular minimal" surfaces).

Variational principle

Theorem

Define the functional E as follows (λ, b: constants):

$$E(\boldsymbol{r}) = \int_\Sigma (-2\lambda \mathcal{H} + \langle \boldsymbol{q}, \boldsymbol{r} \rangle + b)\, dA. \tag{16}$$

Then, the first variation of E (for boundary-fixed variations) is given by:

$$\delta E = \int_\Sigma (2\lambda \mathcal{K} - 2\mathcal{H}(\langle \boldsymbol{q}, \boldsymbol{r} \rangle + b) + \langle \boldsymbol{q}, \boldsymbol{N} \rangle) \langle \delta \boldsymbol{r}, \boldsymbol{N} \rangle\, dA. \tag{17}$$

The Euler-Lagrange equation gives the out-of-plane equation.

Note: if $\lambda = 0$, then E becomes the gravity under the area constraint condition (discussed in Koiso-Palmer (2005)).

Problems for shape generation

Problems

- Can we generate various shapes using the "form diagram $\boldsymbol{r}$" and "force diagram $\overline{\boldsymbol{r}}$ (Combescure transform)" as Airy stress functions???
- Can we construct the variational principle in a general case?
- Can we discretize these formulations with "interesting" mathematics?

Figure: Examples of "discrete hanging membranes" by circular net.

A summary of this talk

In this talk, we introduced (mini) examples of

Mathematics Motivated by Architectural Design.

They consisted of the following contents:

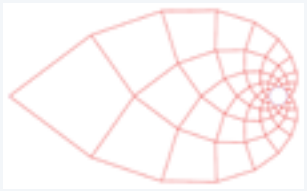

Figure: Michell-Prager type structures and discrete isothermic surfaces

Figure: Formulation of Hanging membranes

Discretization of quadrics and of elliptic coordinates

Yuri B. Suris
Institut für Mathematik, Technische Universität Berlin, Germany

Abstract

In this talk, I will review a recently found discretization of classical elliptic coordinate systems. These systems became prominent after Jacobi used them for integrating several famous problems of classical mechanics, including the two centers problem and the geodesics on an ellipsoid. A structure preserving discretization of these coordinate systems remained open for a long time and was finally tackled in Refs. [1, 2]. I will closely follow the history of this discovery. On the first step [1], a construction based on an integrable discretization of the Euler-Poisson-Darbox equation was used. The coordinate functions of the resulting discrete nets are given in terms of gamma functions. These nets enjoy separability property, their two-dimensional subnets being Koenigs nets with an additional novel discrete analog of the orthogonality property (thus, discrete isothermic, in a sense). On the second step [2], the novel orthogonality concept was put at the very basis of a more general construction. The latter is geometric, via polarity with respect to a sequence of classical confocal quadrics. The coordinate functions of discrete confocal quadrics were computed explicitly. This opens the possibility to close the cycle of historic development by applying discrete elliptic coordinate systems to discretize corresponding problems in classical mechanics in the structure preserving fashion.

References

[1] A.I. Bobenko, W. Schief, Yu.B. Suris, J. Techter. On a discretization of confocal quadrics. I. An integrable systems approach. *J. Integrable Systems*, 2016, **1**, No. 1, xyw005, 34 pp.

[2] A.I. Bobenko, W. Schief, Yu.B. Suris, J. Techter. On a discretization of confocal quadrics. II. A geometric approach to general parametrizations. *Internat. Math. Research Notices*, 2020, **2020**, No. 24, 10180-10230.

Discretization of quadrics and of elliptic coordinates

Yuri B. Suris

(Technische Universität Berlin)

Evolving Design and Discrete Differential Geometry
- towards Mathematics Aided Geometric Design,
Fukuoka, 11.03.2025

Plan

Part 1: Discretizing equations. Based on:

A.I. Bobenko, W. Schief, Yu.B. Suris, J. Techter. On a discretization of confocal quadrics. I. An integrable systems approach. *J. Integrable Systems*, 2016, 1, No. 1, xyw005, 34 pp.

Part 2: Discretizing geometry. Based on:

A.I. Bobenko, W. Schief, Yu.B. Suris, J. Techter. On a discretization of confocal quadrics. II. A geometric approach to general parametrizations. *Internat. Math. Research Notices*, 2020, No. 24, 10180-10230.

Part 1: Discretizing equations

Confocal quadrics

One-parameter family of quadrics: for given $a_1 > \dots > a_N > 0$,

$$\mathcal{Q}_\lambda = \left\{ \boldsymbol{x} = (x_1, \dots, x_N) \in \mathbb{R}^N : \sum_{k=1}^{N} \frac{x_k^2}{a_k + \lambda} = 1 \right\}, \quad \lambda \in \mathbb{R}.$$

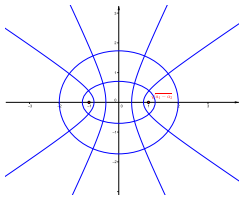

Confocal coordinates

For a given point $\boldsymbol{x} \in \mathbb{R}^N$ with $x_1 x_2 \dots x_N \neq 0$, equation $\sum_{k=1}^{N} x_k^2/(a_k + \lambda) = 1$ for λ has N real roots $u_1, \dots, u_N$ in

$$\mathcal{U} = \{ \boldsymbol{u} \in \mathbb{R}^N : -a_1 < u_1 < -a_2 < u_2 < \dots < -a_N < u_N \}.$$

They correspond to the N confocal quadrics that intersect at $\boldsymbol{x}$:

$$\sum_{k=1}^{N} \frac{x_k^2}{a_k + u_i} = 1, \quad i = 1, \dots, N \quad \Leftrightarrow \quad \boldsymbol{x} \in \bigcap_{i=1}^{N} Q_{u_i}.$$

The coordinates $(u_1, \dots, u_N)$ are called *confocal coordinates* (or *elliptic coordinates*, following Jacobi (1826)).
Expression of x_k^2 through $u_1, \dots, u_N$:

$$x_k^2 = \frac{\prod_{i=1}^{N} (u_i + a_k)}{\prod_{i \neq k} (a_k - a_i)}, \quad k = 1, \dots, N$$

(defines x_k up to sign).

Example: $N = 2$

$$x_1 = \frac{\sqrt{a_1 + u_1}\sqrt{a_1 + u_2}}{\sqrt{a_1 - a_2}}, \quad x_2 = \frac{\sqrt{-(a_2 + u_1)}\sqrt{a_2 + u_2}}{\sqrt{a_1 - a_2}}.$$

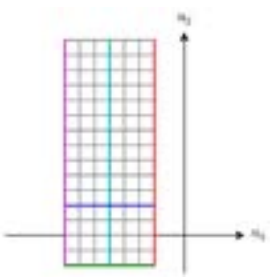

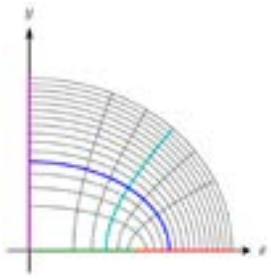

General properties

- The net $\boldsymbol{x} : \mathcal{U} \to \mathbb{R}^N_+$ satisfies the Euler-Poisson-Darboux system

$$\frac{\partial^2 \boldsymbol{x}}{\partial u_i \partial u_j} = \frac{\gamma}{u_i - u_j}\left(\frac{\partial \boldsymbol{x}}{\partial u_j} - \frac{\partial \boldsymbol{x}}{\partial u_i}\right) \qquad (\mathrm{EPD}_\gamma)$$

  with $\gamma = \frac{1}{2}$. All two-dimensional coordinate surfaces of $\boldsymbol{x}$ are Koenigs nets.
- The net $\boldsymbol{x} : \mathcal{U} \to \mathbb{R}^N_+$ is orthogonal:

$$\left\langle \frac{\partial \boldsymbol{x}}{\partial u_i}, \frac{\partial \boldsymbol{x}}{\partial u_j} \right\rangle = 0.$$

  All two-dimensional coordinate surfaces of $\boldsymbol{x}$ are curvature line parametrized.

All two-dimensional coordinate surfaces of $\boldsymbol{x}$ are isothermic.

Characterization

Theorem. Confocal coordinates $\boldsymbol{x} : \mathcal{U} \to \mathbb{R}^N_+$ are *characterized* by the following properties:

- All $x_k : \mathcal{U} \to \mathbb{R}_+$ $(k = 1, \dots, N)$ are separable solutions of (EPD_γ) with $\gamma = \frac{1}{2}$ satisfying boundary conditions

$$\lim_{u_k \searrow (-a_k)} x_k(u_1, \dots, u_N) = 0 \quad \text{for} \quad k = 1, \dots, N,$$
$$\lim_{u_{k-1} \nearrow (-a_k)} x_k(u_1, \dots, u_N) = 0 \quad \text{for} \quad k = 2, \dots, N.$$

- The net $\boldsymbol{x} : \mathcal{U} \to \mathbb{R}^N_+$ is orthogonal:

$$\left\langle \frac{\partial \boldsymbol{x}}{\partial u_i}, \frac{\partial \boldsymbol{x}}{\partial u_j} \right\rangle = 0.$$

Discrete Euler-Poisson-Darboux equation

An integrable discretization of (EPD_γ):

$$\Delta_i \Delta_j \boldsymbol{x} = \frac{\gamma}{n_i + \epsilon_i - n_j - \epsilon_j}(\Delta_j \boldsymbol{x} - \Delta_i \boldsymbol{x}). \qquad (\mathrm{dEPD}_\gamma)$$

Introduced by Konopelchenko-Schief (2014).

Integrable in the sense of multidimensional consistency.

All two-dimensional subnets are Koenigs.

Discrete confocal coordinates

Definition. For $\alpha_1, \dots, \alpha_N \in \mathbb{Z}$ with $\alpha_1 > \alpha_2 > \dots > \alpha_N > 0$, set

$$\mathcal{U} = \mathbb{Z}^N \cap U, \quad \mathcal{U}^* = (\mathbb{Z}^*)^N \cap U,$$

where $\mathbb{Z}^* = \mathbb{Z} + \frac{1}{2}$ and

$$U = \{\boldsymbol{u} \in \mathbb{R}^N : -\alpha_1 \le u_1 \le -\alpha_2 \le u_2 \le \dots \le -\alpha_N \le u_N\},$$

Discrete confocal coordinate system is a net $\boldsymbol{x} : \mathcal{U} \cup \mathcal{U}^* \to \mathbb{R}^N_+$ such that

- all $x_k : \mathcal{U} \to \mathbb{R}_+$ $(k = 1, \dots, N)$ are separable solutions of (dEPD$_\gamma$) with $\gamma = \frac{1}{2}$, satisfying boundary conditions

$$x_k|_{n_k = -\alpha_k} = 0 \quad \text{for} \quad k = 1, \dots, N,$$
$$x_k|_{n_{k-1} = -\alpha_k} = 0 \quad \text{for} \quad k = 2, \dots, N;$$

- all $x_k : \mathcal{U}^* \to \mathbb{R}_+$ $(k = 1, \dots, N)$ are separable solutions of (dEPD$_\gamma$) with $\gamma = \frac{1}{2}$ given by the same formulas as $x_k : \mathcal{U} \to \mathbb{R}_+$, extended to $\mathcal{U}^*$;

Discrete confocal coordinates

and

- the net $\boldsymbol{x}$ is *orthogonal* in the sense that each edge of $\boldsymbol{x}(\mathcal{U}^*)$ is orthogonal to the dual facet of $\boldsymbol{x}(\mathcal{U})$ (and vice versa).

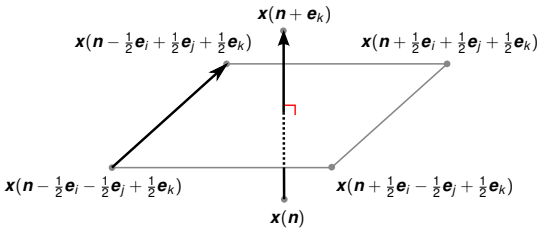

Explicit formulas

Discrete confocal coordinate systems are given by

$$x_k(n_1, \dots, n_N) = D_k \prod_{i<k} (-n_i - \alpha_k - \tfrac{k-i}{2} + \tfrac{1}{2})_{1/2} \prod_{i \ge k} (n_i + \alpha_k + \tfrac{k-i}{2})_{1/2},$$

where the *discrete square root function* is defined by

$$(u)_{1/2} = \frac{\Gamma(u + \frac{1}{2})}{\Gamma(u)},$$

and

$$D_k^{-1} = \prod_{i<k} \sqrt{\alpha_i - \alpha_k + \tfrac{i-k}{2}} \cdot \prod_{i>k} \sqrt{\alpha_k - \alpha_i + \tfrac{k-i}{2}}.$$

Example: $N = 2$

Discrete elliptic coordinates in the plane:

$$x_1(\boldsymbol{n}) = \frac{(n_1+\alpha_1)_{1/2}(n_2+\alpha_2-\frac{1}{2})_{1/2}}{\sqrt{\alpha_1-\alpha_2-\frac{1}{2}}},$$

$$x_2(\boldsymbol{n}) = \frac{(-n_1-\alpha_2)_{1/2}(n_2+\alpha_2)_{1/2}}{\sqrt{\alpha_1-\alpha_2-\frac{1}{2}}},$$

where

$$n_1, n_2 \in \tfrac{1}{2}\mathbb{Z}.$$

Example: $N = 2$ ($\alpha_1 = 5$, $\alpha_2 = 1$)

$$\boldsymbol{x} : (\tfrac{1}{2}\mathbb{Z})^2 \cap U \to \mathbb{R}^2_+$$

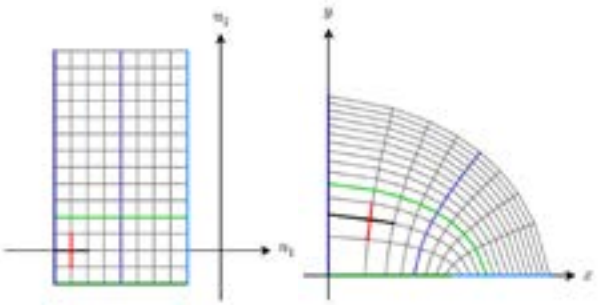

Example: $N = 2$ ($\alpha_1 = 5$, $\alpha_2 = 1$)

On two dual sublattices: $\boldsymbol{x} : (\mathbb{Z}^2 \cup (\mathbb{Z}^*)^2) \cap U \to \mathbb{R}^2_+$

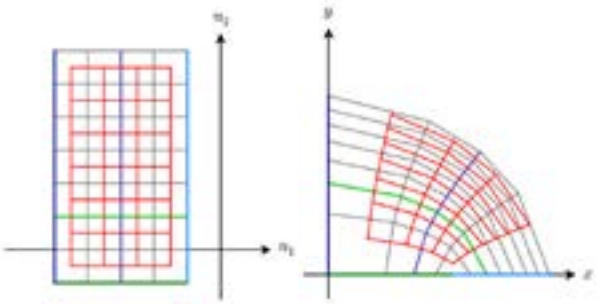

Example: $N = 3$ ($\alpha_1 = 4$, $\alpha_2 = 2$, $\alpha_3 = 0$)

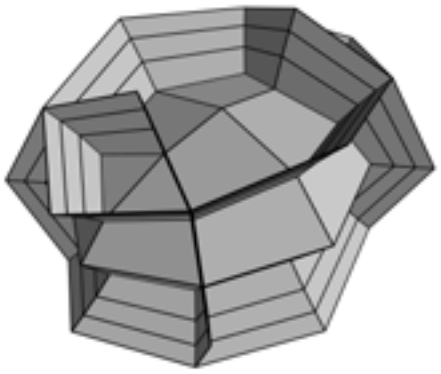

Example: $N = 3$ ($\alpha_1 = 20$, $\alpha_2 = 10$, $\alpha_3 = 0$)

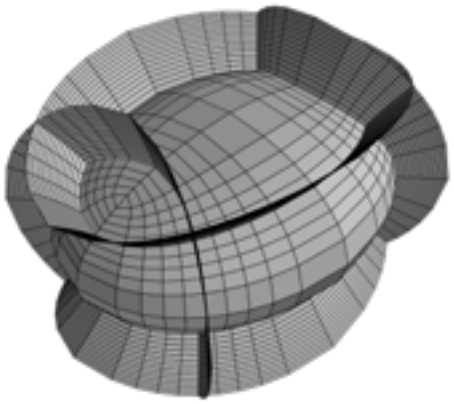

Part 2: Discretizing geometry in arbitrary parametrization

Re-parametrizations

Useful to achieve single-valuedness and periodicity of the functions involved.

Example $N = 2$: in

$$x_1 = \frac{\sqrt{a_1 + u_1}\sqrt{a_1 + u_2}}{\sqrt{a_1 - a_2}}, \quad x_2 = \frac{\sqrt{-(a_2 + u_1)}\sqrt{a_2 + u_2}}{\sqrt{a_1 - a_2}}$$

set

$$u_1 = -a_1 \sin^2 s_1 - a_2 \cos^2 s_1, \quad u_2 = a_1 \sinh^2 s_2 - a_2 \cosh^2 s_2,$$

then

$$x_1 = \sqrt{a_1 - a_2}\, \cos s_1 \cosh s_2, \quad x_2 = \sqrt{a_1 - a_2}\, \sin s_1 \sinh s_2.$$

Example. $N = 2$

Classical elliptic coordinate system in the plane in terms of trigonometric/hyperbolic functions with $a_1 = 2$, $a_2 = 1$:

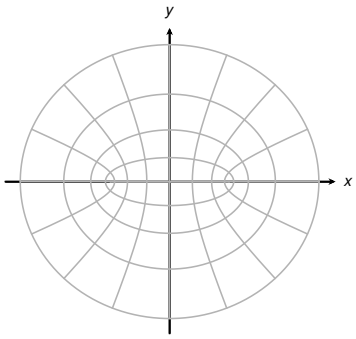

Fundamental restriction of DDG

For functions of a discrete variable, there is no natural notion of re-parametrization!

To find natural discrete analogs of confocal coordinates in arbitrary parametrization, need new ideas.

The main idea: a novel characterization of confocal coordinates, not based on (EPD$_\gamma$) in a special parametrization.

Novel characterization of confocal coordinates

Theorem. If a coordinate system $\boldsymbol{x} : \mathbb{R}^N \supset U \to \mathbb{R}^N$ satisfies two conditions:

i) $\boldsymbol{x}(\boldsymbol{s})$ *factorizes*, in the sense that

$$\begin{cases} x_1(\boldsymbol{s}) = f_1^1(s_1) f_2^1(s_2) \cdots f_N^1(s_N), \\ x_2(\boldsymbol{s}) = f_1^2(s_1) f_2^2(s_2) \cdots f_N^2(s_N), \\ \dots \\ x_N(\boldsymbol{s}) = f_1^N(s_1) f_2^N(s_2) \cdots f_N^N(s_N), \end{cases}$$

with all $f_i^k(s_i) \neq 0$ and $\left(f_i^k\right)'(s_i) \neq 0$;

ii) $\boldsymbol{x}$ is *orthogonal*, that is,

$$\langle \partial_i \boldsymbol{x}, \partial_j \boldsymbol{x} \rangle = 0 \quad \textit{for} \quad i \neq j,$$

then all coordinate hypersurfaces are confocal quadrics.

Discrete confocal coordinates

As often in DDG, we turn a smooth theorem into a discrete definition.

Definition. A discrete coordinate system $\boldsymbol{x} : \left(\frac{1}{2}\mathbb{Z}\right)^N \supset \mathcal{U} \to \mathbb{R}^N$ is called *a discrete confocal coordinate system* if it satisfies two conditions:

i) $\boldsymbol{x}(\boldsymbol{n})$ *factorizes*, in the sense that for any $\boldsymbol{n} \in \mathcal{U}$

$$\begin{cases} x_1(\boldsymbol{n}) = f_1^1(n_1) f_2^1(n_2) \cdots f_N^1(n_N), \\ x_2(\boldsymbol{n}) = f_1^2(n_1) f_2^2(n_2) \cdots f_N^2(n_N), \\ \dots \\ x_N(\boldsymbol{n}) = f_1^N(n_1) f_2^N(n_2) \cdots f_N^N(n_N), \end{cases}$$

with all $f_i^k(n_i) \neq 0$ and $\bar{\Delta} f_i^k(n_i) = f_i^k(n_i) - f_i^k(n_i - 1) \neq 0$;

ii) $\boldsymbol{x}$ is *discrete orthogonal* in the above sense.

Reminder: discrete orthogonality

Recall that we call a net $\boldsymbol{x}$ is *orthogonal* if, for each edge $[\boldsymbol{n}, \boldsymbol{n} + \boldsymbol{e}_k]$, all 2^{N-1} vertices of the dual facet,

$$\boldsymbol{x}(\boldsymbol{n} + \tfrac{1}{2}\boldsymbol{\sigma}) \quad \textit{for all} \quad \boldsymbol{\sigma} = (\sigma_1, \dots, \sigma_N) \in \{\pm 1\}^N \quad \textit{with} \quad \sigma_k = 1,$$

lie in a hyperplane orthogonal to the line $(\boldsymbol{x}(\boldsymbol{n}), \boldsymbol{x}(\boldsymbol{n} + \boldsymbol{e}_k))$:

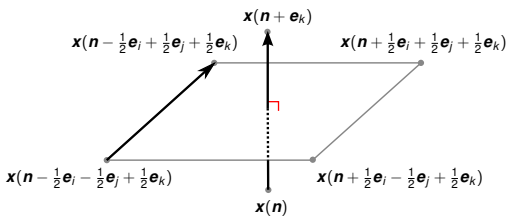

Discretization of confocal quadrics equation

Theorem. For a discrete confocal coordinate system, there exist N real numbers a_k, $1 \le k \le N$, and N sequences $u_i : \frac{1}{2}\mathbb{Z} + \frac{1}{4} \to \mathbb{R}$ such that the following equations are satisfied for any $\boldsymbol{n} \in \mathcal{U}$ and for any $\boldsymbol{\sigma} \in \{\pm 1\}^N$:

$$\sum_{k=1}^{N} \frac{x_k(\boldsymbol{n}) x_k(\boldsymbol{n} + \frac{1}{2}\boldsymbol{\sigma})}{a_k + u_i} = 1, \quad u_i = u_i(n_i + \tfrac{1}{4}\sigma_i), \quad i = 1, \dots, N.$$

Equivalently,

$$x_k(\boldsymbol{n}) x_k(\boldsymbol{n} + \tfrac{1}{2}\boldsymbol{\sigma}) = \frac{\prod_{j=1}^{N}(u_j + a_k)}{\prod_{j \ne k}(a_k - a_j)}, \quad u_j = u_j(n_j + \tfrac{1}{4}\sigma_j), \quad k = 1, \dots, N.$$

Converse statement

Theorem. For given sequences $u_i : \frac{1}{2}\mathbb{Z} + \frac{1}{4} \to \mathbb{R}$, $1 \le i \le N$, consider functions $f_i^k(n_i)$ as solutions of the respective difference equations

$$f_i^k(n_i) f_i^k(n_i + \tfrac{1}{2}) = \begin{cases} u_i(n_i + \frac{1}{4}) + a_k, & k \le i, \\ -\big(u_i(n_i + \frac{1}{4}) + a_k\big), & k > i. \end{cases}$$

The functions f_i^k, $k = 1, \dots, N$ are defined uniquely by prescribing their values at one point. Then, $\boldsymbol{x}$ defined by

$$x_k(\boldsymbol{n}) = \frac{\prod_{j=1}^{N} f_j^k(n_j)}{\prod_{i=1}^{k-1} \sqrt{a_i - a_k} \prod_{i=k+1}^{N} \sqrt{a_k - a_i}}, \quad k = 1, \dots, N$$

constitutes a discrete confocal coordinate system.

Geometric interpretation

The main formula

$$\sum_{k=1}^{N} \frac{x_k(\boldsymbol{n}) x_k(\boldsymbol{n} + \frac{1}{2}\boldsymbol{\sigma})}{a_k + u_i} = 1, \quad u_i = u_i(n_i + \tfrac{1}{4}\sigma_i), \quad i = 1, \dots, N,$$

admits a remarkable geometric interpretation:

the point $\boldsymbol{x}(\boldsymbol{n} + \frac{1}{2}\boldsymbol{\sigma})$ lies in the intersection of the polar hyperplanes of $\boldsymbol{x}(\boldsymbol{n})$ with respect to the (smooth) confocal quadrics $Q(u_i)$, $i = 1, \dots, N$:

$$\boldsymbol{x}(\boldsymbol{n} + \tfrac{1}{2}\boldsymbol{\sigma}) = \bigcap_{i=1}^{N} Pol_{Q(u_i)}(\boldsymbol{x}(\boldsymbol{n})), \quad u_i = u_i(n_i + \tfrac{1}{4}\sigma_i).$$

Geometric construction

Input data.

- N sequences of quadrics of the confocal family is chosen, with the parameters

$$u_i : \left(\tfrac{1}{2}\mathbb{Z} + \tfrac{1}{4}\right) \cap \mathcal{I}_i \to \mathbb{R},$$

  indexed by $n_i + \frac{1}{4} \in \mathcal{I}_i$, where $n_i \in \frac{1}{2}\mathbb{Z}$. Let $\mathcal{V}$, $\mathcal{V}^*$ be the parts of the respective lattices $\mathbb{Z}^N$, $(\mathbb{Z} + \frac{1}{2})^N$ lying in the region $\prod_{i=1}^N \mathcal{I}_i$.
- An arbitrary point $\boldsymbol{x}(\boldsymbol{n}_0)$ for $\boldsymbol{n}_0 \in \mathcal{V} \cup \mathcal{V}^*$.

Recurrent construction

Suppose that $\boldsymbol{x}(\boldsymbol{n}) = \boldsymbol{x}$ is already known. Then for any neighboring vertex of the dual sublattice,

$$\boldsymbol{n}^* = \boldsymbol{n} + \tfrac{1}{2}\boldsymbol{\sigma}, \quad \boldsymbol{\sigma} = (\sigma_1, \dots, \sigma_N), \quad \sigma_i = \pm 1,$$

the point $\boldsymbol{x}(\boldsymbol{n}^*) = \boldsymbol{x}^*$ is constructed as the intersection of N polar hyperplanes

$$\boldsymbol{x}^* := \bigcap_{i=1}^{N} Pol_{Q(u_i)}(\boldsymbol{x}), \quad u_i = u_i(n_i + \tfrac{1}{4}\sigma_i).$$

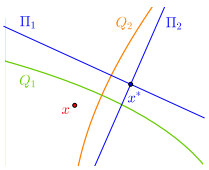

Origin of discrete orthogonality

Lemma. Let Π be a hyperplane. Then the poles of Π with respect to all quadrics of the confocal family lie on a line ℓ. This line ℓ is orthogonal to Π.

Example $N = 2$: if P_2 is related to P_1 via polarity in two confocal conics, that is, $\Pi = Pol_{Q_1}(P_1)$ and $P_2 = Pol_{Q_2}(\Pi)$, then the line through P_1 and P_2 is orthogonal to Π.

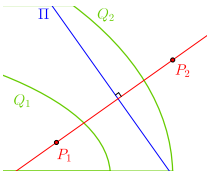

Example: $N = 2$

Discrete elliptic coordinates in the plane, in terms of triginometric/hyperbolic functions:

$$x_1(\boldsymbol{n}) = \sqrt{\frac{a_1 - a_2}{\cos(\frac{\delta_1}{2})\cosh(\frac{\delta_2}{2})}}\cos(\delta_1 n_1)\cosh(\delta_2 n_2),$$

$$x_2(\boldsymbol{n}) = \sqrt{\frac{a_1 - a_2}{\cos(\frac{\delta_1}{2})\cosh(\frac{\delta_2}{2})}}\sin(\delta_1 n_1)\sinh(\delta_2 n_2).$$

Example: $N = 2$ ($a_1 = 2$, $a_2 = 1$, $\delta_1 = \delta_2 = \frac{2\pi}{m}$, $m = 8$)

$$\boldsymbol{x} : \left(\tfrac{1}{2}\mathbb{Z}\right)^2 \to \mathbb{R}^2$$

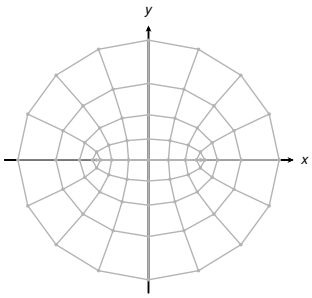

Example: $N = 2$ ($a_1 = 2$, $a_2 = 1$, $\delta_1 = \delta_2 = \frac{2\pi}{m}$, $m = 8$)

Two pairs of dual orthogonal sublattices:

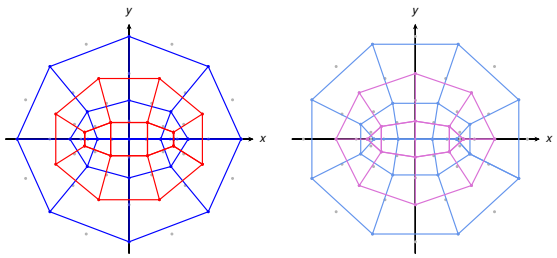

Left: Sublattice on $\mathbb{Z}^2$ in blue and on $\left(\mathbb{Z} + \frac{1}{2}\right)^2$ in red.
Right: Sublattice on $\mathbb{Z} \times (\mathbb{Z} + \frac{1}{2})$ in blue and on $(\mathbb{Z} + \frac{1}{2}) \times \mathbb{Z}$ in pink.

Example: $N = 3$, smooth confocal coordinates

Elliptic coordinates in the 3D space, in terms of elliptic functions:

$$\begin{pmatrix} x_1 \\ x_2 \\ x_3 \end{pmatrix} = \sqrt{a_1 - a_3} \begin{pmatrix} \mathrm{sn}(s_1, k_1)\,\mathrm{dn}(s_2, k_2)\,\mathrm{ns}(s_3, k_3) \\ \mathrm{cn}(s_1, k_1)\,\mathrm{cn}(s_2, k_2)\,\mathrm{ds}(s_3, k_3) \\ \mathrm{dn}(s_1, k_1)\,\mathrm{sn}(s_2, k_2)\,\mathrm{cs}(s_3, k_3) \end{pmatrix},$$

where

$$k_1^2 = k_3^2 = \frac{a_1 - a_2}{a_1 - a_3}, \quad k_2^2 = \frac{a_2 - a_3}{a_1 - a_3} = 1 - k_1^2.$$

Example: $N = 3$, $a_1 = 8$, $a_2 = 4$, $a_3 = 0$

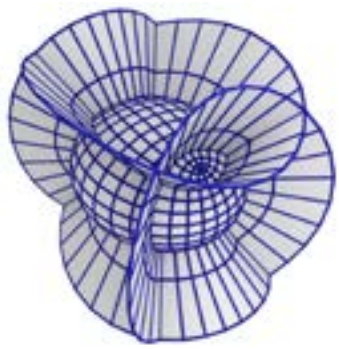

Example: $N = 3$, discrete confocal coordinates

Discrete elliptic coordinates $\boldsymbol{x} : \left(\frac{1}{2}\mathbb{Z}\right)^3 \to \mathbb{R}^3$ in terms of elliptic functions:

$$\begin{aligned} x_1(\boldsymbol{n}) &= \alpha_1\alpha_2\alpha_3\,\mathrm{sn}(\delta_1 n_1, k_1)\,\mathrm{dn}(\delta_2 n_2, k_2)\,\mathrm{ns}(\delta_3 n_3, k_3), \\ x_2(\boldsymbol{n}) &= \beta_1\beta_2\beta_3\,\mathrm{cn}(\delta_1 n_1, k_1)\,\mathrm{cn}(\delta_2 n_2, k_2)\,\mathrm{ds}(\delta_3 n_3, k_3), \\ x_3(\boldsymbol{n}) &= \gamma_1\gamma_2\gamma_3\,\mathrm{dn}(\delta_1 n_1, k_1)\,\mathrm{sn}(\delta_2 n_2, k_2)\,\mathrm{cs}(\delta_3 n_3, k_3), \end{aligned}$$

where the moduli k_1, k_2, k_3 are defined as solutions of the following transcendental equations:

$$k_1^2 = \frac{a_1 - a_2}{a_1 - a_3} \cdot \frac{\mathrm{dn}^2(\frac{\delta_1}{2}, k_1)}{\mathrm{cn}^2(\frac{\delta_1}{2}, k_1)}, \quad k_2^2 = \frac{a_2 - a_3}{a_1 - a_3} \cdot \frac{\mathrm{dn}^2(\frac{\delta_2}{2}, k_2)}{\mathrm{cn}^2(\frac{\delta_2}{2}, k_2)}.$$

$$k_3^2 = \frac{a_1 - a_2}{a_1 - a_3} \cdot \frac{\mathrm{dn}^2(\frac{\delta_3}{2}, k_3)}{\mathrm{cn}^2(\frac{\delta_3}{2}, k_3)}.$$

Example: $N = 3$ ($a_1 = 8$, $a_2 = 4$, $a_3 = 0$, $\delta_i = \mathrm{K}(k_i)/4$)

Discrete quadrics from the pair of dual orthogonal sublattices $\mathbb{Z}^3$ and $\left(\mathbb{Z} + \frac{1}{2}\right)^3$ are shown in blue and red respectively:

- two two-sheeted hyperboloids for $n_1 = 1, 2$ ($n_2, n_3 \in \mathbb{Z}$),
- two one-sheeted hyperboloids for $n_2 = 1, 2$ ($n_1, n_3 \in \mathbb{Z}$),
- one ellipsoid for $n_3 = 3/2$ ($n_1, n_2 \in \mathbb{Z} + \frac{1}{2}$).

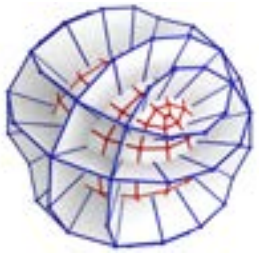

Surface generation for confidence-based data-driven computing in elasticity with application to reliability-based truss topology optimization

Yoshihiro Kanno
The University of Tokyo, Japan

Abstract

Data-driven computational elasticity is an emerging field of computational mechanics. This study presents a method predicting a bound for structural response, where the material responses are supposed to possess uncertainty. The uncertainty set is constructed by generating piecewise affine surfaces from a data set of material responses. We show that the problems for finding upper and lower bounds for the structural response can be recast as a mixed-integer linear programming problem, which can be solved globally with a branch-and-cut method. Then a fundamental property of the order statistics guarantees the confidence level for the probability that the obtained bound includes the structural response is no smaller than the target reliability. Furthermore, we discuss application to the reliability-based design optimization of truss structures.

Surface Generation for Confidence-based Data-driven Computing in Elasticity with Application to Reliability-based Truss Topology Optimization

Yoshihiro Kanno
(The University of Tokyo)

March 10–13, 2025
(Evolving Design and Discrete Differential Geometry:
towards Mathematics Aided Geometric Design)

outline

- data-driven method for computational elasticity
- uncertainty in material behavior
  - a data set of stress–strain observations
  - no modeling of probability distribution
- to find lower & upper bounds for QoI,
  - segmented least squares for nonlinear material behaviour
  - mixed-integer programming for guarantee of tightness of the bound

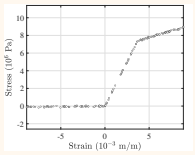

material data set


structure

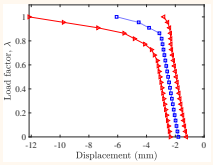

bound for QoI

data-driven equilibrium analysis in elasticity

- T. Kirchdoerfer, M. Ortiz: Data-driven computational mechanics. *Comp. Meth. Appl. Mech. Engrg.*, **304**, pp. 81–101 (2016).
  - use data of material experiments directly
    - instead of constitutive law (i.e., stress–strain relation)

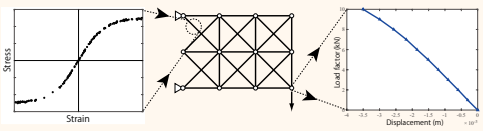

  - subsequent related studies (a lot): [Kirchdoerfer & Ortiz '17], [Ibañez *et al.* '17], [Wang & Sun '18], [Nguyen & Keip '18], [Ayensa-Jiménez, Doweidar, Sanz-Herrera & Doblaré '18]
  - tries to find "the closest point" in a data set
    - combinatorial property from optim. view → difficult to solve

[Kirchdoerfer & Ortiz '16]: influence of outliers

- iterative method
- for one-bar example,
  - find stress satisfying equilibrium with external force: $\sigma \leftarrow p/a$.
  - move to the closest data point from current (ε, σ) .

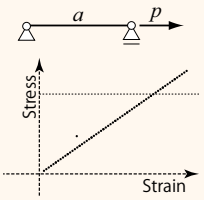

data set w/ an outlier [K. '19]

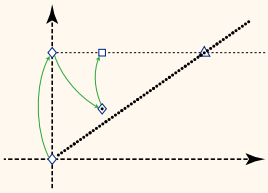

- initial point: origin
- □ : obtained by [KO '16]
  → affected by the outlier
- △ : globally min. distance soln.
  (also, convincing soln.)

a remedy [K. '21a, '21b]

- detecting a surface (i.e., manifold) on which data points (approx.) lie
  - 2-dim. manifold in $\mathbb{R}^3$

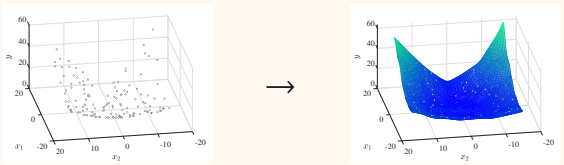

  - 1-dim. manifold in $\mathbb{R}^3$ (as the intersection of two curved surfaces)

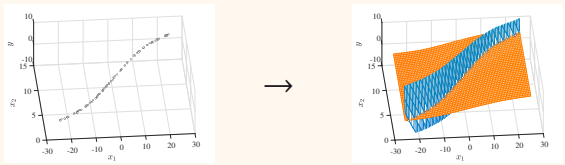

ex.) material data set

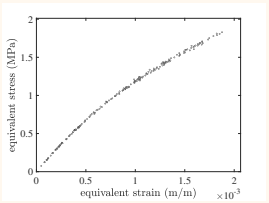

- nonlinear isotropic
- $E = 2\left(\frac{3}{2} - \frac{1}{1+\exp(-10^3 \varepsilon^{\mathrm{eq}})}\right)$,
  $\nu = 0.3$, w/ some noise
- 200 data points

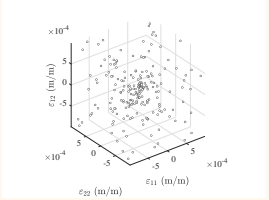

strain

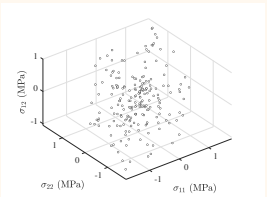

stress

ex.) load–displacement relation

- —— □ proposed (surface generation) · · · · · ○ reference solution
- – – – ◇ [Kirchdoerfer & Ortiz '16] – – – ◇ local linear regression

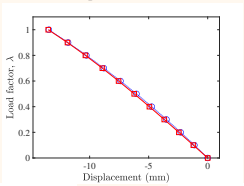

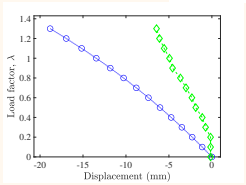

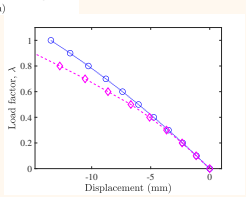

ex.) stress–strain pairs at numerical integration points

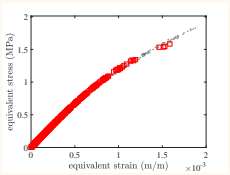

proposed (surface generation)

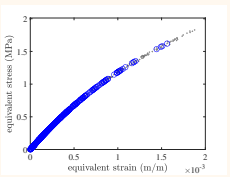

reference solution

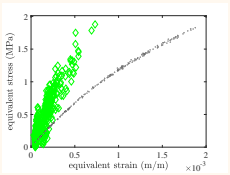

[Kirchdoerfer & Ortiz '16]

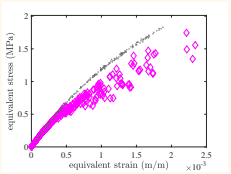

kNN linear regression

ex.) robustness against data set

- for 50 data sets, plot angle between principal axes of stress and strain

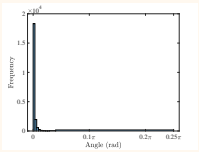

proposed (surface generation)

- isotropy ⇔ angle = 0

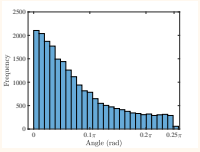

[Kirchdoerfer & Ortiz '16]

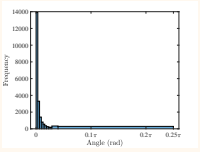

kNN linear regression

[Guo, Du, Liu & Tang '21]: another remedy using uncertainty analysis

- "A new uncertainty analysis-based framework for data-driven computational mechanics." *J. Appl. Mech.*, **88**, 111003 (2021).
  - construct an ellipsoid (an uncertainty set) including data points, and
  - find upper & lower bounds for structural response.
  - avoid influence of outliers.

material data and uncertainty set

- [Guo *et al.* '21]: a set including all ($= r$) data points
- [K. '23]: a set C including $\tilde{p}$ points among r data points
  - $\tilde{p}$:= minimum natural number s. t. $\sum_{k=\tilde{p}}^{r} {}_r\mathrm{C}_k (1-\epsilon)^k \epsilon^{r-k} \le \delta$
  - $\overline{s} := \max\{\mathrm{QoI} \mid (\varepsilon, \sigma) \in C \cap M\}$,
    $\underline{s} := \min\{\mathrm{QoI} \mid (\varepsilon, \sigma) \in C \cap M\}$. ← bounds
    - M : compatibility & force-balance

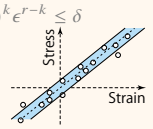

uncertainty set C

  - Fundamentals of order statistics yield

$$\underbrace{\mathrm{P}_F\Big\{\overbrace{\mathrm{P}_{(\varepsilon,\sigma)\sim F}\{s \in [\underline{s}, \overline{s}]\} \ge 1-\epsilon}^{\text{reliability under } F}\Big\}}_{F \text{ is unknown (uncertain)}} \ge 1-\delta\,.$$

    - $1-\epsilon$: target reliability $\quad 1-\delta$: confidence level
    - RBDO w/ uncertain distrib. [Moon *et al.* '17, '18], [Ito, Kim, & Kogiso '18]

material data and uncertainty set

- [Guo *et al.* '21]: a set including all ($= r$) data points
- [K. '23]: a set C including $\tilde{p}$ points among r data points
  - $\tilde{p}$:= minimum natural number s. t. $\sum_{k=\tilde{p}}^{r} {}_r\mathrm{C}_k (1-\epsilon)^k \epsilon^{r-k} \le \delta$
  - $\overline{s} := \max\{\mathrm{QoI} \mid (\varepsilon, \sigma) \in C \cap M\}$, (♣)
    $\underline{s} := \min\{\mathrm{QoI} \mid (\varepsilon, \sigma) \in C \cap M\}$. (♠)
    - M : compatibility & force-balance

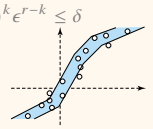
uncertainty set C

- on local vs. global optimality
  - "local opt. of (♣)" : underestimate of "max. value of QoI"
    - ↑ non-conservative bound ☹
  - global optimality
    - this talk: use mixed-integer programming for guarantee
    - w/ segmented least squares (C defined by piecewise-linear ineq.)

fiding a piecewise affine function fitting given data points

- unknown:
  - partition of the points
  - coefficients of each affine function
- minimizing "(sum of squared errors) + γ(#affine functions)"
  $\gamma > 0$: penalty parameter
  - → MIQP (mixed-integer quadratic programming) → global optim.

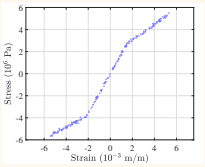

material data set
(stress–strain pairs)

→

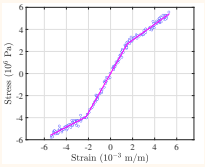

segmented least squares
(piecewise regression)

finding bound for structural response $s(\boldsymbol{u}, \boldsymbol{\sigma})$

- upper bound: (lower bound: found by minimization)

$$\begin{array}{lll} \text{Max.} & s(\boldsymbol{u}, \boldsymbol{\sigma}) & \\ \text{s. t.} & \boldsymbol{\varepsilon} = B\boldsymbol{u}\,, & \text{(compatibility)} \\ & B\boldsymbol{\sigma} = \boldsymbol{f}\,, & \text{(force-balance)} \\ & (\varepsilon_i, \sigma_i) \in C\,. & \text{(inclusion in uncertainty set)} \end{array}$$

- can be reduced to MIP (mixed-integer programming) → global optim.!

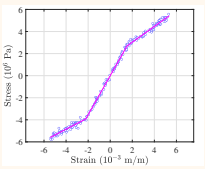

segmented least squares
(piecewise regression)

→

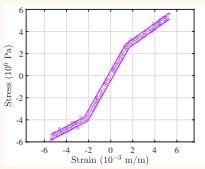

uncertainty set C
(including $\bar{p}$ data points)

uncertainty set C w/ piecewise linear boundary

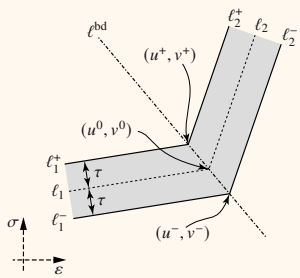

- single breakpoint case (for simplicity)
- boundary of C consists of
  - ℓ_1^+, ℓ_2^+ : $\alpha_i\varepsilon + \beta_i\sigma = \gamma_i - \tau$
  - ℓ_1^-, ℓ_2^- : $\alpha_i\varepsilon + \beta_i\sigma = \gamma_i + \tau$
  - $(\alpha_i,\ \beta_i,\ \gamma_i$: have been obtained by segmented least sq.)
- ℓ^{bd} : $p\varepsilon + q\sigma = r$
  - $(p, q, r$: can be found by elementary calculation)

- $(\varepsilon, \sigma) \in C$ iff

$$(\varepsilon, \sigma) \in \begin{cases} \text{btwn. } \ell_1^+ \text{ \& } \ell_1^- & \text{if } p\varepsilon + q\sigma \le r\,, \\ \text{btwn. } \ell_2^+ \text{ \& } \ell_2^- & \text{if } p\varepsilon + q\sigma \ge r\,. \end{cases}$$

idea for MIP (= mixed-integer prog.) reduction

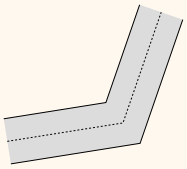

This set can be represented by
0-1 variables & linear inequalities!

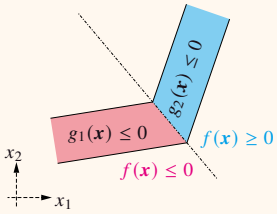

- $f(\boldsymbol{x}) \le 0 \quad \Rightarrow \quad g_1(\boldsymbol{x}) \le 0$
  $f(\boldsymbol{x}) \ge 0 \quad \Rightarrow \quad g_2(\boldsymbol{x}) \le 0$
- w/ variable $s \in \{0, 1\}$ & sufficiently large constant M, we have

$$f(\boldsymbol{x}) \le Ms\,, \qquad g_1(\boldsymbol{x}) \le Ms\,,$$
$$f(\boldsymbol{x}) \ge M(s-1)\,, \qquad g_2(\boldsymbol{x}) \le M(1-s)\,.$$

f, g_1, g_2 : expressed by some linear inequalities (prev. slide)

ex.) truss (1/3)

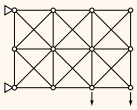

- 29-bar truss

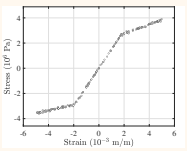

material data (200 data points)

- problem setting: target reliability $1 - \epsilon = 0.9$, confidence level $1 - \delta = 0.9$

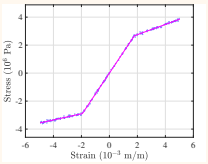

segmented least squares

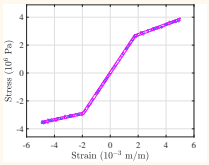

uncertainty set (including 186 pts.)

ex.) truss (2/3)

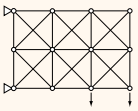

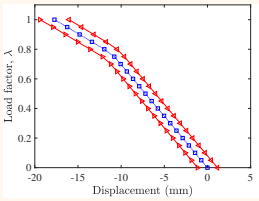

obtained bounds for nodal displacement w.r.t. variation in load factor λ
(□ : reference solution)

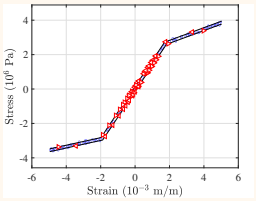

stress–strain of each member at $\lambda = 1$

ex.) truss (3/3)

- stress analysis

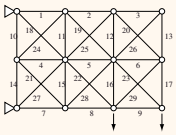

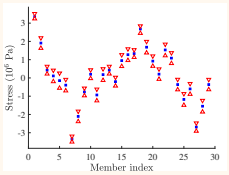

obtained bounds (■ : reference sol.)

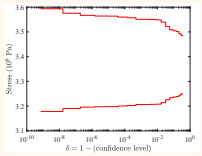

variations in the bound w.r.t. confidence $1 - \delta$ ($1 - \epsilon$ is fixed)

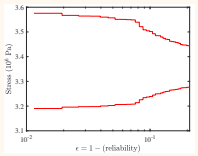

variations in the bound w.r.t. reliability $1 - \epsilon$ ($1 - \delta$ is fixed)

ex.) cable–strut structure (1/2)

- cable
  - thin member,
  - can sustain only tensile force.
- strut
  - sustains compressive & tensile force.

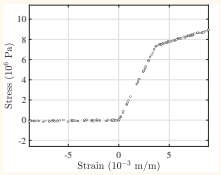

data set for cables

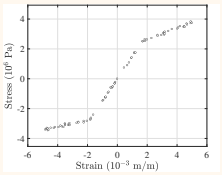

data set for struts

ex.) cable–strut structure (2/2)

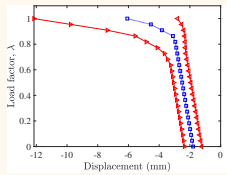

obtained bounds for nodal displacement w.r.t. variation in load factor λ

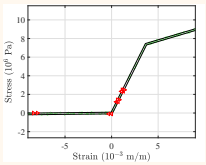

stress–strain of each cable

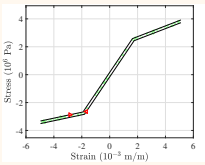

stress–strain of each strut

towords truss design optimization

- constraint under uncertainty
  - uncertainty: material behavior (w/ unknown prob. distr.)
  - $\boldsymbol{x}$: design var. (member cross-section areas)
  - $\pi(\boldsymbol{x})$: compliance (a measure of structural flexibility)
    → random var.

$$\mathrm{P}_F\Big\{\overbrace{\mathrm{P}_{(\varepsilon,\sigma)}\{\pi(\boldsymbol{x}) \le \bar{\pi}\} \ge 1-\epsilon}^{\text{reliability w/ fixed distribution}}\Big\}_{\text{treating uncertainty in distribution}} \ge 1-\delta\,.$$

  - $1-\epsilon$: target reliability $1-\delta$: confidence level of reliability

- reliability-based design optim. w/ uncertain input distribution
  [Moon *et al.* '17, '18], [Ito, Kim, & Kogiso '18]
  [Jung, Cho, & Lee '19], [Jung, Cho, Duan, & Lee, 20]
  [Wang, Hao, Yang, Wang, & Gao '20], [Hao *et al.* '22]

reduction of compliance constraint

$$\mathrm{P}_{F_D}\big\{\mathrm{P}_D\{\pi(\boldsymbol{x}) \le \bar{\pi}\} \ge 1-\epsilon\big\} \ge 1-\delta\,.$$

- sufficient condition (w/ uncertainty set C):

$$\begin{aligned} \bar{\pi} \ge \quad & \max \quad \boldsymbol{f}^\top \boldsymbol{u} && \text{(worst-case external work)} \\ & \text{s. t.} \quad \boldsymbol{\varepsilon} = B\boldsymbol{u}\,, && \text{(compatibility)} \\ & \qquad\quad H(\boldsymbol{x})\boldsymbol{\sigma} = \boldsymbol{f}\,, && \text{(force-balance)} \\ & \qquad\quad (\varepsilon_i, \sigma_i) \in C\,. && \text{(inclusion in uncertainty set)} \end{aligned}$$

  - var.: member strains $\boldsymbol{\varepsilon}$, member stresses $\boldsymbol{\sigma}$, nodal displacements $\boldsymbol{u}$
  - difficulty: constraint on optimal value (of linear programming)

- strong duality of LP yields equivalent cstr.:

$$\exists\text{"Lagrange multiplier"}, \quad \text{(dual objective value)} \le \bar{\pi}\,.$$

  - ↑ can be treated with conventional nonlinear programming!

ex.) w/ continuous design variables (1/2)

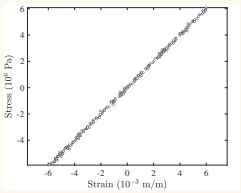

300 data points

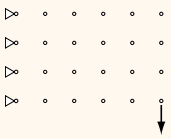

ground structure
(188 members)

- w/ interior-point method
  (nonlinear programming)
- $1-\epsilon = 0.95$ reliability
- $1-\delta = 0.95$ confidence level
- $\tilde{p} = 292$ points are included
  in the uncertainty set.

ex.) w/ continuous design variables (1/2)

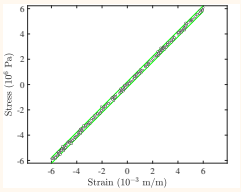

300 data points & uncertainty set

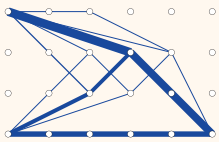

nominal optimal solution
(w/ linear regression result)

- w/ interior-point method
  (nonlinear programming)
- $1-\epsilon = 0.95$ reliability
- $1-\delta = 0.95$ confidence level
- $\bar{p} = 292$ points are included
  in the uncertainty set.

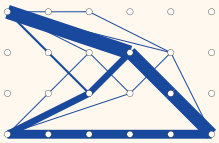

proposed method

ex.) w/ continuous design variables (2/2)

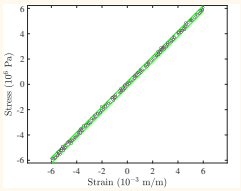

300 data points & uncertainty set

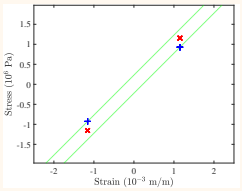

close up

- × : nominal optimal solution
  - all existing members have common absolute value of stresses
    (well-known fact for volume min. under compliance cstr.)
- + : proposed method
  - all existing members have
    common worst-case absolute value of stresses (not proved yet)

ex.) w/ discrete design variables (1/2)

- discrete member cross-section areas
  - selected from predetermined values
- reduced to MIP (mixed-integer linear programming)
  - idea: similar to conventional truss optim.
  - global opt. by MIP solver (branch-and-cut)

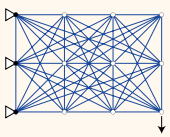

problem setting

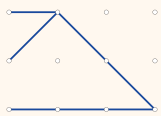

nominal

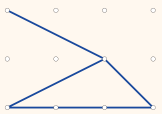

proposed

ex.) w/ discrete design variables (2/2)

- discrete member cross-section areas
  - selected from predetermined values
- reduced to MIP (mixed-integer linear programming)
  - idea: similar to conventional truss optim.
  - global opt. by MIP solver (branch-and-cut)

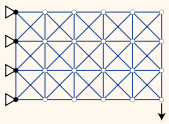

problem setting

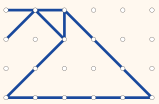

nominal

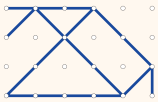

proposed

conclusion

- data-driven computational mechanics [Kirchdoerfer & Ortiz '16]
- introduction of uncertainty analysis [Guo, Du, Liu & Tang '21]
  - upper & lower bounds for structural response
- use of order statistics
  - confidence for reliability that the structural response belongs to the obtained bound
- segmented regression for nonlinear material data
- mixed-integer programming
  - can find a bound w/ global optimality☺
  - ↔ local opt. sol.: underestimate☹ of the structural response
- application to truss design optimization
  - reduction to nonlinear programming via duality of linear programming

Optimization methods for continuum and latticed shells consisting of developable parts

Makoto Ohsaki
Kyoto University, Japan

Abstract

To reduce the cost and time for construction of continuum shells and latticed shells for covering large architectural space, it is important to design the structures as an assembly of developable parts. For this purpose, this presentation summarizes the following three optimization methods developed as part of the JST CREST ED^{3}GE project:

1. A meshless and non-parametric two-level optimization approach is proposed for design of shell surfaces consisting of approximately developable patches. Developability is measured by the area of local Gauss map at the grid points. In the lower-level problem, the developability conditions are relaxed at some grid points to generate internal boundaries between approximately developable surface patches. In the upper-level problem, stiffness under the specified vertical loads is maximized. The design variables are the heights of the selected grid points, where developability conditions of some grid points are automatically relaxed. This way, a new class of structural shape optimization problem of shell surfaces consisting of piecewise developable surfaces is proposed to design shells with desirable geometrical characteristics in view of fabrication and construction.

2. In the design of latticed shell consisting of straight beams, it is important to have planarity of beam plates and surface panels while avoiding kinks at the joints. For this purpose, a hexagonal mesh consisting of straight beams connected at joints without torsion or kink is generated from Koebe mesh on a unit sphere obtained by spherical inversion in Möbius geometry. The parameters for Möbius transformation are optimized to obtain the latticed shell close to the target surface.

3. The cost and time for construction of gridshells consisting of quadrilateral meshes can be reduced by designing the shell as an assembly of planar beams. A gridshell with a planar quadrilateral mesh and planar curves is generated by discretizing an L-isothermic surface, where the directions of principal stresses coincide with the directions of principal curvatures under the uniform pressure load. The cross-sectional areas of gridshells are optimized to have the desired distribution of axial forces.

References

[1] K. Hayakawa, M. Ohsaki and J. Y. Zhang, Meshless non-parametric shape design of piecewise approximately developable surfaces using discretized local Gauss map, J. Int. Assoc. Shell Spatial. Struct., Vol. 64, No. 1, pp. 5-14, 2024.

[2] K. Kabaki, K. Hayakawa, M. Ohsaki, Y. Jikumaru and Y. Yokosuka, Design of gridshells consisting of planar curves using Laguerre geometry, Proc. IASS Symposium 2024, Zurich, Switzerland, Int. Assoc. Shell and Spatial Struct., Paper No. 340, 2024.

[3] R. Watada and M. Ohsaki, Sequential generation method for hexagonal lattice shells with edge offset mesh, Proc. IASS Symposium 2024, Zürich, Int. Assoc. Shell and Spatial Struct., Paper No. 365, 2024.

[4] M. Ohsaki, K. Hayakawa and J. Y. Zhang, Non-parametric structural shape optimization of piecewise developable surfaces using discrete differential geometry, Proc. Asian Congress of Structural and Multidisciplinary Optimization (ACSMO 2024), Zhengzhou, China, Paper B40314, 2024.

Optimization methods for continuum and latticed shells consisting of developable parts

Makoto Ohsaki (Kyoto University)
Jingyao Zhang (Kyoto University)
Ryo Watada (Osaka Sangyo University)
Kentaro Hayakawa (Nihon University)
Kohei Kabaki (Kyoto University)

Outline of presentation

- Three topics from Kyoto Group of Crest project
  Related to "Optimization of shells consisting of developable parts"

1. Design of gridshells using Laguerre geometry
2. Design of latticed shells with hexagonal mesh using Möbius geometry
3. Structural optimization of shells consisting of piecewise developable parts

Design of gridshells using Laguerre geometry

Lie sphere geometry

- Union of Möbius geometry and Laguerre geometry
- Directed sphere and plate in 5 or 6-dimensional vector
- Laguerre transformation:
  Expressed by 5 × 5 matrix satisfying condition in bilinear form

$$\mathbf{x} \mapsto \mathbf{x}' = \begin{pmatrix} 1 & 0 \\ \mathbf{t} & \lambda A \end{pmatrix} \mathbf{x} \qquad \mathbf{t} \in \mathbb{R}^4, \lambda \in \mathbb{R}$$

Condition for transformation

$$A^T E_{pe} A = E_{pe}, \quad E_{pe} = \begin{pmatrix} 1 & 0 & 0 & 0 \\ 0 & 1 & 0 & 0 \\ 0 & 0 & 1 & 0 \\ 0 & 0 & 0 & -1 \end{pmatrix}$$

11 parameters in t and *A*

Expression by 5-dimensional vector

$$\begin{pmatrix} 1 \\ x_1 \\ x_2 \\ x_3 \\ x_4 \end{pmatrix} \quad \text{Center} \quad \text{Signed radius} \qquad \text{Sphere}$$

$$\begin{pmatrix} 0 \\ x_1 \\ x_2 \\ x_3 \\ \sqrt{x_1^2 + x_2^2 + x_3^2} \end{pmatrix} \quad \text{Normal vector} \qquad \text{Plate}$$

4

Purpose

- Design a grid shell with preferred axial force distribution
  ⇒ Assign target force distribution and solve optimization problem
  ⇒ Difficult to assign feasible distribution of axial forces at equilibrium for specified loads

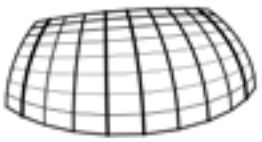

- Design the shape based on Laguerre geometry
- In most of mathematical approaches, deformation against loads (material property) is not considered.
  ⇒ Investigate effect of deformation by structural analysis

5

L-minimal generalized Dupin cyclide

W K Schief, A Szereszewski and C Rogers (2009)

- Envelop of sphere of variable radius translated along Cycloid (one parameter family of sphere)
- One of the curvature lines is a circle
- Both of the curvature lines are planar

$$\mathbf{r} = \frac{\cos\alpha}{2(a_0 - c_0 \cos\alpha \cos u)} \begin{pmatrix} \cos\alpha \\ a_0 \sin\alpha \\ \cos\alpha \sin u \end{pmatrix} + \frac{1}{4} \begin{pmatrix} -a_0 \\ 2\alpha \\ 0 \end{pmatrix}$$

$$(a_0^2 - c_0^2 = 1)$$

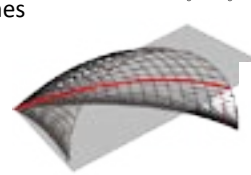

Constant *u*

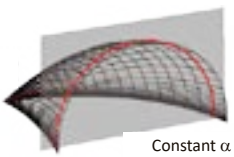

Constant α

Parameter (*u*, α) along curvature lines

6

Membrane forces against uniform normal loads

- Equilibrium to uniform normal load Z with membrane forces
- Principal stresses T_1 and T_2 in the directions of principal curvature lines
- 3rd fundamental form is ithothermic w.r.t. curvature lines
  ⇒ L-isothermic surface
  ⇒ T_1 and T_2 are obtained explicitly from local surface shape and has one arbitrary parameter

$$T_1 = -\frac{Z}{2\kappa_2} - \frac{I_0}{\kappa_2 A_2^2}$$

$$T_2 = -\frac{Z}{2\kappa_1}\left(1 - \frac{(A_2 - A_1)^2}{A_1}\right) + \frac{I_0}{\kappa_1 A_1^2}$$

Arbitrary parameter

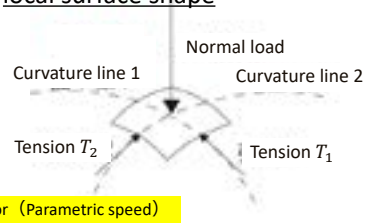

W K Schief, A Szereszewski and C Rogers (2009)

A_1 , A_2 : Norm of tangent vector （Parametric speed）
κ_1, κ_2: Principal curvatures

7

Assignment of parameter

- Assign I_0 to have specific force distribution.
- Example: Force in one direction can vanish at a specific point

$$T_1 = 0 \Leftrightarrow I_0 = -\frac{1}{2}A_2^2 Z$$

$$T_2 = 0 \Leftrightarrow I_0 = \frac{1}{2}(2A_1A_2 - A_2^2)Z$$

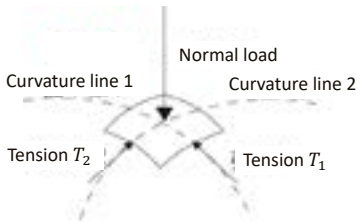

8

Target membrane force (continuum shell)

- Force in one direction vanishes at the center of upper boundary edge

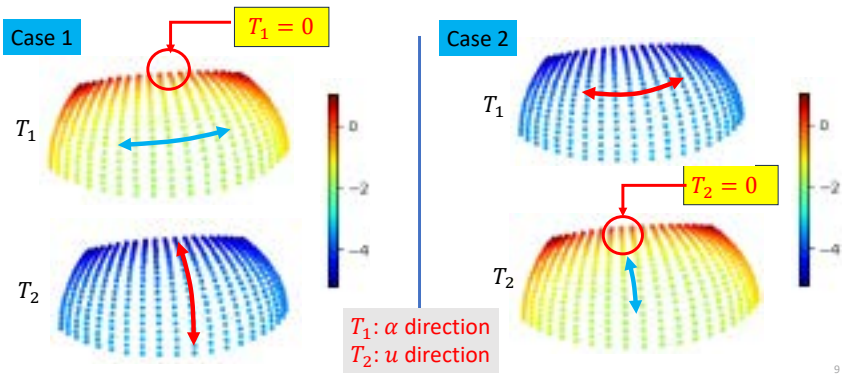

9

Target axial force (gridshell)

- Convert target membrane stress to target axial force
- Zero membrane force ⇒ Zero axial force

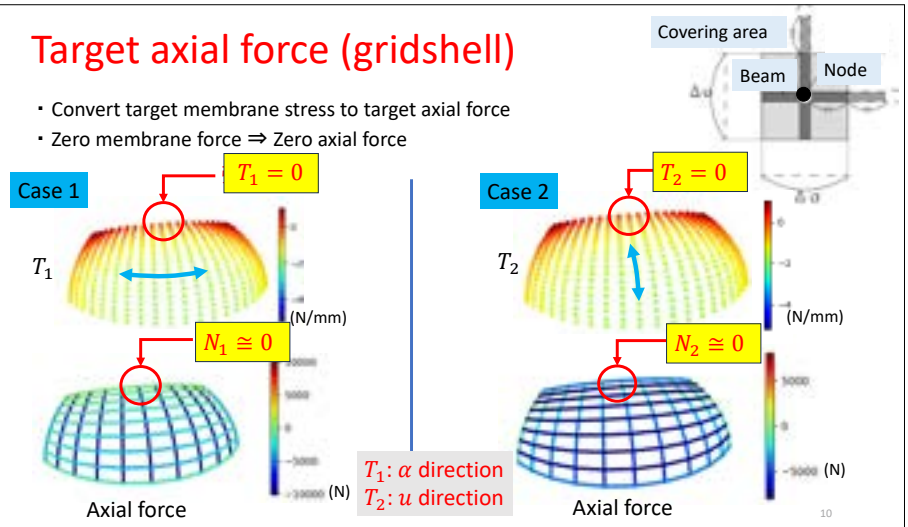

10

Structural optimization

Material property ⇒ Compatibility of deformation
⇒ Bending moment and out-of-plane shear force
⇒ No axial force exactly same as target value

Continuous beams have same section

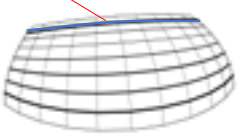

- Objective function: Mean squared error of axial force
- Design variable: Radius of circular pipe of beam
  (thickness = constant)

$$\begin{aligned} &\text{Find} && \mathbf{d} \\ &\text{Minimize} && \|\mathbf{N} - \mathbf{N}_0\|^2 \\ &\text{subject to} && 20 \leq d_i \leq 150 \end{aligned}$$

$\mathbf{d}$: Vector of beam radius
$\mathbf{N}$: Axial force vector
$\mathbf{N}_0$: Vector of target axial force

11

Optimization results (Case 2)

Cross-section radius

Uniform section

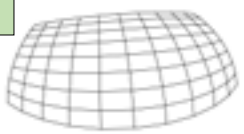

Optimal solution

$N_2 = 0$

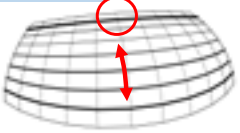

Error from target axial force

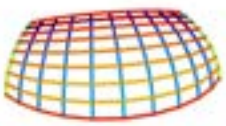

Small error in interior region

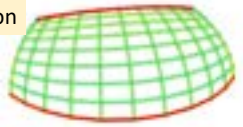

Release support along upper boundary (Case 2)

Zero axial force at upper boundary ⇒ Release support at upper boundary

	Mean axal force error (N)	Mean ratio of shear force to load
Initial (Pin)	2948	4.11%
(Free)	463	24.6%
Optimal (Pin)	218	2.94%
(Free)	394	18.9%

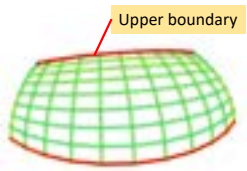

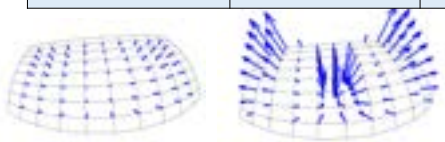

Pin Free

Displacement of initial uniiform solution

Pin Free

Displacement of optimal solution

13

Laguerre transformation of surface

- Cannot transform point to point
- Define point on the surface as contact point between directed sphere and plate
- Apply Laguerre transformation on sphere and plane
- Find contact point between transformed sphere and plane

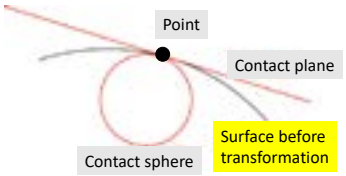

Transformation

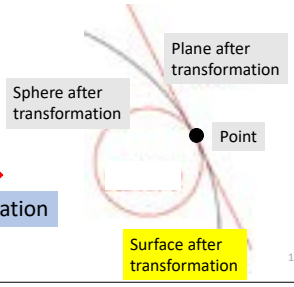

14

Laguerre transformation of surface

- Preserve invariants of Laguerre geometry
  ⇒ Favorable properties of surface are preserved
  ⇒ Curvature lines are transformed to curvature lines
  ⇒ Constructability is maintained

$$\mathbf{x} \mapsto \mathbf{x}' = \begin{pmatrix} 1 & 0 \\ \mathbf{t} & \lambda A \end{pmatrix} \mathbf{x} \qquad \mathbf{t} \in \mathbb{R}^4, \lambda \in \mathbb{R}$$

Condition of transformation

$$A^T E_{pc} A = E_{pc}, \quad E_{pc} = \begin{pmatrix} 1 & 0 & 0 & 0 \\ 0 & 1 & 0 & 0 \\ 0 & 0 & 1 & 0 \\ 0 & 0 & 0 & -1 \end{pmatrix}$$

Expression by 5-dimensional vector

$$\begin{pmatrix} 1 \\ x_1 \\ x_2 \\ x_3 \\ x_4 \end{pmatrix}$$ Center, Signed radius — Sphere

$$\begin{pmatrix} 0 \\ x_1 \\ x_2 \\ x_3 \\ \sqrt{x_1^2 + x_2^2 + x_3^2} \end{pmatrix}$$ Normal vector — Plate

15

Conversion by Laguerre transformation

- Inner product: $\langle \mathbf{x}, \mathbf{y} \rangle_{\mathrm{pe}} = \langle A\mathbf{x}, A\mathbf{y} \rangle_{\mathrm{pe}}$
- Directed sphere contacting the surface at $\mathbf{p}$: $\begin{pmatrix} \mathbf{p} \\ 0 \end{pmatrix} + a \begin{pmatrix} \mathbf{n} \\ -1 \end{pmatrix}$
- Laguerre transformation of directed sphere:

$$A\left[\begin{pmatrix} \mathbf{p} \\ 0 \end{pmatrix} + a \begin{pmatrix} \mathbf{n} \\ -1 \end{pmatrix}\right] = A \begin{pmatrix} \mathbf{p} \\ 0 \end{pmatrix} + a \begin{pmatrix} \hat{\mathbf{n}} \\ -\|\hat{\mathbf{n}}\| \end{pmatrix}$$

- L-isothermic surface: $\langle \mathbf{n}_x, \mathbf{n}_x \rangle = \langle \mathbf{n}_y, \mathbf{n}_y \rangle = e^{2\theta}, \langle \mathbf{n}_x, \mathbf{n}_y \rangle = 0$
- Laguerre transformation of 3rd fundamental form (x, y: parameters) :

$$\mathrm{III} = \langle d\mathbf{n}, d\mathbf{n} \rangle = e^{2\theta}\left(dx^2 + dy^2\right)$$
$$\widehat{\mathrm{III}} = \langle d\hat{\mathbf{n}}, d\hat{\mathbf{n}} \rangle = e^{2\hat{\theta}}\left(dx^2 + dy^2\right),\ \hat{\theta} = \theta - \log \|\hat{\mathbf{n}}\|$$

16

Examples of Laguerre transformation

Black: before transformation

Red: after transformation

Rotation

Scaling

Rotation w.r.t. hyperbolic function in projective space

17

Stress distribution after transformation (Case 1)

T_1 T_2 Equilibrium $\kappa_1 T_1 + \kappa_2 T_2 + Z$

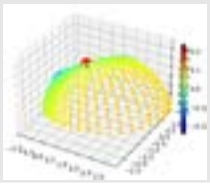
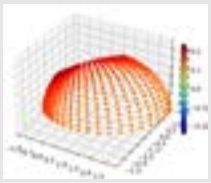
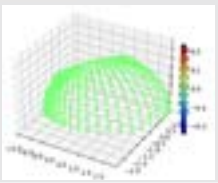
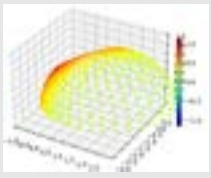
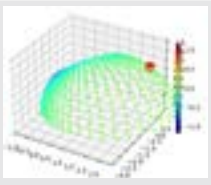
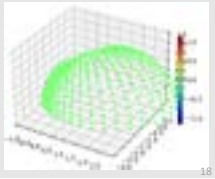

18

Design of latticed shells with hexagonal mesh using Möbius transformation

19

Edge-offset (EO) mesh

Mesh with the same edge offset value

・Edge offset mesh:
Planar beam with same height
Planar face

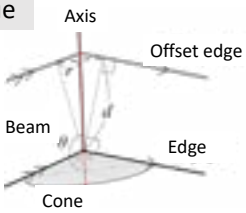

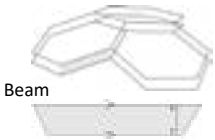

EO mesh
・Vertex axis = Axis of cone
・Edge on cone

20

Generating EO mesh

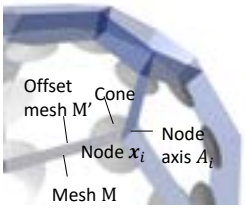

Koebe mesh

- All edges contact to a unit sphere
- Generated from circle packing on the sphere
- EO mesh is parallel to Koebe mesh
- All edges contact the cone at vertex

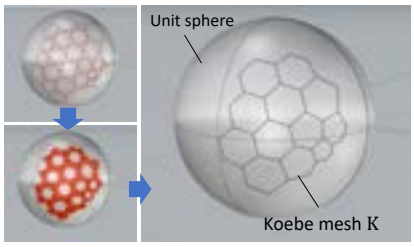

Mesh parallelity

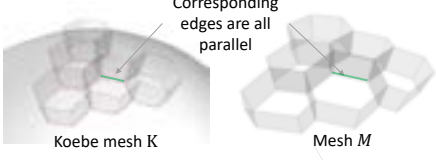

Generating Koebe mesh

Projection of circle packing on a plane to unit sphere
⇒ Modify circle packing ⇒ Modify Koebe mesh

Möbius transformation:

$$f(z) = \frac{az+b}{cz+d},\ (a,b,c,d \in \mathbb{C}, ad-bc \neq 0)$$

or

$$f(z) = \rho e^{i\theta}\left(\frac{1}{z+\alpha}+\beta\right),\quad (\alpha,\beta \in \mathbb{C}, \rho > 0, -\pi \leq \theta < \pi)$$

- $\alpha = \alpha_R + i\alpha_I, \beta = \beta_R + i\beta_I,$

  ⇒ Mobius transformation can be determined by six real parameters $\alpha_R, \alpha_I, \beta_R, \beta_I, \rho, \theta \in \mathbb{R}$

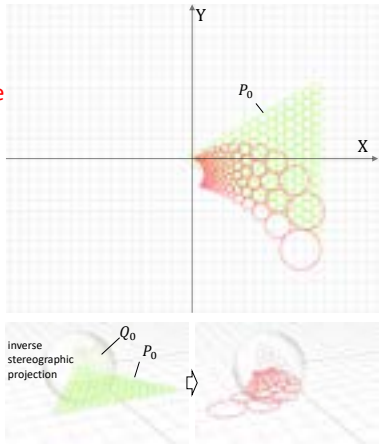

Mobius transformation

Möbius transformation

$$f(z) = \rho e^{i\theta}\left(\frac{1}{z+\alpha}+\beta\right),\quad (\alpha,\beta \in \mathbb{C}, \rho > 0, -\pi \leq \theta < \pi)$$

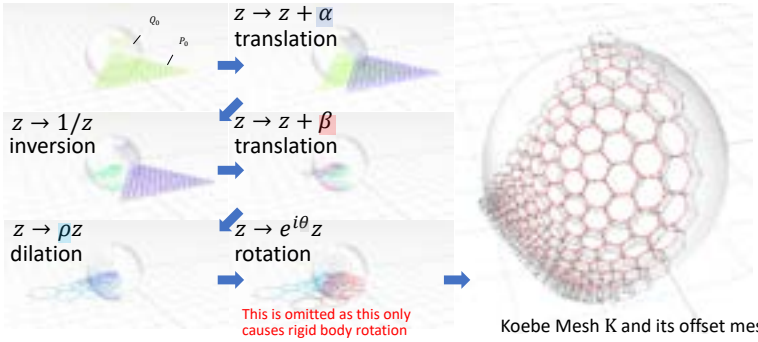

Koebe Mesh K and its offset mesh

Sequential generation of EO mesh

The number of neighboring faces: 1
→ variables : $\xi_{f1}, \xi_{f2}, \eta_f$

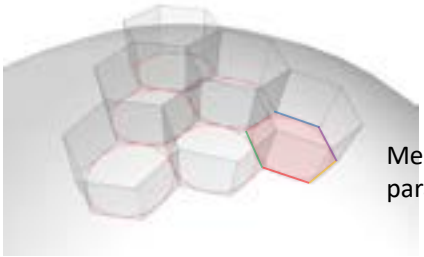

Pre-fixed Koebe mesh K

Mesh M
parallel to K

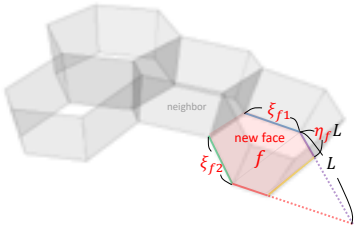

Generated EO mesh M

Surface approximation

- **Sequential optimization:**
  Minimization of mean squared error of normal vector
- Variables: : $\xi_{f1}, \xi_{f2}, \eta_f$ $(f \in F_g)$
  (F_g: surfaces considering symmetry)

minimize $\Phi_g = \sum_{i \in I_f, f \in F_g} \|\boldsymbol{n}_i - \hat{\boldsymbol{n}}_i\|^2$
subject to $\|\boldsymbol{x}_i - \hat{\boldsymbol{x}}_i\| - D^U \leq 0 \ (i \in I_f, f \in F_g)$
Bounds for $\eta_f, \xi_{f1}, \xi_{f2}$

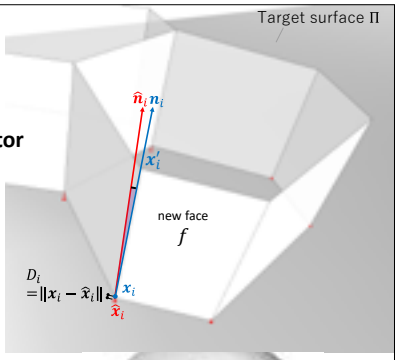

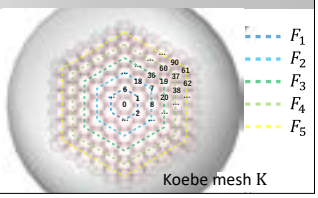

$\boldsymbol{n}_i$: Unit Vertex axis vector at vertex $\boldsymbol{x}_i$
$\hat{\boldsymbol{n}}_i$: Unit normal vector at $\hat{\boldsymbol{x}}_i$ on surface
$\hat{\boldsymbol{x}}_i$: Point on surface nearest to $\boldsymbol{x}_i$

Number of variables: $|F_g| \times 3$ at maximum (about 15)

Numerical example

Target surface shape

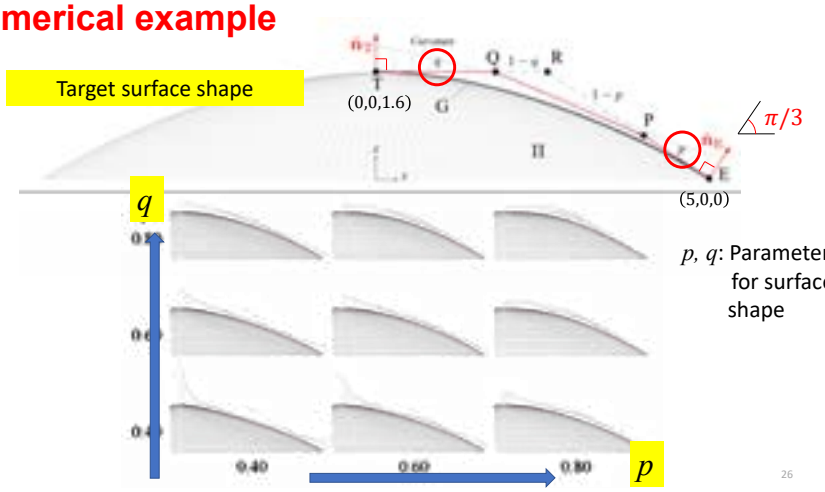

p, q: Parameter for surface shape

Effect of shape parameters

$D^U = 0.10$
Beam height : 0.30

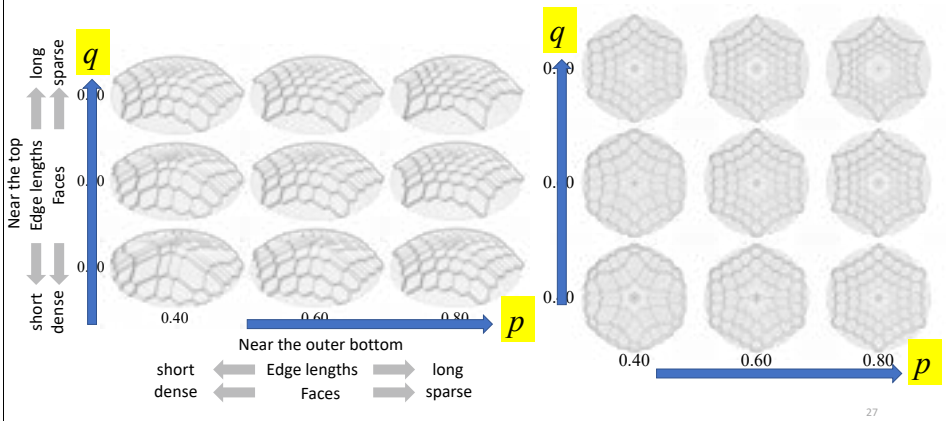

Structural performance

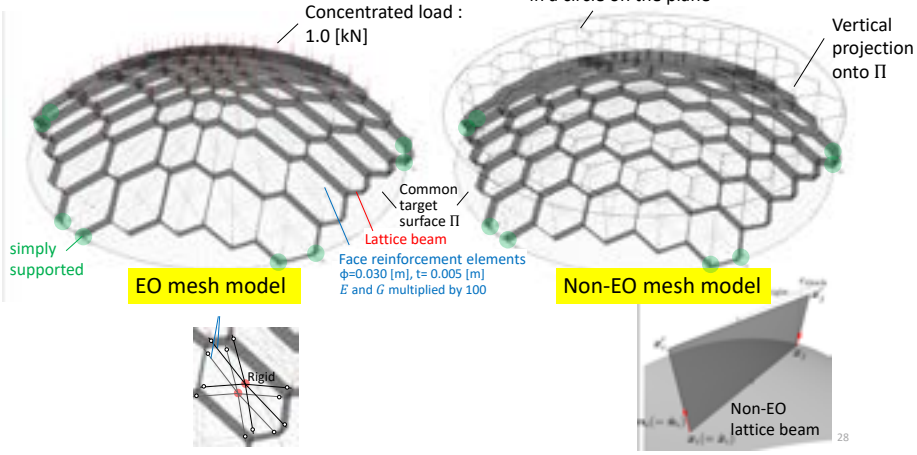

28

Effect of beam torsion (small deformation)

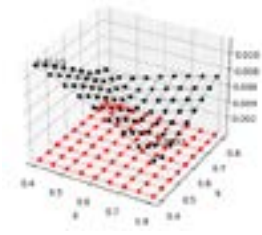

Maximum deviation e_{thick} in the thickness direction [m]

Torsional deformation

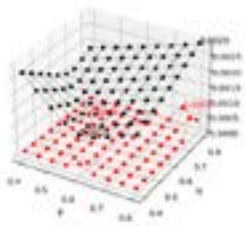

Average of $|M_{xx}|$ [kN · m/m]

Bending moment

● EO lattice
● non-EO lattice

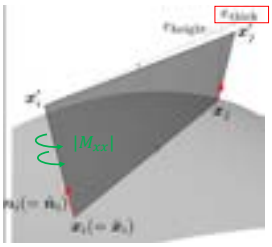

Load-Displacement

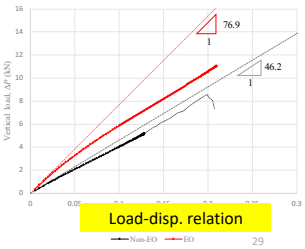

Load-disp. relation

29

Local deformation

EO mesh reduces local deformation

● EO lattice
● non-EO lattice

$(p, q) = (0.5, 0.7)$
EO: 0.004239 ←Minimum
Non-EO: 0.004368

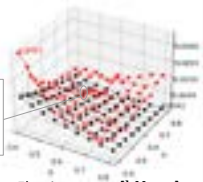

Elastic energy [kN · m]

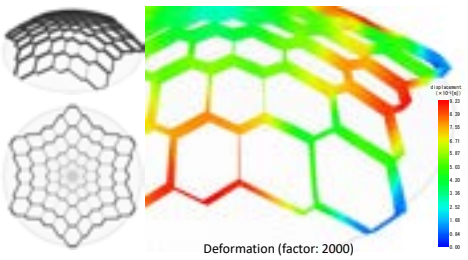

Deformation (factor: 2000)

EO lattice (Min. strain energy)
$(p, q) = (0.50, 0.70)$
$E = 0.004239$

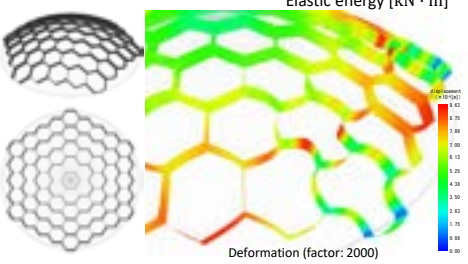

Deformation (factor: 2000)

Non-EO lattice
$(p, q) = (0.50, 0.70)$
$E = 0.004368$

30

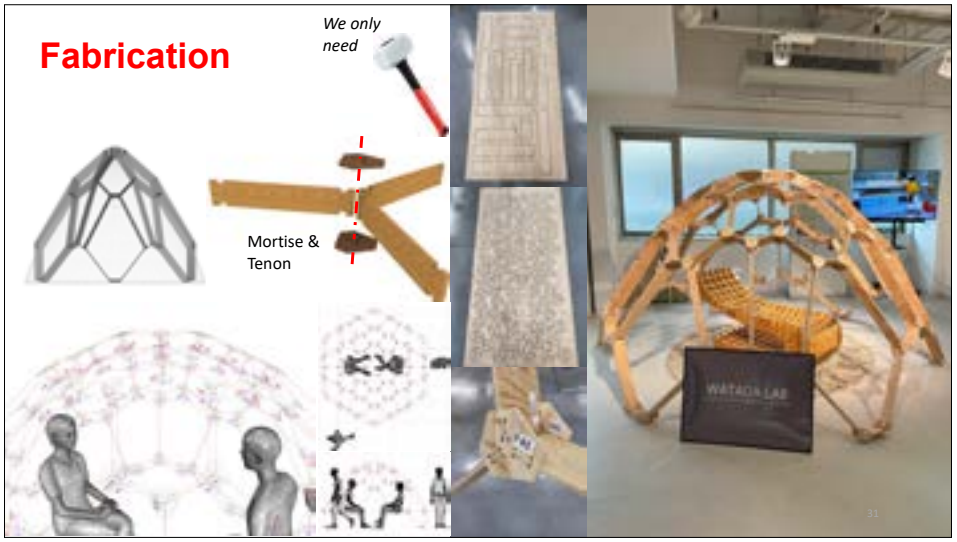

Structural optimization of shells consisting of piecewise developable surface

32

Background

Many methods for designing free-form shells for architectural roof and façade

Large construction cost:

- cost for formwork for reinforced concrete (RC) shell

Developable surface for cost reduction:

- generated by bending plate

Use same mesh for design, analysis and optimization:

- dependency of solutions on triangular mesh discretization

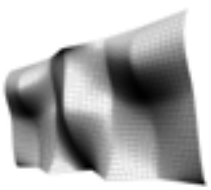

Assemblage of developable Bézier surface [1]

Discrete developable surfaces [2]

[1] J. Cui and M. Ohsaki, J. Int. Assoc. Shell. Spatial Struct., Vol. 59 (3), pp. 199-214, 2018.
[2] M. Ohsaki and K. Hayakawa, J. Int. Assoc. Shell. Spatial Struct., Vol. 62 (2), pp. 93-101, 2021.

33

Purpose

Two-level shape optimization method of curved surfaces:

limited class of surface:

piecewise developable surfaces

Developability of the polyhedral surface:

- vanishing area of discretized local Gauss map at each vertex

Optimize locations of selected points on the surface:

- minimize compliance (maximize stiffness)

34

Gauss map and developable surface

Gauss map:

- mapping from point on the surface to a point on the unit sphere of unit normal vector

Vanishing area of Gauss map → developable surface:

- plane: point
- cylinder: arc
- cone: arc

Gauss map of non-developable surface

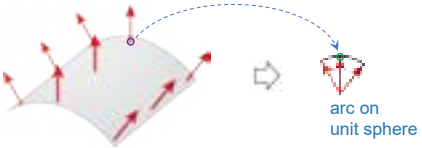

Gauss map of developable surface

35

Meshless approach

Surface represented by grid points

- Mesh structure (global connectivity of edges): not specified.
- Auxiliary edges: tentatively arranged to construct a locally triangulated surface.
- Gauss map: defined locally at each interior grid point.

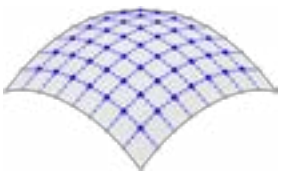

surface with grid points

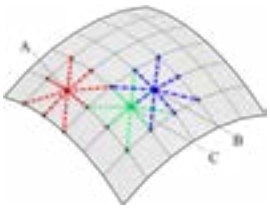

grid points A, B, C and auxiliary edges connecting to their neighborhood points

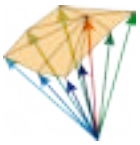

Local gauss map

36

Discrete (polyhedral) Gauss map

Unit normal vector of triangular region between edges *j* and *j*+1

$$\mathbf{n}_j^{\mathrm{f}} = \frac{\hat{\mathbf{n}}_j^{\mathrm{f}}}{\left\|\hat{\mathbf{n}}_j^{\mathrm{f}}\right\|} \qquad \hat{\mathbf{n}}_j^{\mathrm{f}} = (\mathbf{q}_j - \mathbf{p}_i)\times(\mathbf{q}_{j+1} - \mathbf{p}_i)$$

Unit normal vector at point *i*

$$\mathbf{n}_i = \frac{\hat{\mathbf{n}}_i}{\left\|\hat{\mathbf{n}}_i\right\|} \qquad \hat{\mathbf{n}}_i = \frac{1}{m_i}\sum_{j=1}^{m_i}\mathbf{n}_j^{\mathrm{f}}$$

Area of local Gauss map

$$a_{ij} = \frac{1}{2}\left\|(\mathbf{n}_j^{\mathrm{f}} - \mathbf{n}_i)\times(\mathbf{n}_{j+1}^{\mathrm{f}} - \mathbf{n}_i)\right\|$$

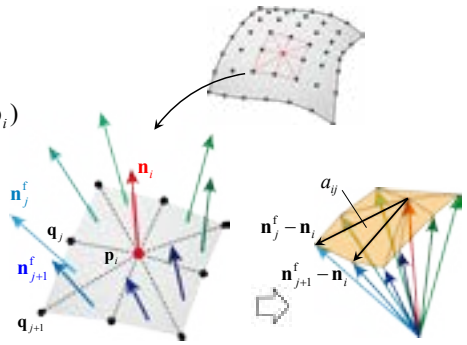

Design surface Local gauss map

37

Lower-level optimization problem: Generate piecewise developable surface

Minimization of the sum of area of local Gauss map

- prevention of divergence of gradients of a_{ij} at $a_{ij} \simeq 0$ by minimizing the sum of $(a_{ij})^2$ (developability error)

Lower level problem

$$\text{Minimize } F(\mathbf{x}) = \sum_{i\in I} A_i$$

$$\text{subject to } \mathbf{x} \in \chi$$

$$A_i = \sum_{j=1}^{m_i}(a_{ij})^2 = 0$$

$$\Rightarrow \text{depelopability condition}$$

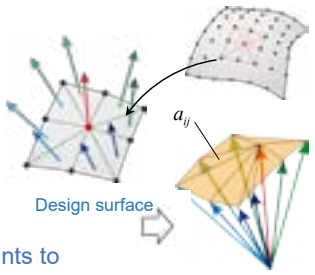

Design surface Local gauss map

- exclusion of developability error at some selected points to generate interior boundaries between patches

⇒ **Piecewise developable surface**

$\mathbf{x}$: vector of variables (selected coordinates of grid points)

I : set of indices of selected grid points

χ : feasible region (upper and lower bounds) of $\mathbf{x}$

38

Two-level shape optimization of surface with limited class

Stiffness maximization of the piecewise developable surface

- Upper problem: Minimization of compliance against static loads
  FE-model: grid points ⇒ quadrilateral mesh
- Lower problem: Generate piecewise developable surface

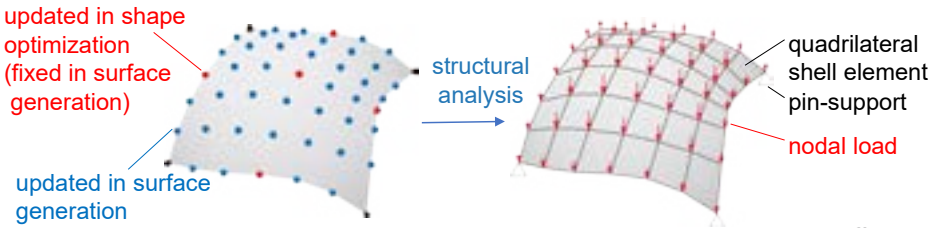

39

Example 1:

Initial shape

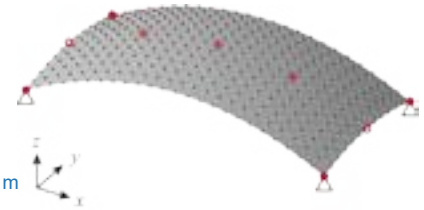

Lower Problem: Generation of piecewise developable surface

bounds for z-coordinates

Structural analysis

Young's modulus, Poisson's ratio: 200 GPa, 0.2

load (self-weight): 1.0×10^2 kN/m^2, Shell thickness: 0.1 m

Upper Problem: Shape optimization by simulated annealing

max. number of steps: 200

neighborhood search:
10 times at each temperature

bounds for z-coordinates

: fixed in lower-level problem

: Ignored developability condition

: updated in upper-level problem

: pin-supported

40

Result of structural optimization

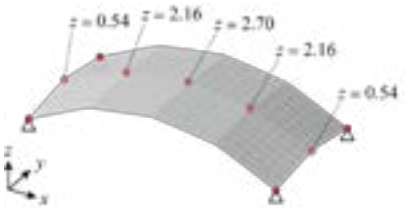

Initial surface for upper-level problem
(solution of lower problem)

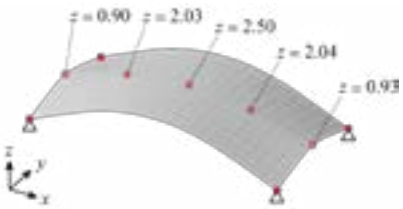

Optimal surface
(solution of upper problem)

✓Initial surface for structural optimization: eight almost planar patches.

✓Optimal surface:
smooth cylindrical patch around center; and two ridges near boundary.

41

Properties of optimal solution

Displacement in z-direction

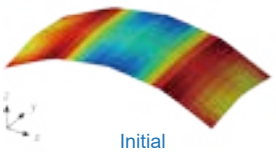

Initial

Optimal

✓Reduced magnitude of displacement in the optimal shape

✓Smoother distribution in the optimal shape

Minimum bending stress

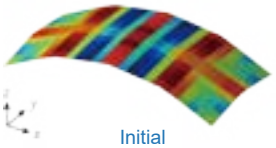

Initial

Optimal

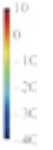

✓Large negative bending stress in the flat region in the initial shape

✓Reduced and smoother moment distribution in the optimal shape

42

Error concentration using tanh function

Difficulty in previous method:

specify points for ignoring developability
⇒ specify approximate locations of internal boundary

⇒ Method without prior assignment of internal boundary

automatic concentration of developability error

Lower problem

$$\text{Minimize } F(\mathbf{x}) = \sum_{i \in I} A_i$$

$$\text{Minimize } F(\mathbf{x}) = \sum_{i \in I_{\text{in}}} \tanh\left(c\sqrt{A_i(\mathbf{x}) + \varepsilon}\right)$$

Parameter

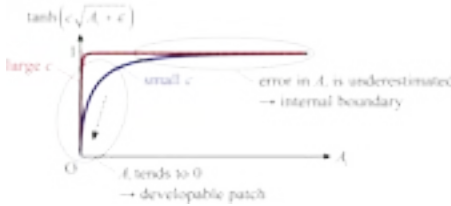

Underestimate large developability error
→ concentrate nondevelopable points

43

Example 2-1 (Shape generation: lower problem)

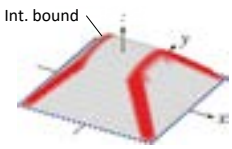

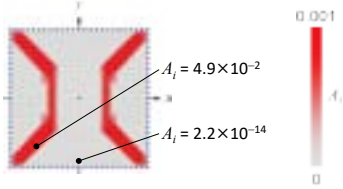

c = 100
Two internal boundaries
Center: cylinder
Side: plane
A_i < 10^{-6}: developable
> 10^{-4}: non-developable
(int. boundary)

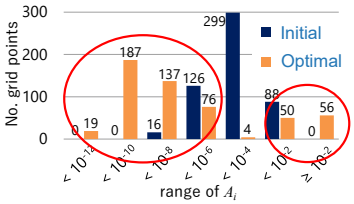

44

Example 2-2 (Shape generation: lower problem)

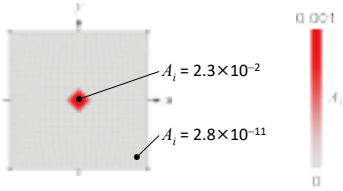

c = 50
Center: non-developable
Interior: 4 planes
A_i : less than 10^{-6}
(developable)
except center

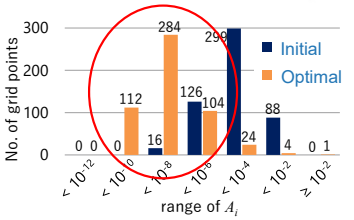

45

Example 3 (Struct. optimization: upper problem)

Initial of initial (W = 4.998 kNm)

Contour: max. bending moment

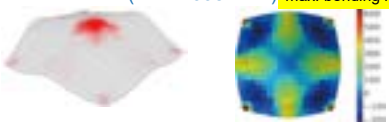

Randomize grid points to have internal boundary in arbitrary directions

Varied in upper problem

Fixed in lower problem

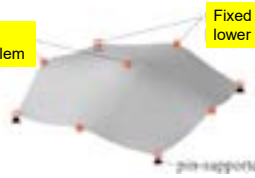

Optimal of initial (W = 5.555 kNm)

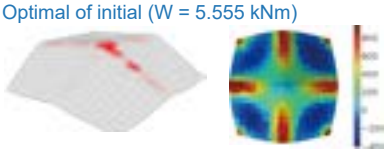

Optimal of optimal (3.386 kNm)

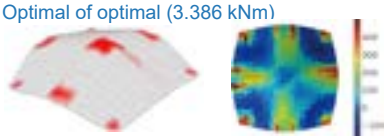

Size on plane: 10 x 10 m
Range of x: initial ±8 m
Range of Z: initial ±1 m
Randomize grid points: regular ±0.015 m
Young's modulus: 200 GPa
Poisson's ratio: 0.3

46

Example 3 (Struct. optimization: upper problem)

Optimal c = 100

Contour: max. bending moment

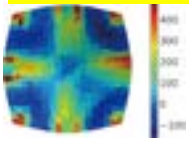

$$F(\mathbf{x}) = \sum_{i \in I_{in}} \tanh\left(c\sqrt{A_i(\mathbf{x}) + \varepsilon}\right)$$

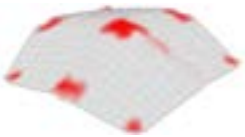

Optimal c = 10

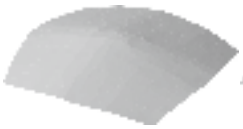

Optimal c = 200

c = 10: Ambiguous internal boundary
c = 100, 200: Corrugated shape near variable points

47

Example 4

Varied in upper problem

Fixed in lower problem

Initial c = 10 (W = 0.4338 kNm)

Contour: max. bending moment

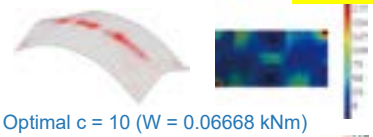

Optimal c = 10 (W = 0.06668 kNm)

Optimal c = 100

Size on plane: 10 x 10 m
Range of x: initial ±8 m
Range of Z: initial ±1 m
Randomize grid points: regular ±0.01 m
Young's modulus: 200 GPa
Poisson's ratio: 0.3

$$F(\mathbf{x}) = \sum_{i \in I_{in}} w_i \tanh\left(c\sqrt{A_i(\mathbf{x}) + \varepsilon}\right)$$

c = 10: Ambiguous internal boundary
c = 100: Clear internal boundary; non-smooth shape near variable points

48

Summary

- Lie spherical geometry can be used to design lattice shells that has high constructability.
- Mathematical formulation does not incorporate the effect of deformation related to material properties that should be considered even for small deformation.
- Laguerre transformation preserves the preferable mechanical properties of L-isothemic surfaces.
- Edge-offset surfaces allow the design of lattice shells with excellent constructability and mechanical properties.
- Piecewise developable surface can be a new class of shell surfaces ensuring efficient structural performance and constructability.

Evolving Design and Discrete Differential Geometry
- towards Mathematics Aided Geometric Design

Development of Bidirectional Circulative Design Platform

Presenter: Kentaro Hayakawa, Nihon Univ.

Concept of Bidirectional Circulative Design Platform

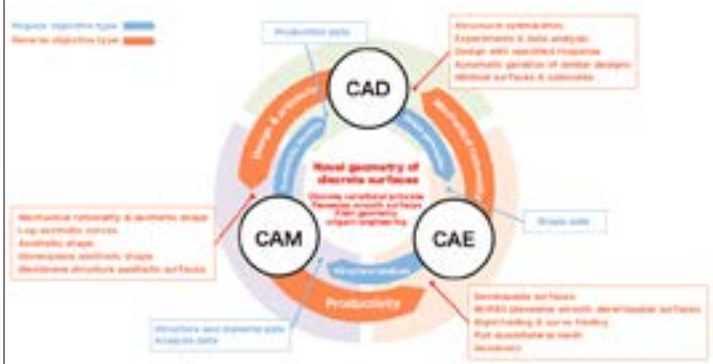

Concept of Bidirectional Circulative Design Platform

Bidirectional

Realize both

1. regular objective type
   (= conventional design)
2. reverse objective type
   (= optimization, inverse design)

design scheme

Circulative

Realize fast, efficient, and seamless rotation of above bidirectional design scheme

Framework

Software

Rhinoceros : widely used modelling and CAD software

Grasshopper : visual programming plugin of Rhinoceros

Python / C# : available in grasshopper

Geometric design tool as a set of components

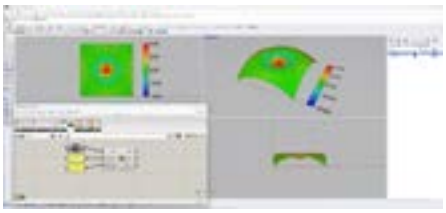

How to Use? What Can We Do?

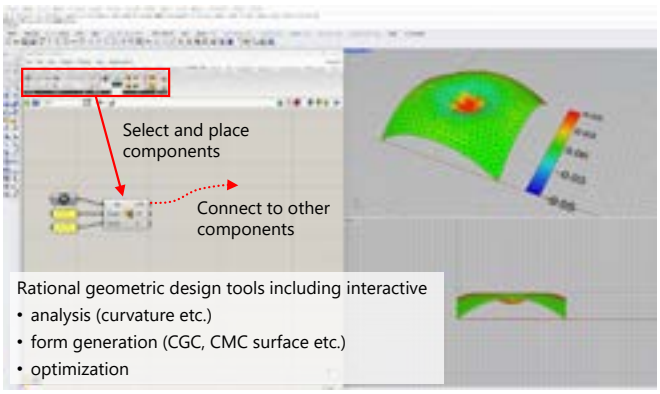

Rational geometric design tools including interactive

- analysis (curvature etc.)
- form generation (CGC, CMC surface etc.)
- optimization

Features of Proposed Design Platform

Easy generation of specific surface classes

Geometry of discrete surfaces

Developable surface, minimal surface, origami surface, etc.

Enhance reverse objective type design scheme for high efficiency, low cost, beauty, security, and safety of structure

Versatility through combination of multiple components inside/outside of platform

Geometry design + physics simulation

Geometry design + structural analysis + optimization

Example of Components

Utility

Constant Curvature Surface

Optimization

Origami

Shell and Membrane Structure

More components will be added.

Demonstrations

Origami surface approximation

Approximate input surface by rigid origami surface developable to plane

Generation of piecewise developable surface and structural optimization

Find positions of grid points to form a surface consisting of developable patches

Surface generation from stress distribution

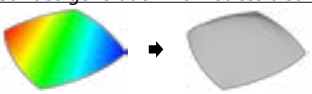

Generate a surface equilibrated with gravity with a specified horizontal stress distribution

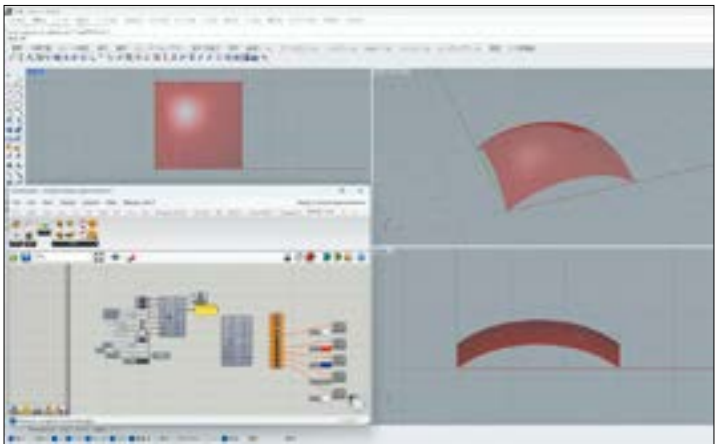

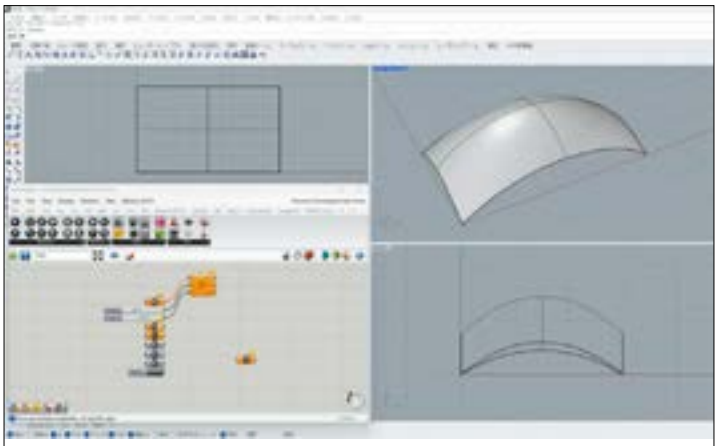

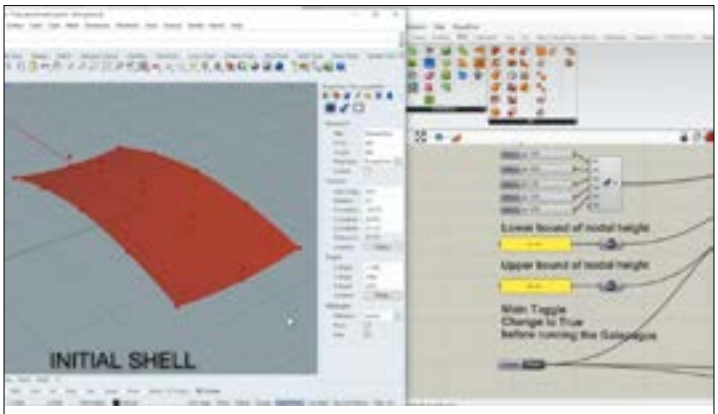
INITIAL SHELL
Lower bound of nodal height
Upper bound of nodal height
Main Toggle
Change to True
before running the Solver

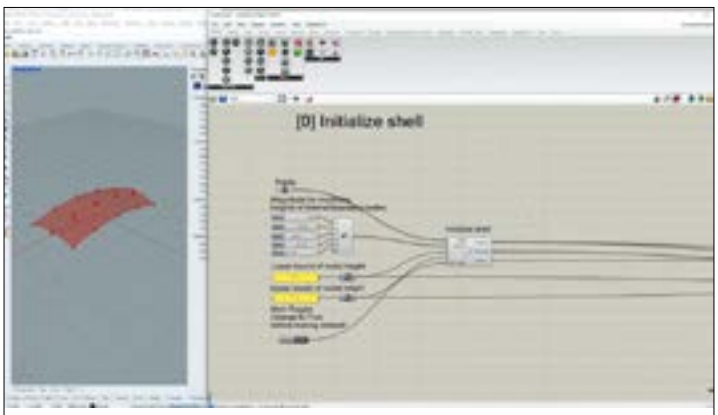
[0] Initialize shell

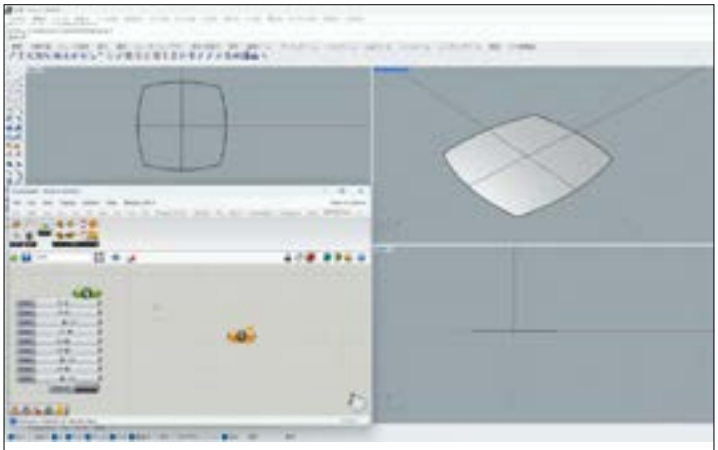

Development of bidirectional circulative design platform – case example (pillow box)

Shun Kumagai
(Hachinohe Institute of Technology, Kajiwara group)

International Conference "Evolving Design and Discrete Differential Geometry
- towards Mathematics Aided Geometric Design"
2025/3/11

Context of this presentation

- This talk presents **a case example** of implementation and actual use of components in the bidirectional circulative design platform.
- The components are designed to handle ``**pillow box**''.
- For theoretical discussions and applications in architecture, please refer to **tomorrow's talks by Prof. Koiso and Prof. Yokosuka**.

Objective: pillow box of maximal volume

A pillow box is a closed, box-shaped surface formed by creasing a double rectangular sheet rigidly along given curves.

Theorem (Koiso). For any $a, b > 0$, there exists a unique pillow box with maximal volume that is isometric to the rectangle with width $2a$ and height $2b$. It is represented by a developable surface that includes the ``**main curve**'' described on the next slide.

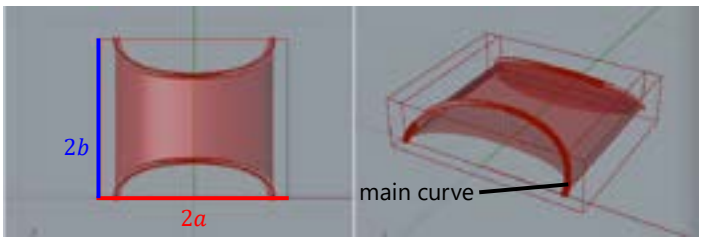

Formula for maximum-volume pillow box

The main curve of the pillow box of input (a, b) is described by :

$$x = x(z) := \pm I_\mu(z) \mp I_\mu(z_0), \quad 0 \le z \le z_0, \quad \left(0 \le x \le I_\mu(z_0)\right)$$

$$I_\mu(z) := \int_0^z \frac{-\mu\zeta\left(1-\frac{\zeta}{b}\right)}{\sqrt{1-\left(\mu\zeta\left(1-\frac{\zeta}{b}\right)\right)^2}}\,d\zeta, \quad z_0 = z_0(\mu) := \frac{b}{2}\left(1-\sqrt{1-\frac{4}{b|\mu|}}\right),$$

where $\mu < 0$ is a solution of the equation $a = \int_0^{z_0(\mu)} \frac{d\zeta}{\sqrt{1-\left(\mu\zeta\left(1-\frac{\zeta}{b}\right)\right)^2}}$.

The configuration can be determined by **any** of the input pairs (a, b), (b, z_0), or $(b, c{:=}x(0))$.

4

Formula for maximum-volume pillow box

The following description of the main curve represents one possible isometric transformation process ($t = 0$: rectangle, $t = 1$: pillowbox) :

$$x_t = x_t(z) := \pm I_{\mu,t}(z) \mp I_\mu(z_{0,t}), \quad 0 \le z \le z_{0,t}, \quad \left(0 \le x \le I_\mu(z_{0,t})\right)$$

$$I_{\mu,t}(z) := \int_0^z \frac{-\mu\zeta\left(1-\frac{\zeta}{b}\right)+t}{\sqrt{1-\left(\mu\zeta\left(1-\frac{\zeta}{b}\right)-t\right)^2}}\,d\zeta, \quad z_{0,t} = z_{0,t}(\mu) := \frac{b}{2}\left(1-\sqrt{1-\frac{4(1-t)}{b|\mu|}}\right),$$

where $\mu < 0$ is a solution of the equation $a = \int_0^{z_{0,t}(\mu)} \frac{d\zeta}{\sqrt{1-\left(\mu\zeta\left(1-\frac{\zeta}{b}\right)-t\right)^2}}$.

Pillow box components include an **interactive solver** for these equations, which corresponds to the given input. (built-in python script)

5

Tool1: regular objective type

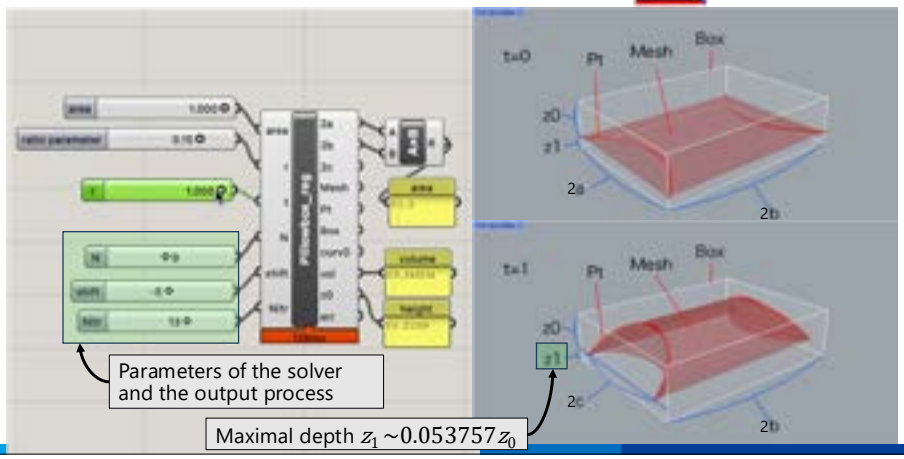

Tool1: regular objective type

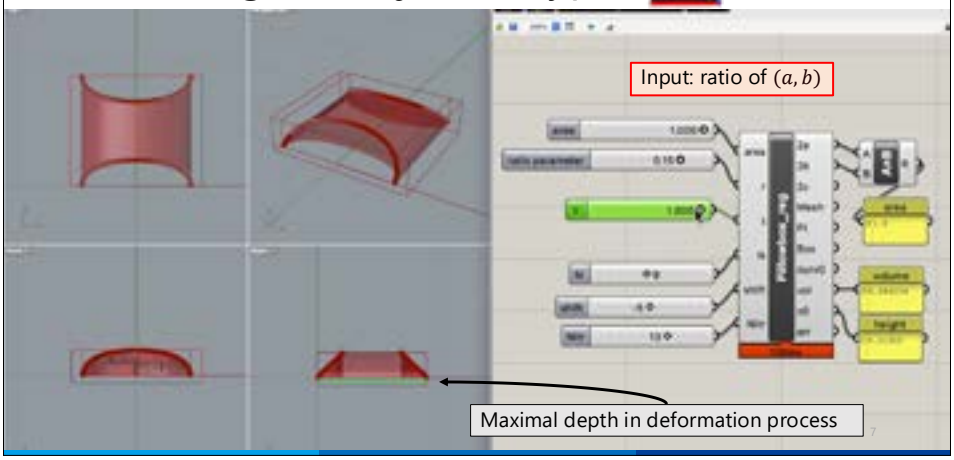

Tool1: regular objective type

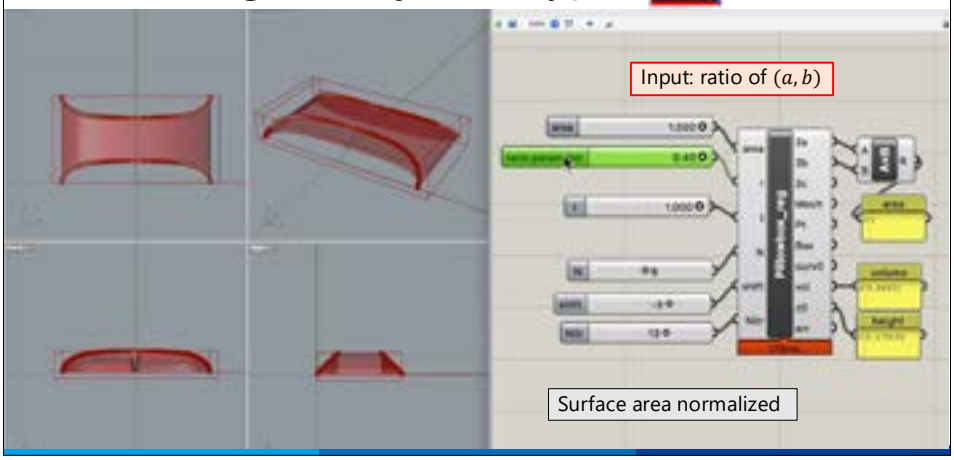

Tool2: reverse objective type (height)

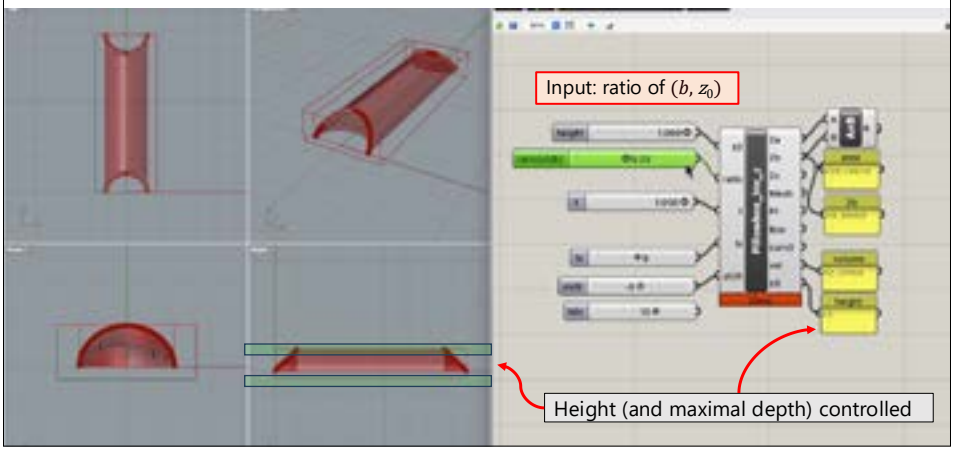

Tool3: reverse objective type (box width)

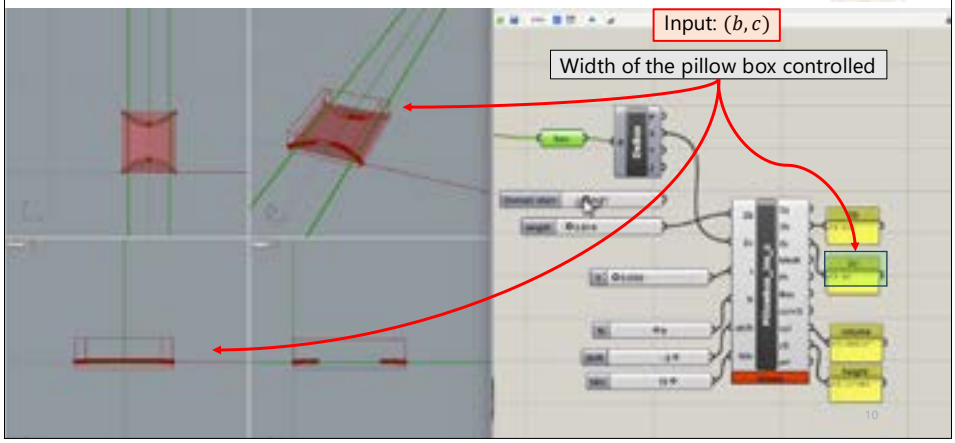

Contents of pillow box tools

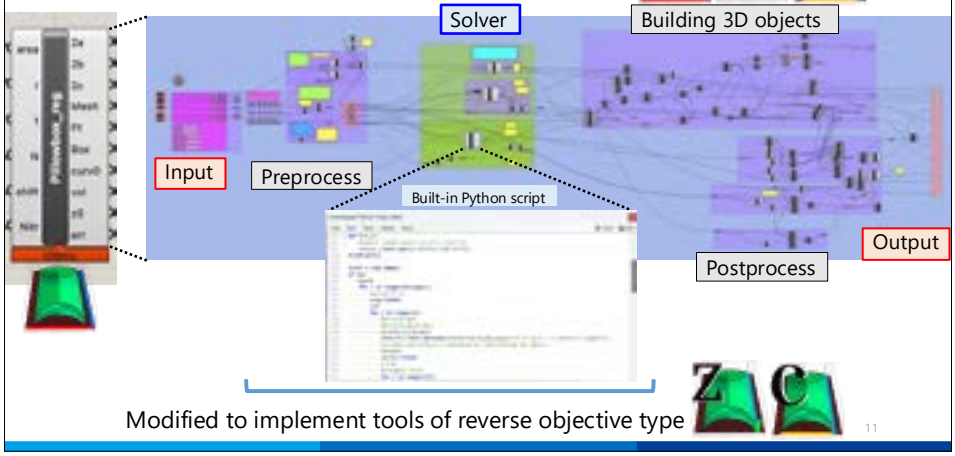

Modified to implement tools of reverse objective type

Example of tool use: printing a pillow box

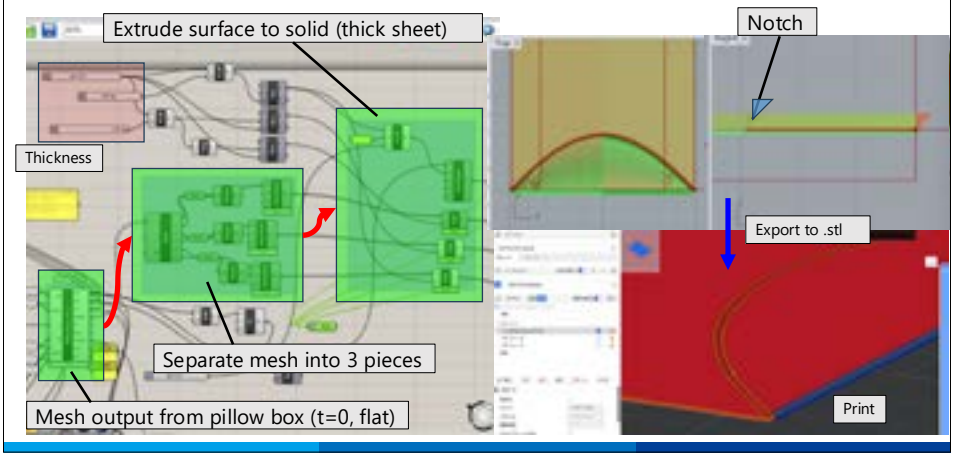

Example of tool use: discretization and optimizing ratio

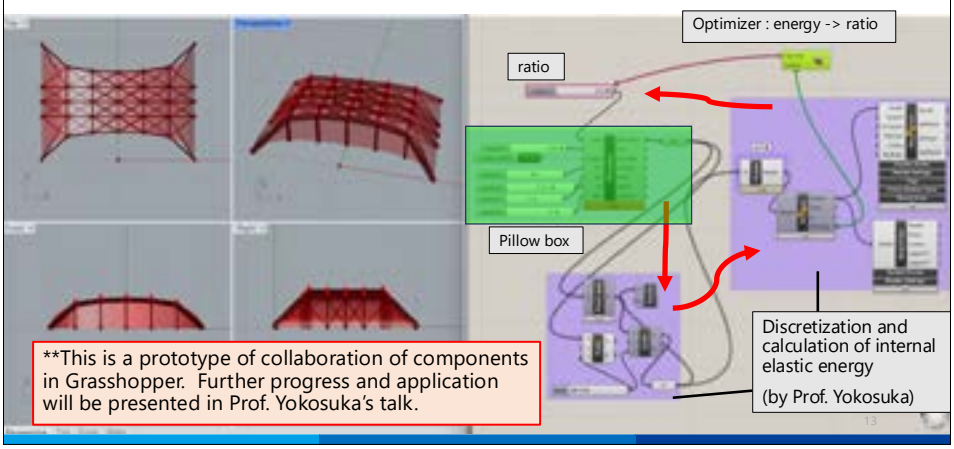

Contents of pillow box tools

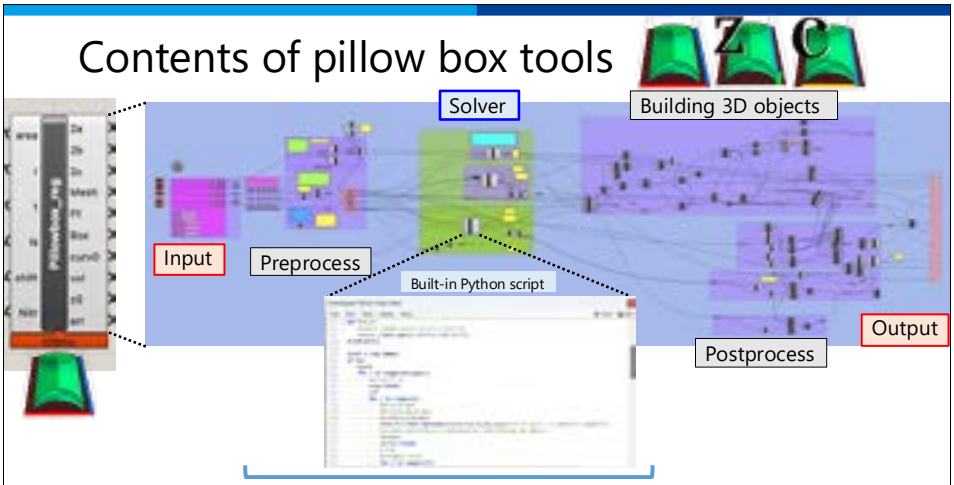

Arrange to fit the objective -> reverse objective type design

Discrete conformality and beyond.
Where geometry meets computer graphics and mathematical physics

Alexander I. Bobenko
Institute of Mathematics, Technische Universität Berlin, Germany

Abstract

Structure-preserving discretization in the field of geometry is the paradigm of discrete differential geometry. In some aspects, the discrete theory turns out to be even richer than its smooth counterpart. It focuses on developing constructive methods. The well-established theory of discrete conformal maps and circle patterns is related to discrete integrable models of mathematical physics and has found applications in geometry processing. We present their generalizations beyond the conformal limit: decorated discrete conformal maps [1, 2] and ring patterns [3, 4], which share the corresponding existence and uniqueness statements. The theory and construction methods are based on convex variational principles related to hyperbolic geometry. We define discrete constant mean curvature (cmc) surfaces (soap bubble surfaces) [5] in terms of sphere packings with orthogonally intersecting circles. These discrete cmc surfaces can be constructed from orthogonal ring patterns. The data used for the construction is purely combinatorial - the combinatorics of the curvature line pattern. Numerous virtual and printed models as well as animation movies will be demonstrated.

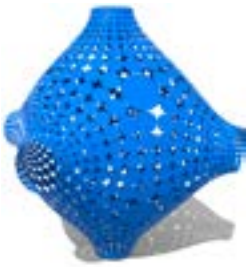

Figure 1: Left: Conformally parametrized tea pot costructed using discrete conformal mappings.
Right: A discrete cmc surface constructed using orthogonal ring patterns [5].

References

[1] A.I. Bobenko, C.O. Lutz, Decorated discrete conformal maps and convex polyhedral cusps, Intern. Math. Research Notices 2024:12 (2024), 9505-0534, doi.org/10.1093/imrn/rnae016

[2] A.I. Bobenko, C. Lutz, Decorated discrete conformal equivalence in non-Euclidean geometries (2023) arXiv:2310.17529 [math.GT]

[3] A.I. Bobenko, T. Hoffmann, T. Rörig, Orthogonal ring patterns in the plane, Geometria Dedicata (2023), doi.org/10.1007/s10711-023-00859-y

[4] A.I. Bobenko, Spherical and hyperbolic orthogonal ring patterns: integrability and variational principles (2024) arXiv:2409.06573 [math.MG] [math.GT]

[5] A.I. Bobenko, T. Hoffmann, N. Smeenk, Constant mean curvature surfaces from ring patterns: Geometry from combinatorics (2024) arXiv:2410.08915 [math.DG]

Discrete conformality and beyond. Where geometry meets computer graphics and mathematical physics

Alexander Bobenko

Technische Universität Berlin

Evolving Design and Discrete Differential Geometry - towards Mathematics Aided Geometric Design, Fukuoka, March 2025

DGD | SFB TRR 109 | Discretization in Geometry and Dynamics

Discrete Differential Geometry.

Development of discrete equivalents of notions and methods of differential geometry.

- Structure preserving discretizations.
- Classical theory as a limit of refinements of the discretization.
- Constructive. Computational
- Applications: computer graphics
- Discrete (integrable) models in physics

Conformal maps

- conformal means *angle preserving*
- infinitesimal lengths scaled by conformal factor

$$|df| = e^u |dx|$$

independent of direction

- in the small like *similarity transformations*
- Problem: surface in space $\xrightarrow{\text{conformally}}$ plane

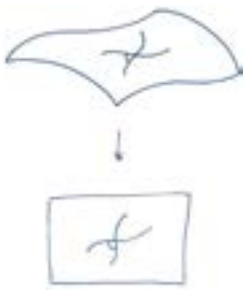

Discrete conformal maps

(Orthogonal) circle patterns

- angle properties
- convergence to conformal maps
- maps in the plane

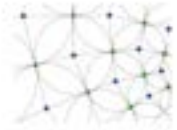

[Thurston, Stephenson, Schramm, He, AB, Springborn ... 1980'-]

Discrete conformal equivalence

- metric properties
- $\tilde{\ell}_{ij} = e^{(u_i+u_j)/2}\,\ell_{ij}$
- works for surfaces

[Luo, Springborn, Pinkall, Schröder, AB, Gu, Sun, Wu ... 2004-]

Generalizations?

Conformal mappings very rigid:

- Computer Graphics: large variations of conformal factor, optimization of conformality and isometry, discretizations of quasi-conformal
- Physics: conformal models $\rightarrow$ massive models.
- Differential geometry: minimal surfaces $\rightarrow$ cmc surfaces

Discrete models with a mathematical theory?

I. Decorated discrete conformal mappings

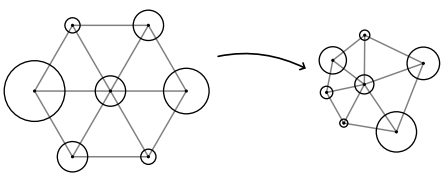

Joint with Carl Lutz

Discrete conformal equivalence

- abstract surface triangulation $M = (V, E, T)$

A *discrete metric* on M is a function

$$\ell : E \to \mathbb{R}_{>0}, \quad ij \mapsto \ell_{ij}$$

satifying all triangle inequalities:

$$\forall\, ijk \in T: \quad \begin{aligned} \ell_{ij} &< \ell_{jk} + \ell_{ki} \\ \ell_{jk} &< \ell_{ki} + \ell_{ij} \\ \ell_{ki} &< \ell_{ij} + \ell_{jk} \end{aligned}$$

Discrete conformal equivalence

Definition [Luo '04]

Two discrete metrics ℓ, $\tilde{\ell}$ on M are *(discretely) conformally equivalent* if

$$\tilde{\ell}_{ij} = e^{\frac{1}{2}(u_i+u_j)}\ell_{ij}$$

for some function $u : V \to \mathbb{R}$

- use $\lambda_{ij} = 2\log \ell_{ij}$
  $\tilde{\lambda}_{ij} = \lambda_{ij} + u_i + u_j$

Mapping problem

- angles sum around vertex i

$$\Theta_i = \sum_{ijk \ni i} \alpha^i_{jk}$$

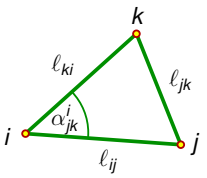

- Given mesh M, metric $\ell_{ij} = e^{\frac{1}{2}\lambda_{ij}}$, and desired angle sums $\widehat{\Theta}_i$

  Find conformally equivalent metric $\tilde{\ell}_{ij}$ with

$$\widetilde{\Theta}_i = \widehat{\Theta}_i$$

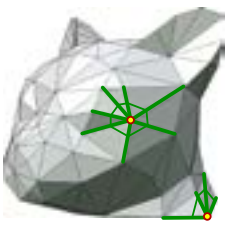

Variational principle

- $S(u) \stackrel{\text{def}}{=} \sum_{ijk \in T} \Big(\tilde{\alpha}_{ij}^{k} \tilde{\lambda}_{ij} + \tilde{\alpha}_{jk}^{i} \tilde{\lambda}_{jk} + \tilde{\alpha}_{ki}^{j} \tilde{\lambda}_{ki} - \frac{\pi}{2} (\tilde{\lambda}_{ij} + \tilde{\lambda}_{jk} + \tilde{\lambda}_{ki}) + 2\,\text{Л}(\tilde{\alpha}_{ij}^{k}) + 2\,\text{Л}(\tilde{\alpha}_{jk}^{i}) + 2\,\text{Л}(\tilde{\alpha}_{ki}^{j}) \Big) + \sum_{i \in V} \widehat{\Theta}_i u_i$
- Milnor's Lobachevsky function

$$\text{Л}(\alpha) = -\int_0^\alpha \log |2 \sin t| \, dt$$

$\tilde{\ell}_{ij} = e^{\frac{1}{2}(\lambda_{ij} + u_i + u_j)}$ solves mapping problem

$\Updownarrow$

$u = (u_1, \ldots, u_n)$ is critical point of $S(u)$

[Springborn-Pinkall-Schröder '08]

Ronkin function. Convexity

- $S(u) = \sum_{ijk \in T} \big(2f(\frac{\tilde{\lambda}_{ij}}{2}, \frac{\tilde{\lambda}_{jk}}{2}, \frac{\tilde{\lambda}_{ki}}{2}) - \pi/2(\tilde{\lambda}_{ij} + \tilde{\lambda}_{jk} + \tilde{\lambda}_{ki}) \big) + \sum_{i \in V} \widehat{\Theta}_i u_i$
- $f(x_1, x_2, x_3) = \alpha_1 x_1 + \alpha_2 x_3 + \alpha_3 x_3 + \text{Л}(\alpha_1) + \text{Л}(\alpha_2) + \text{Л}(\alpha_3)$
- Ronkin function; free energy of the thermodynamic limit of a dimer model on hexagonal grid
  [Kenyon-Okounkov-Sheffield '06]
- convex

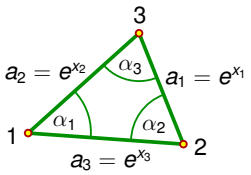

How it works: Riemann mapping theorem

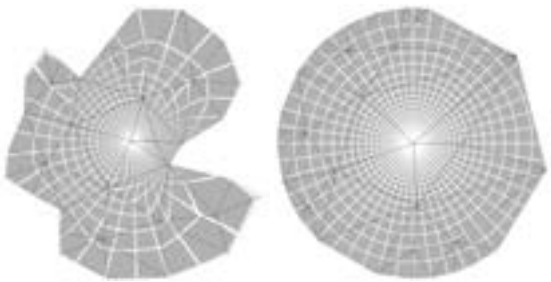

[AB-Pinkall-Springborn '15]

How it works: Riemann mapping theorem

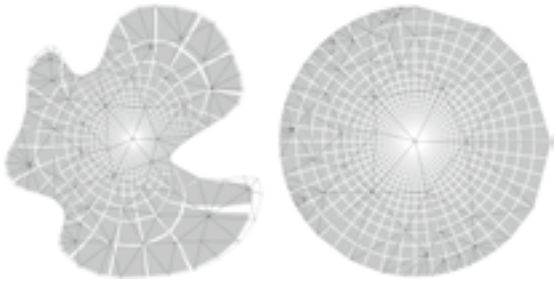

[AB-Pinkall-Springborn '15]

How it works: Riemann mapping theorem

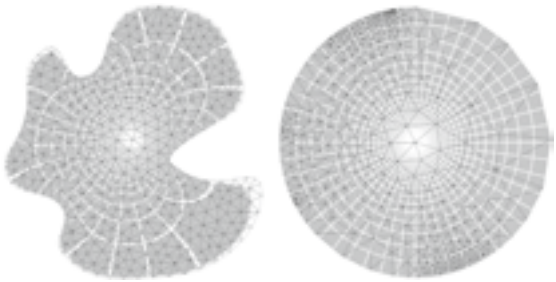

[AB-Pinkall-Springborn '15]

How it works: Conformal parametrization of surfaces

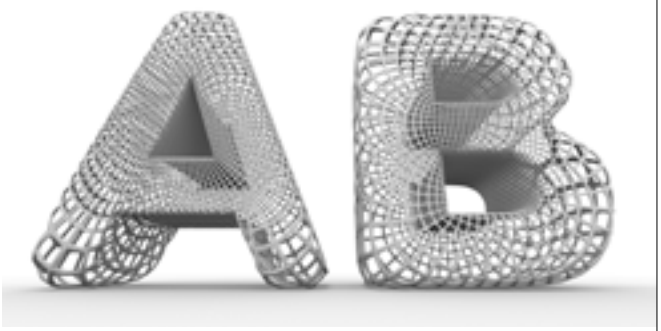

Discrete conformal KPM tea pot

Discrete conformal KPM tea pot

Discrete conformal KPM tea pot

Discrete conformal KPM tea pot

Induced hyperbolic metric

Origin: Hyperbolic geometry interpretation
[AB, Pinkall, Springborn '15]

- circumcircle induces hyperbolic metric (Klein model)
- euclidean triangle $\rightarrow$ ideal hyperbolic triangle
- vertices at infinity (cusps)
- conformally equivalent discrete metrics $\Leftrightarrow$ same hyperbolic metric (with cusps)
- Definition of conformally equivalent metrics **with different triangulations** $\Leftrightarrow$ same hyperbolic metric

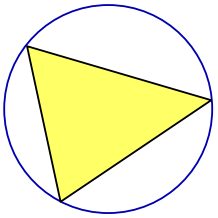

Discrete Uniformization

Theorem. (Gu-Luo-Sun-Wu 2018)

For any piecewise euclidean metric on a surface of genus g with n marked points and for any Θ_i satisfying the Gauss-Bonnet condition

$$\frac{1}{2\pi}\sum \Theta_i = 2g - 2 + n$$

there exists a discretely conformally equivalent metric with the cone angles Θ_i. It is uniquely determined up to scale.

- **DG** [Gu-Luo-Sun-Wu '18] sequence of Delaunay triangulations.
- **CG** [Gillespie-Springborn-Crane '21] effective numerical realization.

Decorated Discrete Conformal (DCE)

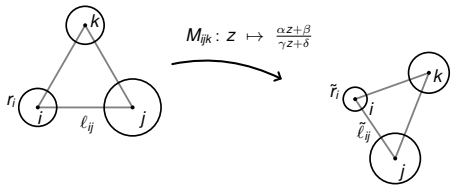

- Möbius equivalent decorated triangles

Decorated Discrete Conformal (DCE)

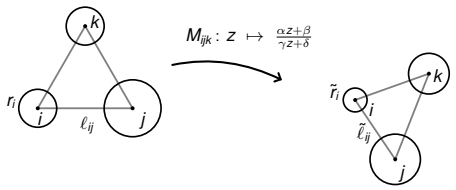

- Möbius equivalent decorated triangles
- Inversive distance invariant $I_{ik} = \frac{\ell_{ik}^2 - r_i^2 - r_k^2}{2 r_i r_k}$
- two decorated triangles are Möbius equivalent iff the inversive distances of their sides coincide

Decorated Discrete Conformal (DCE)

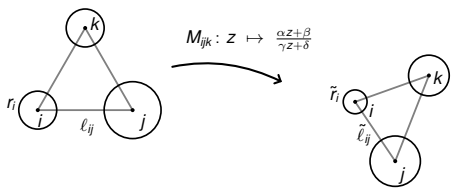

- Möbius equivalent decorated triangles
- Inversive distance invariant $I_{ik} = \frac{\ell_{ik}^2 - r_i^2 - r_k^2}{2 r_i r_k}$
- two decorated triangles are Möbius equivalent iff the inversive distances of their sides coincide

Decorated Discrete Conformal (DCE)

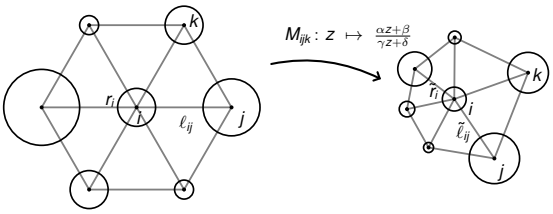

- Möbius equivalent decorated triangles
- $\tilde{r}_i = e^{u_i} r_i$
  $\tilde{\ell}_{ij}^2 = (e^{2u_i} - e^{(u_i+u_j)}) r_i^2 + e^{(u_i+u_j)} \ell_{ij}^2 + (e^{2u_j} - e^{(u_i+u_j)}) r_j^2$
- discretely conformally equivalent triangulated decorated PE-surfaces (same combinatorics)

Discrete Conformal as Special Case

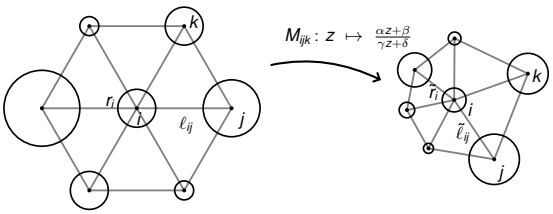

- any two triangles are Möbius equivalent, no inversive distance for $r = 0$
- infinitesimal circles $r_i \to 0$
- $\tilde{\ell}_{ij} = e^{(u_i+u_j)/2} \ell_{ij}$

Decorated Discrete Conformal Maps

- Discrete conformal maps of inversive distance circle patterns [Bowers-Stephenson '04]. Existence and uniqueness?
- Numerical computations [Bowers-Hurdal '03]
- Unified discrete Ricci flow [Zhang et al. '14]
- Discrete conformal structures via duality structures [Glickenstein '11]
- Decorated discrete conformal maps [AB-Lutz '23]. Variable combinatorics. Existence and uniqueness theorems

Decorated Discrete Conformal Mapping Problem

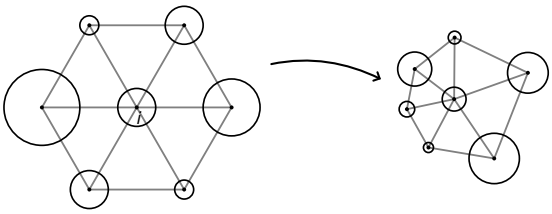

- ***Given***:
  - a triangulation $\mathcal{T}$ of the surface $\mathcal{S}_g$,
  - a decorated PE-metric (ℓ, r),
  - and a desired angel sums Θ_i.
- ***Find***: u_i such that the DCE-changed metric *w.r.t.* u_i has angle sums Θ_i.

Decorated Discrete Conformal Mapping Problem

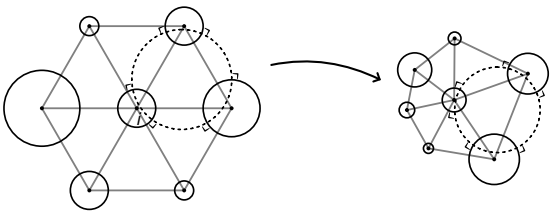

Varying Combinatorics

- Consider PE-metrics $(\mathcal{T}, \ell) \leftrightarrow \mathrm{dist}_{\mathcal{S}_g}$
- if circles non-intersecting, there exist weighted Delaunay triangulations (wDt), empty disc property
- sequences of wDts
- non-decorated [Gu-Luo-Sun-Wu '18, Springborn '19]

Uniformization theorem (AB, Lutz 2023)

Theorem

Given a hyperideally decorated PE-metric $(\mathrm{dist}_{\mathcal{S}_g}, r)$ *on the closed marked genus g surface* $(\mathcal{S}_g, V)$*. Then*

- *(existence) a decorated PE-metric DCE to* $(\mathrm{dist}_{\mathcal{S}_g}, r)$ *realizing* $\Theta \in \mathbb{R}^V_{>0}$ *exists iff* Θ *satisfies the Gauß–Bonnet condition*

$$\frac{1}{2\pi}\sum \Theta_i \;=\; 2g - 2 + |V|.$$

- *(uniqueness) there exists at most one decorated PE-metric DCE to* $(\mathrm{dist}_{\mathcal{S}_g}, r)$ *realizing* $\Theta \in \mathbb{R}^V_{>0}$*, up to scale.*
- *(variational principle)* $u \in \mathbb{R}^V$ *giving the change of metric minimizes the discrete convex Hilbert–Einstein functional (volume of a hyperideal hyperbolic tetrahedron).*

The uniformization theorem by [Gu-Luo-Sun-Wu '18] is $r = 0$.

II. Orthogonal ring patterns

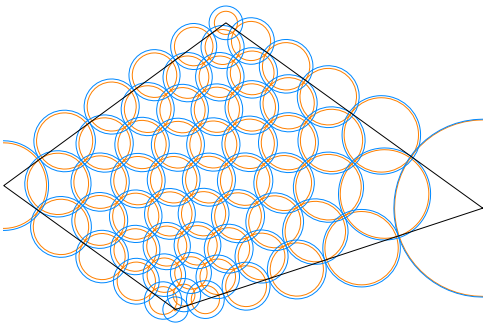

Joint with Tim Hoffmann, Nina Smeenk

Orthogonal circle patterns

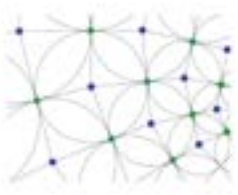

- Orthogonal circle patterns as discrete complex analysis
  [Schramm '97]
- Convergence to conformal maps
- Integrable equations

$$|f_x| = |f_y|, \quad f_x \perp f_y.$$

Orthogonal circle patterns

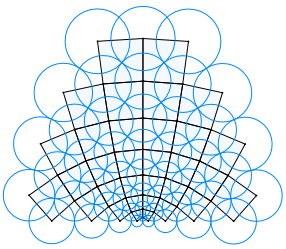

- Orthogonal circle patterns as discrete complex analysis
  [Schramm '97]
- Convergence to conformal maps
- Integrable equations

$$|f_x| = |f_y|, \quad f_x \perp f_y.$$

Orthogonally intersecting rings

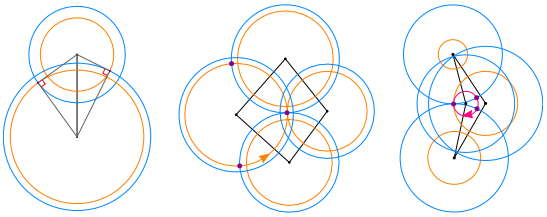

- A ring is a pair of concentric circles C_i, c_i of radii: r_i and R_i
- The outer circle C_i intersects the inner circle c_j orthogonally
- Orthogonal rings have the same area

Orthogonal ring patterns in a sphere [AB '24]

- $q = \frac{\cos R}{\cos r}$ is global invariant
- circle pattern limit $q \to 1$
- parametrization in elliptic functions of modulus $q \leq 1$, $\sin r = \mathrm{cn}(\rho, q),\ \sin R = \mathrm{dn}(\rho, q)$

Q4 integrable equation

$$\frac{\mathrm{sn}\,\frac{1}{2}(\rho+\rho_1+iK')}{\mathrm{sn}\,\frac{1}{2}(\rho-\rho_1+iK')}\frac{\mathrm{sn}\,\frac{1}{2}(\rho+\rho_2+iK')}{\mathrm{sn}\,\frac{1}{2}(\rho-\rho_2+iK')}\times \\ \frac{\mathrm{sn}\,\frac{1}{2}(\rho+\rho_3+iK')}{\mathrm{sn}\,\frac{1}{2}(\rho-\rho_3+iK')}\frac{\mathrm{sn}\,\frac{1}{2}(\rho+\rho_4+iK')}{\mathrm{sn}\,\frac{1}{2}(\rho-\rho_4+iK')}=1.$$

- Radii of spherical (hyperbolic) orthogonal ring patterns
- Master integrable equation in the ABS-classification ['09]
- $\Delta u \pm \sinh u = 0$ in the smooth limit
- Variational principle [AB '24]. Elliptic generalization of dilogarithms, hyperbolic volumes?

Koebe polyhedra and orthogonal circle patterns

- Orthogonal circle pattern$\leftrightarrow$ Koebe polyheder
- Circumscribed polyhedron with touching edges

[Koebe, Andreev, Thurston,...]

Koebe polyhedra and minimal surfaces

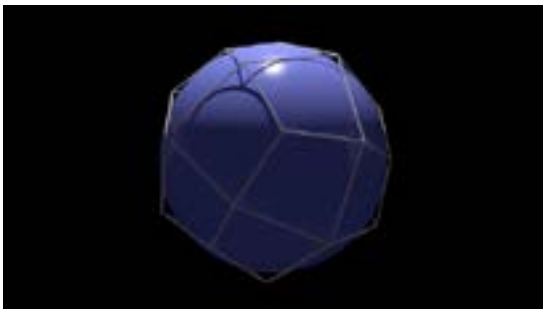

- Koebe polyhedron as Gauss map of minimal surface
  [AB-Hoffmann-Springborn, Annals '06]
- Animation film [AB-Newjoto-Techter '18]

Koebe polyhedra and minimal surfaces

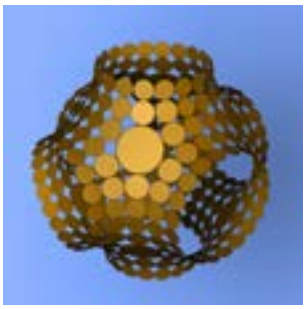

- Koebe polyhedron as Gauss map of minimal surface
  [AB-Hoffmann-Springborn, Annals '06]
- Animation film [AB-Newjoto-Techter '18]

Gauss maps. Orthogonal ring (circle) patterns

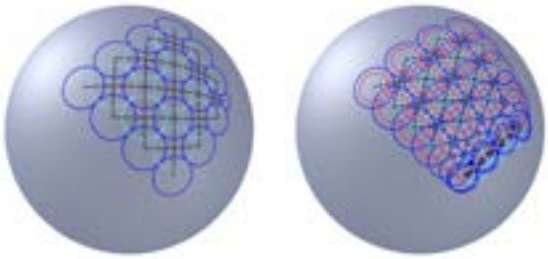

minimal cmc

Discrete cmc surfaces

cmc minimal cmc

- circle patterns $\Rightarrow$ minimal surfaces
- ring patterns $\Rightarrow$ cmc surfaces

C^∞-convergence?

smooth cmc
[AB-Heller-Schmitt '21]

discrete cmc
[AB-Hoffmann-Smeenk '24]

C^∞-convergence?

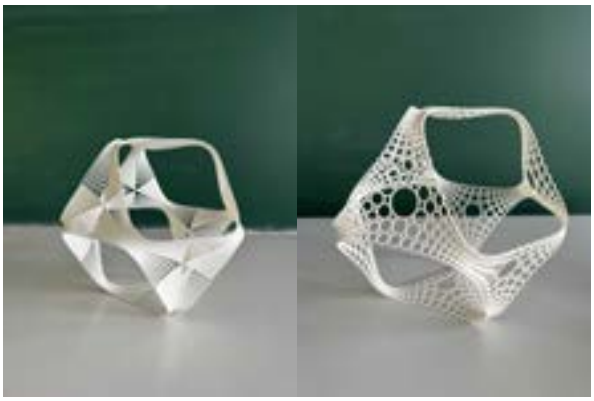

smooth cmc
[AB-Heller-Schmitt '21]

discrete cmc
[AB-Hoffmann-Smeenk '24]

C^∞-convergence?

C^∞-convergence?

smooth cmc
[AB-Heller-Schmitt '21]

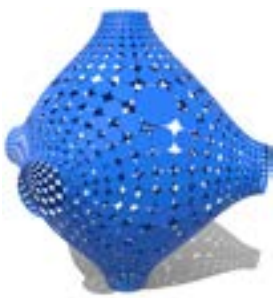

discrete cmc
[AB-Hoffmann-Smeenk '24]

Papers

- AB, Lutz, Decorated discrete conformal maps and convex polyhedral cusps, IMRN 2024:12 (2024)
- AB, Lutz, Decorated discrete conformal equivalence in non-Euclidean geometries, DCG (2025)
- AB, Hoffmann, Rörig, Orthogonal ring patterns in the plane, Geom. Dedicata (2023)
- AB, Spherical and hyperbolic orthogonal ring patterns: Integrability and variational principles (2024) arXiv:2409.06573
- AB, Hoffmann, Smeenk, Constant mean curvature surfaces from ring patterns: Geometry from combinatorics (2024) arXiv:2410.08915
- AB, Heller, Schmitt, Constant mean curvature surfaces based on fundamental quadrilaterals, MPAG (2021)

Interactive Design and Efficient Simulation of Developable Surfaces with Curved Folds

Jun Mitani
University of Tsukuba, Japan

Abstract

Developable surfaces with curved folds are widely used in engineering, architecture, digital fabrication, and computational design. However, their strict geometric constraints make both modeling and simulation non-trivial tasks. This talk introduces two complementary research approaches that address these challenges by focusing on interactive 3D modeling and efficient crease pattern-based simulation.

The first approach, proposed by Mitani and Ohashi [1], presents an interactive 3D modeling framework that enables users to directly manipulate curved fold structures in three-dimensional space. This method introduces a novel user interface based on a *handle curve*, which serves as an auxiliary control element for shaping the developable surface. By specifying both a crease curve (the curved fold) and a handle curve, users can intuitively deform the surface while ensuring developability and avoiding ruling collisions. This technique provides direct control over the 3D shape, making it particularly useful for interactive design applications in CAD modeling and digital fabrication.

In contrast, the second approach, developed by Sasaki and Mitani [2], focuses on efficiently generating 3D folded structures from 2D crease patterns. Instead of direct 3D manipulation, this method takes a given crease pattern, approximates curved folds using polylines, and applies a ruling-aware triangulation to construct a 3D model that accurately simulates the folded state. Implemented in a web-based Origami Simulator [3], this approach enables fast and computationally efficient simulation, making it ideal for applications where the input is a crease pattern rather than a predefined 3D model. The method allows for quick evaluation of different folding scenarios and helps designers explore complex curved fold structures without manual 3D adjustments.

By integrating these two methods—interactive modeling and efficient simulation—we provide a powerful framework for designing and analyzing developable surfaces with curved folds. This talk will discuss the theoretical foundations, algorithmic implementations, and potential applications of these techniques in digital fabrication, CAD modeling, and origami design.

References

[1] Jun Mitani, Kaoru Ohashi, “Interactive Curved Fold Modeling using a Handle Curve”, Computer-Aided Design and Applications, **20(2)** (2022) 275–289, https://doi: 10.14733/cadaps.2023.275-289.

[2] Kosuke Sasaki, Jun Mitani, “Simple implementation and low computational cost simulation of curved folds based on ruling-aware triangulation”, Computers & Graphics, **102** (2021) 213–219, https://doi:10.1016/j.cag.2021.09.012.

[3] Amanda Ghassaei, Erik D. Demaine, Neil Gershenfeld, “Fast interactive origami simulation using gpu computation”, Origami **7** (2018) 1151–66.

筑波大学

Interactive Design and Efficient Simulation of Developable Surfaces with Curved Folds

Jun Mitani
University of Tsukuba, JAPAN

1

Today's talk

- Provide topics related to shape modeling of origami.
- The main focus is on introducing several origami design applications that we have developed so far.
- There will be no novel points in view of mathematics (sorry), but focusing on interactive design approach for origami shapes.

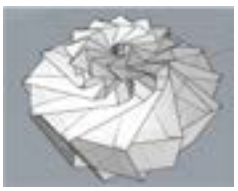

6

Geometry of ruled surfaces

The trajectory traced by the continuous movement of a straight element (ruling).

$$\boldsymbol{X}(\mathrm{s},\mathrm{t}) = \boldsymbol{p}(\mathrm{s}) + t \cdot \boldsymbol{e}(\mathrm{s})$$

$\boldsymbol{p}(\mathrm{s})$: A curve that represents the movement of a straight line.

$\boldsymbol{e}(\mathrm{s})$: A unit vector representing the direction of a straight line.

s: arc length

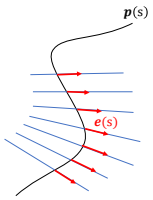

Ex: Hyperbolic Paraboloid

$$X(\mathrm{s},\mathrm{t}) = p(\mathrm{s}) + t(q(\mathrm{s}) - p(s))$$

p(s) and q(s) are two skew lines.

Developable surface

$$\mathbf{X}(\mathrm{s},\mathrm{t}) = \boldsymbol{p}(s) + t \cdot \frac{\boldsymbol{p}''(s) \times \boldsymbol{p}'''(s)}{|\boldsymbol{p}''(s)|^2}$$

geodesic on a surface — direction of rulings

p": principal normal direction

Another expression $r(s) = \tau T + \kappa B$

τ: torsion, κ: curvature, T: unit tangent vector, B: unit binormal vector

$$X(s,t) = p(s) + t(p''(s) \times p'''(s))$$

Geometry of Curved Folds

(1) $\kappa_{2D}(s) = \kappa(s)\cos\alpha(s)$

(2) $\cot\beta_L(s) = \dfrac{\alpha(s)' - \tau(s)}{\kappa(s)\sin\alpha(s)}$

(3) $\cot\beta_R(s) = \dfrac{-\alpha(s)' - \tau(s)}{\kappa(s)\sin\alpha(s)}$

[Tachi 2011]

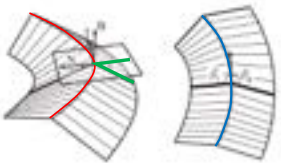

(a) 3D crease curve (defined by $\kappa(s)$ and $\tau(s)$)
(b) 2D crease curve (defined by $\kappa_{2D}(s)$)
(c) Fold angle ($\alpha(s)$)

Two of above parameters (a),(b),and(c) define the other one.

15

Even though the mathematics of curve fold geometry is revealed, we still do not know how to design *attractive* curved origami.

Following Topics

1. Three design tools we developed before
2. Curved folds on Origami Simulator
3. Design interface for a space curved fold

How can we make a sphere with a single sheet of paper?

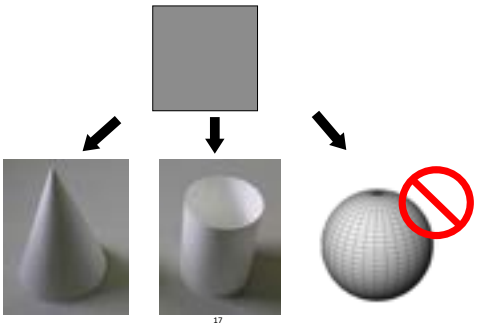

17

A square sheet wraps around the sphere.
The presence of fine wrinkles allows the paper to deform flexibly.

18

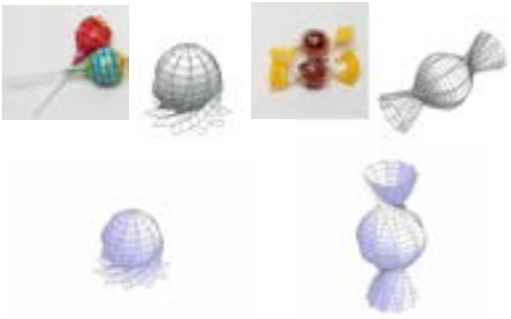

19

Basic idea

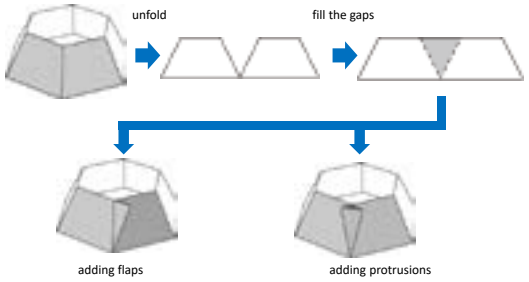

20

Unfold of a sphere

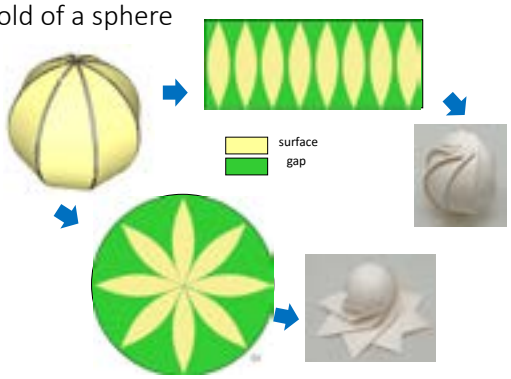

ORI-REVO

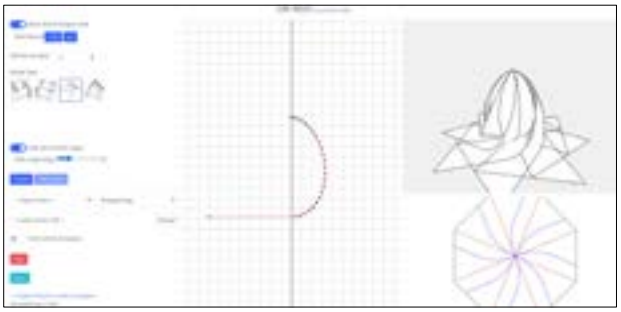

https://mitani.cs.tsukuba.ac.jp/ja/software/orirevo/

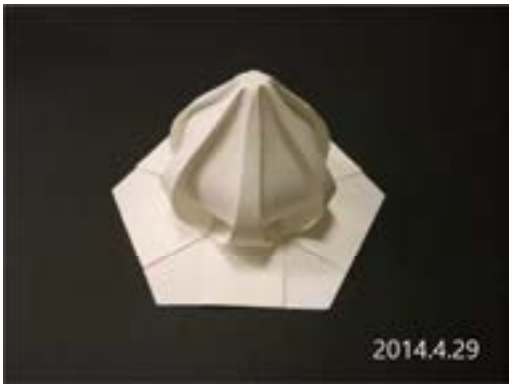

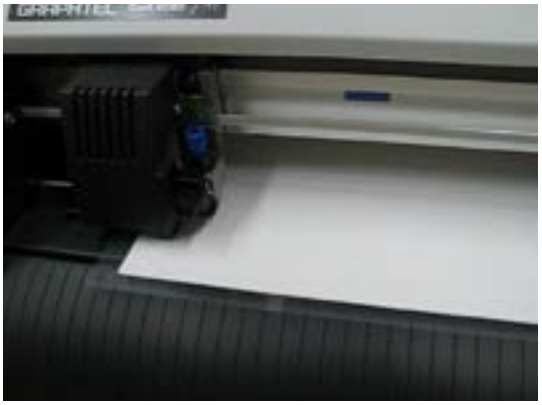

Interactive Design of Planar Curved Folding by Reflection

Demo

A fold can be added to a developable surface by reflecting a part of the surface by an intersecting plane.

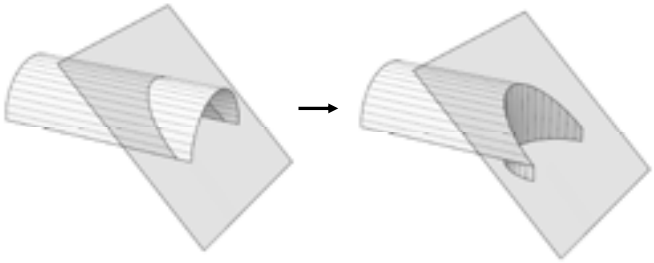

Mirror operation adds a planer curve fold.

A set of mirror operations

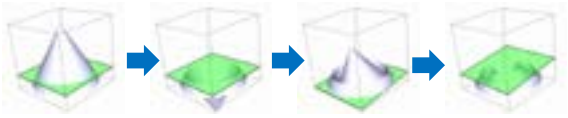

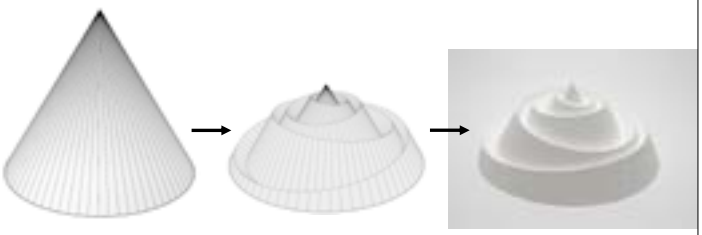

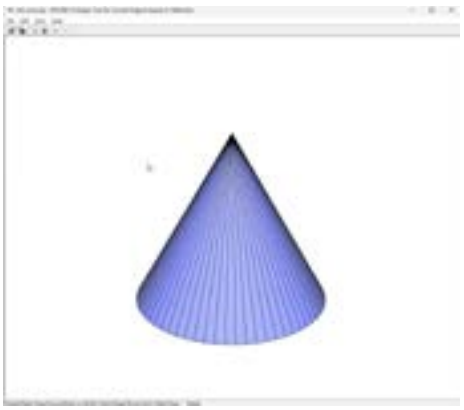

Design tool for curved folds based on reflection

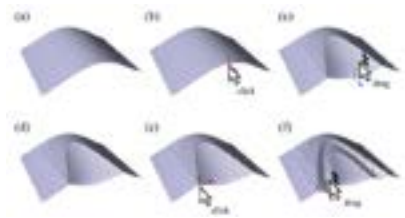

DEMO

Demo

37

The perpendicular bisector of the line segment connecting the initial coordinates of the vertex and the coordinates after moving is taken as the mirror plane.

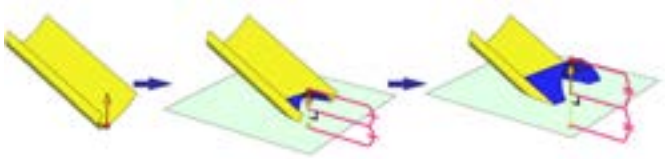

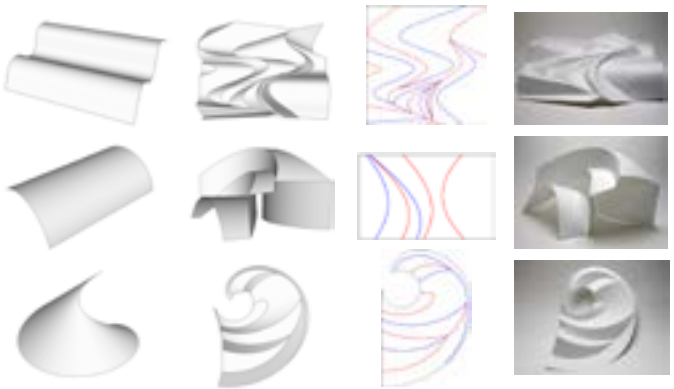

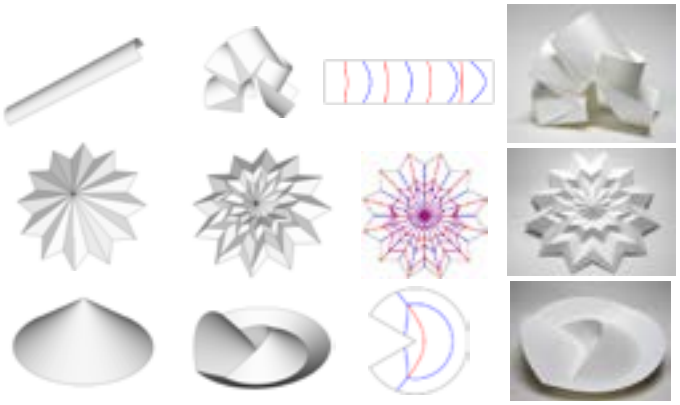

Column-shaped Origami Design Based on Mirror Reflections

Making a cylindrical surface by a sweep operation

- Elements deciding the shape
  - **Profile polyline**: lying on a vertical plane
  - **Trajectory path**: perpendicular to the vertical plane

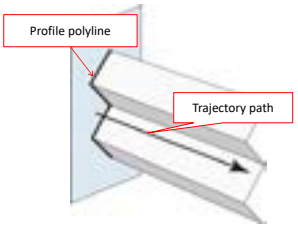

Add a fold by a reflection

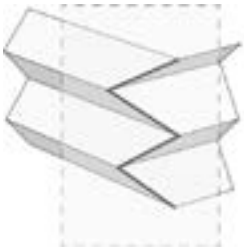

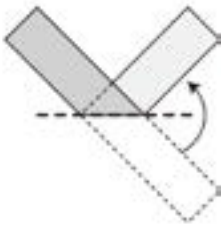

Top view

Reflection planes are placed according to the Trajectory path

- A reflection plane is positioned so that each corner of the polyline lies on it.
- Then the reflection plane is orientated so that its normal vector coincides with the bisector of the corner angle.

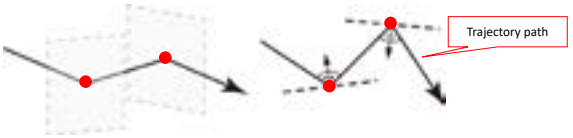

Trajectory path looks like a bounce trajectory of light rays by reflection planes.

The profile polyline and the trajectory path defines the shape

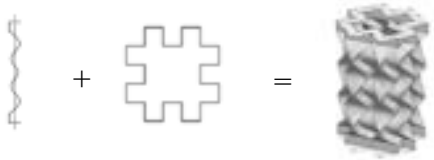

Profile polyline Trajectory path

The Trajectory path represents the final shape as seen from above

Reconstruction of known patterns : **Miura pattern**

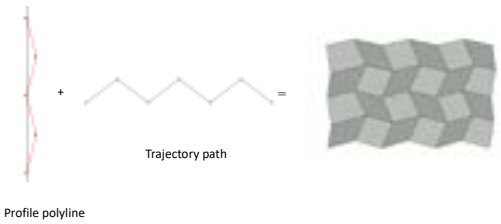

Reconstruction of known patterns : **Yoshimura Pattern**

- Degenerated line elements exist.

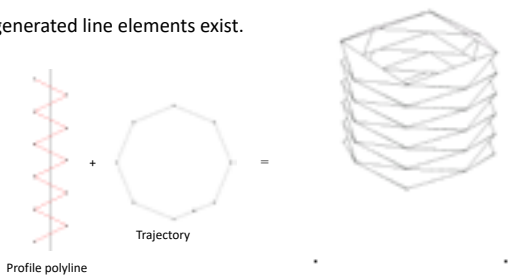

Implemented system

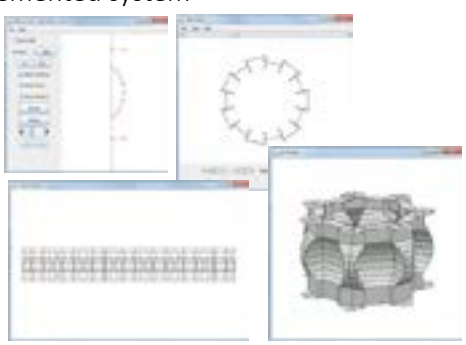

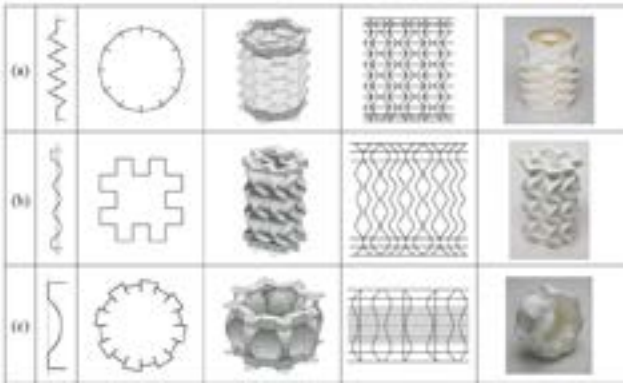
(a)
(b)
(c)

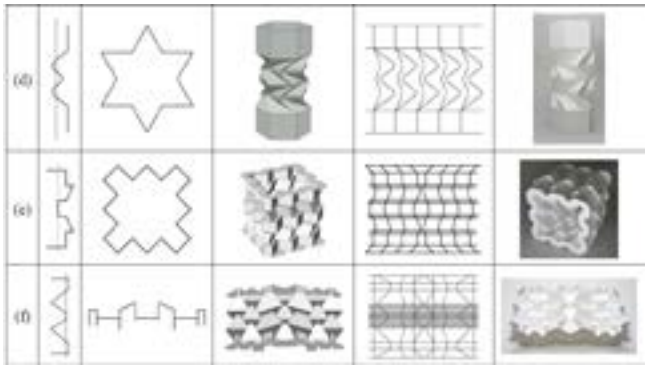
(d)
(e)
(f)

Curved folds on Origami Simulator

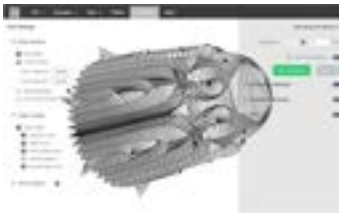

Kosuke Sasaki, and Jun Mitani. Simple implementation and low computational cost simulation of curved folds based on ruling-aware triangulation. Computers & Graphics, 2021.

Origami Simulator used to support only straight folds

https://origamisimulator.org/

developed by Amanda Ghassaei

62

Simulation on the past Origami Simulator

Crease pattern

Ear clipping algorithm

Triangular mesh

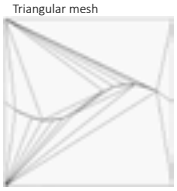

63

Simulation on the current Origami Simulator

Crease pattern

Ruling-aware triangulation

Triangular mesh

Better triangular mesh for curved folds

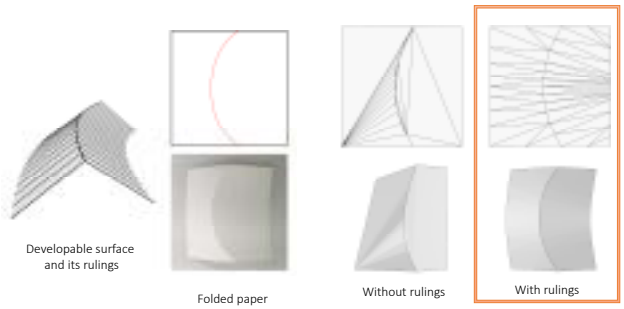

65

Outline of the proposed method

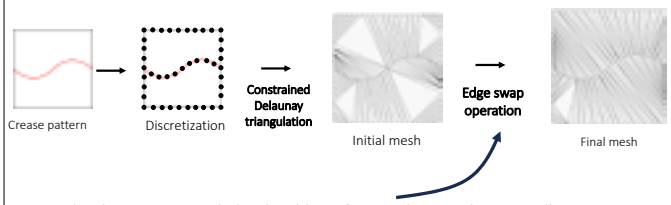

1) Rulings on a smooth developable surface tend not to align conically.
2) Rulings and the curved creases tend to align orthogonally on the unfolded pattern.

69

Edge swap operation

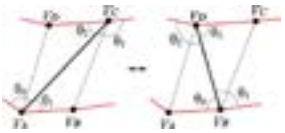

1. Find edges that meet:
   - ① Neither crease line nor borderline
   - ② No more than three edges share the vertex V_B and V_D.
   - ③ The value of $\boldsymbol{E}$ becomes smaller by the edge-swap operation.
     E is the value by which to evaluate the orthogonality between rulings and creases on the planar state.
     Smaller E values indicate more orthogonality.
     $E = (\theta_0 - \theta_1)^2 + (\theta_2 - \theta_3)^2$
2. The edge-swap operation is applied to the edge that has the smallest value of E after the edge-swap operation.

72

Results of triangulation

Crease pattern Initial mesh Final mesh

73

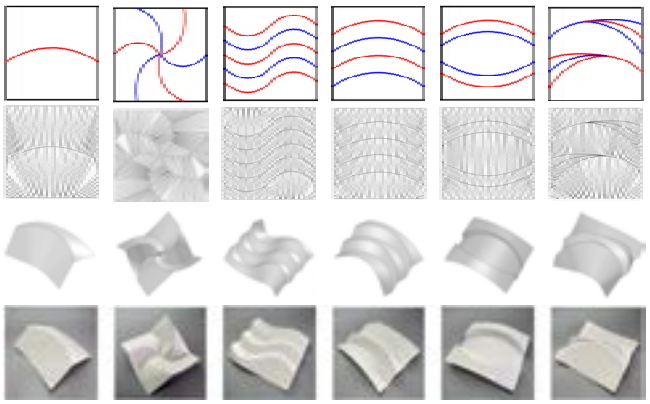

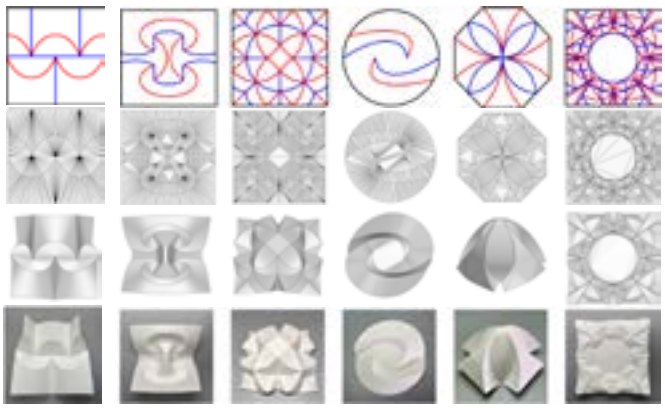

76

Interactive Curved Fold Modeling using a Handle Curve

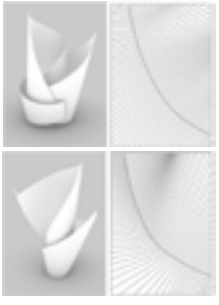

Jun Mitani and Kaoru Ohashi, Interactive Curved Fold Modeling using a Handle Curve, CAD Conference 2022, July 11-13, Beijing

79

Target shape

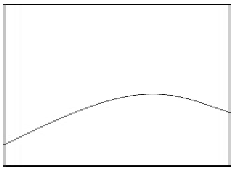

Developable surfaces with a single curved fold (not limited a planer curved fold but a space curved fold is allowed)

80

This shape is also made with a single crease curve

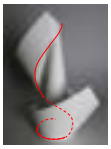

Q: How can we create this 3D model on a CAD/CG software?

Proposed method

Input : (1) Crease curve

(2) Handle curve ← a copy of the crease curve

Edit: Handle curve

Output: Curved surface such that the handle curve <u>almost</u> rides on it with the specified crease curve.

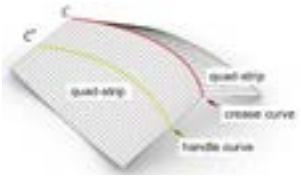

84

pseudo-ruling

Lines connect the points on the crease curve and the handle curve.

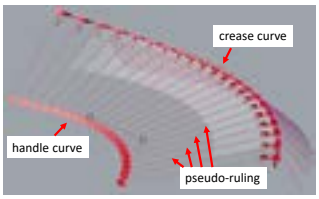

85

crease curve + handle curve

↓

pseudo-rulings

↓

fold angle

↓

rulings

identical when the crease curve and the handle curve are similar

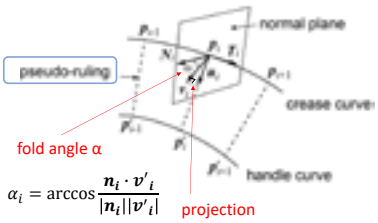

$$\alpha_i = \arccos \frac{\boldsymbol{n_i} \cdot \boldsymbol{v'}_i}{|\boldsymbol{n_i}||\boldsymbol{v'}_i|}$$

86

Shape and orientation of the handle curve

$$\mathrm{C}' = s\mathrm{C} + \boldsymbol{t}$$

$s = 1$

congruent

→ cylindrical surface

$s \neq 1$

similar

→ conical surface

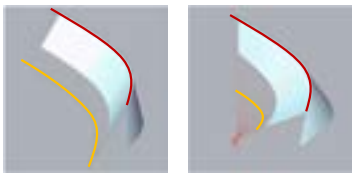

87

User Interface

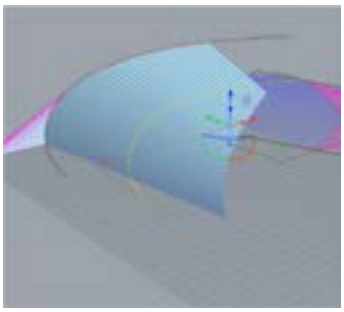

90

Congruent handle curve

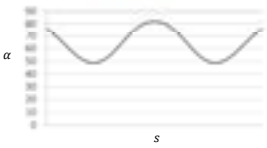

91

Similar handle curve

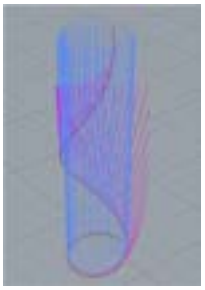

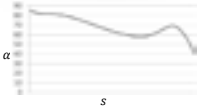

←It is impossible to specify this function manually

93

Examples

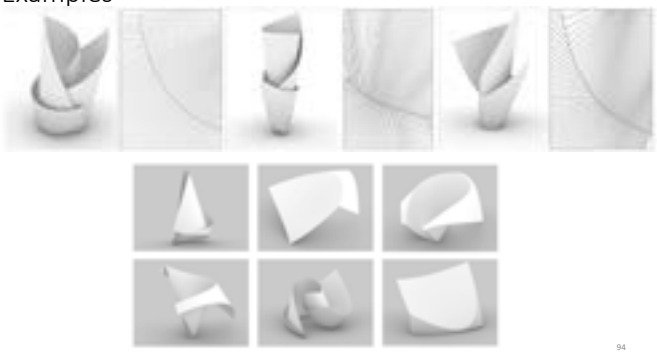

94

Summery

- The geometry of curve folding has become quite clear in mathematics.
- A user interface is crucial for designing artistic shapes.
- We developed several design tools for curved folds, and created various shapes.

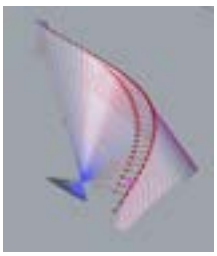

96

Future Work

- Many artworks are made by the minute expansion and contraction at the folds to achieve expressive shapes
- A shape modeling tool that allows for minute distortion in folds is desirable
- Research and development using heat-deforming materials that take into account manufacturing processes such as self-folding is desirable

97

Jun MITANI
University of Tsukuba, JAPAN
http://mitani.cs.tsukuba.ac.jp/

Modeling of Discrete Developable Surfaces with a Break Using Trace Diagrams on the Gaussian Sphere

Kosuke Horiuchi
University of Tsukuba, Japan

Jun Mitani
University of Tsukuba, Japan

Abstract

In recent years, industries such as manufacturing and architecture have increasingly adopted CAD software for shape modeling and product design. This shift minimizes the cost and effort associated with physical prototyping. Despite advancements, designing developable surfaces while maintaining intuitive and precise interfaces remains a challenge. Developable surfaces, characterized by zero Gaussian curvature, are created by twisting or bending unstretchable sheet materials. They are represented through a trajectory of straight line elements called rulings. One remarkable technique is "Non-Crease", which generates complex curvature without traditional folds by creating indentations called breaks, which are degenerated creases with zero length. By enabling the computational design of Non-Crease surfaces, it is expected to facilitate the digital archiving, analysis, and creation of art pieces.

This research aims to support the design of developable surfaces with a break by proposing an interface that integrates Gauss sphere-based trace diagrams[1]. These diagrams map the behavior of surface normal vectors onto the Gauss sphere, aiding in the visualization of curvature distribution around vertices. A key property of trace diagrams on the Gauss sphere for developable surfaces is that the areas enclosed by the traces sum to zero. By editing these diagrams, users can intuitively create and modify developable surfaces with breaks.

The methodology involves starting with a predefined template for developable surfaces with a break. The trace diagram corresponding to this template is visualized and editable. Users adjust trace lengths and angles to create their desired shapes, with the system performing optimizations to ensure the areas enclosed by traces on the Gauss sphere sum to zero, a key constraint of developable surfaces. Trace intersections and the enclosed areas are calculated in real-time to guide this process. Post-editing, the interface generates a crease pattern. Finaly, crease pattern is validated 3D shape and physical realization, supported by Origami Simulator[2].

Results show that this interface enables effective control over the ruling angles and the creation of various developable surface shapes. Optimizations minimize area discrepancies in trace diagrams, enhancing the accuracy of the resultant designs.

Future work will address extending the system to handle shapes with multiple convex and concave regions, improving usability, and reducing optimization errors. This study highlights the potential of trace diagram-based modeling as a powerful tool for designing intricate and mathematically accurate developable surfaces.

References

[1] David Huffman, "Curvature and Creases: A Primer on Paper", IEEE Trans. on Computer, Vol. C-25, No. 10, pp. 1010–1019, 1976.

[2] Amanda Ghassaei, Erik D. Demaine, Neil Gershenfeld, "Fast, Interactive Origami Simulation using GPU computation", Origami, Vol. 7, pp. 1151–1166, 2018.

Modeling of Discrete Developable Surfaces with a Break Using Trace Diagrams on the Gaussian Sphere

Kosuke Horiuchi Jun Mitani
University of Tsukuba, JAPAN

Background

- Shape modeling products such as CAD have become widespread.
- This research proposes an interface to support the design of developable surface modeling.
- A developable surface is a type of curved surface created by twisting and bending a single, inextensible sheet of material.
- It is represented by the trajectory of straight-line elements called "rulings."

Background

- **Non-Crease**: A technique that enables the complex curvature of paper by creating indentations called "breaks“, which are degenerated creases with zero length instead of folds.
- Expected applications in archiving artworks and design production.

Discrete representation using triangles with rulings as edges, then unfolded.

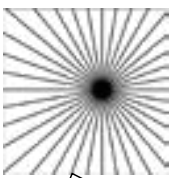

Rulings radiate from the center of the break.

Background

- However, existing CAD software makes it difficult to intuitively design surfaces while maintaining developable surface constraints.
- "Non-Crease" shapes are created using trace diagrams on the Gaussian sphere [1].
- These diagrams help understand the curvature distribution and shape around a single vertex.
- The method is well-suited for "Non-Crease" design, where surfaces curve around a break.

[1] David. Huffman, ``Curvature and Creases: A Primer on Paper'', IEEE Trans. on Computer, Vol. C-25, No. 10, pp. 1010-1019, 1976.

Trace Diagram on the Gaussian Sphere

- A mapping of how surface normal vectors change in space, projected onto a unit-radius Gaussian sphere.

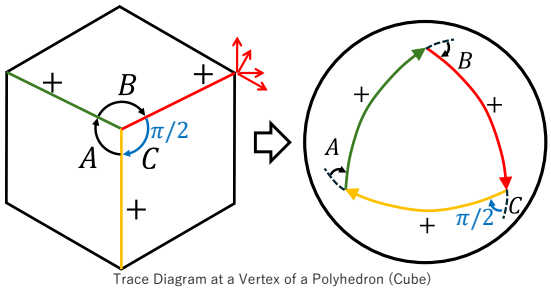

＋：Convex
－：Concave
A, B, C：Sector Angles

Trace Diagram at a Vertex of a Polyhedron (Cube)

Trace Diagram on the Gaussian Sphere

- A mapping of how surface normal vectors change in space, projected onto a unit-radius Gaussian sphere.

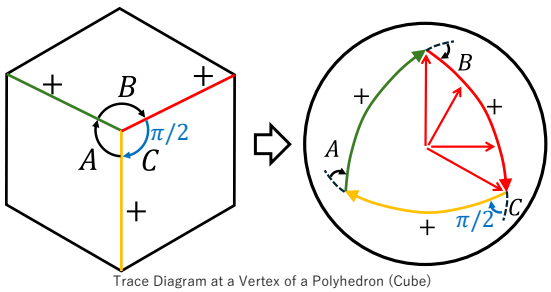

＋：Convex
－：Concave
A, B, C：Sector Angles

Trace Diagram at a Vertex of a Polyhedron (Cube)

Trace Diagram on the Gaussian Sphere

- The area enclosed by a trace represents Gaussian curvature, clockwise is positive, counterclockwise : negative
- At any point on a developable surface, Gaussian curvature is 0, and the sum of sector angles is 2π.

＋：Convex　－：Concave　A, B, C：Sector Angles

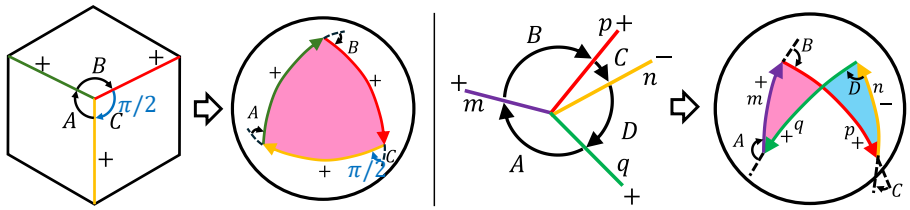

Trace Diagrams at a Vertex of a Polyhedron (Cube) and a Developable Surface Vertex

Overview of the Interface and Modeling Process

1. The user selects a base shape template.
2. The system renders the trace diagram.
3. The user edits the trace diagram.
4. The system optimizes the trace diagram.
5. The final shape is output as a crease pattern.

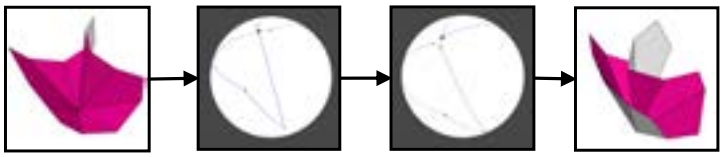

Trace Diagram Rendering

Other shapes will be considered at the end.

- Prepare the template trace diagram.
- The developable surface used has one convex and one concave part.
- Crease pattern consists of 12 rulings.
- Sector angles (angles between rulings) are all 360/12 = 30°.

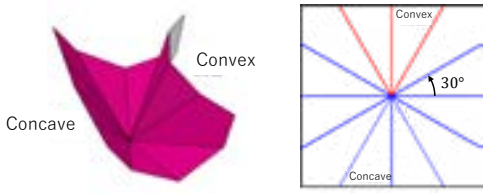

Template Shape and Its crease pattern

Trace Diagram Rendering

1. Compute the normal vectors of each developable surface face.
$$\boldsymbol{n_i} = \boldsymbol{p_i} \times \boldsymbol{p_{i+1}}$$
2. Connect vertices corresponding to normal vectors in order.

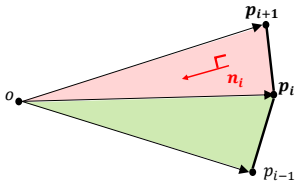

Vertices Constituting the Developable Surface

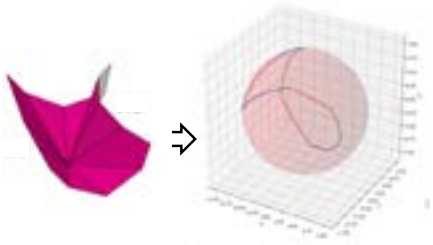
Trace Diagram of the Template shape

Trace Diagram Region Segmentation

- The trace diagram forms a figure-eight shape.
- Two regions exist, and their areas indicate curvature.
- To compute the area of each region, segmentation is performed.
- Each region is divided by intersection points of traces.

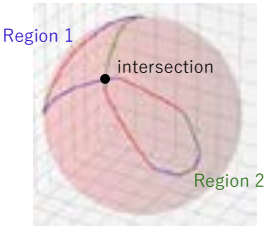

Intersection Determination Procedure

Input: List of vertex coordinates plotting traces in connection order.

1. Check for intersections between all trace pairs.
2. After finding an intersection, determine whether the point belongs to both traces.

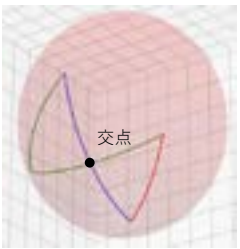

Intersection Determination Procedure

Input: List of vertex coordinates plotting traces in connection order.

1. Check for intersections between all trace pairs.
   - Let the endpoints of two traces be p_1, p_2 and q_1, q_2, respectively.
   - If the two traces intersect, the intersection line of their planes passes through the center of the sphere.
   - The direction vector L of this intersection line is given by the cross product of the normal vectors of the two planes.

     $\boldsymbol{L = n_1 \times n_2} \quad \left(\boldsymbol{n_1 = p_1 \times p_2}, \quad \boldsymbol{n_2 = q_1 \times q_2}\right)$
   - The intersection line L has two intersection points $\boldsymbol{I_1}$ and $\boldsymbol{I_2}$.

     $\boldsymbol{I_1 = \frac{L}{|L|}}, \boldsymbol{I_2 = -I_1}$

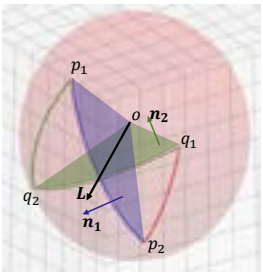

Intersection Determination Procedure

2. After finding an intersection, determine whether the point belongs to both traces.

$|\theta_{\text{arc}} - (\theta_1 + \theta_2)| < \epsilon$

$\theta_{arc} = \cos^{-1}\left(\frac{\boldsymbol{p_1 \cdot p_2}}{|p1||\boldsymbol{p_2}|}\right)$

$\theta_1 = \cos^{-1}\left(\frac{\boldsymbol{p_1 \cdot I_1}}{|\boldsymbol{p_1}||\boldsymbol{I_1}|}\right)$

$\theta_2 = \cos^{-1}\left(\frac{\boldsymbol{p_2 \cdot I_1}}{|\boldsymbol{p_2}||\boldsymbol{I_1}|}\right)$

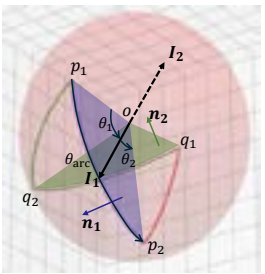

Region Segmentation

After computing intersection points, traces are divided into positive and negative regions.

Insert intersection coordinates into the vertex list.

Split the coordinate list into sections based on the intersection points.

$[p_1,\ p_2,\ q_1,\ q_2]$

$[p_1,\ I,\ p_2, q_1,\ I, q_2]$

$[p_1,\ I,\ p_2, q_1,\ I, q_2]$

$[I,\ p_2, q_1]$ $\quad$ $[I, q_2,\ p_1]$

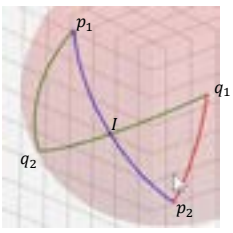

Result of Region Segmentation

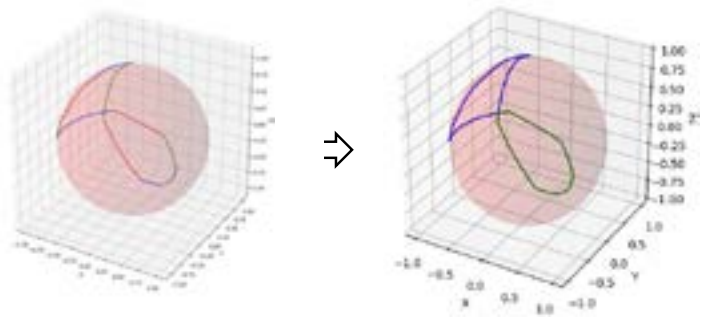

Trace Diagram Area Calculation

- The enclosed region in a trace diagram forms a spherical polygon, and its area is computed using spherical excess.
- The interior angle a_i of a spherical polygon is obtained from the dot product of adjacent normal vectors $\boldsymbol{n_{i-1}}$ and $\boldsymbol{n_i}$.
- The area A of a spherical polygon is calculated as:

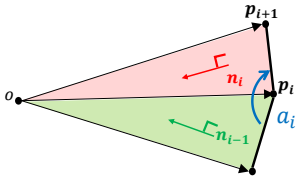

$$A = \sum_{i=1}^{n} a_i - (n-2)\pi$$

(n : number of vertices in the spherical polygon)

Result of Trace Diagram Area Calculation

- The areas of the two enclosed regions in a trace diagram should be equal, but discrepancies arise.
- These differences are likely due to surface shape errors and rounding errors in computation.
- Sector angles result in multiples of 30°.

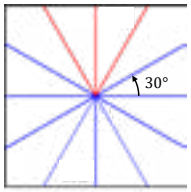

Region 1 : 0.5592
Region 2 : 0.5953
Area difference : 0.0061

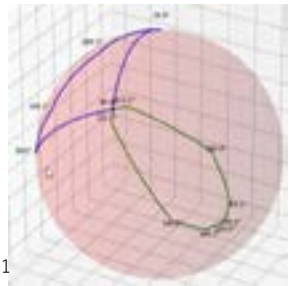

Trace Diagram Optimization

- Objective Function

$$f(\mathbf{v}) = |A_1(\mathbf{v}) - A_2(\mathbf{v})| + \lambda_1 P_{\text{angle}}(\mathbf{v}) + \lambda_2 P_{\text{distance}}(\mathbf{v})$$

trace vertices — Areas of the two regions — Penalty for violating angle constraints — Penalty for vertex movement distance

- Angle constraint penalty:
  Enforce angle constraints so that adjacent trace angles belong to $T = \{30, 150, 210, 330°\}$

$$P_{\text{angle}}(\mathbf{v}) = \sum_{i=1}^{m} \min_{t \in T} |\phi_i - t|$$

m : Number of Vertices of the Spherical Polygon
ϕ_i : Magnitude of the Interior Angles of the Spherical Polygon

Trace Diagram Optimization

- Distance constraint penalty:
  To minimize displacement from initial vertex positions, a penalty function is used.

$$P_{\text{distance}}(\mathbf{v}) = \sum_{i=1}^{m} |\mathbf{v}_i - \mathbf{v}_i^0|^2$$

m : Number of Vertices of the Spherical Polygon

- Vertex positions are updated using gradient descent.

$$\mathbf{v}_i^{(k+1)} = \mathbf{v}_i^{(k)} - \alpha \nabla f(\mathbf{v})$$

Vertex Coordinate at Step k for the i-th Vertex — Learning Rate — Gradient of the Objective Function

Trace Diagram Optimization

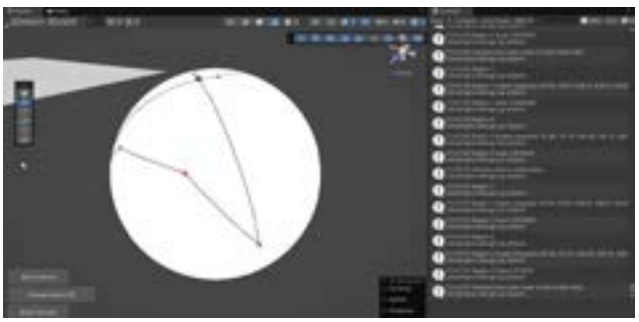

Before Editing

After Editing & Optimization

Trace Diagram Optimization

Before Editing

After Editing

After Optimization

	Before Editing	After Editing	After Optimization
Region 1 [rad]	0.5592	0.7111	0.8172
Region 2 [rad]	0.5953	0.6144	0.8236
Difference [rad]	0.0061	0.0967	0.0064

Controlling Rulings and Development Diagram Output

- Origami Simulator is used to specify fold angles along rulings.
- Mountain folds are red, and valley folds are blue.
- Fold angle magnitude is represented by transparency.

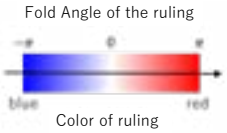

Correspondence Between Ruling Fold Angle and Color

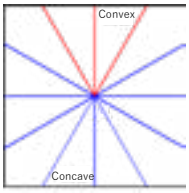

Output crease pattern

Comparison of Surface Before and After Editing

- The development diagram is observed using Origami Simulator.

Before Editing

After Editing & Optimization

Shapes Created with the Proposed Interface

- Example with 36 rulings.

Other shapes – 2 convex and 2 concave

Render trace diagrams for various shapes and consider optimization methods

1. 2 convex and 2 concave

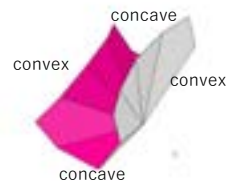

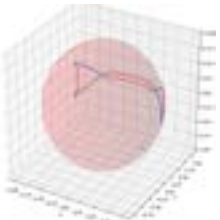

trace diagram

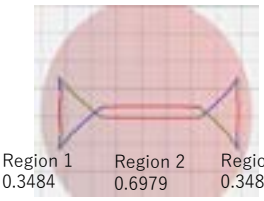

Region 1 + Region 3 - Region 2 = -0.0015

Other shapes – 3 convex and 3 concave

2. 3 convex and 3 concave

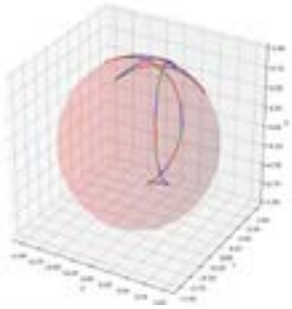

Other shapes – 3 convex and 3 concave

2. 3 convex and 3 concave

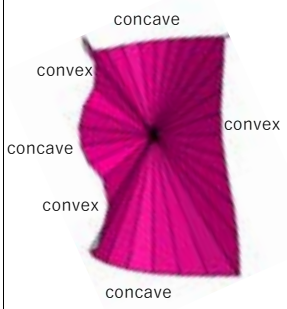

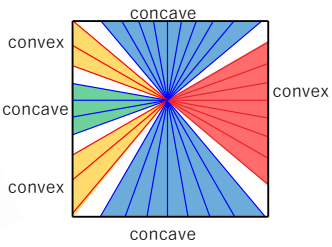

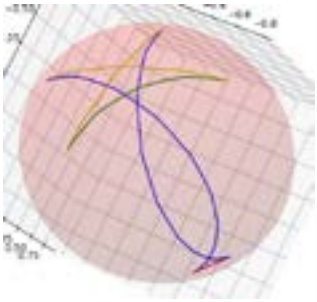

Other shapes – 3 convex and 3 concave

To region segmentation,

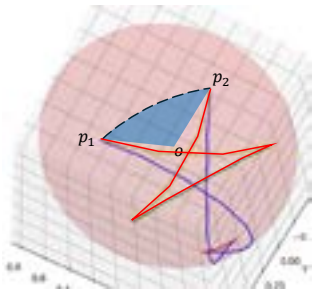

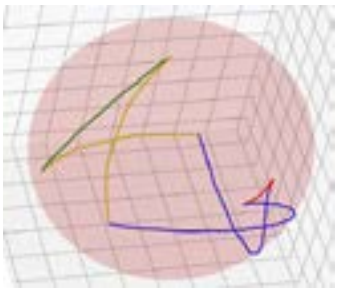

Summary

- This research proposed a shape modeling method for developable surfaces using trace diagrams.
- Implemented functionalities for rendering, editing, and optimizing trace diagrams.
- Confirmed that ruling control and developable surface creation are possible through trace diagram editing.

Future Work

- Further minimize the area difference between trace regions.
- Support for various shapes (currently limited to one convex and one concave part).
- Implement partial shape modification.
- Evaluate and improve usability.

Parametric Design Tools for 3D Curved-Origami Shapes in Conceptual and Prototype Architectural Design

Aida Safary
University of Tsukuba, Japan

Jun Mitani
University of Tsukuba, Japan

Abstract

In this research, we produce digital parametric tools of 3D origami-based architectural elements, enabling the users to modify and manipulate basic geometrical features of these tools to explore and create extended geometric variability options of the mentioned structures. In our first project, we designed a module for the One-Fold project by Patkau architects with specific options for changing the shape parameters to give users the ability to generate various structures of architectural shelters of the same 3D shape. The One-Fold project consists of a rectangular or square plane with a single fold as of its diagonal line, which creates conic curve borders when folded [1]. As our second research project, we developed a digital system for the parametric design of David Huffman's design with ellipses of two-degree two-vertices. In this design tool, we apply parameters for changing the fold angle, the size of the structure, and the rotation of curved lines inside our 3D shape. In this design tool, we applied an approach similar to the additive algorithm method for generating our shape step by step as a quad mesh structure [2, 3]. In our future research project, we intend to compare our digital tools with physical prototypes using 3D scanners, evaluate the Elastica curves of both models and use the RMSE method for surface error analysis.

References

[1] Aida Safary, Hamid Shafieasl, and Jun Mitani, "Geometric design tool for One-Fold, a curved origami with a single fold", J. Geom. Graph., **28** (2024) 89–101.

[2] Erik D. Demaine, Martin L. Demaine, and Duks Koschitz, "Reconstructing David Huffman's legacy in curved-crease folding", Origami **5** (2011) 39–52.

[3] Levi H. Dudte, Gary P. T. Choi, and L. Mahadevan, "An additive algorithm for origami design", Proc. Natl. Acad. Sci., **118** (2021) e2019241118.

筑波大学
University of Tsukuba

Parametric Design Tools for 3D Curved-Origami Shapes in Conceptual and Prototype Architectural Design

University of Tsukuba
2025.03.11

Aida SAFARY-Mitani Lab

1

Research Background and Objective:

- The primary aim of this research is to develop digital parametric tools for 3D origami-inspired architectural components, allowing users to adjust and customize fundamental geometric characteristics of these tools to investigate and generate a broader range of geometric variations for the structures described.

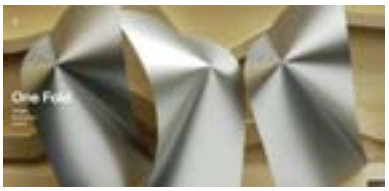

https://www.patkau.ca/projects/one-fold

Demaine, Erik D., Martin L. Demaine, and Duks Koschitz. "Reconstructing David Huffman's legacy in curved-crease folding." *Origami* 5 (2011): 39-52.

2

Table of Contents- Research Projects

3

Research Title:

Geometric Design Tool for One-Fold, a Curved Origami with a Single Fold.

4

Main Idea-Objective

To replicate the original pavilion model called one-fold, inspired by Paul Jackson's "One-Crease" artwork, By Patkau Architects, as A digital model.

Original Prototype

Our Digital System Render

5

Steps of Methodology

1. Creation of Direction-Curve.
2. The apex would be the vertex of a cone.
3. Creation of Direction Surface.
4. Creation of Direction Vectors.
5. Creation of Final Surface.

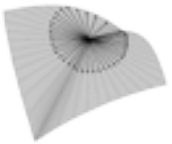

6

Direction Sectors(Curves)

Consider an arc of a circle with measure of θ where $\theta > 180°$. The condition of being larger than 180° is important to be able to see that in the neighborhood of the fold line there is concavity. Then we change (the amount of α is given by the user) and transfer the sector of the circle such a way that it lies in the set .

$$\{(x, y, z) : x, z \in R \ \& \ y \in [0, +\infty)\}$$

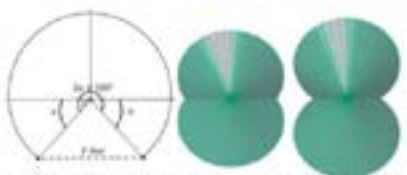

The value of 2α is inversely proportional to the length of the $f-line$.

7

Finding the apex

After rotation of the circle we should find the apex point in a way that it would connect the sectors of the semicircle structure to the most appropriate point in the z-axis.

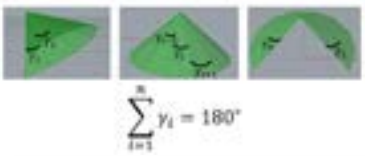

$$\sum_{i=1}^{n} \gamma_i = 180°$$

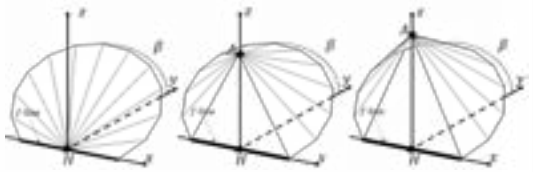

Finding the apex point.

8

Diagram of Process-Direction Surface vs Direction Vectors

The steps of emerging Direction-Surface can be seen from left to right . The right surface appears upon when the apex is found and the Direction-Vectors are the vectors that overlaps on the indicated line on it.

9

Direction vectors-Direction Vector Unitization

Direction-Vectors = connecting the apex point with vertices of the Direction-Curve.

Direction-Vectors give direction to the final surface's ruling lines.

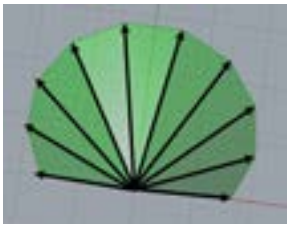

Final Surface = Unitize direction-vectors to lengths from 2D plane.

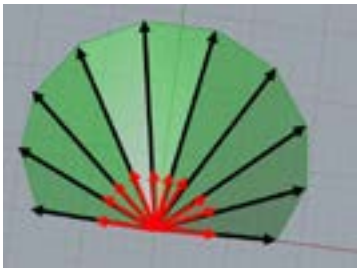

10

Conic Structures

Applying first developability condition.

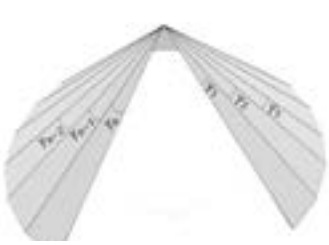

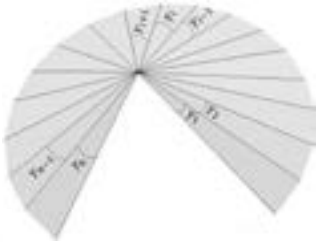

$$\sum_{i=1}^{n} \gamma_i = 180^\circ$$

11

Direction-Surface

Reflexing the surface on the other side of the z-axis to create the overall completed Direction-Surface.

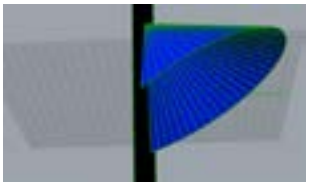

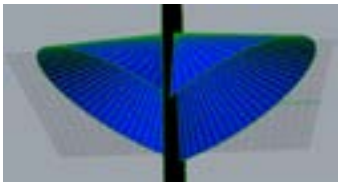

12

Any Possible Quadrilaterals

Consider an arbitrary quadrilateral as below and divide half of it via [r, s]

The value of angles are obtained from Direction-Surface.

We extend the direction vectors on 3D surface using the length that we obtained from 2D surface, for instance in the following figure $AB = A'B', AC = A'C'$ and *two edges and one angle* guarantee the congruence of triangles ABC, and $A'B'C'$, as well.

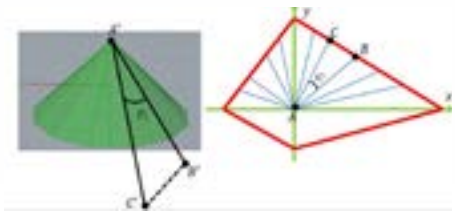

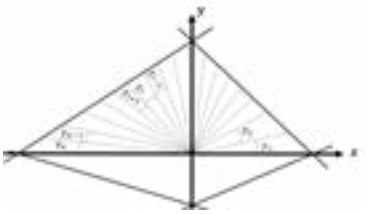

13

Direction-Surface vs Final Surface

Final surfaces are according to the orientation of Direction-Vectors. Upper surfaces indicate the Direction-Surface and the lower surfaces are final surfaces.

14

Geometric Features

3 main geometric features define our shape:

-α.

-β.

-*Apex movement*.

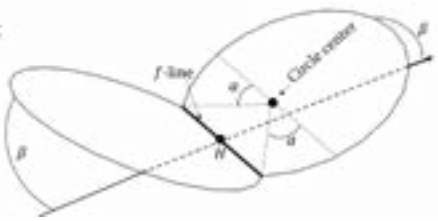

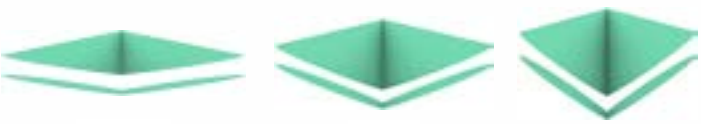

$\beta = 10°$ $\beta = 25°$ $\beta = 40°$

15

Process Renders

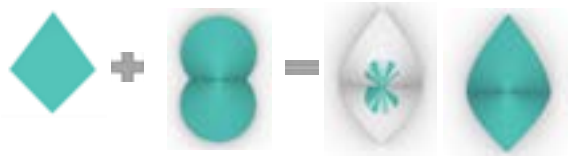

α value changes.

β value changes.

$X - C$ parameter changes.

16

Only quadrilaterals?

The system also works for convex - 2D planes, Star-shaped polygons.

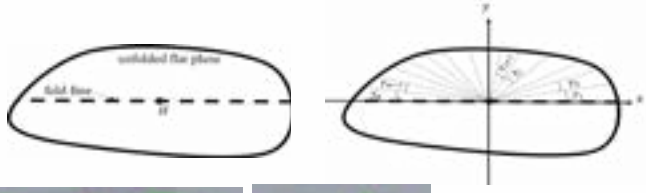

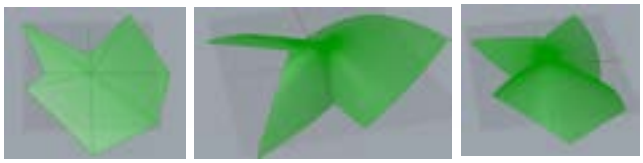

17

One-Fold System

18

Construction of Physical Model

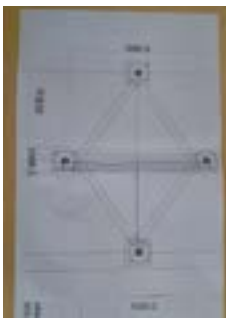

Base part

Side part

Front Part

19

Construction of Physical Model

Final Level

20

Research Title:

Parameterized Folded State Shape Modeling of David Huffman's Ellipse.

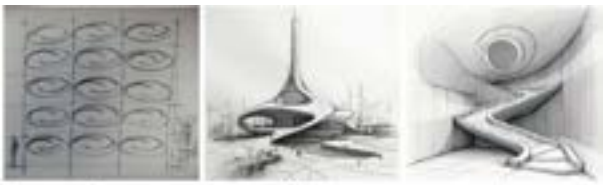

21

Huffman design using ellipses with 2 degree-2 vertices.

Demaine, Erik D., Martin L. Demaine, and Duks Koschitz. "Reconstructing David Huffman's legacy in curved-crease folding." *Origami* 5 (2011): 39-52.

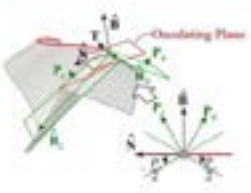

22

We decided to take a different approach.

A new approach called the Additive algorithm method.

Related paper:

Dudte, Levi H., Gary PT Choi, and L. Mahadevan. "An additive algorithm for origami design." *Proceedings of the National Academy of Sciences* 118.21 (2021): e2019241118.

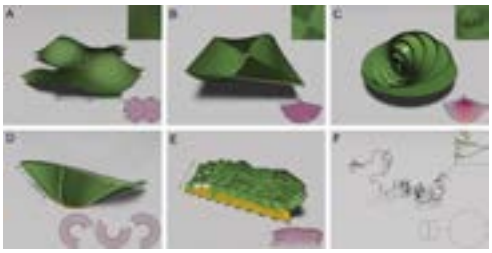

23

What is the idea of additive algorithm? What are the Steps?

The initial seed and extension of the seed are based on specific defined rules.

Consider our initial seed as the first raw of the crease pattern and x_i as our initial point.

Parameters of x_i and e_i ,$\theta_{i,3}$,$\theta_{i,4}$ are confirmed by default. we give the parameters for flap angle α_0 and β_i .

For the next seed creation the flap angle α and β are determined automatically.

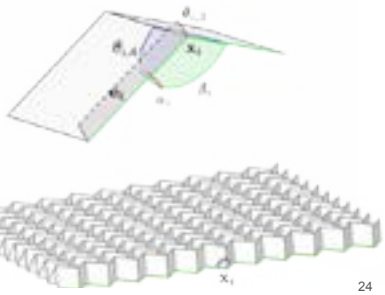

24

Step 1: Dividing the crease pattern.

Dividing crease pattern

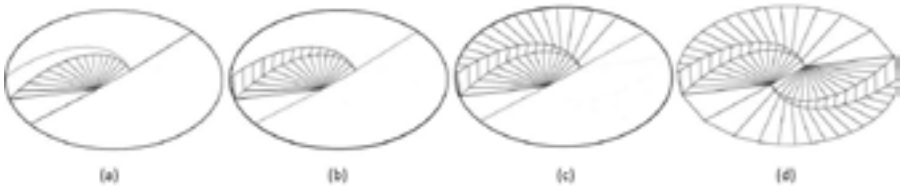

25

Step 2:

We select one of the following pieces:

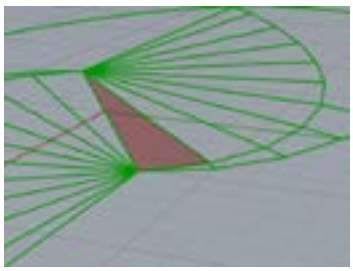

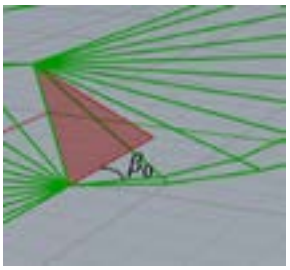

As the first user parameter:β_0 We rotate the selected piece by β_0

26

Step 3:

Select the following new piece in second strip and rotate it by (flap angle) α_0.

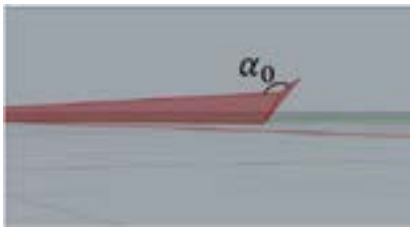

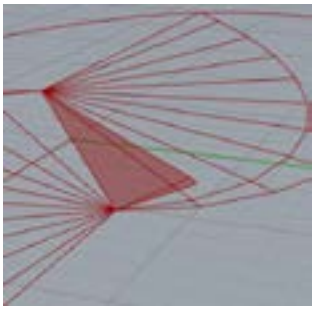

27

The angles θ_i's could be attained via $2D$ surface. Now, we set the value of β_1 according to the below formulas:

Additive Method

$$\cos\theta_2 = \cos\theta_1\cos\beta + \sin\theta_1\sin\beta\cos\alpha,$$

$$\beta = \cos^{-1}\left(\frac{\cos\theta_2\cos\theta_1 \pm \sin\theta_1\cos\alpha\sqrt{\cos^2\theta_1 - \cos^2\theta_2 + \sin^2\theta_1\cos^2\alpha}}{\cos^2\theta_2 + \cos^2\theta_1}\right).$$

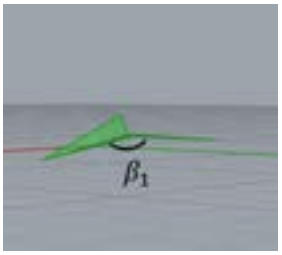

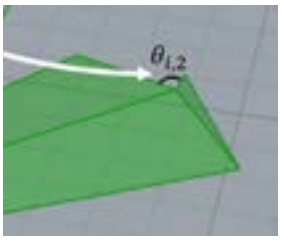

28

We use the three points shown in the left figure and find the fourth point shown in the right figures according to the corresponding lengths of unfolded surface.

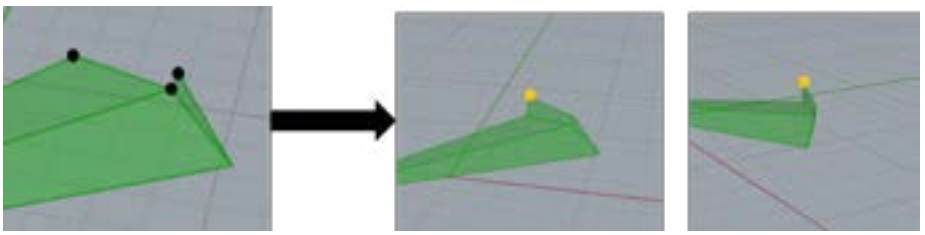

29

We follow the same process until the end until we get the desired shape.

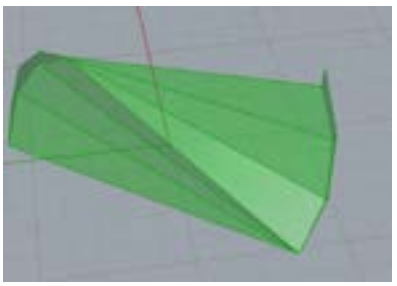

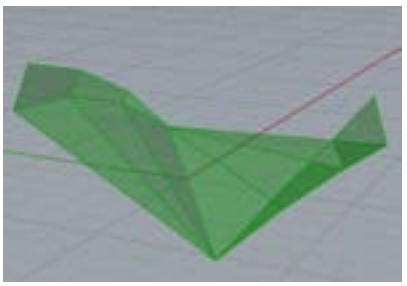

30

For the outer side of the ellipse.

First, we evaluated the following angles (δ, γ) in the $2D$ state.
The first 3D line (Vector u) should be positioned in a state that the angles will be preserved in 3D state. Subsequently we rotate our first quad in region S around vector v in such a way that the mentioned angles after folding would be preserved.

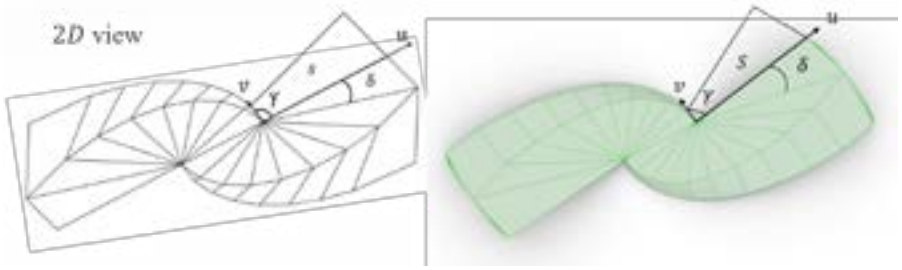

31

Find the $4th$ point in the $3D$ surface(black point) according to 3 points of quadrilateral(yellow points) as before and create the surface.

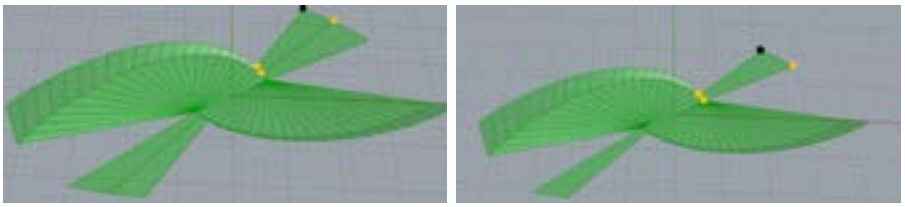

32

Repeating the process until the end.

We also evaluated the 360 ◦ condition around the points on left-up and right-down, and the error is zero(see instances in the figure), and it is expected due to the nature of the implemented method.

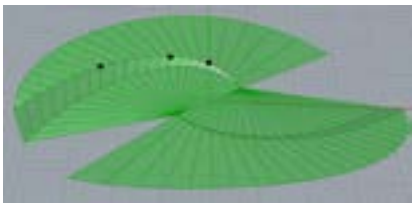

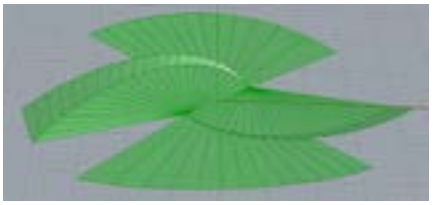

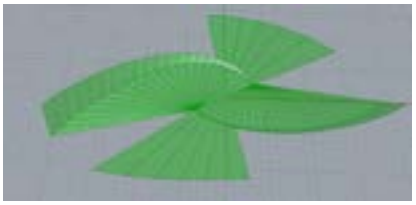

33

Final renders

The angle condition on each vertice is preserved.

34

Huffman's Ellipse System:

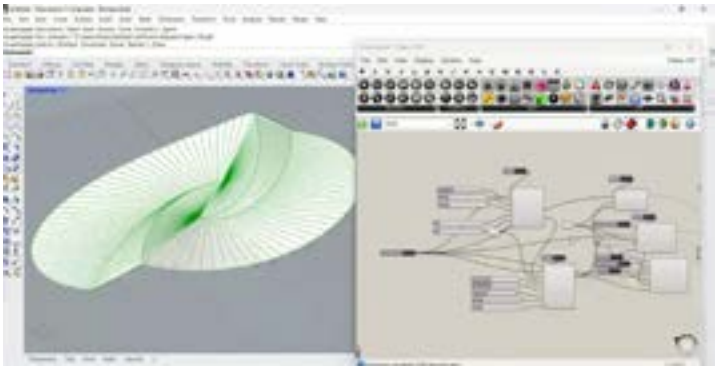

35

Research Title:

Comparison and Calculation of Error Value Between Digital Models and Physical Prototypes of Our Designed Digital Systems .

36

Types of Prototypes

Different techniques:

1-Traditional Physical Models.

2-Modern Digital Models (CAD models).

3-3D printing.

Archdaily.com

37

Prototype that we intended to create.

Patkau.ca

One-Fold: The original project is made of metal sheets but we deal with fabric in our own prototype.

38

From concept and sketches to prototyping:

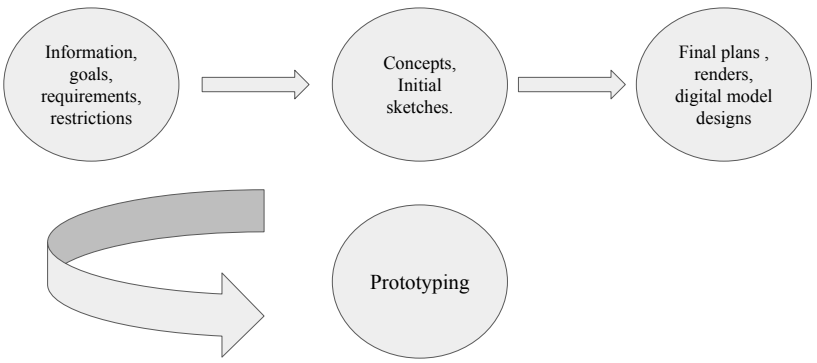

39

Our example:

Fabric Structure,

Joint finishing master slim cables.

White sheet roll fabric.

40

3D printing and Error Evaluation

1-3D scanning, collecting data points, surface reconstruction.

2- Adjusting the scales of 3D printed digital model with the original digital model.

3-Using Cloud compare software to calculate the error value.

$$RMSE = \sqrt{\frac{1}{n}\sum_{i=1}^{n}(y_i - \hat{y}_i)^2}$$

Where:

- n is the number of observations,
- y_i is the actual observed value,
- $\hat{y}_i$ is the predicted value.

Digital Model

Scanned Model of Physical Prototype

41

Cloud-compare Evaluation

1-Loading the models, selecting the models, aligning models.

2- Model alignment.

One model should be used as a reference, one model should be an aligned target.

42

Energy Minimization & Bending energy

Smoothing energy = minimization.

Minimize energy = minimize area.

The goal is to minimize the energy of a membrane, which corresponds to minimizing its surface area. This is mathematically expressed through the integrals shown in the image.

Elastica curves describe the equilibrium shape of thin, flexible rods or plates under bending.
The energy associated with these curves is **bending energy**, given by:

$$E_b = \frac{1}{2}\int K^2\,ds$$

where K is the curvature, and ds is the arc length.

$$\int_S ds \rightarrow \min$$

$$\downarrow$$

$$\int_\Omega \|\mathbf{p}_u\|^2 + \|\mathbf{p}_v\|^2\,du dv \rightarrow \min$$

$$\downarrow$$

$$\Delta \mathbf{p} = 0$$

We developed a Related Grasshopper Algorithm

They key to formulas used in this script are elliptical integrals of the first kind, $k(m)$ and the second kind $E(m)$.

K: The modulus (or eccentricity parameter), $0 \leq K \leq 1$

θ: Tangent angle of the bending beam.

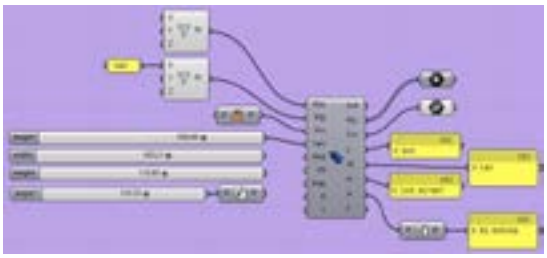

$$K(k) = \int_0^{\pi/2} \frac{d\theta}{\sqrt{1 - k^2 \sin^2\theta}}$$

$$E(k) = \int_0^{\pi/2} \sqrt{1 - k^2 \sin^2\theta}\,d\theta$$

We developed a Related Grasshopper Algorithm

X (protype) = 98.99

X (digital) = 98.99

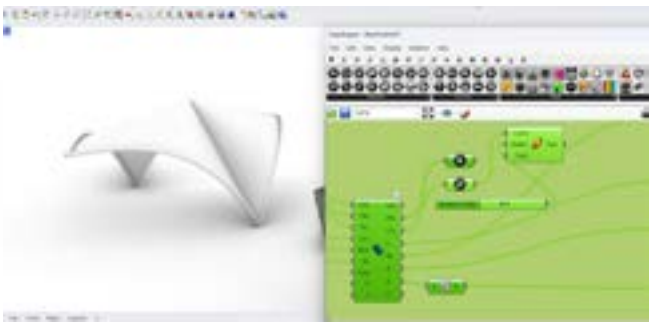

Conclusion and Future Work

1-Our project illustrated the efficiency of combining digital and physical prototyping in architectural design.

2-Challenges included considering the accuracy of construction or the complexity of the surfaces.

3-In the future, certain refinements will be undertaken in our methods and materials to continue the advancement of design and construction..

46

Hoberman's Scissor Mechanism and Digital fabrication

Higa Miyashiro Pamela
University of Tsukuba, Japan

Yiyang Jia
Japan Women's University, Japan

Mitani Jun
University of Tsukuba, Japan

Abstract

The Hoberman mechanism, developed by Chuck Hoberman, is renowned for its applications in toys and architecture. The Hoberman Sphere, a collapsible toy, exemplifies the mechanism's versatility through its use of circular elements with scissor-like linkages to expand and contract. These linkages are fundamental to the mechanism's deployment, which is also evident in architectural applications, most notably in the Hoberman Arch, showcased at the 2002 Winter Olympics. This structure, composed of segmented arcs arranged in multiple layers, highlights the scalability and adaptability of the mechanism. Our research on the Hoberman mechanism spans geometric principles, movement profiles, and deployment constraints [1, 2, 3]. In this study, we combine theoretical research, digital modeling, and physical prototyping. Using tools such as Rhinoceros and Grasshopper, we facilitated digital simulations of scissor mechanisms. Additionally, we employed digital fabrication techniques to create physical prototypes. We tested three configurations: an irregular polyline, a regular dodecagon, and a circumscribed irregular dodecagon. These models allowed us to explore how geometry impacts movement and to address the challenges posed by irregular configurations. We focused specifically on the irregular dodecagon model, as its closed and irregular geometry highlights the constraints of the method. By maintaining proportional link lengths and angular relationships, we ensured proper deployment of the mechanism. A physical prototype of the irregular dodecagon was fabricated, and its movement matched the predictions from the simulations. Inspired by the Hoberman Arch, which incorporates multiple layers of Hoberman mechanisms into a discretized semicircle, we added additional layers to the irregular dodecagon model. However, the multi-layered design exhibited resistance and deformation during movement, suggesting the presence of over-constraints in the model. To further investigate, we simulated the movement of the double-layered irregular dodecagon. The simulation, combined with an in-depth geometric analysis, revealed that multi-layered designs using irregular polygons inherently lead to over-constraints. Overall, our study demonstrates the Hoberman mechanism's adaptability in toys, architecture, and deployable structures. However, we also identified limitations in the shapes that can successfully support multi-layered Hoberman mechanisms, particularly in irregular configurations.

References

[1] Gomez, Alfonso, "Deployable Domes Based on Angulated Scissors: A Method of Design Based on Geometrical Construction", The International Journal of Designed Objects, **9** (2015) 1.

[2] Asefi, Maziar, Ebadia, Atefeh, and Ghasemib, Azam, "Geometry feasibility of angulated scissor-like elements in a constant perimeter", (2019).

[3] Sun, Xuemin, Yao, Yan-An, and Li, Ruiming, "Novel method of constructing generalized Hoberman sphere mechanisms based on deployment axes", Frontiers of Mechanical Engineering, **15** (2020) 89–99.

Hoberman's Scissor mechanism and its fabrication.

CREST ED3GE meeting 2025

Higa Pamela
CGG Mitani Group
2025/03

筑波大学

1

Scissor Mechanism

Scissor mechanism unit

- Forms an X shape
- Pair of interconnected rigid links.
- Links joined by a pivot point

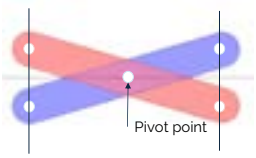

Multiple connected units

- Deployable structures
- Controlled transformation
- One degree of freedom

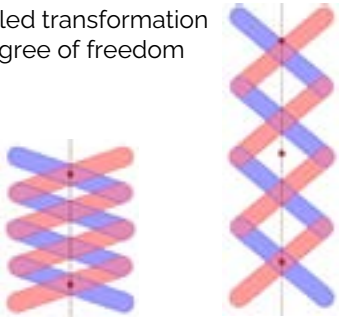

2

Origami and Scissor Mechanism

- Origami and scissor mechanism have similar movement behavior.
- Long term goal is to develop a system for hybrid structure: Scissor mechanism and origami

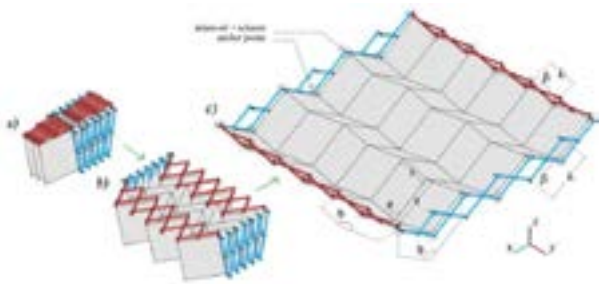

Image from Vlachaki et al., 2021 (Hybrid Deployable Structures)

3

Hybrid Deployable Structures

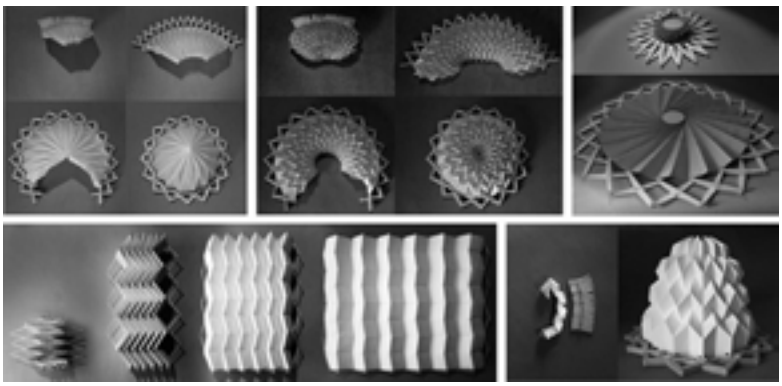

Image from Vlachaki & Liapi, 2024 (Hybrid Origami-Linkage Structures)

4

Scissor mechanism in Micro robotics

Video from Teoh et al., 2018 (Rotary-Actuated Folding Polyhedrons)

5

Large-Scale Deployable Structures

Hoberman Arch - Olympic Medals Plaza in Salt Lake City (2002). Image source: https://www.hoberman.com/

6

Research Goals

- Study and understand Scissor mechanism, specifically Hoberman's scissor mechanism for close polygons and close polyhedral with radial movement.
- Simulate movement trajectories and analyze constraints.
- Fabricate physical models to compare with simulation

7

Scissor Mechanism movements profiles

- Linear movement

- Polar movement

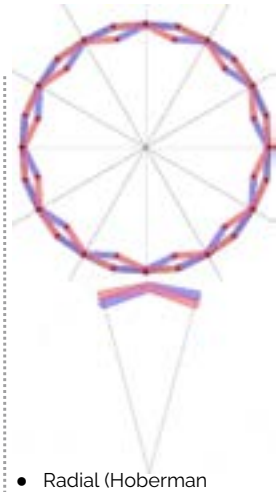

- Radial (Hoberman Scissor mechanism)

8

Hoberman's Scissor Mechanism and the Hoberman Sphere

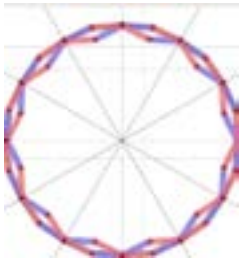

Expanded circle

Contracted circle

Spherical icosidodecahedron

Hoberman Sphere

- Single degree of freedom

9

Hoberman's Arch

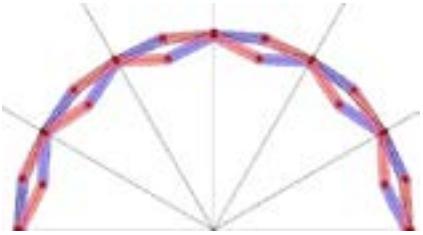

Hoberman's arch Scissor mechanism, one layer

Hoberman's arch Scissor mechanism, multilayered

Generalized Angulated Elements

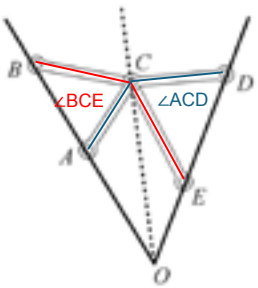

Lineal movement
∠BCE = ∠ACD = π
BC = AC
DC= EC

Polar movement
∠BCE = ∠ACD = π
BC = DC
AC = EC
BC≠ AC

Radial movement (Hoberman's Scissor mechanism)
BC/AC = EC/DC=m
∠ACD = ∠BCE = π - ∠BOD.

Generalized angulated element. (GAE)

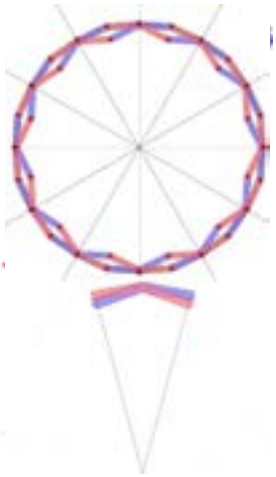

Two angulated elements

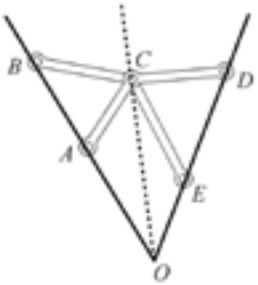

Radial movement
BC/AC = EC/DC=m
∠ACD = ∠BCE = π - ∠BOD.

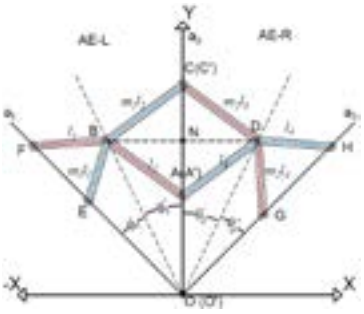

Two angulated elements for a Radial Movement

Constraints

$$l_2 = l_3$$

$$\theta_1'' = \theta_2'$$

$$m_1 = m_2$$

Pantographic Grasshopper script

To study the movement of Hoberman Mechanism, we used a modified version of Pantographic script for Rhinoceros- Grasshopper.

Input: polyline

The script takes the points of the polyline and places them as pivot points, and the midpoints of each polyline segment as the connections between units.

13

Construction irregular dodecagon

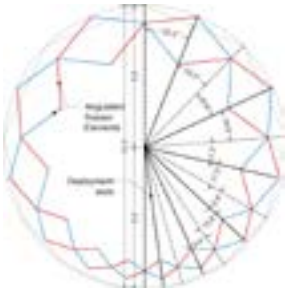

Geometry construction

Movement simulation with trajectory path.

Physical model

14

Two layered Irregular dodecagon

Hoberman's arch

Physical model
-Presented resistance to movement.

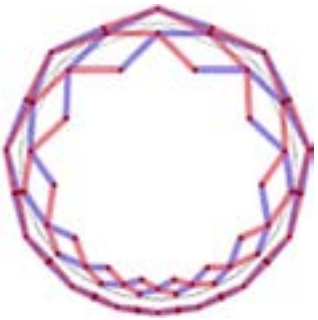

Simulation
- Gaps between rings during movement

15

Irregular Polygon Over-Constraint

Multilayered Scissor mechanism. (Hoberman's arch)

Angled elements Lateral pair

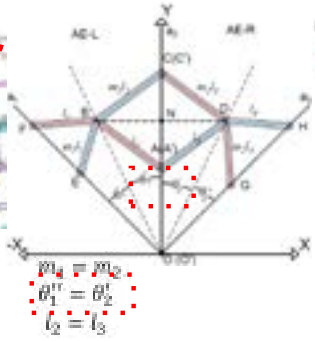

Angled elements Axial pair

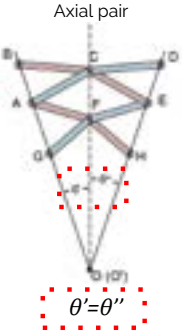

$\theta'=\theta''$

$$\theta_0 = \theta_1 = \theta_{2...} = \theta_n$$

$$\sum_{i=0}^{N} \theta_i = 2\pi$$

Only regular polygons can be multilayered.

Physical model Vs Mathematical Model

Physical model

- Gap at the pivot point provides enough flexibility to accommodate the over-constraint.

Radial movement

- Any pivot point that lies on the circle will move towards the center of the circumcircle

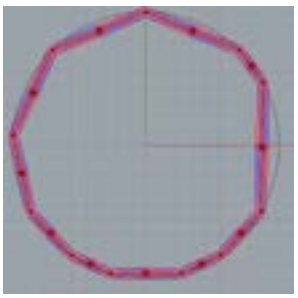

Circumscribed Polygon with Random Tangent Points

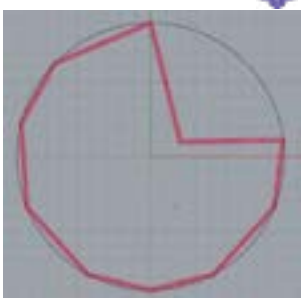

Polygon with all but one vertex on a circle.

Irregular sphere

- Exploring Irregularity:
- Applied irregular polygon concepts to create a polyhedral structure with radial movement toward the circumscribed sphere's center.
- Construction Process: Arranged circles of equal radius around a common circumcenter.
- Circumscribed irregular polygons around these circles to form the structure.

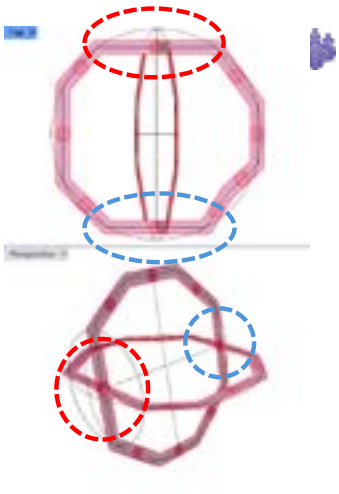

19

Irregular sphere – Joints constraints

Pivot point and joints between units trajectory simulations.

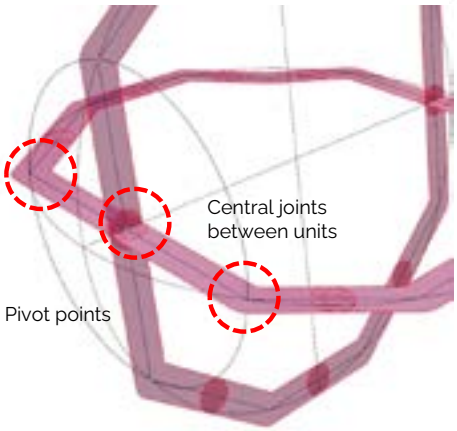

20

Irregular sphere – Joints constraints

Pivot point and joints between units trajectory simulations.

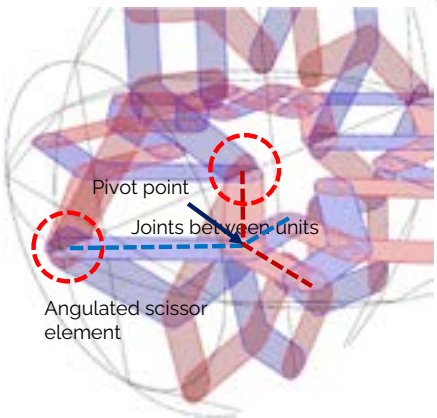

21

Irregular sphere – Joints constraints

The central joints connects four units.

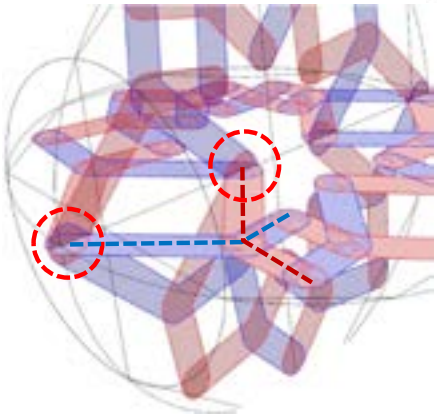

22

Irregular sphere – Joints constraints

To prevent the joint from being over constrained, these four pivot points must be equidistant from the central joint

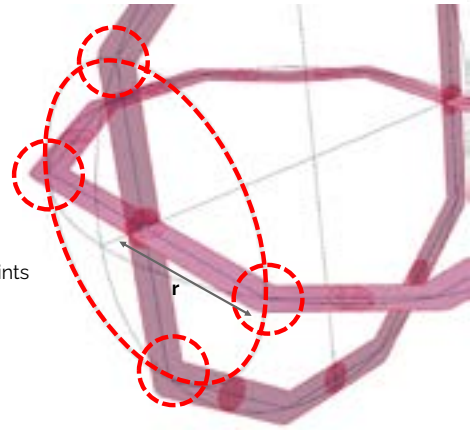

23

Irregular sphere – Joints constraints

Example of non-equidistant pivot points from the central joint

24

Sphere from irregular polygons for fabrication

- A sphere was designed to show irregularity limits in a Hoberman mechanism.
- The sphere is made of three irregular polygons.
- Two polygons lie on planes that are not perpendicular to each other.
- One polygon has a concave corner.

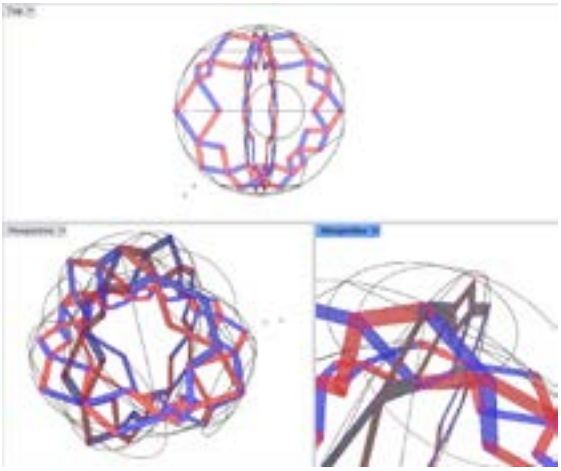

25

Sphere Fabrication – Joint Desing

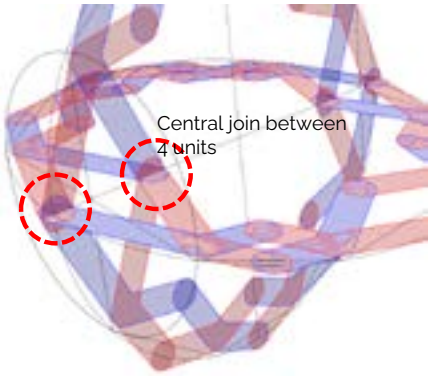

26

Sphere Fabrication – Joint Desing

- The joint adds degrees of freedom to the movement when the joint is considered independently.
- But when the whole system is assembled, the system has 1 degree of freedom.

27

Physical model of regular sphere

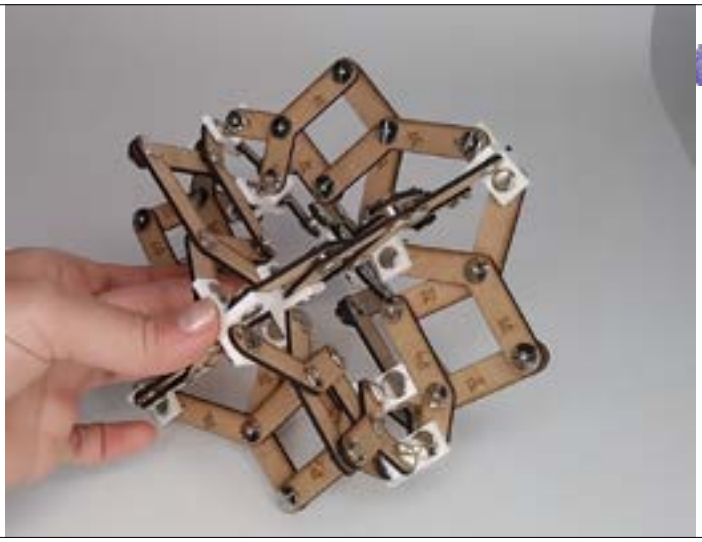

28

Summary

This work is in an early stage of development. This section of the research aimed to understand the degree of irregularity achievable with shapes constructed with Hoberman mechanism.

- Found limitations for the multilayer mechanism.
- Study the joints constraints for a polyhedral
- Fabricated irregular polyhedral.

29

Future work

- Study the movement and trajectory path of scissor mechanism that includes lineal, polar and radial movement.
- Apply the method on to wide variety of irregular shapes.
- Wider the possibilities for origami + Scissor mechanism hybrid structures.

30

Surface Rationalization and Optimization in Structural Engineering Practice

Toby Mitchell
Thornton Tomasetti, Chicago, United States

Abstract

In this talk, we examine the nuances and challenges of deploying the techniques of architectural geometry and discrete differential geometry in commercial structural engineering practice. By contrast to the academic context, structural design of surface structures in building practice involves multiple overlapping optimization objectives, many of which are not easily quantifiable, and many of which are not fully clear at the outset of the design process. Instead, the particular mathematical techniques appropriate for a given design problem must be uncovered by engineers working together with architects and other specialists in an iterative design process that integrates structural and construction performance goals with other technical objectives as well as subjective design intent. The author will examine approaches that have proven successful in his work on practical engineering projects, such as

1. The use of graphic statics in the design of the flat-paneled negatively-curved grid shell of the Hangzhou Greenland Center (which recently won the CTBUH's Best Tall Building award in the Asian region [1]).

2. The use of the Airy stress function in structural design of the flat-paneled quad-dominant grid shell of the Columbus, Ohio John Glenn airport renovation, and the utility of self-Airy shells in incorporating multiple panelization objectives while retaining structural performance [2].

3. The use of the static-kinematic duality in the design of rigidly-foldable structural origami such as SOM's MAK pavilion, and in the design of doubly-curved flat-paneled cable nets [3]

In addition to discussing the specific mathematical techniques used in these projects, the author will focus on the practical aspects of deploying architectural geometry and structural form-finding in design practice, such as the need to educate engineers on specialized techniques that are not typically part of their education, the need to solicit buy-in and facilitate authorship of architectural designers, the phasing of project development that necessitates the use of "lightweight" mathematical methods that do not rely on extensive information that will not be available in the early phases of design development, and the need to respond to input from contractors which often comes at the very end of a design process and may necessitate substantial design revisions.

References

[1] "SOM Wins Seven Awards of Excellence from the Council on Tall Buildings and Urban Habitat", https://www.som.com/news/ctbuh-awards-24/.

[2] Cameron Millar, Toby Mitchell, Arek Mazurek, Ashpica Chhabra, Alessandro Beghini, Jeanne N. Clelland, Allan McRobie, and William F. Baker, On designing plane-faced funicular gridshells, Int. J. Space Structures, vol. 38, issue 1 (2022), https://doi.org/10.1177/09560599221126656.

[3] Toby Mitchell, Arek Mazurek, Christian Hartz, Masaaki Miki, and William F. Baker, Structural Applications of the Graphics Statics and Static-Kinematic Dualities: Rigid Origami, Self-Centering Cable Nets, and Linkage Meshes, Proceedings of IASS Annual Symposia, IASS 2018 Boston Symposium: Graphic statics, pp. 1-8(8)

Variable Projection (VarPro) Method and Form-finding of Tension-compression Mixed Shells

Masaaki Miki
The University of Tokyo, Japan

Abstract

This presentation reviews recent advances in the form-finding of tension-compression mixed shells. Although purely compressive stress states are traditionally considered ideal for shell structures, we propose that allowing a mix of tension and compression can expand the range of feasible shell geometries. The key challenge lies in the fact that the equilibrium problem becomes a hyperbolic boundary value problem, which is notoriously difficult to solve. We point out that the introduction of the Airy's stress function reveals that the equilibrium equation is a bilinear partial differential equation (PDE). We then indicate that this PDE can be solved using the Variable Projection (VarPro) method—developed specifically for bilinear problems. We also demonstrate that the alignment of stress and curvature directions is governed by a bilinear PDE, which can be solved concurrently with the equilibrium equation using the VarPro method.

THREE SIGGRAPH PAPERS (2015, 2022 SA, 2024)

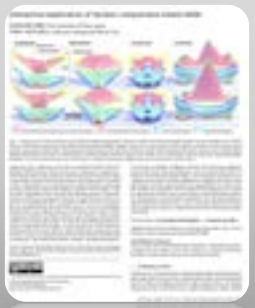

SIGGRAPH 2015

[Miki et al., 2015] Parametric self-supporting surfaces via direct computation of Airy stress functions, *Transactions on Graphics*, 2015

Form-finding of pure-compression shells using Airy stress function and NURBS

SIGGRAPH ASIA 2022

[Miki and Mitchell, 2022] Interactive exploration of tension–compression mixed shells, *Transactions on Graphics*, 2022

Form-finding of T/C mixed shells using Airy stress function and NURBS

- Reported that the problem can be solved using the Variable Projection (VarPro) method, a Least-squares and Gauss-Newton based method specifically designed to solve a system of bilinear equations.

SIGGRAPH 2024

[Miki et al., 2024] Alignment conditions for NURBS-based design of mixed tension–compression grid shells, *Transactions on Graphics*, 2024

Alignment of conjugate stress and curvature nets in a NURBS-based T/C mixed shell form-finding

Reported that the alignment condition can be solved using VarPro as well.

BACKGROUND

SYSTEM

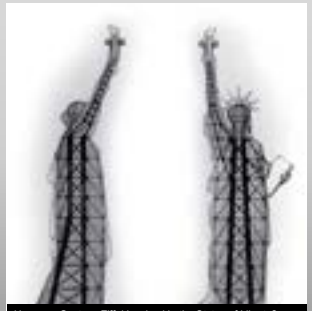

How was Gustave Eiffel Involved in the Statue of Liberty? https://www.thecollectcr.com/how-gustave-eiffel-involved-in-statue-of-liberty/

A system is a structure based on a simple and stable geometry, assembled with repeating and easily manufactured components and standardized detailing; it allows to create a variety of shapes.

Left: a skeleton inside the Statue of Liberty, engineered by Gustave Eiffel.

WHAT DO WE SEE VALUE IN

Generated by DALL-E

A good system allows us to build arbitrary shapes effectively. If the statue of Liberty is possible, the Stanford Bunny at an architectural scale should also be possible.

However, this is not what “we” do, because “we” don’t see any value in it.

Buildepedia

“Zaha Hadid’s Heydar Aliyev Cultural Centre: Turning a Vision into Reality”

I THINK THIS IS BEAUTIFUL. IT FOLLOWS THE PRINCIPLES OF MECHANICS, RIGHT?. CAN WE DO THIS? – NO. –

TENSION-COMPRESSION-BENDING

We don't want bending

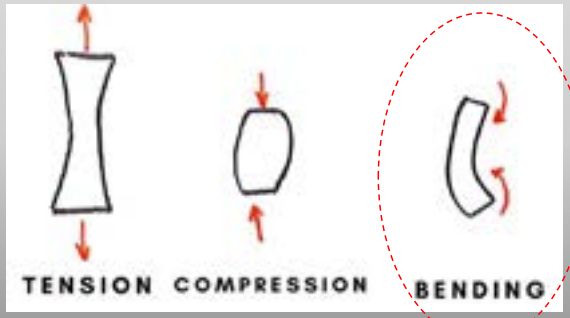

https://www.youtube.com/watch?v=4Am6myjNpEw
Internal Forces, StructruePlanet

STRUCTURALLY EFFICIENT SHAPES

Munich Olympic Stadium (Frie Otto)

Olympiastadion (Munich) (2024, June 3). From Wikipedia https://en.wikipedia.org/wiki/Olympiastadion_(Munich)

Jefferson National Expansion Memorial (Eero Saarinen)

Gateway Arch National Park (2024, May 21). From Wikipedia https://en.wikipedia.org/wiki/Gateway_Arch_National_Park

"We" see value in shapes that follow the principles of mechanics.

There are a few existing precedents whose geometry follows the principles of mechanics. However, they are extremely rare because their construction is too expensive. They cost too much because they lack systems easy to construct.

WHAT IS A GOOD DESIGN IN ARCHITECTURE?

Shanghai International F1 Circuit (Taiyo Kogyo)

https://www.taiyokogyo.co.jp/en/works/50495/

Good architecture should involve both

1. a structurally efficient shape, and
2. a good system that is easy to construct

For example,

Minimal surface = a structurally efficient shape

Partitioning with geodesic lines = a good system that is easy to construct

FORM-FINDING USING SOAP FILM (TENSION)

Frie Otto film, Youtube

www.archdaily.com

https://www.archdaily.com/610531/frei-otto-and-the-importance-of-experimentation-in-architecture

www.isaa.org

COMPUTATION FORM-FINDING OF TENSION STRUCTURES

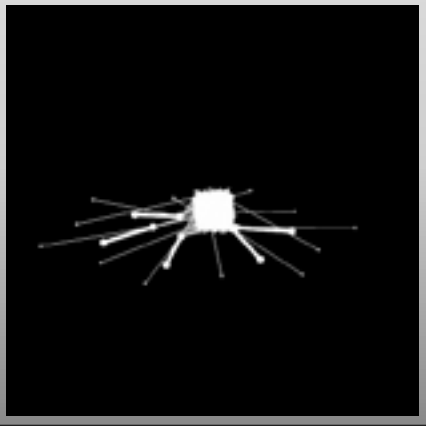

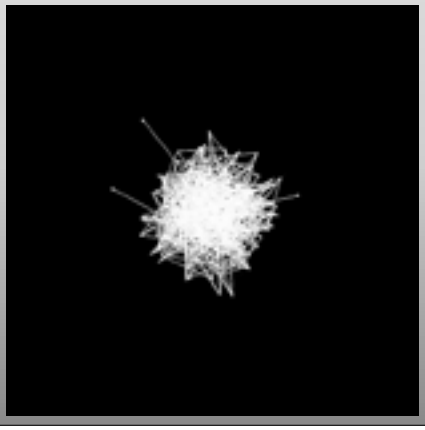

PHYSICAL MODEL MAKING

CATENARY ARCH (COMPRESSION)

The Gateway Arch, Earo Saarinen, St. Louis

FORM-FINDING BY INVERTED HANGING EXPERIMENTS (COMPRESSION)

Heinz Isler

Highway service area, Solothurn, Switzerland

H. Isler, Typologie und Technik der modernen Schalen, 1983

FORM-FINDING BY INVERTED HANGING EXPERIMENTS (COMPRESSION)

KK Clark, https://adventures-of-kk.blogspot.com/2012/05/day-8-bike-tour-gaudi.html

Sagrada Familia, Bernard Gagnon, 2009, Licensed under CC BY-SA 3.0 via Wikimedia Commons

COMPUTATIONAL FORM-FINDING OF PURE-COMPRESSION SHELLS

A simulation of the inverted hanging experiments.

© Designboom, MARC FORNES/THEVERYMANY fabricates vaulted willow pavilion in edmonton

PURE-COMPRESSION DOMES

Masterpieces by engineers

Eduardo Torroja

Eduardo Torroja (2024, March 4). From Wikipedia https://en.wikipedia.org/wiki/Eduardo_Torroja

Pier Luigi Nervi

Pier Luigi Nervi (2024, June 29). From Wikipedia https://en.wikipedia.org/wiki/Pier_Luigi_Nervi

SHELL-LIKE STRUCTURES BY ARCHITECTS

Perhaps they are not pure shells, but they are beautiful.

TWA Flight Center at JFK Airport (Eero Saarinen)

TWA Flight Center (2024, May 17). From Wikipedia https://en.wikipedia.org/wiki/TWA_Flight_Center

Sydney Opera House (Jørn Utzon)

Sydney Opera House (2024, June 20). From Wikipedia. https://en.wikipedia.org/wiki/Sydney_Opera_House

WHAT IF A MIX OF TENSION AND COMPRESSION IS ALLOWED?

Felix Candela

Amancio Williams

* Courtesy of Amancio Williams funds, Canadian Centre for Architecture, Gift of the children of Amancio Williams

T/C MIXED SHELLS = UNEXPLORED FRONTIER

T/C

The complete set of special class of surfaces that can withstand gravity with no-bending

Pure-compression

Already explored

ISN'T IT BENDING? – NO –

This is T/C mixed

This is bending

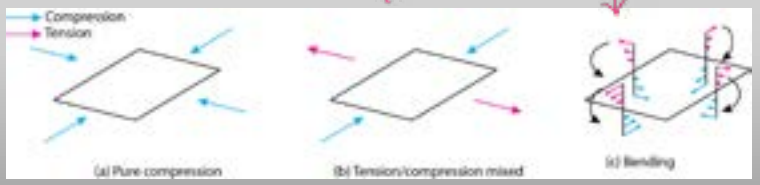

CORE CONCEPTS IN SHELL FORM-FINDING

AIRY STRESS FUNCTION

Positive Gaussian curvature

Pure compression

Negative Gaussian curvature

Tension-compression mixed

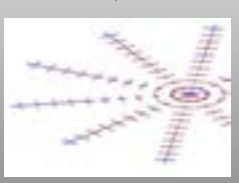

FORM-FINDING USING AIRY STRESS FUNCTION

Positive Gaussian curvature

Pure compression shell

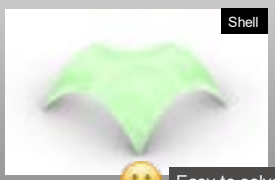

Easy to solve.

Negative Gaussian curvature

Mixed tension-compression shell

The old books say it is notoriously difficult to solve.

BOUNDARY CONDITION – FREE EDGE –

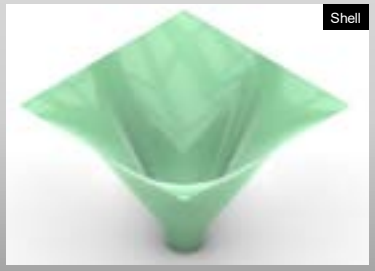

(VERTICAL) EQUILIBRIUM EQUATION OF A SHELL

$\bar{\phi}(x,y)$, Airy stress function (given)

$\bar{\rho}(x,y)$, vertical load (given)

$z(x,y)$, shell (unknown to be identified)

$$\frac{\partial^2\bar{\phi}}{\partial y^2}\frac{\partial^2 z}{\partial x^2}-2\frac{\partial^2\bar{\phi}}{\partial x\partial y}\frac{\partial^2 z}{\partial x\partial y}+\frac{\partial^2\bar{\phi}}{\partial x^2}\frac{\partial^2 z}{\partial y^2}=-\bar{\rho}$$

TYPES OF 2ND-ORDER PDES

Pure compression: elliptical
Easy to solve.

T/C mixed: hyperbolic
Notoriously difficult to solve.

TYPES OF 2ND-ORDER PDES

Elliptic problem

e.g., $\frac{\partial^2 z}{\partial x^2} + \frac{\partial^2 z}{\partial y^2} = 1$ Laplace's equation

The nature of those two types of PDEs are surprisingly different

Hyperbolic problem

e.g., $\frac{\partial^2 z}{\partial x^2} - \frac{\partial^2 z}{\partial y^2} = 1$ Wave equation

LAPLACE EQUATION

$$\frac{\partial^2 z}{\partial x^2} + \frac{\partial^2 z}{\partial y^2} = 1$$

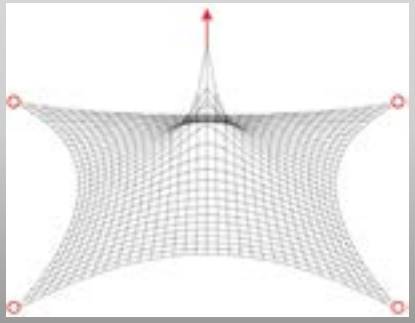

- Typically solved as a boundary value problem.
- A solution is a smooth averaging between the boundary values in general.
- Easy to solve.

WAVE EQUATION

$$\frac{\partial^2 z}{\partial x^2} - \frac{\partial^2 z}{\partial y^2} = 1$$

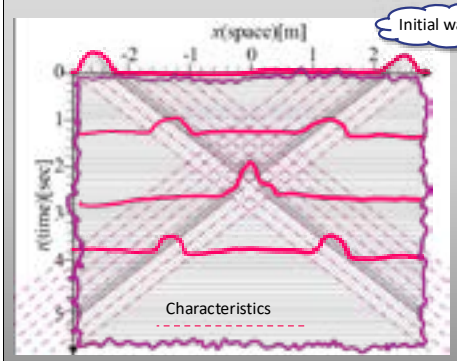

- Typically solved as an initial value problem.
- A solution is a wave propagation over time.
- In the time-space domain, the waves run along characteristic lines (diagonal lines in the left figure)
- Normally solved by incrementing the state of the wave step by step by incrementing the time with a small time step.
- Normally, it is not a good idea to solve it as a boundary value problem because you cannot prescribe the past and future at the same time.
- Unfortunately, a T/C mixed form-finding is a hyperbolic boundary value problem

CHARACTERISTIC LINES = ASYMPTOTIC LINES OF AIRY STRESS FUNCTION

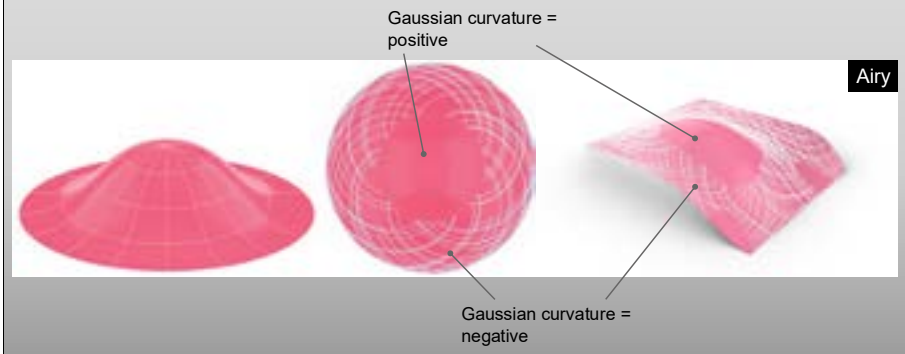

COMPATIBLE BOUNDARY CONDITIONS

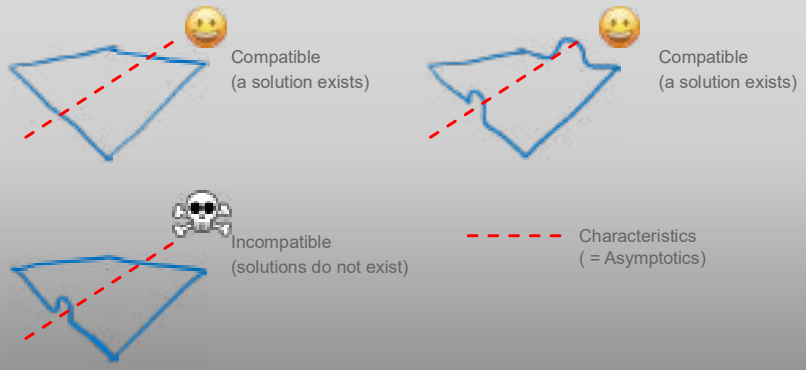

WHEN THE PROBLEM DOES NOT HAVE SOLUTIONS

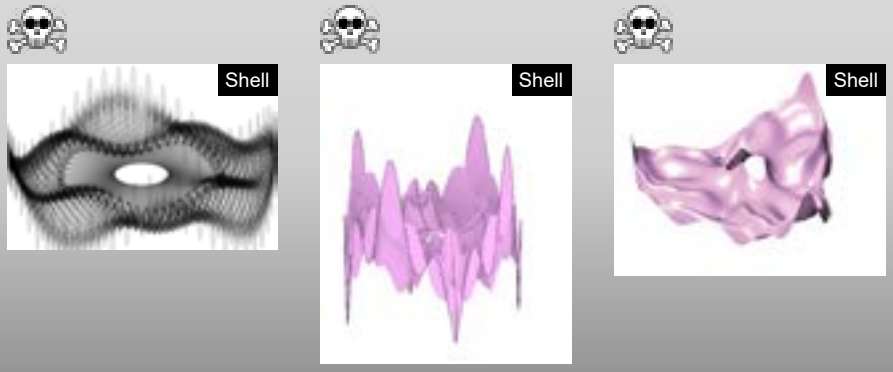

WHEN THE PROBLEM DOES HAVE A SOLUTION

**This study was supervised by Chris J. K. Williams

Stress function ϕ

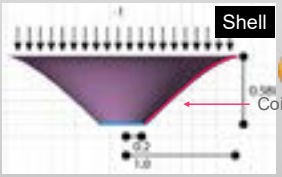

Shell z (numerical solution)

Coincide!

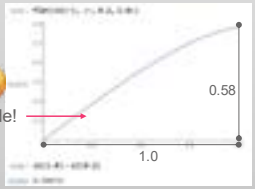

Shell z (Analytical solution)

When solution exists, it is easy to solve numerically.

FORM-FINDING (OUR APROACH)

RECIPROCAL STRUCTURE

$\bar{\phi}$: Airy stress function, z: shell

Pin $\bar{\phi}$, find z

$$\frac{\partial^2\bar{\phi}}{\partial x^2}\frac{\partial^2 z}{\partial y^2} - 2\frac{\partial^2\bar{\phi}}{\partial x\partial y}\frac{\partial^2 z}{\partial x\partial y} + \frac{\partial^2\bar{\phi}}{\partial y^2}\frac{\partial^2 z}{\partial x^2} = \rho$$

Linear

Pin $\bar{z}$, find ϕ

$$\frac{\partial^2\phi}{\partial x^2}\frac{\partial^2\bar{z}}{\partial y^2} - 2\frac{\partial^2\phi}{\partial x\partial y}\frac{\partial^2\bar{z}}{\partial x\partial y} + \frac{\partial^2\phi}{\partial y^2}\frac{\partial^2\bar{z}}{\partial x^2} = \rho$$

Linear

IDEA: UNPIN STRESS FUNCTION

ϕ: stress function (unknown function to be identified)
z: shell (unknown function to be identified)

$$\frac{\partial^2\phi}{\partial x^2}\frac{\partial^2 z}{\partial y^2} - 2\frac{\partial^2\phi}{\partial x\partial y}\frac{\partial^2 z}{\partial x\partial y} + \frac{\partial^2\phi}{\partial y^2}\frac{\partial^2 z}{\partial x^2} = \rho$$

We now have two unknown functions against one condition. This means there are many solutions.

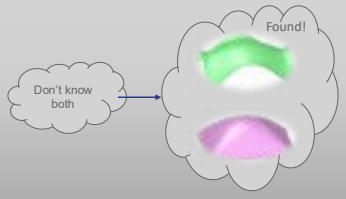

CONCLUSION: IT IS A BILINEAR PDE

$$\frac{\partial^2\phi}{\partial x^2}\frac{\partial^2 z}{\partial y^2} - 2\frac{\partial^2\phi}{\partial x\partial y}\frac{\partial^2 z}{\partial x\partial y} + \frac{\partial^2\phi}{\partial y^2}\frac{\partial^2 z}{\partial x^2} = \rho$$

with one condition for two unknown functions.

BILINEAR LEAST SQAURES PROBLEM

Full Problem (Bilinear)

Find $\{\phi, z\}$ such that $\int \left(\frac{1}{g}(\nabla_{11}\phi\nabla_{22}z - \nabla_{12}\phi\nabla_{12}z + \nabla_{22}\phi\nabla_{11}z) + \rho\frac{\sqrt{\det g_{ij}}}{\sqrt{\det \bar{g}_{ij}}} \right)^2 \mathrm{da} \rightarrow \min$

Primal Subproblem (Linear)

Given $\bar{\phi}$, find z such that $\int \left(\frac{1}{g}(\nabla_{11}\bar{\phi}\nabla_{22}z - \nabla_{12}\bar{\phi}\nabla_{12}z + \nabla_{22}\bar{\phi}\nabla_{11}z) + \rho\frac{\sqrt{\det g_{ij}}}{\sqrt{\det \bar{g}_{ij}}} \right)^2 \mathrm{da} \rightarrow \min$

Dual Subproblem (Linear)

Given $\bar{z}$, find ϕ such that $\int \left(\frac{1}{g}(\nabla_{11}\phi\nabla_{22}\bar{z} - \nabla_{12}\phi\nabla_{12}\bar{z} + \nabla_{22}\phi\nabla_{11}\bar{z}) + \rho\frac{\sqrt{\det g_{ij}}}{\sqrt{\det \bar{g}_{ij}}} \right)^2 \mathrm{da} \rightarrow \min$

ALTERNATING APPROACH (ALT)

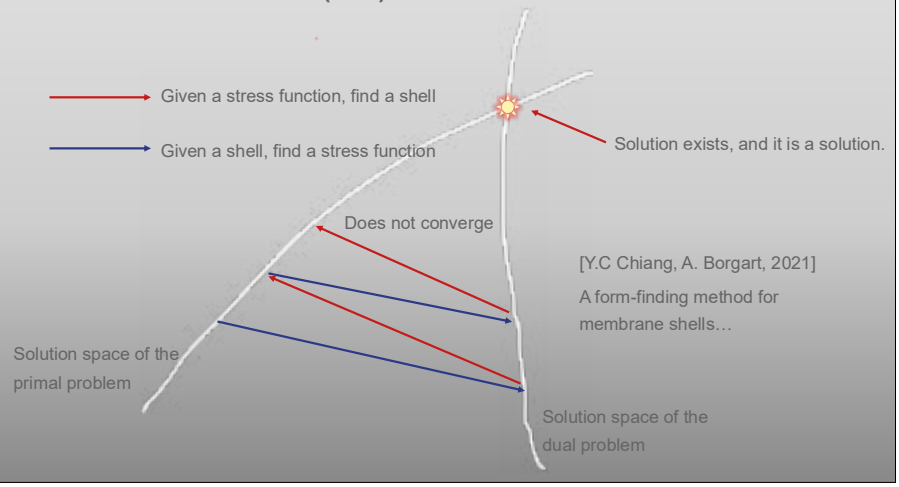

VARIABLE PROJECTION (VARPRO)

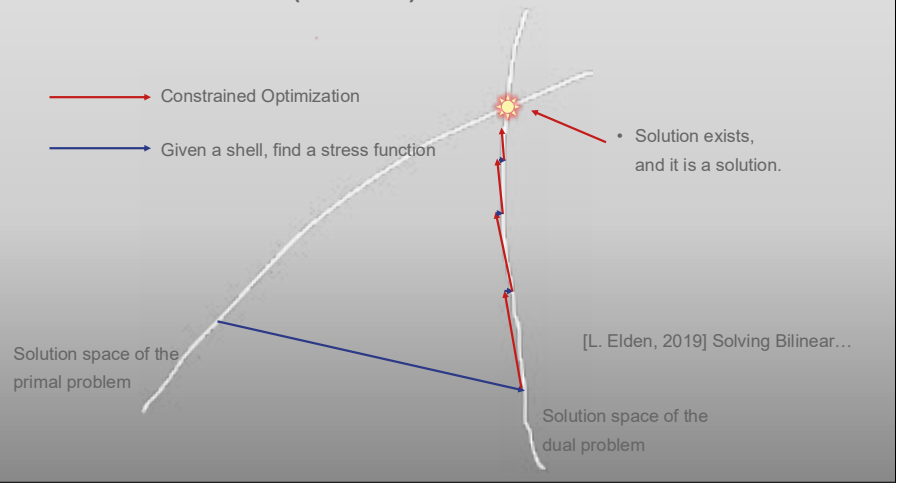

T/C MIXED SHELL FORM-FINDING USING VARPRO

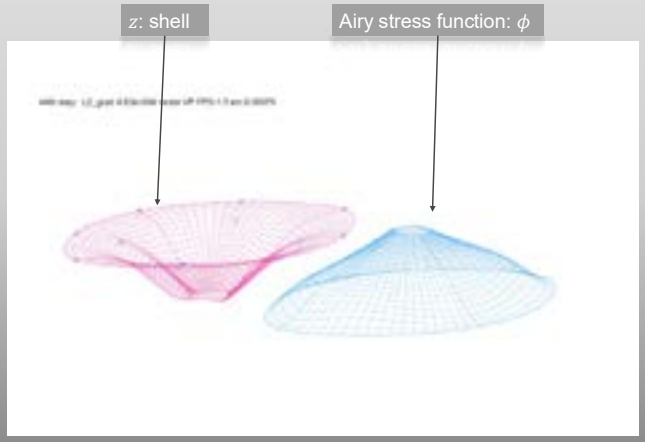

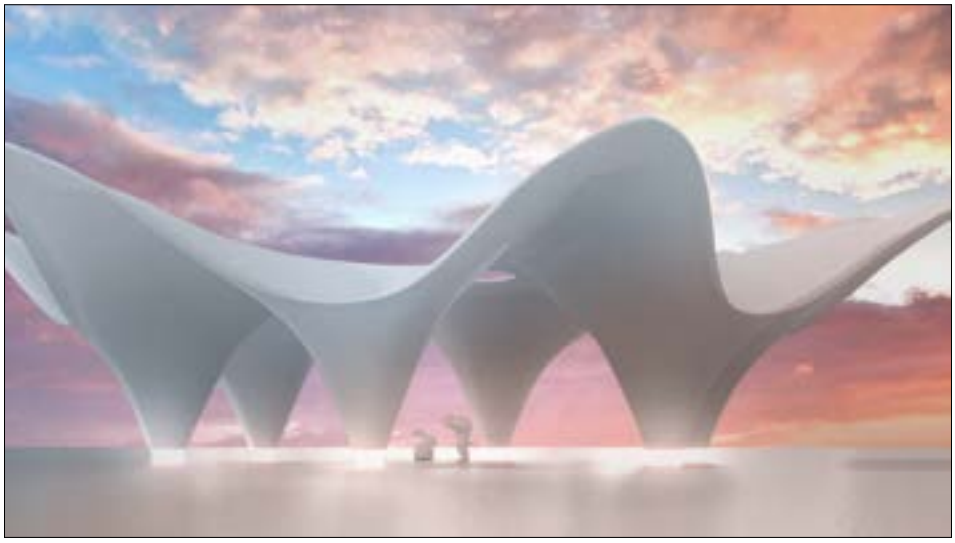

ALIGNMNET CONDITION

CONJUGATE CURVATURE NET

- Tracings of local frames on a surface that gives no local warping → Can be used for planar quadrilateral panelization.
- Lines of curvature are special conjugate curvature nets in which two directions intersect orthogonally.

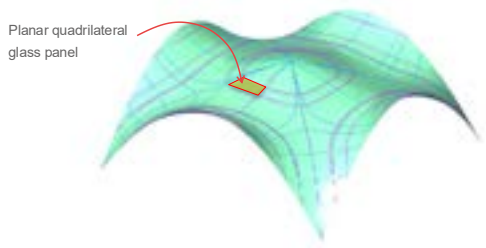

CONJUGATE STRESS NET

- Tracings of local frames on a surface that give no shear stress → Can be used for the basis geometry of a bending-free grid shell.
- Principal stress trajectories are a special case of conjugate stress net in which two directions intersect orthogonally.
- It is a conjugate curvature net of an Airy stress function.

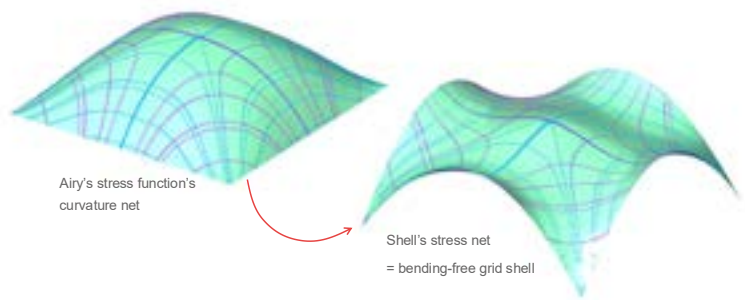

ALIGNING TWO SYMMETRIC MATRICES

A: 2x2 real symmetric matrix
B: 2x2 real symmetric matrix
$A + B$ is symmetric
$A - B$ is symmetric
AB is *not* symmetric

$$AB = \text{symm}$$

⇔ When AB is symmetric, it represents a special state in which eigenvectors of two matrices point to the same directions.

$$\begin{bmatrix}1 & 0\\0 & 3\end{bmatrix}\begin{bmatrix}2 & 0\\0 & 1\end{bmatrix} = \begin{bmatrix}2 & 0\\0 & 3\end{bmatrix}\text{(symm)}$$

$$\begin{bmatrix}1 & 2\\2 & 1\end{bmatrix}\begin{bmatrix}-2 & 3\\3 & -2\end{bmatrix} = \begin{bmatrix}4 & -1\\-1 & 4\end{bmatrix}\text{(symm)}$$

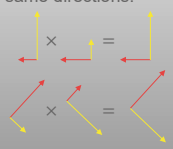

ALIGNMENT BETWEEN THREE MATRICES

A: 2x2 real symmetric matrix

B: 2x2 real symmetric matrix

E: 2x2 real symmetric positive (semi) definite matrix

e: $R_{90}ER_{90}^T$

$$AEB = \text{symm}$$

⇔ When E is positive (semi)definite, a conjugate pair that is simultaneously conjugate with A,B and e exists.

CONTROLLING THE ALIGNMENT THROUGH $\bar{E}$

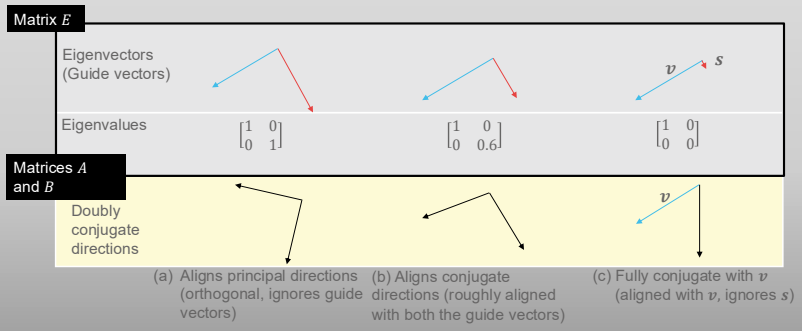

(a) Aligns principal directions (orthogonal, ignores guide vectors)

(b) Aligns conjugate directions (roughly aligned with both the guide vectors)

(c) Fully conjugate with v (aligned with v, ignores s)

BILINEAR PDES

Equilibrium equation:

$$\frac{\partial^2 z}{\partial x \partial x}\frac{\partial^2 \phi}{\partial y \partial y} - 2\frac{\partial^2 z}{\partial x \partial y}\frac{\partial^2 \phi}{\partial x \partial y} + \frac{\partial^2 z}{\partial y \partial y}\frac{\partial^2 \phi}{\partial x \partial x} = \rho$$

Alignment condition:

$$\frac{\partial^2 z}{\partial x \partial x}\bar{E}_{xx}\frac{\partial^2 \phi}{\partial x \partial y} + \frac{\partial^2 z}{\partial x \partial x}\bar{E}_{xy}\frac{\partial^2 \phi}{\partial y \partial y} + \frac{\partial^2 z}{\partial x \partial y}\bar{E}_{yx}\frac{\partial^2 \phi}{\partial x \partial y} + \frac{\partial^2 z}{\partial x \partial y}\bar{E}_{yy}\frac{\partial^2 \phi}{\partial y \partial y} = \frac{\partial^2 z}{\partial y \partial x}\bar{E}_{xx}\frac{\partial^2 \phi}{\partial x \partial x} + \frac{\partial^2 z}{\partial y \partial x}\bar{E}_{xy}\frac{\partial^2 \phi}{\partial y \partial x} + \frac{\partial^2 z}{\partial y \partial y}\bar{E}_{yx}\frac{\partial^2 \phi}{\partial x \partial x} + \frac{\partial^2 z}{\partial y \partial y}\bar{E}_{yy}\frac{\partial^2 \phi}{\partial y \partial x}$$

- Both conditions are bilinear PDEs.
- Can be solved using VarPro.

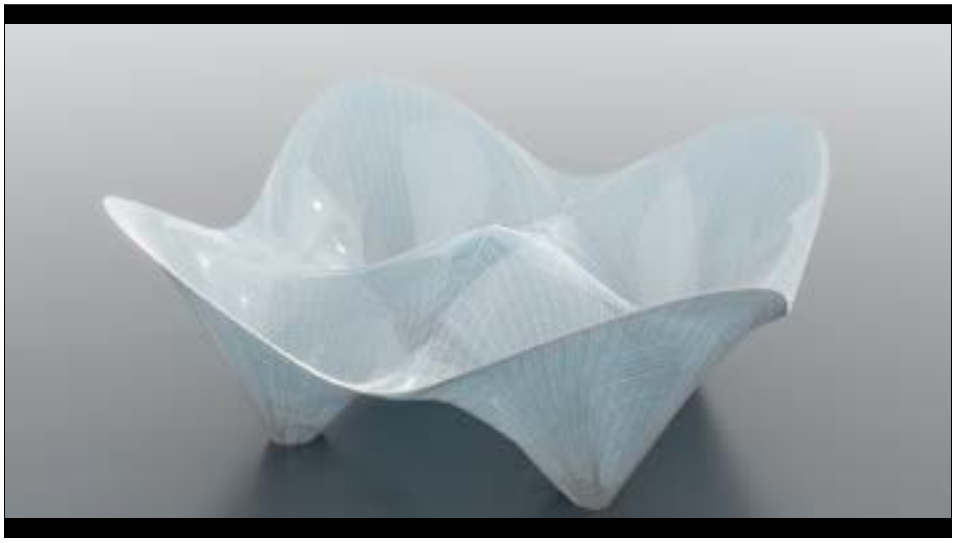

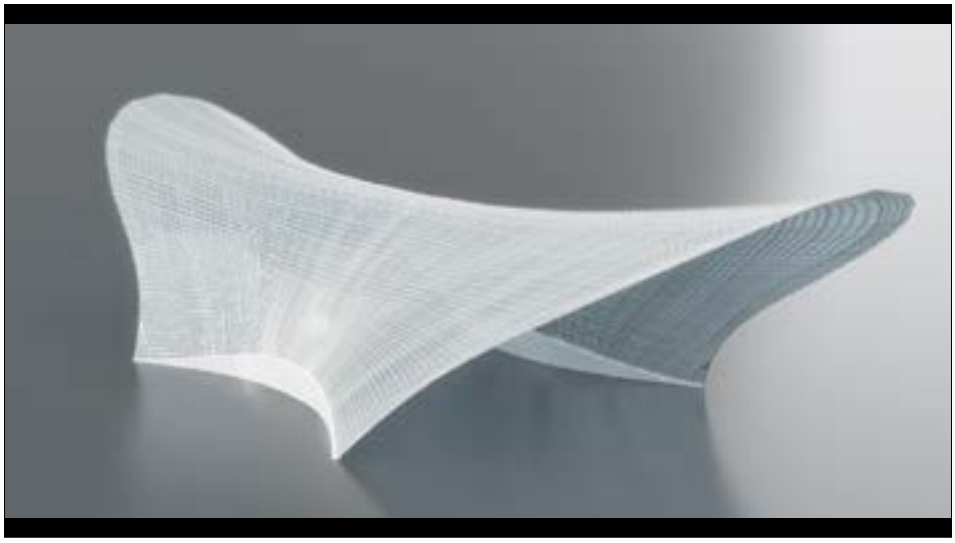

FABRICATION

STARFISH_B

TESTING MATERIAL SAMPLES

BUILDING A FORMWORK

ASSEMBLING DEVELOPABLE STRIPS

FORMWORK ASSEMBLY IS READY

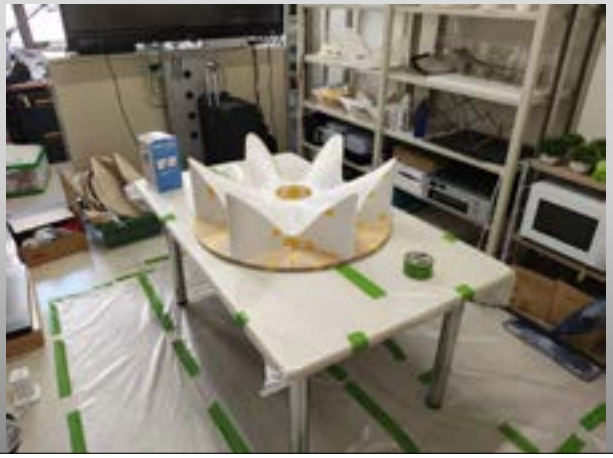

INGREDIENTS

Cement

Steel fibers
(Staples)

Tough binder
(Nylon fibers)

CONCRETE PLACEMENT

CONCRETE PLACEMENT

24HRS

48HRS

FORMWORK REMOVAL

CLEANING

A MINIATURE T/C MIXED CONCRETE SHELL

A MINIATURE T/C MIXED CONCRETE SHELL

THANK YOU!

CONTACT: MASAAKI.MIKI@MMIKI.JP

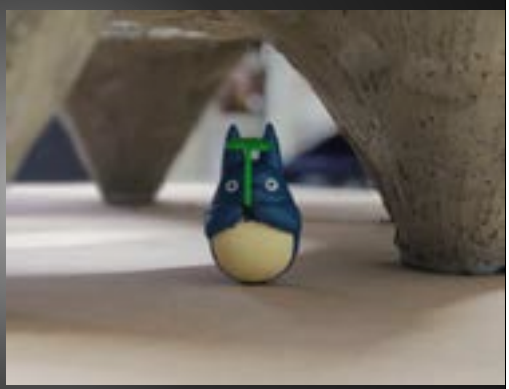

Curved Surface Structures with Excellent Mechanical Rationality and Constructability/Fabricability

Yohei Yokosuka
Kagoshima University, Japan

Abstract

There are geometrically defined classes of surfaces and curves suitable for each surface shape, such as membrane structures that resist tensile stress and shell structures that resist compressive stress. These surface and curve classes are categorized as mechanically motivated and those motivated by constructability and member fabrication. From a mechanical point of view, F. Otto uses an extremely minimal curved surface for the membrane structure and H. Isler applied a suspended curved surface for the shell structure, designing a curved surface structure that is mechanically rational. F. Candela uses HP curved surfaces in curved structures, designing curved structures that are superior from constructability. In recent years, there has been progress in research on the design of curved surface structures that rediscover the properties of both the mechanical and constructional perspectives from geometry by means of discrete differential geometry. This presentation will introduce a class of surfaces and curves that can be applied to curved structures in architecture.

International Conference "Evolving Design and Discrete Differential Geometry - towards Mathematics Aided Geometric Design"

Curved Surface Structures with Excellent Mechanical Rationality and Constructability/Fabricability

Yohei YOKOSUKA[1)], Yoshiki JIKUMARU[2)], Kazuki HAYASHI[3)],
Kentaro HAYAKAWA[4)], Yusuke SAKAI[5)]

1) Graduate School of Science and Engineering, Kagoshima University
2) Information Networking for Innovation And Design, Toyo University
3) Graduate School of Engineering, Kyoto University
4) College of Industrial Technology Department of Conceptual Design, Nihon University
5) Sony Computer Science Laboratories, Inc

■ Overview

1. Close relationship between shell and spatial structures and geometry

2. Research Case Studies

   2.1 Discrete isothermic minimal surfaces
   2.2 Discrete membrane O surface
   2.3 Willmores surface and Möbius transformation
   2.4 Airy stress function and Laguerre geometry

3. Conclusion

Curved Surface Structures with Excellent Mechanical Rationality and Constructability/Fabricability

1. Close relationship between shell and spatial structures and geometry

○ Geometry ○ Shell and Spatial Structures
(Static Mechanics・ Constructability/Fabricability)

Classical Surfaces Classes

Minimal surface	⇔ Suspension Membrane Structure: Pure tension
Geodesic line	⇔ Membrane cutting line and cable placement: Shear free
CMC surface	⇔ Pneumatic membrane structures: Pure tension
Catenary curve	⇔ Reversed Hanging curve/membrane: Pure compression
Hyperbolic paraboloid surface	⇔ Shell structures: Doubly ruled surface
Rotational hyperboloid	⇔ Cooling tower, Tower: Doubly ruled surface
Ruled surface	⇔ Beam structures: Ruled surface

Curved Surface Structures with Excellent Mechanical Rationality and Constructability/Fabricability

1. Close relationship between shell and spatial structures and geometry

○ Geometry　　○ Shell and Spatial Structures
(Static Mechanics・ Constructability/Fabricability)

Minimal surface	⇔ Suspension Membrane Structure: Pure tension
Geodesic line	⇔ Membrane cutting line and cable placement: Shear free
CMC surface	⇔ Pneumatic membrane structures: Pure tension
Catenary curve	⇔ Reversed Hanging curve/membrane: Pure compression

How can these surfaces be characterized?

Curved Surface Structures with Excellent Mechanical Rationality and Constructability/Fabricability

1. Close relationship between shell and spatial structures and geometry

○ Geometry　　○ Shell and Spatial Structures
(Static Mechanics)

Minimal surface	⇔ Suspension Membrane Structure: Pure tension
Geodesic line	⇔ Membrane cutting line and cable placement: Shear free
CMC surface	⇔ Pneumatic membrane structures: Pure tension
Catenary curve	⇔ Reversed Hanging curve/membrane: Pure compression

How can these surfaces be characterized?
⇒ Critical points for variational problems
⇒ At arbitrary boundary conditions, a certain functional is defined and the solution that minimizes the functional is obtained.

Curved Surface Structures with Excellent Mechanical Rationality and Constructability/Fabricability

1. Close relationship between shell and spatial structures and geometry

○ Geometry　　○ Shell and Spatial Structures
(Static Mechanics)

Minimal surface	⇔ Minimization of curved surface area
Geodesic line	⇔ Minimization of curve length on a surface
CMC surface	⇔ Minimize curved surface area by specifying inner volume
Catenary curve	⇔ Minimization of gravitational potential

How can these surfaces be characterized?
⇒ Critical points for variational problems
⇒ At arbitrary boundary conditions, a certain functional is defined and the solution that minimizes the functional is obtained.

Curved Surface Structures with Excellent Mechanical Rationality and Constructability/Fabricability

1. Close relationship between shell and spatial structures and geometry

○ Geometry　　○ Shell and Spatial Structures (Constructability/Fabricability)

Hyperbolic paraboloid surface	⇔ Shell structures: Doubly ruled surface
Rotational hyperboloid	⇔ Cooling tower, Tower: Doubly ruled surface
Ruled surface	⇔ Beam structures: Ruled surface

How can these surfaces be characterized?

Curved Surface Structures with Excellent Mechanical Rationality and Constructability/Fabricability

1. Close relationship between shell and spatial structures and geometry

○ Geometry　　○ Shell and Spatial Structures (Constructability/Fabricability)

Hyperbolic paraboloid surface	⇔ Shell structures: Doubly ruled surface
Rotational hyperboloid	⇔ Cooling tower, Tower: Doubly ruled surface
Ruled surface	⇔ Beam structures: Ruled surface

How can these surfaces be characterized?

⇒ Focusing on the direction of coordinate lines are taken, coordinate lines with zero normal curvature are chosen.

⇒ Asymptotic direction, which is limited to the case when Gaussian curvature is negative.

Curved Surface Structures with Excellent Mechanical Rationality and Constructability/Fabricability

1. Close

We would like to sample a finite number of points for practical use.
⇒ Inherently, a discrete surface that is not smooth is not differentiable at a point
⇒ Discrete Differential Geometry

★ Context of Variations and Coordinates

・Study of variational problems with triangular polyhedral meshes by introducing the concept of curvature consistent between continuous and discrete surfaces
・A comprehensive treatment of a class of surfaces with flat quadrilaterals as shape elements and good properties (Integrable geometry)

negative.

2. Research Case Studies
2.1 Discrete isothermic minimal surfaces

■ **Architecture：** **Form-finding of membrane structure**
Otto, F. (1973) : Application to tension structures
Schek, H.J (1974) : Force density method
Barnes, M.R (1977) : Dynamic relaxation

■ **Mathematics**
Courant, R(1950) : Problem to minimize Dirichlet integration (Dirichlet energy)
Hinata, M., Shimasaki, M., and Kiyono, T(1974) :Discretization by finite element method
Tsuchiya, T(1992) :Discretization of Dirichlet energy by finite element method
Pinkall, U., Polthier, K.(1993) : Dirichlet energy discretization (cotan formula)

Curved Surface Structures with Excellent Mechanical Rationality and Constructability/Fabricability

2. Research Case Studies
2.1 Discrete isothermic minimal surfaces

Functional (Dirichlet energy)

$$E = \frac{1}{2}\iint_{\Omega}\left(f_u^{\,2} + f_v^{\,2}\right)dudv \qquad (1)$$

f_u, f_v **: Tangent vector of** u, v **coordinates on the surface**

Curved Surface Structures with Excellent Mechanical Rationality and Constructability/Fabricability

2. Research Case Studies
2.1 Discrete isothermic minimal surfaces

Minimal surface ⇔ **Minimization of curved surface area**
⇔ **Dirichlet energy minimization and isothermic**
⇔ **Mean curvature is 0 and isothermic**
★ Coordinates issue

- **Isothermic properties of continuous curved surfaces**

$$f_u \perp f_v, \left\|f_u\right\| = \left\|f_v\right\| \qquad (1)$$

f_u, f_v **: Tangent vector of** u, v **coordinates on the surface**

2. Research Case Studies

2.1 Discrete isothermic minimal surfaces

・ Bobenko et al. constructed a Koebe polyhedron with a three-dimensional sphere $\mathbb{S}^2$ from known minimal surfaces, and showed that it is possible to construct different discrete isothermic minimal surfaces by giving their Christoffel duals (transformations).

⇒ Christoffel's theorem that a surface constructed from a Gauss map of minimal surfaces by a transformation preserving isothermality is a minimal surface.

Koebe polyhedron　　Discrete isothermal minimal surfaces

Bobenko, A.I., Hoffmann T., Springborn B. A., Minimal surfaces from circle patterns: Geometry from combinatorics, Annals of Mathematics, 164, pp.231–264, 2006

Curved Surface Structures with Excellent Mechanical Rationality and Constructability/Fabricability

2. Research Case Studies

Note:

・This method showed that different minimal surfaces can be obtained by applying a coordinate-preserving transformation.

⇒ Transformation itself is essential.

Koebe polyhedron　　Discrete isothermal minimal surfaces

Bobenko, A.I., Hoffmann T., Springborn B. A., Minimal surfaces from circle patterns: Geometry from combinatorics, Annals of Mathematics, 164, pp.231–264, 2006

Curved Surface Structures with Excellent Mechanical Rationality and Constructability/Fabricability

2. Research Case Studies

Note

Circle Pattern:
Corresponds to discretization of curvature line coordinates (discrete curvature line network)

Isothermic curvature line coordinates:
Corresponds to the condition that cross-ratio is equal to -1

Koebe polyhedron　　Discrete isothermal minimal surfaces

Bobenko, A.I., Hoffmann T., Springborn B. A., Minimal surfaces from circle patterns: Geometry from combinatorics, Annals of Mathematics, 164, pp.231–264, 2006

2. Research Case Studies
2.2 Membrane O surfaces

・**The canopy of Tokyo Midtown** is composed of **multi-layered curved surfaces** and **vertical members** connecting between the curved surfaces. The **orientation** of the **curved surface members** adopts the **principal direction,** and in one compartment, **four sides** are **flat surfaces.**

Principal direction - curvature line coordinates in the direction that follows the principal curvature

The canopy of Tokyo Midtown

2. Research Case Studies
2.2 Membrane O surfaces

・**Discrete curvature line network ⇒** A curved surface covered by **quadrilaterals to which a circle is circumscribed.** The quadrilateral connecting the intersections is flat.
・**Vertex Offset ⇒** In a **discrete curvature line network,** the **normals** defined by the points are **mirrored** in the **plane orthogonal to the edge**, and **the sides spanned** by the **normals** are **flat without torsion.**

・Curved surface structures consisting of flat quadrilaterals have excellent properties in the view of **Constructability/Fabricability.**

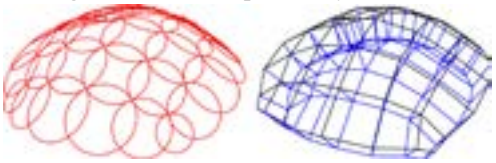

Assembled beam with discrete curvature line network and normal

Schief, W. K.: Integrable structure in discrete shell membrane theory, Proc. R. Soc. A (2014) 470: 20130757, 2014

2. Research Case Studies
2.2 Membrane O surfaces

・ **Membrane O surfaces ⇒** A class of curved surfaces that are equilibrium by **in-plane membrane stress** without **bending moment** and **in-plane shear** when a **constant load** is applied in the **normal direction**.
・**Equilibrium equation of in-plane**
⇒ **Dual surface** exists in the **Combescure transformation**
⇒ Corresponds to the **force diagram** and **form diagram** of **Graphic statics**

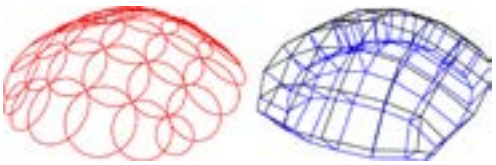

Assembled beam with discrete curvature line network and normal

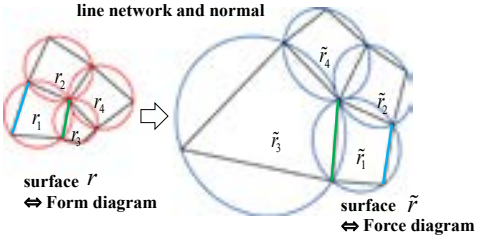

Combescure transformation (Parallel translation of edges)

2. Research Case Studies
2.2 Membrane O surfaces

Discrete Membrane O surfaces

・ A discrete curvature line network always has a surface $\tilde{r}$.

・ The out-of-plane equilibrium equation is expressed by the orthogonal conditionals for surfaces r and $\tilde{r}$.

・ Mem
of curve
by **in-pl**
bending
when a
normal
・ Equil
⇒ **I**
⇒ Corresponds to the **force diagram** and **form diagram** of **Graphic statics**

ure

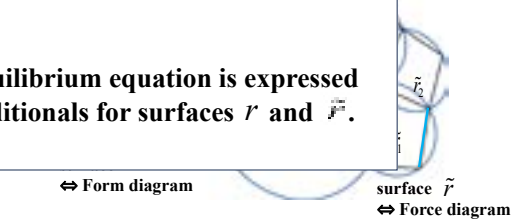

⇔ Form diagram

surface $\tilde{r}$
⇔ Force diagram

Combescure transformation (Parallel translation of edges)

2. Research Case Studies
2.3 Willmore surface and Möbius transformation

・Klein geometry
⇒A geometry characterized by transformations and invariants in those transformations.
Möbius geometry is a type of Klein geometry.

・Möbius transformation
⇒ A transformation that maps a circle to a circle, and cross-ratio is invariant under the Möbius transformation.
⇒ A discrete curvature line network can be mapped to a discrete curvature line network.

Felix C. Klein (1849-1925)

2. Research Case Studies
2.3 Willmore surface and Möbius transformation

・ Inversion ⇒ Typical operations with Möbius tranformation

$$\begin{cases} C, M, M' \ aligned \\ |CM||CM'| = k \end{cases} \quad (2)$$

C : **Center of a circle**
M: **Points before transformation**
M': **Points after transformation**
$\sqrt{|k|}$: **Radius of circle**

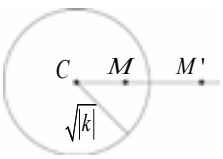

Inversion

Mesnil, R., Douthe, C., Baverel, O., Leger, B.: Generalised Cyclidic Nets for Shape Modelling in Architecture, International Journal of Architectural Computing, Volume 15, Issue 2, pp.1-22, 2017

2. Research Case Studies
2.3 Willmore surface and Möbius

・**Willmore Energy**
⇒ **Invariant functional with Möbius transformation**

$$\Omega = \int_S H^2 - K\, dA \qquad (3)$$

H: **Mean Curvature** K: **Gaussian Curvature**

・**Willmore surface**
⇒ **Critical point of Willmore energy**
⇒ **Möbius transformation allows Willmore surfaces to be mapped to Willmore surfaces.**

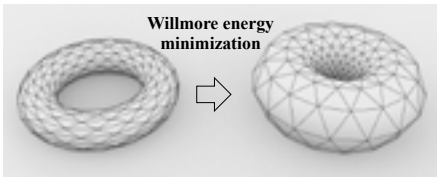

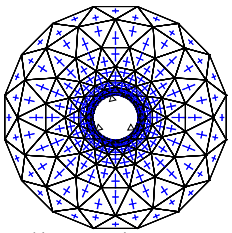

・pressure load: 100 N/m²
・membrane thickness: 1.0 mm
・elastic modulus : 100 N/mm²
・shear elastic modulus: 60 N/mm²
・ratio of poisson : 0.3

	σmax (N/mm²) Principal stress	σmin (N/mm²) Principal stress
max	1.4643	0.4123
min	0.5832	0.2668

Bobenko, A.I., Schröder, P., Discrete Willmore Flow, Eurographics Symposium on Geometry Processing, 2005

Curved Surface Structures with Excellent Mechanical Rationality and Constructability/Fabricability

2. Research Case Studies
2.3 Willmore surface and Möbius

・**Willmore Energy**
⇒ **Invariant functional with Möbius transformation**

$$\Omega = \int_S H^2 - K\, dA \qquad (3)$$

H: **Mean Curvature** K: **Gaussian Curvature**

・**Willmore surface**
⇒ **Critical point of Willmore energy**
⇒ **Möbius transformation allows Willmore surfaces to be mapped to Willmore surfaces.**

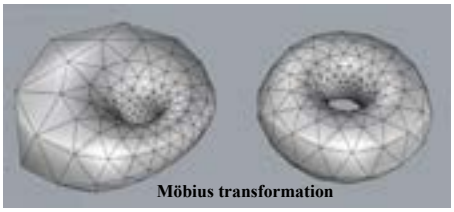

ARK NOVA (Arata Isozaki, Anish Kapoor)

Bobenko, A.I., Schröder, P., Discrete Willmore Flow, Eurographics Symposium on Geometry Processing, 2005

Curved Surface Structures with Excellent Mechanical Rationality and Constructability/Fabricability

2. Research Case Studies

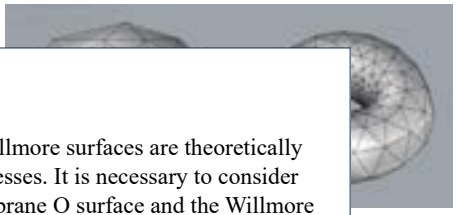

Note:

・It is not guaranteed that the Willmore surfaces are theoretically equilibrium by the membrane stresses. It is necessary to consider the connection between the membrane O surface and the Willmore surface.

・**Willmore Energy**
⇒ **Invariant functional with Möbius transformation**

H: **Mea**

・**Willmore surface**
⇒ **Critical point of Willmore energy**
⇒ **Möbius transformation allows Willmore surfaces to be mapped to Willmore surfaces.**

Arknova (Arata Isozaki, Anish Kapoor)

Bobenko, A.I., Schröder, P., Discrete Willmore Flow, Eurographics Symposium on Geometry Processing, 2005

2. Research Case Studies
2.4 Airy stress function and Laguerre geometry

・Hanging membrane
■ Architecture
Ramm, E., Bletzinger, K.-U., Reitinger, R.(1993) : Minimization of Shell structures
Block, P. and Ochsendorf, J.(2007) :Thrust Network Analysis
Miki, M., Igarashi, Block, P. (2015) : Airy stress function in parametric surface

■ Mathematics
Vouga, E. Höbinger, M. Wallner, J. Pottmann, H.(2012) :Isotropic geometry
Koiso, M., Palmer, B.(2005) :Smooth hanging curve and Euler-Lagrange equation
Jikumaru, Y., Yokosuka, Y.(2022):Hanging membrane of isotropic stress

Curved Surface Structures with Excellent Mechanical Rationality and Constructability/Fabricability

2. Research Case Studies
2.4 Airy stress function and Laguerre geometry

・Laguerre geometry
⇒ The object of Laguerre geometry is a plane.
⇒ The normal is defined and the plane is the set of points that have the same perpendicular distance from the origin.
⇒ Laguerre transform acts on a plane

・Laguerre functional
⇒ invariant functional of Laguerre transformation

$$\Omega = \int_S \frac{H^2 - K}{K} dA \qquad (4)$$

H: **Mean Curvature** K: **Gaussian Curvature**

・Airy stress function
⇒ Stress function equilibrium by in-plane membrane stress when a constant vertical load is applied to a curved surface

Curved Surface Structures with Excellent Mechanical Rationality and Constructability/Fabricability

2. Research Case Studies
2.4 Airy stress function and Laguerre geometry

・Pottmann et al. showed the relationship between L-minimal surfaces and Airy stress functions minimizing the Laguerre functional.

Airy stress function is biharmonic function ⇔ **L-minimal surface expressed by isotropic model is biharmonic function**

・Isotropic geometry
⇒ Geometry of a surface represented as a function graph of $z = f(x, y)$
⇒ No distance metering in height direction

[42] Pottmann, H., Grohs, P., Mitra, N., J. : Laguerre minimal surfaces, isotropic geometry and linear elasticity, Advances in Computational Mathematics volume 31, Article number: 391, pp.391-419, 2009

2. Research Case Studies
2.4 Airy stress function and Laguerre geometry

・Mean curvature and Gaussian curvature in isotropic geometry

$$K_i = \det(\nabla^2 f) = f_{xx} + f_{yy} - f_{xy}^2 \quad (9)$$

$$2H_i = \mathrm{trace}(\nabla^2 f) = f_{xx} + f_{yy} \quad (10)$$

・Equilibrium equations and compatibility conditionals introducing Airy stress functions

$$\mathrm{div}(M\nabla s) = F,\ \mathrm{div}M = 0 \quad (11)$$

$$M = \mathrm{adj}\left(\nabla^2 \phi\right) \quad (12)$$

$\Leftrightarrow$

・Equilibrium equations in isotropic geometry

$$2K_\phi H^{rel} = F \quad (13)$$

S：**height** ϕ：**Airy stress function**
M：**stress tensor** F：**vertical load**

Fraternali, et al

Vouga, et al

Curved Surface Structures with Excellent Mechanical Rationality and Constructability/Fabricability

2. Research Case Studies
2.4 Airy stress function and Laguerre geometry

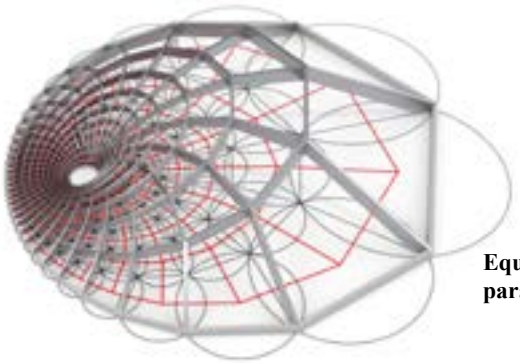

・Möbius transformation allows circles to be mapped to circles.

・Lines of connecting the center of circles become force diagram.

⇩

Equilibrium in plane can be obtained parametrically by Möbius transformation.

Temporary Structures with Curved Folding

Conclusion

・This presentation introduces four topics: discrete isothermal minimal surfaces, discrete membrane O surfaces, Willmore surfaces and Möbius transforms, Airy stress functions and Laguerre geometry.

・The viewpoints and representations of surfaces in non-Euclidean geometry are important not only in conventional Euclidean geometry, but also in non-Euclidean geometry, showing that invariant quantities and properties in transformations, and the "transformations" themselves that preserve these properties, are of great importance.

Lie Spherical Geometry and Design of Curved Surface Structures

Yohei Yokosuka
Kagoshima University, Japan

Abstract

The purpose of this study is to employ discrete surfaces as shape elements and to construct a design method for curved surface structures by parametric deformation using Lie spherical transformations. NURBS surfaces and Bézier surfaces are useful parametric surface generation methods as surface design tools. However, the properties of the cross ratio and the developability of the surfaces covered by the coordinate lines are not preserved. Lie spherical geometry can perform Lie spherical transformation, which maps curvature line coordinates to curvature line coordinates. Curvature line coordinates can be represented by discrete surfaces filled with circles on the surface; the Möbius transform, one of the Lie spherical transforms, allows transformations that preserve the cross ratio, and isothermal coordinates can be mapped to isothermal coordinates. This presentation will describe the method of generating 3-D and 2-D surfaces and the mechanical properties of isothermal coordinates.

International Conference "Evolving Design and Discrete Differential Geometry - towards Mathematics Aided Geometric Design"

Lie Sphere Geometry and Design of Curved Surface Structures

Yohei YOKOSUKA[1)], Junichi INOGUCHI[2)], Makoto OHSAKI[3)], Toshio HONMA[1)]
Yoshiki JIKUMARU[5)]

1) Graduate School of Science and Engineering, Kagoshima University
2) Department of Mathematics, Hokkaido University
3) Graduate School of Engineering, Kyoto University
4) Information Networking for Innovation And Design, Toyo University

Lie Sphere Geometry and Design of Curved Surface Structures

- **Recent studies on discrete surfaces**
  - It is possible to generate discrete curved surfaces with extremely good properties by Möbius geometry and Laguerre geometry.
  - These curved surface with excellent fabricability and constructability can be constructed.

A. I. Bobenko and Yu. B. Suris, Discrete differential geometry: Integrable structure, Graduate studies in mathematics Vol. 98, AMS, 2008
Y. Liu, H. Pottmann, J. Wallner, Y.-L. Yang, and W. Wang, Geometric modelling with conical meshes and developable surfaces, ACM Trans. Graphics 25, no. 3, pp.681–689, 2006

Lie Sphere Geometry and Design of Curved Surface Structures

- **Recent studies on discrete surfaces**
  - It is possible to generate discrete curved surfaces with extremely good properties by Möbius geometry and Laguerre geometry.
  - These curved surface with excellent fabricability and constructability can be constructed.

  - In this presentation, we introduce the formulation of Lie sphere geometry and the method of modelling for gridshell structures.
  - we demonstrate the structural analysis of curved surface found by Lie sphere geometry whether the curved surface has the similar mechanical performance.

A. I. Bobenko and Yu. B. Suris, Discrete differential geometry: Integrable structure, Graduate studies in mathematics Vol. 98, AMS, 2008
Y. Liu, H. Pottmann, J. Wallner, Y.-L. Yang, and W. Wang, Geometric modelling with conical meshes and developable surfaces, ACM Trans. Graphics 25, no. 3, pp.681–689, 2006

Lie Sphere Geometry and Design of Curved Surface Structures

- **Klein geometry**

  Klein geometry classifies geometry by the operation of transformations on a set.

- **Lie sphere geometry**

  Lie sphere geometry has a large group in Klein geometry.
  Lie sphere geometry considers points and planes as part of spheres.
  The curvature line coordinates are conserved by the Lie sphere transformation.

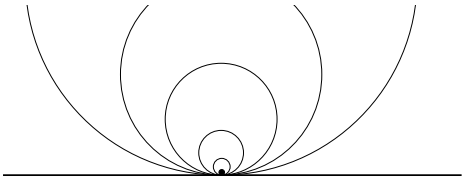

Lie Sphere Geometry and Design of Curved Surface Structures

- **Oriented sphere**: $S(c,r)$

$$S(c,r)=\{x\in\mathbb{R}^3;|x-c|=r\} \quad (1)$$

$$S(c,r)=\{x\in\mathbb{R}^3;|x-c|^2=r^2\} \quad (2)$$

x : point c : center point r : signed radius

- **Oriented plane**: $P(\nu,d)$

$$P(\nu,d)=\{x\in\mathbb{R}^3;\nu\cdot x=d\} \quad (3)$$

ν : unit normal (inward) d : signed height

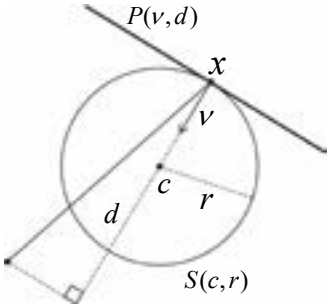

A. I. Bobenko and Yu. B. Suris, Discrete differential geometry: Integrable structure, Graduate studies in mathematics Vol. 98, AMS, 2008
Y. Liu, H. Pottmann, J. Wallner, Y.-L. Yang, and W. Wang, Geometric modelling with conical meshes and developable surfaces, ACM Trans. Graphics 25, no. 3, pp.681–689, 2006

Lie Sphere Geometry and Design of Curved Surface Structures

- **Natural basis**:

$$e_1=(1,0,0,0,0,0),e_2=(0,1,0,0,0,0),e_3=(0,0,1,0,0,0),$$
$$e_4=(0,0,0,1,0,0),e_5=(0,0,0,0,1,0),e_6=(0,0,0,0,0,1) \quad (4)$$

- **Vector**: $\hat{s}$

$$\hat{s}=(c_1,c_2,c_3,\frac{1}{2}(1-|c|^2+r^2),\frac{1}{2}(1-|c|^2-r^2),r) \quad (5)$$

A. I. Bobenko and Yu. B. Suris, Discrete differential geometry: Integrable structure, Graduate studies in mathematics Vol. 98, AMS, 2008
Y. Liu, H. Pottmann, J. Wallner, Y.-L. Yang, and W. Wang, Geometric modelling with conical meshes and developable surfaces, ACM Trans. Graphics 25, no. 3, pp.681–689, 2006

Lie Sphere Geometry and Design of Curved Surface Structures

- **Natural Basis**:

$$c_1^2 + c_2^2 + c_3^2 + \{\frac{1}{2}(1-|c|^2+r^2)\}^2 - \{\frac{1}{2}(1-|c|^2-r^2)\}^2 - r^2 = 0$$

introduce an scalar product

- **Vecto**

$$\langle x, y\rangle = x_1y_1 + x_2y_2 + x_3y_3 + x_4y_4 - x_5y_5 - x_6y_6$$

$$\langle \hat{s}, \hat{s}\rangle = 0$$

A. I. Bobenko and Yu. B. Suris, Discrete differential geometry: Integrable structure, Graduate studies in mathematics Vol. 98, AMS, 2008
Y. Liu, H. Pottmann, J. Wallner, Y.-L. Yang, and W. Wang, Geometric modelling with conical meshes and developable surfaces, ACM Trans. Graphics 25, no. 3, pp.681–689, 2006

Lie Sphere Geometry and Design of Curved Surface Structures

- **Natural basis**:

$$e_1 = (1,0,0,0,0,0), e_2 = (0,1,0,0,0,0), e_3 = (0,0,1,0,0,0),$$
$$e_4 = (0,0,0,1,0,0), e_5 = (0,0,0,0,1,0), e_6 = (0,0,0,0,0,1) \quad (4)$$

- **Vector**: $\hat{s}$ **an oriented sphere**

$$\hat{s} = (c_1, c_2, c_3, \frac{1}{2}(1-|c|^2+r^2), \frac{1}{2}(1-|c|^2-r^2), r) \quad (5)$$

A. I. Bobenko and Yu. B. Suris, Discrete differential geometry: Integrable structure, Graduate studies in mathematics Vol. 98, AMS, 2008
Y. Liu, H. Pottmann, J. Wallner, Y.-L. Yang, and W. Wang, Geometric modelling with conical meshes and developable surfaces, ACM Trans. Graphics 25, no. 3, pp.681–689, 2006

Lie Sphere Geometry and Design of Curved Surface Structures

- Two oriented spheres S_1 and S_2 are in oriented contact if and only if

$$\langle \hat{s}_1, \hat{s}_2\rangle = 0.$$

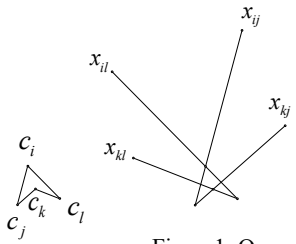

Figure1: One unit

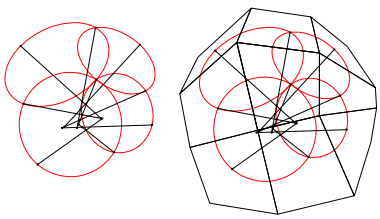

Figure2: Möbius and Laguerre geometry

Lie Sphere Geometry and Design of Curved Surface Structures

・**Equations generating Circular nets**

$$\langle \hat{s}_i, \hat{s}_j \rangle = 0 \quad \langle \hat{s}_j, \hat{s}_k \rangle = 0 \quad \langle \hat{s}_k, \hat{s}_l \rangle = 0 \quad \langle \hat{s}_l, \hat{s}_i \rangle = 0 \qquad (6)$$

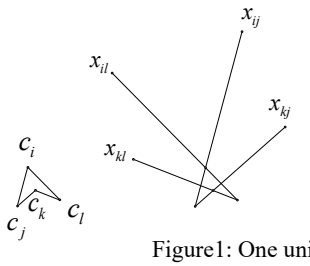

Figure1: One unit

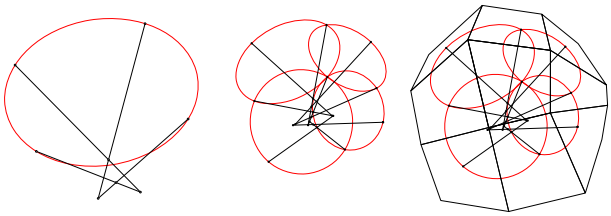

Figure2: Möbius and Laguerre geometry

Lie Sphere Geometry and Design of Curved Surface Structures

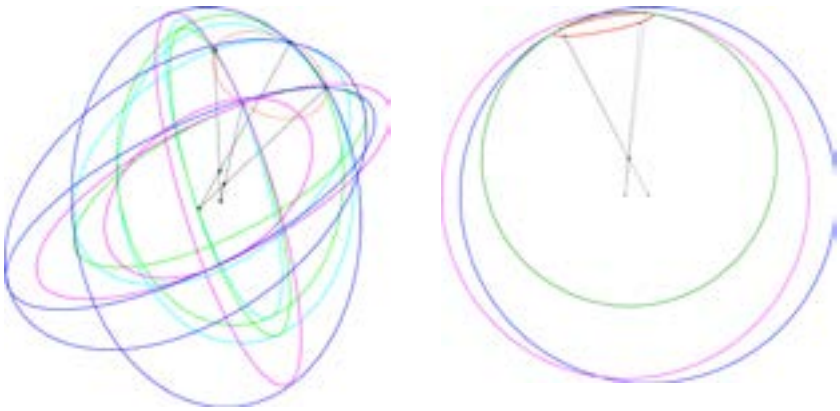

Great circle of spheres tangent to a point

Lie Sphere Geometry and Design of Curved Surface Structures

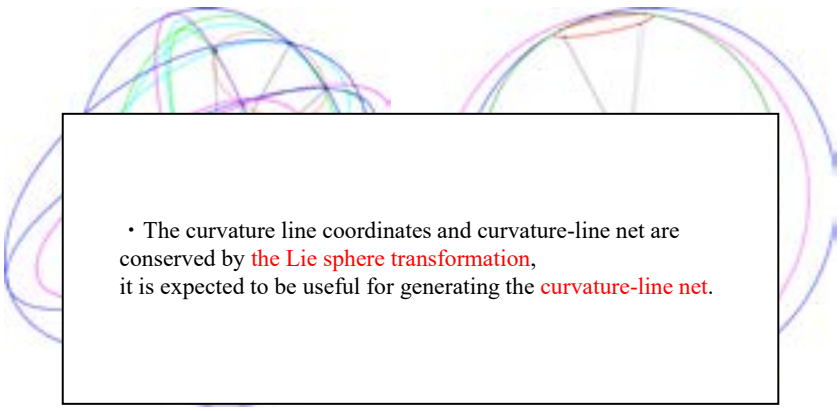

・The curvature line coordinates and curvature-line net are conserved by the Lie sphere transformation, it is expected to be useful for generating the curvature-line net.

Great circle of spheres tangent to a point

Lie Sphere Geometry and Design of Curved Surface Structures

• How to configure Circular net

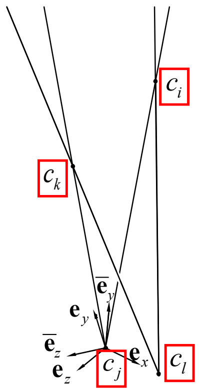

1. The set of four center points constitute minimum unit.
2. The network of center points are expanded to two directions of X, Y.
3. When the network expand, the plane including the center point is rotated. To solve the equation, find a new center point.
4. If all center points are found, all radius can be found also. the constituent nodes of the circular nets can be found.

Figure 3: center points and orthonomal basis vector

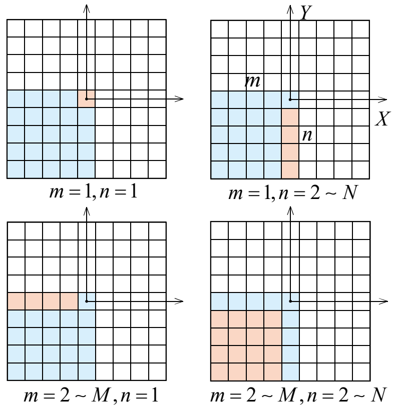

Figure 4: grid number and symmetry condition

Lie Sphere Geometry and Design of Curved Surface Structures

• How to configure Circular net

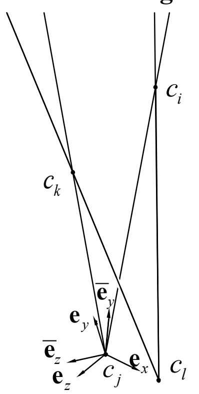

1. The set of four center points constitute minimum unit.
2. The network of center points are expanded to two directions of X, Y.
3. When the network expand, the plane including the center point is rotated. To solve the equation, find a new center point.
4. If all center points are found, all radius can be found also. the constituent nodes of the circular nets can be found.

Figure 3: center points and orthonomal basis vector

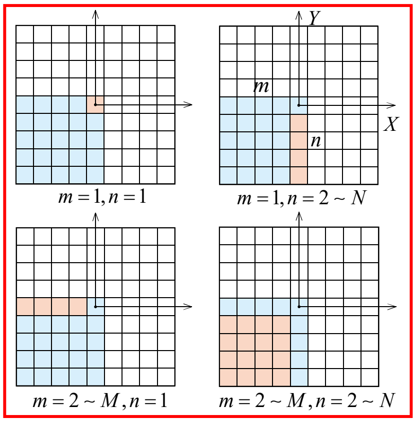

Figure 4: grid number and symmetry condition

Lie Sphere Geometry and Design of Curved Surface Structures

• How to configure Circular net

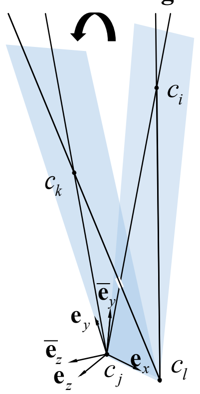

1. The set of four center points constitute minimum unit.
2. The network of center points are expanded to two directions of X, Y.
3. When the network expand, the plane including the center point is rotated. To solve the equation, find a new center point.
4. If all center points are found, all radius can be found also. the constituent nodes of the circular nets can be found.

Figure 3: center points and orthonomal basis vector

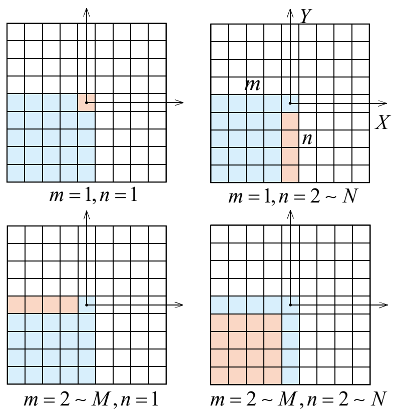

Figure 4: grid number and symmetry condition

Lie Sphere Geometry and Design of Curved Surface Structures

- **How to configure Circular net**

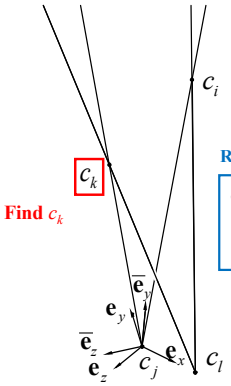

For example:

$m = 2 \sim M,\ n = 1$

Rotation of a plane

$$\mathbf{e}_y^{m,n} = \mathbf{R}\left(\mathbf{e}_x^{m,n}, \theta^{m,n}\right)\bar{\mathbf{e}}_y^{m,n}$$

$\mathbf{R}(\mathbf{e}_x, \theta)$: Rodrigues's rotation matrix

Figure 3: center points and orthonomal basis vector

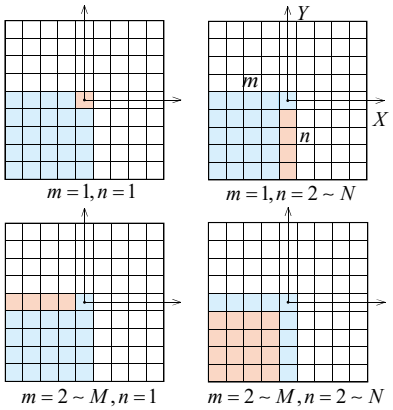

Figure 4: grid number and symmetry condition

Lie Sphere Geometry and Design of Curved Surface Structures

- **How to configure Circular net**

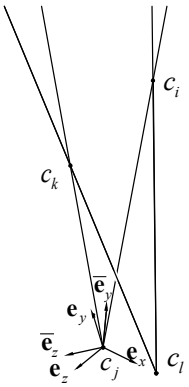

1. The set of four center points constitute minimum unit.
2. The network of center points are expanded to two directions of X,Y.
3. When the network expand, the plane including the center point is rotated. To solve the equation, find a new center point.
4. If all center points are found, all radius can be found also. The constituent nodes of the circular nets can be found.

Figure 3: center points and orthonomal basis vector

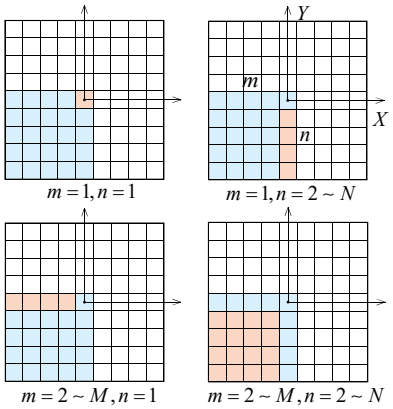

Figure 4: grid number and symmetry condition

Lie Sphere Geometry and Design of Curved Surface Structures

- **How to configure Circular net**

Table1: Symbols

$f_1, f_2, f_3, f_4 \in \mathbb{R}$:Nonlinear equation contact to oriented sphere	$\hat{s}_i, \hat{s}_j, \hat{s}_k, \hat{s}_l \in \mathbb{R}^{4,2}$: Projective model of oriented sphere
$c_i, c_j, c_k, c_l \in \mathbb{R}^3$: Center point of oriented sphere	$r_i, r_j, r_k, r_l \in \mathbb{R}$: Signed radius of the oriented sphere
$\bar{r} \in \mathbb{R}$: Reference radius	m, n : Grid number in X,Y direction
M, N : Number of grids in X,Y direction	$\mathbf{e}_x, \mathbf{e}_y \in \mathbb{R}^3$: Orthonormal basis vector
$x, y \in \mathbb{R}$: Unkwon parameter in 2D plane	$\theta \in \mathbb{R}$: Specified angle
$\mathbf{R}(\mathbf{e}_x, \theta)$: Rodrigues's rotation matrix	$\alpha, \beta, \gamma \in \mathbb{R}$: Specified parameter
$\xi \in \mathbb{R}$: Unkwon parameter in 1D line	$x_{ij}, x_{il}, x_{kj}, x_{kl} \in \mathbb{R}^3$: Constituent nodes of circular nets

Lie Sphere Geometry and Design of Curved Surface Structures

・**How to configure Circular net** • $m=1, n=1$

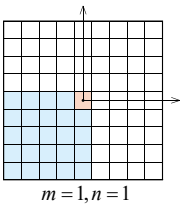

Initial values (radius and center point):

$$\overline{r}, c_i^{1,1}, c_j^{1,1}, c_k^{1,1}, c_l^{1,1}, r_i^{1,1}=\overline{r}, r_j^{1,1}=\overline{r}+\left|c_i^{1,1}-c_j^{1,1}\right|, r_k^{1,1}=\overline{r}, r_l^{1,1}=\overline{r}+\left|c_i^{1,1}-c_l^{1,1}\right| \quad (7)$$

Specified values: $\alpha^{1,1}, \beta^{1,1}$

Define next initial value: $c_i^{2,1}$, $c_j^{2,1}$, $c_l^{2,1}, r_i^{2,1}, r_j^{2,1}, r_l^{2,1}$

$$c_i^{2,1}=c_k^{1,1},\ c_j^{2,1}=c_j^{1,1}+\alpha^{1,1}\frac{c_j^{1,1}-c_k^{1,1}}{\left|c_j^{1,1}-c_k^{1,1}\right|},\ c_l^{2,1}=c_l^{1,1}+\beta^{1,1}\frac{c_l^{1,1}-c_k^{1,1}}{\left|c_l^{1,1}-c_k^{1,1}\right|} \quad (8)$$

$$r_i^{2,1}=r_k^{1,1},\ r_j^{2,1}=r_i^{2,1}+\left|c_i^{2,1}-c_j^{2,1}\right|,\ r_l^{2,1}=r_i^{2,1}+\left|c_i^{2,1}-c_l^{2,1}\right| \quad (9)$$

Lie Sphere Geometry and Design of Curved Surface Structures

・**How to configure Circular net** • $m=2\sim M, n=1$

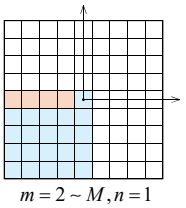

Equations(Nonlinear equations):

$$f_3=\left\langle \hat{s}_k^{m,1}, \hat{s}_j^{m,1}\right\rangle=\left\langle c_k^{m,1}, c_j^{m,1}\right\rangle-\frac{1}{2}\left\{\left|c_k^{m,1}\right|^2+\left|c_j^{m,1}\right|^2-(r_k^{m,1})^2-(r_j^{m,1})^2\right\}-r_k^{m,1}r_j^{m,1}=0$$

$$f_4=\left\langle \hat{s}_k^{m,1}, \hat{s}_l^{m,1}\right\rangle=\left\langle c_k^{m,1}, c_l^{m,1}\right\rangle-\frac{1}{2}\left\{\left|c_k^{m,1}\right|^2+\left|c_l^{m,1}\right|^2-(r_k^{m,1})^2-(r_l^{m,1})^2\right\}-r_k^{m,1}r_l^{m,1}=0 \quad (10)$$

Specified values: $\theta^{m,1}, \alpha^{m,1}, \beta^{m,1}, r_k^{m,1}$

Unkown value: x, y $\quad c_k^{m,1}=c_j^{m,1}+x\mathbf{e}_x^{m,1}+y\mathbf{e}_y^{m,1}$ (11)

Define next initial value: $c_i^{m+1,1}, c_j^{m+1,1}, c_l^{m+1,1}, r_i^{m+1,1}, r_j^{m+1,1}, r_l^{m+1,1}$

$$c_i^{m+1,1}=c_k^{m,1},\ c_j^{m+1,1}=c_j^{m,1}+\alpha^{m,1}\frac{c_j^{m,1}-c_k^{m,1}}{\left|c_j^{m,1}-c_k^{m,1}\right|},\ c_l^{m+1,1}=c_l^{m,1}+\beta^{m,1}\frac{c_l^{m,1}-c_k^{m,1}}{\left|c_l^{m,1}-c_k^{m,1}\right|} \quad (12)$$

$$r_i^{m+1,1}=r_k^{m,1},\ r_j^{m+1,1}=r_i^{m+1,1}+\left|c_i^{m+1,1}-c_j^{m+1,1}\right|,\ r_l^{m+1,1}=r_i^{m+1,1}+\left|c_i^{m+1,1}-c_l^{m+1,1}\right|$$

Lie Sphere Geometry and Design of Curved Surface Structures

・**How to configure Circular net** • $m=1, n=2\sim N$

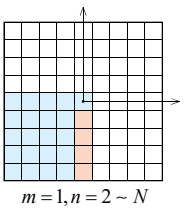

Equations(Nonlinear equations):

$$f_1=\left\langle \hat{s}_i^{1,n}, \hat{s}_j^{1,n}\right\rangle=\left\langle c_i^{1,n}, c_j^{1,n}\right\rangle-\frac{1}{2}\left\{\left|c_i^{1,n}\right|^2+\left|c_j^{1,n}\right|^2-(r_i^{1,n})^2-(r_j^{1,n})^2\right\}-r_i^{1,n}r_j^{1,n}=0$$

$$f_3=\left\langle \hat{s}_k^{1,n}, \hat{s}_j^{1,n}\right\rangle=\left\langle c_k^{1,n}, c_j^{1,n}\right\rangle-\frac{1}{2}\left\{\left|c_k^{1,n}\right|^2+\left|c_j^{1,n}\right|^2-(r_k^{1,n})^2-(r_j^{1,n})^2\right\}-r_k^{1,n}r_j^{1,n}=0 \quad (13)$$

Specified values: $\theta^{1,n}, \alpha^{1,n}, \beta^{1,n}, r_j^{1,n}$

Unkown value: x, y $\quad c_j^{1,n}=c_i^{1,n}+x\mathbf{e}_x^{1,n}+y\mathbf{e}_y^{1,n}$ (14)

Define next initial value: $c_i^{1,n+1}, c_k^{1,n+1}, c_l^{1,n+1}, r_i^{1,n+1}, r_k^{1,n+1}, r_l^{1,n+1}$

$$c_i^{1,n+1}=c_i^{1,n}+\alpha^{1,n}\frac{c_i^{1,n}-c_j^{1,n}}{\left|c_i^{1,n}-c_j^{1,n}\right|},c_k^{1,n+1}=c_k^{1,n}+\beta^{1,n}\frac{c_k^{1,n}-c_j^{1,n}}{\left|c_k^{1,n}-c_j^{1,n}\right|},c_l^{1,n+1}=c_j^{1,n} \quad (15)$$

$$r_i^{1,n+1}=r_j^{1,n}-\left|c_l^{1,n+1}-c_i^{1,n+1}\right|,r_k^{1,n+1}=r_j^{1,n}-\left|c_k^{1,n+1}-c_l^{1,n+1}\right|,\ r_l^{1,n+1}=r_j^{1,n}$$

Lie Sphere Geometry and Design of Curved Surface Structures

- **How to configure Circular net** • $m=2\sim M, n=2\sim N$

Equations(Nonlinear equations):

$$f_1=\left\langle \hat{s}_i^{m,n},\hat{s}_j^{m,n}\right\rangle=0,\ f_3=\left\langle \hat{s}_k^{m,n},\hat{s}_j^{m,n}\right\rangle=0,\ f_4=\left\langle \hat{s}_k^{m,n},\hat{s}_l^{m,n}\right\rangle=0 \qquad (16)$$

Specified values: γ

Unkown value: ξ, r_j, r_k

$$c_j^{m,n}=c_i^{m,n}+\xi\mathbf{e}_\xi^{m,n},\ \mathbf{e}_\xi^{m,n}=\frac{c_j^{m-1,n}-c_i^{m,n}}{\left|c_j^{m-1,n}-c_i^{m,n}\right|}$$

$$c_k^{m,n}=c_l^{m,n}+(\xi+\gamma)\mathbf{e}_\eta^{m,n},\ \mathbf{e}_\eta^{m,n}=\frac{c_k^{m,n-1}-c_l^{m,n}}{\left|c_k^{m,n-1}-c_l^{m,n}\right|} \qquad (17)$$

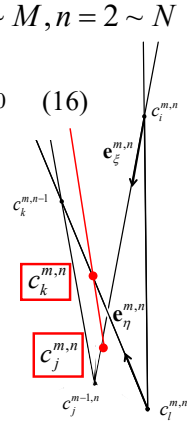

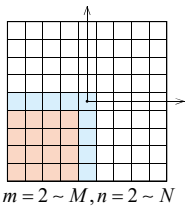

Lie Sphere Geometry and Design of Curved Surface Structures

- **How to configure Circular net**

The constituent nodes of the circular net $x_{ij}, x_{il}, x_{kj}, x_{kl}$:

$$x_{ij}^{m,n}=c_i^{m,n}+r_i^{m,n}\frac{c_i^{m,n}-c_j^{m,n}}{\left|c_i^{m,n}-c_j^{m,n}\right|},\ x_{il}^{m,n}=c_i^{m,n}+r_i^{m,n}\frac{c_i^{m,n}-c_l^{m,n}}{\left|c_i^{m,n}-c_l^{m,n}\right|}$$

$$x_{kj}^{m,n}=c_k^{m,n}+r_k^{m,n}\frac{c_k^{m,n}-c_j^{m,n}}{\left|c_k^{m,n}-c_j^{m,n}\right|},\ x_{kl}^{m,n}=c_k^{m,n}+r_k^{m,n}\frac{c_k^{m,n}-c_l^{m,n}}{\left|c_k^{m,n}-c_l^{m,n}\right|} \qquad (18)$$

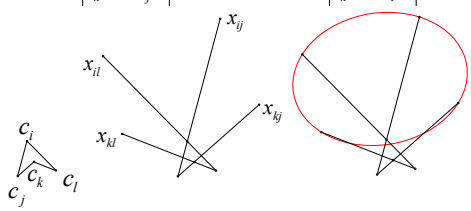

Lie Sphere Geometry and Design of Curved Surface Structures

- **Numerical result of circular nets**

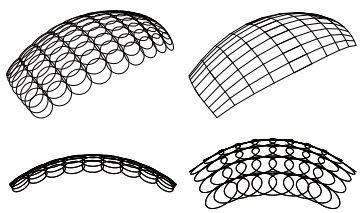

$\theta^{m,1}=0.15$ $\alpha^{m,1}=0$ $\theta^{1,n}=-0.15$ $\alpha^{1,n}=0$
$\beta^{m,1}=0$ $r_k^{m,1}=10$ $\beta^{1,n}=0$ $\gamma=0$

a. Model-1

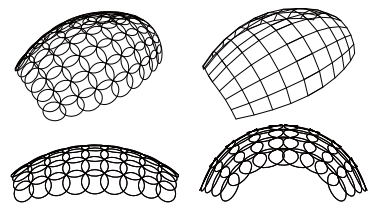

$\theta^{m,1}=0.15$ $\alpha^{m,1}=0$ $\theta^{1,n}=-0.30$ $\alpha^{1,n}=0$
$\beta^{m,1}=0$ $r_k^{m,1}=10$ $\beta^{1,n}=0$ $\gamma=0$

b. Model-2

Lie Sphere Geometry and Design of Curved Surface Structures

- **Numerical result of circular nets**

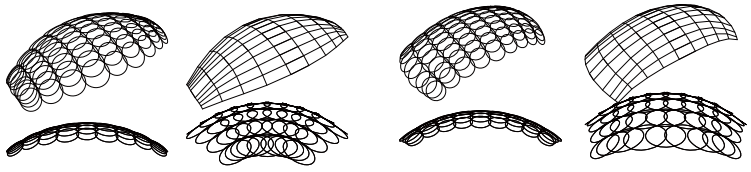

c. Model-3　　d. Model-4

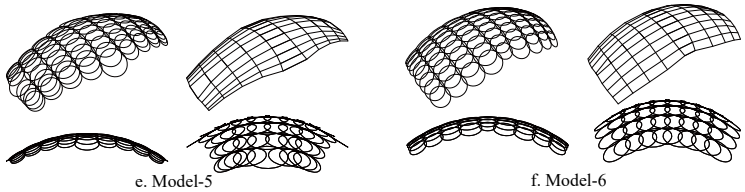

e. Model-5　　f. Model-6

Lie Sphere Geometry and Design of Curved Surface Structures

- **Subdivision**

1. Create circles with half the diameter at the same position.
2. Draw a line (spoke) connecting the four nodes, which are the intersections of adjacent circles, with the center of the circle.
3. Draw a circle that passes through the four intersections (A, B, C, D) where the spoke and the half circle intersect.
4. Repeat step1-3 to generate a gridshell structure.

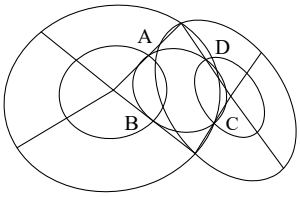

Subdivision

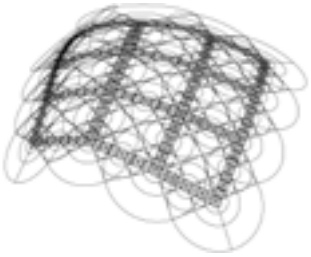

Result of 3 times subdivision

Lie Sphere Geometry and Design of Curved Surface Structures

- **Subdivision**

1. Create circles with half the diameter at the same position.
2. Draw a line (spoke) connecting the four nodes, which are the intersections of adjacent circles, with the center of the circle.
3. Draw a circle that passes through the four intersections (A, B, C, D) where the spoke and the half circle intersect.
4. Repeat step1-3 to generate a gridshell structure.

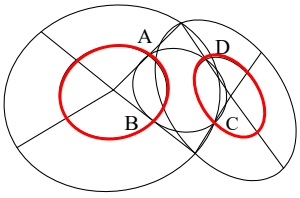

Subdivision

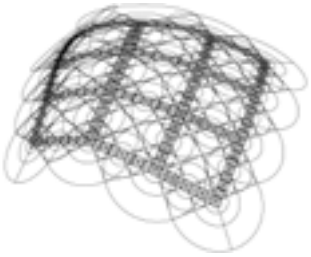

Result of 3 times subdivision

Lie Sphere Geometry and Design of Curved Surface Structures

- **Subdivision**

1. Create circles with half the diameter at the same position.
2. Draw a line (spoke) connecting the four nodes, which are the intersections of adjacent circles, with the center of the circle.
3. Draw a circle that passes through the four intersections (A, B, C, D) where the spoke and the half circle intersect.
4. Repeat step1-3 to generate a gridshell structure.

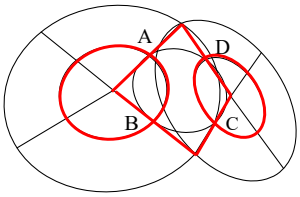

Subdivision

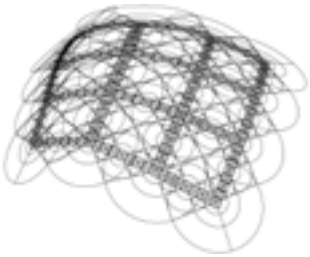

Result of 3 times subdivision

Lie Sphere Geometry and Design of Curved Surface Structures

- **Subdivision**

1. Create circles with half the diameter at the same position.
2. Draw a line (spoke) connecting the four nodes, which are the intersections of adjacent circles, with the center of the circle.
3. Draw a circle that passes through the four intersections (A, B, C, D) where the spoke and the half circle intersect.
4. Repeat step1-3 to generate a gridshell structure.

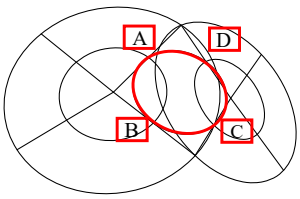

Subdivision

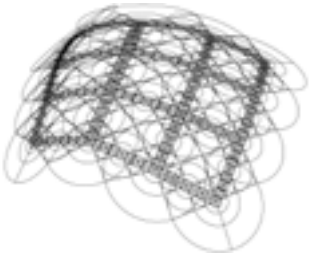

Result of 3 times subdivision

Lie Sphere Geometry and Design of Curved Surface Structures

- **Subdivision**

1. Create circles with half the diameter at the same position.
2. Draw a line (spoke) connecting the four nodes, which are the intersections of adjacent circles, with the center of the circle.
3. Draw a circle that passes through the four intersections (A, B, C, D) where the spoke and the half circle intersect.
4. Repeat step1-3 to generate a gridshell structure.

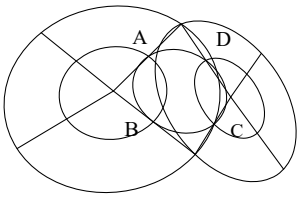

Subdivision

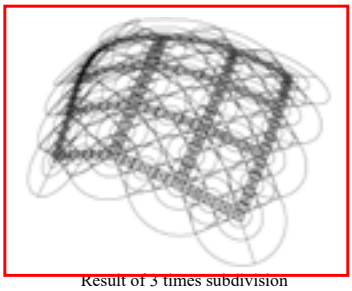

Result of 3 times subdivision

Lie Sphere Geometry and Design of Curved Surface Structures

・**Subdivision** Gaussian curvature distribution (almost zero)

This result is considered as a discrete curvature line in which the discrete curved surface is subdivided along the curvature line. Therefore, it is possible to construct a curved member by bending only one axis.

This gridshell structure has a property of excellent fabricability of members.

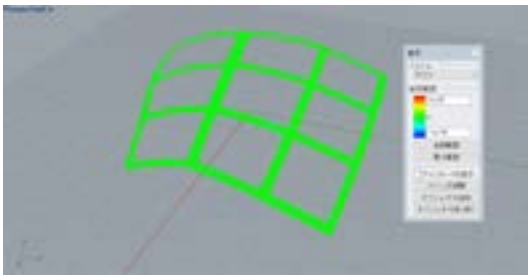

Lie Sphere Geometry and Design of Curved Surface Structures

・**Lie Sphere Transformation**

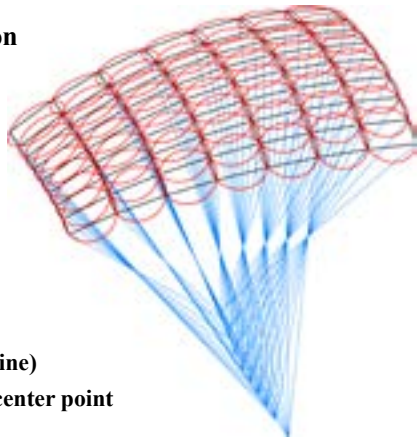

Circular net (red line and black line)

Line connecting a point and the center point of the sphere (blue line)

Lie Sphere Geometry and Design of Curved Surface Structures

・**Lie Sphere Transformation**

・**Conical net**

Lie Sphere geometry includes Möbius and Laguerre geometry, with Möbius geometry constituting **Circular nets** and Laguerre geometry **Conical nets**.

The definition of a conical net is four planes having one shared point and tangent to a cone.

Once the circular net is constructed, the normals $\nu_{ij},\nu_{jk},\nu_{kl},\nu_{li}$ are obtained by the following equation.

$$\nu_{ij}=-\frac{x_{ij}-c_i}{\left|x_{ij}-c_i\right|}=-\frac{x_{ij}-c_j}{\left|x_{ij}-c_j\right|},\nu_{jk}=-\frac{x_{jk}-c_j}{\left|x_{jk}-c_j\right|}=-\frac{x_{jk}-c_k}{\left|x_{jk}-c_k\right|}$$

$$\nu_{kl}=-\frac{x_{kl}-c_k}{\left|x_{kl}-c_k\right|}=-\frac{x_{kl}-c_l}{\left|x_{kl}-c_l\right|},\nu_{li}=-\frac{x_{li}-c_l}{\left|x_{li}-c_l\right|}=-\frac{x_{li}-c_i}{\left|x_{li}-c_i\right|} \quad (19)$$

Lie Sphere Geometry and Design of Curved Surface Structures

- **Lie Sphere Transformation**
- **Conical net**

The height $d_{ij}, d_{jk}, d_{kl}, d_{li}$ are obtained by the following equation

$$d_{ij} = \langle v_{ij}, x_{ij} \rangle, d_{jk} = \langle v_{jk}, x_{jk} \rangle, d_{kl} = \langle v_{kl}, x_{kl} \rangle, d_{li} = \langle v_{li}, x_{li} \rangle \qquad (20)$$

Conical nets are obtained by solving the following simultaneous equations for each circle in the circular nets

$$\begin{bmatrix} v_{ij} & v_{jk} & v_{kl} \end{bmatrix}^T \begin{Bmatrix} x \\ y \\ z \end{Bmatrix} = \begin{Bmatrix} d_{ij} \\ d_{jk} \\ d_{kl} \end{Bmatrix} \qquad (21)$$

Note that any three of the four planes are chosen, but any of the equations may be chosen.

Lie Sphere Geometry and Design of Curved Surface Structures

- **Lie Sphere Transformation**
- **Conical net**

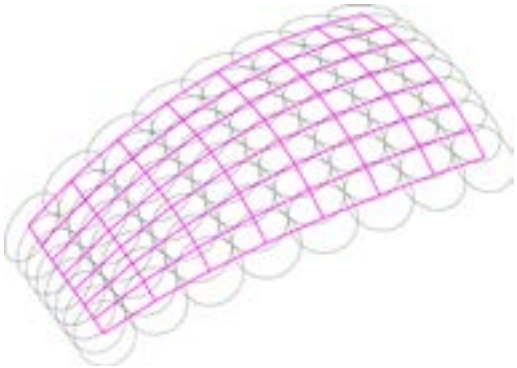

Circles of circular nets and conical net points form a cone.

Lie Sphere Geometry and Design of Curved Surface Structures

- **Lie Sphere Transformation**

The Lie Sphere transformation is used for the coefficient matrix of the quadratic form of the projective space.
As $x, y \in \mathbb{R}^{4,2}$, consider a linear transformation $x \mapsto Ax$ that satisfies the following inner product

$$\langle Ax, Ay \rangle = \langle x, y \rangle \qquad (22)$$

However, limited to

$$A^T E_{4,2} A = E_{4,2} \qquad (23)$$

In this case A is the **Lie Sphere transformation**.

$$E_{4,2} = \begin{bmatrix} 1 & 0 & 0 & 0 & 0 & 0 \\ 0 & 1 & 0 & 0 & 0 & 0 \\ 0 & 0 & 1 & 0 & 0 & 0 \\ 0 & 0 & 0 & 1 & 0 & 0 \\ 0 & 0 & 0 & 0 & -1 & 0 \\ 0 & 0 & 0 & 0 & 0 & -1 \end{bmatrix}$$

T. E. Cecil, Lie Sphere Geometry with Applications to Submanifolds second edition, Springer New York, 2008.
G. R. Jensen, E. Musso, L. Nicolodi, Surfaces in Classical Geometries : A Treatment by Moving Frames, Springer, 2016.

Lie Sphere Geometry and Design of Curved Surface Structures

- **Lie Sphere Transformation**

Inversion

The inversion of the Lie Sphere transformation acts on the point $\mathbb{R}^3$. The mapping from $\mathbb{R}^3$ to $\mathbb{S}^3$ is obtained by

$$A_I = f_+^{-1} \circ T_I \circ f_+ : \mathbb{R}^3 \mapsto \mathbb{S}^3$$

$$f_+(x) = x + 1\cdot e_0 + |x|^2 e_\infty + 0\cdot e_6$$

$$= x + \frac{1-|x|^2}{2} e_4 + \frac{1+|x|^2}{2} e_5 + 0\cdot e_6$$

$$T_I = \begin{bmatrix} I_3 & 0 & 0 & 0 \\ 0 & 1 & 0 & 0 \\ 0 & 0 & -1 & 0 \\ 0 & 0 & 0 & 0 \end{bmatrix}$$

$$f_+^{-1}(x + ue_4 + ve_5) = \frac{1}{v}(x + ue_4) \qquad (24)$$

Lie Sphere Geometry and Design of Curved Surface Structures

- **Lie Sphere Transformation**

Inversion

The inversion of the Lie Sphere transformation acts on the point $\mathbb{R}^3$. The mapping from $\mathbb{R}^3$ to $\mathbb{S}^3$ is obtained by

$$A_I = f_+^{-1} \circ T_I \circ f_+ : \mathbb{R}^3 \mapsto \mathbb{S}^3$$

$$f_+(x) = x + 1\cdot e_0 + |x|^2 e_\infty + 0\cdot e_6$$

$$= x + \frac{1-|x|^2}{2} e_4 + \frac{1+|x|^2}{2} e_5 + 0\cdot e_6$$

$$f_+^{-1}(x + ue_4 + ve_5) = \frac{1}{v}(x + ue_4) \qquad (24)$$

$$A_I(x) = \left(\frac{2x}{1+|x|^2} + \frac{1-|x|^2}{1+|x|^2} e_4 \right)$$

This mapping can be regarded as a Möbius transformation that maps point $x \in \mathbb{R}^3$ onto $\mathbb{S}^3$ (the unit sphere) on $\mathbb{R}^4$ using a sphere of radius $\sqrt{2}$ and center (0,0,0,1)

Lie Sphere Geometry and Design of Curved Surface Structures

- **Lie Sphere Transformation**

Inversion

$y \in \mathbb{R}^4$ is pulled back to $\mathbb{R}^3$ by the following transformation.

$$y \mapsto s + \frac{\rho^2}{|y-s|^2}(y-s) \qquad (25)$$

$s = (0,0,0,1), \rho = \sqrt{2}$ Alternatively, you can use $s = (0,0,0,-1)$

Note that Inversion maps a point on the sphere of Lie Sphere geometry to a point on the sphere, **but the center point of the sphere does not map to the center point of the sphere**.

Lie Sphere Geometry and Design of Curved Surface Structures

- **Lie Sphere Transformation**

Inversion

Cross-ratios are preserved.

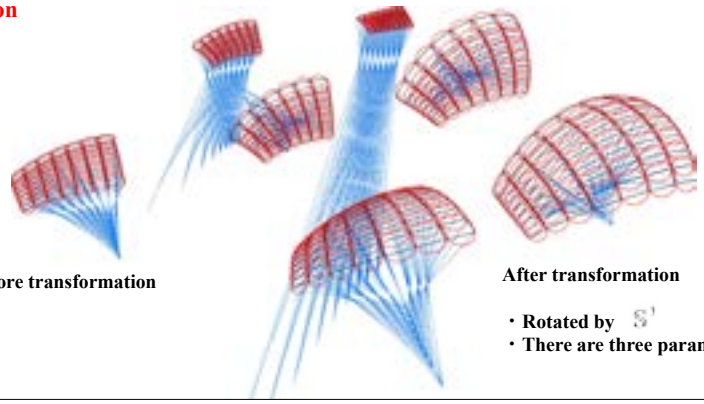

Before transformation

After transformation

- **Rotated by** $\mathbb{S}^1$
- **There are three parameters.**

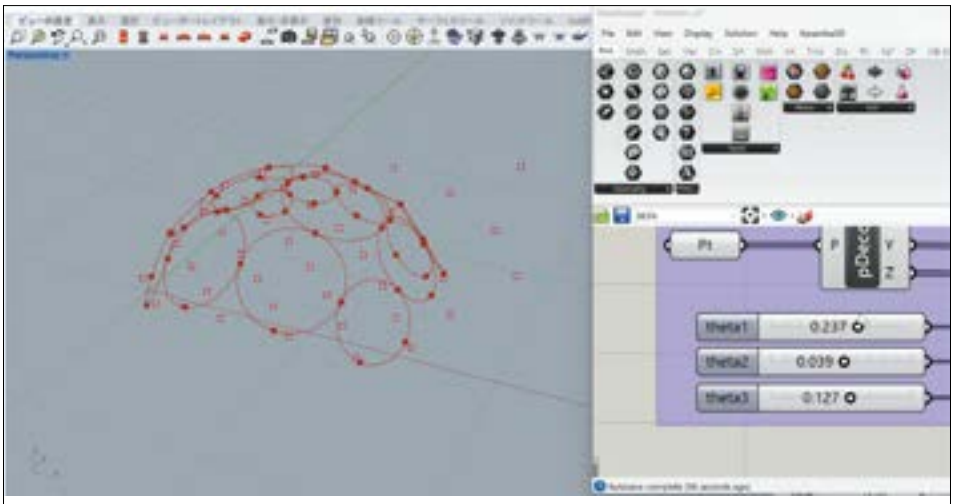

Lie Sphere Geometry and Design of Curved Surface Structures

- **Lie Sphere Transformation**

Offset

The Offset of the Lie Sphere transformation acts on the **oriented plane**, which is a pair of **normals** and **points**.
The following map is acted on $\hat{p}$ using the natural basis of the 6-dimensional space $\mathbb{R}^6$.

$$T_O = \begin{bmatrix} I_3 & 0 & 0 & 0 \\ 0 & 1+\frac{t^2}{2} & \frac{t^2}{2} & t \\ 0 & -\frac{t^2}{2} & 1-\frac{t^2}{2} & -t \\ 0 & t & t & 1 \end{bmatrix}$$

$$\hat{p} = v + 0 \cdot e_0 + 2de_\infty + 1 \cdot e_6 = v - 2de_4 + 2de_5 + 1 \cdot e_6$$

Lie Sphere Geometry and Design of Curved Surface Structures

- **Lie Sphere Transformation**

Offset

The Offset of the Lie Sphere transformation acts on the **oriented plane**, which is a pair of **normals** and **points**.
The following map is acted on $\hat{p}$ using the natural basis of the 6-dimensional space $\mathbb{R}^6$.

$$T_O = \begin{bmatrix} I_3 & 0 & 0 & 0 \\ 0 & 1+\frac{t^2}{2} & \frac{t^2}{2} & t \\ 0 & -\frac{t^2}{2} & 1-\frac{t^2}{2} & -t \\ 0 & t & t & 1 \end{bmatrix}$$

The height d obtained in $T_O(\hat{p})$ is used to obtain the coordinate values directly in the equation that forms the conical net.

$$\begin{bmatrix} v_\gamma & v_\beta & v_\alpha \end{bmatrix}^T \begin{Bmatrix} x \\ y \\ z \end{Bmatrix} = \begin{Bmatrix} d_\gamma \\ d_\beta \\ d_\alpha \end{Bmatrix}$$

$$\hat{p} = v + 0 \cdot e_0 + 2de_\infty + 1 \cdot e_6 = v - 2de_4 + 2de_5 + 1 \cdot e_6$$

Lie Sphere Geometry and Design of Curved Surface Structures

- **Lie Sphere Transformation**

Offset

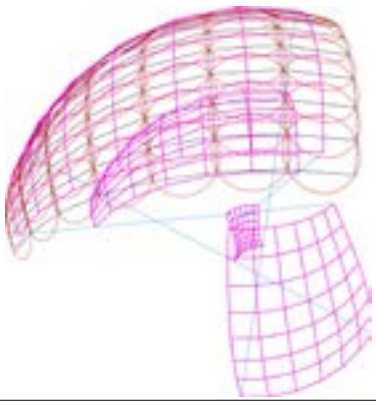

Constant face offset
Face Offset Mesh

It is possible to obtain a surface with the sign of the Gauss curvature reversed.

Lie Sphere Geometry and Design of Curved Surface Structures

- **Lie Sphere Transformation**

Offset

Note:

・It was shown that various shapes can be obtained by manipulating Inversion and Offset.

・The number of parameters is only four: Inversion-3 and Offset-1.The Lie Sphere transformation can also be used as a parametric surface with fabricability properties.

n a
of the
ersed.

Lie Sphere Geometry and Design of Curved Surface Structures

Christoffel Transformation

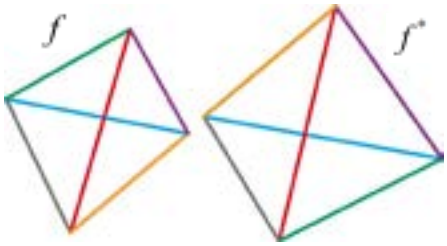

- **Transformation that hold when the cross-ratio is -1**
- **Lines of the same color parallel to each other**
- **Gaussian curvature from positive to negative**

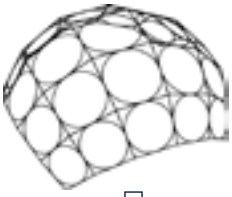

Koebe Polyhedron
Quadrilateral sides touching a Sphere surface.

⇩ **Christoffel transformation**

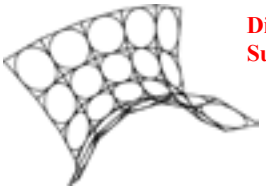

Discrete Minimal Surface

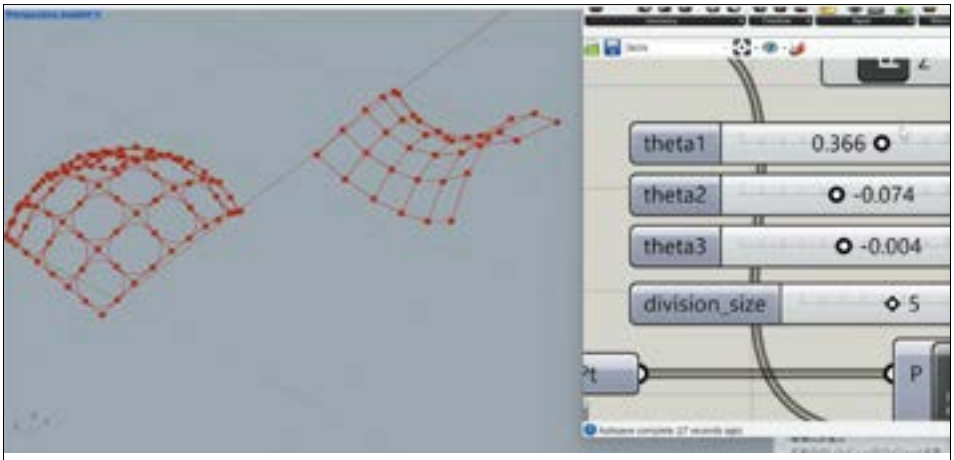

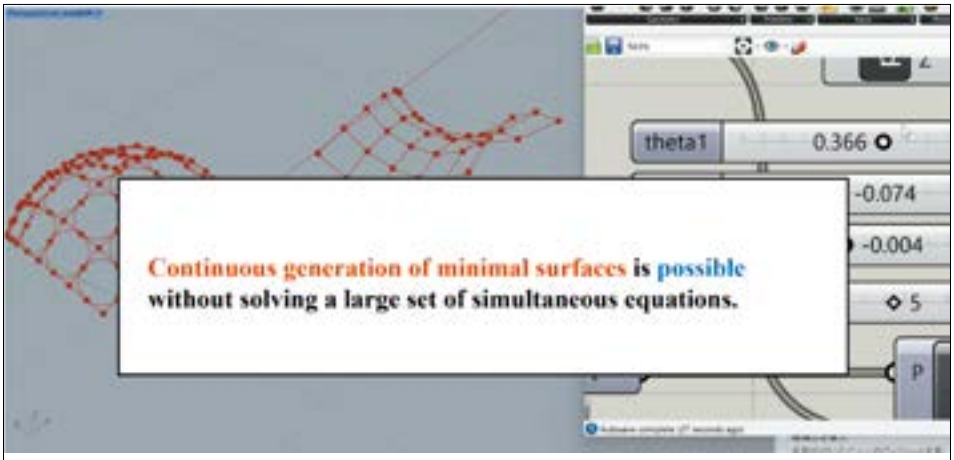

Lie Sphere Geometry and Design of Curved Surface Structures

Numerical results

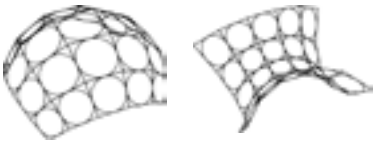

Case1: $t_1 = 0.50$, $t_2 = 0.00$, $t_3 = 0.00$

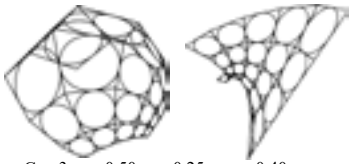

Case3: $t_1 = 0.50$, $t_2 = 0.25$, $t_3 = -0.40$

Case2: $t_1 = 0.50$, $t_2 = -0.25$, $t_3 = 0.10$

a. Koebe Polyhedron **b. Discrete minimal surface**

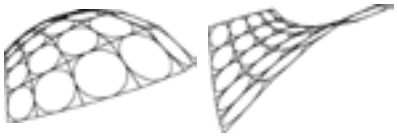

Case4: $t_1 = 0.25$, $t_2 = -0.25$, $t_3 = 0.10$

a. Koebe Polyhedron **b. Discrete minimal surface**

Lie Sphere Geometry and Design of Curved Surface Structures

Conclusion

・We introduced Lie sphere geometry, and indicated importance of Lie quadric to generate discrete curvature line. Next, we present the modeling technique of circular nets based on Lie sphere geometry.

・ The following items regarding Lie sphere geometry were explained.
How to construct a surface by Lie Sphere geometry.
How to construct a conical net.
The inversion and offset transformations of the Lie Sphere transformation are shown.

・We confirmed that various surfaces with discrete curvature line coordinates can be constructed by using only four parameters, three for inversion and one for offset.

Form-finding of Composite Tensile Structures by Finite Element Technique based on Nodal Coordinate Assumption

Yohei Yokosuka
Kagoshima University, Japan

Abstract

In general, the finite element method used in structural analysis uses a finite element method assumed displacement in which the displacement of a node is formulated as an unknown function. On the other hand, the finite element technique based on nodal coordinate assumption can formulate the coordinates of nodes themselves as unknown functions and perform stress-deformation analysis and form-finding analyses. In this presentation, I derive a virtual work equation using embedded coordinates and explain the differences in strain and stress derived from the equilibrium equation after deformation. In the equilibrium equation, the displacement assumption corresponds to the first Piola-Kirchhoff stress tensor and the coordinate assumption corresponds to the Cauchy stress tensor. Therefore, when the before deformed configuration is used as the reference configuration, proposed method presents a natural formulation and is suitable for nonlinear analysis using the total Lagrange method. In addition, the form-finding analysis of composite tensile structures with beam, truss, and membrane elements using the nodal coordinate assumption based on finite element technique will be explained.

International Conference "Evolving Design and Discrete Differential Geometry - towards Mathematics Aided Geometric Design"

Form-finding of Hybrid Tensile Structures with Active Bending Using Finite Element Technique Assuming Nodal Coordinates

Yohei YOKOSUKA[1)]
Sakura TORIGOE[2)]
Toshio HONMA[1)]

1) Graduate School of Science and Engineering, Kagoshima university
2) Shimizu Corporation

1. Overview

- **Bending-active structures**[1-2)]
  - It is possible to realize a lightweight structure with a self-equilibrium shape due to the tension of the membrane and cable and the temporary external force during construction.

1) Lienhard, J., Alpermann, H., Gengnagel, C. and Knippers, J., Active Bending, A Review on Structures where Bending is used as a Self-Formation Process, Inter-national Journal of Space Structures, Vol.28, No. 3&4, pp.187-196, 2013. https://doi.org/10.1260/0266-3511.28.3-4.187
2) Lienhard, J., Knippers, J., Bending-active Textile Hybrid, Journal of the International Association for Shell and Spatial Structures, 56 (1), pp.37-48, 2015.

1

1. Overview

- **Bending-active structures**[1-2)]
  - Two types of numerical analysis are required:
    1. Form-finding to obtain a self-equilibrium shape
    2. Stress displacement analysis to verify the structural performance when an external force is applied

1) Lienhard, J., Alpermann, H., Gengnagel, C. and Knippers, J., Active Bending, A Review on Structures where Bending is used as a Self-Formation Process, Inter-national Journal of Space Structures, Vol.28, No. 3&4, pp.187-196, 2013. https://doi.org/10.1260/0266-3511.28.3-4.187
2) Lienhard, J., Knippers, J., Bending-active Textile Hybrid, Journal of the International Association for Shell and Spatial Structures, 56 (1), pp.37-48, 2015.

2

1. Overview

- **Bending-active structures**[1-2)]
  - Two types of numerical analysis are required:
    1. Form-finding to obtain a self- equilibrium shape
    2. [illegible] when an [illegible]

  - Inheritance of residual stress of beam elements by active bending is important in stress displacement analysis to verify structural performance.

1) Lienhard, J., Alpermann, H., Gengnagel, C. and Knippers, J., Active Bending, A Review on Structures where Bending is used as a Self-Formation Process, Inter-national Journal of Space Structures, Vol.28, No. 3&4, pp.187-196, 2013. https://doi.org/10.1260/0266-3511.28.3-4.187
2) Lienhard, J., Knippers, J., Bending-active Textile Hybrid, Journal of the International Association for Shell and Spatial Structures, 56 (1), pp.37-48, 2015.

1. Overview

- **Finite Element Technique Assuming Nodal Coordinates**[3-4)]
  - Finite Element Technique Assuming Nodal Coordinates is a technique for form-finding of tension structures, and is a finite element technique in which coordinate values are directly unknown.

  - In this presentation, we introduce the discretization formulation of beam elements[5)], and apply it to the form-finding problem of the composite tension structure by beam, membrane, and cable elements.

3) Honma, T., Ataka, N., Geometorically Nonlinear Structural Analysis by FEM Using the Coordinate Value on a Deformed Body, INFORMATION, 7(5), pp.569-583, 2004.
4) Honma, T., Gouda, Y., Ataka, N, A Method of Tension Structure Analysis by Finite Element Technique Using the Coordinate Value on a Deformed Body, Journal of Structural and Construction Engineering (Transactions of AIJ), Vol.71, No.602, pp.161-169, 2006 (in Japanese)
5) Torigoe, S., Yokosuka, Y. and Honma, T.: From-finding and Formula-tions of Finite Element Technique Assuming Nodal Coordinates,15th Colloquium Analysis and Generation of Structural Shapes and Systems, pp.47-52, 2020 (in Japanese)

2. Formulation of beam elements

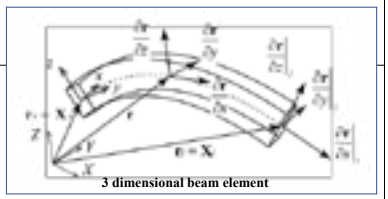
3 dimensional beam element

- **position coordinate vector** $\mathbf{r}$

$$\mathbf{r}(x,y,z)=\mathbf{S}(x,y,z)\mathbf{X}=\begin{bmatrix} r_X & r_Y & r_Z \end{bmatrix}^T \quad (1)$$

- **shape function** $\mathbf{S}$

$$\overset{3\times 24}{\mathbf{S}}=\begin{bmatrix} \overline{\mathbf{S}} & \mathbf{0} & \mathbf{0} \\ \mathbf{0} & \overline{\mathbf{S}} & \mathbf{0} \\ \mathbf{0} & \mathbf{0} & \overline{\mathbf{S}} \end{bmatrix} \quad (2)$$

$$\overline{\mathbf{S}}=\begin{bmatrix} S_1 & S_2 & S_3 & S_4 & S_5 & S_6 & S_7 & S_8 \end{bmatrix}$$

$$S_1=2\xi^3-3\xi^2+1 \qquad S_2=L\left(\xi^3-2\xi^2+\xi\right)$$
$$S_3=L(1-\xi)\eta \qquad S_4=L(1-\xi)\zeta$$
$$S_5=-2\xi^3+3\xi^2 \qquad S_6=L\left(\xi^3-\xi^2\right)$$
$$S_7=L\xi\eta \qquad S_8=L\xi\zeta \quad (3a\text{-}i)$$

x,y,z : local coordinates, X,Y,Z : global coordinates,
L : initial length, $\xi=x/L$, $\eta=y/L$, $\zeta=z/L$: normalized coordinates

- **generalized nodal coordinate vector** $\mathbf{X}$

$$\overset{24\times 1}{\mathbf{X}}=\left[X_i \left.\frac{\partial r_X}{\partial x}\right|_i \left.\frac{\partial r_X}{\partial y}\right|_i \left.\frac{\partial r_X}{\partial z}\right|_i X_j \left.\frac{\partial r_X}{\partial x}\right|_j \left.\frac{\partial r_X}{\partial y}\right|_j \left.\frac{\partial r_X}{\partial z}\right|_j \right.$$
$$Y_i \left.\frac{\partial r_Y}{\partial x}\right|_i \left.\frac{\partial r_Y}{\partial y}\right|_i \left.\frac{\partial r_Y}{\partial z}\right|_i Y_j \left.\frac{\partial r_Y}{\partial x}\right|_j \left.\frac{\partial r_Y}{\partial y}\right|_j \left.\frac{\partial r_Y}{\partial z}\right|_j$$
$$\left. Z_i \left.\frac{\partial r_Z}{\partial x}\right|_i \left.\frac{\partial r_Z}{\partial y}\right|_i \left.\frac{\partial r_Z}{\partial z}\right|_i Z_j \left.\frac{\partial r_Z}{\partial x}\right|_j \left.\frac{\partial r_Z}{\partial y}\right|_j \left.\frac{\partial r_Z}{\partial z}\right|_j \right]^T \quad (4)$$

2. Formulation of beam elements

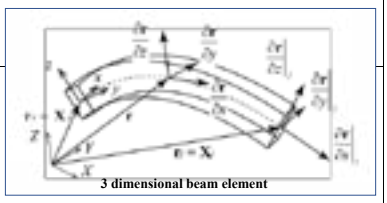

・**Green-Lagrange strain** γ_x

$$\gamma_x = \frac{1}{2}\left(\frac{\partial \mathbf{r}}{\partial x}^T \frac{\partial \mathbf{r}}{\partial x} - 1\right) = \frac{1}{2L^2}\mathbf{X}^T\mathbf{G}\mathbf{X} - \frac{1}{2} \qquad (5)$$

・**curvature** κ_y, κ_z

$$\kappa_y = -\frac{\partial \mathbf{r}}{\partial z}^T \frac{\partial^2 \mathbf{r}}{\partial x^2} = -\frac{1}{2L^3}\mathbf{X}^T\mathbf{H}_y\mathbf{X}$$

$$\kappa_z = \frac{\partial \mathbf{r}}{\partial y}^T \frac{\partial^2 \mathbf{r}}{\partial x^2} = \frac{1}{2L^3}\mathbf{X}^T\mathbf{H}_z\mathbf{X} \qquad (6a,b)$$

$\mathbf{G}, \mathbf{H}_y, \mathbf{H}_z$ ：constant matrix

・**strain-nodal coordinate relation, strain increment-nodal coordinate increment relation**

$$\gamma_x = \mathbf{B}_\gamma \mathbf{X} - C \qquad \delta\gamma_x = \mathbf{B}_\gamma^* \delta\mathbf{X}$$

$$\kappa_y = \mathbf{B}_{\kappa y}\mathbf{X} \qquad \delta\kappa_y = \mathbf{B}_{\kappa y}^* \delta\mathbf{X}$$

$$\kappa_z = \mathbf{B}_{\kappa z}\mathbf{X} \qquad \delta\kappa_z = \mathbf{B}_{\kappa z}^* \delta\mathbf{X} \qquad (7a\text{-}f)$$

2. Formulation of beam elements

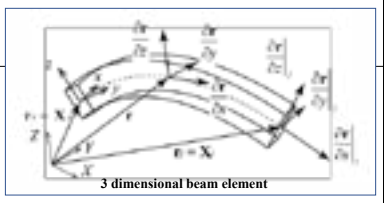

・**virtual work equation**

$$\int_V \delta\gamma_x(\mathbf{X},\xi)\tau(\mathbf{X},\xi)dV + \int_L \delta\kappa_y(\mathbf{X},\xi)m_y(\mathbf{X},\xi)dx + \int_L \delta\kappa_z(\mathbf{X},\xi)m_z(\mathbf{X},\xi)dx = \delta\mathbf{X}^T\lambda\mathbf{f} \qquad (8)$$

・**discretized equilibrium equation**

$$EAL\int_0^1 \mathbf{B}_\gamma^{*T}\gamma_x d\xi + EI_yL\int_0^1 \mathbf{B}_{\kappa y}^{*\ T}\kappa_y d\xi + EI_zL\int_0^1 \mathbf{B}_{\kappa z}^{*\ T}\kappa_z d\xi - \lambda\mathbf{f} = \mathbf{0} \qquad (9)$$

・**constitutive equation**

$$\tau = E\gamma_x \qquad m_y = EI_y\kappa_y \qquad m_z = EI_z\kappa_z \qquad (10a\text{-}c)$$

τ ：axial stress

m_y, m_z ：bending moment

2. Formulation of beam elements

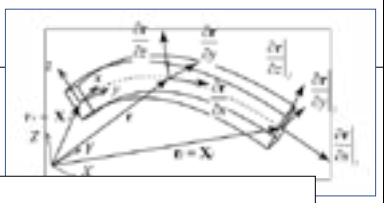

・**virtual work equation**

$$\int_V \delta\gamma_x(\mathbf{X},\xi)\tau(\mathbf{X},\xi)dV + \int_L \delta\kappa_y(\mathbf{X},\xi)m_y(\mathbf{X},\xi)dx$$

$$+\int_L \delta\kappa_z(\quad$$

・**discretiz**

$$EAL\int_0^1 \mathbf{I}$$

$$+EI_zL\int$$

Notes on numerical calculation

・Gauss's three-point integration is adopted

・Reference arrangement by this formulation follows the solution by the total Lagrange method.

・Degree of freedom is reduced the reduction operation of $\partial\mathbf{r}/\partial y$, $\partial\mathbf{r}/\partial z$

Characteristics

・Strain and curvature cannot be separated into linear and nonlinear terms.

・No coordinate transformation required.

10a-c)

m_y, m_z ：bending moment

3. Comparison of numerical and analytical result (beam in 2D plane)

- **second-order differential equation (post buckling)**

$$EI\frac{d^2v/dx^2}{\left\{1+\left(dv/dx\right)^2\right\}^{3/2}}=P\left(\delta-v\right) \qquad (11)$$

Material property

Elastic modulus	Cross-Sectional area	Moment of inertia	Beam length	Buckling load
2.05×10^8 kN/m^2	1.0×10^{-2} m^2	1.333×10^{-6} m^4	10 m	26.97 kN

Exact solution

- Analytical result is expressed by using curvature as rigorous definition.
- Elliptic integral required.

Numerical solution

- Numerical analysis uses finite element technique assuming nodal coordinates to trace the equilibrium path by the arc-length method.
- Initial imperfection of the shape sin function is given.
- Divide into 50 elements

9

3. Comparison of numerical and analytical result (beam in 2D plane)

- **second-order differential equation**

$$EI\frac{d^2v/dx^2}{\left\{1+\left(dv/dx\right)^2\right\}^{3/2}}=P\left(\delta-v\right) \qquad (11)$$

Material property

Elastic modulus	Cross-Sectional area	Moment of inertia	Beam length	Buckling load
2.05×10^8 kN/m^2	1.0×10^{-2} m^2	1.333×10^{-6} m^4	10 m	26.97 kN

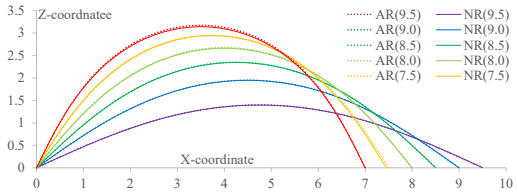

Buckling forms of numerical results (NR) and analytical results (AR)

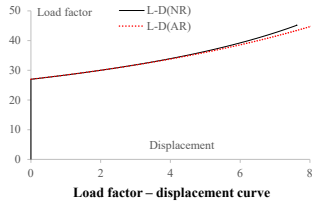

Load factor – displacement curve

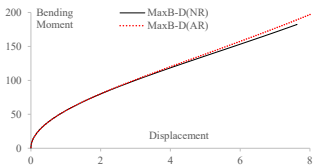

Bending moment – displacement curve

10

3. Comparison of numerical and analytical result (beam in 2D plane)

- **second-order differential equation**

$$EI\frac{d^2v/dx^2}{\left\{1+\left(dv/dx\right)^2\right\}^{3/2}}=P\left(\delta-v\right) \qquad (11)$$

Material property

Elastic modulus	Cross-Sectional area	Moment of inertia	Beam length	Buckling load
2.05×10^8 kN/m^2	1.0×10^{-2} m^2	1.333×10^{-6} m^4	10 m	26.97 kN

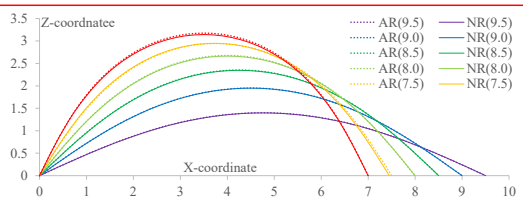

Buckling forms of numerical results (NR) and analytical results (AR)

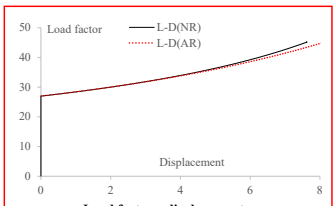

Load factor – displacement curve

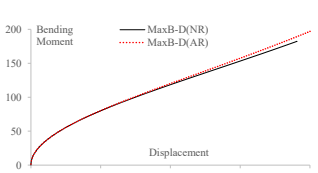

Bending moment – displacement curve

10

4. Form-finding of Hybrid Tensile Structures with Active Bending

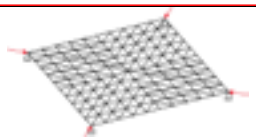

△: *X*, *Y*-free boundary, *Z*-fixed boundary

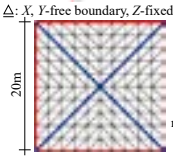

beam

cable

△ membrane

Initial form

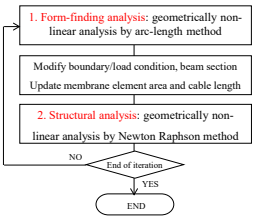

Analysis flow

Form-finding analysis
(laminated beams with flat bars that allows shear slip)

Structural analysis
(composite beams with bolt joint that does not allow shear slip)

Analysis cases (sectional property of beam elements)

	case1		case2		case3	
Cross-sectional shape	40mm×400mm - 3 layers		40mm×400mm - 4 layers		32mm×400mm - 5 layers	
	Form-finding	Structural analysis	Form-finding	Structural analysis	Form-finding	Structural analysis
Moment of inertia (m^4)	6.40e-6	5.76e-5	8.53e-6	1.37e-4	5.46e-6	1.37e-4
Section modulus (m^3)	3.20e-4	9.60e-4	4.27e-4	1.71e-3	3.41e-4	1.71e-3
Allowable bending (kNm)	69.3	208.0	92.4	370.0	74.0	370.0

Material property of membrane, cable element

Membrane element			
Elastic modulus	Shear modulus	Thickness	Poisson ratio
1.0e+5 kN/m^2	6.0e+4 kN/m^2	1.0e-3 m	0.3
Cable element			
Elastic modulus		Sectional area	
2.05e+8 kN/m^2		3.95e-5 m^2	

11

4. Form-finding of Hybrid Tensile Structures with Active Bending

△: *X*, *Y*-free boundary, *Z*-fixed boundary

beam

cable

△ membrane

Initial form

Analysis flow

Form-finding analysis
(laminated beams with flat bars that allows shear slip)

Structural analysis
(composite beams with bolt joint that does not allow shear slip)

Analysis cases (sectional property of beam elements)

	case1		case2		case3	
Cross-sectional shape	40mm×400mm - 3 layers		40mm×400mm - 4 layers		32mm×400mm - 5 layers	
	Form-finding	Structural analysis	Form-finding	Structural analysis	Form-finding	Structural analysis
Moment of inertia (m^4)	6.40e-6	5.76e-5	8.53e-6	1.37e-4	5.46e-6	1.37e-4
Section modulus (m^3)	3.20e-4	9.60e-4	4.27e-4	1.71e-3	3.41e-4	1.71e-3
Allowable bending (kNm)	69.3	208.0	92.4	370.0	74.0	370.0

Material property of membrane, cable element

Membrane element			
Elastic modulus	Shear modulus	Thickness	Poisson ratio
1.0e+5 kN/m^2	6.0e+4 kN/m^2	1.0e-3 m	0.3
Cable element			
Elastic modulus		Sectional area	
2.05e+8 kN/m^2		3.95e-5 m^2	

11

4. Form-finding of Hybrid Tensile Structures with Active Bending

△: *X*, *Y*-free boundary, *Z*-fixed boundary

beam

cable

△ membrane

Initial form

Analysis flow

Form-finding analysis
(laminated beams with flat bars that allows shear slip)

Structural analysis
(composite beams with bolt joint that does not allow shear slip)

Analysis cases (sectional property of beam elements)

	case1		case2		case3	
Cross-sectional shape	40mm×400mm - 3 layers		40mm×400mm - 4 layers		32mm×400mm - 5 layers	
	Form-finding	Structural analysis	Form-finding	Structural analysis	Form-finding	Structural analysis
Moment of inertia (m^4)	6.40e-6	5.76e-5	8.53e-6	1.37e-4	5.46e-6	1.37e-4
Section modulus (m^3)	3.20e-4	9.60e-4	4.27e-4	1.71e-3	3.41e-4	1.71e-3
Allowable bending (kNm)	69.3	208.0	92.4	370.0	74.0	370.0

Material property of membrane, cable element

Membrane element			
Elastic modulus	Shear modulus	Thickness	Poisson ratio
1.0e+5 kN/m^2	6.0e+4 kN/m^2	1.0e-3 m	0.3
Cable element			
Elastic modulus		Sectional area	
2.05e+8 kN/m^2		3.95e-5 m^2	

11

4. Form-finding of Hybrid Tensile Structures with Active Bending

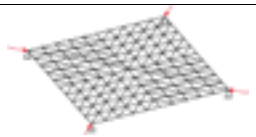

△: *X*, *Y*-free boundary, *Z*-fixed boundary

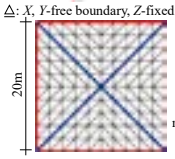

Initial form

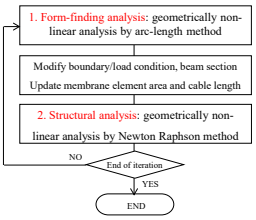

Analysis flow

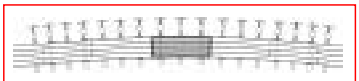

Form-finding analysis
(laminated beams with flat bars that allows shear slip)

Structural analysis
(composite beams with bolt joint that does not allow shear slip)

Analysis cases (sectional property of beam elements)

	case1		case2		case3	
Cross-sectional shape	40mm×400mm - 3 layers		40mm×400mm - 4 layers		32mm×400mm - 5 layers	
	Form-finding	Structural analysis	Form-finding	Structural analysis	Form-finding	Structural analysis
Moment of inertia (m^4)	6.40e-6	5.76e-5	8.53e-6	1.37e-4	5.46e-6	1.37e-4
Section modulus (m^3)	3.20e-4	9.60e-4	4.27e-4	1.71e-3	3.41e-4	1.71e-3
Allowable bending (kNm)	69.3	208.0	92.4	370.0	74.0	370.0

Material property of membrane, cable element

Membrane element			
Elastic modulus	Shear modulus	Thickness	Poisson ratio
1.0e+5 kN/m^2	6.0e+4 kN/m^2	1.0e-3 m	0.3
Cable element			
Elastic modulus		Sectional area	
2.05e+8 kN/m^2		3.95e-5 m^2	

4. Form-finding of Hybrid Tensile Structures with Active Bending

△: *X*, *Y*-free boundary, *Z*-fixed boundary

20m
beam
cable
△
membrane

Initial form

1. Form-finding analysis: geometrically non-linear analysis by arc-length method
Modify boundary/load condition, beam section
Update membrane element area and cable length
2. Structural analysis: geometrically non-linear analysis by Newton Raphson method
NO
End of iteration
YES
END

Analysis flow

Form-finding analysis
(laminated beams with flat bars that allows shear slip)

Structural analysis
(composite beams with bolt joint that does not allow shear slip)

Analysis cases (sectional property of beam elements)

	case1		case2		case3	
Cross-sectional shape	40mm×400mm - 3 layers		40mm×400mm - 4 layers		32mm×400mm - 5 layers	
	Form-finding	Structural analysis	Form-finding	Structural analysis	Form-finding	Structural analysis
Moment of inertia (m^4)	6.40e-6	5.76e-5	8.53e-6	1.37e-4	5.46e-6	1.37e-4
Section modulus (m^3)	3.20e-4	9.60e-4	4.27e-4	1.71e-3	3.41e-4	1.71e-3
Allowable bending (kNm)	69.3	208.0	92.4	370.0	74.0	370.0

Material property of membrane, cable element

Membrane element			
Elastic modulus	Shear modulus	Thickness	Poisson ratio
1.0e+5 kN/m^2	6.0e+4 kN/m^2	1.0e-3 m	0.3
Cable element			
Elastic modulus		Sectional area	
2.05e+8 kN/m^2		3.95e-5 m^2	

11

4. Form-finding of Hybrid Tensile Structures with Active Bending

△: *X*, *Y*-free

20m

Form-finding analysis

・Concentrated force which induces buckling acts and the equilibrium path is traced by the arc-length method.

・Cables and membranes are not considered elastic stiffness. Cable tension and membrane tension are constant at 10 kN and 1 kN/m, respectively.

Structural analysis

・Release the concentrated force and change the roller support to a pin support.
・Change the section property from a laminated beam to a composite beam.
・Inherit the bending / axial stress at the time of structural analysis.
・Apply self weight (snow load + dead load) and solve by Newton-Raphson method.

	case1		case2		case3	
Cross-sectional shape	40mm×400mm - 3 layers		40mm×400mm - 4 layers		32mm×400mm - 5 layers	
	Form-finding	Structural analysis	Form-finding	Structural analysis	Form-finding	Structural analysis
Moment of inertia (m^4)	6.40e-6	5.76e-5	8.53e-6	1.37e-4	5.46e-6	1.37e-4
Section modulus (m^3)	3.20e-4	9.60e-4	4.27e-4	1.71e-3	3.41e-4	1.71e-3
Allowable bending (kNm)	69.3	208.0	92.4	370.0	74.0	370.0

Membrane element			
Elastic modulus	Shear modulus	Thickness	Poisson ratio
1.0e+5 kN/m^2	6.0e+4 kN/m^2	1.0e-3 m	0.3
Cable element			
Elastic modulus		Sectional area	
2.05e+8 kN/m^2		3.95e-5 m^2	

12

4. Form-finding of Hybrid Tensile Structures with Active Bending

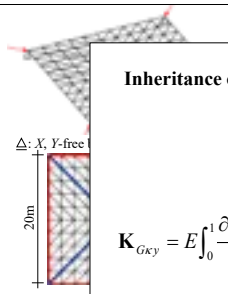

Inheritance of stress for geometric stiffness matrix in structural analysis

$$\mathbf{K}_{G\gamma} = EA\int_0^1 \frac{\partial \mathbf{B}_{\gamma}^{*T}}{\partial \mathbf{X}}\left(\boxed{L_0\gamma_{x0}}+\boxed{L\gamma_x}\right)d\xi$$

Form-finding **Structural analysis**

$$\mathbf{K}_{G\kappa y} = E\int_0^1 \frac{\partial \mathbf{B}_{\kappa y}^{*T}}{\partial \mathbf{X}}\left(\boxed{I_{y0}L_0\kappa_{y0}}+\boxed{I_yL\kappa_y}\right)d\xi \quad \mathbf{K}_{G\kappa z} = E\int_0^1 \frac{\partial \mathbf{B}_{\kappa z}^{*T}}{\partial \mathbf{X}}\left(\boxed{I_{z0}L_0\kappa_{z0}}+\boxed{I_zL\kappa_z}\right)d\xi$$

Cross-sectional shape	40mm×400mm - 3 layers		40mm×400mm - 4 layers		32mm×400mm - 5 layers	
	Form-finding	Structural analysis	Form-finding	Structural analysis	Form-finding	Structural analysis
Moment of inertia (m^4)	6.40e-6	5.76e-5	8.53e-6	1.37e-4	5.46e-6	1.37e-4
Section modulus (m^3)	3.20e-4	9.60e-4	4.27e-4	1.71e-3	3.41e-4	1.71e-3
Allowable bending (kNm)	69.3	208.0	92.4	370.0	74.0	370.0

Elastic modulus	Shear modulus	Thickness	Poisson ratio
1.0e+5 kN/m²	6.0e+4 kN/m²	1.0e-3 m	0.3

Cable element	
Elastic modulus	Sectional area
2.05e+8 kN/m²	3.95e-5 m²

12

4. Form-finding of Hybrid Tensile Structures with Active Bending

・**Numerical results**

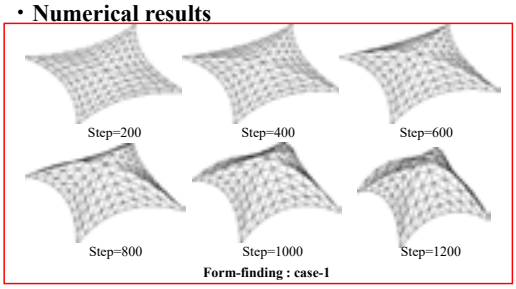

Form-finding : case-1

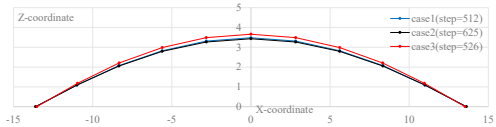

solution with maximum rise among allowable solutions

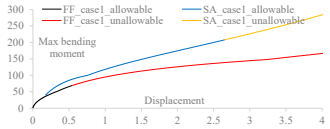

Max bending – displacement : case-1

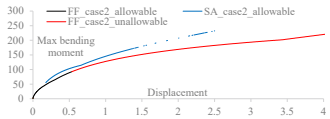

Max bending – displacement : case-2

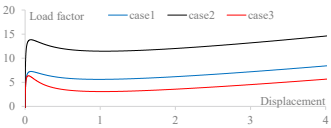

Load factor – displacement : case-1-3

13

4. Form-finding of Hybrid Tensile Structures with Active Bending

・**Numerical results**

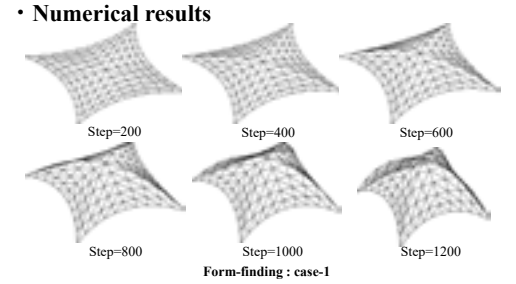

Form-finding : case-1

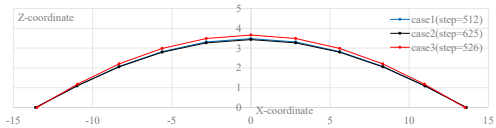

solution with maximum rise among allowable solutions

Max bending – displacement : case-1

Max bending – displacement : case-2

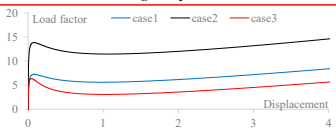

Load factor – displacement : case-1-3

13

4. Form-finding of Hybrid Tensile Structures with Active Bending

・**Numerical results**

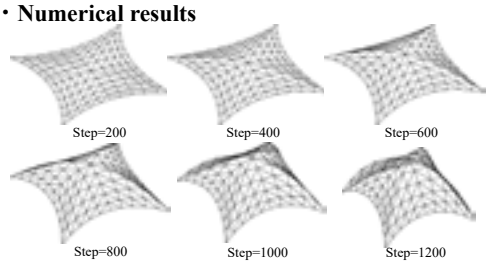

Form-finding : case-1

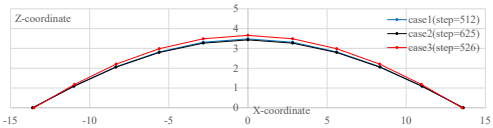

solution with maximum rise among allowable solutions

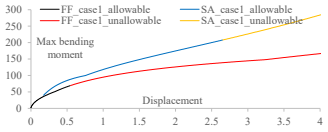

Max bending – displacement : case-1

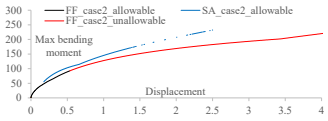

Max bending – displacement : case-2

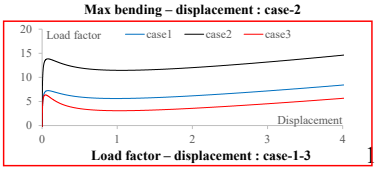

Load factor – displacement : case-1-3

13

4. Form-finding of Hybrid Tensile Structures with Active Bending

・**Numerical results**

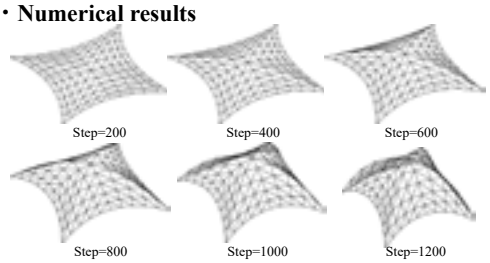

Form-finding : case-1

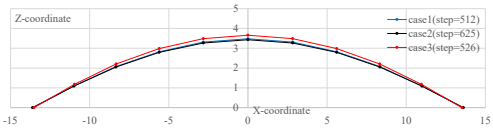

solution with maximum rise among allowable solutions

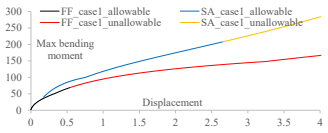

Max bending – displacement : case-1

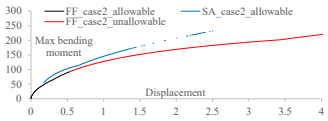

Max bending – displacement : case-2

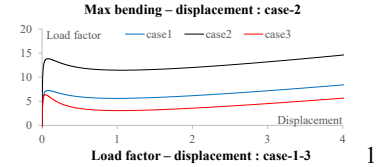

Load factor – displacement : case-1-3

13

5. Conclusion

・We show the formulation of the beam element of the finite element technique assuming nodal coordinates, and show the validity of this method by comparing the analytical solution of the buckling form of the beam in the two-dimensional plane and the result of numerical analysis.

・We showed that allowable solutions for each analysis can be obtained by performing form-finding and stress displacement analysis of the hybrid tensile structure, and proposed a bending-active structure by using this method.

・ It is possible to inherit the axial stress and bending stress by active bending even if the cross-sectional shape changes in each analysis by dividing it into two stages.

14

Nonlinear Finite Element Method by Embedded Coordinates : Membrane Elements

Yohei YOKOSUKA
Graduate School of Science and Engineering, Kagoshima university

1.1 Coordinate systems and position vectors

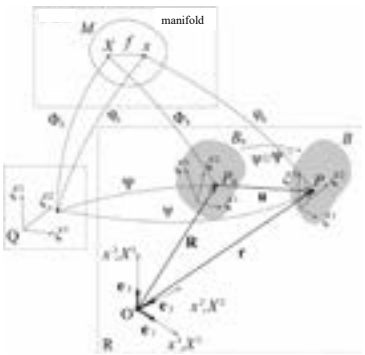

The interior region of an object is regarded as a manifold M .
An embedded coordinate system Q is given as local coordinates that describe arbitrary positions and physical quantities inside an object.
The global (Cartesian) coordinate system R is given as the coordinates in which the object is placed.

・Deformation :

$$x = f(X) \tag{1}$$

・Embedded coordinates of points X, x are equal :

$$\Phi_{\mathrm{Q}}(X) = \varphi_{\mathrm{Q}}(f(X)) \tag{2}$$

・Mapping from embedded coordinates to global coordinates before/after deformation:

$$\Psi = \Phi_{\mathrm{R}} \circ \Phi_{\mathrm{Q}}^{-1},\ \psi = \varphi_{\mathrm{R}} \circ \varphi_{\mathrm{Q}}^{-1} \tag{3}$$

1.1 Coordinate systems and position vectors

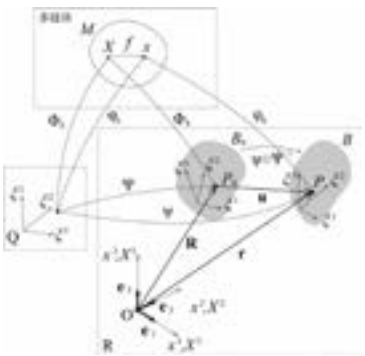

・Global coordinate system

$$X^1, X^2, X^3 \tag{4}$$

・Orthonormal basis in global

$$\mathbf{e}_1, \mathbf{e}_2, \mathbf{e}_3 \tag{5}$$

・Embedded coordinates

$$\xi^1, \xi^2, \xi^3 \tag{6}$$

・Position vectors before deformation

$$\mathbf{R} = X^i \mathbf{e}_i \tag{7}$$

・Position vectors after deformation

$$\mathbf{r} = x^i\left(X^1, X^2, X^3\right)\mathbf{e}_i \tag{8}$$

・Displacement vectors

$$\mathbf{u} = \mathbf{r} - \mathbf{R} \tag{9}$$

・Representation of Embedded coordinates

$$X^i = X^i\left(\xi^1, \xi^2, \xi^3\right)$$
$$x^i = x^i\left(\xi^1, \xi^2, \xi^3\right) \tag{10}$$

1.2 Strain

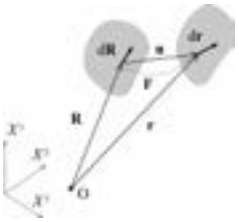

・Transformation of continuum

Let the material point $\mathbf{R}$ and its neighborhood $\mathbf{R}+\mathrm{d}\mathbf{R}$ be a point.

Infinitesimal vector $\mathrm{d}\mathbf{R}$:

$$\frac{\partial \mathbf{R}}{\partial X^i}=\mathbf{e}_i,\ \ \mathrm{d}\mathbf{R}=\frac{\partial \mathbf{R}}{\partial X^i}dX^i=dX^i\mathbf{e}_i \tag{11}$$

The infinitesimal vector after deformation is represented as a linear mapping of the infinitesimal vector before deformation as follows

Infinitesimal vector $\mathrm{d}\mathbf{r}$:

$$\mathrm{d}\mathbf{r}=\mathbf{F}\cdot\mathrm{d}\mathbf{R} \tag{12}$$

$\mathbf{F}$: Deformation gradient tensor

Deformation gradient tensor $\mathbf{F}$:

$$\mathbf{F}=\frac{\partial x^j}{\partial X^j}\mathbf{e}_i\otimes\mathbf{e}_j \tag{131}$$

1.2 Strain

・Green-Lagrange strain1 (coordinate type)

Strain is defined as the difference in the inner product of an infinitesimal vector before and after deformation.

$$\begin{aligned}\mathrm{d}\mathbf{r}\cdot\mathrm{d}\mathbf{r}-\mathrm{d}\mathbf{R}\cdot\mathrm{d}\mathbf{R}&=\left(\mathbf{F}\cdot\mathrm{d}\mathbf{R}\right)\cdot\left(\mathbf{F}\cdot\mathrm{d}\mathbf{R}\right)-\mathrm{d}\mathbf{R}\cdot\mathrm{d}\mathbf{R}\\&=\mathrm{d}\mathbf{R}^T\left(\mathbf{F}^T\mathbf{F}\right)\mathrm{d}\mathbf{R}-\mathrm{d}\mathbf{R}^T\mathrm{d}\mathbf{R}\\&=\mathrm{d}\mathbf{R}^T\left(\mathbf{F}^T\mathbf{F}-\mathbf{I}\right)\mathrm{d}\mathbf{R}\end{aligned} \tag{14}$$

Green-Lagrange strain $\mathbf{E}$:

$$\mathbf{E}\equiv\frac{1}{2}\left(\mathbf{F}^T\mathbf{F}-\mathbf{I}\right) \tag{15}$$

Green-Lagrange strain can be expressed in coordinates only, but the linear and nonlinear parts cannot be separated; when Green-Lagrange strain is employed, it becomes a nonlinear finite element method.

1.2 Strain

・Green-Lagrange strain2 (displacement type)

Deformation gradient tensor $\mathbf{Z}$:

$$\mathbf{Z}\equiv\nabla\otimes\mathbf{u}=\frac{\partial u_i}{\partial X^j}\mathbf{e}_i\otimes\mathbf{e}_j \tag{16}$$

$$\nabla\equiv\frac{\partial}{\partial X^j}\mathbf{e}_j \tag{17}$$

Whereas,

$$\begin{aligned}\mathbf{Z}\cdot\mathrm{d}\mathbf{R}&=\left(\frac{\partial u_i}{\partial X^j}\mathbf{e}_i\otimes\mathbf{e}_j\right)\cdot\mathrm{d}X^k\mathbf{e}_k=\frac{\partial u_i}{\partial X^j}\mathrm{d}X^k\left(\mathbf{e}_i\otimes\mathbf{e}_j\right)\cdot\mathbf{e}_k=\frac{\partial u_i}{\partial X^j}\cdot\mathrm{d}X^k\delta_{jk}\mathbf{e}_i\\&=\frac{\partial u_i}{\partial X^j}\cdot\mathrm{d}X^j\mathbf{e}_i=\frac{\partial \mathbf{u}}{\partial X^j}\cdot\mathrm{d}X^j=\mathrm{d}\mathbf{u}\end{aligned} \tag{18}$$

Therefore,

$$\left(\mathbf{I}+\mathbf{Z}\right)\cdot\mathrm{d}\mathbf{R}=\mathrm{d}\mathbf{R}+\mathrm{d}\mathbf{u}=\mathrm{d}\left(\mathbf{R}+\mathbf{u}\right)=\mathrm{d}\mathbf{r},\ \ \left(\mathbf{I}+\mathbf{Z}\right)=\mathbf{F} \tag{19}$$

1.2 Strain

・Green-Lagrange strain2 (displacement type)

Green-Lagrange strain $\mathbf{E}$:

$$\begin{aligned}\mathbf{E} &= \frac{1}{2}\left\{\nabla\otimes\mathbf{u} + (\nabla\otimes\mathbf{u})^T + (\nabla\otimes\mathbf{u})^T\cdot(\nabla\otimes\mathbf{u})\right\} \\ &= \frac{1}{2}\left(\frac{\partial u_i}{\partial X^j} + \frac{\partial u_j}{\partial X^i} + \frac{\partial u_k}{\partial X^i}\frac{\partial u_k}{\partial X^j}\right)\mathbf{e}_i\otimes\mathbf{e}_j\end{aligned} \tag{20}$$

1.3 Embedded coordinates and covariant and contravariant bases

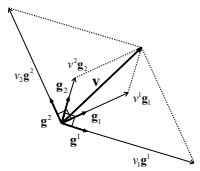

Covariant and Contravariant basis vectors

・Covariant and Contravariant basis vectors

Let the material point $\mathbf{R}$ and its neighborhood $\mathbf{R}+\mathrm{d}\mathbf{R}$ be a point.

Covariant basis vectors $\mathbf{g}_i$,

Contravariant basis vectors $\mathbf{g}^i$:

$$\begin{aligned}&\mathbf{g}^i\cdot\mathbf{g}_j = \delta^i_j,\ \begin{cases}\delta^i_j = 1, & i = j\\ \delta^i_j = 0, & i\neq j\end{cases}\\ &\mathbf{g}^i\cdot\mathbf{g}^j = g^{ij},\ \ \mathbf{g}_i\cdot\mathbf{g}_j = g_{ij}\\ &\mathbf{g}_i = g_{ij}\mathbf{g}^j,\ \ \mathbf{g}^i = g^{ij}\mathbf{g}_j\end{aligned} \tag{21}$$

The other basis vector is determined by determining $\mathbf{g}_i$ or $\mathbf{g}^i$ from the geometric relationship. The vector $\mathbf{v}$ in the figure can be expressed in two ways.

$$\begin{aligned}&\mathbf{v} = v_i\mathbf{g}^i = v^i\mathbf{g}_i\\ &v_i = g_{ij}v^j,\ v^i = g^{ij}v_j\end{aligned} \tag{22}$$

1.3 Embedded coordinates and covariant and contravariant bases

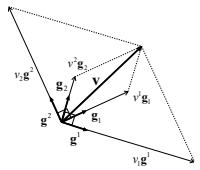

Covariant and Contravariant basis vectors

・Covariant and Contravariant basis vectors

$$\mathbf{g}^i = \frac{\mathbf{g}_j\times\mathbf{g}_k}{(\mathbf{g}_1\times\mathbf{g}_2)\cdot\mathbf{g}_3},\ (i,j,k) = (1,2,3),(2,3,1),(3,1,2) \tag{23}$$

1.3 Embedded coordinates and covariant and contravariant bases

The components of the infinitesimal vector $d\xi^i$, dX^i, dx^i have the following relationship

$$d\xi^i = \frac{\partial \xi^i}{\partial X^j} dX^j, \quad dX^i = \frac{\partial X^i}{\partial \xi^j} d\xi^j, \quad dx^i = \frac{\partial x^i}{\partial \xi^j} d\xi^j, \quad d\xi^i = \frac{\partial \xi^i}{\partial x^j} dx^j \tag{24}$$

Covariant and contravariant basis vectors before transformation $\mathbf{G}_i, \mathbf{G}^i$:

$$\mathbf{G}_i = \frac{\partial X^j}{\partial \xi^i}\mathbf{e}_j = \frac{\partial \mathbf{R}}{\partial \xi^i}, \quad \mathbf{G}^i = \frac{\partial \xi^i}{\partial X^j}\mathbf{e}^j = G^{ij}\mathbf{G}_j \tag{25}$$

Infinitesimal vector with embedded coordinates before deformation $\mathrm{d}\mathbf{R}$:

$$\mathrm{d}\mathbf{R} = \mathbf{G}_i d\xi^i = \mathbf{G}^i d\xi_i \tag{26}$$

Covariant and contravariant basis vectors after transformation $\mathbf{g}_i, \mathbf{g}^i$:

$$\mathbf{g}_i = \frac{\partial x^j}{\partial \xi^i}\mathbf{e}_j = \frac{\partial \mathbf{r}}{\partial \xi^i}, \quad \mathbf{g}^i = \frac{\partial \xi^i}{\partial x^j}\mathbf{e}^j = g^{ij}\mathbf{g}_j \tag{27}$$

Infinitesimal vector with embedded coordinates after deformation $\mathrm{d}\mathbf{r}$:

$$\mathrm{d}\mathbf{r} = \mathbf{g}_i d\xi^i = \mathbf{g}^i d\xi_i \tag{28}$$

1.3 Embedded coordinates and covariant and contravariant bases

Product of covariant basis vectors before and after transformation

$$\mathbf{G}_i \cdot \mathbf{G}_j = G_{ij}, \ \mathbf{g}_i \cdot \mathbf{g}_j = g_{ij} \tag{29}$$

Green-Lagrange strain $\mathbf{E}$:

$$E_{ij} = \frac{1}{2}\left(g_{ij} - G_{ij}\right), \ \mathbf{E} = \frac{1}{2}\left(g_{ij} - G_{ij}\right)\left(\mathbf{G}^i \otimes \mathbf{G}^j\right) \tag{30}$$

This can be considered as follows.

$$\begin{aligned}
&\mathrm{d}\mathbf{R} = \mathbf{G}_i d\xi^i, \ \mathrm{d}\mathbf{r} = \mathbf{g}_i d\xi^i \\
&\mathbf{g}_i = \left(\mathbf{g}_i \otimes \mathbf{G}^i\right) \cdot \mathbf{G}_i \\
&\mathrm{d}\mathbf{r} = \mathbf{g}_i d\xi^i = \left(\mathbf{g}_i \otimes \mathbf{G}^i\right) \cdot \mathbf{G}_i d\xi^i = \mathbf{F}\mathrm{d}\mathbf{R} \\
&\mathbf{F} = \mathbf{g}_i \otimes \mathbf{G}^i, \ \mathbf{F}^T\mathbf{F} = \left(\mathbf{G}^i \otimes \mathbf{g}_i\right)\left(\mathbf{g}_j \otimes \mathbf{G}^j\right) = \mathbf{g}_i \cdot \mathbf{g}_j \left(\mathbf{G}^i \otimes \mathbf{G}^j\right) = g_{ij}\left(\mathbf{G}^i \otimes \mathbf{G}^j\right) \\
&\mathbf{I} = \left(\mathbf{G}^i \otimes \mathbf{G}_i\right)\left(\mathbf{G}_j \otimes \mathbf{G}^j\right) = \mathbf{G}_i \cdot \mathbf{G}_j \left(\mathbf{G}^i \otimes \mathbf{G}^j\right) = G_{ij}\left(\mathbf{G}^i \otimes \mathbf{G}^j\right)
\end{aligned} \tag{31}$$

2.1 Equilibrium of force

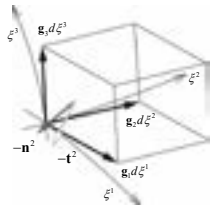

Parallel Hexahedron equilibrium

The equilibrium of force after deformation acting on a parallel hexahedron with a width of $\mathrm{d}\xi^i$ in the direction from point $\left(\xi^1_{s0}, \xi^2_{s0}, \xi^3_{s0}\right)$ to ξ^i in the object is

$$\left(\mathbf{t}^i + \frac{\partial \mathbf{t}^i}{\partial \xi^i}\mathrm{d}\xi^i\right)\mathrm{d}s_i - \mathbf{t}^i \mathrm{d}s_i + \rho \mathbf{f}\mathrm{d}v = \mathbf{0} \tag{32}$$

where $\mathbf{t}^i$: Cauchy stress vector, $\mathbf{f}$: force in unit volume, ρ : density.

・Cauchy stress tensor $\mathbf{T}$

$$T^{ij}\left(\mathbf{g}_i \otimes \mathbf{g}_j\right) \equiv \mathbf{T}, \ \mathbf{T}\mathbf{n}^i = \mathbf{t}^i \tag{33}$$

・Equilibrium equation

$$\frac{\partial \mathbf{T}}{\partial \xi^i}\mathbf{n}^i \mathrm{d}s_i \mathrm{d}\xi^i + \rho \mathbf{f}\mathrm{d}v = \mathbf{0} \tag{34}$$

2.1 Equilibrium of force

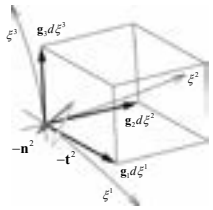

Parallel Hexahedron equilibrium

・Equilibrium equation

From the relation of the following equation

$$\mathbf{n}^i \mathrm{d}s_i \mathrm{d}\xi^i = \mathbf{g}^i \mathrm{d}v \tag{35}$$

The equilibrium equation becomes

$$\frac{\partial \mathbf{T}}{\partial \xi^i} \mathbf{g}^i \mathrm{d}v + \rho \mathbf{f} \mathrm{d}v = \mathbf{0} \tag{36}$$

Furthermore, from the following formula defining nabla,

$$\nabla \equiv \mathbf{g}^j \frac{\partial}{\partial \xi^j} \tag{37}$$

The equilibrium equation becomes

$$\left(\nabla \cdot \mathbf{T} + \rho \mathbf{f}\right) \mathrm{d}v = \mathbf{0} \tag{38}$$

2.2 Second Piola-Kirchhoff Stress

The Cauchy stress tensor represents stress in a equilibrium state after deformation.
The second Piola-Kirchhoff stress is used to express stresses with respect to the shape before deformation. Consider pulling the Cauchy stress tensor back to its before deformation state.

The pullback of $\mathbf{t}^a ds$ multiplied by the Cauchy stress vector multiplied by a infinitesimal area is

$$\mathbf{F}^{-1}\mathbf{T}\mathbf{n}\mathrm{d}s = \mathbf{S}\mathbf{N}\mathrm{d}S \tag{39}$$

The following Nanson formula is used here.

$$\mathbf{n}\mathrm{d}s = \left(\det \mathbf{F}\right)\mathbf{F}^{-\mathrm{T}}\mathbf{N}\mathrm{d}S \tag{40}$$

From equations (39) and (40), the following equation can be derived

$$\mathbf{F}^{-1}\mathbf{T}\left(\det \mathbf{F}\right)\mathbf{F}^{-\mathrm{T}}\mathbf{N}\mathrm{d}S = \mathbf{S}\mathbf{N}\mathrm{d}S \tag{41}$$

The stress tensor $\mathbf{S}$ becomes

$$\begin{aligned}\mathbf{S} &= \mathbf{F}^{-1}\mathbf{T}\left(\det \mathbf{F}\right)\mathbf{F}^{-\mathrm{T}} \\ &= \left(\det \mathbf{F}\right)T^{ij}\left(\mathbf{G}_i \otimes \mathbf{g}^i\right)\left(\mathbf{g}_i \otimes \mathbf{g}_j\right)\left(\mathbf{g}^j \otimes \mathbf{G}_j\right) = \left(\det \mathbf{F}\right)T^{ij}\left(\mathbf{g}^i \cdot \mathbf{g}_i\right)\left(\mathbf{g}_j \cdot \mathbf{g}^j\right)\left(\mathbf{G}_i \otimes \mathbf{G}_j\right) \\ &= \left(\det \mathbf{F}\right)T^{ij}\left(\mathbf{G}_i \otimes \mathbf{G}_j\right)\end{aligned} \tag{42}$$

2.2 Second Piola-Kirchhoff Stress

$\mathbf{S}$ is the second Piola-Kirchhoff stress. If the component S^{ij} of $\mathbf{S}$, we obtain the following equation.

$$\mathbf{S} = S^{ij}\left(\mathbf{G}_i \otimes \mathbf{G}_j\right) \tag{43}$$

The basis of the second Piola-Kirchhoff stress tensor shows a correspondence with the Green-Lagrange strain.

3.1 Constitutive equation of linear elastic body

From the relationship between the second Piola-Kirchhoff stress and Green-Lagrange strain components, the constitutive equation can be expressed as follows.

$$S^{ij} = C^{ijkl} E_{kl} \tag{44}$$

where the second Piola-Kirchhoff stress tensor $\mathbf{S}$ and Green-Lagrange $\mathbf{E}$ strain are expressed as

$$\mathbf{S} = S^{ij}\left(\mathbf{G}_i \otimes \mathbf{G}_j\right),\ \mathbf{E} = E_{ij}\left(\mathbf{G}^i \otimes \mathbf{G}^j\right) \tag{45}$$

The elasticity tensor is expressed as

$$\mathbf{C} = C^{ijkl}\left(\mathbf{G}_i \otimes \mathbf{G}_j \otimes \mathbf{G}_k \otimes \mathbf{G}_l\right) \tag{46}$$

The constitutive equation can be expressed as follows

$$\mathbf{S} = \mathbf{C} : \mathbf{E} \tag{47}$$

$$\begin{aligned}
\mathbf{C} : \mathbf{E} &= \left(C^{ijkl}\mathbf{G}_i \otimes \mathbf{G}_j \otimes \mathbf{G}_k \otimes \mathbf{G}_l\right) : \left(E_{mn}\mathbf{G}^m \otimes \mathbf{G}^n\right) \\
&= C^{ijkl}E_{mn}\left(\mathbf{G}_i \otimes \mathbf{G}_j \otimes \mathbf{G}_k \otimes \mathbf{G}_l\right) : \left(\mathbf{G}^m \otimes \mathbf{G}^n\right) \\
&= C^{ijkl}E_{mn}\left(\mathbf{G}_i \otimes \mathbf{G}_j\right)\left(\mathbf{G}_k \cdot \mathbf{G}^m\right)\left(\mathbf{G}_l \cdot \mathbf{G}^n\right) \\
&= C^{ijkl}E_{mn}\delta_k^m\delta_l^n\left(\mathbf{G}_i \otimes \mathbf{G}_j\right) = C^{ijkl}E_{kl}\left(\mathbf{G}_i \otimes \mathbf{G}_j\right)
\end{aligned} \tag{48}$$

3.2 Constitutive equation of linear elastic body

・Generalized Hooke's law

$$C^{ijkl} = \lambda\delta_{ij}\delta_{kl} + \mu\left(\delta_{ij}\delta_{kl} + \delta_{ik}\delta_{jl}\right) \tag{49}$$

where λ, μ are Lame constants, can be expressed using the elastic modulus E and Poisson's ratio ν as follows.

$$\begin{cases} \lambda = \dfrac{\nu E}{(1+\nu)(1-2\nu)} \\ \mu = \dfrac{E}{2(1+\nu)} \end{cases} \tag{50}$$

4.1 principle of virtual work

・Principle of virtual work

$$\int_\Omega \left(\nabla \cdot \mathbf{T} + \rho\mathbf{f}\right) \cdot \delta\mathbf{r}\,\mathrm{d}v = 0 \tag{51}$$

where $\delta\mathbf{r}$: virtual displacement, Ω : area of the object.
The following relationship exists.

$$\nabla \cdot \left(\mathbf{T}\delta\mathbf{r}\right) = \mathbf{T} : \left(\nabla \otimes \delta\mathbf{r}\right) + \left(\nabla \cdot \mathbf{T}\right) \cdot \delta\mathbf{r} \tag{52}$$

Using the above equation and Gauss' divergence theorem, the internal force work of the virtual work becomes

$$\int_\Omega \left(\nabla \cdot \mathbf{T}\right) \cdot \delta\mathbf{r}\,\mathrm{d}v = -\int_\Omega \mathbf{T} : \left(\nabla \otimes \delta\mathbf{r}\right)\mathrm{d}v + \int_\Omega \nabla \cdot \left(\mathbf{T}\delta\mathbf{r}\right)\mathrm{d}v \tag{53}$$

The principle of virtual work is as follows.

$$\begin{aligned}
&-\int_\Omega \mathbf{T} : \left(\nabla \otimes \delta\mathbf{r}\right)\mathrm{d}v + \int_\Omega \nabla \cdot \left(\mathbf{T}\delta\mathbf{r}\right)\mathrm{d}v + \int_\Omega \rho\mathbf{f} \cdot \delta\mathbf{r}\,\mathrm{d}v = 0 \\
&\Leftrightarrow \int_\Omega \mathbf{T} : \left(\nabla \otimes \delta\mathbf{r}\right)\mathrm{d}v = \int_\Omega \nabla \cdot \left(\mathbf{T}\delta\mathbf{r}\right)\mathrm{d}v + \int_\Omega \rho\mathbf{f} \cdot \delta\mathbf{r}\,\mathrm{d}v \\
&\Leftrightarrow \int_\Omega \mathbf{T} : \left(\nabla \otimes \delta\mathbf{r}\right)\mathrm{d}v = \int_\Gamma \mathbf{n} \cdot \left(\mathbf{T}\delta\mathbf{r}\right)\mathrm{d}s + \int_\Omega \rho\mathbf{f} \cdot \delta\mathbf{r}\,\mathrm{d}v
\end{aligned} \tag{54}$$

4.1 principle of virtual work

From the symmetry of $\mathbf{T}$, we obtain

$$\begin{aligned}&\mathbf{T}:(\nabla\otimes\delta\mathbf{r})=\frac{1}{2}\mathbf{T}:(\nabla\otimes\delta\mathbf{r})+\frac{1}{2}\mathbf{T}^T:(\nabla\otimes\delta\mathbf{r})^T\\&=\frac{1}{2}\mathbf{T}:(\nabla\otimes\delta\mathbf{r})+\frac{1}{2}\mathbf{T}:(\nabla\otimes\delta\mathbf{r})^T=\mathbf{T}:\frac{1}{2}\left\{\left[(\nabla\otimes\delta\mathbf{r})+(\nabla\otimes\delta\mathbf{r})^T\right]\right\}\end{aligned} \tag{55}$$

The mechanical and geometric boundary conditions are given as follows

$$\mathbf{Tn}=\bar{\mathbf{t}}\quad(\text{on }\Gamma_t),\ \mathbf{r}=\bar{\mathbf{r}}\quad(\text{on }\Gamma_x) \tag{56}$$

From the geometric boundary conditions, the following relationship holds

$$\delta\mathbf{r}=\mathbf{0}\quad(\text{on }\Gamma_x) \tag{57}$$

Based on the above, the principle of virtual work becomes

$$\int_\Omega\mathbf{T}:\left\{\frac{1}{2}\left[(\nabla\otimes\delta\mathbf{r})+(\nabla\otimes\delta\mathbf{r})^T\right]\right\}\mathrm{d}v=\int_{\Gamma_t}\bar{\mathbf{t}}\cdot\delta\mathbf{r}\,\mathrm{d}s+\int_\Omega\rho\mathbf{f}\cdot\delta\mathbf{r}\,\mathrm{d}v \tag{58}$$

4.2 Pulling back the principle of virtual work

Next, we derive the principle of virtual work in a microvolume before deformation.
The surface force vector $\bar{\mathbf{t}}\mathrm{d}s$ in a infinitesimal can be expressed as

$$\bar{\mathbf{t}}\mathrm{d}s=\mathbf{T}\mathbf{n}\mathrm{d}s=\mathbf{T}(\det\mathbf{F})\mathbf{F}^{-T}\mathbf{N}\mathrm{d}S=\frac{1}{\det\mathbf{F}}\mathbf{FSF}^T(\det\mathbf{F})\mathbf{F}^{-T}\mathbf{N}\mathrm{d}S=\mathbf{FSN}\mathrm{d}S \tag{59}$$

From the law of conservation of mass before and after deformation, density ρ satisfies the following relation with density ρ_0 before deformation.

$$\rho\mathrm{d}v=\rho_0\mathrm{d}V \tag{60}$$

As the interior region Ω_0 and boundary region Γ_{0t},Γ_{0x} before deformation, the mechanical and geometric boundary conditions can be expressed as follows

$$\begin{aligned}&\mathbf{FSN}=\tilde{\mathbf{t}}\quad(\text{on }\Gamma_{0t})\\&\mathbf{r}=\bar{\mathbf{r}}\quad(\text{on }\Gamma_{0x})\end{aligned} \tag{61}$$

4.2 Pulling back the principle of virtual work

Based on the above, the principle of virtual work becomes.

$$\int_\Omega\mathbf{T}:\left\{\frac{1}{2}\left[(\nabla\otimes\delta\mathbf{r})+(\nabla\otimes\delta\mathbf{r})^T\right]\right\}\mathrm{d}v=\int_{\Gamma_{0t}}\tilde{\mathbf{t}}\cdot\delta\mathbf{r}\,\mathrm{d}S+\int_{\Omega_0}\rho_0\mathbf{f}\cdot\delta\mathbf{r}\,\mathrm{d}V \tag{62}$$

The internal force work on the left side can be expressed as

$$\begin{aligned}&\mathbf{T}:\left\{\frac{1}{2}\left[(\nabla\otimes\delta\mathbf{r})+(\nabla\otimes\delta\mathbf{r})^T\right]\right\}\mathrm{d}v\\&=\left(\frac{1}{\det\mathbf{F}}\mathbf{FSF}^T\right):\left\{\frac{1}{2}\left[\left(\mathbf{g}^i\frac{\partial}{\partial\xi^i}\otimes\delta\mathbf{r}\right)+\left(\delta\mathbf{r}\otimes\mathbf{g}^i\frac{\partial}{\partial\xi^i}\right)\right]\right\}(\det\mathbf{F})\mathrm{d}V\\&=\left(\frac{1}{\det\mathbf{F}}\mathbf{FSF}^T\right):\left\{\frac{1}{2}\left[\left(\mathbf{g}^i\otimes\frac{\partial\delta\mathbf{r}}{\partial\xi^i}\right)+\left(\frac{\partial\delta\mathbf{r}}{\partial\xi^i}\otimes\mathbf{g}^i\right)\right]\right\}(\det\mathbf{F})\mathrm{d}V\\&=\left(\frac{1}{\det\mathbf{F}}\mathbf{FSF}^T\right):\left\{\frac{1}{2}\left[\left(\mathbf{g}^i\otimes\delta\mathbf{g}_i\right)+\left(\delta\mathbf{g}_i\otimes\mathbf{g}^i\right)\right]\right\}(\det\mathbf{F})\mathrm{d}V\\&=\left(\mathbf{FSF}^T\right):\left\{\frac{1}{2}\left[\left(\mathbf{g}^i\otimes\delta\mathbf{g}_i\right)+\left(\delta\mathbf{g}_i\otimes\mathbf{g}^i\right)\right]\right\}\mathrm{d}V\end{aligned} \tag{63}$$

4.2 Pulling back the principle of virtual work

Transform the term $\left[\left(\mathbf{g}^i\otimes\delta\mathbf{g}_i\right)+\left(\delta\mathbf{g}_i\otimes\mathbf{g}^i\right)\right]$.

$$\begin{aligned}
&\frac{1}{2}\left[\left(\mathbf{g}^i\otimes\delta\mathbf{g}_i\right)+\left(\delta\mathbf{g}_i\otimes\mathbf{g}^i\right)\right]\\
&=\frac{1}{2}\left[\left(\mathbf{g}^k\otimes\mathbf{g}_k\right)\left(\mathbf{g}^i\otimes\delta\mathbf{g}_i\right)\left(\mathbf{g}_l\otimes\mathbf{g}^l\right)+\left(\mathbf{g}^i\otimes\mathbf{g}_i\right)\left(\delta\mathbf{g}_l\otimes\mathbf{g}^l\right)\left(\mathbf{g}_k\otimes\mathbf{g}^k\right)\right]\\
&=\frac{1}{2}\left[\delta_k^i\left(\delta\mathbf{g}_i\cdot\mathbf{g}_l\right)\left(\mathbf{g}^k\otimes\mathbf{g}^l\right)+\left(\mathbf{g}_i\cdot\delta\mathbf{g}_l\right)\delta_k^i\left(\mathbf{g}^l\otimes\mathbf{g}^k\right)\right]\\
&=\frac{1}{2}\left[\left(\delta\mathbf{g}_i\cdot\mathbf{g}_l\right)\left(\mathbf{g}^i\otimes\mathbf{g}^l\right)+\left(\mathbf{g}_l\cdot\delta\mathbf{g}_i\right)\left(\mathbf{g}^l\otimes\mathbf{g}^i\right)\right]\\
&=\frac{1}{2}\left[\left(\delta\mathbf{g}_i\cdot\mathbf{g}_j\right)\left(\mathbf{g}^i\otimes\mathbf{g}^j\right)+\left(\mathbf{g}_j\cdot\delta\mathbf{g}_i\right)\left(\mathbf{g}^j\otimes\mathbf{g}^i\right)\right]\\
&=\frac{1}{2}\left[\left(\delta\mathbf{g}_i\cdot\mathbf{g}_j\right)\left(\mathbf{g}^i\otimes\mathbf{g}^j\right)+\left(\mathbf{g}_i\cdot\delta\mathbf{g}_j\right)\left(\mathbf{g}^i\otimes\mathbf{g}^j\right)\right]=\frac{1}{2}\left(\delta\mathbf{g}_i\cdot\mathbf{g}_j+\mathbf{g}_i\cdot\delta\mathbf{g}_j\right)\left(\mathbf{g}^i\otimes\mathbf{g}^j\right)
\end{aligned}\tag{64}$$

Here, the following relationship is used

$$\left(\mathbf{g}^i\otimes\mathbf{g}_i\right)\left(\mathbf{g}_j\otimes\mathbf{g}^j\right)=\mathbf{g}_i\cdot\mathbf{g}_j\left(\mathbf{g}^i\otimes\mathbf{g}^j\right)=\mathbf{I}\tag{65}$$

4.2 Pulling back the principle of virtual work

It can be expressed as a deformation gradient tensor $\mathbf{F}^T=\mathbf{G}^i\otimes\mathbf{g}_i,\mathbf{F}=\mathbf{g}_i\otimes\mathbf{G}^i$, and the internal force work can be expressed as

$$\begin{aligned}
&\mathbf{T}:\left\{\frac{1}{2}\left[\left(\nabla\otimes\delta\mathbf{r}\right)+\left(\nabla\otimes\delta\mathbf{r}\right)^T\right]\right\}\mathrm{d}v\\
&=\left(\mathbf{FSF}^T\right):\left[\frac{1}{2}\left(\delta\mathbf{g}_i\cdot\mathbf{g}_j+\mathbf{g}_i\cdot\delta\mathbf{g}_j\right)\left(\mathbf{g}^i\otimes\mathbf{g}^j\right)\right]\mathrm{d}V\\
&=\mathbf{S}:\mathbf{F}^T\left[\frac{1}{2}\left(\delta\mathbf{g}_i\cdot\mathbf{g}_j+\mathbf{g}_i\cdot\delta\mathbf{g}_j\right)\left(\mathbf{g}^i\otimes\mathbf{g}^j\right)\right]\mathbf{F}\mathrm{d}V\\
&=\mathbf{S}:\left[\frac{1}{2}\left(\delta\mathbf{g}_i\cdot\mathbf{g}_j+\mathbf{g}_i\cdot\delta\mathbf{g}_j\right)\left(\mathbf{G}^i\otimes\mathbf{g}_i\right)\left(\mathbf{g}^i\otimes\mathbf{g}^j\right)\left(\mathbf{g}_j\otimes\mathbf{G}^j\right)\right]\mathrm{d}V\\
&=\mathbf{S}:\left[\frac{1}{2}\left(\delta\mathbf{g}_i\cdot\mathbf{g}_j+\mathbf{g}_i\cdot\delta\mathbf{g}_j\right)\left(\mathbf{G}^i\otimes\mathbf{G}^j\right)\right]\mathrm{d}V\\
&=\mathbf{S}:\left[\frac{1}{2}\delta\left(\mathbf{g}_i\cdot\mathbf{g}_j\right)\left(\mathbf{G}^i\otimes\mathbf{G}^j\right)\right]\mathrm{d}V
\end{aligned}\tag{68}$$

4.2 Pulling back the principle of virtual work

Here, from the definition of Green-Lagrange strain, the internal force work can be expressed as follows

$$\begin{aligned}
&E_{ij}=\frac{1}{2}\left(\mathbf{g}_i\cdot\mathbf{g}_j-\mathbf{G}_i\cdot\mathbf{G}_j\right)=\frac{1}{2}\left(\mathbf{g}_i\cdot\mathbf{g}_j-(\text{constant})\right),\\
&\mathbf{S}:\left[\frac{1}{2}\delta\left(\mathbf{g}_i\cdot\mathbf{g}_j\right)\left(\mathbf{G}^i\otimes\mathbf{G}^j\right)\right]\mathrm{d}V\\
&=\mathbf{S}:\left[\delta E_{ij}\left(\mathbf{G}^i\otimes\mathbf{G}^j\right)\right]\mathrm{d}V=\mathbf{S}:\delta\mathbf{E}\mathrm{d}V
\end{aligned}\tag{69}$$

From the above, the principle of virtual work in a small volume before deformation becomes

$$\int_{\Omega_0}\mathbf{S}:\delta\mathbf{E}\mathrm{d}V=\int_{\Gamma_{\sigma_0}}\tilde{\mathbf{t}}\cdot\delta\mathbf{r}\,\mathrm{d}S+\int_{\Omega_0}\rho_0\mathbf{f}\cdot\delta\mathbf{r}\,\mathrm{d}V\tag{70}$$

where a: virtual strain tensor. From the above equation deformation, we obtain from the balancing equation expressed in terms of the Cauchy stress tensor referring to after deformation, the second Piola-Kirchhoff stress tensor referring to before deformation, and the virtual work principle expressed in terms of Green-Lagrange strain.

4.2 Pulling back the principle of virtual work

Next, consider pulling back the equilibrium equation to the before deformation state using the virtual displacement $\delta\mathbf{u}$. However, instead of the Cauchy stress, the first Piola-Kirchhoff stress tensor is given by $\mathbf{\Pi}$. $\mathbf{\Pi}$ is the stress tensor, which represents the force acting on the face element after deformation as a stress vector translated before deformation and not including rotation.

$$\mathbf{\Pi} = \det(\mathbf{F})\mathbf{F}^{-1}\mathbf{T} = \mathbf{S}\mathbf{F}^{T} \tag{71}$$

$\mathbf{\Pi}$ is not a symmetric tensor. Therefore, from Eq. (55),

$$\begin{aligned}
&\left(\frac{1}{\det\mathbf{F}}\mathbf{\Pi}\right)^{T} : (\nabla \otimes \delta\mathbf{u})\mathrm{d}v \\
&= \mathbf{\Pi}^{T} : (\nabla \otimes \delta\mathbf{u})\mathrm{d}V = \left(\mathbf{S}\mathbf{F}^{T}\right)^{T} : \delta\mathbf{Z}\mathrm{d}V = \left(\mathbf{S}\mathbf{F}^{T}\right)^{T} : \delta\mathbf{F}\mathrm{d}V \\
&= \mathbf{S}^{T} : \mathbf{F}^{T}\delta\mathbf{F}\mathrm{d}V = \mathbf{S} : \mathbf{F}^{T}\delta\mathbf{F}\mathrm{d}V = \mathbf{S} : \delta\left(\frac{1}{2}\mathbf{F}^{T}\mathbf{F}\right)\mathrm{d}V \\
&= \mathbf{S} : \delta\mathbf{E}\mathrm{d}V
\end{aligned} \tag{72}$$

4.2 Pulling back the principle of virtual work

Following the strict formulation, $\delta\mathbf{r}$ obtain the clearer result.
The total Lagrange method with the reference configuration as the initial configuration is suitable for case $\delta\mathbf{r}$, and the updated Lagrange method with the reference configuration as the current configuration is suitable for case $\delta\mathbf{u}$.

5 References

1) Miyazaki, Y., An introduction Gossamer multi-body dynamics (in Japanese) https://stage.tksc.jaxa.jp/taurus/member/miyazaki/old/lecture/GMD.pdf
2) Yasuhisa Noguchi, Toshiaki Hisada, Fundamentals and Applications of Nonlinear Finite Element Methods, Matuzen, 1995 (in Japanese)
3) Green, A.E., W,Zerna, Theoretical Elasticity, 1968

Piecewise constant mean curvature surfaces

Kazuki Hayashi (Kyoto University)
Yoshiki Jikumaru (Toyo University)
Makoto Ohsaki (Kyoto University)
Takashi Kagaya (Muroran Institute of Technology)
Yohei Yokosuka (Kagoshima University)

Kazuki Hayashi, Yoshiki Jikumaru, Makoto Ohsaki, Takashi Kagaya, Yohei Yokosuka (2023) Mean curvature flow for generating discrete surfaces with piecewise constant mean curvatures, *Computer Aided Geometric Design*, Volume 101, No. 102169.

Mean curvature flow

- Move vertex positions using mean curvature and normal vector

$$\nabla \mathbf{p}_i = -(H_i - \bar{H})\vec{\mathbf{n}}_i$$

$\nabla \mathbf{p}_i$: Change in the location of node i

H_i : Mean curvature at node i

$\bar{H}$: Target mean curvature

$\vec{\mathbf{n}}_i$: Unit normal vector at node i

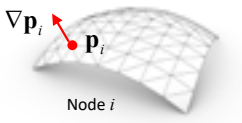

- The stationary point of mean curvature flow has a constant mean curvature (CMC) $\bar{H}$ at each vertex

Can we benefit from constant mean curvatures?

- Bezier, NURBs, T-spline etc. (params.: control net)

We can create almost any surface (≠ feasible as structural design)

↕

- Mean curvature flow (params.: target mean curvatures)

→ satisfy equilibrium condition for pressure load

Hayashi et al. "Mean curvature flow for generating discrete surfaces with piecewise constant mean curvatures", *Computer Aided Geometric Design*, 2023. 4

CMC with internal boundary

- The resulting surfaces are too simple when mean curvature flow is applied to a single closed surface
- By allowing G0 continuous internal boundaries, various shapes can be generated

Double bubble

Shintoyosu Brillia Running Stadium, Japan

⇒Derive curvature flow to obtain piecewise CMC (p-CMC) surfaces based on the variational principle

Variational problem (continuous case)

- Define a plane P and two patches M_1 and M_2
- Define another plane M_3 bounded by P and patch intersection
- Determine surface transformation from the variation of energy functional E

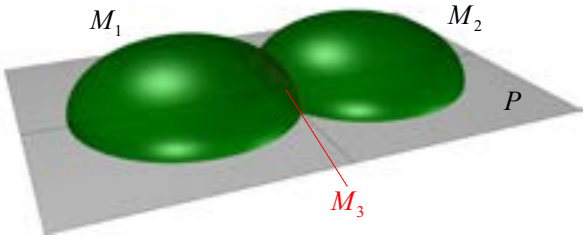

Volume of enclosed domain (positive in concave direction)

$$E = V(M_1, M_2, P) + \sum_{i=1}^{3} \alpha_i A(M_i)$$

Area

Arbitrary value

Stationary condition

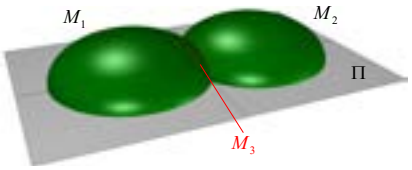

arbitrary value, area, volume

$$E = \sum_{i=1}^{3} \alpha_i A(M_i) - V(M_1, M_2, \Pi)$$

velocity vector, outer pointing unit normal vector

$$\delta E = \sum_{i=1}^{2} \int_{M_i} \mathbf{v} \cdot (1 + 2\alpha_i H_i)\mathbf{v}_i dA$$

$$- \int_{M_3} \mathbf{v} \cdot (2\alpha_3 H_3)\mathbf{v}_3 dA$$

co-normal vector on the intersection

$$+ \int_{\partial M_1 \cap \partial M_2 \cap \partial M_3} \mathbf{v} \cdot \sum_{i=1}^{3} (\alpha_i \mathbf{n}_i)\, ds$$

$$+ \int_{\partial M_3 \cap P} \mathbf{v} \cdot (\alpha_3 \mathbf{n}_3)\, ds$$

stationary condition $(\delta E = 0)$

$$H_1 = \frac{-1}{2\alpha_1} \text{ on } M_1, \quad H_2 = \frac{-1}{2\alpha_2} \text{ on } M_2$$

$$H_3 = 0 \text{ on } M_3$$

$$\sum_{i=1}^{3} \alpha_i \mathbf{n}_i = 0 \text{ on } \partial M_1 \cap \partial M_2 \cap \partial M_3$$

$$\mathbf{t}_3 \perp P \text{ on } \partial M_3 \cap P$$

Obtained variation of E and its stationary point

Stationary condition

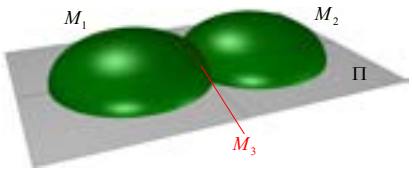

$$E = \overbrace{V(M_1, M_2, \Pi)}^{\text{volume}} + \sum_{i=1}^{3} \overbrace{\alpha_i}^{\text{arbitrary value}} \overbrace{A(M_i)}^{\text{area}}$$

stationary condition $(\delta E = 0)$

$$H_1 = \frac{-1}{2\alpha_1} \text{ on } M_1, \quad H_2 = \frac{-1}{2\alpha_2} \text{ on } M_2$$

$$H_3 = 0 \text{ on } M_3$$

$$\sum_{i=1}^{3} \alpha_i \mathbf{n}_i = 0 \text{ on } \partial M_1 \cap \partial M_2 \cap \partial M_3$$

$$\mathbf{t}_3 \perp P \text{ on } \partial M_3 \cap P$$

→

Shape at the stationary point is

- M_1 has a constant MC $-1/(2\alpha_1)$
- M_2 has a constant MC $-1/(2\alpha_2)$
- M_3 has zero MC
- $\frac{\sin\theta_1}{\alpha_1} = \frac{\sin\theta_2}{\alpha_2} = \frac{\sin\theta_3}{\alpha_3}$

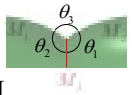

- M_3 is orthogonal Π

The solution that satisfies the above uniquely exists
= Mean curvature flow is stable

8

Discretization of energy

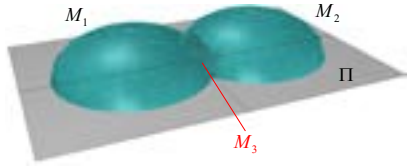

$$E = \overbrace{V(M_1, M_2, \Pi)}^{\text{volume}} + \sum_{i=1}^{3} \alpha_i \overbrace{A(M_i)}^{\text{area}}$$

discretize ↓

$$E_{\mathrm{d}} = \sum_{T(\mathbf{p},\mathbf{q},\mathbf{r}) \in M_1 \cup M_2} \frac{1}{6} \langle \mathbf{p}, \mathbf{q} \times \mathbf{r} \rangle + \sum_{i=1}^{3} \alpha_i \sum_{T(\mathbf{p},\mathbf{q},\mathbf{r}) \in M_i} \frac{1}{2} \left\| (\mathbf{q}-\mathbf{p}) \times (\mathbf{r}-\mathbf{p}) \right\|$$

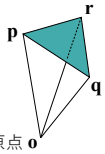

cone volume

$$\frac{1}{2} \cdot \frac{1}{3} \langle \mathbf{p}, (\mathbf{q}-\mathbf{p}) \times (\mathbf{r}-\mathbf{p}) \rangle$$

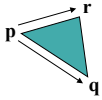

The norm of the outer product of two vectors = 2 × (area)

→ Discrete version of mean curvature flow can be obtained

9

Discretization of energy variation

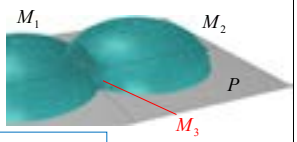

$$E_{\mathrm{d}} = -\sum_{T(\mathbf{p},\mathbf{q},\mathbf{r}) \in M_1 \cup M_2} \frac{1}{6} \langle \mathbf{p}, \mathbf{q} \times \mathbf{r} \rangle + \sum_{i=1}^{3} \alpha_i \sum_{T(\mathbf{p},\mathbf{q},\mathbf{r}) \in M_i} \frac{1}{2} \left\| (\mathbf{q}-\mathbf{p}) \times (\mathbf{r}-\mathbf{p}) \right\|$$

$$\delta E_{\mathrm{d}} = \sum_{p} \langle \nabla E(p), \mathbf{n}_p \rangle$$

If node p is inside mesh M_1

Denoted as **J**

$$\nabla E_{\mathrm{d}}(p) = \sum_{j=1}^{n_p} \left(-\frac{1}{6} \mathbf{q}_j \times \mathbf{q}_{j+1} + \frac{\alpha_1}{2} \frac{(\mathbf{q}_j - \mathbf{p}) \times (\mathbf{q}_{j+1} - \mathbf{p})}{\left\| (\mathbf{q}_j - \mathbf{p}) \times (\mathbf{q}_{j+1} - \mathbf{p}) \right\|} \times (\mathbf{q}_{j+1} - \mathbf{q}_j) \right)$$

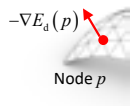

10

How to move the nodes?

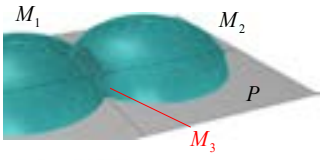

If node p is inside mesh M_1:

$$\nabla E(p)=\sum_{j=1}^{n_p}\left(-\frac{1}{6}\mathbf{q}_j\times\mathbf{q}_{j+1}+\frac{\alpha_1}{2}\mathbf{J}\times\left(\mathbf{q}_{j+1}-\mathbf{q}_j\right)\right)$$

If node p is inside mesh M_2:

$$\nabla E(p)=\sum_{j=1}^{n_p}\left(-\frac{1}{6}\mathbf{q}_j\times\mathbf{q}_{j+1}+\frac{\alpha_2}{2}\mathbf{J}\times\left(\mathbf{q}_{j+1}-\mathbf{q}_j\right)\right)$$

If node p is inside mesh M_3:

$$\nabla E(p)=\sum_{j=1}^{n_p}\left(\frac{\alpha_3}{2}\mathbf{J}\times\left(\mathbf{q}_{j+1}-\mathbf{q}_j\right)\right)$$

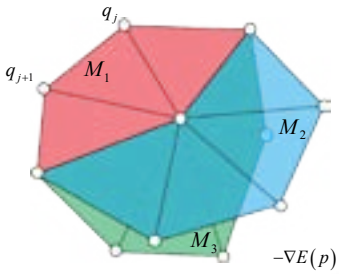

If node p is on $M_1 \cap M_2 \cap M_3$:

$$\nabla E(p)=\sum_{i=1}^{2}\sum_{j=1}^{n_{p,M_i}}\left(-\frac{1}{6}\mathbf{q}_j\times\mathbf{q}_{j+1}+\frac{\alpha_1}{2}\mathbf{J}\times\left(\mathbf{q}_{j+1}-\mathbf{q}_j\right)\right)+\sum_{j=1}^{n_{p,M_3}}\left(\frac{\alpha_3}{2}\mathbf{J}\times\left(\mathbf{q}_{j+1}-\mathbf{q}_j\right)\right)$$

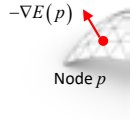

11

Example

Structurally preferable shapes can be obtained through pure mathematic techniques

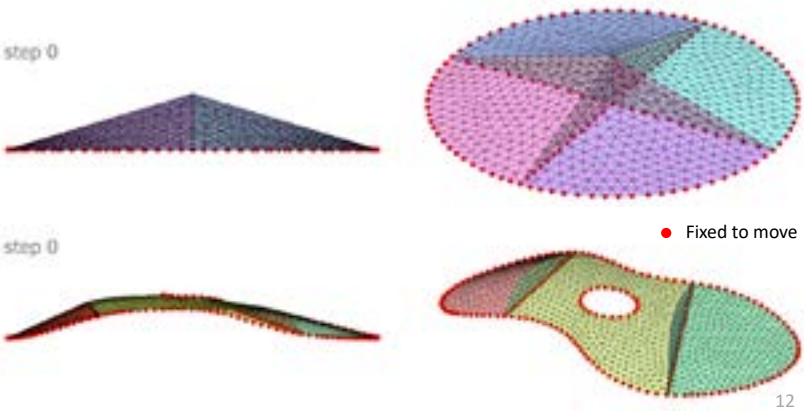

12

Example

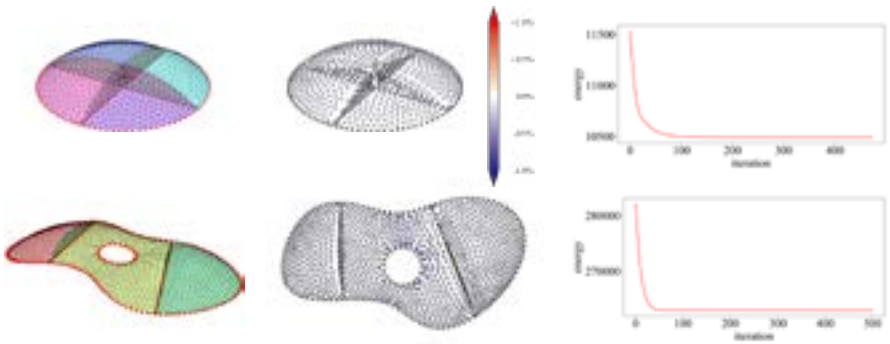

Final geometry
➡ Piecewise smooth

Error to the target mean curvature
➡ Precisely approximate the target shape

Energy functional history
➡ Good convergence

13

Example

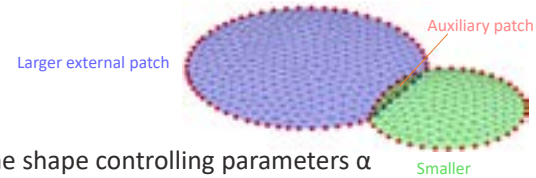

- Convergence depends on the shape controlling parameters α

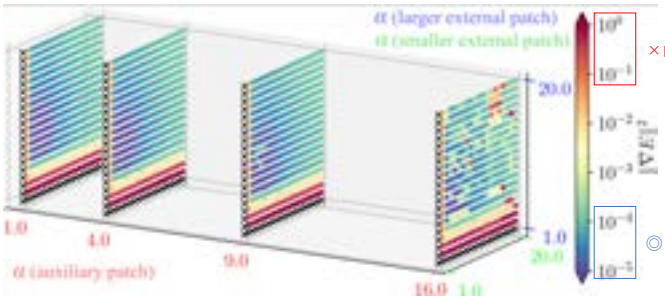

14

Conclusion

- Formulated mean curvature flow for meshes with internal boundaries
- Parametrically generated various piecewise CMC discrete surfaces
- Convergence property depends on the boundary condition
- Transformation behavior depends on hyperparameters

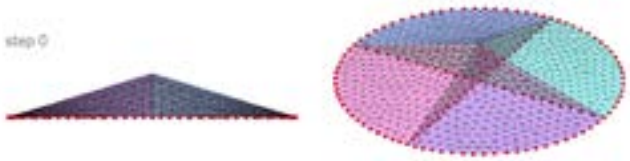

Kazuki Hayashi, Yoshiki Jikumaru, Makoto Ohsaki, Takashi Kagaya, Yohei Yokosuka (2023) Mean curvature flow for generating discrete surfaces with piecewise constant mean curvatures, *Computer Aided Geometric Design*, Volume 101, No. 102169. 15

Evolving Design and Discrete Differential Geometry
- towards Mathematics Aided Geometric Design

Form Generation of Rigid Origami for Approximating a Curved Surface

Kentaro Hayakawa

Kyoto Group, Nihon University

*Joint work with M. Ohsaki
@ Kyoto Univeristy

Previous Studies

Generalization of typical crease patterns

Dudte et al. 2016, Tachi 2013, Zhao et al. 2018

Large DOFs of mechanism in many examples

Low approximation accuracy in sparse crease patterns

Dudte et al. 2016

Zhao et al. 2018

⇒ Design flexibility: High, Constructability: Low

Rigid foldable quadrilateral mesh

Tachi 2010, He and Guest 2020

Rigid foldability for general quad mesh（Tachi 2009）

Single DOF mechanism

⇒ Design flexibility: Low, Constructability: High

He and Guest. 2020

Purpose

Surface approximation by developable rigid origami with small DOF

Approximation error function reflecting appearance of origami surface

Use of an arbitrary initial crease pattern (not depend on typical crease patterns)

Small degrees of freedom of mechanism for controllability of folding motion obtained by sequentially removing (fixing) crease lines

Selection criterion of fixed crease lines reflecting shape and folding mechanism to avoid undesirable locking phenomenon

2025/3/13 4

Origami Surface as a Triangular Mesh

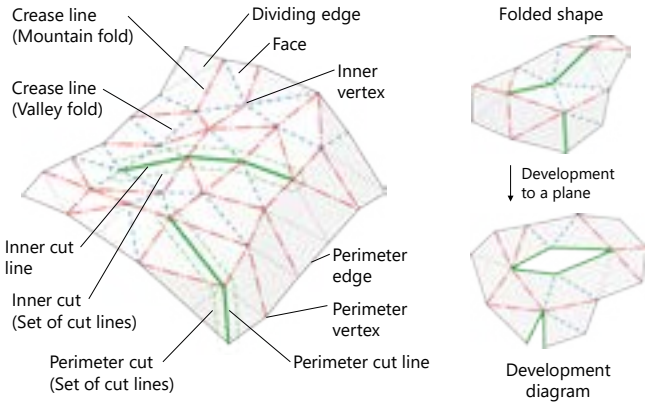

2025/3/13 5

Overview of Form Generation Procedure

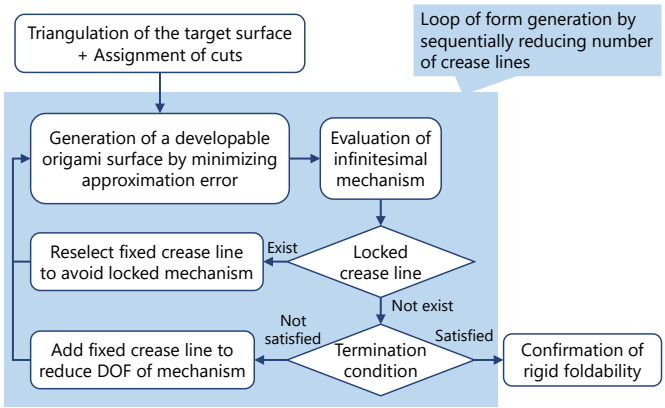

2025/3/13 6

Developability Conditions

Gaussian curvature at a vertex not on a cutting lines

$$\kappa_v = 2\pi - \sum_{i=1}^{n_v^{\text{edge}}} \theta_{i,v} = 0$$

κ_v: Gaussian curvature at vertex v

$\theta_{i,v}$: angle between adjacent edges

n_v^{edge}: number of edges around vertex v

Normal vectors of a pair of faces adjacent to a dividing edge

$$\left\| \mathbf{v}_{f_1} \times \mathbf{v}_{f_2} \right\| = 0$$

$\mathbf{v}_{f_1}$, $\mathbf{v}_{f_2}$: unit normal vectors of faces f_1 and f_2

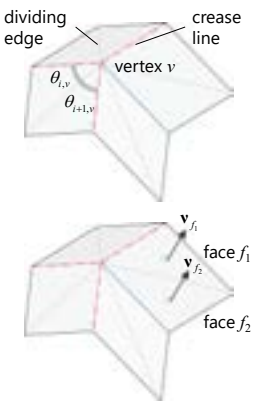

Developability Conditions

Direction vector of the edge going round a cutting line

$$\mathbf{u}_{c,i+1} = \mathbf{R}(\varphi_{c,i} - \pi)\mathbf{u}_{c,i}$$

$$\downarrow \longleftarrow \mathbf{u}_{c,2n_c^{\mathrm{cut}}+1} = \mathbf{u}_{c,1}$$

$$\sum_{v \in V_c^{\mathrm{cut}}} \kappa_v = 2(1-k)\pi$$

$\mathbf{u}_{c,i}$: direction vector of edge i
$\varphi_{c,i}$: rotation angle between edge i and i+1
$\mathbf{R}(\theta)$: rotation matrix about angle θ
n_c^{cut}: number of edges of cutting line c
V_c^{cut}: set of vertices on cutting line c

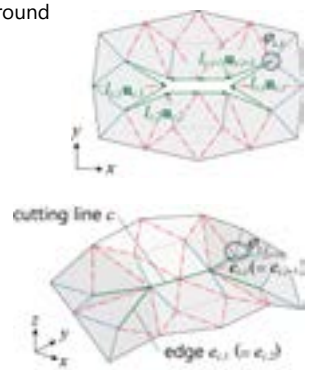

Developability Conditions

Closed loop of cutting lines on the development diagram

$$\sum_{i=1}^{2n_c^{\mathrm{cut}}} l_{c,i}\mathbf{u}_{c,i} = \mathbf{0}$$

$$\downarrow$$

$$\begin{cases} l_{c,1} + \sum_{i=1}^{2n_c^{\mathrm{cut}}-1} (-1)^i l_{c,i+1} \cos\left(\sum_{j=1}^{i} \varphi_{c,j}\right) = 0 \\ \sum_{i=1}^{2n_c^{\mathrm{cut}}-1} (-1)^i l_{c,i+1} \sin\left(\sum_{j=1}^{i} \varphi_{c,j}\right) = 0 \end{cases}$$

$l_{c,i}$: length of edge i

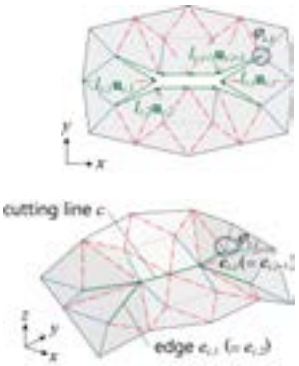

Definition of Design Variables

Target surface: **Bézier surface**.

Parameters representing the position of vertex v :
Bézier parameters ξ_v, ψ_v that define a point on the surface
Offset distance ζ_v in the direction normal to the Bézier surface.

$$\underbrace{\mathbf{r}(\xi_v,\psi_v,\zeta_v)}_{\text{vertex } v} = \underbrace{\overline{\mathbf{r}}(\xi_v,\psi_v)}_{\substack{\text{point on} \\ \text{Bézier surface}}} + \underbrace{\zeta_v \overline{\mathbf{v}}(\xi_v,\psi_v)}_{\text{offset}}$$

$\mathbf{r}(\xi_v,\psi_v,\zeta_v)$: position vector of vertex v
$\overline{\mathbf{r}}(\xi_v,\psi_v)$: position vector of the point on the target surface
$\overline{\mathbf{v}}(\xi_v,\psi_v)$: unit normal vector at point $\overline{\mathbf{r}}(\xi_v,\psi_v)$

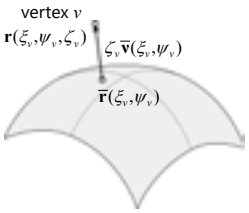

Definition of Approximation Error Function

Distance between vertices and target surface

$$G_{\mathrm{D}} = \frac{1}{2}\sum_{v\in V}\zeta_v^2$$

Surface area

$$G_{\mathrm{A}} = \left|A - \bar{A}\right|$$

Unit normal vectors of faces and target surface

$$G_{\mathrm{N}} = \sum_{f\in F}\left\|\mathbf{v}_f - \bar{\mathbf{v}}_f^{\mathrm{ref}}\right\|^2$$

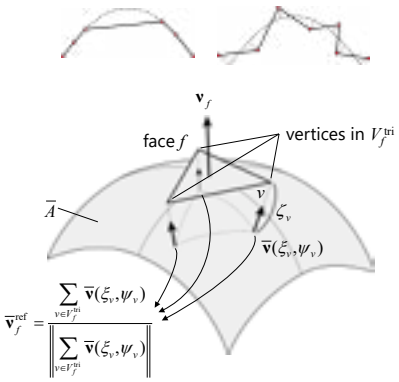

Optimization Problem for Form Generation

$$\min_{\mathbf{X}}\ G(\mathbf{X}) = G_{\mathrm{D}}(\mathbf{X}) + w_{\mathrm{A}}G_{\mathrm{A}}(\mathbf{X}) + w_{\mathrm{N}}G_{\mathrm{N}}(\mathbf{X})$$

s.t. Developability conditions

$$\kappa_v = 0$$
$$\left\|\mathbf{v}_{f_1}\times\mathbf{v}_{f_2}\right\| = 0$$
$$\sum_{v\in V_c^{\mathrm{cut}}}\kappa_v = 0$$
$$l_{c,1} + \sum_{i=1}^{2n_c^{\mathrm{cut}}-1}(-1)^i l_{c,i+1}\cos\left(\sum_{j=1}^{i}\varphi_{c,j}\right) = 0$$
$$\sum_{i=1}^{2n_c^{\mathrm{cut}}-1}(-1)^i l_{c,i+1}\sin\left(\sum_{j=1}^{i}\varphi_{c,j}\right) = 0$$

$l_e(\mathbf{X}) \geq l_{\min}$
: lower bounds of edge length

$\theta_{\min} \leq \theta_{v,i}(\mathbf{X}) \leq \theta_{\max}$
: bounds of inner angles

$\mathbf{v}_f(\mathbf{X})\cdot\bar{\mathbf{v}}_f^{\mathrm{ref}}(\mathbf{X}) \geq 0$
: avoidance of face flipping

$\mathbf{X}\in\chi$: bounds of design variables

$\mathbf{X}$: parameters for determining the positions of the vertices of the rigid origami

Overview of Form Generation Procedure

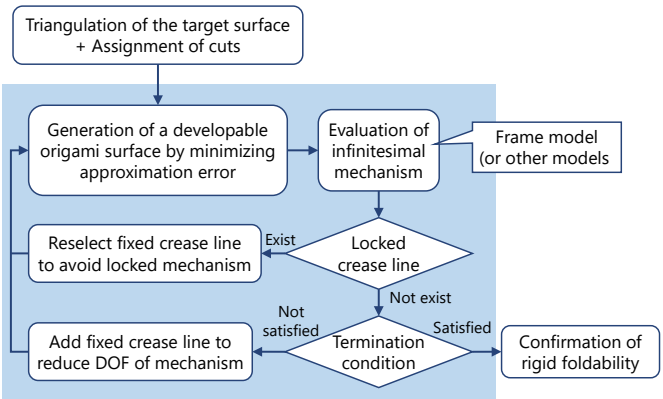

Selection Criterion of Fixed Crease lines

Folding angle criterion

Fix a crease line with small folding angle
⇒ Small shape difference

$$\sigma_h^{\mathrm{S}} = \frac{\rho_h}{\sum_{j=1}^{N_{\mathrm{H}}} \rho_j} \quad \leftarrow \text{The smaller the better}$$

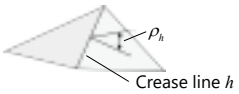

Infinitesimal mechanism criterion

Fix a crease line with a large rotation in the infinitesimal mechanism
⇒ Small possibility of locking phenomenon

$$\sigma_h^{\mathrm{F}} = \frac{\max_i \left(\phi_{ih}^2\right)}{\sum_{j=1}^{N_{\mathrm{H}}} \max_i \left(\phi_{ij}^2\right)} \quad \leftarrow \text{The larger the better}$$

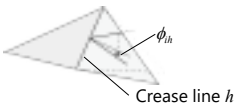

Selection Criterion of Fixed Crease lines

Mixed Criterion

Fix one or several crease lines with smallest scores

$$\sigma_h = \frac{\sigma_h^{\mathrm{S}}}{\sigma_h^{\mathrm{F}}} = \frac{(\text{Shape criterion})}{(\text{Mechanism criterion})}$$

- Small shape difference
- Small possibility of locking phenomenon

⇒ High possibility of successful termination in the succeeding optimization step without locked crease lines

⇒ Reduction in the number of times to solve optimization problems

Examples of HP Surface

Design variables are selected so that the symmetry of the surface is preserved.

Optimization parameters are set as:

$w_{\mathrm{A}} = 0.2$, $w_{\mathrm{N}} = 1.0$

$l_{\min} = 1.0$, $\theta_{\min} = \pi/6$, $\theta_{\max} = 5\pi/6$, $-5 \le \zeta_v \le 5$

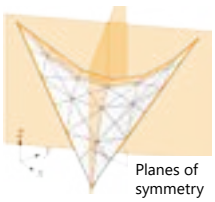
Planes of symmetry

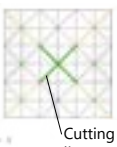

Pattern X

Pattern E

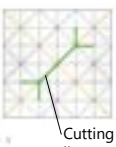

Pattern H

2025/3/13 16

Examples of HP Surface

Without cut

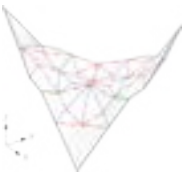

Pattern E

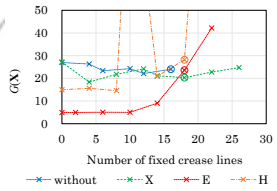

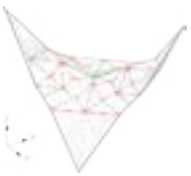

Pattern X

Pattern H

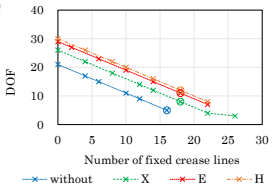

2025/3/13 17

Examples of HP Surface

Fixed crease lines: 16, DOF: **5**, $G(\mathbf{X})$ = 24.0

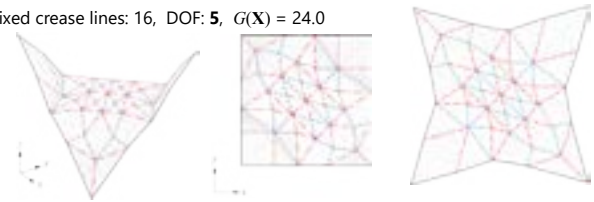

Fixed crease lines: 18, DOF: 8, $G(\mathbf{X})$ = **20.3**

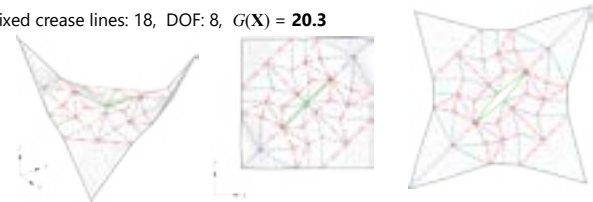

2025/3/13 18

Examples of HP Surface

Fixed crease lines: 18, DOF: 11, $G(\mathbf{X})$ = 23.6

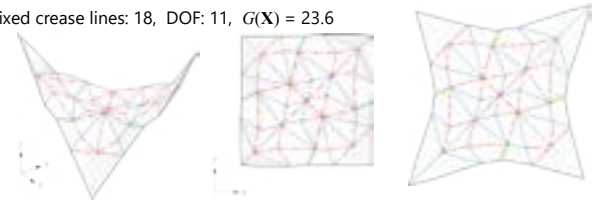

Fixed crease lines: 18, DOF: 12, $G(\mathbf{X})$ = **28.2**

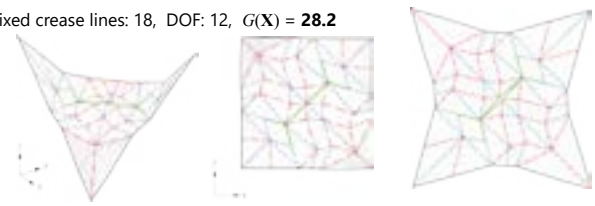

Examples of Dome Surface

Design variables are selected so that the symmetry of the surface is preserved.

Optimization parameters are set as:

$w_A = 0.2,\ \ w_N = 1.0$

$l_{min} = 1.0,\ \theta_{min} = \pi/6,\ \theta_{max} = 5\pi/6,\ -7.5 \le \zeta_v \le 7.5$

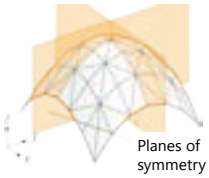

Planes of symmetry

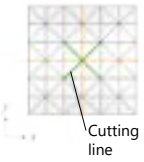

Pattern X

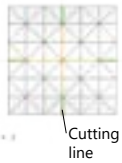

Pattern E

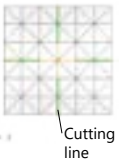

Pattern EE

Examples of Dome Surface

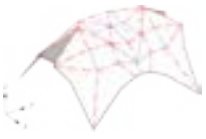

Without cut

Pattern E

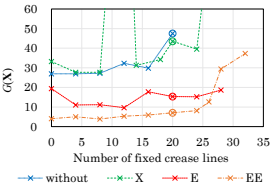

Pattern X

Pattern EE

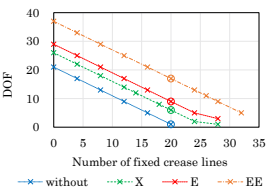

Examples of Dome Surface

Fixed crease lines: 20, DOF: **1**, $G(\mathbf{X}) = 47.5$

Fixed crease lines: 20, DOF: 6, $G(\mathbf{X}) = 43.5$

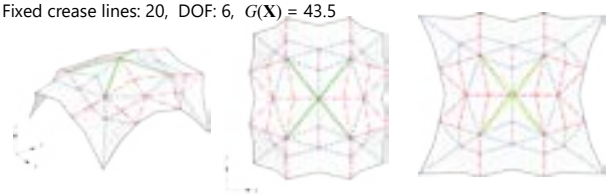

Examples of Dome Surface

Fixed crease lines: 20, DOF: 9, $G(\mathbf{X})$ = **15.4**

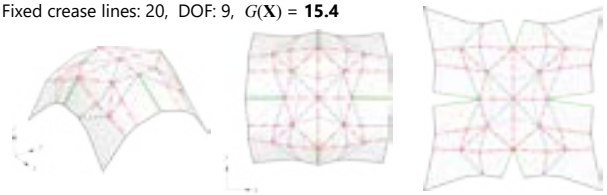

Fixed crease lines: 20, DOF: **17**, $G(\mathbf{X})$ = **7.07**

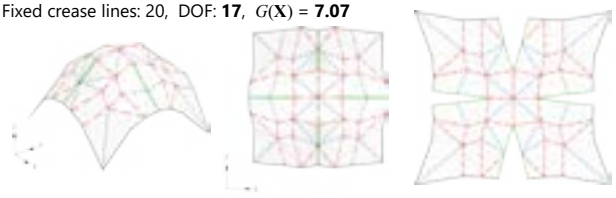

Conclusions

Optimization approach for surface approximation by rigid origami

Developability conditions for an origami surface

Approximation error function reflecting the appearance of the surface

Selection criterion of the crease lines to be fixed for high possibility of successful termination in the succeeding optimization step without locked crease lines

Cut lines may improve the approximation accuracy but increase the degrees of freedom of mechanism

Pillow boxes as developable surfaces with curved foldings

Miyuki Koiso
Institute of Mathematics for Industry, Kyushu University, Japan

Abstract

Pillow boxes are surfaces created by folding a double rectangle. They are often used for gift boxes and packaging, and have architectural applications. In this talk, first we give the existence, uniqueness, and representation formula of the pillow box which encloses the largest volume among pillow boxes made out of a double rectangle with an arbitrary fixed size. The second topic is relating to a rigidity problem that is whether a piecewise smooth closed surface can be isometrically-deformed changing the enclosed volume. By definition, a pillow box is isometric to a double rectangle. We can construct a continuous isometric deformation of a half of any pillow box into a (single) rectangle which fixes the "crease pattern". However, we prove under a certain natural symmetry assumption that there is no global isometric deformation of the whole pillow box into the double rectangle which fixes the "crease pattern". This talk consists of a recent joint research with Hiroyuki Kitahata (Chiba U.), and another joint research with Atsufumi Honda (Yokohama National U.).

International Conference "Evolving Design and Discrete Differential Geometry - towards Mathematics Aided Geometric Design"

Pillow boxes as developable surfaces with curved folds *

Miyuki Koiso
（Kyushu University, Japan）

March 12, 2025, Nishijin Plaza, Kyushu University

*This work is supported by JST CREST Grant Number JPMJCR1911 and JSPS KAKENHI Grant Number JP20H01801.

Collaborators and papers

- I learned a lot on pillow boxes from Prof. Jun Mitani (U. of Tsukuba).
- Components of the bidirectional circulative design platform on the optimal pillow boxes were introduced and explained by Prof. Shun Kumagai yesterday.
- In the next talk, Prof. Yohei Yokosuka will explain discretization of pillow boxes and an application of them to temporary housing.

This talk includes some results from the following two papers.
[1] A. Honda and M. Koiso, Isometric deformations of pillow boxes, preprint.
[2] H. Kitahata and M. Koiso, Optimal pillow boxes (tentative title), in preparation.

Plan of the talk

1. Introduction
2. A variational problem for developable surfaces “Find the optimal pillow box ! ”
3. Continuous isometric (i.e. not expanding,not contracting) deformation from a planar double rectangle to a pillow box
4. Future works
5. Summary

1. Introduction: Developable surfaces

Def. 1. A piecewise (PW)-smooth surface M is said to be developable if it is isometric to a planar region R (that is, there exists a Lipschitz continuous bijective mapping F from M onto R that preserves the length of each curve).

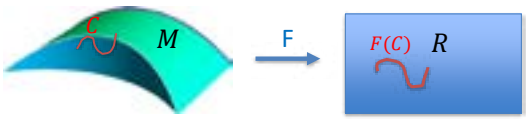

Remark 1. It is well-known that a smooth surface M is developable if and only if the Gaussian curvature $K(p)$ of M vanishes at any point $p \in M$.

4

Real analytic developable surfaces (C^ω surfaces with 0-Gaussian curvature)

Fact 1. Real analytic developable surfaces in $\mathbb{E}^3$ are the following: (1) cylinders, (2) cones, (3) tangent developable surfaces.

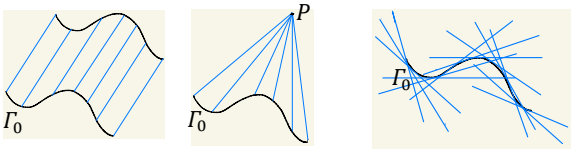

cylinder cone tangent developable surface

Since developable surfaces can be constructed by bending a flat sheet, they are important in manufacturing objects from sheet metal, cardboard, and plywood. Developable surfaces with curved folds (Ex. Pillow boxes) are also important!

5

2. A variational problem for developable surfaces "Find the optimal pillow box ! "

What is a pillow box?

A double flat rectangle (topologically, 2-spere S^2) made of paper

Fold along curves

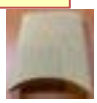

Pillow box

Def. 2 (Pillow box). A pillow box is a compact PW-smooth surface without boundary with genus 0 that consists of four parts of cylinders whose generators are parallel to either the y-axis or the z-axis and that is isometric to a double rectangle.

Q: For a given double rectangle, find the pillow box with the maximal volume. A: We will give a (rigorous) answer.

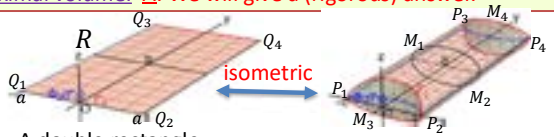

A double rectangle Pillow box

6

Existence and uniqueness of the optimal pillow box

Theorem 1 (K) : For any given double rectangle $R(2a, 2b)$ with width $2a$ and height $2b$ (see the picture below) there exists a unique pillow box $M(2a, 2b)$ (which we call the optimal pillow box) that encloses the largest volume. It has an explicit representation using elliptic integrals. It consists of four (generalized) cylinders (of C^∞ class) of which the base curves (the top and the bottom half of Γ_0 and two blue curves in the picture below right) are congruent and they are elastic curves.

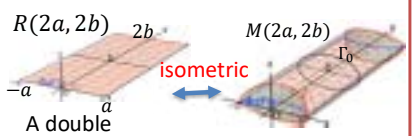

A double rectangle

Pillow box

Remark 2.
(1) $\lim_{b\to\infty} M(2a, 2b) =$ a right circular cylinder with radius $2a/\pi$.
(2) $\lim_{a\to\infty} M(2a, 2b) =$ two parallel rectangles with width $2b$ and infinite length.

Remark on the optimal pillow box

Remark (Kitahata-K.) : By numerical computation, we observe that, if $a > b$, then the volume of $M(2a, 2b)$ is bigger than the volume of $M(2b, 2a)$.

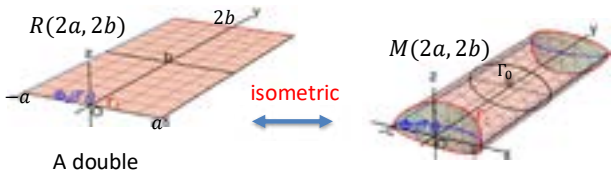

A double rectangle

Pillow box

Representation of the optimal pillow box (I) --- base curves---

The base curve $\Gamma_0 : z = f(x)$ of the optimal pillow box is represented as follows.

$$\begin{cases} x = -I_\mu(z) + c, & 0 \le z \le z_0, \quad (0 \le x \le c) \\ x = I_\mu(z) - c, & 0 \le z \le z_0, \quad (-c \le x \le 0) \end{cases} \quad \cdots (2)$$

where, $I_\mu(z) := \int_0^z \frac{-\mu\zeta\left(1-\frac{\zeta}{b}\right)}{\sqrt{1-\left(\mu\zeta\left(1-\frac{\zeta}{b}\right)\right)^2}} d\zeta > 0, (0 < z < b)$, $z_0 := \frac{b}{2}\left(1 - \sqrt{1 - \frac{4}{b|\mu|}}\right)$,

$c := I_\mu(z_0)$. $\mu\ (< 0)$ is the curvature of Γ_0 at the end points that is determined by the following.

$$a = \int_0^{z_0} \frac{d\zeta}{\sqrt{1-\left(\mu\zeta\left(1-\frac{\zeta}{b}\right)\right)^2}} \quad \cdots (3)$$

The crease Γ_1 is $(x, f(x), f(x))$, $(-c \le x \le c)$.

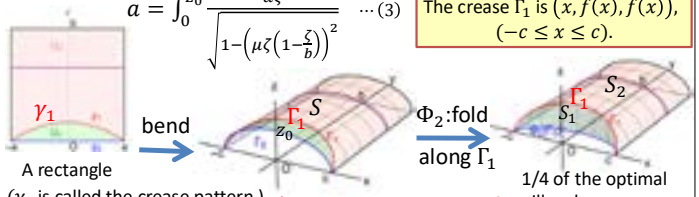

A rectangle (γ_1 is called the crease pattern.)

(Γ_1 is called the crease.)

1/4 of the optimal pillow box.

Representation of the optimal pillow box (II)
--- surface and volume ---

Let $\Gamma_0: z = f(x)$ be the base curve of the optimal pillow box given in the previous slide.

The parts S_1, S_2 of the ¼ of the optimal pillow box are represented as

$$\begin{cases} S_1 = \{(x, f(x), z); -c \le x \le c, 0 \le z \le f(x)\} \\ S_2 = \{(x, y, f(x)); -c \le x \le c, f(x) \le y \le b\} \end{cases} \quad \cdots (4)$$

Hence, the volume $V(f)$ of the optimal pillow box is

$$V(f) = 4\int_{-c}^{c} f(x)\big(b - f(x)\big)\,dx \quad \cdots (5)$$

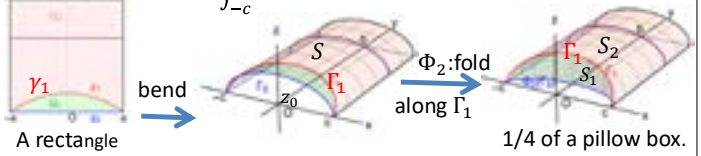

A rectangle 1/4 of a pillow box.

(γ_1 is called the crease pattern.) (Γ_1 is called the crease.)

10

3.Continuous isometric (i.e. not expanding,not contracting) deformation from a planar double rectangle to a pillow box

Theorem 2 (K). We can deform the initial double rectangle R to any given pillow box M that is isometric to R continuously and isometrically if the crease pattern is permitted to be changed.

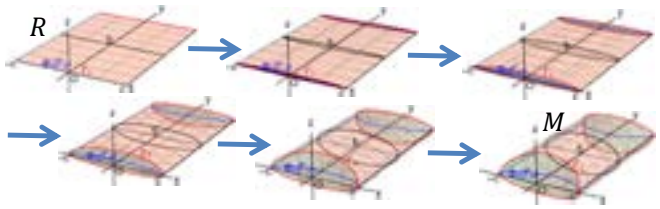

An isometric deformation from R to M. Here the crease pattern is changed, which is not good for application!

11

Theorem 2 (Honda-K.). There exists no continuous isometric deformation from a double rectangle to any pillow box without changing crease pattern.

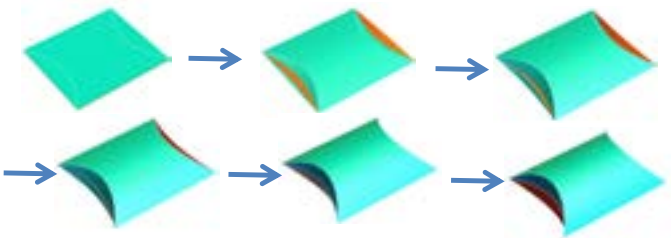

A continuous isometric deformation from a double rectangle to a pillow box without changing the crease pattern. However, at each stage, the upper half and the lower half are separated and they intersect each other except the beginning and the end.

12

Future work

Prove the following conjecture:

Conjecture (a generalization of Bellows Conjecture). If a closed embedded piecewise-smooth surface M is deformed continuously and isometrically without changing the crease pattern, then the enclosed volume is preserved. Therefore, M can not be deformed to a planar region.

Remark. Pillow boxes are good examples for the above conjecture.

Remark. If a closed embedded polyhedron is deformed continuously and isometrically without changing the crease pattern (edges and vertices), then the enclosed volume is preserved (Connelly, R.; Sabitov, I.; and Walz, A. "The Bellows Conjecture." *Contrib. Algebra Geom.* **38**, 1-10, 1997).

13

Summary

- We gave the definition of developable surfaces and pillow boxes.
- We gave the existence, uniqueness, and representation formula of the optimal pillow box.
- We gave a continuous isometric deformation from a planar region to a pillow box with changing the crease pattern.
- We explained the non-existence of continuous isometric deformation from a planar region to any pillow box without changing the crease pattern.
- We mentioned a generalization of the Bellows Conjecture as a future work.

14

Temporary structures with curved folding

Yohei Yokosuka
Kagoshima University, Japan

Abstract

Temporary housing needs to provide a large number of houses quickly after a disaster, so it is useful to have temporary structures using curved folds that are superior in space-saving stocking, portability, and quick construction, and can immediately expand flat plates into a three-dimensional structure. Koiso et al. derive an explicit expression for the maximum volume solution of the pillow box and show that the bottom curve of the pillow box is an elastic curve. In this presentation, a scaled experimental model of a temporary structure with curve folding is fabricated to show that curve folding is possible with rigid body deformation. Furthermore, an example of numerical analysis is shown where the generation of a curved surface shape that is the solution to the maximum volume of a pillow box is linked to structural analysis and applied to a multi-objective optimization problem where the volume evaluated as architectural planning performance and the maximum displacement evaluated as structural performance are used as indices.

International Conference "Evolving Design and Discrete Differential Geometry - towards Mathematics Aided Geometric Design"

Temporary Structures with Curved Folding

Yohei YOKOSUKA[1)], Miyuki KOISO[2)], Kento OKUDA[3)], Shun KUMAGAI[4)], Toshio HONMA[1)], Jun MITANI[5)], Yudai HIYOSHI[1)]

1) Graduate School of Science and Engineering, Kagoshima University
2) Institute of Mathematics for Industry, Kyushu University
3) National Institute of Technology, Sasebo College
4) Hachinohe Institute of Technology
5) Information and Systems, University of Tsukuba

Temporary Structures with Curved Folding

Propose temporary structures with excellent portability and stiffness using the curve folding in origami engineering.
In times of disaster, **temporary tents and housing** with safety need to be provided quickly and in large quantities.
This presentation shows a form-finding and potential applications for structures suitable for temporary housing by utilizing stiffness due to **curved surfaces formed by curve folding**.

Portable state　　Unfolding state　　Completed state

Temporary Structures with Curved Folding

Outline of Temporary Structures (Emergency Temporary Housing)

1995 Great Hanshin earthquake

Construction period − 32.43 days (Average)
Number of houses built − 245.9 houses/day
Worker − 7.4 persons/house
Total number of construction − 48,300 houses

2011 Tōhoku earthquake

Total number of construction − 52,513 houses
(Rental type emergency housing 67,877 houses)

Temporary Structures with Curved Folding

Types of Emergency Temporary Housings

- **Construction Type Emergency Housing**
  ⇒ This type is possible to supply housing with excellent living performance.
  Difficult to provide it quickly.

- **Rental Type Emergency Housing**
  ⇒ Local governments lease private housing.
  Difficult to secure numbers.

- **Others（Container House, Trailer house）**
  ⇒ Need to secure a place to stock.

Temporary Structures with Curved Folding

Temporary Structures of Curved Folding

Portable state

Unfold

Unfolding state

Lift up

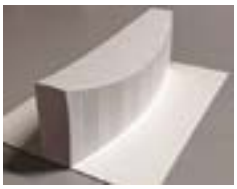

Completed state

- **Space-saving stock in portable condition**
- **Rapid construction of roof structures**

Pillow box shape to maximize internal volume
Jun MITANI, Miyuki KOISO, Kento OKUDA,

Temporary Structures with Curved Folding

Maximum solution for internal volume of pillow box

i) curvature κ in Γ_0 ii) curvature μ at both ends points in curve Γ_0
Γ_0 is orthogonal to x-axis at both end points

$$\kappa = \frac{\mu}{b}(b-2z)$$

iii) integral $I_\mu(z)$, $\mu < 0, 0 < z < b$

$$I_\mu(z) := \int_0^z \frac{\mu\zeta\left(1-\frac{\zeta}{b}\right)}{\left[1-\left(\mu\zeta\left(1-\frac{\zeta}{b}\right)\right)^2\right]^{1/2}} d\zeta$$

$$z_0 := \frac{b}{2}\left(1-\sqrt{1-\frac{4}{b|\mu|}}\right), c := I_\mu(z_0)$$

Rectangle in plane Ω

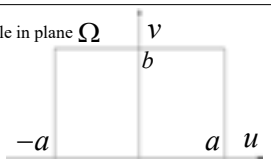

Cylindrical surface S

$\Gamma_0 : z = f(x)$

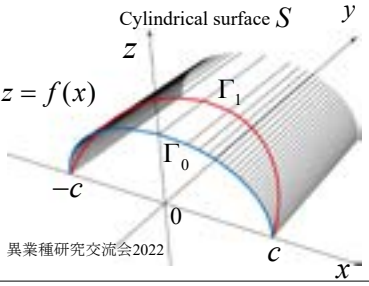

奥田 健斗, 小磯 深幸,ピロー型ボックスの体積最大解の存在と一意性, 異分野・異業種研究交流会2022
https://www.isc.meiji.ac.jp/~mathcareer2022/posterfiles/ps13.pdf

Temporary Structures with Curved Folding

Maximum solution for internal volume of pillow box

Rectangle in plane Ω

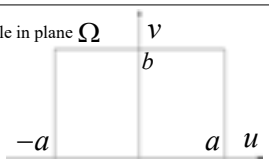

iv) Let μ satisfy the following equation

$$a=\int_0^{z_0}\left[1-\left(\mu\zeta\left(1-\frac{\zeta}{b}\right)\right)^2\right]^{-1/2}d\zeta$$

v) Γ_0 is given by the following equation

$$\begin{cases}x=-I_\mu(z)+c, 0\le z\le z_0\ (0\le x\le c)\\ x=I_\mu(z)+c, 0\le z\le z_0\ (-c\le x\le 0)\end{cases}$$

Integral $I_\mu(z)$ is elliptic integral,
Γ_0 is characterized by an elasticity curve

Cylindrical surface S

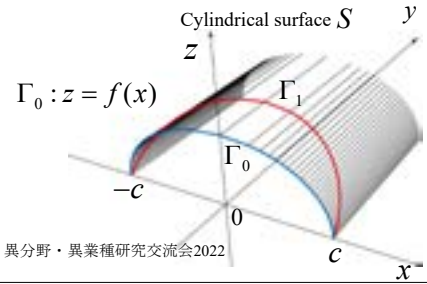

奥田 健斗, 小磯 深幸,ピロー型ボックスの体積最大解の存在と一意性, 異分野・異業種研究交流会2022
https://www.isc.meiji.ac.jp/~mathcareer2022/posterfiles/ps13.pdf

Temporary Structures with Curved Folding

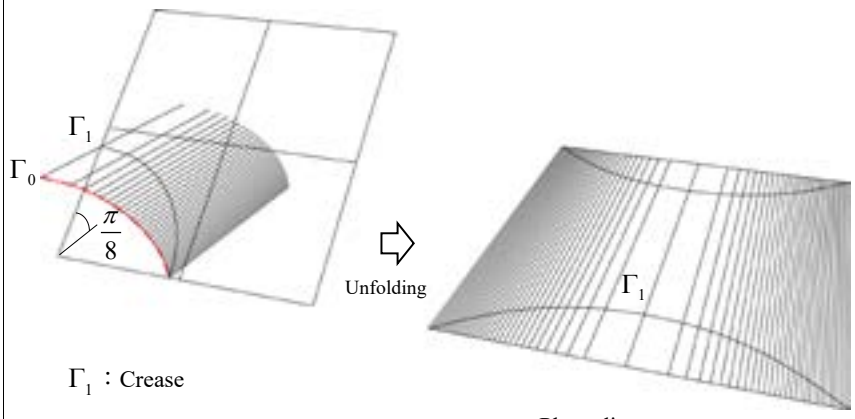

Γ_1 : Crease

Plane diagram

Temporary Structures with Curved Folding

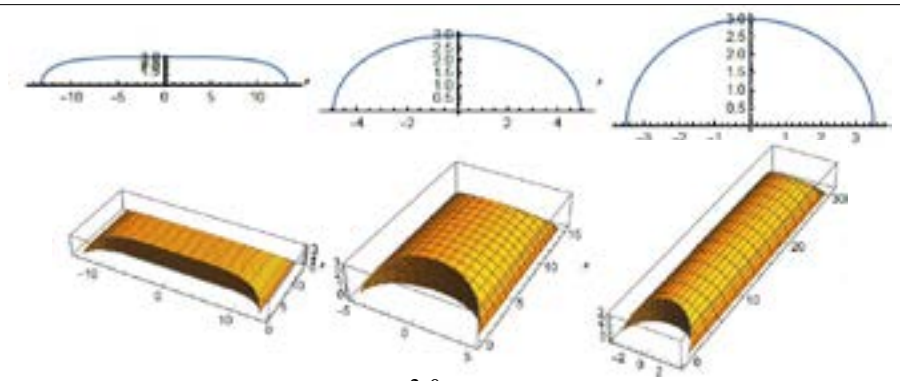

$z_0=3.0$ $b=6.015$ $a=14.558$

$z_0=3.0$ $b=7.5$ $a=6.304$

$z_0=3.0$ $b=15.0$ $a=5.099$

Maximum solution for internal volume

Temporary Structures with Curved Folding

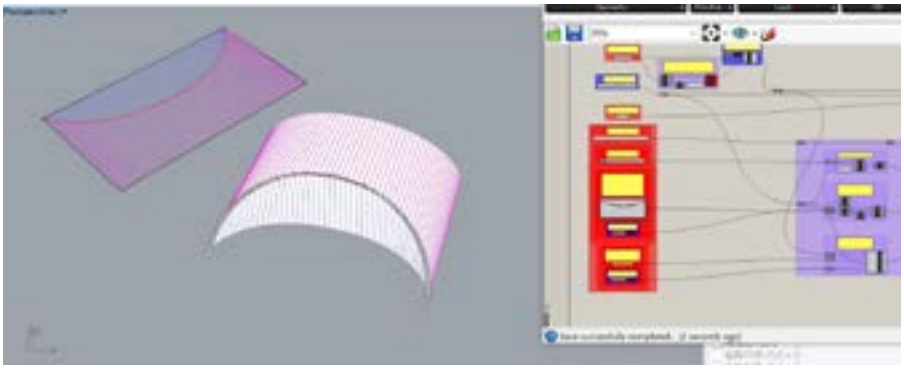

Simulation of Plane diagram including curved folding (Jun MITANI)

Kosuke Sasaki, Jun Mitani, Simple implementation and low computational cost simulation of curved folds based on ruling-aware triangulation, Computers & Graphics, Volume 102, February 2022, Pages 213-219

Temporary Structures with Curved Folding

Problems of temporary structures with curved folding

1. **Possibility of Rigid folding (Continuous isometric deformation)**
2. **Mechanism of Curved folding**
3. **Curved folding with thick surfaces**
4. **Structural stiffness**

Temporary Structures with Curved Folding

1. Possibility of Rigid folding (Continuous isometric deformation)
If the cross-sectional curve of the surface is Crease, the folded shape can be generated by mirror-reversing the surface on one side. However, it is generally unknown that it is capable of continuous rigid folding.

・Continuous surface
Koiso and Okuda parameterized continuously isometric deformable surfaces with boundary conditions only if they are cylindrical surface (ruling is parallel).

・Discrete surface
Numerically rigid folding is possible.

⇨ **Rigid folding simulation with generalized inverse matrix can realize continuous isometric deformation.**

Temporary Structures with Curved Folding

1. Possibility of Rigid folding (Continuous isometric deformation)

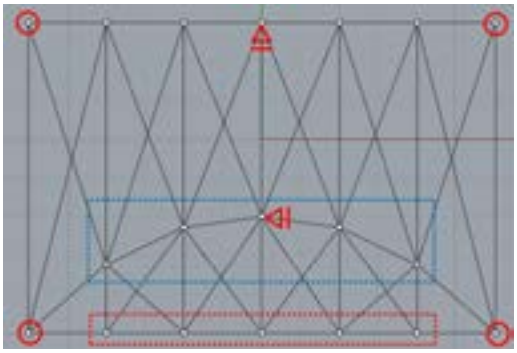

Number of nodes：19
Number of elements：50
Number of boundary conditions：6
Degree of freedom：51

51−50 = 1

Model with one rigid body displacement mode

－Fixed in Z direction
－Fixed in Y direction
－Fixed in X direction

・半谷裕彦, 川口健一, 形態解析　一般逆行列とその応用, 培風館, 1991

Temporary Structures with Curved Folding

1. Possibility of Rigid folding (Continuous isometric deformation)

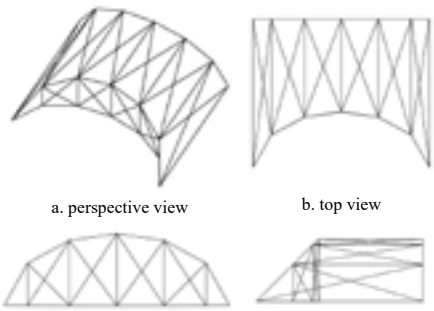

a. perspective view　b. top view　c. front view　d. right view

Numerical results

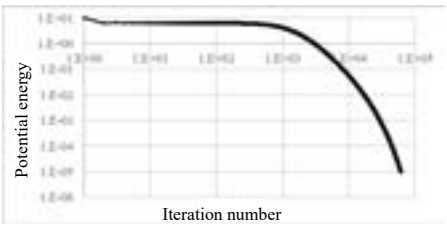

Convergence History

2. Mechanism of Curved folding

・Figure represents 1/4 region

・The pink line is the original curve.

・The rotation axes of the red lines are all parallel.
→ Possible if the curved surface is a cylindrical surface

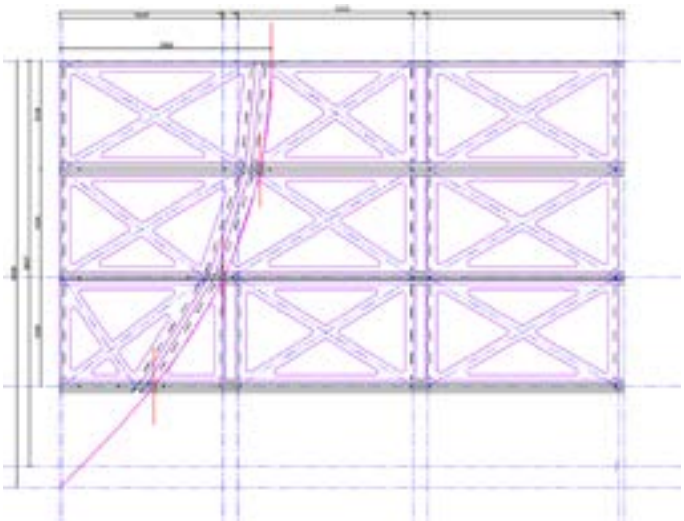

Temporary Structures with Curved Folding

3. Curved folding with thick surfaces

・Members that become columns and beams are displaced without tilting.

・The neutral plane of the blue line is rigid and displaced.

・The cross-sectional shape of the box composed of braces allows for shear deformation. These boxes are connected to the columns and beams by hinges.

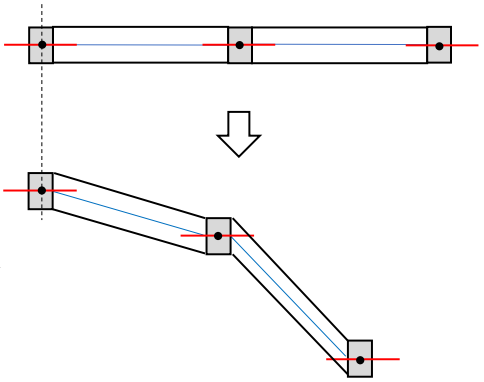

Temporary Structures with Curved Folding

3. Curved folding with thick surfaces

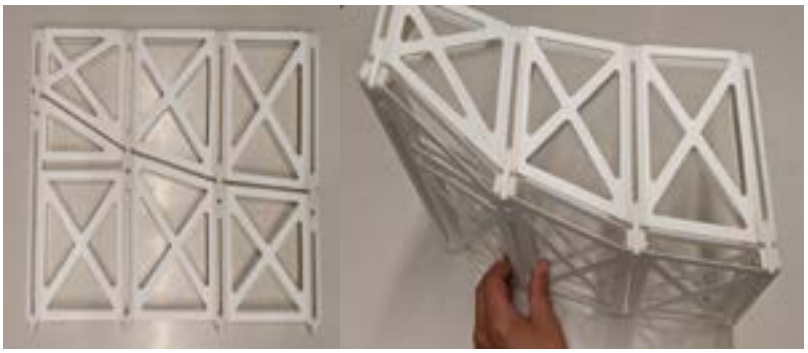

Scaled model

4. Structural stiffness

Member :
・Beam and Column
2-38 × 184 mm (Wood: SPF)

・Brace
12 × 100 mm (Wood: plywood)

Model-A Total weight 1328 kgf

Model-B Total weight 1360 kgf

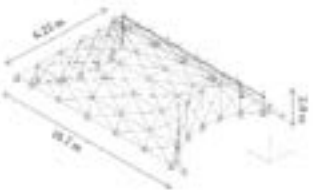

Model-C Total weight 1267 kgf

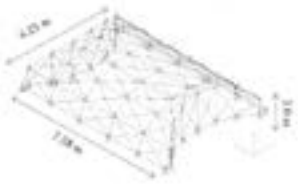

Model-D Total weight 1395 kgf

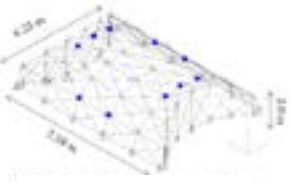

Blue points: Reinforcement by columns

Type-1

Max displacement

Max bend. Moment bend. stress

Max comp. force comp. stress

Max tension force tens. stress

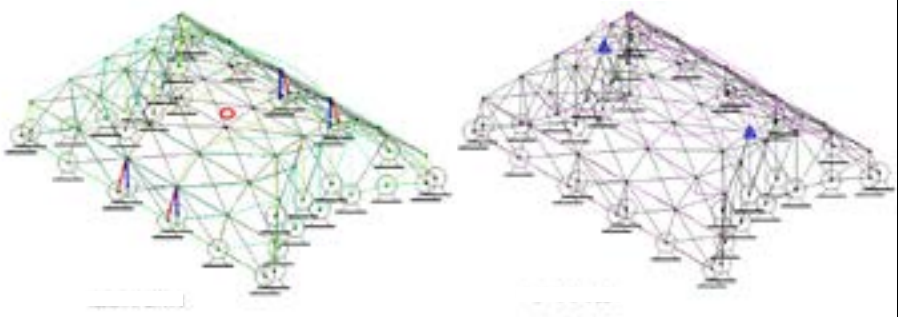

Displacement and axial force

Bending moment

These results show that allowable solutions of structural stiffness are obtained.

Temporary Structures with Curved Folding

plan view

・Experimental model (1:3 scale)

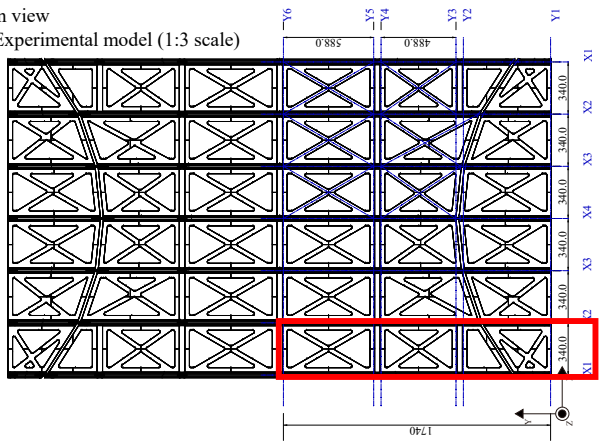

Temporary Structures with Curved Folding

X方向断面図

・Actual model

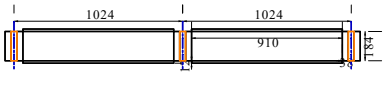

post and beam member：2×8

brace：plywood (12*mm*)

・Experimental model (1:3 scale)

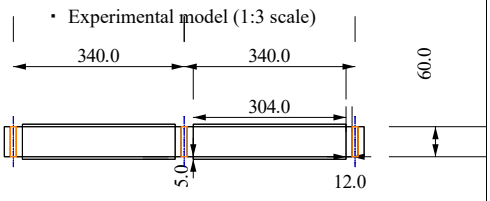

column post and beam member： plywood (12mm)

brace ：plywood (5mm)

Temporary Structures with Curved Folding

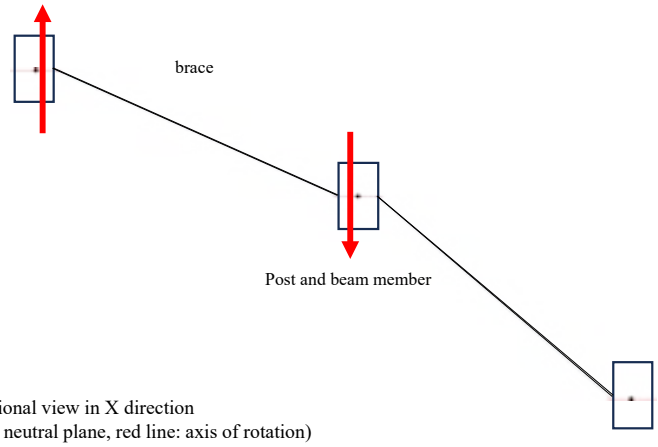

Cross-sectional view in X direction
(Blue line: neutral plane, red line: axis of rotation)

Temporary Structures with Curved Folding

Cutting of parts and materials

Cutting of brace member

Processing of post and beam member

Assembling the unit

Fabrication of the foundation

Connecting units

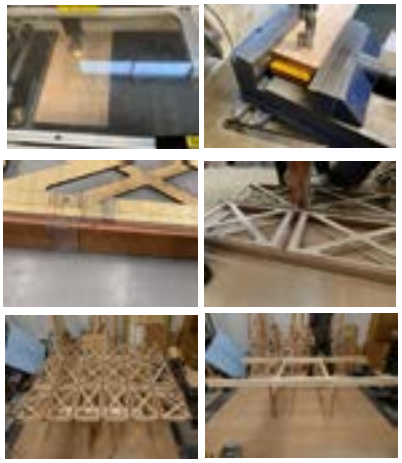

Temporary Structures with Curved Folding

Assembling the unit

- belt hinge

Two belts support both sides of the brace

Temporary Structures with Curved Folding

Assembling the unit
- Fixing belt hinges


One unit


Temporarily fixed with a tacker


Wood, glue, and bolts to fix the main structure

Temporary Structures with Curved Folding

Fabrication of the foundation


Installation image


Foundation for beam material


Foundation for post material

Temporary Structures with Curved Folding

Connecting units

Connect at the position of the spacer
Rotation axis through steel pipe


Connecting units


Adjustment of rotary shaft


Installation of rotary shaft

Temporary Structures with Curved Folding

Connecting units

Connecting units

Pre-drilled spacers

Installation of rotary shaft

Temporary Structures with Curved Folding

Connecting units

Parallel installation on the foundation and unit connection

Installation on the foundation

Connection between units

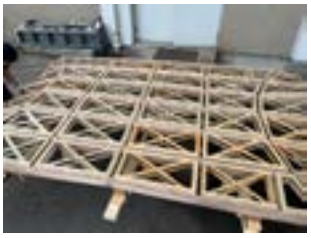

Installation of the whole area

Temporary Structures with Curved Folding

ユニット設置

土台とモデルの間にコロを挟む

コロ（台車）を介して設置

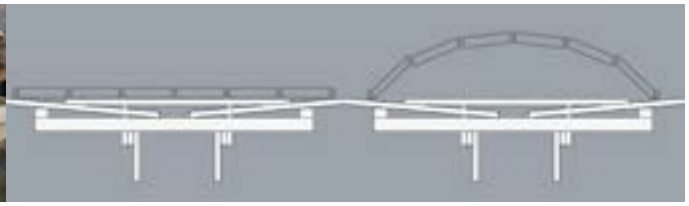

立ち上げ前断面

立ち上げ後断面

Temporary Structures with Curved Folding

Experimental result:

・Thick models can be folded rigidly.
・push-up by a small number of people

Shape after bending

Front view

Side view

Temporary Structures with Curved Folding

Multi-objective optimization

Building planning performance

・Space Utilization Efficiency

The most flattened surface of the pneumatic membrane structure with the condition that the rise at the boundary is vertical so that no dead space is created near the boundary.

・Main level living

In general, living area levels are recommended based on the number of household members.

⇒ Maximum solution for inner volume with constant surface area

⇒ There is a maximum solution for the inner volume that varies with $r := a / b$.

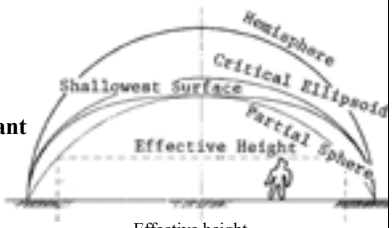

Effective height

川口衞, 空気膜構造におけるしわなし最偏平回転曲面, 日本建築学会学術講演会梗概集, pp.1053-1054, 1978
Mamoru KAWAGUCHI, Wrinkle-free most flattened rotational surface in pneumatic membrane structure, 1978

Temporary Structures with Curved Folding

Multi-objective optimization
Structural performance

・**Maximum Deflection** $w_{\max}$
The structural form adopted is a beam structures in the **depth (*b*) direction**.
The larger the span (*b*) of the frame, the **greater the deformation and deflection** due to its self-weight, and thus the **lower the structural performance**.

⇒ The maximum solution for **the inner volume tends to increase** in volume as *b* increases.
⇒ There is a trade-off between **structural performance** and **building planning performance**, and a **Pareto solution** must be obtained through multi-objective optimization.

Temporary Structures with Curved Folding

Multi-objective optimization formulation

$$\textit{Find} \qquad r := a / b \tag{1}$$

$$\textit{Minimize} \qquad f_1(r) := w_{\max} / (b - z_0),\ f_2(r) := 1/V \tag{2}$$

$$\textit{Subject to} \qquad \Gamma_0 : z = f(x),\ \begin{cases} x = -I_\mu(z) + c, 0 \le z \le z_0\ (0 \le x \le c) \\ x = I_\mu(z) + c, 0 \le z \le z_0\ (-c \le x \le 0) \end{cases} \tag{3.a,b}$$

$$z_0(\mu) := \frac{b}{2}\left(1 - \sqrt{1 - \frac{4}{b|\mu|}}\right),\ c := I_\mu(z_0),\ I_\mu(z) := \int_0^z \frac{\mu\zeta\left(1 - \frac{\zeta}{b}\right)}{\left[1 - \left(\mu\zeta\left(1 - \frac{\zeta}{b}\right)\right)^2\right]^{1/2}} d\zeta,\ A(S) = \bar{A} \tag{3.c-f}$$

However, μ is the curvature of the endpoints of Γ0determined from equation (4).

$$a = \int_0^{z_0} \left[1 - \left(\mu\zeta\left(1 - \frac{\zeta}{b}\right)\right)^2\right]^{-1/2} d\zeta \tag{4}$$

Temporary Structures with Curved Folding

Implementation of multi-objective optimization (Rhinoceros + Kramba3D + Wallacei)

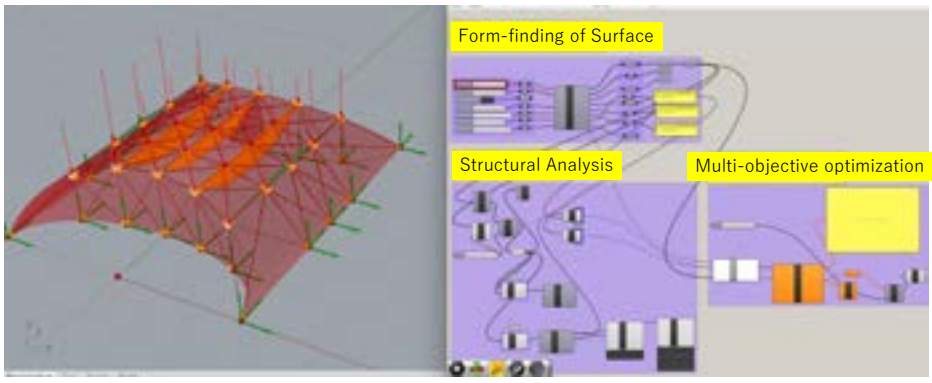

bidirectional circulative design platform（Planning + Structure + Construction）

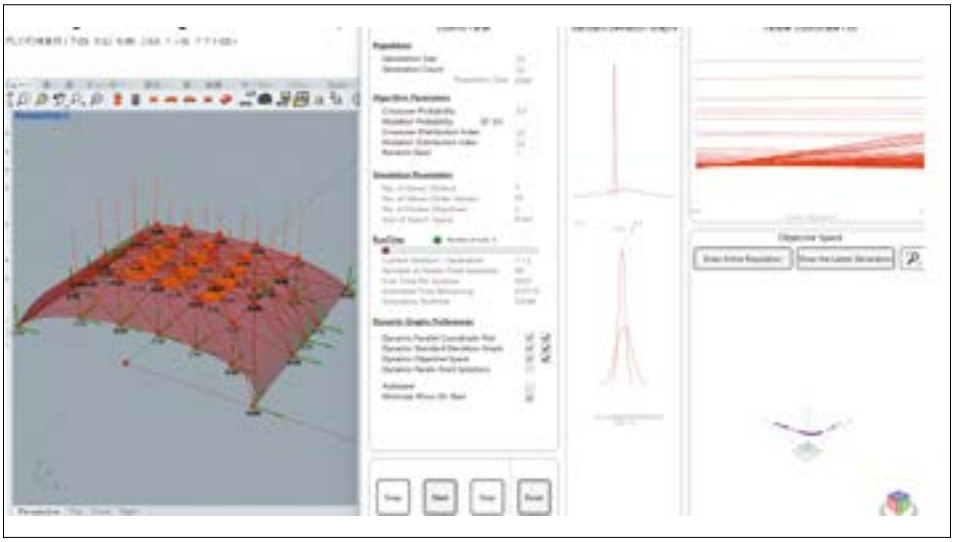

Temporary Structures with Curved Folding

Multi-objective optimization (Wallacei)

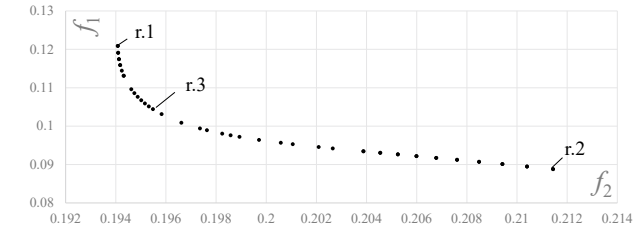

Pareto solution

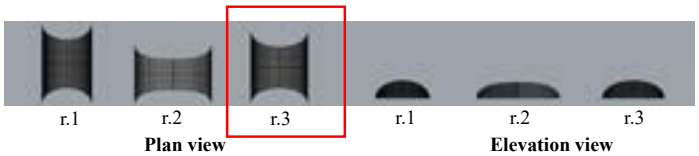

Plan view **Elevation view**

Temporary Structures with Curved Folding

Conclusion

・The possibility concerning the application of temporary buildings by means of curve folding is presented.

・Rigid foldable curved surfaces and thickness should be considered.

・A model with simplified joints was proposed.

・We presented an example of multi-objective optimization of a temporary structure with a pillow box curve folding geometry by using bidirectional circulative design platform.

Local & Global Property Quantification With Persistent Homology

R. U. Gobithaasan
School of Mathematical Sciences, Universiti Sains Malaysia, Penang, Malaysia.

Kenjiro T. Miura
Graduate School of Science and Technology, Shizuoka University, Hamamatsu, Shizuoka, Japan.

Abstract

Topological Data Analysis (TDA) is a powerful algebraic topology framework that aims to understand the shape and structure of complex datasets, particularly those with high dimensionality point cloud data $X \in R^d$ [1]. It has been successfully used for various types of Machine Learning tasks [2, 3]. Persistent Homology (PH), the main methodology in TDA, quantifies the shape and structure of complex datasets by representing the topological dan geometrical information of data in the form of Persistence Diagram denoted as $D_k(X)$. A $D_k(X)$ consisting of a set of 2-tuple $(b_i, d_i) \in R^2$, corresponds to a pairing between the births of k^{th} homology class at b_i and its death at d_i along the filtration of X. $D_k(X)$ can be converted in the form of vector spaces that can be directly used as features for machine learning (ML) pipelines. It is known that topological features manifest as long-lived birth-death pairs in the $D_k(X)$, indicating their presence across multiple spatial scales. Recently it was found that (b_i, d_i) close to diagonal encodes the geometrical feature of X [4, 5]. The first part of this talks delves the law of composition [6] which makes an art beautiful and its relation to the types of shape analysis tools developed; hence leading to the development of Persistent Homology. We will then review the variety of framework for capturing geometrical and topological features across different spatial scales for understanding the underlying structure and relationships within the data. Overall, this talk provides insight into the implementation of PH framework not just as ML tasks, but also for the development of visually pleasing products.

References

[1] G. Carlsson, "Topology and data", Bull. Amer. Math. Soc. **46**, 255–308, (2009).

[2] R. U. Gobithaasan, Zabidi Abu Hasan, et al., "Clustering Selected Terengganu's Rainfall Stations Based on Persistent Homology", Thai Journal of Mathematics, 197–211, (2022).

[3] A. S. Shakthi Aswin, R. U. Gobithaasan, Kelin Xia, Kenjiro T. Miura. "The Efficacy of Weight Control in Persistence Vectors Detecting Geometrical and Topological Features from Point Cloud", AIP Journal Proceedings, to appear.

[4] Peter Bubenik, Michael Hull, Dhruv Patel, and Benjamin Whittle, "Persistent homology detects curvature". Inverse Problems, **36**(2): 025008, (2020).

[5] Renata Turkeš and Guido Montúfar and Nina Otter, "On the effectiveness of persistent homology", 2206.10551, arXiv, (2023).

[6] John Ruskin, "The Elements of Drawing: In Three Letters to Beginners", https://www.gutenberg.org/files/30325/30325-h/30325-h.htm.

Local & Global Property Quantification With Persistent Homology

from Shape Quantification to Product Design

Miura Group

School of Mathematical Sciences, Universiti Sains Malaysia, Malaysia.
Graduate School of Science and Technology, Shizuoka University, Japan.

10^{th} March. – 13^{th}March 2025

This talk covers on

1. **Part I**: Fr Designer's Perspective to Mathematical defs.
   - Visually Pleasing Shapes at various resolution.
   - Shape Descriptors.
2. **Part II** : Intro to Topological Data Analysis:
   - One-Parameter
   - Multi-Parameter PH.
3. **Part III**: **WIP**
   - Framework for Aesthetic Design.

Moving Forward: Simplified Life cycle of Aesthetic Design

Ideal Setup for Aesthetic Design (AD):

Solving the Puzzle: Putting Them Together

John Ruskin: philosopher, art historian and art critic

Laws of composition

- **Global characteristics**
- **Local characteristics**
- **Loc. + Glo. characteristics**

- **Principality**: dominant element
- **Repetition**: recurring shapes/colours or forms
- **Continuity**: natural visual flow
- **Curvature**: curved lines adds grace rather than rigid straight lines
- **Radiation**: emanate outward from a central point.
- **Contrast**: use of opposing elements.
- **Interchange**: elements are arranged to support one another.
- **Consistency**: in style and visual treatment.
- **Harmony**: shapes, lines, colors, light/ shadow—work together to create a pleasing visual.

frametitle Local Vs. Global Characteristics

- **Local Characteristics: Geometry = Fine Details**
- **Global Characteristics: Topology =Global Properties**

Figure: Great Wave off Kanagawa (Hokusai)

Shape Analysis: Local to Global Descriptors

- Shape analysis focuses on quantifying the properties of shapes to analyze, compare, and classify shapes. Three types of shape descriptors:

1. **Geometrical Descriptors**: Local descriptors that are invariant under rigid motions: geometric properties of a shape: area, perimeter and **curvature**
2. **Neighborhood Descriptors** : based on geodesic distance on the manifold around a point, e.g. **density function**
3. **Topological Descriptors**: analyze shapes based on their connected components and holes: Morphological Analysis, and **Persistent Homology** .

Geometrical Descriptors: Curvature

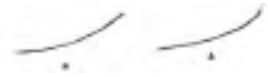

- Ruskin's proposal: beautiful curves [3]

- Farin's idea on fair curves: few monotonic curvature segments.

- Logarithmic Curvature Graph (LCG):

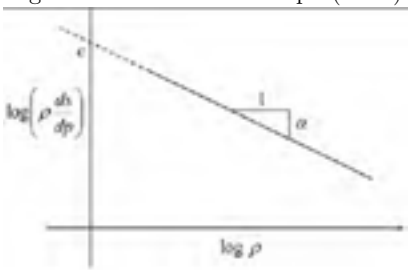

- Fundamental Equation of LAC: $log(\rho\frac{ds}{d\rho}) = \alpha\log(\rho) + C$

Neighbourhood Descriptors: Density Function

- Gaussian kernel density estimate (KDE)[1]

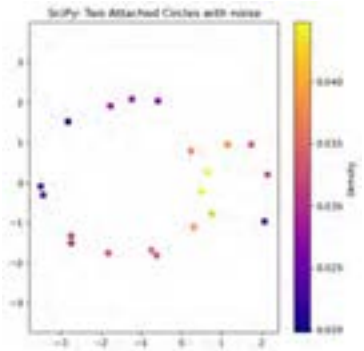

- Distance-To-Measure (DTM) employs KDTRee Nearest Neighbor's Algo [2]

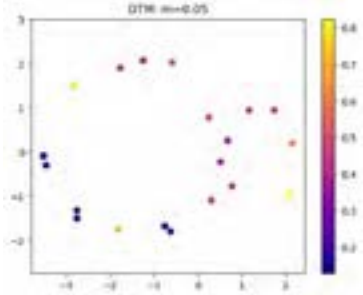

[a] SciPy: gaussian_kde

[b] GUDHI's DTM: $m \longrightarrow 1 \approx \frac{1}{KDE}$

Topological Descriptors: Connectivity & $n^{th}D$ holes

Topological Data Analysis (TDA)

- **TDA's theme: Data has shape, shapes has meaning**.

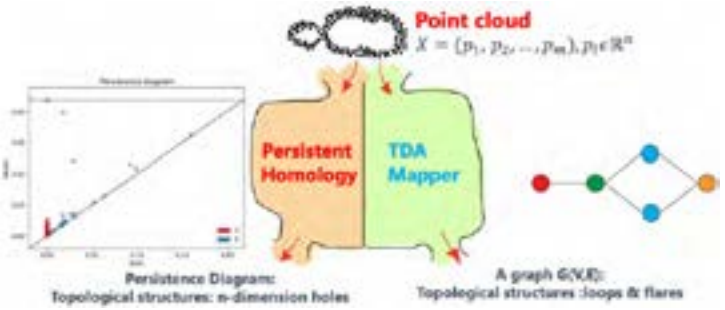

Topological Descriptors: Euler Characteristics

Definition (Euler Characteristics)

Let $\mathcal{K}$ be a a simplical complex with $\beta_0, \beta_1, \beta_2, \ldots$ as Betti numbers denoting k^{th} dimensional holes. Then we define the Euler characteristic to be the alternating sum : $\chi(\mathcal{K}) = \sum_0^n (-1)^n \beta_n$.

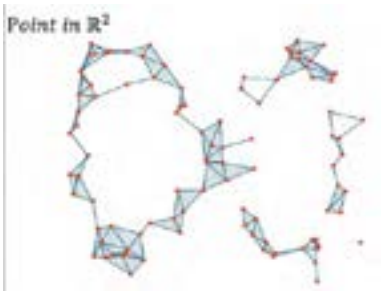

$\chi(\mathcal{K}) = 5 - 3 + 0 = 2$

- Alternatively, we can directly compute $\chi(\mathcal{K}) = \sum_0^n (-1)^n |\mathcal{K}^n|$, where $|\mathcal{K}^n|$ denotes the carnality of set of n-simplices.

Persistent Homology: One-Parameter Persistence

Input: (X, δ_X):

1. Geometric Realization

construct an increasing family (X_t) of simplicial complex with single scale parameter $t \geq 0$.

2.Algebraic Topology

Compute the d-th homology vector spaces $\{H_d(X_t) | t \geq 0\}$.

3.Representation Theory

Output: produce a barcode or Persistence diagram $\mathcal{D}_D$

output: $\mathcal{D}_D = \{[b_1, d_1), \ldots, [b_k, d_k)\}$, where b_i & d_i are birth and death of features, respectively.

- Lifespan $= d_i - b_i$.

Handcrafted Persistence Signatures (Vectors) for ML

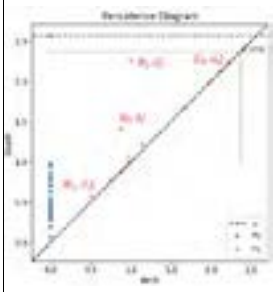

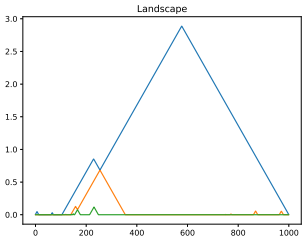

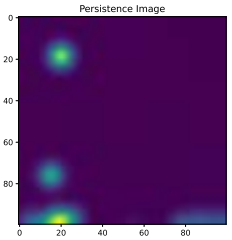

- Persistence Landscape: Peter Bubenik (Uni. Florida).
- Persistence Image: Hendry Adams et. al (Colorado State Uni.)

Topological Machine Learning (TML)

- **(Many success stories) of TML in various field of study.**

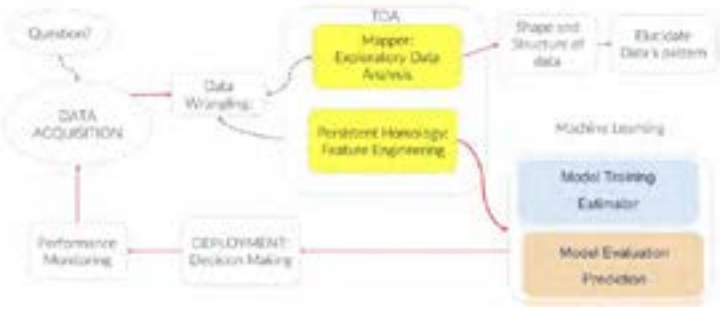

Why One-parameter PH is effective?

1. PH detects topological information:
   - connected components & k^{th} dimensional holes.
   - **Long lifespan detects topological information**
2. Also detects geometric information:
   - **curvature**: (Bubenik et. al (2019) and Turkes et.al (2022))
   - **(many) short lifespan detects geometrical information.**
   - **Accuracy**: Outperformed PointNet & NN Deep.
3. **Highly tunable one-parameter PH** for ML: {Signal (L+G), one-filtration (Types of Simplicial Complex), Signature(Types of Persistence Vectors)}

Example: Classification Point Cloud

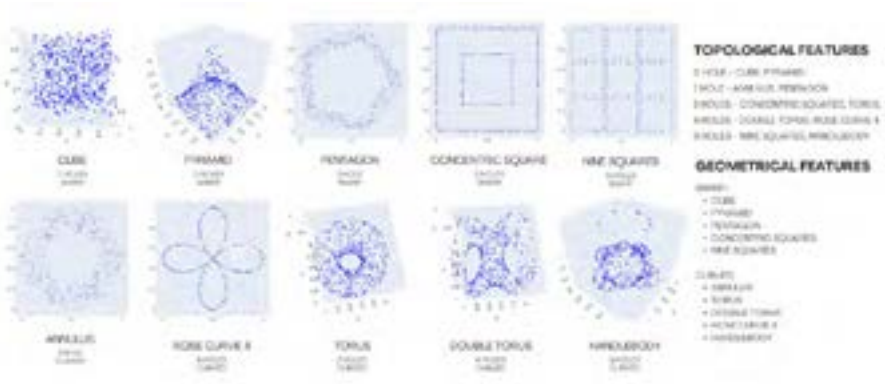

Example: Classification Framework

Standard:

Persistent Homology:

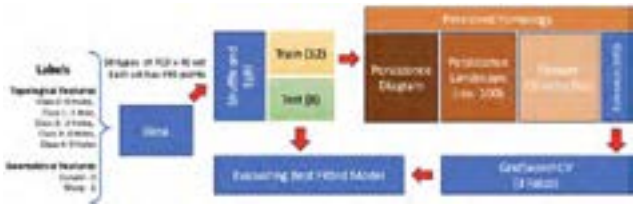

Example: Classification Results

Feature	SVM	RFC	L. Reg	k-NN	PointNet	PH
Geo	80.00	66.67	53.54	47.71	**85.93**	**95.00**
Topo	61.04	47.5	32.29	30.00	**68.73**	**98.75**

1. **Can we push further?**
   - {Signal, ~~**one-filtration**~~ **Multi-filtration**, Signature}

Persistent Homology: **Multi-parameter Persistence**

Input: (X, δ_X^t):

1. Geometric Realization

construct a family $\mathcal{F} = (\mathcal{F}_t)_{t\in\mathbb{R}^m}$ of subcomplexes $\mathcal{F}_t \subseteq \mathcal{K}$ that is increasing with respect to inclusions, i.e., such that $\mathcal{F}_t \subseteq \mathcal{F}_{t'}$ for any $t, t' \in \mathbb{R}^m$ with $t \leq t'$.

2.Alg. Topology & Repr. Theory

The *Euler Characteristic Transform (ECT) ; also known as EC Profile* of an *m-parameter* filtration $\mathcal{F}$ is the map:

$$\text{ECT} \quad \chi_{\mathcal{F}} : t \in \mathbb{R}^m \mapsto \chi(\mathcal{F}_t)$$

variations of output $\chi_{\mathcal{F}}$ include:

- *Euler characteristic curve* (ECC) of $\mathcal{F}$ when m = 1,
- *Euler characteristic surface* (ECS) of $\mathcal{F}$ when m = 2.
- *Smooth ECP* (SECT) [Munch et. al., Mic. St. Uni, USA]& *Differentiable ECT* (DECT) [Reick, et. al., TUM, Germany].

Bi-filtration: Alpha Complex (radius) Vs. Density

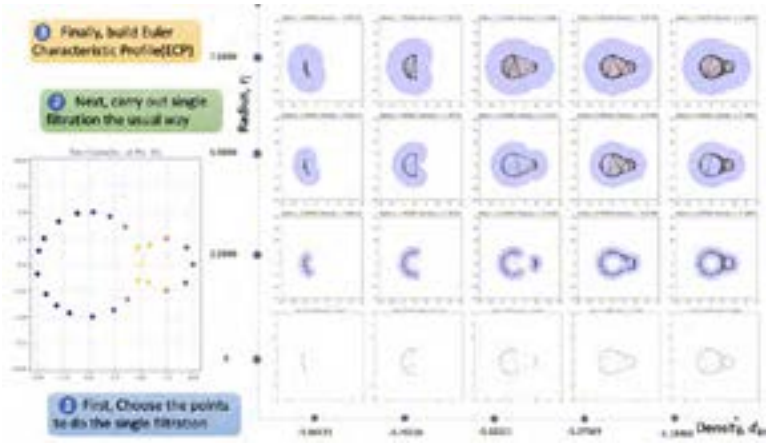

$m = 2$: Euler Characteristic Surface

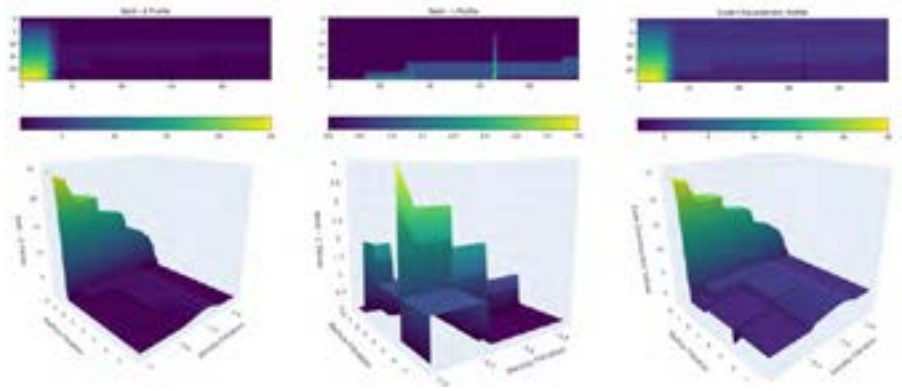

Scalable Curvature Estimate Beyond: $X \in R^3$

Idea: Principal Component Analysis (PCA)

1. Define **a local neighborhood** N_p **for each point** p (e.g., k-NN or fixed radius).
2. Calculate the covariance matrix C_p for points in N_p and compute its eigenvalues $\lambda_1 \leq \lambda_2 \leq \lambda_3$ and eigenvectors v_1, v_2, v_3.
3. Estimate Curvature type I: $\kappa_I = \lambda_1$
4. Estimate Curvature type II: $\kappa_{II} = \frac{\lambda_1}{\lambda_1+\lambda_2+\lambda_3}$ (Normalized)
5. Radius of curvature, 2D:$(\rho_i = \frac{1}{\kappa_i})$, and 3D: $(\rho_i = \frac{1}{\sqrt{\kappa_i}})$ where $i =$ I or II.

Wavy Surface: Est. Curvature Vs Gaussian/Mean Curvature

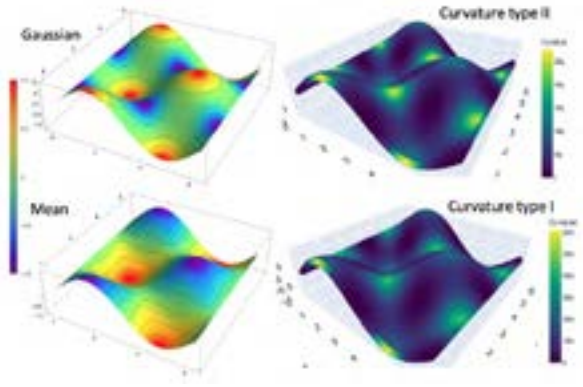

Two-Circle: Est. Curvature Type II with its Histogram

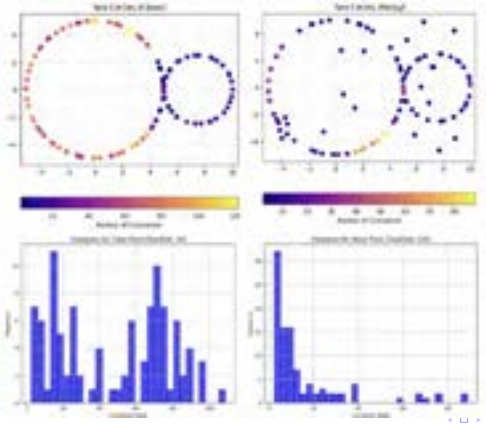

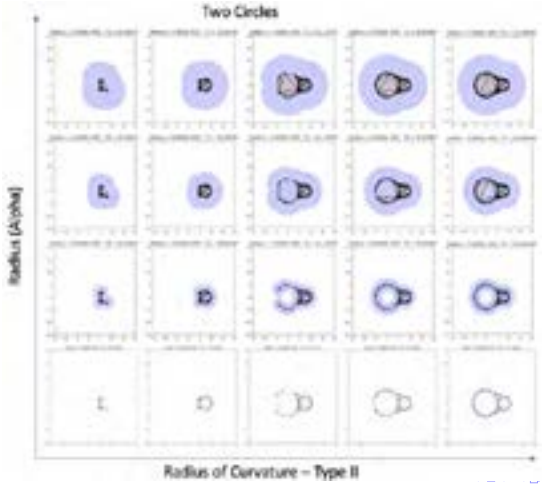

ML: Predicting Curvature with One-Parameter PH

Bubenik et.al(2019), Turkes et.al(2022)

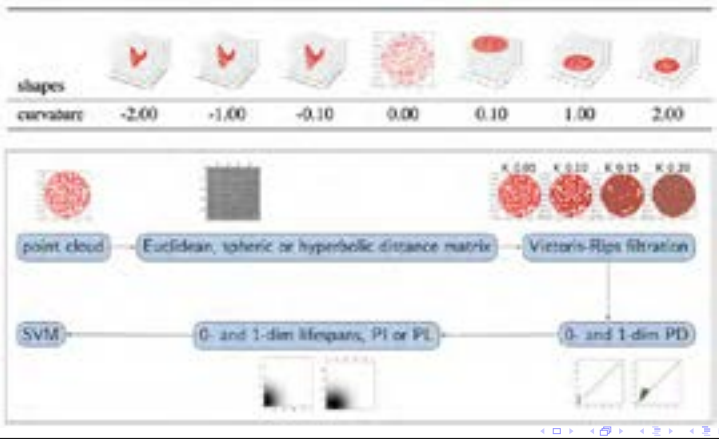

Result: Predicting Curvature with **One**-Parameter PH

Turkes et.al(2022): SVR and its Mean Squared Error (MSE)

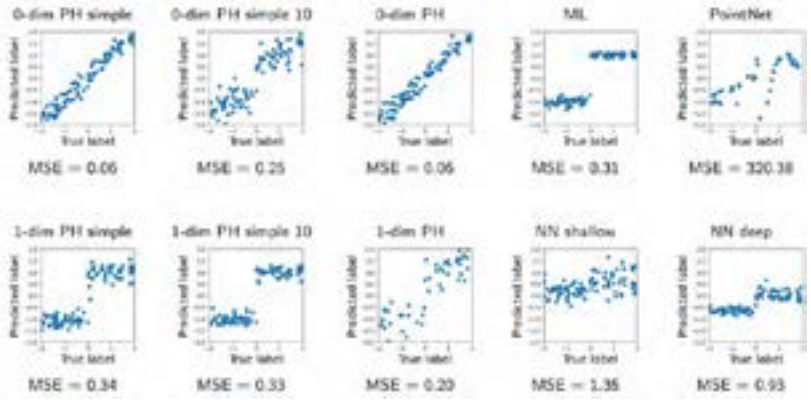

Framework: Predicting Curvature with : **Multi**-Parameter PH

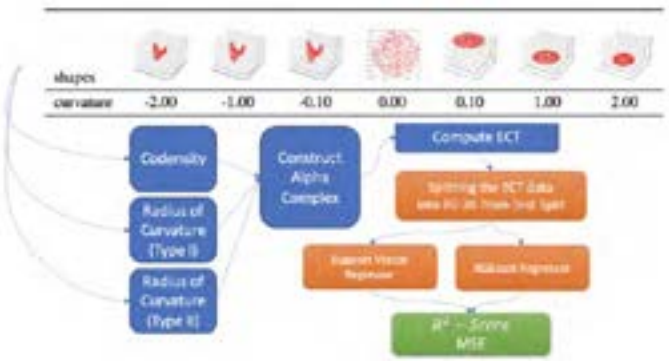

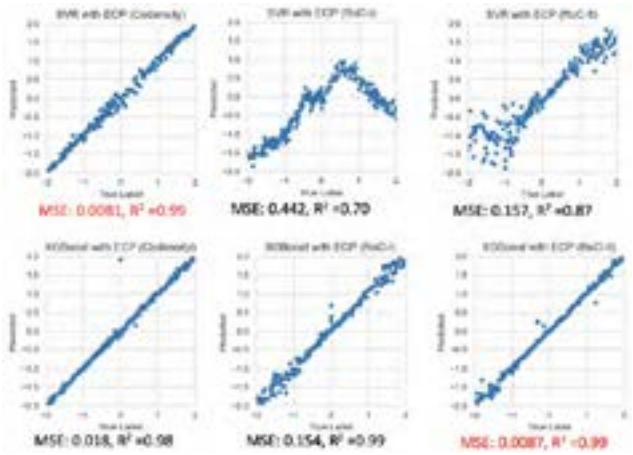

Moving Forward: Aesthetic Generative Design (AGD)

Towards for Aesthetic Design (AD):

$$\overbrace{\underbrace{\text{Shape Descriptor}}_{\text{Persistent Homology}}}^{\text{LCG}} \rightarrow \overbrace{\underbrace{\text{Signal}}_{\text{Local + Neigh.+ Global}}}^{\text{Local Characteristics}} \rightarrow \text{Aesthetic Design}$$

Towards Aesthetic Generative Model

1. **ANN as a Computational Building Block**
   - **Generative Adversarial Network (GAN)**.
2. **ANN** as a Universal Function Approximator (UFA): $|f(x) - \hat{f}(x)| < \epsilon$
   - **Topological & Geometrical Loss**.

Towards Aesthetic Generative Design (AGD) Framework

1. **Computational Building Block of GAN = Generator + Discriminator**

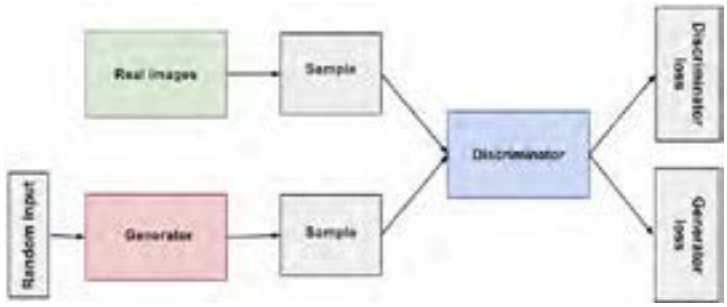

Figure: https://developers.google.com/machine-learning/gan/gan_structure

Towards Aesthetic Generative Design (AGD) Framework

1. **GAN's Function Approximator: Topological & Geometrical Loss.**

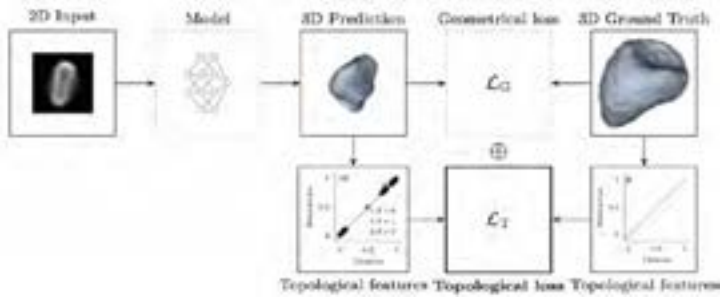

Figure: Waibel et al., 2022, Capturing Shape Information with Multi-Scale Topological Loss Terms for 3D Reconstruction

Ideal Aesthetic Generative Design (AGD) Framework

$$\underbrace{\text{Shape Design}}_{\text{LCG}} \leftrightarrow \underbrace{\text{Signal}}_{\text{Local Char.}} \leftrightarrow \underbrace{\text{Structure Analysis}}_{\text{Strength}}$$

Multi-Param PH | Local + Neigh.+ Global | Local + Neigh.+ Global

Solving the Puzzle: Seamless + Scalable

Thank You

- For your attention.
- Prof. Kenjiro Miura: for having me in the team
- CREST Team: Grant Number JPMJCR1911, Japan Science and Technology (JST) Agency.

References

Main References

- Peter Bubenik, Michael Hull, Dhruv Patel, and Benjamin Whittle. Persistent homology detects curvature. Inverse Problems, 36(2):025008, (2020).
- Renata Turkeš and Guido Montúfar and Nina Otter, On the effectiveness of Persistent Homology, 2206.10551, arXiv, (2023).
- John Ruskin, The Elements of Drawing: In Three Letters to Beginners, `https://www.gutenberg.org/files/30325/30325-h/30325-h.htm`
- Olympio Hacquard and Vadim Lebovici, Euler Characteristic Tools for Topological Data, Journal of Machine Learning Research 25 (2024) 1-39 Analysis
- Erik J Amézquita et al., Quantifying the shape of barley seeds using the Euler characteristic transform, in silico Plants, 4(1), 2022.
- Waibel et al., 2022, Capturing Shape Information with Multi-Scale Topological Loss Terms for 3D Reconstruction, arXiv, 2203.01703v3, 2022.
- Ernst Roell and Bastian Rieck, Differentiable Euler Characteristic Transforms for Shape Classification, 2310.07630, arXiv, 2024.
- Elizabeth Munch, An Invitation to the Euler Characteristic Transform, 2310.10395, arXiv, 2023.
- Ghasemi P, Yuan C, Marion T, Moghaddam M. DCG-GAN: design concept generation with generative adversarial networks. Design Science. 2024.

Advancing Precision and Smoothness of Shape Preserving with Quintic Trigonometric Bézier Curve

Md Yushalify Misro
School of Mathematical Sciences, Universiti Sains Malaysia, 11800 Gelugor, Pulau Pinang, Malaysia.

Abstract

This study integrates an optimization technique into positivity- and monotonicity-preserving interpolation methods to enhance curve smoothness by refining free shape parameters. These parameters play a pivotal role in defining curve geometry, granting users the flexibility to fine-tune the final shape. However, selecting them arbitrarily can compromise both aesthetics and accuracy, leading to undesired results. To address this challenge, an optimization-driven approach is introduced to systematically determine the optimal shape parameters. Within this framework, three smoothness metrics —arc length minimization, strain energy minimization, and curvature variation energy minimization— are employed. The resulting curves are analyzed and compared to assess their ability to preserve data while maintaining smoothness. The findings affirm that this method not only optimizes free shape parameters effectively but also surpasses conventional techniques in computational efficiency.

Advancing Precision and Smoothness of Shape Preserving Interpolation with Quintic Trigonometric Bézier Curves

CREST SIMPOSIUM, Fukuoka | 10 – 13 March 2025

Associate Professor Dr. Md Yushalify Misro
School of Mathematical Sciences,
Universiti Sains Malaysia

Shape Preserving Interpolation

Shape-preserving interpolation used to **maintain certain geometric properties of the original data**

Ensures the interpolated function for **positive data remains positive**

Data visualization
Avoid undesired oscillations

Misinterpretation of data

Unrealistic results

CAGD
Generate **smooth curves** and **surfaces** while maintaining nature of data

Mimic smooth transition of most physical phenomena

More stable for numerical computation

Image interpolation
Retain original edges, textures and overall structure.

2

Shape Preserving Types

Positivity-preserving interpolation

Convexity-preserving interpolation

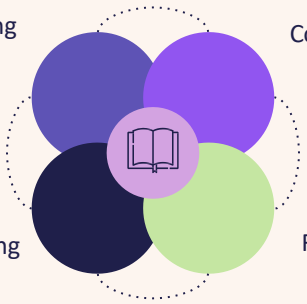

Monotonicity-preserving interpolation

Range-restricted interpolation

3

Positivity-preserving interpolation

Dougherty *et al.* (1989)	• Used **cubic and quintic Hermite** interpolations. • To guarantee positivity, **modifications on the derivative values** in the curve segments that are negative are required.
Butt and Brodlie (1993)	• Used piecewise **cubic Hermite** interpolation. • **Insertion extra intermediate knots** for curve segments that are not positive is necessary.
Harim *et al.* (2020), Zhu (2018)	• **Rational quartic interpolation** spline with shape parameters • Positivity preserving condition was **derived on one shape parameter**. • The developed interpolant are C^1 and C^2 continuous, respectively.
Hussain *et al.* (2018)	• **Rational quintic function** with 3 shape parameter to achieve C^2 continuity. • Has 2 free parameters.

4

Range-restricted interpolation

Sarfraz *et al.* (2015)	• Preserved the shape of range-restricted data using **quadratic trigonometric spline** with three parameters. • Derived shape preserving **constraints on two parameters**
Karim *et al.* (2019)	• **Rational cubic spline function** (cubic/quadratic). • Consists of three shape parameters with **two free parameters** to allow flexibility for curve enhancement.
Zakaria *et al.* (2016)	• **Rational cubic Ball functions** in the form of (cubic/quadratic). • Used the **arithmetic mean approach** to estimate the derivative values in this study. • The generated interpolation are **C^1 continuous.**
Tyada *et al.* (2021)	• C^1 **rational cubic over cubic trigonometric fractal interpolation functions** with 4 shape parameters. • Data dependent constraints for shape preservation were derived on the scaling factors and shape parameters.

5

Monotonicity-preserving interpolation

Karim (2016), Tahat *et al.* (2016)	• Developed monotonicity-preserving interpolation schemes using **rational cubic Ball function** with three and four shape parameters. • One shape parameter was constrained for shape preservation. • C^1 continuity
Ahmad and Misro (2022)	• Integrated a **rational cubic Ball curve**. • Examined the **curvature profile to test the smoothness** of their interpolations.
Ahmad *et al.* (2017)	• Used **multiquadric quasi-interpolation**. • Multiquadric quasi-interpolation was inappropriate for interpolating the dataset and did not generate a smooth curve.
Vijay and Chand (2023)	• Proposed novel method based on **rational quadratic trigonometric fractal interpolation function** constructed through iterated function system. • Developed interpolant is C^1 continuous and offers no free parameter.

6

Convexity-preserving interpolation

Hussain et al. (2016)	• Used **cubic polynomial interpolation with two shape parameters** in Ball form. • Convexity preserving **constraints were developed on both** parameters.
Han (2015)	• Developed C^2 interpolant using **rational quartic spline** with one shape parameter.
Han (2018)	• Presented a united form of the **classical Hermite interpolation** with up to C^3 **order continuity**. • Convexity is preserved by setting the parameter on each subinterval with the given values.
Jena (2021)	• Developed **nonlinear Hermite interpolatory subdivision scheme** based on quadratic rational Bernstein Bezier curves for curve interpolation. • Conditions were developed for the limit curve to preserve convexity of data. • The limit curve is C^1 **continuous**.

7

Optimization

Hu et al. (2023) Zheng et al. (2022)	• Optimize the shapes of rational quartic interpolation splines and quintic generalized Hermite interpolation curves • Enhanced Tunicate Swarm Algorithm and Improved Grey Wolf Algorithm were implemented
Li and Li (2020)	• Solved the nonlinear curve fitting problem by incorporating the Particle Swarm Optimization • Optimization was used to find the optimal number of hidden knots with is the key factor to achieve a good generalization.
Hu et al. (2021)	• Optimized the shape of shape-adjustable generalized cubic developable Ball surfaces by using an Improved Marine Predators Algorithm

As of now, there is still lack of studies on the implementation of optimization in shape preserving interpolation.

8

Problem Statement

Hussain et al. (2018) developed a shape-preserving scheme using a rational quintic function. However, the scheme is complex due to the rational form, which can make it more challenging to implement and compute

01

02

Previous studies on shape-preserving interpolation, such as Karim (2016) and Tahat et al. (2016), assessed the smoothness of their interpolation curves through visual comparison. However, this method is inadequate because visual assessments can be subjective and do not provide the precise metrics needed for a thorough analysis of the smoothness of the curves

9

Problem Statement

03

The technique for selecting free shape parameters in previous studies relied on visual comparison. This technique is prone to bias and may result in non-smooth interpolation curves.

04

There is lack of research on the use of optimization techniques in shape-preserving interpolation, thus efficiency of this implementation is unexplored and required further study.

10

Optimized Shape Preserving Interpolation

Shape-preserving interpolation + Optimization method

- Implementation of optimization method in finding the optimal free shape parameter values → Optimal curves in terms of smoothness
- Procedure to find the best possible solution to a given problem with minimal effort.
- Optimization algorithms have been applied across various fields.

11

Objectives

01 To **develop shape preserving algorithms** on quintic trigonometric Bézier curves to **preserve data shape**

02 To **assess the smoothness of interpolation** by analyzing **three different smoothness metrics**

03 To **apply optimization methods** in finding the optimal free shape parameter values

04 To **compare the efficiency of optimization algorithm** in preserving data shape by implementing different optimization methods

12

Research Methodology

This study will implement the **quintic trigonometric Bézier curve with two shape parameters** introduced by Misro et al. (2017) given by:

$$x(\theta) \equiv x_i(\theta) = \sum_{j=0}^{5} B_{j,5} f_j(\theta), \qquad (1)$$

$$\begin{aligned}
f_0(\theta) &= (1-\sin\theta)^5 (1-\alpha_i \sin\theta),\\
f_1(\theta) &= \sin\theta (1-\sin\theta)^4 (4+\alpha_i-\alpha_i \sin\theta),\\
f_2(\theta) &= (1-\sin\theta)^2 (1-\cos\theta)(8\sin\theta+3\cos\theta+9),\\
f_3(\theta) &= (1-\cos\theta)^2 (1-\sin\theta)(8\cos\theta+3\sin\theta+9),\\
f_4(\theta) &= \cos\theta (1-\cos\theta)^3 (4+\beta_i-\beta_i\cos\theta),\\
f_5(\theta) &= (1-\cos\theta)^4 (1-\beta_i\cos\theta),
\end{aligned}$$

Satisfy all the geometric properties of Bezier Curves:

1. **Non-negativity**
2. **Symmetry**
3. **Partition of unity**

where $\theta = \frac{\pi(x-x_i)}{2h_i}$ with $\theta \in [0, \frac{\pi}{2}]$.

The shape parameters $\alpha_i, \beta_i \in (-4,1]$ are responsible in controlling each end of the curve.

13

Research Methodology

To ensure continuity (up to C^2 continuous), the following interpolating conditions will be applied to find the unknown control

$$\begin{aligned}
x(x_i) &= y_i, & x(x_{i+1}) &= y_{i+1},\\
x'(x_i) &= d_i, & x'(x_{i+1}) &= d_{i+1},\\
x''(x_i) &= D_i, & x''(x_{i+1}) &= D_{i+1}.
\end{aligned}$$

Arithmetic Mean Method (AMM)

It is straightforward to establish that

$$\begin{aligned}
B_0 &= y_i,\\
B_1 &= y_i + \frac{2h_i d_i}{(4+\alpha_i)n},\\
B_2 &= y_i + \frac{h_i\{(4+\alpha_i)D_i h_i + 4d_i + \alpha_i d_{i+1}\pi\}}{3(4+\alpha_i)n^2},\\
B_3 &= y_{i+1} - \frac{h_i\{(\beta_i-4)D_{i+1}h_i + 4d_{i+1} + \beta_i d_i \pi\}}{3(4+\beta_i)n^2},\\
B_4 &= y_{i+1} - \frac{2h_i d_{i+1}}{(4+\beta_i)n},\\
B_5 &= y_{i+1}.
\end{aligned} \qquad (2)$$

where $h_i = x_{i+1} - x_i$.

14

Research Methodology

Arithmetic Mean Method (AMM)

- The first-order and second-order derivatives formula are obtained from Hussain *et al*. (2018).

First-order derivatives

$$\begin{aligned}
d_1 &= \Delta_0 + (\Delta_1 - \Delta_0)\frac{h_1}{h_1+h_2},\\
d_i &= \frac{\Delta_i + \Delta_{i-1}}{2} \text{ for } i = 2, 3, \ldots, n-1,\\
d_n &= \Delta_{n-1} + (\Delta_{n-1} - \Delta_{n-2})\frac{h_{n-1}}{h_{n-1}+h_{n-2}},\\
&\text{where } \Delta_i = \frac{y_{i+1} - y_i}{h_i}.
\end{aligned}$$

Second-order derivatives

$$\begin{aligned}
D_1 &= M_1 + (M_1 - M_2)\frac{h_1}{h_1+h_2},\\
D_i &= \frac{M_i + M_{i-1}}{2} \text{ for } i = 2, 3, \ldots, n-1,\\
D_n &= M_{n-1} + (M_{n-1} - M_{n-2})\frac{h_{n-1}}{h_{n-1}+h_{n-2}},\\
&\text{with } M_i = \frac{d_{i+1} - d_i}{h_i}.
\end{aligned}$$

15

Methodology

The C^2 quintic trigonometric Bézier curve with two shape parameters in Eq (1) defined over each subinterval I_i can be written as:

$$s(x) = \sum_{j=0}^{5} B_{i,j} f_j(x) = y_i (1-\sin\theta)^4 (1-\alpha_i \sin\theta) + \left\{ y_i + \frac{2h_i d_i}{(4+\alpha_i)\pi} \right\} \sin\theta (1-\sin\theta)^3$$
$$(4+\alpha_i - \alpha_i \sin\theta) + \left\{ y_i + \frac{h_i ((4+\alpha_i)D_i h_i + 4(3+\alpha_i)d_i \pi)}{3(4+\alpha_i)\pi^2} \right\} (1-\sin\theta)^2 (1-\cos\theta)$$
$$(8\sin\theta + 3\cos\theta + 9) + \left\{ y_{i+1} + \frac{h_i ((4+\beta_i)D_{i+1} h_i - 4(3+\beta_i)d_{i+1}\pi)}{3(4+\beta_i)\pi^2} \right\} (1-\cos\theta)^2$$
$$(1-\sin\theta)(8\cos\theta + 3\sin\theta + 9) + \left\{ y_{i+1} - \frac{2h_i d_{i+1}}{(4+\beta_i)\pi} \right\} \cos\theta (1-\cos\theta)^3$$
$$(4+\beta_i - \beta_i \cos\theta) + y_{i+1} (1-\cos\theta)^4 (1-\beta_i \cos\theta), \quad (3)$$

Shape Preserving Constraints

- The interpolant in Eq (3) does not guarantee to preserve the shape of data.
- This section derive data dependent constraints on the shape parameter α_i for the four shape preservation.
- Four theorems for shape preservation are provided.

Positivity Preserving Interpolation

Theorem 1

The C^2 quintic trigonometric Bézier curves interpolation defined over the interval $[x_1, x_n]$ preserve the positivity of positive data if the shape parameters α_i, β_i in each subinterval I_i satisfy the following sufficient conditions:

$\beta_i \in [-4, 1]$ that produce positive and smooth interpolating curve,

$$\alpha_i \geq \max\left\{ \frac{-2h_i d_i}{\pi y_i}, \frac{4\pi h_i d_i}{3\pi^2 y_i + h_i (4\pi d_i + D_i h_i)} \right\}$$

with $k_i = \frac{h_i}{h_n}$ and $k_i \geq \max\left\{ 0, \frac{-2d_i h_i + \sqrt{4d_i^2 h_i^2 - 3D_i y_i h_i^2}}{3\pi y_i} \right\}$.

Proof: Mahzir, S. S., & Misro, M. Y. (2023). Shape preserving interpolation of positive and range-restricted data using quintic trigonometric bézier curves. *Alexandria Engineering Journal*, *80*, 122-133.

Positivity Preserving Interpolation

Remark

The sufficient conditions in Theorem 1 can be rewritten as:

$\beta_i \in [-k, k]$ that produce positive and smooth interpolating curve,

$$\alpha_i = \max\left\{\frac{-2\bar{\lambda}_i d_i}{\pi y_i}, \frac{4\pi\bar{\lambda}_i d_i}{3\pi^2 y_i + \bar{\lambda}_i(4\pi d_i + D_i\bar{\lambda}_i)}\right\} + w$$

$$\text{with } \bar{\lambda}_i = \frac{\lambda_i}{k_i} \text{ and } k_i = \max\left\{0, \frac{-2d_i\bar{\lambda}_i + \sqrt{4d_i^2\bar{\lambda}_i^2 - 3D_i y_i \bar{\lambda}_i^2}}{3\pi y_i}\right\} + w.$$

The free parameters w and w are positive real numbers added to inequalities (12) and (13) so that the more than signs ">" can be changed to the equal signs "=".

19

Range-restricted Interpolation

Theorem 2

For data lying above a straight line, the C^2 quintic trigonometric Bézier interpolating spline curve defined over the interval $[x_0, x_n]$ also lies above the straight line if the shape parameters α_i, β_i in each subinterval satisfy the following sufficient conditions:

$\beta_i \in [-k, k]$ which produce smooth interpolating curve that lies above the straight line,

$$\alpha_i > \max\left\{\frac{2\bar{\lambda}_i(d_i - m)}{-(y_i - a_i)\pi}, \frac{4\pi\bar{\lambda}_i(d_i - m)}{3\pi^2(y_i - a_i) + 4\pi d_i\bar{\lambda}_i + D_i\bar{\lambda}_i^2 - 4\pi m\bar{\lambda}_i}\right\},$$

$$\begin{cases} \bar{\lambda}_i = \lambda_i^* = \dfrac{\lambda_i}{k_i}, & \text{if } d_i < 0 \text{ and } D_i < 0, \\ \bar{\lambda}_i = \dfrac{\lambda_i}{k_i}, \lambda_i^* = k_i, & \text{if } d_i < 0 \text{ and } D_i > 0, \\ \bar{\lambda}_i = \lambda_i^* = \lambda_i, & \text{otherwise.} \end{cases}$$

$$k_i > \max\left\{0, \frac{-2\bar{\lambda}_i(d_i - m) + \sqrt{\bar{\lambda}_i^2(4(d_i - m)^2 - 3D_i(y_i - a_i))}}{3\pi(y_i - a_i)}\right\}.$$

Proof: Mahzir, S. S., & Misro, M. Y. (2023). Shape preserving interpolation of positive and range-restricted data using quintic trigonometric bézier curves. *Alexandria Engineering Journal*, *80*, 122-133.

20

Range-restricted Interpolation

Remark 2

The sufficient conditions in Theorem 2 can be rewritten as:

$\beta_i \in [-k, k]$ which produce a smooth interpolating curve that lies above the straight line,

$$\alpha_i = \max\left\{\frac{2\bar{\lambda}_i(d_i - m)}{-(y_i - a_i)\pi}, \frac{4\pi\bar{\lambda}_i(d_i - m)}{3\pi^2(y_i - a_i) + 4\pi d_i\bar{\lambda}_i + D_i\bar{\lambda}_i^2 - 4\pi m\bar{\lambda}_i}\right\} + w,$$

$$\begin{cases} \bar{\lambda}_i = \lambda_i^* = \dfrac{\lambda_i}{k_i}, & \text{if } d_i < 0 \text{ and } D_i < 0, \\ \bar{\lambda}_i = \dfrac{\lambda_i}{k_i}, \lambda_i^* = k_i, & \text{if } d_i < 0 \text{ and } D_i > 0, \\ \bar{\lambda}_i = \lambda_i^* = \lambda_i, & \text{otherwise.} \end{cases}$$

$$k_i = \max\left\{0, \frac{-2\bar{\lambda}_i(d_i - m) + \sqrt{\bar{\lambda}_i^2(4(d_i - m)^2 - 3D_i(y_i - a_i))}}{3\pi(y_i - a_i)}\right\} + w.$$

21

Monotonicity Preserving Interpolation

Theorem 3

The C^2 quintic trigonometric Bézier curves will preserve the monotonicity of monotone data if the parameters α_i, β_i, δ_i, and δ_i^* in each subinterval satisfy the following conditions:

$\beta_i \in (-4, 1]$, which produces a monotone curve, and $\alpha_i \in [L_i, u_i]$ for

$$L_i = \max\left\{0, \frac{-2h_i d_i}{\sigma_{Y_i}} - 4, \frac{4\sigma h_i d_i}{3\sigma^2 Y_i + 4\sigma d_i \beta_i + D_i \beta_i^2} - 4\right\},$$

$$u_i = \max\left\{0, \frac{-2h_i d_i}{\sigma_{Y_i}}, \frac{4\sigma h_i d_i}{3\sigma^2 Y_i + 4\sigma d_i \beta_i + D_i \beta_i^2}\right\}.$$

Let b_j for $j = 1, 2, 3, 4$ be the second terms in B_j

$$\begin{cases} \delta_i = \frac{b_1}{d_i}, & \text{if } b_1 > \frac{d_{Y_i}}{2} \text{ or } b_2 > \frac{d_{Y_i}}{2}, \\ \delta_i^* = \frac{b_4}{d_i}, & \text{if } b_3 > \frac{d_{Y_i}}{2} \text{ or } b_4 > \frac{d_{Y_i}}{2}, \\ \delta_i = \delta_i^* = \delta_i, & \text{elsewhere,} \end{cases}$$

where L_i, U_i^* satisfy Eqs (11) and (12).

Proof: Mahzir, S. S., Misro, M. Y., & Miura, K. T. (2024). Preserving monotone or convex data using quintic trigonometric Bézier curves. *AIMS Mathematics*, *9*(3), 5971-5994.

Convexity-Preserving Interpolation

Theorem 4

The C^2 quintic trigonometric Bézier curves defined will preserve the convexity of convex data if the parameters α_i, β_i, δ_i, and δ_i^* in each subinterval satisfy the following conditions:

$\beta_i \in (-4, 1]$, which produces a smooth and convex curve, and $\alpha_i \in [L_i, u_i]$, where

$$L_i = \frac{-2h_i d_i}{\sigma_{Y_i}} - 4,$$

$$u_i = \max\left\{0, \frac{-2h_i d_i}{\sigma_{Y_i}}, \frac{4\sigma h_i d_i}{h_i^2 D_i + 4\sigma h_i d_i + 3\sigma^2 Y_i}\right\}.$$

Let b_j for $j = 1, 2, 3, 4$ be the second terms of Eq (2). If $d_i > 0$,

$$\begin{cases} \delta_i = \frac{b_1}{d_i}, & \text{if } b_1 > \frac{d_{Y_i}}{2} \text{ or } b_2 > \frac{d_{Y_i}}{2}, \\ \delta_i^* = \frac{b_4}{d_i}, & \text{if } b_3 > \frac{d_{Y_i}}{2} \text{ or } b_4 > \frac{d_{Y_i}}{2}, \\ \delta_i = \delta_i^* = \delta_i, & \text{elsewhere,} \end{cases}$$

where L_i, U_i^* are defined as (15) and (16). If $d_i < 0$,

$$\begin{cases} \delta_i = \frac{b_1}{d_i}, & \text{if } b_1 < \frac{d_{Y_i}}{2} \text{ or } b_2 < \frac{d_{Y_i}}{2}, \\ \delta_i^* = \frac{b_4}{d_i}, & \text{if } b_3 < \frac{d_{Y_i}}{2} \text{ or } b_4 < \frac{d_{Y_i}}{2}, \\ \delta_i = \delta_i^* = \delta_i, & \text{elsewhere,} \end{cases}$$

for L_i, U_i^* given in Eqs (17) and (18).

Proof: Mahzir, S. S., Misro, M. Y., & Miura, K. T. (2024). Preserving monotone or convex data using quintic trigonometric Bézier curves. *AIMS Mathematics*, *9*(3), 5971-5994.

Flowchart

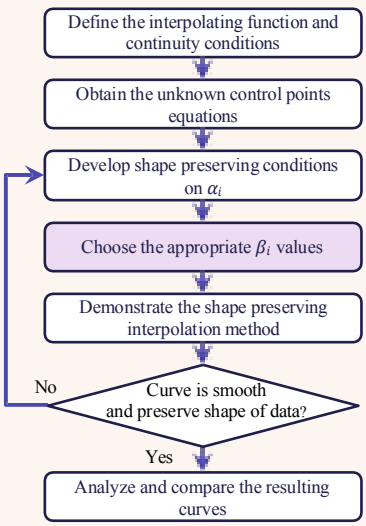

Example 1 – Positivity-preserving Interpolation

Table 1: Amount of creatinine in the blood of six individuals from Hussain et al. (2018)

i	1	2	3	4	5	6
x_i (years)	20	30	32	35	37	39
y_i (mg/dl)	1.51	0.18	1.06	0.6	0.51	47

The normal creatinine level for an adult should be between 0.50 – 1.10 mg/dL.

25

Results

Fig 4a: C^2 quintic trigonometric Bézier curve interpolation

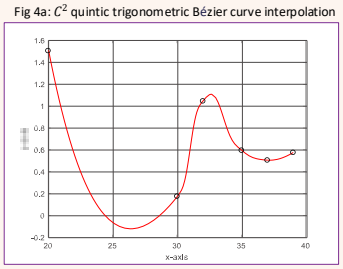

Fig 4b: Positivity-preserving interpolation for several β values

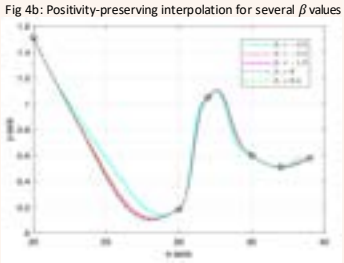

Fig 4c: Positivity-preserving interpolation

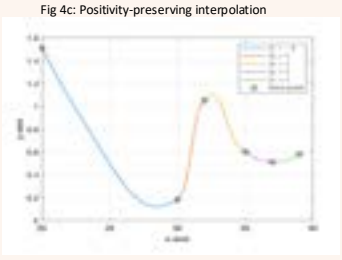

Fig 4d: Comparison with existing scheme

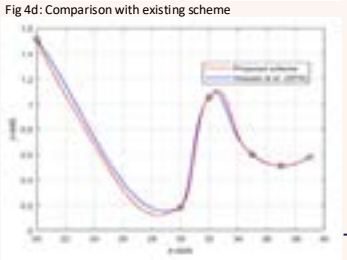

Example 2 – Range-restricted Interpolation

Table 3: Data lying above $y = x + 2$ from Hussain et al. (2018)

i	1	2	3	4	5
x_i	0	4	21	30	32
y_i	22.8	8	33.9	38.9	43.6

27

Results

Fig 6a: C^2 quintic trigonometric Bézier curve interpolation

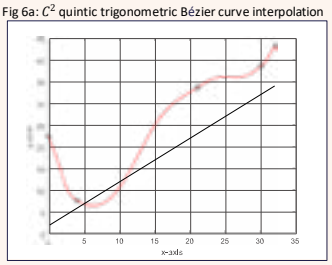

Fig 6b: Range-restricted interpolation for several β values

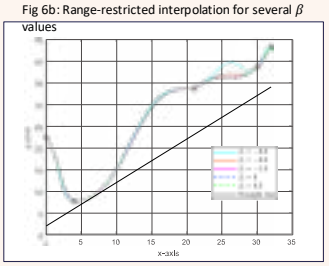

Fig 6c: Range-restricted interpolation

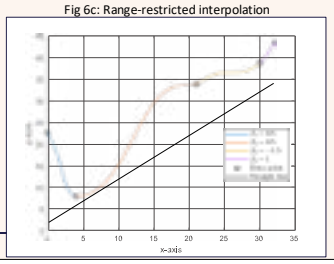

Fig 6d: Comparison with existing scheme

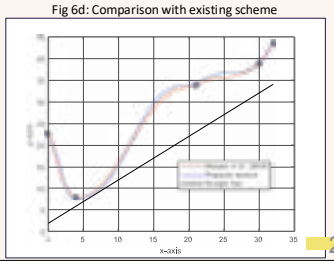

28

Example 3: Monotonicity-preserving Interpolation

Table 5: Monotone data set taken from Karim and Kong (2012).

i	1	2	3	4	5
x_i	0	6	10	29.5	30
y_i	0	15	15	25	30

29

Results

Fig 8a: C^2 quintic trigonometric Bézier curve interpolation

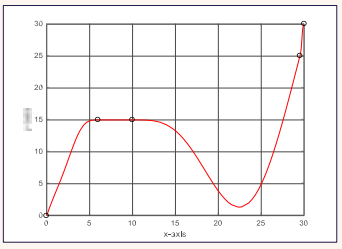

Fig 8b: Monotonicity-preserving interpolation for several β values

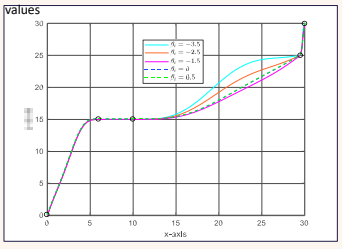

Fig 8c: Monotonicity-preserving interpolation

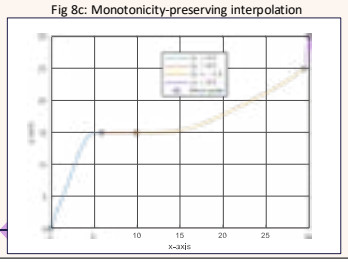

Fig 8d: Comparison with existing scheme

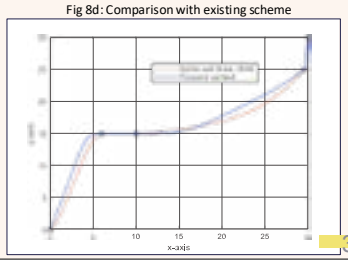

30

Example 4: Convexity-preserving Interpolation

Table 7: Convex data set taken from Hussain et al. (2014)

i	1	2	3	4
x_i	3	4	5	7
y_i	7	0.4	0.4	2.5

31

Results

Fig 10a: C^2 quintic trigonometric Bézier curve interpolation

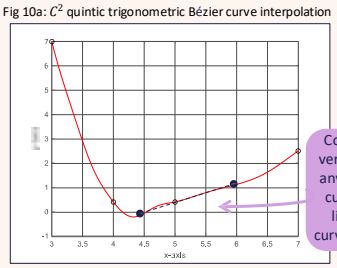

Convex curve can be verified by connecting any two points on the curve. If none of the lines lie below the curve, then it is convex.

Fig 10b: Convexity-preserving interpolation for several β values

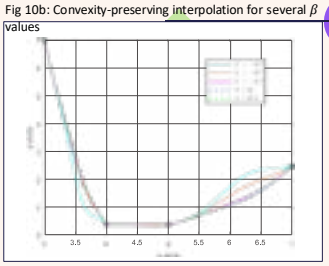

Fig 10c: Convexity-preserving interpolation

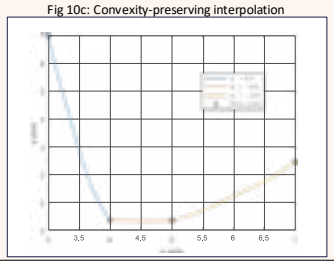

Fig 10d: Comparison with existing scheme

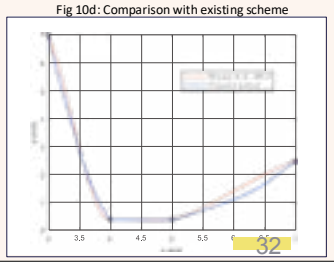

32

Conclusion

1. This study developed shape preserving conditions on the quintic trigonometric Bezier curves
2. This method reduced the complexity of previous study
3. Optimization method ensure optimal β_i values and helps in reducing time

Future Works

1. To apply optimization methods for α_i parameter and compare their effectiveness
2. Can be extended to shape preservation of surfaces

55


Thank you !
56

Extension of κ-curve

Kenjiro T. Miura
Graduate School of Science and Technology, Shizuoka University, Japan

Abstract

The κ-curve[1, 2] is a recently published interpolating spline which consists of quadratic Bézier segments passing through input points at the loci of local curvature extrema. We extend this representation to control the magnitudes of local maximum curvature in a new scheme called *extended-* or $\epsilon\kappa$-curves.

κ-curves have been implemented as the curvature tool in Adobe Illustrator® and Photoshop®, and are highly valued by professional designers. However, because of the limited degrees of freedom of quadratic Bézier curves, it provides no control over the curvature distribution.

We propose new methods that enable the modification of local curvature at the interpolation points by degree elevation of the Bernstein basis as well as application of generalized trigonometric basis functions. By using $\epsilon\kappa$-curves, designers acquire much more ability to produce a variety of expressions, as illustrated by our examples.

References

[1] Yan, Z., Schiller, S., Wilensky, G., Carr, N., Schaefer, "κ-curves: Interpolation at local maximum curvature", ACM Transactions on Graphics **36**(4), Article 129 (2017).

[2] Yan, Z., Schiller, S., Schaefer, S., "Circle reproduction with interpolatory curves at local maximal curvature points". Computer Aided Geometric Design **72**(6), 98–110 (2019).

Log-aesthetic Curve and Similarity Geometry + κ-Curve

Kenjiro T. Miura
Shizuoka University, Japan

Kenjiro T. Miura, Dai Shibuya, R.U. Gobithaasan, Shin Usuki, "Designing Log-aesthetic Splines with G2 Continuity," Computer-Aided Design & Applications, Vol.10, No.6, pp.1021-1032, 2013, DOI: 10.3722/cadaps.2013.1021-1032.

1

Today's talk

Two topics

a. Log-aesthetic curve + Similarity geometry:

Standard curve for aesthetic design

b. κ-curve

1. Aesthetic curve

2. Cute curve

2

Examples of aesthetic surfaces : Sculpture

David statue

Basara statue（伐折羅）

3

Examples of aesthetic curve : Japanese sord

種別 太刀, 国 備前, 時代 平安時代後期～鎌倉時代初期, 法量 二尺四寸五分, 銘文 正恒

種別 脇差, 国 山城, 時代 江戸時代初期[安土桃山時代], 法量 一尺三寸, 銘文 平安城藤原弘幸

種別 刀, 国 肥後国, 時代 江戸時代後期, 法量 二尺三寸一分 銘文 肥後同田貫小山延寿太郎藤原宗廣 文久三年十月日

4

Examples of aesthetic curve : Wings of butterfly

ミカドアゲハ

ヒメギフチョウ

オオムラサキ

キチョウ

5

Impressions of curve and surface

＜Different impressions＞

・David and F355 ⇨ Divergent curve

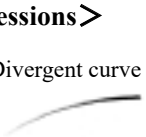

・Basara and Celica ⇨ Convergent curve

David (left) and Basara (right)

Depend on designers' Kansei

So far mathematical approaches has been avoided.

Celica (top) and F355(bottom) 6

Researches on aesthetic curves and surfaces

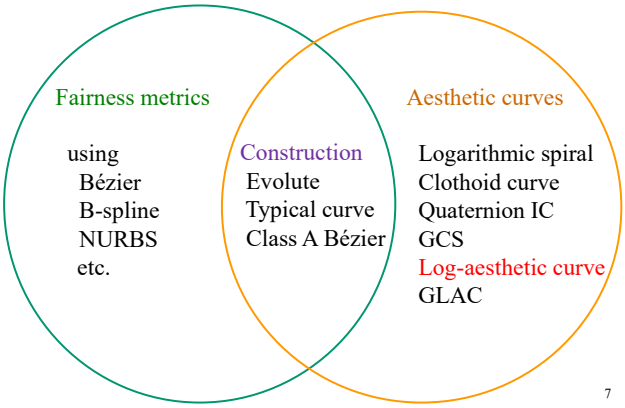

7

Aesthetic curves

- Clothoid curve

  D. S. Meek and D. J. Walton, The use of Cornu spirals in drawing planar curves of controlled curvature, Journal of Computational and Applied Mathematics 25(1989), 69-78.

- GCS (generalized Cornu spiral)

  A. Jamaludin et al., The generalised Cornu spiral and its application to span generation, Journal of Computational and Applied Mathematics Vol.102, No.1, P-37-47, 1999.

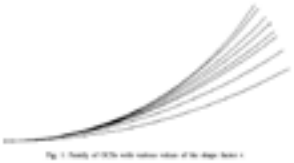

8

GCS

The curvature profile is given by

$$\kappa(s) = \frac{p + qs}{s + rs}$$

where κ: curvature, s : arc length, S:total length, p, q, r : cnst > 1

The domain of the curve $0 \leqq s \leqq S$.

The sign of the curvature derivative is always positive or negative, so the curvature is monotonically increasing/ decreasing.

$$\frac{d\kappa(s)}{ds} = \frac{sq - pr}{(s + rs)^2}$$

9

Unit Quaternion Integral Curve

K.T. Miura, Unit Quaternion Integral Curve: a new type of fair free-form curves, CAGD, 17(2000) 39-58.

$$C(t) = P_0 + \int_0^t q(t) v q(t)^{-1} dt$$

where q is a unit quaternion.

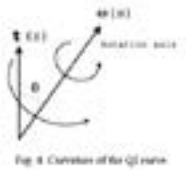

Miura, K.T., "Unit Quaternion Integral Curve: A New Type of Fair Free-Form Curves," Computer Aided Geometric Design, vol.17, no.1, pp.39-58, 2000

10

GLAC

Gobithaasan, R.U. (2010). The Development of Planar Curves with High Aesthetic Value (Doctoral dissertation, Universiti Sains Malaysia, Jan. 2010).

Radius of curvature-shifted GLAC

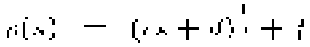

Curvature-shifted GLAC

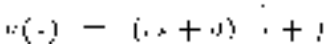

Difference

Directional angle of ROC-shifted GLAC : hypergeometric function

Directional angle of curvature-shifted GLAC : integrable

11

Example of aesthetic curves

Typical example of aesthetic curves
logarithmic (equiangular) spiral

Nautilus

Logarithmic spiral

Counterexample:
Archimedean spiral

$r = r_0 + a\theta$

Logarithmic spiral

Logarithmic spiral

General expression

$$C(t) = e^{(a+ib)t}, \quad (t \geq 0)$$

Main property

$$\rho = c_0 s + c_1$$

ρ : radius of curvature,

s : arc length

Self-similarity

$$C'(t) = C(t+1)$$
$$= e^a e^{ib} C(t)$$

13

Reasons to be aesthetic

Self-similarity

Golden ratio

$$\phi = \frac{\sqrt{5}+1}{2} = 1.618033989...$$

「Golden section connects art and mathematics」

Golden spiral : a kind of logarithmic spirals

About the fixed point (intersection of red lines) rotate by 90 degrees clockwise and scale by $1/\phi$

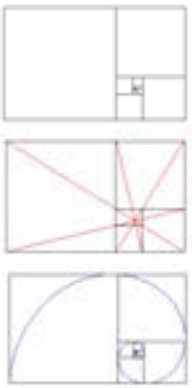

Golden spiral

14

Clothoid curve

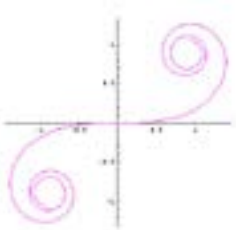

Clothoid curve

General expression

$$C(t) = \int_0^t e^{iat^2} dt, \quad (t \geq 0)$$

Main property

$$\rho^{-1} = c_0 s + c_1$$

ρ : roc, s : arc length

Self-affinity

Reparametarize as $s(t) = c_1(e^{\beta t} - 1)/c_0$

$$\rho'(t) = e^{-\beta} \rho(t+1)$$
$$s'(t) = s(t+1) - s(1) = e^{\beta} s(t)$$

15

Circle involute curve

Circle involute curve

General expression

$$C(t) = (\cos t + t \sin t, \sin t - r \cos t)$$

Main property

$$\rho^2 = c_0 s + c_1$$

ρ : roc, s : arc length

Self-affinity

Reparametrize as $t = c_1(e^{\beta t} - 1)/c_0$

$$\rho'(t) = \rho(t+1) = e^{\beta/2}\rho(t)$$

$$s'(t) = s(t+1) - s(1) = e^{\beta} s(t)$$

16

Involute gear

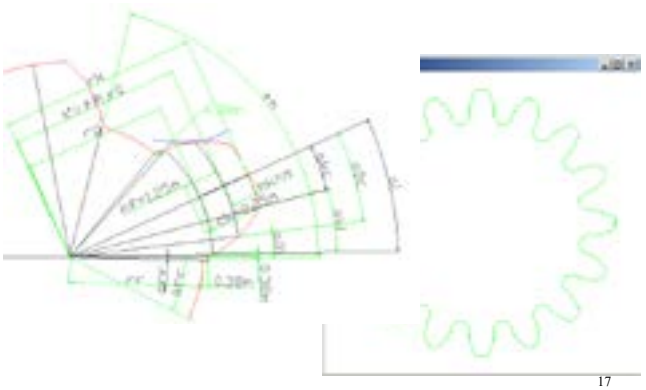

17

Self-affinity

[Ref: Mathematics of shape, Ryuji Takagi]

Extension #2 Self-affinity

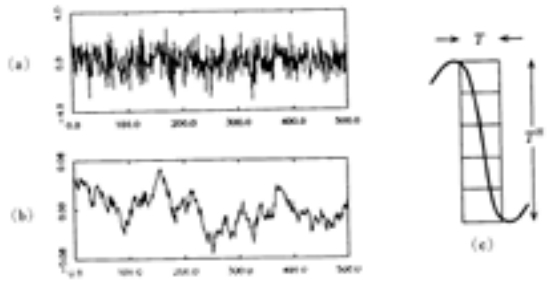

図 2.24 乱雑信号

(a), (b) コンピューターによる波形 (Turcotte, 1988)[20], (c) 波形の統覆.

18

Logarithmic Curvature Histogram #1

Logarithmic curvature histogram

Horizontal axis : log of radius of curvature
Vertical axis : log of small change of arc length with respect to small change of log of radius of curvature

$$\log(\frac{ds}{d(\log\rho)})$$

rhythm	α	elem. func.	impressions
simple	−	sin, cubic cur.	sharp, strong
	0	(not found)	stable
	+	parabola, log, log. spiral	gathering centripetal
complex	+ → −	sin	diverge to converge
	− → +	(not found)	converge to diverge

Table 1: LCH lines' slopes α and their impressions

19

Logarithmic Curvature Histogram #2

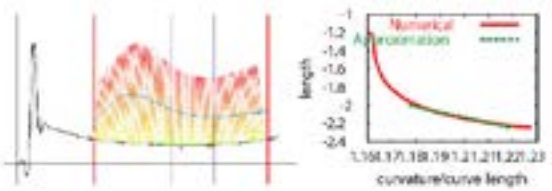

20

A general equation of aesthetic curves

$$\log(\rho\frac{ds}{d\rho}) = \alpha\log\rho + C, \quad \rho^{\alpha} = c_0 s + c_1, \quad \rho = c_0 e^{c_1 s}$$

The fundamental equation of aesthetic curves

Logarithmic spiral α=1

Clothoid curve α= -1

Circle involute α= 2

Nielsen's spiral α= 0

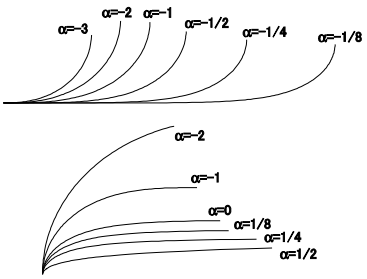

21

Parametric expression

$$\rho(s) = (c_0 s + c_1)^{\frac{1}{\alpha}}$$

$$\frac{dx}{ds} = \cos\theta, \quad \frac{dy}{ds} = \sin\theta$$

$$\frac{d\theta}{ds} = (c_0 s + c_1)^{-\frac{1}{\alpha}}$$

$$C(s) = P_0 + e^{ic_2} \int_0^s e^{i\frac{\alpha(c_0 s + c_1)^{\frac{\alpha-1}{\alpha}}}{(\alpha-1)c_0}} ds$$

Extended clothoid curve

22

Self-affinity

Main property

$\rho^{\alpha} = c_0 s + c_1$

ρ : radius of curvature, s : arc length

Self-affinity

$\rho'(t) = e^{\frac{\beta}{\alpha}} \rho(t+1)$

$s'(t) = s(t+1) - s(1) = e^{\beta} s(t)$

where $s(t) = c_1(e^{\beta t} - 1)/c_0$

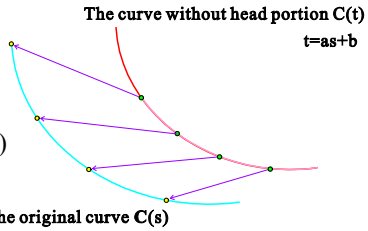

23

Butterfly's wings

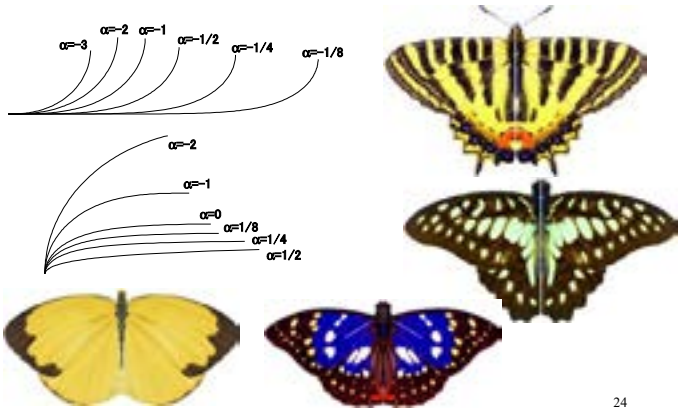

24

N. Yoshida and T. Saito, Interactive Aesthetic Curve Segments, The Visual Computer (Pacific Graphics), Vol. 22, No.9-11, pp.896-905, 2006.

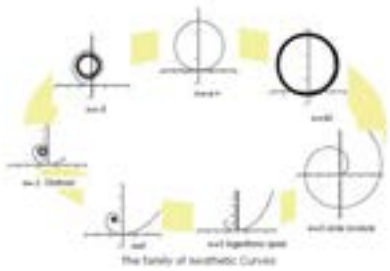

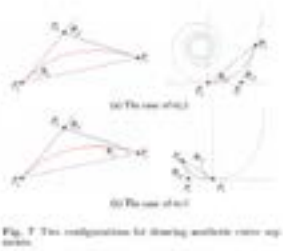

25

INTERACTIVE DESIGN USING LAC

26

Compound-Rhythm LAC

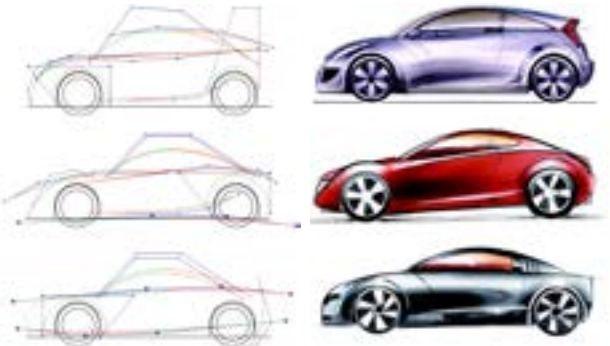

Kenjiro T. Miura, Dai Shibuya, R.U. Gobithaasan, Shin Usuki, "Designing Log-aesthetic Splines with G2 Continuity," Computer-Aided Design & Applications, Vol.10, No.6, pp.1021-1032, 2013, DOI: 10.3722/cadaps.2013.1021-1032

27

G^2 C-Shape & S-Shape with LAC triplets

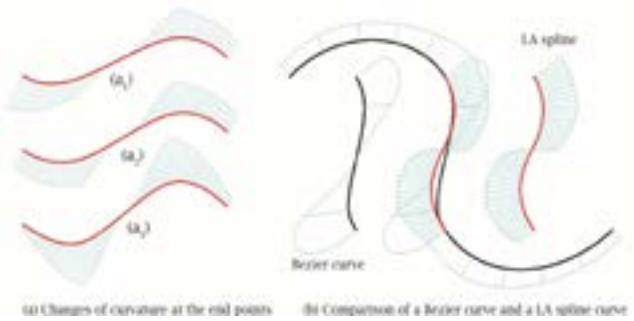

(a) Changes of curvature at the end points (b) Comparison of a Bezier curve and a LA spline curve

Kenjiro T. Miura, Dai Shibuya, R.U. Gobithaasan, Shin Usuki, "Designing Log-aesthetic Splines with G2 Continuity," Computer-Aided Design & Applications, Vol.10, No.6, pp.1021-1032, 2013, DOI: 10.3722/cadaps.2013.1021-1032

28

LAC as plugin for Rhino 3D

(a) Isoparametric lines and zebra mapping (b) Rendering (c) Mock-up

Kenjiro T. Miura, Dai Shibuya, R.U. Gobithaasan, Shin Usuki, "Designing Log-aesthetic Splines with G2 Continuity," Computer-Aided Design & Applications, Vol.10, No.6, pp.1021-1032, 2013, DOI: 10.3722/cadaps.2013.1021-1032.

29

Design examples

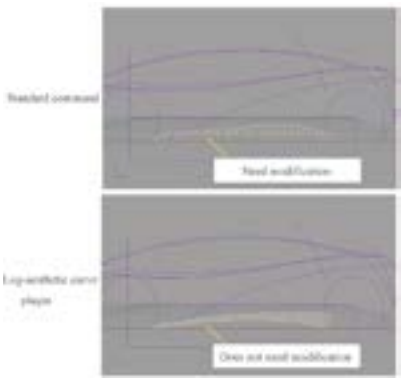

30

Applications for Archtecture

31

SIMILARITY GEOMETRY

32

Similarity Geometry of the Plane Curve #1

Since we know that the arc length s may vary, thus the representation of plane curves is parameterized by direction angle θ which is invariant by scaling.

We assume the curve is not a straight line. Let a plane curve be given as a function of its direction angle by $\boldsymbol{C}(\theta)$ and let a unit tangent vector $\boldsymbol{T}^{sim}$ and a unit normal vector $\boldsymbol{N}^{sim}$. Then

$$\boldsymbol{T}^{sim}(\theta) = \frac{d\boldsymbol{C}}{ds}\frac{ds}{d\theta} = \frac{1}{\kappa(s)}\boldsymbol{T}(s)$$

$$\boldsymbol{N}^{sim}(\theta) = \frac{1}{\kappa(s)}\boldsymbol{N}(s)$$

33

Similarity Geometry of the Plane Curve #2

Similarity Frenet frame $F^{sim}(\theta) = (T^{sim}(\theta), N^{sim}(\theta))$

$$\frac{d}{d\theta}F^{sim}(\theta) = F^{sim}(\theta)\begin{pmatrix} -\kappa^{sim}(\theta) & -1 \\ 1 & -\kappa^{sim}(\theta) \end{pmatrix}$$

where

Similarity curvature $S(\theta) = \kappa^{sim}(\theta) = \frac{1}{\kappa^2}\frac{d\kappa}{ds} = -\frac{d\rho}{ds} = -\frac{1}{\rho}\frac{d\rho}{d\theta}$

Similarity curvature is a similarity geometry invariant!

34

Similarity Curvature of LAC and its evolute

$$\frac{dS}{d\theta} = (\alpha - 1)S^2$$

LAC: general solution $S(\theta) = L(\alpha, \lambda; \theta) = -\frac{\lambda}{(\alpha-1)\lambda\theta+1}$

$$\frac{dS(\theta)}{d\theta} = S(\theta)^2 - T\left(\theta + \frac{\pi}{2}\right)S(\theta)$$

where $S(\theta)$: similarity curvature of LAC, $T(\theta+\pi/2)$:that of its evolute

Assume that $T(\theta+\pi/2)=(2-\alpha)L(\alpha, \lambda, \theta)=L(1/(2-\alpha), (2-\alpha)\lambda, \theta)$.
ROC-shift GLAC: general solution

$$S(\theta) = \frac{L(\alpha,\lambda;\theta)}{1+C((\alpha-1)\lambda\theta+1)^{\frac{1}{1-\alpha}}} = \frac{L(\alpha,\lambda;\theta)}{1+\nu((\alpha-1)\lambda\theta+1)^{\frac{1}{1-\alpha}}}$$

Sato, M.; Shimizu, Y.: The log-aesthetic curve and Riccati equations from the viewpoint of similarity geometry, Proc. JSIAM2014, 2014.

35

Similarity Radius of Curvature

$$\frac{dV}{d\theta} = 1 - \alpha$$

LAC: general solution $V(\theta) = M(\alpha, \lambda; \theta) = -\frac{(\alpha-1)\lambda\theta+1}{\lambda}$

$$\frac{dV(\theta)}{d\theta} = T\left(\theta + \frac{\pi}{2}\right)V(\theta) - 1$$

where $V(\theta)$=1/$S(\theta)$: Similarity ROC of LAC

General solution of $V(\theta)$: $V(\theta) = \frac{1+C((\alpha-1)\lambda\theta+1)^{\frac{1}{1-\alpha}}}{L(\alpha,\lambda;\theta)}$

Similarity ROC of Curvature-shift GLAC:

$$V_{K-GALC}(\theta) = -\frac{((\alpha-1)\lambda\theta+1)^{\frac{\alpha}{\alpha-1}}(v+((\alpha-1)\lambda\theta+1)^{\frac{1}{1-\alpha}})}{\lambda}$$

$$V(-\theta) = -\frac{((\beta-1)\lambda\theta+1)^{\frac{\beta}{\beta-1}}\left(C+((\beta-1)\lambda\theta+1)^{\frac{1}{1-\beta}}\right)}{\lambda} = M(\beta,\lambda;-\theta)(1+\nu((1-\beta)\lambda\theta+1)^{\frac{1}{\beta-1}})$$

36

where β=2-α

Kenjiro T. Miura, R.U. Gobithaasan, Sho Suzuki, Shin Usuki, Reformulation of Generalized Log-aesthetic Curves with Bernoulli Equations, Computer-Aided Design and Applications , Volume 13, Issue 2, pages 265-269, 2016. DOI:10.1080/16864360.2015.1084200.

Similarity Curvature of Typical Curve

$$\frac{dS}{d\theta} = -\frac{-1}{n+1}S^2 - \frac{n+1}{(n-1)^2}$$

where n is degree of the curve.

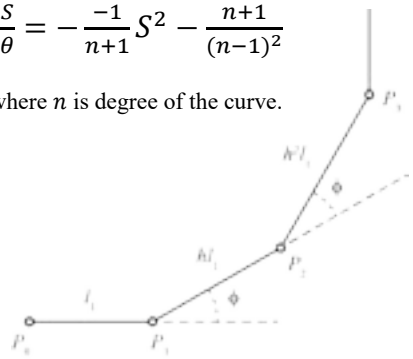

Sato, M., & Shimizu, Y. (2016). Generalization of log-aesthetic curves by Hamiltonian formalism. JSIAM Letters, 8, 49-52.

37

σ-Curve and τ-Curve

Fig. 3. A Venn diagram illustrating relationship between σ-curve and τ-curve.

Kenjiro T. Miura, Sho Suzuki, R.U. Gobithaasan, Shin Usuki, Jun-ichi Inoguchi, Masayuki Sato, Kenji Kajiwara, Yasuhiro Shimizu, "Fairness metric of plane curves defined with similarity geometry invariants," Computer-Aided Design and Applications, DOI:10.1080/16864360.2017.1375677, 2017.

K.T. Miura, S. Suzuki, S. Usuki, R.U. Gobithaasan, τ-curve -Introduction of Cusps to Aesthetic Curves, Journal of Computational Design and Engineering, 2020, 7(2), 155-164.

38

σ-Curve

We define σ curve by its Cesàro equation as follows:

$$\sigma = \rho^{\alpha} = a_n s^n + a_{n-1}s^{n-1} + \cdots + a_1 s + a_0 \qquad (5.13)$$

In the above equation, $\sigma = \rho^{\alpha}$ is given by a polynomial function of arc length s.

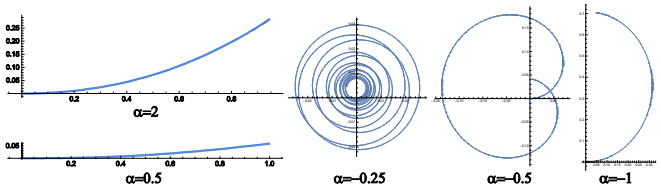

39

σ-Curve

$$\kappa^{-\alpha} = as^2 + bs + c$$

where a, b and c are constants. By differentiating both sides of the above equation with respect to s three times and assuming $\kappa \neq 0$, we obtain

$$-(\alpha+1)(\alpha+2)\kappa_s^3 + 3(\alpha+1)\kappa\kappa_s\kappa_{ss} - \kappa^2\kappa_{sss} = 0 \quad (69)$$

From Eq.(23) $\kappa_s = d\kappa/ds = \kappa^2 S$ and

$$\kappa_{ss} = \frac{d^2\kappa}{ds^2} = \kappa^3(S_\theta + 2S^2)$$

$$\kappa_{sss} = \frac{d^3\kappa}{ds^3} = \kappa^4(6S^3 + 7SS_\theta + S_{\theta\theta}) \quad (70)$$

By substituting the above equations in Eq.(69), we have the following second-order nonlinear ordinary differential equation for S.

$$S_{\theta\theta} + (4 - 3\alpha)SS_\theta + (\alpha - 1)(\alpha - 2)S^3 = 0 \quad (71)$$

40

τ-Curve

According to the discussion so far, it is desirable to use direction angle $\theta(s)$ to introduce points with infinite curvature to a curve. Similar to the σ-curve definition, the power β of $\theta(s)$ is given by a polynomial function of arc length s, i.e.

$$\operatorname{sgn}(\theta)|\theta|^\beta = b_n s^n + b_{n-1}s^{n-1} + \cdots + b_1 s + b_0 \quad (19)$$

Supposing $\theta \geq 0$,

$$\theta = \left[b_n s^n + b_{n-1}s^{n-1} + \cdots + b_1 s + b_0\right]^{\frac{1}{\beta}} \quad (20)$$

In this research, the curve whose direction angle $\theta(s)$ is given in this way is called τ-curve. Similar to σ-curve n is called the degree of τ-curve.

K.T. Miura, S. Suzuki, S. Usuki, R.U. Gobithaasan, τ-curve -Introduction of Cusps to Aesthetic Curves, Journal of Computational Design and Engineering, 2020, 7(2), 155-164.

41

τ-Curve

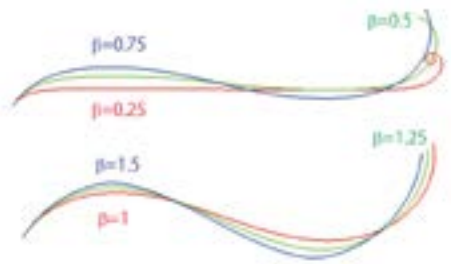

Figure 9. Quadratic τ-curve: length=4.5, $\theta^\beta = (s^2 - 4s + 3)/3 = (s-1)(s-3)/3$.

K.T. Miura, S. Suzuki, S. Usuki, R.U. Gobithaasan, τ-curve -Introduction of Cusps to Aesthetic Curves, Journal of Computational Design and Engineering, 2020, 7(2), 155-164.

42

τ-Curve

The direction angle θ of a quadratic τ-curve powered by β is given by

$$\theta^{\beta} = as^2 + bs + c \qquad (101)$$

where a and b are constants. As in the quadratic θ-curve, by differentiating both sides of the above equation with respect to s three times and assuming $\kappa' \neq 0$, we obtain the following first-order nonlinear ordinary differential equation:

$$(\beta-1)(\beta-2)+3(\beta-1)\theta\tilde{s}_\theta+\theta^2\tilde{s}_\theta^2=0$$

Even though the above differential equation is non-linear, fortunately we can get its analytical solution as follows:

$$\tilde{s} = \frac{-\frac{2\sqrt{\beta^2-3\beta+4}}{\sqrt{\theta^{\beta}}}+\sqrt{\beta^2-3\beta+4}}{b} \qquad (102)$$

43

K-CURVE

Kawaii Engineering

Kawaii Engineering, editor: Michiko Ohkura, Springer 2019.

Japanese word: “かわいい”
English word: cute, lovable, charming, (cool)

For 2D and 3D objects, kawaii preference for curved shape is in common.

Zhipei Yan, Stephen Schiller, Gregg Wilensky, Nathan Carr, Scott Schaefer, “k-Curves: Interpolation at Local Maximum Curvature,” TOG, 36(4), 129, 2017.

εκ-Curves:
Controlled Local Curvature Extrema

K.T. Miura et al. εκ-Curves: Controlled Local Curvature Extrema, The Visual Computer, 2021.

Kenjiro T. Miura[1]
R.U. Gobithaasan[2]
Péter Salvi[3]
Dan Wang[1]
Tadashi Sekine[1]
Shin Usuki[1]
Jun-ichi Inoguchi[4]
Kenji Kajiwara[5]
[1]Shizuoka University
[2]University Malaysia Terenggan
[3]Budapest U. of T. and E.
[4]University of Tsukuba
[5]Kyushu University

46

κ-curves

The κ-curve is a recently published interpolating spline which consists of quadratic Bézier segments passing through input points at the loci of local curvature extrema. [Yan2017]. It has the following properties:

1. It passes through all input point.
2. All the curvature extremum points are input points.
3. Curvature continuity (G^2 continuity) is guaranteed except for inflection points.

Zhipei Yan, Stephen Schiller, Gregg Wilensky, Nathan Carr, Scott Schaefer, "κ-Curves: Interpolation at Local Maximum Curvature," TOG, 36(4), 129, 2017.

47

κ-curves examples

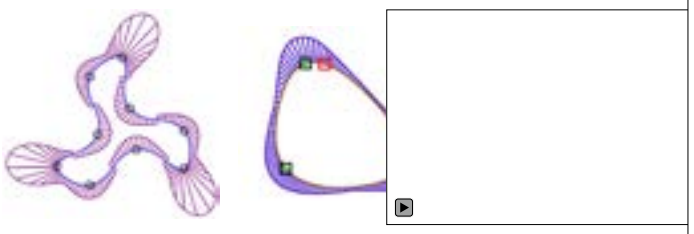

48

Disadvantages of κ-curves and its improvement

The values of curvature extrema can't be controlled !

[Yan2019]
Increase DOF by using rational quadratic Bézier curve.

Proposed method
Increase DOF by elevating degree from quadratic to cubic.

Advantage
Not only rational quadratic Bézier, but also other various type of curves

Z. Yan, S. Schiller, and S. Schaefer, "Circle reproduction with interpolatory curves at local maximal curvature points," Computer Aided Geometric Design, vol. 72, no. 6, pp. 98–110, 2019.

49

εκ-curves: extended κ-curves

Constrained cubic curve

$\frac{d\kappa}{dt} = 0$: polynomial of degree 9 in terms of parameter t

For one curve segment

1. Proof of at most one curvature extremum[1]

2. Uniqueness of the solution passing the input point[2]

[1] K. T. Miura, "One peak," November 2020. [Online]. Available: https://mc2-lab.com/KTMiuraOnePeak.pdf

[2]K. T. Miura , "Unique solution," November 2020. [Online]. Available: https://mc2-lab.com/KTMiuraUniqueSolution.pdf

50

εκ-curves: Local modifications

51

εκ-curves: Global modifications

εκ-curves: Comparison with Log-Aesthetic Curves

Log-aesthetic curves

εκ-curves

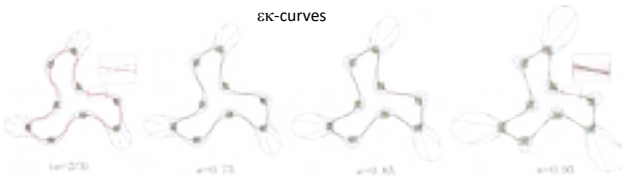

εκ-curves: Sample code in Julia and Movie file

Contributions

1. Inherent nice properties of κ-curve
2. Applicable for various curves(polynomial, rational, trigonometric, etc.)
3. Not necessary to increase # of input points to control curvature extrema
4. Global and local control of curvature extrema
5. As fast as κ-curves

Prototype in Julia
P. Salvi, (2020, November) εκ-curves. [Online] Available: https://github.com/salvipeter/ekcurves/tree/master

Movie file
[Online] Available: https://mc2-lab.com/ek-curves.mp4

εκ-curves: Movie file

55

Future works

Surface

1. Log-aesthetic surface?
2. Not K-surface, but κ-surface?

K-Surfaces: Bézier-Splines Interpolating at Gaussian Curvature Extrema (2023)
Tobias Djuren, Maximilian Kohlbrenner, Marc Alexa
ACM Transactions on Graphics (Proc. of Siggraph Asia)

56

Intrinsic and extrinsic singularities and curvatures of piecewise smooth surfaces

Miyuki Koiso
Institute of Mathematics for Industry, Kyushu University, Japan

Abstract

We study piecewise-smooth (PS in short) surfaces which are two-dimensional topological manifolds made by connecting finitely many smooth surfaces. We discuss intrinsic and extrinsic singular points of such surfaces and give new definitions which represent curvature and sharpness at each point in the 'edges' and at each 'vertex' of such a surface. Especially, the intrinsic singularities are defined intrinsically by using a generalization of the classical Bertrand-Puiseux Theorem, which gives a power series expansion of the length of the geodesic circle with respect to the radius. Then, as an application of the new concepts mentioned above, we represent the well-known Gauss-Bonnet Theorem that gives a relationship between curvatures and topology for surfaces in a simple form. We discuss also the definition and characterization of PS developable surfaces which are locally isometric to planar domains. Our definitions of intrinsic curvatures can estimate how far a PW-smooth surface is from being developable.

International Conference "Evolving Design and Discrete Differential Geometry - towards Mathematics Aided Geometric Design"

Intrinsic and extrinsic singularities and curvatures of piecewise smooth surfaces*

Miyuki Koiso
（IMI, Kyushu University, Japan）

March 13, 2025, Nishijin Plaza, Kyushu University

*This work is supported by JST CREST Grant Number JPMJCR1911 and JSPS KAKENHI Grant Number JP20H01801.

Plan of talk

1. Motivation
2. Bertrand-Puiseux Theorem and its generalization
3. Definitions of intrinsic singular points and curvatures
4. Gauss-Bonnet Theorem.
5. Idea of the proof of the generalized Bertrand-Puiseux Theorem
6. Summary

1.Motivation

Definition（Piecewise smooth surface）.
Let $M = \bigcup_{i=1}^{k} M_i$ be a 2-dim. connected oriented C^∞- manifold included in $\mathbb{R}^3$. If M satisfies the following conditions (i) - (iii), we call M a piecewise smooth (PW-smooth in short) surface in $\mathbb{R}^3$.

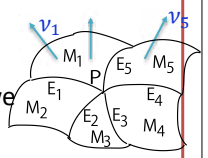

(i) Each M_i is an oriented connected smooth submanifold with piecewise smooth boundary ∂M_i and unit normal vector field ν_i in $\mathbb{R}^3$.
(ii) If $i \neq j$, then $M_i \cap M_j = \partial M_i \cap \partial M_j$ holds.
(iii) For each i, the unit normal ν_i satisfies the following condition: For any local coordinates (u_1, u_2), $\left\{\frac{\partial}{\partial u_1}, \frac{\partial}{\partial u_2}, \nu_i\right\}$ gives the canonical orientation of $\mathbb{R}^3$.

1.Motivation (continuation)

Definition (Extrinsic singular points).
Let $M = \cup_{i=1}^{k} M_i$ be a PW-smooth surface.
(i) If $M_i \cap M_j \neq \phi$ and $i \neq j$, then $M_i \cap M_j$ is called an extrinsic edge (or simply, edge) of M.
(ii) If $p = M_1 \cap \cdots \cap M_N \in M^o$ (M_1, ..., M_N are all different, and $N \geq 3$) is called an extrinsic vertex (or simply, vertex) of M.

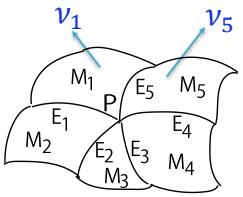

4

1.Motivation (continuation)

Def. 1. A piecewise (PW)-smooth surface M is said to be developable if it is isometric to a planar region R (that is, there exists a Lipschitz continuous bijective mapping F from M onto R that preserves the length of each curve).

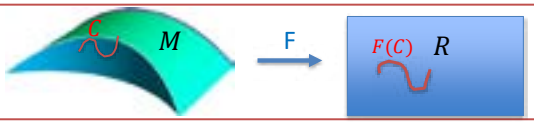

Remark 1. It is well-known that a smooth surface M is developable if and only if the Gaussian curvature $K(p)$ of M vanishes at any point $p \in M$.

Question. Estimate how far a PW-smooth surface is from being developable.

5

2. Bertrand–Puiseux Theorem and its generalization

Let M be a PW-smooth surface. For $p, q \in M$, $\mathrm{dist}(p,q) :=$ the smallest length of PW C^∞ curves connecting p and q in M.

Remark. A shortest path is not necessarily smooth!

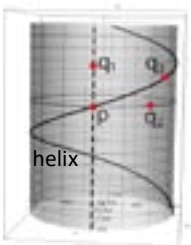

Cylinder and geodesics

pA is a straight line segment.

Aq is a part of a helix.

Cylinder covered with a disc and its non-smooth shortest path connecting p, q.

6

2. B–P Theorem and its generalization (continuation)

Let M be a PW–smooth surface. The Gaussian curvature of M at a regular point $p \in M$ is denoted by $K(p)$. The geodesic circle in M with center at p and radius r is defined as $C(p;r) = \{q \in M | \mathrm{dist}(q,p) = r\}$, and the length of $C(p;r)$ is denoted by $L(p;r)$.

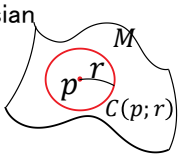

Bertrand (1848. For general R-mfd, Gray1974). If $p \in M$ is a regular point, then for small $r > 0$, $L(p;r) = 2\pi r - \frac{\pi}{3} K(p) r^3 + o(r^3)$.

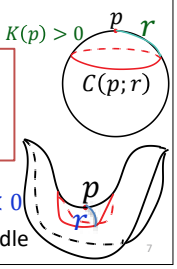

Rem. If M is a plane, $C(p;r)$ is a round circle with radius r and $L(p;r) = 2\pi r$.

2. B–P Theorem and its generalization (continuation)

Next, let $M = \bigcup_j M_j$ be a PW–smooth surface.

And let $p = M_1 \cap \cdots \cap M_N$.

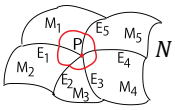

$N = 5$

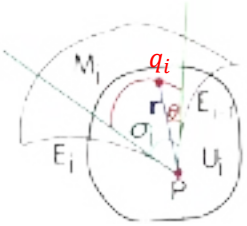

In a neighborhood U_i of a point $p \in M_i$, we use the geodesic polar coordinate (r,θ) to represent any point as $q_i = q(r,\theta) \in M_i \cap U_i$, $(\vartheta_1^i(r) \le \theta \le \vartheta_2^i(r))$.

σ_i is the inner angle of M_i at p, $K_i(p)$ is the Gaussian curvature of M_i at p, $k_{g1}^i(\mathrm{r})$ is the signed geodesic curvature of the edge $M_i \cap M_{i-1}$ and $k_{g2}^i(\mathrm{r})$ is that of $M_i \cap M_{i+1}$.

2. B–P Theorem and its generalization (continuation)

Let $M = \bigcup_j M_j$ be a PW smooth surface. And let $p \in M^o$.

Theorem 1 (Koiso) (1) Let $p = M_1 \cap \cdots \cap M_N$ be a vertex of M. then $L(p;r) = \left(\sum_{i=1}^N \sigma_i\right) r - \frac{1}{2}\sum_{i=1}^N \left(k_{g1}^i(0) + k_{g2}^i(0)\right) r^2 - \frac{1}{6}\sum_{i=1}^N \left(K_i(p)\sigma_i + (k_{g1}^i)'(0) + (k_{g2}^i)'(0)\right) r^3 + o(r^3)$.

(2) Let p be an interior point of an edge $E = M_1 \cap M_2$. Denote by $k_j(p)$ the geodesic curvature of $E \subset M_j$ at p w.r.t. the inner normal. Then, $L(p;r) = 2\pi r - \left(k_1(p) + k_2(p)\right) r^2 - \frac{\pi}{6}\left(K_1(p) + K_2(p)\right) r^3 + o(r^3)$.

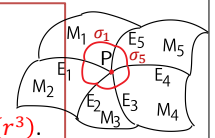

Cor. 1. The area of geodesic discs are given by integrating $L(p;r)$ with respect to r.

2. B–P Theorem and its generalization (continuation)

For a regular arc $\gamma \subset M$, the signed geodesic curvature k_g is expressed as $k_g = \dfrac{\det(\dot\gamma\ \ddot\gamma\ \nu)}{|\dot\gamma|^3}$.

Example 1. $M = M_1 \cup M_2 \cup M_3$, $p \in E = M_1 \cap M_2$, where M_1 is a part of a cylinder with radius R, M_2 and M_3 are flat disks with radius R. Then,

$$L(p;r) = 2\pi r - \frac{1}{R}r^2 + o(r^4).$$

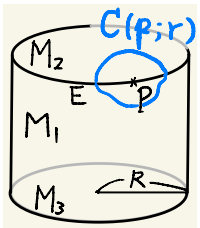

10

2. B–P Theorem and its generalization (continuation)

Example 2. Let M be a cube. Then, for each vertex p, $L(p;r) = \frac{3}{2}\pi r$.

Example 3. $M = M_1 \cup M_2$, $p \in E = M_1 \cap M_2$,

$$L(p;r) = 2\pi r - 2\frac{\cot\theta}{R}r^2 - \frac{\pi}{3R^2}r^3 + o(r^3)$$

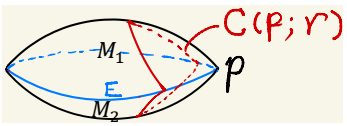

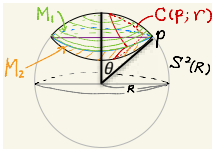

11

3. Definition of intrinsic singular points and curvatures (cont.)

Let $M = \cup_j M_j$ be a PW–smooth surface. Let $p \in M^o$. Represent the length $L(p;r)$ of the geodesic circle $C(p;r)$ in M with center at p and radius r as $L(p;r) = a_1(p)r + a_2(p)r^2 + a_3(p)r^3 + o(r^3)$.

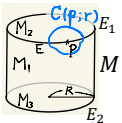

Cylinder $M = \sum_{j=1}^{3} M_j$
(E_1, E_2 : edges of M)

Def. 1(K). (i) If $a_1(p) \neq 2\pi$, we call p an intrinsic vertex of M.
(ii) We call the set of points that satisfy both $a_1(p) = 2\pi$ and $a_2(p) \neq 0$ intrinsic edges of M.

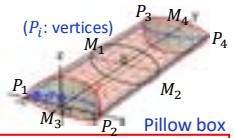

(P_i: vertices)

Pillow box

Def. 2 (K). (i) We call $S(p) := 2\pi - a_1(p)$ the sharpness of M at p.
(ii) We call $k_e(p) := -a_2(p)$ the edge curvature of M at p.
(iii) We call $K(p) := -(3/\pi)a_3(p)$ the Gaussian curvature of M at p.

Theorem 2 (K). A PW-smooth surface is locally developable. $\Leftrightarrow S(p) = k_e(p) = K(p) = 0, \forall p \in M$.

12

4. Gauss-Bonnet Theorem

The classical Gauss-Bonnet Theorem can be represented as follows.

Proposition 1 (K). Let M be a closed PW-smooth surface with Euler characteristic χ. And let $\tilde{E}$ be the union of all intrinsic edges of M. Then, it holds that

$$\int_M K\, dA + \int_{\tilde{E}} k_e\, ds + \sum_{p\in M} S(p) = 2\pi\chi,$$

where dA is the area element of M and ds is the line element at regular points of $\tilde{E}$.

13

5. Idea of the proof of the generalized Bertrand–Puiseux Theorem

Let M be a PW–smooth surface. And let $p = M_1 \cap \cdots \cap M_N \in M^o$. Near the point $p \in M_i$, we use the geodesic polar coordinate (r,θ) to represent any point as $q_i = q(r,\theta)$, $(\vartheta_1^i(r) \le \theta \le \vartheta_2^i(r))$, and metric $ds^2 = dr^2 + h^2 d\theta^2$, where $h = (q_\theta \cdot q_\theta)^{\frac{1}{2}}$. Then, $L(p;r) \approx \sum_{i=1}^N \int_{\vartheta_1^i(r)}^{\vartheta_2^i(r)} h(r,\theta)d\theta$.

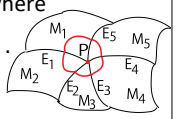

Let
$L(p;r) = a_1(p)r + a_2(p)r^2 + a_3(p)r^3 + o(r^3)$.
Then, using L'Hopital's rule, we obtain

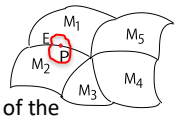

$a_1 = \lim_{r\to 0} \frac{1}{r}\left(\sum_{i=1}^N \int_{\vartheta_1^i(r)}^{\vartheta_2^i(r)} h(r,\theta)d\theta\right) =$
$\lim_{r\to 0}\left(\sum_{i=1}^N \int_{\vartheta_1^i(r)}^{\vartheta_2^i(r)} h_r d\theta\right) = \sum_{i=1}^N \left(\vartheta_2^i - \vartheta_1^i\right)$ =the sum of the inner angles around p, here we used $\lim_{r\to+0} h_r = 1$.

14

5. Idea of the proof of the generalized Bertrand–Puiseux Theorem (continuation)

Recall the length of the geodesic circle $C(p;r)$ is
$L(r) := L(p;r) = a_1(p)r + a_2(p)r^2 + a_3(p)r^3 + o(r^3)$

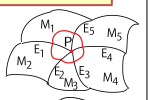

$\approx \sum_{i=1}^N \int_{\vartheta_1^i(r)}^{\vartheta_2^i(r)} h(r,\theta)d\theta$. Then, using L'Hopital's rule again,

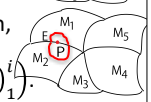

$a_2 = \lim_{r\to+0} \frac{L(r)-a_1 r}{r^2} = \lim_{r\to+0} \frac{L''(r)}{2} = \frac{-1}{2}\sum_{i=1}^N \left((k_g)_2^i + (k_g)_1^i\right)$.

$$a_3 = \lim_{r\to+0} \frac{L(r) - a_1 r - a_2 r^2}{r^3} = \lim_{r\to+0} \frac{L''(r) - 2a_2}{6r}$$

$$= -\frac{1}{6}\sum_{i=1}^N \left(\sigma_i K_i(p) + \lim_{r\to 0}\left((k_{g1}^i)'(r) + (k_{g2}^i)'(r)\right)\right),$$

where σ_i is the inner angle of M_i at p. Moreover we estimate the error term. From these we obtain the result.

15

6. Summary

- We generalized the classical Bertrand–Puiseux Theorem to PW-smooth surfaces (say M). For example,

let $p = M_1 \cap \cdots \cap M_N$ be a vertex of M. Then the length of the geodesic circle $C(p;r)$ in M with center at p and radius r is

$$L(p;r) = \left(\sum_{i=1}^{N} \sigma_i\right) r - \frac{1}{2}\sum_{i=1}^{N}\left(k_{g1}^{i}(0) + k_{g2}^{i}(0)\right) r^2 - \frac{1}{6}\sum_{i=1}^{N}\left(K_i(p)\sigma_i + (k_{g1}^{i})'(0) + (k_{g2}^{i})'(0)\right) r^3 + o(r^3),$$

where K_i is the Gauss. curvature, and k_{gj}^{i} is the geodesic curvature.

- We defined intrinsic singular points (edges and vertices) and curvatures of PW-smooth surfaces.
- We gave a simple representation of the Gauss-Bonnet Theorem using the intrinsic singular points at curvatures there.
- We explained ideas of the proof of the main result.

16

Geometric shape generation for ideal lighting

Yoshiki Jikumaru
Faculty of Information Networking for Innovation And Design, Toyo University, Japan

Kentaro Hayakawa
Department of Conceptual Design, College of Industrial Technology, Nihon University, Japan

Kazuki Hayashi
Department of Architecture and Architectural Engineering, Graduate School of Engineering, Kyoto University, Japan

Miyuki Koiso
Institute of Mathematics for Industry, Kyushu University, Japan

Shun Kumagai
Hachinohe Institute of Technology, Japan

Abstract

In this talk, we propose a geometric shape generation of roof design for ideal lighting. The idea is based on the variational problem for anisotropic energy, originally proposed as a mathematical model for crystal growth. In our implementation, users can intuitively specify the direction in which they want to improve lighting. Moreover, our approach allows us to generate shapes with natural "internal boundary". While the main idea will be introduced in the smooth setting, we also propose a discretization for triangulated surfaces and shape generations.

Let $\mathbb{S}^2$ be the unit sphere in the 3-dimensional Euclidean space $\mathbb{R}^3$ and $\gamma : \mathbb{S}^2 \to \mathbb{R}$ be a positive-valued smooth function. For a smooth surface M in $\mathbb{R}^3$, we define the *anisotropic energy* $\mathcal{F}_\gamma(M)$ as follows:

$$\mathcal{F}_\gamma(M) = \int_M \gamma(N)\, dA,$$

where N denotes the unit normal vector field along M and dA denotes the area element. The minimizer of the anisotropic energy among all closed "surfaces" enclosing the same volume is called the *Wulff shape*. Moreover, a critical point of the anisotropic energy under volume-preserving variations can be characterized as a "constant anisotropic curvature" condition. If $\gamma \equiv 1$, the functional gives the area, and therefore, this situation can be regarded as a generalization of constant mean curvature (CMC) surfaces, which gives a mathematical model of soap bubbles. The above model of "generalization of soap bubbles" is useful for shape generation in the following two ways:

- While soap bubbles are "homogeneous", Wulff shapes, in general, "change the size of the faces according to the direction of the normal vector", which can be used to specify the "direction of lighting".
- While soap bubbles have "no edges", Wulff shapes generally have "edges", and natural "internal boundaries" can be generated without connecting several surface pieces.

References

[1] Miyuki Koiso and Bennett Palmer, Geometry and stability of surfaces with constant anisotropic mean curvature, Indiana University Mathematics Journal **54** (2005), 1817–1852.

Information Networking for Innovation And Design

Geometric shape generation for ideal lighting

CREST ED3GE International Conference

Yoshiki Jikumaru (Toyo University)

Collaborators: Kazuki Hayashi (Kyoto University), Kentaro Hayakawa (Nihon University), Miyuki Koiso (Kyushu University), Shun Kumagai (Hachinohe Institute of Technology)

Faculty of Information Networking for Innovation And Design
Toyo University

March 13, 2025

The "target" objects

Figure: London City Hall

Figure: Entrance of Metro Bilbao

https://hash-casa.com/2021/09/08/londoncityhall/

A "summary" of this talk

A "summary" of this talk

- Shape generation with "corners" without connecting surface patches.
- The user specifies the direction in which they want to create more faces by changing the parameters ("ideal lighting").
- The idea came from the geometry of anisotropic energy, which originates the crystal growth model.

Introduction: Isoperimetric problem

Isoperimetric problem (2D, 等周問題)

The following problems are equivalent and called the isoperimetric problem:

Isoperimetric problem (Queen Dido's problem)

- Among all "closed curves" in the plane of fixed perimeter, which curve maximizes the area of its enclosed region?
- Among all "closed curves" in the plane enclosing a fixed area, which curve minimizes the perimeter?

Isoperimetric problem (2D, 等周問題)

The following problems are equivalent and called the isoperimetric problem:

Isoperimetric problem (Queen Dido's problem)

- Among all "closed curves" in the plane of fixed perimeter, which curve maximizes the area of its enclosed region?
- Among all "closed curves" in the plane enclosing a fixed area, which curve minimizes the perimeter?

The answer is the circle.
(the "most symmetric" shape)

Mathematically, we must clarify the class of "curves".

Isoperimetric problem (3D)

Isoperimetric problem (“Mathematical soap bubbles”)

Among all “closed surfaces” enclosing a fixed volume, which surface minimizes the area?

“Anisotropic” isoperimetric problem

Can we consider the following types of “anisotropic” objects (e.g., crystals)?

Figure: A salt crystal

Figure: An alum crystal

https://mmlnp.exblog.jp/28347204/, https://kyokoippoppo.hatenablog.com/entry/2021/04/18/083916

They have some “preferred” directions (faces) → “anisotropic” energy

“Anisotropic” isoperimetric problem

Anisotropic isoperimetric problem (“Mathematical crystals”)

Among all “closed surfaces” enclosing a fixed volume,
which surface minimizes the “anisotropic” energy?

→ the answer is called the Wulff shape (“anisotropic sphere”).

A mathematical formulation

A brief review of the area functional

Let M be a 2-dimensional manifold and $\boldsymbol{r} : M \to \mathbb{R}^3$ be an immersion.
For the (local) coordinates (x, y), define the area element dA as follows:

$$dA = \|\boldsymbol{r}_x \times \boldsymbol{r}_y\| \, dxdy. \tag{1}$$

The area A and (algebraic) volume V enclosed by the surface are defined as follows:

$$A = \int_M dA, \quad V = \frac{1}{3} \int_M \langle \boldsymbol{r}, \boldsymbol{N} \rangle \, dA, \tag{2}$$

where $\boldsymbol{N}$ denotes the unit normal.

"Solution" of the isoperimetric problem

Among all "closed surfaces" enclosing a fixed volume, the sphere minimizes the area.

A brief review of the area functional

Theorems

- For a small perturbation (variation) $\boldsymbol{r}_\varepsilon = \boldsymbol{r} + \varepsilon \boldsymbol{V} + O(\varepsilon^2)$, we have

$$\left. \frac{d}{d\varepsilon} \right|_{\varepsilon=0} A(\boldsymbol{r}_\varepsilon) = \lim_{\varepsilon \to 0} \frac{A(\boldsymbol{r}_\varepsilon) - A(\boldsymbol{r})}{\varepsilon} = -2 \int_M \mathcal{H} \langle \boldsymbol{V}, \boldsymbol{N} \rangle \, dA, \tag{3}$$

  for boundary-fixed variations. Here $\mathcal{H}$: mean curvature, $\boldsymbol{N}$: unit normal.
- A stationary point of the area for volume-preserving variations must be CMC.
- If a closed CMC surface $\boldsymbol{r}$ is "stable (2nd var. ≥ 0)", then $\boldsymbol{r}$ must be the sphere.

J. L. Barbosa and M. do Carmo, Stability of hypersurfaces with constant mean curvature. Math Z. 185, 339–353 (1984).

Anisotropic energy

Definition (anisotropic energy)

For a function $\gamma : S^2 \to \mathbb{R}_{>0}$, the anisotropic energy $\mathcal{F}_\gamma$ for a surface $\boldsymbol{r}$ is defined by

$$\mathcal{F}_\gamma(\boldsymbol{r}) = \int_M \gamma(\boldsymbol{N})\, dA. \tag{4}$$

Theorem (J. E. Taylor, 1978)

Among all "closed surfaces" enclosing a fixed volume, the minimizer of $\mathcal{F}_\gamma$ is given by the Wulff shape:

$$W_\gamma = \partial \bigcap_{N \in S^2} \{x \in \mathbb{R}^3 \mid \langle x, N \rangle \le \gamma(N)\}. \tag{5}$$

Examples

A trivial choice: $\gamma = 1$. Then $\mathcal{F}_\gamma = A$, and W_γ becomes the sphere.

$\gamma = |N_1| + |N_2| + |N_3|$:

Figure: Wulff shape

$\gamma = 1$:

Figure: Wulff shape

$\gamma = (N_1^8 + N_2^8 + N_3^8)^{1/8}$:

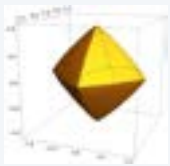

Figure: Wulff shape

→ The anisotropy naturally generates the "corners" (without connecting patches).

Cahn-Hoffman map

The Cahn-Hoffman map gives a "parametrization" of the Wulff shape.

Definition (Cahn-Hoffman, 1972)

For a function $\gamma : \mathbb{S}^2 \to \mathbb{R}_{>0}$, define the Cahn-Hoffman map ξ_γ as follows:

$$\xi_\gamma(\boldsymbol{N}) = D\gamma + \gamma(\boldsymbol{N})\boldsymbol{N}, \quad \boldsymbol{N} \in \mathbb{S}^2, \tag{6}$$

where $D\gamma$ denotes the gradient on $\mathbb{S}^2$ at $\boldsymbol{N}$.

Trivial example: if $\gamma = 1$, then $\xi_\gamma(\boldsymbol{N}) = \boldsymbol{N}$.

L^p-norm example: if $\gamma(N_1, N_2, N_3) = (N_1^p + N_2^p + N_3^p)^{1/p}$, then

$$\xi_\gamma(\boldsymbol{N}) = \xi_\gamma(N_1, N_2, N_3) = (N_1^p + N_2^p + N_3^p)^{(1-p)/p}(N_1^{p-1}, N_2^{p-1}, N_3^{p-1}). \tag{7}$$

CAMC condition

Proposition and Definition

The first variation of the anisotropic energy (fixed boundary):

$$\left.\frac{d}{d\varepsilon}\right|_{\varepsilon=0} \mathcal{F}_\gamma = -2\int_M \Lambda\langle \boldsymbol{V}, \boldsymbol{N}\rangle \, dA. \tag{8}$$

Here, Λ is called anisotropic mean curvature.
As in the "soap bubble" case, a stationary point of $\mathcal{F}_\gamma$ under volume-preserving variations must have constant anisotropic mean curvature (CAMC).

M. Koiso and B. Palmer. Geometry and stability of surfaces with constant anisotropic mean curvature. Indiana Univ. Math. J. 54 (2005), 1817–1852

$\rightarrow$ a story analogous to CMC surfaces!

A discretization

Discrete anisotropic energy

For a triangular mesh M in $\mathbb{R}^3$, the anisotropic energy $\mathcal{F}_\gamma$ is given by

$$\mathcal{F}_\gamma = \sum_T \gamma(\boldsymbol{N}_T) A(T), \tag{9}$$

where $A(T)$ is the area of the triangle T.

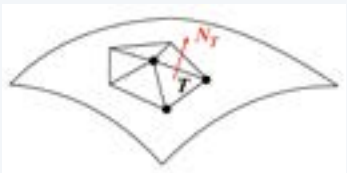

Figure: A triangular mesh and the unit normal $\boldsymbol{N}_T$ on a triangle T.

First variation

Let us consider a variation of vertices (v_p: "variation vector"):

$$p(\varepsilon) = p + \varepsilon v_p + O(\varepsilon^2). \tag{10}$$

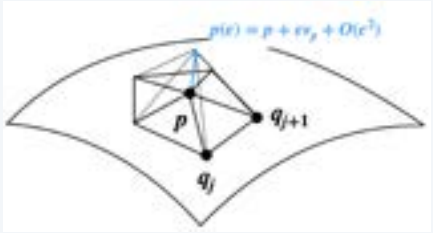

Figure: A variation of vertices

First variation

Theorem

Then, the first variation formula can be written as follows:

$$\left.\frac{d}{d\varepsilon}\right|_{\varepsilon=0} \mathcal{F}_\gamma = \sum_p \langle \nabla_p \mathcal{F}_\gamma, v_p \rangle,$$

$$\nabla_p \mathcal{F}_\gamma = \frac{1}{2} \sum_{T=(p,q_j,q_{j+1}) \in \mathrm{star}\,(p)} \xi_\gamma(\boldsymbol{N}_j) \times (q_{j+1} - q_j).$$

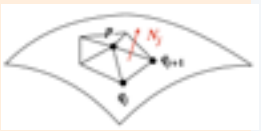

Note: if $\gamma = 1$, the privileged cotangent formula is retrieved.

Y. Jikumaru, Geometry of equilibrium curves and surfaces for discrete anisotropic energy, JSIAM Lett. 14 (2022) 57–60.

U. Pinkall and K. Polthier, Computing discrete minimal surfaces and their conjugates, Exper. Math. 2(1): 15–36 (1993).

Discrete CAMC surface

Definition

For a given constant Λ_0, a triangular mesh is called CAMC-Λ_0 if

$$\nabla_p \mathcal{F}_\gamma + 2\Lambda_0 \nabla_p V = 0, \tag{11}$$

holds away from the boundary.

The CAMC-Λ_0 condition is defined without defining the discrete anisotropic mean curvature. The idea originates discrete CMC surfaces by Polthier-Rossman.

K. Polthier and W. Rossman, Discrete constant mean curvature surfaces and their index J. reine und angew. Math. 549(549):47–77 (2002).

Basic properties

Theorem

For a closed CAMC-Λ_0 surface, the Minkowski-type formula holds:

$$\sum_T (\gamma(\boldsymbol{N}_T) + \Lambda_0 \langle p, \boldsymbol{N}_T \rangle) A(T) = 0 \iff \mathcal{F}_\gamma + 3\Lambda_0 V = 0. \tag{12}$$

Theorem

Let $\gamma : \mathbb{S}^2 \to \mathbb{R}_{>0}$ be of class C^2 and "convex". If a discrete CAMC surface has only one interior vertex, then the second variation is non-negative.

Y. Jikumaru, Geometry of equilibrium curves and surfaces for discrete anisotropic energy, JSIAM Lett. 14 (2022) 57–60.

Example of shape generation: $\gamma = (N_1^8 + N_2^8 + N_3^8)^{1/8}$

For each triangle, we can compute the Cahn-Hoffman map:

$$\xi_\gamma(\boldsymbol{N}) = \xi_\gamma(N_1, N_2, N_3) = (N_1^8 + N_2^8 + N_3^8)^{-7/8}(N_1^7, N_2^7, N_3^7). \tag{13}$$

The energy gradient:

$$\nabla_p \mathcal{F}_\gamma = \frac{1}{2} \sum_{T=(p,q_j,q_{j+1})} \xi_\gamma(\boldsymbol{N}_j) \times (q_{j+1} - q_j). \tag{14}$$

Technical part for shape generation

General setting

In general, if the unit normal $\boldsymbol{N}$ is parametrized by

$$\boldsymbol{N} = (N_1, N_2, N_3) = (\cos x \cos y, \cos x \sin y, \sin x), \tag{15}$$

then the Cahn-Hoffman map for $\gamma = \gamma(x, y)$ is given by

$$\xi_\gamma = \gamma_x \boldsymbol{X} + \frac{\gamma_y}{\sqrt{N_1^2 + N_2^2}} \boldsymbol{Y} + \gamma \boldsymbol{N}, \tag{16}$$

where the unit tangent vectors $\boldsymbol{X}, \boldsymbol{Y}$ are given

$$\boldsymbol{X} = \left(-\frac{N_1 N_3}{\sqrt{N_1^2 + N_2^2}}, -\frac{N_2 N_3}{\sqrt{N_1^2 + N_2^2}}, \sqrt{N_1^2 + N_2^2} \right), \quad \boldsymbol{Y} = \left(-\frac{N_2}{\sqrt{N_1^2 + N_2^2}}, \frac{N_1}{\sqrt{N_1^2 + N_2^2}}, 0 \right). \tag{17}$$

$\rightarrow$ if $\gamma = \gamma(x, y)$ is given, we can compute ξ_γ.

Energy density determined by the Gielis formula

We use the so-called Gielis' (super)formula to generate various shapes in a parameter-controllable setting.

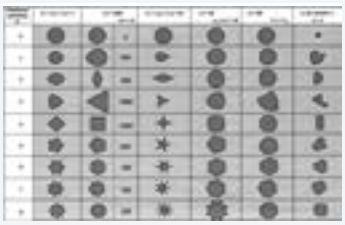

Figure: Various shapes generated by the formula, motivated by botany.

J. Gielis, A generic geometric transformation that unifies a large range of natural and abstract shapes, Amer. J. Botany, 90(3), 333–338 (2003).

Energy density determined by the Gielis formula

For example, define r_1 and r_2 as follows:

$$r_1 = ((N_1^2 + N_2^2)^{k_1} + N_3^{2k_1})^{1/(2l_1)}, \quad r_2 = \left(\frac{N_1^{2k_2} + N_2^{2k_2}}{(N_1^2 + N_2^2)^{k_2}} \right)^{1/(2l_2)}. \tag{18}$$

In this case, the user can specify 4 parameters.

Then for the energy density $\gamma = r_1 r_2$, we have

$$\xi = A r_2 \boldsymbol{X} + \frac{r_1 B}{\sqrt{N_1^2 + N_2^2}} \boldsymbol{Y} + r_1 r_2 \boldsymbol{N}. \tag{19}$$

Here, A and B are given on the next page:

Energy density determined by the Gielis formula

Although the expressions are complicated, all quantities can be computed explicitly.

$$A = \frac{k_1}{l_1}((N_1^2+N_2^2)^{k_1}+N_3^{2k_1})^{1/(2l_1)-1}\left(N_3^{2k_1-1}\sqrt{N_1^2+N_2^2}-N_3(N_1^2+N_2^2)^{k_1-\frac{1}{2}}\right),$$

$$B = \frac{k_2}{l_2}\left(\frac{N_1^{2k_2}+N_2^{2k_2}}{(N_1^2+N_2^2)^{k_2}}\right)^{1/(2l_2)-1}\left(\frac{N_1N_2^{2k_2-1}-N_1^{2k_2-1}N_2}{(N_1^2+N_2^2)^{k_2}}\right),$$

$$r_1 = ((N_1^2+N_2^2)^{k_1}+N_3^{2k_1})^{1/(2l_1)}, \quad r_2 = \left(\frac{N_1^{2k_2}+N_2^{2k_2}}{(N_1^2+N_2^2)^{k_2}}\right)^{1/(2l_2)}.$$

$$\boldsymbol{X} = \left(-\frac{N_1N_3}{\sqrt{N_1^2+N_2^2}}, -\frac{N_2N_3}{\sqrt{N_1^2+N_2^2}}, \sqrt{N_1^2+N_2^2}\right), \quad \boldsymbol{Y} = \left(-\frac{N_2}{\sqrt{N_1^2+N_2^2}}, \frac{N_1}{\sqrt{N_1^2+N_2^2}}, 0\right).$$

Which direction do you want to create larger faces?

The direction in which the user wants to create more surfaces becomes “bigger”:

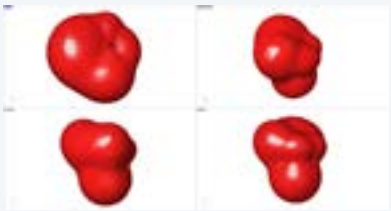

The surface is called the Frank shape.

- Convex direction: large faces (“preferable” directions).
- Concave direction: small faces (“unpreferable” directions).

Demonstration video

Let’s take a look at a demonstration (link).

Summary

Summary

- Shape generation with “corners” without connecting surface patches.
- The user specifies the direction in which they want to create more faces by changing the parameters (“ideal lighting”).
- The idea came from the geometry of anisotropic energy, which originates the crystal growth model.

Geometric Shape Generation by Singular Generalized Miura-ori with Canonical and Non-canonical Arrangements

Hiroyuki Tagawa
Department of Architecture, Mukogawa Women's University, Japan

Abstract

Generalized Miura-ori with the canonical arrangement, including well-known Miura-ori as well as proposed arc- and spiral-shaped Miura-ori [1], can be folded flat without causing self-intersections. A total of 26 patterns of singular generalized Miura-ori, which is defined as the generalized Miura-ori that has symmetry and regularity in included angles to enable rigid flat-foldability with linked one degree-of-freedom motion, is counted for the canonical arrangement as follows: 11 patterns for $K_1 = K_4$, $K_2 = K_3$, 11 patterns for $K_1 = K_2$, $K_3 = K_4$, and 4 patterns for $K_1 = K_2 = K_3 = K_4$ [2]. Among 26 patterns, the arc- and spiral-shaped Miura-ori, which are classified as $K_1 = K_2$, $K_3 = K_4$, are the only patterns in which all the fold lines are not parallel to each other.
Non-canonical arrangement is obtained by exchanging the included angles at the diagonal positions of the Units 2 and 3 in the canonical arrangement and accordingly changing the mountain and valley folding directions as shown in Fig. 1. These exhibit 3D cylindrical or vault shape while satisfying the linked folding conditions. A total of 17 patterns of singular generalized Miura-ori is counted for the above non-canonical arrangement as follows: 11 patterns for $K_1 = K_4$, $K_2' = K_3'$, 2 patterns for $K_1 = K_2'$, $K_3' = K_4$, and 4 patterns for $K_1 = K_2' = K_3' = K_4$. Huffman tessellation and the dual of Miura-ori (Hourglass mode) are classified as $K_1 = K_2' = K_3' = K_4$. Cylindrical closed shape is obtained by the optimization on included angles of the quadrilaterals and deployment angle as shown in Fig. 2.

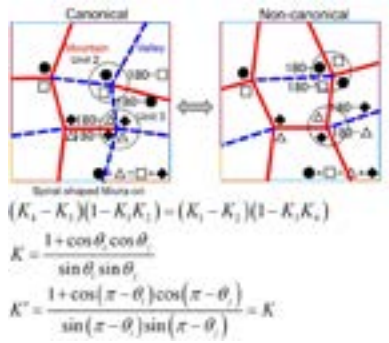

Fig. 1 Dual conversions

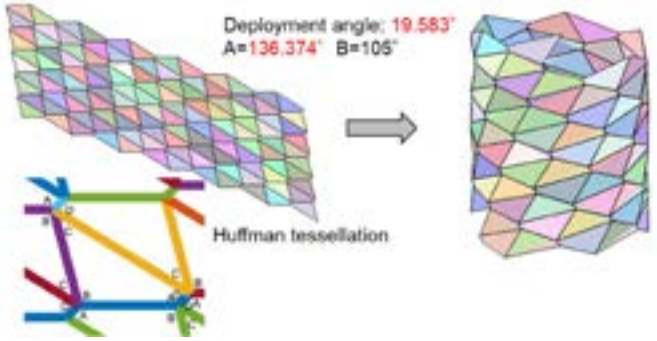

Figure 3: *
Fig. 2 Cylindrical closed shape obtained by optimization

References

[1] H. Tagawa, N. Yoshioka, T. Suzuki, "Proposal of arc- and spiral-shaped Miura-ori and its application to the design of large roof architecture", Proceedings of the IASS symposium 2022, Beijing, China, 2022.

[2] H. Tagawa, A. Sugimura, A. Mukai, K. Inomata, "Counting-up and classification of all combination patterns of singular generalized Miura-ori", Proceedings of the IASS symposium 2024, Zurich, Switzerland, 2024.

MI レクチャーノートシリーズ刊行にあたり

本レクチャーノートシリーズは、文部科学省 21 世紀 COE プログラム「機能数理学の構築と展開」（H15-19 年度）において作成した COE Lecture Notes の続刊であり、文部科学省大学院教育改革支援プログラム「産業界が求める数学博士と新修士養成」（H19-21 年度）および、同グローバル COE プログラム「マス・フォア・インダストリ教育研究拠点」（H20-24 年度）において行われた講義の講義録として出版されてきた。平成 23 年 4 月のマス・フォア・インダストリ研究所（IMI）設立と平成 25 年 4 月の IMI の文部科学省共同利用・共同研究拠点として「産業数学の先進的･基礎的共同研究拠点」の認定を受け、今後、レクチャーノートは、マス・フォア・インダストリに関わる国内外の研究者による講義の講義録、会議録等として出版し、マス・フォア・インダストリの本格的な展開に資するものとする。

2022 年 10 月
マス・フォア・インダストリ研究所
所長　梶原 健司

2024年度採択分　九州大学マス･フォア･インダストリ研究所 共同利用研究集会

設計の新パラダイムを拓く新しい離散的な曲面の幾何学

発　行　2025年 10 月 1 日
編　集　大崎　純 , 軸丸　芳揮
発　行　九州大学マス・フォア・インダストリ研究所
九州大学大学院数理学府
〒819-0395 福岡市西区元岡744
九州大学数理・IMI 事務室
TEL 092-802-4402　FAX 092-802-4405
URL https://www.imi.kyushu-u.ac.jp/

印　刷　城島印刷株式会社
〒810-0012 福岡市中央区白金 2 丁目 9 番 6 号
TEL 092-531-7102　FAX 092-524-4411

シリーズ既刊

Issue	Author／Editor	Title	Published
COE Lecture Note	Mitsuhiro T. NAKAO Kazuhiro YOKOYAMA	Computer Assisted Proofs - Numeric and Symbolic Approaches - 199pages	August 22, 2006
COE Lecture Note	M.J.Shai HARAN	Arithmetical Investigations - Representation theory, Orthogonal polynomials and Quantum interpolations- 174pages	August 22, 2006
COE Lecture Note Vol.3	Michal BENES Masato KIMURA Tatsuyuki NAKAKI	Proceedings of Czech-Japanese Seminar in Applied Mathematics 2005 155pages	October 13, 2006
COE Lecture Note Vol.4	宮田　健治	辺要素有限要素法による磁界解析 - 機能数理学特別講義 21pages	May 15, 2007
COE Lecture Note Vol.5	Francois APERY	Univariate Elimination Subresultants - Bezout formula, Laurent series and vanishing conditions - 89pages	September 25, 2007
COE Lecture Note Vol.6	Michal BENES Masato KIMURA Tatsuyuki NAKAKI	Proceedings of Czech-Japanese Seminar in Applied Mathematics 2006 209pages	October 12, 2007
COE Lecture Note Vol.7	若山　正人 中尾　充宏	九州大学産業技術数理研究センター キックオフミーティング 138pages	October 15, 2007
COE Lecture Note Vol.8	Alberto PARMEGGIANI	Introduction to the Spectral Theory of Non-Commutative Harmonic Oscillators 233pages	January 31, 2008
COE Lecture Note Vol.9	Michael I.TRIBELSKY	Introduction to Mathematical modeling 23pages	February 15, 2008
COE Lecture Note Vol.10	Jacques FARAUT	Infinite Dimensional Spherical Analysis 74pages	March 14, 2008
COE Lecture Note Vol.11	Gerrit van DIJK	Gelfand Pairs And Beyond 60pages	August 25, 2008
COE Lecture Note Vol.12	Faculty of Mathematics, Kyushu University	Consortium “MATH for INDUSTRY” First Forum 87pages	September 16, 2008
COE Lecture Note Vol.13	九州大学大学院 数理学研究院	プロシーディング「損保数理に現れる確率モデル」 ― 日新火災・九州大学 共同研究2008年11月 研究会 ― 82pages	February 6, 2009

シリーズ既刊

Issue	Author／Editor	Title	Published
COE Lecture Note Vol.14	Michal Beneš, Tohru Tsujikawa Shigetoshi Yazaki	Proceedings of Czech-Japanese Seminar in Applied Mathematics 2008 77pages	February 12, 2009
COE Lecture Note Vol.15	Faculty of Mathematics, Kyushu University	International Workshop on Verified Computations and Related Topics 129pages	February 23, 2009
COE Lecture Note Vol.16	Alexander Samokhin	Volume Integral Equation Method in Problems of Mathematical Physics 50pages	February 24, 2009
COE Lecture Note Vol.17	矢嶋　　徹 及川　正行 梶原　健司 辻　　英一 福本　康秀	非線形波動の数理と物理 66pages	February 27, 2009
COE Lecture Note Vol.18	Tim Hoffmann	Discrete Differential Geometry of Curves and Surfaces 75pages	April 21, 2009
COE Lecture Note Vol.19	Ichiro Suzuki	The Pattern Formation Problem for Autonomous Mobile Robots —Special Lecture in Functional Mathematics— 23pages	April 30, 2009
COE Lecture Note Vol.20	Yasuhide Fukumoto Yasunori Maekawa	Math-for-Industry Tutorial: Spectral theories of non-Hermitian operators and their application 184pages	June 19, 2009
COE Lecture Note Vol.21	Faculty of Mathematics, Kyushu University	Forum “Math-for-Industry” Casimir Force, Casimir Operators and the Riemann Hypothesis 95pages	November 9, 2009
COE Lecture Note Vol.22	Masakazu Suzuki Hoon Hong Hirokazu Anai Chee Yap Yousuke Sato Hiroshi Yoshida	The Joint Conference of ASCM 2009 and MACIS 2009: Asian Symposium on Computer Mathematics Mathematical Aspects of Computer and Information Sciences 436pages	December 14, 2009
COE Lecture Note Vol.23	荒川　恒男 金子　昌信	多重ゼータ値入門 111pages	February 15, 2010
COE Lecture Note Vol.24	Fulton B.Gonzalez	Notes on Integral Geometry and Harmonic Analysis 125pages	March 12, 2010
COE Lecture Note Vol.25	Wayne Rossman	Discrete Constant Mean Curvature Surfaces via Conserved Quantities 130pages	May 31, 2010
COE Lecture Note Vol.26	Mihai Ciucu	Perfect Matchings and Applications 66pages	July 2, 2010

シリーズ既刊

Issue	Author／Editor	Title	Published
COE Lecture Note Vol.27	九州大学大学院 数理学研究院	Forum “Math-for-Industry” and Study Group Workshop Information security, visualization, and inverse problems, on the basis of optimization techniques　100pages	October 21, 2010
COE Lecture Note Vol.28	ANDREAS LANGER	MODULAR FORMS, ELLIPTIC AND MODULAR CURVES LECTURES AT KYUSHU UNIVERSITY 2010　62pages	November 26, 2010
COE Lecture Note Vol.29	木田　雅成 原田　昌晃 横山　俊一	Magma で広がる数学の世界　157pages	December 27, 2010
COE Lecture Note Vol.30	原　　隆 松井　　卓 廣島　文生	Mathematical Quantum Field Theory and Renormalization Theory 201pages	January 31, 2011
COE Lecture Note Vol.31	若山　正人 福本　康秀 高木　　剛 山本　昌宏	Study Group Workshop 2010 Lecture & Report　128pages	February 8, 2011
COE Lecture Note Vol.32	Institute of Mathematics for Industry, Kyushu University	Forum “Math-for-Industry” 2011 “TSUNAMI-Mathematical Modelling” Using Mathematics for Natural Disaster Prediction, Recovery and Provision for the Future　90pages	September 30, 2011
COE Lecture Note Vol.33	若山　正人 福本　康秀 高木　　剛 山本　昌宏	Study Group Workshop 2011 Lecture & Report　140pages	October 27, 2011
COE Lecture Note Vol.34	Adrian Muntean Vladimír Chalupecký	Homogenization Method and Multiscale Modeling　72pages	October 28, 2011
COE Lecture Note Vol.35	横山　俊一 夫　　紀恵 林　　卓也	計算機代数システムの進展　210pages	November 30, 2011
COE Lecture Note Vol.36	Michal Beneš Masato Kimura Shigetoshi Yazaki	Proceedings of Czech-Japanese Seminar in Applied Mathematics 2010 107pages	January 27, 2012
COE Lecture Note Vol.37	若山　正人 高木　　剛 Kirill Morozov 平岡　裕章 木村　正人 白井　朋之 西井　龍映 栄　伸一郎 穴井　宏和 福本　康秀	平成23年度 数学・数理科学と諸科学・産業との連携研究ワークショップ　拡がっていく数学　～期待される “見えない力” ～ 154pages	February 20, 2012

シリーズ既刊

Issue	Author／Editor	Title	Published
COE Lecture Note Vol.38	Fumio Hiroshima Itaru Sasaki Herbert Spohn Akito Suzuki	Enhanced Binding in Quantum Field Theory 204pages	March 12, 2012
COE Lecture Note Vol.39	Institute of Mathematics for Industry, Kyushu University	Multiscale Mathematics: Hierarchy of collective phenomena and interrelations between hierarchical structures 180pages	March 13, 2012
COE Lecture Note Vol.40	井ノ口順一 太田　泰広 筧　三郎 梶原　健司 松浦　望	離散可積分系・離散微分幾何チュートリアル2012 152pages	March 15, 2012
COE Lecture Note Vol.41	Institute of Mathematics for Industry, Kyushu University	Forum “Math-for-Industry” 2012 “Information Recovery and Discovery” 91pages	October 22, 2012
COE Lecture Note Vol.42	佐伯　修 若山　正人 山本　昌宏	Study Group Workshop 2012 Abstract, Lecture & Report 178pages	November 19, 2012
COE Lecture Note Vol.43	Institute of Mathematics for Industry, Kyushu University	Combinatorics and Numerical Analysis Joint Workshop 103pages	December 27, 2012
COE Lecture Note Vol.44	萩原　学	モダン符号理論からポストモダン符号理論への展望 107pages	January 30, 2013
COE Lecture Note Vol.45	金山　寛	Joint Research Workshop of Institute of Mathematics for Industry (IMI), Kyushu University “Propagation of Ultra-large-scale Computation by the Domain-decomposition-method for Industrial Problems (PUCDIP 2012)” 121pages	February 19, 2013
COE Lecture Note Vol.46	西井　龍映 栄　伸一郎 岡田　勘三 落合　啓之 小磯　深幸 斎藤　新悟 白井　朋之	科学・技術の研究課題への数学アプローチ ―数学モデリングの基礎と展開― 325pages	February 28, 2013
COE Lecture Note Vol.47	SOO TECK LEE	BRANCHING RULES AND BRANCHING ALGEBRAS FOR THE COMPLEX CLASSICAL GROUPS 40pages	March 8, 2013
COE Lecture Note Vol.48	溝口　佳寛 脇　隼人 平坂　貢 谷口　哲至 島袋　修	博多ワークショップ「組み合わせとその応用」 124pages	March 28, 2013

シリーズ既刊

Issue	Author／Editor	Title	Published
COE Lecture Note Vol.49	照井　章 小原　功任 濱田　龍義 横山　俊一 穴井　宏和 横田　博史	マス・フォア・インダストリ研究所　共同利用研究集会 II 数式処理研究と産学連携の新たな発展　137pages	August 9, 2013
MI Lecture Note Vol.50	Ken Anjyo Hiroyuki Ochiai Yoshinori Dobashi Yoshihiro Mizoguchi Shizuo Kaji	Symposium MEIS2013: Mathematical Progress in Expressive Image Synthesis　154pages	October 21, 2013
MI Lecture Note Vol.51	Institute of Mathematics for Industry, Kyushu University	Forum “Math-for-Industry” 2013 “The Impact of Applications on Mathematics”　97pages	October 30, 2013
MI Lecture Note Vol.52	佐伯　修 岡田　勘三 髙木　剛 若山　正人 山本　昌宏	Study Group Workshop 2013 Abstract, Lecture & Report　142pages	November 15, 2013
MI Lecture Note Vol.53	四方　義啓 櫻井　幸一 安田　貴徳 Xavier Dahan	平成25年度　九州大学マス・フォア・インダストリ研究所 共同利用研究集会　安全・安心社会基盤構築のための代数構造 ～サイバー社会の信頼性確保のための数理学～　158pages	December 26, 2013
MI Lecture Note Vol.54	Takashi Takiguchi Hiroshi Fujiwara	Inverse problems for practice, the present and the future　93pages	January 30, 2014
MI Lecture Note Vol.55	栄　伸一郎 溝口　佳寛 脇　隼人 渋田　敬史	Study Group Workshop 2013 数学協働プログラム Lecture & Report 98pages	February 10, 2014
MI Lecture Note Vol.56	Yoshihiro Mizoguchi Hayato Waki Takafumi Shibuta Tetsuji Taniguchi Osamu Shimabukuro Makoto Tagami Hirotake Kurihara Shuya Chiba	Hakata Workshop 2014 ~ Discrete Mathematics and its Applications ~　141pages	March 28, 2014
MI Lecture Note Vol.57	Institute of Mathematics for Industry, Kyushu University	Forum “Math-for-Industry” 2014: “Applications + Practical Conceptualization + Mathematics = fruitful Innovation”　93pages	October 23, 2014
MI Lecture Note Vol.58	安生健一 落合啓之	Symposium MEIS2014: Mathematical Progress in Expressive Image Synthesis　135pages	November 12, 2014

シリーズ既刊

Issue	Author／Editor	Title	Published
MI Lecture Note Vol.59	西井　龍映 岡田　勘三 梶原　健司 髙木　　剛 若山　正人 脇　　隼人 山本　昌宏	Study Group Workshop 2014 数学協働プログラム Abstract, Lecture & Report　196pages	November 14, 2014
MI Lecture Note Vol.60	西浦　　博	平成26年度九州大学 IMI 共同利用研究・研究集会（I） 感染症数理モデルの実用化と産業及び政策での活用のための新たな展開　120pages	November 28, 2014
MI Lecture Note Vol.61	溝口　佳寛 Jacques Garrigue 萩原　　学 Reynald Affeldt	研究集会 高信頼な理論と実装のための定理証明および定理証明器 Theorem proving and provers for reliable theory and implementations (TPP2014)　138pages	February 26, 2015
MI Lecture Note Vol.62	白井　朋之	Workshop on “β-transformation and related topics”　59pages	March 10, 2015
MI Lecture Note Vol.63	白井　朋之	Workshop on “Probabilistic models with determinantal structure” 107pages	August 20, 2015
MI Lecture Note Vol.64	落合　啓之 土橋　宜典	Symposium MEIS2015: Mathematical Progress in Expressive Image Synthesis　124pages	September 18, 2015
MI Lecture Note Vol.65	Institute of Mathematics for Industry, Kyushu University	Forum “Math-for-Industry” 2015 “The Role and Importance of Mathematics in Innovation”　74pages	October 23, 2015
MI Lecture Note Vol.66	岡田　勘三 藤澤　克己 白井　朋之 若山　正人 脇　　隼人 Philip Broadbridge 山本　昌宏	Study Group Workshop 2015 Abstract, Lecture & Report 156pages	November 5, 2015
MI Lecture Note Vol.67	Institute of Mathematics for Industry, Kyushu University	IMI-La Trobe Joint Conference “Mathematics for Materials Science and Processing” 66pages	February 5, 2016
MI Lecture Note Vol.68	古庄　英和 小谷　久寿 新甫　洋史	結び目と Grothendieck-Teichmüller 群 116pages	February 22, 2016
MI Lecture Note Vol.69	土橋　宜典 鍛治　静雄	Symposium MEIS2016: Mathematical Progress in Expressive Image Synthesis　82pages	October 24, 2016
MI Lecture Note Vol.70	Institute of Mathematics for Industry, Kyushu University	Forum “Math-for-Industry” 2016 “Agriculture as a metaphor for creativity in all human endeavors” 98pages	November 2, 2016
MI Lecture Note Vol.71	小磯　深幸 二宮　嘉行 山本　昌宏	Study Group Workshop 2016 Abstract, Lecture & Report　143pages	November 21, 2016

シリーズ既刊

Issue	Author／Editor	Title	Published
MI Lecture Note Vol.72	新井　朝雄 小嶋　　泉 廣島　文生	Mathematical quantum field theory and related topics　133pages	January 27, 2017
MI Lecture Note Vol.73	穴田　啓晃 Kirill Morozov 須賀　祐治 奥村　伸也 櫻井　幸一	Secret Sharing for Dependability, Usability and Security of Network Storage and Its Mathematical Modeling　211pages	March 15, 2017
MI Lecture Note Vol.74	QUISPEL, G. Reinout W. BADER, Philipp MCLAREN, David I. TAGAMI, Daisuke	IMI-La Trobe Joint Conference Geometric Numerical Integration and its Applications　71pages	March 31, 2017
MI Lecture Note Vol.75	手塚　　集 田上　大助 山本　昌宏	Study Group Workshop 2017 Abstract, Lecture & Report　118pages	October 20, 2017
MI Lecture Note Vol.76	宇田川誠一	Tzitzéica 方程式の有限間隙解に付随した極小曲面の構成理論 ―Tzitzéica 方程式の楕円関数解を出発点として―　68pages	August 4, 2017
MI Lecture Note Vol.77	松谷　茂樹 佐伯　　修 中川　淳一 田上　大助 上坂　正晃 Pierluigi Cesana 濵田　裕康	平成29年度　九州大学マス・フォア・インダストリ研究所 共同利用研究集会（I） 結晶の界面，転位，構造の数理　148pages	December 20, 2017
MI Lecture Note Vol.78	瀧澤　重志 小林　和博 佐藤憲一郎 斎藤　　努 清水　正明 間瀬　正啓 藤澤　克樹 神山　直之	平成29年度　九州大学マス・フォア・インダストリ研究所 プロジェクト研究　研究集会（I） 防災・避難計画の数理モデルの高度化と社会実装へ向けて 136pages	February 26, 2018
MI Lecture Note Vol.79	神山　直之 畔上　秀幸	平成29年度　AIMaP チュートリアル 最適化理論の基礎と応用　96pages	February 28, 2018
MI Lecture Note Vol.80	Kirill Morozov Hiroaki Anada Yuji Suga	IMI Workshop of the Joint Research Projects Cryptographic Technologies for Securing Network Storage and Their Mathematical Modeling　116pages	March 30, 2018
MI Lecture Note Vol.81	Tsuyoshi Takagi Masato Wakayama Keisuke Tanaka Noboru Kunihiro Kazufumi Kimoto Yasuhiko Ikematsu	IMI Workshop of the Joint Research Projects International Symposium on Mathematics, Quantum Theory, and Cryptography　246pages	September 25, 2019
MI Lecture Note Vol.82	池森　俊文	令和2年度　AIMaP チュートリアル 新型コロナウイルス感染症にかかわる諸問題の数理 145pages	March 22, 2021

シリーズ既刊

Issue	Author／Editor	Title	Published
MI Lecture Note Vol.83	早川健太郎 軸丸　芳揮 横須賀洋平 可香谷　隆 林　　和希 堺　　雄亮	シェル理論・膜理論への微分幾何学からのアプローチと その建築曲面設計への応用　49pages	July 28, 2021
MI Lecture Note Vol.84	Taketoshi Kawabe Yoshihiro Mizoguchi Junichi Kako Masakazu Mukai Yuji Yasui	SICE-JSAE-AIMaP Tutorial Advanced Automotive Control and Mathematics　110pages	December 27, 2021
MI Lecture Note Vol.85	Hiroaki Anada Yasuhiko Ikematsu Koji Nuida Satsuya Ohata Yuntao Wang	IMI Workshop of the Joint Usage Research Projects Exploring Mathematical and Practical Principles of Secure Computation and Secret Sharing　114pages	February 9, 2022
MI Lecture Note Vol.86	濱田　直希 穴井　宏和 梅田　裕平 千葉　一永 佐藤　寛之 能島　裕介 加葉田雄太朗 一木　俊助 早野　健太 佐伯　　修	2020年度採択分　九州大学マス・フォア・インダストリ研究所 共同利用研究集会 進化計算の数理　135pages	February 22, 2022
MI Lecture Note Vol.87	Osamu Saeki, Ho Tu Bao, Shizuo Kaji, Kenji Kajiwara, Nguyen Ha Nam, Ta Hai Tung, Melanie Roberts, Masato Wakayama, Le Minh Ha, Philip Broadbridge	Proceedings of Forum “Math-for-Industry” 2021 -Mathematics for Digital Economy-　122pages	March 28, 2022
MI Lecture Note Vol.88	Daniel PACKWOOD Pierluigi CESANA, Shigenori FUJIKAWA, Yasuhide FUKUMOTO, Petros SOFRONIS, Alex STAYKOV	Perspectives on Artificial Intelligence and Machine Learning in Materials Science, February 4-6, 2022　74pages	November 8, 2022

シリーズ既刊

Issue	Author／Editor	Title	Published
MI Lecture Note Vol.89	松谷　茂樹 落合　啓之 井上　和俊 小磯　深幸 佐伯　　修 白井　朋之 垂水　竜一 内藤　久資 中川　淳一 濵田　裕康 松江　　要 加葉田雄太朗	2022年度採択分 九州大学マス・フォア・インダストリ研究所 共同利用研究集会 材料科学における幾何と代数 III　356pages	December 7, 2022
MI Lecture Note Vol.90	中山　尚子 谷川　拓司 品野　勇治 近藤　正章 石原　　亨 鍛冶　静雄 藤澤　克樹	2022年度採択分 九州大学マス・フォア・インダストリ研究所 共同利用研究集会 データ格付けサービス実現のための数理基盤の構築　58pages	December 12, 2022
MI Lecture Note Vol.91	Katsuki Fujisawa Shizuo Kaji Toru Ishihara Masaaki Kondo Yuji Shinano Takuji Tanigawa Naoko Nakayama	IMI Workshop of the Joint Usage Research Projects Construction of Mathematical Basis for Realizing Data Rating Service 610pages	December 27, 2022
MI Lecture Note Vol.92	丹田　　聡 三宮　　俊 廣島　文生	2022年度採択分 九州大学マス・フォア・インダストリ研究所 共同利用研究集会 時間・量子測定・準古典近似の理論と実験 ～古典論と量子論の境界～　150pages	Janualy 6, 2023
MI Lecture Note Vol.93	Philip Broadbridge Luke Bennetts Melanie Roberts Kenji Kajiwara	Proceedings of Forum “Math-for-Industry” 2022 -Mathematics of Public Health and Sustainability-　170pages	June 19, 2023
MI Lecture Note Vol.94	國廣　　昇 池松　泰彦 伊豆　哲也 穴田　啓晃 縫田　光司	2023年度採択分 九州大学マス・フォア・インダストリ研究所 共同利用研究集会 現代暗号に対する安全性解析・攻撃の数理　260pages	Janualy 11, 2024
MI Lecture Note Vol.96	澤田　茉伊	2023年度採択分 九州大学マス・フォア・インダストリ研究所 共同利用研究集会 デジタル化時代に求められる斜面防災の思考法　70pages	March 18, 2024

シリーズ既刊

Issue	Author／Editor	Title	Published
MI Lecture Note Vol.97	Shariffah Suhaila Syed Jamaludin Zaiton Mat Isa Nur Arina Bazilah Aziz Taufiq Khairi Ahmad Khairuddin Shaymaa M.H.Darwish Ahmad Razin Zainal Abidin Norhaiza Ahmad Zainal Abdul Aziz Hang See Pheng Mohd Ali Khameini Ahmad	International Project Research-Workshop (I) Proceedings of 4th Malaysia Mathematics in Industry Study Group (MMISG2023)　172pages	March 28, 2024
MI Lecture Note Vol.98	中澤　　嵩	2024 年度採択分 九州大学マス・フォア・インダストリ研究所 共同利用研究集会 自動車性能の飛躍的向上を目指す Data-Driven 設計　92pages	January 30, 2025
MI Lecture Note Vol.99	Jacques Garrigue	2024 年度採択分 九州大学マス・フォア・インダストリ研究所 共同利用研究集会 コンピュータによる定理証明支援とその応用　308pages	March 17, 2025
MI Lecture Note Vol.100	Yutaka Jitsumatsu Masayoshi Ohashi Akio Hasegawa Katsutoshi Shinohara Shintaro Mori	IMI Workshop of the Joint Usage Research Projects Mathematics for Innovation in Information and Communication Technology 274pages	March 19, 2025

九州大学マス・フォア・インダストリ研究所
九州大学大学院 数理学府
〒819-0395 福岡市西区元岡744　TEL 092-802-4402　FAX 092-802-4405
URL https://www.imi.kyushu-u.ac.jp/